CONF-780765
SLAC-215
(T/E)
UC-34d

PROCEEDINGS

OF

SUMMER INSTITUTE ON PARTICLE PHYSICS

July 10-21, 1978

WEAK INTERACTIONS -- PRESENT AND FUTURE

Program Directors

Frederick J. Gilman

and

David W. G. S. Leith

Ed. by Martha C. Zipf

Sponsored by Stanford University and Stanford Linear Accelerator Center under contract with the U. S. Department of Energy. Contract EY-76-C-03-0515.

November 1978

Printed in the United States of America. Available from National Technical Information Service, U.S. Department of Commerce, 5285 Port Royal Road, Springfield, Va. 22161. Prices: Printed copy $14.50; Microfiche $3.00.

PREFACE

The SLAC Summer Institute on Particle Physics met again in 1978 to concentrate on Weak Interactions -- Present and Future. Three hundred and twenty-nine theoretical and experimental physicists, representing fourteen countries, sat through seven days of pedagogy broken by afternoons of speculation on future machine possibilities. As in previous years, this was followed by a three-day topical conference with presentations on state-of-the-art experiments.

None of the speakers from the panel which led the discussions on the machines of the future chose to render their opinions in writing for inclusion in these Proceedings; therefore, without mention here, the reader might never know that these sessions took place. Those who participated were E. Picasso (Chairperson), R. Schwitters (Introduction and Large Electron-Positron Colliding Rings), R. Diebold (High Energy Proton-Proton Colliding Rings), M. Davier (Electron-Proton Colliding Rings), F. Sciulli (Fixed Target High Energy Experiments), and, halted momentarily in intraplanetary flight, C. Rubbia (Antiproton-Proton Colliding Beams). These were lively and well attended sessions, and we thank both E. Picasso for chairing them and the panel members for sharing their ideas.

The topical conference was again a very good meeting with lots of exciting new data and vigorous interchanges of ideas among the proponents. It was, as usual, crashed by several unregistered physicists, all unidentified in the list of participants. The supply of these Proceedings will closely match the number of registered participants, so we expect that in future years such behavior will be a less frequent problem.

Finally, we would like to thank the Institute's Coordinator, Martha C. Zipf, who once again survived the circumstances that arise at such meetings, managed to keep the sessions going, and provided the smooth operation and friendly atmosphere that has become the trademark of these meetings. She joins us in thanking all of you for making it what it was!

Frederick J. Gilman and David W. G. S. Leith

Program Directors

Table of Contents

PART II. Topical Conference (continued)

ACCELERATOR NEUTRINO EXPERIMENTS

D.H. Perkins
Department of Nuclear Physics
Oxford.

1. INTRODUCTION

These lectures are not intended to be a comprehensive review of accelerator neutrino physics Instead, I have selected three widely disparate topics in the field, on the basis of current interests and developments, and blind personal prejudice.

To introduce the subject I first discuss briefly the production and monitoring of neutrino beams, and the characteristics and limitations of the detectors employed. Especially now that single experiments can accumulate thousands or even hundreds of thousands of events, sources of systematic error which one could happily ignore at the hundred event level, become crucially important in the more detailed analyses which are now possible.

Next I consider the so-called inclusive charged-current neutrino reactions:- ν, $\bar{\nu}$ + nucleon → muon + anything. For such reactions, the weak interaction itself is very well understood, being of the V-A form mediated by single vector particle ($W^{\pm}$) exchange. Here, the emphasis is on using neutrino beams as a tool to probe the structure of the nucleon target, that is, to study the nature of the strong interactions. The particular advantages of neutrino beams are well known. Since $M_{W^{\pm}} \sim 80$ GeV, the propagator term does not damp down the cross-section for q^2 up to 100 GeV^2 or so, in contrast to the $1/q^4$ propagator in electron and muon scattering. The second peculiar advantage of such beams is that they are naturally spin-polarized, the left-handed neutrinos scattering preferentially off quarks, and the right-handed antineutrinos off anti-quarks. Hence, the contributions of quark and antiquark constituents to the scattering can be separated. Another feature of inelastic lepton

scattering is that, whereas the scattering of electrons and muons is determined by the square of the target charge, the neutrino scattering is determined by the change in the isospin (third component) or strangeness of the target, according to the Cabibbo (or GIM) coupling. The neutrino results thus complement those from electron scattering.

First results from the analysis of differential deep inelastic cross-sections, the structure functions and their moments are in surprisingly good quantitative agreement with the simplest (first-order in α_s) predictions of quantum chromodynamics (QCD) describing the quark-gluon constitution of hadrons. Other, more tentative, predictions of QCD relate to the distributions of secondary hadrons, interpreted as the fragmentation products of the struck partons (gluons and quarks) from the primary collision. There is a lot of activity, both theoretical and experimental, in this sector. Theoretically, it is not straightforward to separate the perturbative, calculable QCD effects from the non-perturbative (and non-calculable) contributions and the best that one could claim at present is that there do seem to be broad trends in the data which, qualitatively at least, are not in disagreement with the model.

The next major topic discussed is the subject of neutral weak currents. There has been considerable progress over the last year or so towards analyses of inclusive neutral current reactions on nucleons which are less susceptible to uncertainties in the hadron models assumed and there is now a whole range of data, from inclusive, semi-inclusive and exclusive reactions, all consistent with the SU2 x U1 (Salam-Weinberg) model with $\sin^2\theta_w \approx 0.20$-$0.25$. The study of the isospin amplitudes of the neutral current (i.e. the isovector/isoscalar admixtures) is on somewhat less solid experimental grounds but again points strongly to the SW model. The cleanest test of models is, however, in the lepton sector, in the process of neutrino-electron scattering. The numbers of events however are modest, because of the very small cross-sections. The recently-reported large $\nu_\mu e^-$ cross-section from the CERN Gargamelle group appears to be an unusual fluctuation, and if one accepts this, the data are consistent with the most popular model and the above value of $\sin^2\theta_w$. However, especially in view of the conflicting results from atomic physics experiments, it is far too early to conclude that we are home and dry on a unified theory of weak and electromagnetic interactions.

Non-conservation of the "strong" quantum numbers is one of the hallmarks of weak interactions, and neutrino experiments have always held out the promise of the discovery of new quark flavours, signalled by their leptonic decay and the observation of multilepton events. Dilepton events - now running into hundreds and thousands - seem to be very well described in terms of charmed hadron production. Trimuon events, on the other hand, seem to be well described in terms of conventional sources. The production of muon pairs at the hadron vertex at the rate observed in hadron-hadron collisions can account for most of the events, and the electromagnetic process of internal bremsstrahlung of a muon pair at the lepton vertex, an accurately calculable QED process, for the remainder. Like-sign dimuon events, at a level significantly above background from pion and kaon decay, might indicate the existence of cascade decay of heavier quarks (e.g. $b \to c \to s$); however, at the present time a singal is not positively established.

Finally, I shall discuss briefly the phenomenon of prompt single lepton (neutrino) production in hadron collisions. The results of these beam dump experiments are not too easy to interpret in terms only of pair production (followed by leptonic decay) of charmed particles. In any case, the bizarre situation that the best present evidence for charmed particle production in hadronic collisions, via the detection of neutrinos

(and of muons) from the leptonic decays, can hardly go unmentioned in a review of neutrino experiments.

2. CHARGED-CURRENT NEUTRINO REACTIONS

2.1 Neutrino Beams

Neutrino beams at proton accelerators are produced by decay in flight ($\pi \to \mu\nu_\mu$, $K \to \mu\nu_\mu$, $K \to \pi e\nu_e$) of secondary pions and kaons generated in a target irradiated by the external proton beam. There are three main components to the beam: (i) the proton target, followed by momentum selecting/focussing elements to direct the pions and kaons from the target down (ii) a decay tunnel in which a proportion (5-20%) of these particles decay in flight; and (iii) a steel (and/or rock/earth) muon shield, whose function is to absorb the hadrons by interaction and muons by ionization loss, leaving a neutrino beam with minimum background (i.e. the hadrons and muons generated by, and in equilibrium with, the neutrino beam as it traverses the shield).

Three types of beam are in common use; the so-called narrowband, wideband and highband systems. For the narrowband (or dichromatic) beam, dipole and quadrupole magnets downstream of the proton target select and focus a beam of pions and kaons with a narrow (±5% typically) momentum range (see Fig. 1). For a truly pencil beam of unique energy E_ν there is a one-to-one correspondence between the decay angle, θ in $\pi\mu 2$ or $K\mu 2$ decay and the neutrino energy: $E_\nu = E_\nu(\max)/(1 + \gamma^2\theta^2)$ where $E_\nu^K(\max) = 0.97E$ and $E_\nu^\pi(\max) = 0.42E$, and $\gamma = E/m_{K,\pi}$. At a fixed distance r from the detector axis, the neutrino spectrum has a width determined by the relative length of the decay tunnel L and shielding D ($L \sim D$ for optimum flux), the momentum bite of the parents and their angular and spatial divergence. A typical energy distribution of events (assuming $\sigma(\text{total}) \propto E$) as a function of radius is shown in Fig. 2 for the CERN

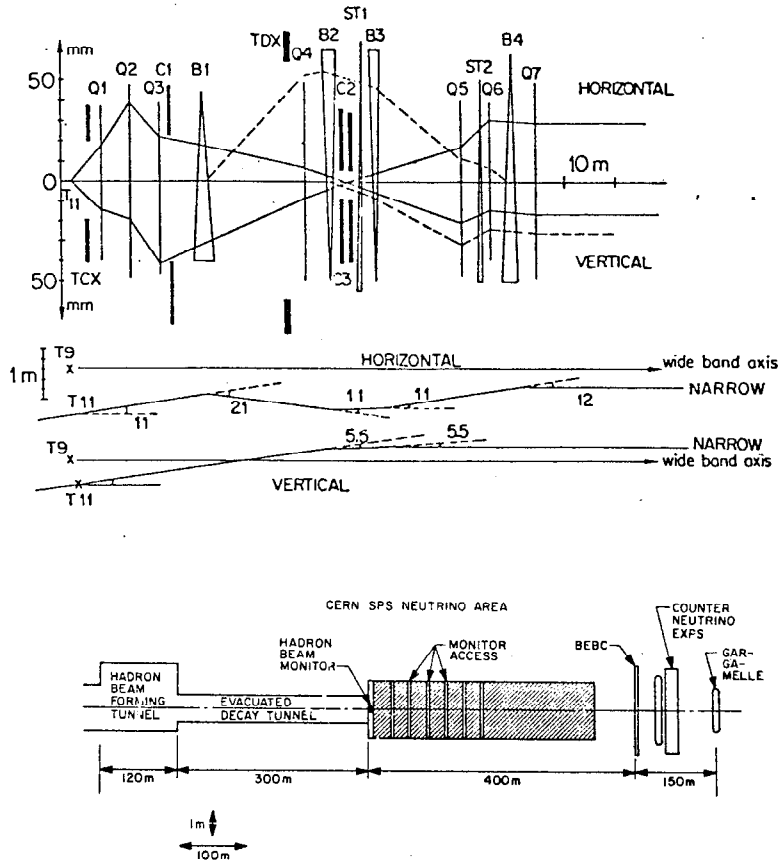

Fig. 1(a) CERN narrowband beam optics. C2/C3 is the momentum-defining collimator. The neutrino beam axis is at 11 mrad with respect to the incident proton beam in both horizontal and vertical planes (to reduce wideband background).

(b) Layout of CERN SPS neutrino area. The steel muon shield is shown shaded, with gaps for muon flux monitoring.

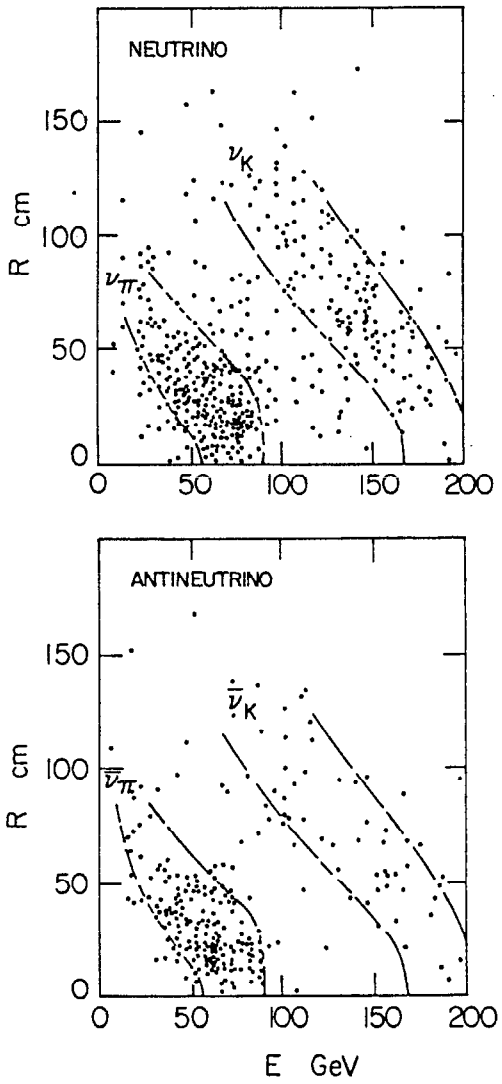

Fig. 2. Dependence of energy on distance from beam axis in CERN NB system, for neutrinos from $\pi\mu 2$ and $K\mu 2$ decay. The dashed curves indicate the limits inside which 90% of events should lie. The dots represent measured event energies in the BEBC experiments. Some events in the "valley" are due to neutrinos from $K\mu 3$ decay.

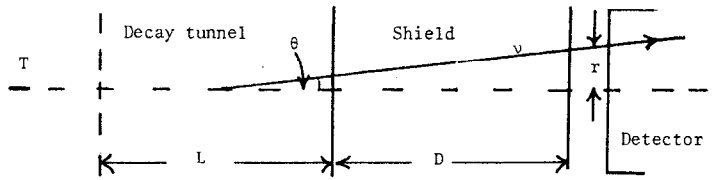

beam. (Not shown in this plot is the background between the $\pi\mu 2$ and $K\mu 2$ contributions, due to $K\mu 3$ decay - of the order of 4%). The whole point of a narrowband experiment is to have information on neutrino energy, within the limits indicated. For this purpose it is necessary to know the momentum bite, composition (K/π ratio) and angular divergence of the parent beam quite accurately, and this is discussed below.

Wideband beams employ aluminium sheet conductors (horns, reflectors) pulsed with currents of order 0.25-0.5 megamps, providing magnetic fields with field lines which are circles about the beam axis. These focus secondaries of one sign, and defocus those of the opposite sign, over a broad momentum band. The optional design of horn and reflector shapes is a highly technical subject which I do not discuss here. It is actually possible to achieve neutrino fluxes (allowing for secondary absorption in the horns, reflectors etc.) which are within a factor of two of "ideal focussing", i.e. that which would be obtained if all secondaries from the target emerged along the axis. The fluxes are, of course, much larger than in the narrowband beam, but peaked to low energy. A comparison of narrowband and wideband spectra is shown in Fig. 3. Wideband beams are essential for experiments involving detectors of low mass (e.g. hydrogen bubble chambers) or in high statistics experiments.

The drawback of wideband beams is that the flux peaks at low energy, and this constitutes a useless background in an experiment which is

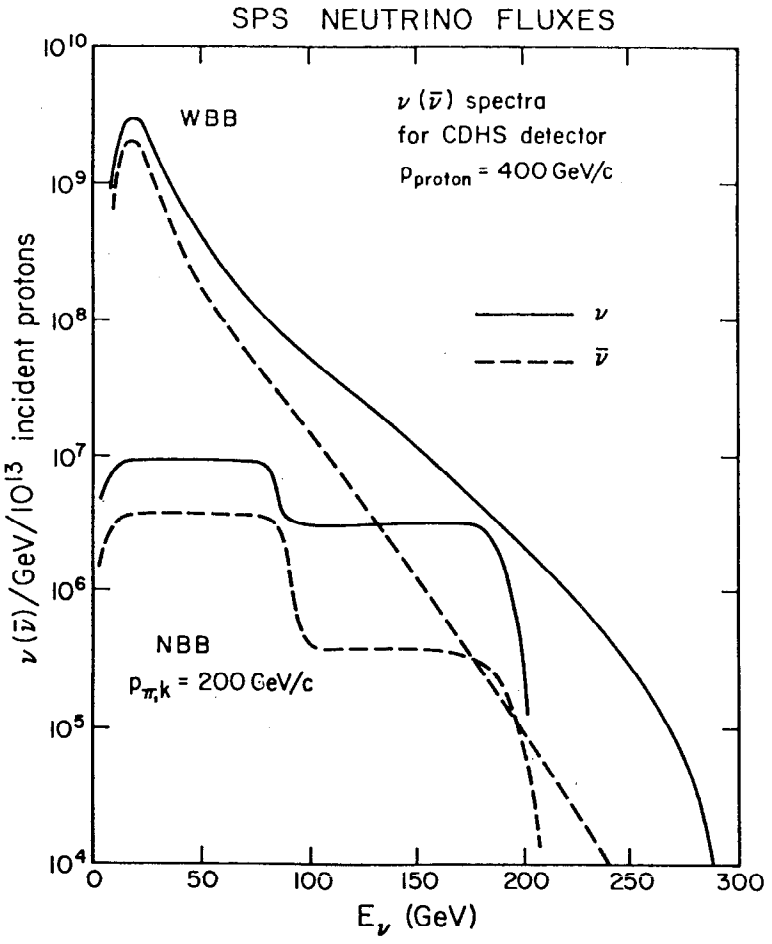

Fig. 3 Comparison of narrowband and wideband fluxes through CDHS detector (CERN SPS).

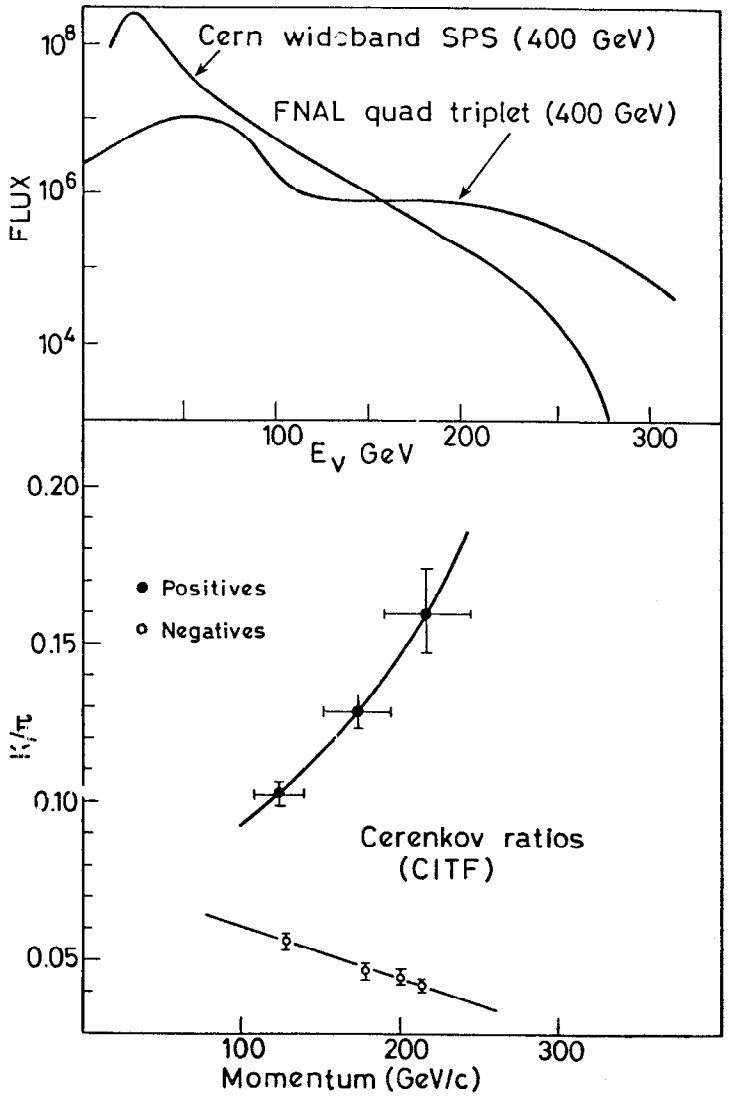

Fig. 4 (a) Comparison of CERN wideband and FNAL highband fluxes.
(b) K/π ratios measured in FNAL narrowband beam.

oriented to the high energy part of the spectrum. The highband beam is designed to optimize the high energy flux and consists simply of a triplet of magnets downstream of the target, to focus and sign select the high energy secondaries. A comparison between the FNAL highband beam and CERN SPS wideband beam is given in Fig. 4.

The monitoring of neutrino beams has been carried out by a variety of methods. One approach, feasible only with narrowband beams, is to measure the total intensity of the parent beam (e.g. by means of a beam current transformer) and the constitution (proportions of pions, kaons, protons) by means of differential gas Cerenkov counters. The neutrino spectra from pion and kaon decay are then computed from the decay kinematics. A second method, which can be used for any type of beam, is to measure the radial distribution of muons as a function of depth in the shield. For a narrowband beam, for example, the muon radial/depth distribution depends on the beam energy and angular divergence, as well of course on the ionization loss and multiple scattering of the muons in the shield. Fig. 5 shows, as an example, the determination of the beam divergence from the radial muon distribution in the CERN SPS experiment. Absolute calibration of the solid-state muon counters is achieved by track-counting in nuclear emulsion (see Fig. 6). Since the muon energy from decay of a pion beam of energy E varies from 0.58E to E, while that from a kaon beam varies from ~0 to E, the muon counting method gives a measure of the pion flux, and the K/π ratio has to be determined by another method (i.e. with a Cerenkov, as described above - see Fig. 4)

The errors associated with neutrino flux measurements, even with the most elaborate monitoring techniques, are in the region of 7-12%. The lower figure applies to neutrinos from pion decay, and the latter to those from kaon decay, where errors in the K/π ratio are dominant.

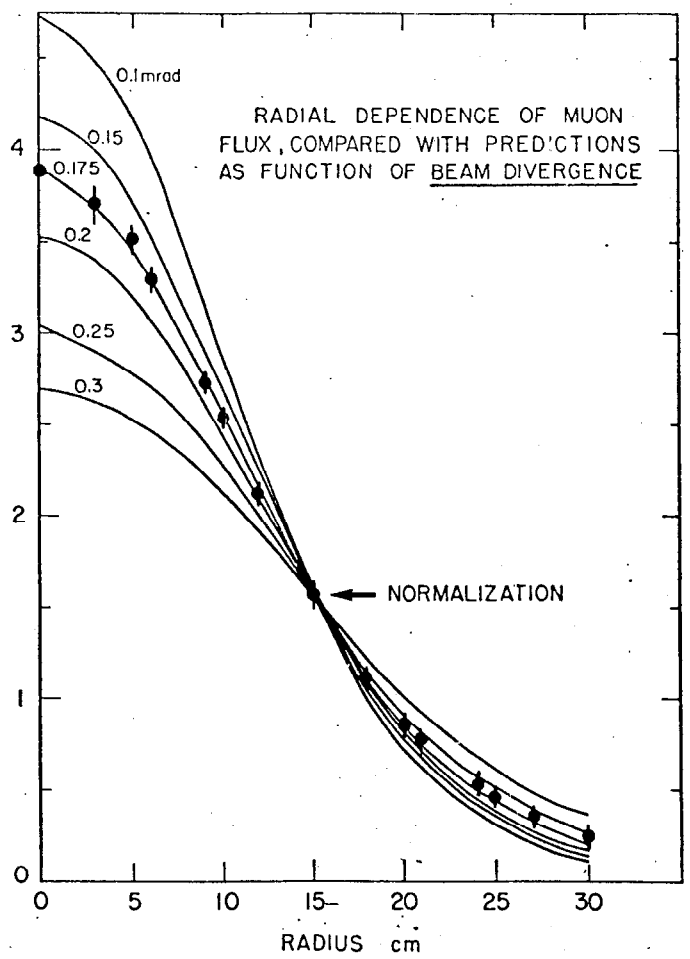

Fig. 5 Radial dependence of muon flux at 30m depth in shield, compared with predicted flux as function of π/K beam divergence (θ = 0.1 → 0.3 mrad).

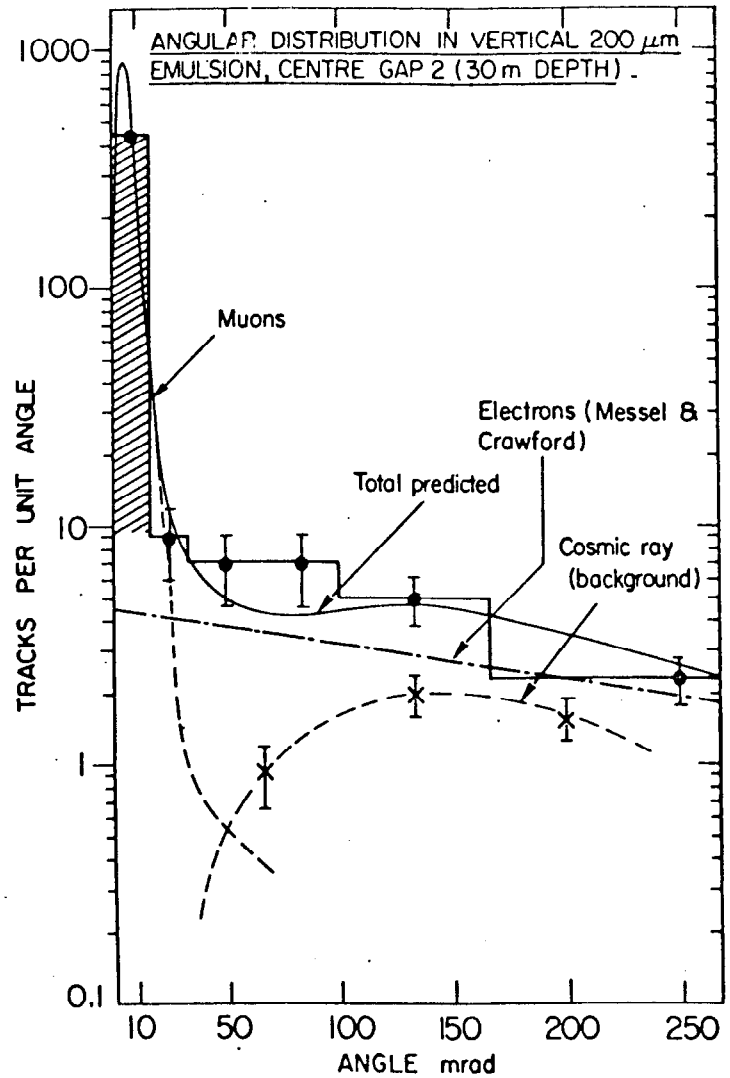

Fig. 6 Results of track-counting in emulsion to calibrate muon flux counters. The forward peak is due to muons, and the broad distribution at wider angles to knock-on electrons from the shielding and cosmic rays.

Wideband beams and highband beams, which rely entirely on focussing action for sign selection, always contain contamination from "wrong-sign" background ($\bar{\nu}$ flux in a ν beam, and vice-versa). For horn-focussed beams, this varies from ∿1% at low energy to ∿10% at high energy. Because of the dominance of $\mu\nu_\mu$ decay modes of the parent pions and kaons, accelerator neutrino beams consist mostly of ν_μ or $\bar{\nu}_\mu$, with a background of order 1% of ν_e (or $\bar{\nu}_e$) from Ke3 and μ-decay. These features are illustrated in Fig. 7.

2.2 Detectors

Because of the small neutrino interaction cross-sections ($\sim 10^{-38} E$ cm^2 nucleon^{-1} GeV^{-1}), detectors must be massive, and a corollary of this is that they are usually of limited resolution.

Counter devices, such as those used by the HPWF, CITF and CDHS groups, have effective target masses of order 100-1000 tons. For example the HPWF apparatus, consists of (i) a target/calorimeter of liquid scintillator, in which the interactions take place and the energy of the secondary hadrons is measured (ii) magnetized iron toroids for measurement of the muon momentum. In the CDHS experiment, the solid scintillator is sandwiched between magnetized iron plates so that the whole volume serves for a target, calorimeter and for muon momentum measurement, (see Fig. 8).

Economy has dictated the use of magnetized iron spectrometers for muon momentum measurement in all the counter experiments and the precision attainable is therefore determined by multiple Coulomb scattering in the iron; in practice, $\Delta p_\mu/p_\mu \approx$ 10-15%. The hadron calorimeters can be calibrated with hadron beams, and give hadron energy resolution $\Delta E_H/E_H \approx 100/\sqrt{E_H}$ %, where E_H is in GeV. Severe fiducial volume cuts are required if the nuclear cascade is to be contained inside the calorimeter, without substantial correction factors.

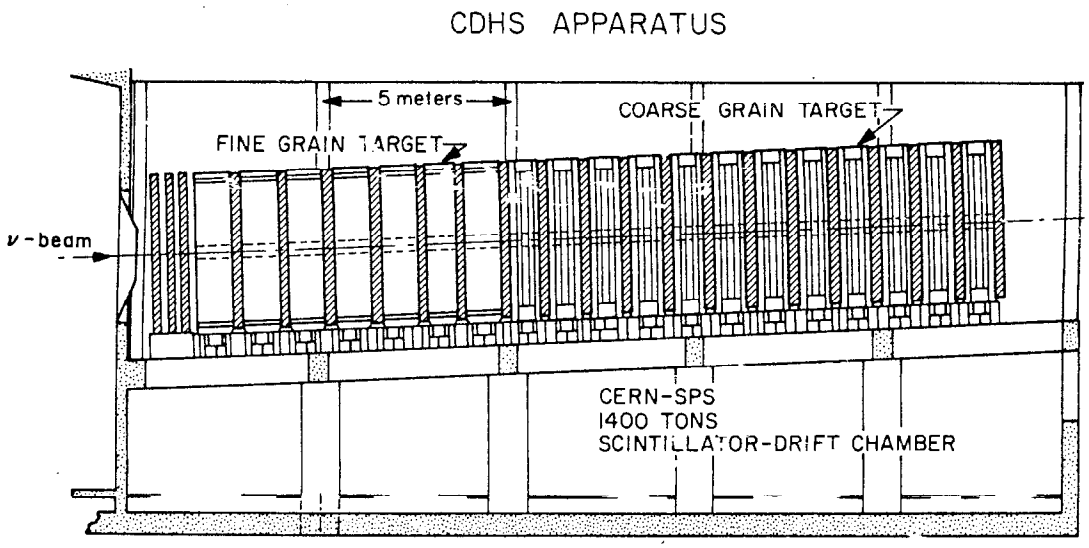

Fig. 8 Counter apparatus used by CDHS group at CERN SPS. It consists of plastic scintillator sandwiched between magnetized iron plates (5cm or 15 cm thick) together with drift chambers.

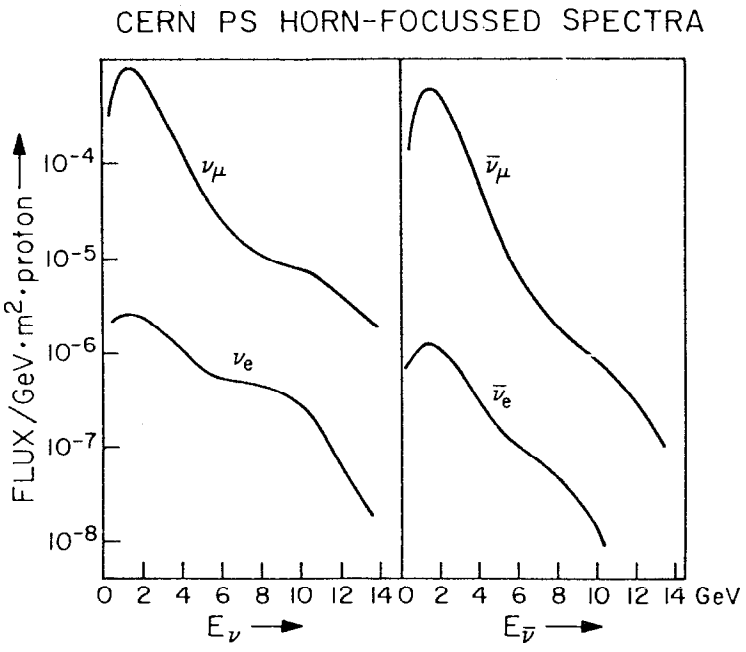

Fig. 7 ν_μ, $\bar{\nu}_\mu$ and ν_e, $\bar{\nu}_e$ fluxes for the CERN PS wideband (horn-focussed) beam.

The large bubble chambers (15' FNAL, 12' ANL, Gargamelle and BEBC (CERN)) used in neutrino physics have useful sensitive volumes up to $\sim$15 m^3 and thus target masses of order 1 ton with hydrogen filling and around 10 tons with heavy liquid (eg Ne/H_2 mixture). The muon momentum resolution is superior to that in the counter experiments. For example BEBC (35 kgauss superconducting magnet) has $\Delta p_\mu/p_\mu$ =4% for E_μ = 100 GeV, and 2 m of track length. Muon secondaries are identified with the help of external muon identifiers (EMI) consisting of one or more planes of MWPCs (150 m^2 area in the case of BEBC, separated from the chamber by $\sim$1 m iron absorber). The muon momentum resolution is improved by using the fringe field of the chamber and the EMI hit coordinates. In comparison with the calorimeters, the hadron energy resolution in the bubble chambers is rather poor at high energy. The charged hadron energy can usually be well measured, but some of the neutral energy may be "lost" - for example, high energy γ-rays from π°-decay may originate in, but convert a long way from, the primary vertex, and could therefore be confused with γ-rays from secondary vertices. To avoid double-counting, distant γ-rays therefore have to be ignored in measuring hadron energy. Furthermore, the energy of charged hadrons interacting close to the primary vertex must be estimated from the visible energy of the products of the interaction, and this also leads to underestimate of the true energy. Fig. 9 illustrates the method employed in the BEBC NE/H_2 experiments. Firstly, in charged-current events, the transverse momentum relative to the beam, of the muon and of the hadrons must balance. Suppose ε = (visible hadron energy)/(true hadron energy). In a sample of events, an arbitrary value of ε is chosen, and thus, from the corrected values of E_ν = $E_\mu + E_H$ (visible)/ε and from p_μ, the expected angle θ_H(calc) of the hadron momentum vector can be computed. On <u>average</u>, the true hadron

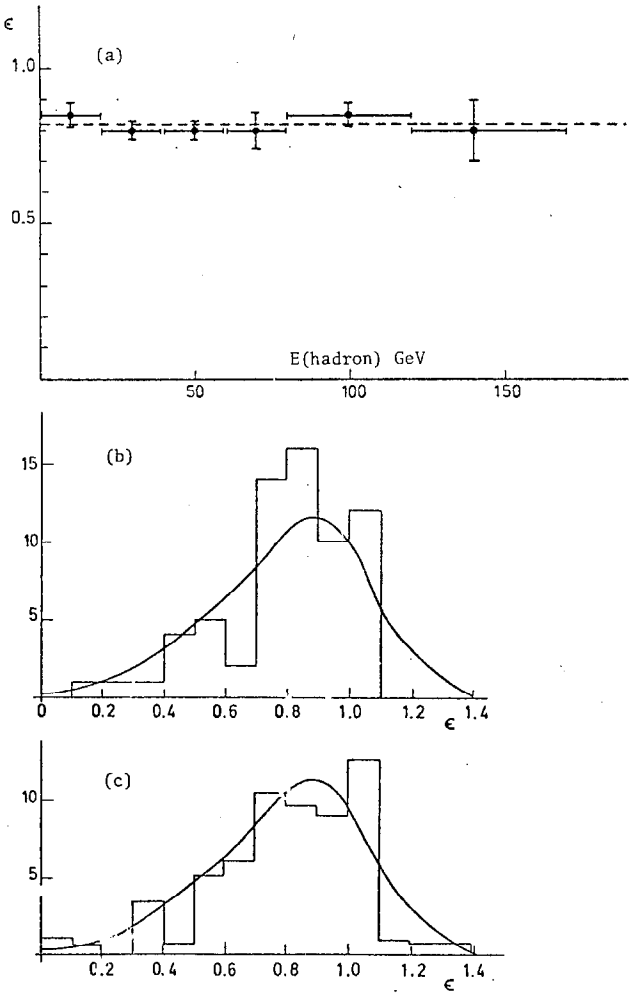

Fig. 9 (a) Mean value of ε= visible hadron energy/true hadron energy, determined from p_T balance in BEBC charged current events.
(b) ε distribution in 70 GeV pion interactions.
(c) ε distribution in 110 GeV pion interactions.

direction cannot be affected by missed energy. Hence, the best value of ϵ is that which makes the mean difference θ_H(vis) - θ_H(calc.) zero. The mean value obtained was $\epsilon = 0.82 \pm .02$, apparently independent of hadron energy. This correction factor was checked by measuring, in the same chamber and by the same technique, the total visible energy in interactions of 70 GeV/c and 110 GeV/c negative pions, as shown in the figures. What is important in these corrections is that, although the rms error in the hadron energy is $\sigma = 20\%$, the distribution is non-Gaussian and skew. This is confirmed by observing the distribution in the transverse momentum ratio of the muon to that of the visible hadrons, in individual events.

The corrections for energy losses and resolution effects are of particular importance in determining absolute values of structure functions, especially at high x where the function is falling steeply as $(1-x)^3$. Since $x = q^2/2ME_H$, quite small errors in E_H can have relatively drastic effects.

There are still eminent physicists in the world who believe the fundamental limitation of accelerator neutrino experiments, on account of the low cross-sections, is of a statistical nature. The fact is that the low cross-sections have dictated the use of massive and relatively crude detectors and the important limitations arise from systematic uncertainties about the detector resolution and biasses, as well as of the neutrino fluxes. The sort of things that can go wrong when these problems are not fully understood is well illustrated by the sad story of y anomalies.

2.3 Total and Differential cross-sections in the Naive Parton Model

In conformity with our experience from weak decay processes, we can describe the inclusive process

$$\nu + \text{nucleon} \rightarrow \mu^- + \text{anything}$$

in terms of the interaction of two currents (J(lepton) and J(hadron)) via single vector particle ($W^{\pm}$) exchange. Provided we do not specify the momentum of an individual hadron, the kinematic variables can be formed from the independent Lorentz invariants q.q, q.P and k.P; q^2 = q.q,

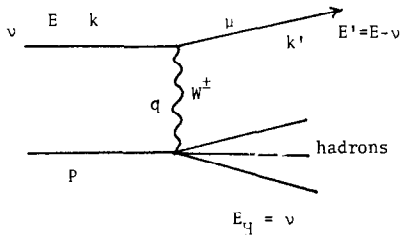

$M\nu$ = P.q and ME = P.K, where k, P, q are the 4-momenta of the neutrino, nucleon and exchanged boson, ν is the energy transfer in the nucleon rest-frame (lab. system) and E is the laboratory neutrino energy. The dimensionless "scaling variables" are $x = 2M\nu/q^2 = 2P.q/q^2$ and $y = \nu/E = P.q/P.k$. We neglect lepton masses ($k'^2 \ll q^2$).

The exchanged $W^{\pm}$ boson has 3 helicity states (±1, 0) and, if the target nucleon is unpolarized, the cross-section can therefore be described in terms of just 3 unknown structure functions describing the hadron vertex.[1] Each must be a function of the two independent scalars containing q: q^2 and ν, or, equivalently, q^2 and x:-

$$\frac{d^2\sigma^{\nu,\bar{\nu}}}{dxdy} = \frac{G^2ME}{\pi}\left[(1-y-\frac{Mxy}{2E})F_2^{\nu,\bar{\nu}}(x,q^2) + \frac{y^2}{2}2xF_1^{\nu,\bar{\nu}}(x,q^2) \pm y(1-\frac{y}{2})xF_3^{\nu,\bar{\nu}}(x,q^2)\right] \quad (2.1)$$

F_1, F_2 and F_3 are different for neutrinos and antineutrinos, and for proton and neutron targets. F_3 is the V-A interference term, which changes sign for neutrinos and antineutrinos. In general therefore, there are 12 unknown functions. A great simplification occurs if we

consider only $\Delta S = \Delta C = 0$ processes (i.e. set the Cabibbo angle $\theta_c \simeq 0$) and isoscalar targets. Then from charge symmetry we obtain

$$F_i^{\nu n} = F_i^{\bar{\nu}p} \quad F_i^{\nu p} = F_i^{\bar{\nu}n} \quad i = 1, 2, 3$$

or $$F_i^{\nu N} = F_i^{\bar{\nu}N}$$

so that, to the extent that $\Delta S = 1$ or $\Delta C = 1$ processes are suppressed by a factor $\tan^2\theta_c \simeq 0.05$, and targets used in inclusive reaction studies are complex nuclei with approximately equal numbers of neutrons and protons, we can describe both neutrino and antineutrino cross-sections in terms of just three structure functions:-

$$\frac{d^2\sigma^{\nu,\bar{\nu}N}}{dxdy} = \frac{G^2ME}{\pi}\left[(1-y-\frac{Mxy}{2E})F_2(x,q^2) + \frac{y^2}{2}.2xF_1(x,q^2) \pm y(1-\frac{y}{2})xF_3(x,q^2)\right] \quad (2.2)$$

Since the irreducible error on neutrino fluxes is at the 5% level at least, this approximation is well justified.

The conjecture of Bjorken[2] in 1968 was that in the limit $q^2 \to \infty$ the structure functions would be scale-invariant:-

$$\underset{q^2 \to \infty}{Lt} \quad F_i(x,q^2) \to F_i(x) \qquad (2.3)$$

i.e. only depend on the dimensionless ratio, x. Immediately SLAC-MIT data on e-p scattering[3] showed that, to within the then experimental precision of ~10%, the data supported Bjorken scaling, at least for $q^2 > 1$ GeV^2. In the case of neutrino scattering, hypothesis (2.3) implies that, if Mxy/2E is small (implying that for the secondary muon, the angle of emission in the LS is such that $\cos^2(\theta_\mu/2) \simeq 1$), the x and y dependence in (2.2) factorizes. Hence, integrating we get

$$\sigma^{\nu,\bar{\nu}} = \frac{G^2ME}{\pi}\int_0^1 F_2dx[\tfrac{1}{2} + \frac{A}{6} \pm \frac{B}{3}]; \quad \frac{\bar{\sigma}}{\sigma} = \frac{3 + A - 2B}{3 + A + 2B} \qquad (2.4)$$

where $A = \int 2xF_1dx/\int F_2dx$, $B = \int xF_3dx/\int F_2dx$. These cross-sections, instead of being written in terms of F_1, F_2, F_3, can be expressed equally in terms of the cross-sections σ_L, σ_R, σ_S for absorption of virtual bosons with helicity -1, +1, 0. Since these σ's must be positive definite, there exist positivity constraints

$$F_2 \geq \frac{2xF_1}{(1 + 4m^2x^2/q^2)} \geq \frac{xF_3}{\sqrt{1 + 4m^2x^2/q^2}} \geq 0 \qquad (2.5)$$

The main prediction of (2.4) is that $\sigma(\text{total}) \propto E$, and this was verified in the early experiments[4] in the 1.2m heavy liquid chamber at the CERN PS (1968) and subsequently in the Gargamelle experiments[5] at the PS, although the mean energies involved ($\langle E\rangle \sim 4$ GeV, $\langle q^2\rangle \sim 1$ GeV^2) were very low - see Fig. 10. A second very important result was that $\bar{\sigma}/\sigma = 0.38 \pm 0.02$ over the range E = 2-10 GeV. From (2.5) we see that $A \geq B$, hence the proximity of $\bar{\sigma}/\sigma$ to $^1/3$ implied, from (2.4), that $A \sim B \sim 1$, i.e. the V, A interference term xF_3 was maximal.

The interpretation of scale invariance in terms of the pointlike nucleon constituents, or partons, of Feynman[6] is well known. Scale invariance follows if these constituents are regarded as quasi-free so that transverse momenta are neglected. In a reference frame where the nucleon has a large 4-momentum P, the partons move in a parallel stream in the direction $\vec{P}$. Let the struck parton carry a 4-momentum ξP. Then

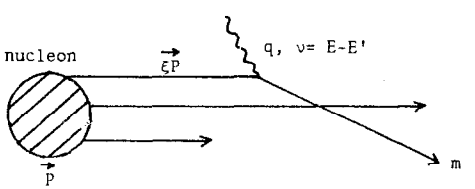

$$(\xi P + q)^2 = -m^2 \qquad (2.6)$$

where m is the mass of the parton. If $q^2 >> m^2$ or $M^2(= -P^2)$ it follows that

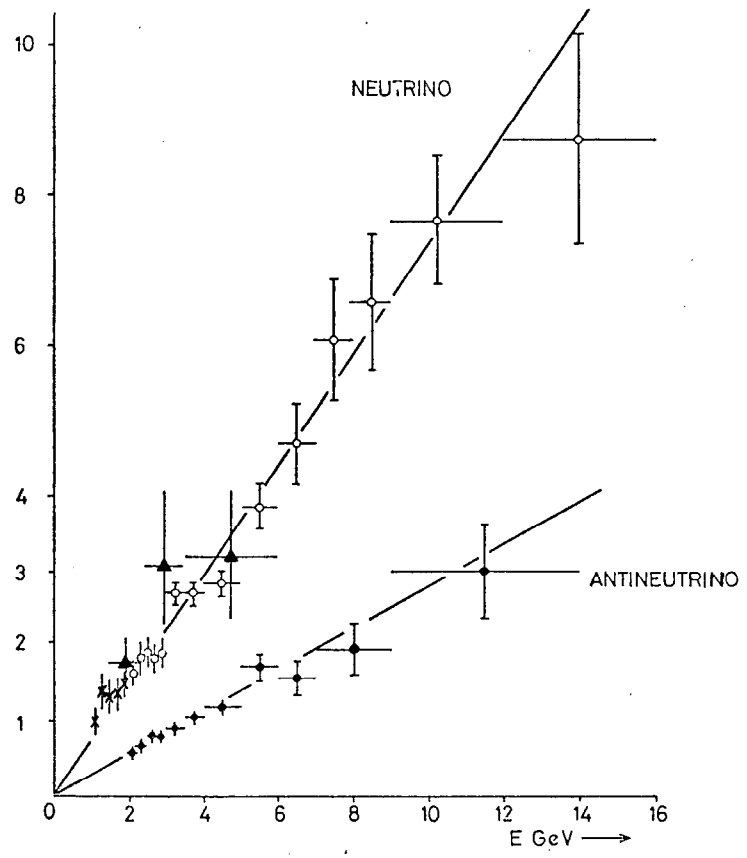

Fig. 10 Neutrino and antineutrino total cross-sections measured in wideband experiments at the CERN PS, using the Gargamelle chamber filled with CF_3Br. Units are 10^{-38} cm^2 per nucleon.

$$\xi = \frac{q^2}{-2P.q} = \frac{q^2}{2M\nu} = x \qquad (2.7)$$

so that x equals the fractional nucleon momentum, ξ, carried by the parton. Alternatively, one can view the absorption of the current in the parton rest-frame, when $q^2 = 2m\nu$ and thus $\xi = x = m/M$ i.e. ξ or x is the fractional mass of the nucleon carried by our hypothetical free parton. If we do not neglect the masses in (2.6) then the positive root is:-

$$\xi_+ = \frac{-\nu + \sqrt{\nu^2 + q^2 + m^2}}{M} = x\left[1 - \left(\frac{M^2x^2 - m^2}{q^2}\right) + \ldots\right] \qquad (2.8)$$

Just retaining the target (nucleon) mass we then obtain the Nachtmann[7] (or light-cone) variable

$$\xi_{\text{Nachtmann}} = \frac{2x}{(1 + \sqrt{1 + 4m^2x^2/q^2})} = x\left(1 - \frac{M^2x^2}{q^2} + \ldots\right) \qquad (2.9)$$

which we shall refer to later on. The main point is that the Bjorken x variable has a simple interpretation only if $q^2 > M^2, m^2$. For modest values of q^2, M^2 cannot be neglected and $\xi < x$; this is also the case when the recoiling parton emerges with appreciable mass, as in the transformation of a d-quark constituent to a c-quark (charmed particle production).

2.4 Physical Interpretation of the Structure Functions

Since we shall be dealing at length with the behaviour of the functions F_1, F_2, F_3 it is perhaps worthwhile discussing the physical meaning of these functions. For F_1 and F_2, it is easiest to start with the analogous process of inelastic electron scattering, for which the form analogous to (2.2) is obtained by the substitution $G^2/\pi \to 8\pi\alpha^2/q^4$, and dropping the term xF_3 (since electromagnetic interactions are parity conserving):-

$$\frac{d^2\sigma^{ep}}{dxdy} = \frac{4\pi\alpha^2}{q^4}\left[(1 - y - \frac{Mxy}{2E})F_2^{ep}(x) + \frac{y^2}{2}2xF_1^{ep}(x)\right]2ME \qquad (2.10)$$

or

$$\frac{d^2\sigma^{ep}}{dq^2dx} = \frac{4\pi\alpha^2}{q^2}\left[(1 - y - \frac{Mxy}{2E})\frac{F_2^{ep}}{x} + \frac{y^2}{2}.2F_1^{ep}(x)\right] \qquad (2.11)$$

in the limit $y \to 0$, that is, forward scattering $\theta \sim 0$, we get

$$\left(\frac{d\sigma}{dq^2}\right)_{\theta\to 0} = \frac{4\pi\alpha^2}{q^4}\int_0^1 \frac{F_2^{ep}(x)dx}{x}$$

which is the Rutherford pointlike scattering formula, so that $\int F_2(x)dx/x = \Sigma Q_i^2$ = sum of squares of the parton charges.

Next, we write down the Dirac cross-section for the elastic scattering of an electron by a spin ½ particle of g = 2, charge ze and mass m

$$\left(\frac{d\sigma}{dq^2}\right)_{Dirac} = \frac{4\pi\alpha^2}{q^4}\frac{E'}{E}(\cos^2\frac{\theta}{2} + \frac{q^2}{2m^2}\sin^2\frac{\theta}{2})z^2 \qquad (2.12)$$

Using the fact that $q^2 = 2EE'(1 - \cos\theta) = 4EE'\sin^2\theta/2 = 2MExy$, $m^2 = x^2M^2$ for free partons of mass m, we obtain

$$\left(\frac{d\sigma}{dq^2}\right)_{Dirac} = \frac{4\pi\alpha^2}{q^4}\left[(1 - y - \frac{Mxy}{2E}) + \frac{y^2}{2}\right]z^2$$

and, comparing with (2.11) gives

$$2xF_1 = F_2$$

Thus, $2xF_1/F_2 = g/2 = 1$ for free, spin ½, pointlike partons; in other words, the Callan-Gross ratio[8] $A = 2xF_1/F_2$ measures the relative magnitude of magnetic and electric scattering, the ratio being unity for a Dirac fermion with g = 2. This equality is supported by the early electron scattering data, for which $0.8 < xF_1/F_2 < 1$.[9]

For the case of neutrino scattering, the formula (2.1) or (2.2) can be usefully compared with that for the V-A scattering of neutrinos (ν_e) by electrons via $W^{\pm}$ exchange, which has the form[10], for E >> m:-

$$\frac{d\sigma^{\nu e}}{dy} = \frac{d\sigma^{\bar\nu\bar e}}{dy} = \frac{2G^2mE}{\pi}\ ; \qquad (2.13)$$

$$\frac{d\sigma^{\bar\nu e}}{dy} = \frac{d\sigma^{\nu\bar e}}{dy} = \frac{2G^2mE}{\pi}(1-y)^2\ ; \qquad (2.14)$$

and

$$\sigma^{\nu e} = \sigma^{\bar\nu\bar e} = 3\sigma^{\bar\nu e} = 3\sigma^{\nu\bar e} = 2G^2mE/\pi$$

where $y = E_e/E$, the fractional recoil energy of the electron. The difference in the cross-sections (2.13) and (2.14) is easily understood on the basis of helicity arguments. The diagrams indicate the

CMS momenta and spin projections of LH neutrino (RH antineutrino) and LH electron.

In the νe case, $J_z = 0$ and the scattering is isotropic, with a flat y distribution as in (2.13). For the $\bar\nu e$ case, $J_z = +1$ and back-scattering (i.e. J_z(final) = -1) is impossible. The angular distribution of the scattered antineutrino is of the form $(1 + \cos\theta^*)^2$, corresponding to a y distribution of the scattered electron as in (2.14).

Thus, for an assembly of spin ½ pointlike particle/antiparticle targets, the neutrino cross-section will be

$$\frac{d\sigma}{dy} = \frac{G^2ME}{\pi}\cdot 2x[q(x) + \bar q(x)(1-y)^2]dx \qquad (2.15)$$

with the antineutrino cross-section obtained by interchanging $q \leftrightarrow \bar q$. Here $x = m/M$ is the ratio of target mass to nucleon mass and $q(x)$, $\bar q(x)$ are the particle/antiparticle densities at x.

Since the neutrino data indicate $A = 2xF_1/F_2 \sim 1$, let us assume $2xF_1 = F_2$ and re-write (2.2) in the form

$$\frac{d\sigma^{\nu,\bar\nu N}}{dy} = \frac{G^2ME}{\pi}\left[(\frac{F_2 \pm xF_3}{2}) + (\frac{F_2 \mp F_3}{2})(1-y)^2\right]dx \qquad (2.16)$$

in the approximation E >> M, and comparing with (2.15) we obtain

$$2xq(x) = \frac{F_2 - xF_3}{2} \qquad F_2(x) = 2x(q(x) + \bar{q}(x))$$

$$2x\bar{q}(x) = \frac{F_2 - xF_3}{2} \qquad xF_3(x) = 2x(q(x) - \bar{q}(x)) \tag{2.17}$$

To summarise; assuming the weak currents are of the pure V-A form for both leptons and partons (i.e. they are both pointlike, spin ½ objects), the quantity $F_2(x)$ measures the fractional momentum content of the sum of partons and antipartons at x, while $xF_3(x)$ measures the difference. In particular, a value $\bar{\sigma}/\sigma = 1/3$ implies $\bar{q}/q \ll 1$ so that the majority of the partons must be fermions rather than antifermions. From (2.15) we have, with $Q = \int x\,q(x)dx$, $\bar{Q} = \int x\bar{q}(x)dx$:-

$$\bar{Q}/(Q + \bar{Q}) = (3R-1)/(2R+2), \qquad R = \bar{\sigma}/\sigma \tag{2.18}$$

For R = 0.40, the relative momentum content of antipartons is $\bar{Q}/(Q + \bar{Q}) = 0.07$. This fraction can also be measured from the y distributions. The value of $d\sigma/dy$ at $y \sim 0$ measures $(Q + \bar{Q})$, while at $y \sim 1$ it measures Q for neutrinos and $\bar{Q}$ for antineutrinos. Typical results

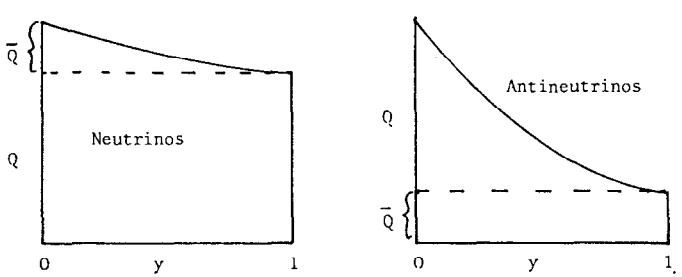

from the CDHS experiment are shown in Figs. 11 and 12. For y > 0.8, the x distribution for antineutrinos will be typical of antipartons $\bar{q}(x)$ and is seen to be peaked to smaller x than the corresponding distribution $q(x)$ for neutrinos.

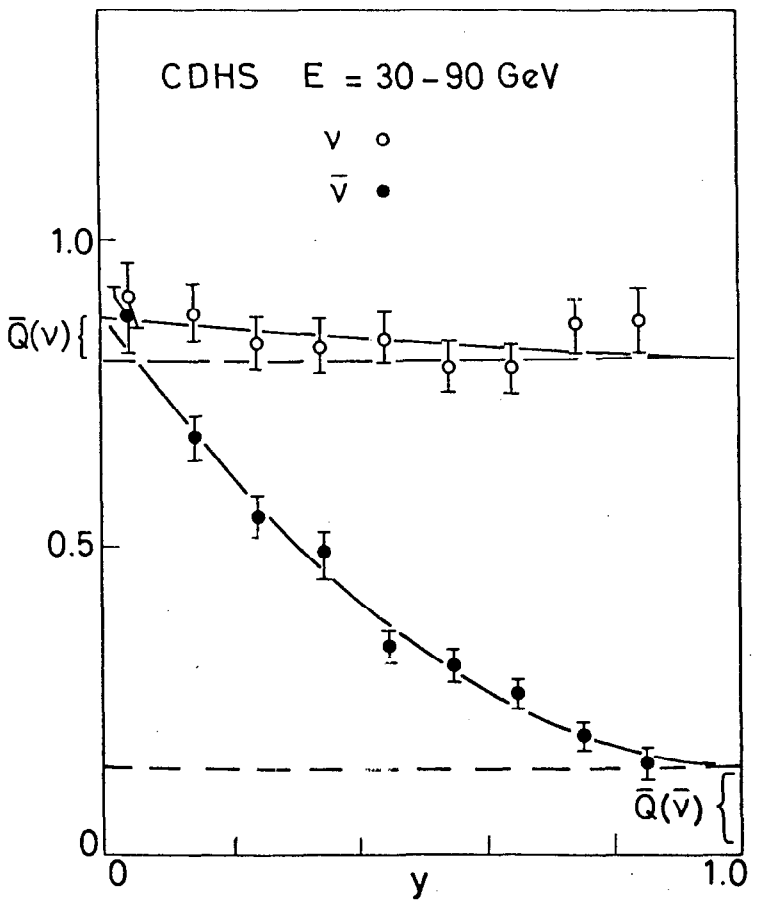

Fig. 11

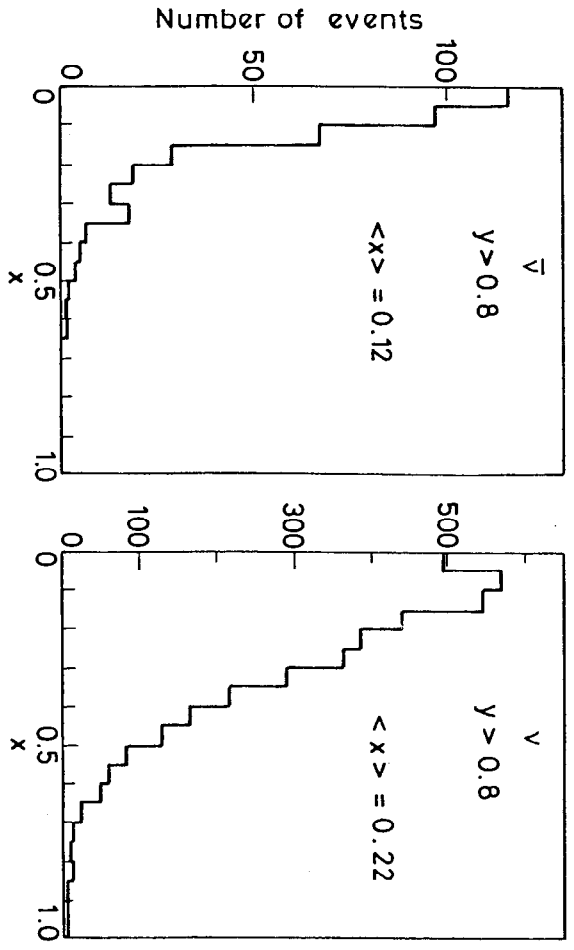

Fig. 12 x-distributions for $y > 0.8$ in the CDHS experiment. For antineutrinos, at left, the x-distribution is typical of the antiquarks, and is narrower than that of the quarks, as indicated from the neutrino distribution.

2.5 Neutrino Cross-Sections in the Quark Model

The hypothesis that the partons can be identified with quarks is best tested by comparing neutrino and electron scattering from nucleons. For neutrinos and antineutrinos, the fundamental processes on non-strange u and d quarks are

$$\begin{aligned} \nu + d &\to \mu^- + u \\ \nu + \bar{u} &\to \mu^- + \bar{d} \\ \bar{\nu} + u &\to \mu^+ + d \\ \bar{\nu} + \bar{d} &\to \mu^+ + \bar{u} \end{aligned} \qquad (2.19)$$

so that from (2.17) we obtain (with $\theta_{\text{Cabibbo}} = 0$):-

$$\begin{aligned} F_2^{\nu p}(x) &= 2x(d(x) + \bar{u}(x)) \\ F_2^{\nu n}(x) &= 2x(u(x) + \bar{d}(x)) \end{aligned}$$

or $$F_2^{\nu N}(x) = x[u(x) + d(x) + \bar{u}(x) + \bar{d}(x)] \qquad (2.20)$$

where u(x), d(x) ... refer, by convention, to the quark densities in the proton, and, by charge symmetry, u(neutron) = d(proton), etc. If we do not neglect the Cabibbo angle and stay below charmed particle threshold (2.20) is modified to

$$F_2^{\nu N}(x) = x\left\{[u + d + \bar{u} + \bar{d}][1 - \tfrac{1}{2}\sin^2\theta] + \sin^2\theta[s + \bar{s}]\right\} \qquad (2.21)$$

while above charmed threshold

$$F_2^{\nu N}(x) = x[u + d + \bar{u} + \bar{d} + s + \bar{s} + c + \bar{c}] \qquad (2.22)$$

where in the last two expressions, F_2 represents the <u>average</u> of $F_2^{\nu N}$ and $F_2^{\bar{\nu}N}$ - which are not equal, as they are in (2.20).

The structure functions in electron scattering are given by the quark densities weighted by the squares of the quark charges, as indicated under (2.11). Thus

$$\begin{aligned} F_2^{ep}(x) &= x[\tfrac{4}{9}(u + \bar{u}) + \tfrac{1}{9}(d + \bar{d}) + \tfrac{1}{9}(s + \bar{s}) \ \ldots] \\ F_2^{en}(x) &= x[\tfrac{4}{9}(d + \bar{d}) + \tfrac{1}{9}(u + \bar{u}) + \tfrac{1}{9}(s + \bar{s}) \ \ldots] \end{aligned}$$

$$F_2^{eN}(x) = \frac{5}{18}x[(u+d+\bar{u}+\bar{d}) + \frac{2}{5}(s+\bar{s}) + \ldots] \qquad (2.23)$$

Comparing (2.23) with (2.20) or (2.21) we obtain

$$F_2^{\nu N}(x) \leqslant \frac{18}{5}F_2^{eN}(x) \qquad (2.24)$$

The early Gargamelle[11] results at low energy (2-10 GeV) were compared with the MIT-SLAC data[12] at 16-20 GeV with the results

SLAC-MIT $\int_{\sim 0}^{1} F_2^{eN}(x)dx = 0.15 \pm .01$

GGM-PS $\int_0^1 F_2^{\nu N}(x)dx = \frac{3}{4G^2ME}(\sigma^{\nu N} + \sigma^{\bar{\nu}N})$

$= 0.49 \pm 0.05$

or $$\int F_2^{\nu N}dx / \int F_2^{eN}dx = 3.3 \pm 0.4 \tilde{\sim} 18/5 \qquad (2.25)$$

Further verification of the quark-parton model is provided by data on the Gross-Llewellyn-Smith sumrule[13]. From 2.17 we obtain

$$\underset{q^2\to\infty}{Lt} \int_0^1 \frac{xF_3^{\nu N}(x)dx}{x} = (u + d - \bar{u} - \bar{d}) = 3 \qquad (2.26)$$

for the number of valence quarks per nucleon. As described later, a lower limit of 2.7 ± 0.4 is obtained for $q^2 > 3$ in the BEBC/SPS experiment.

2.6 Deviations from Scaling in Neutrino Reactions

As long ago as 1973, evidence was presented for small deviations from exact Bjorken scaling, in inelastic muon scattering.[14] By now, all groups involved in lepton (e, μ, ν) scattering agree, at least qualitatively, that the deviations are there. Hints of these effects can be obtained without a sophisticated analysis. Fig. 13 gives a compilation of data on total cross-sections σ/E and $\bar{\sigma}$/E by various groups. While σ/E seems to be fairly constant for antineutrinos, there is an apparent decrease with E in the value for neutrinos. A second

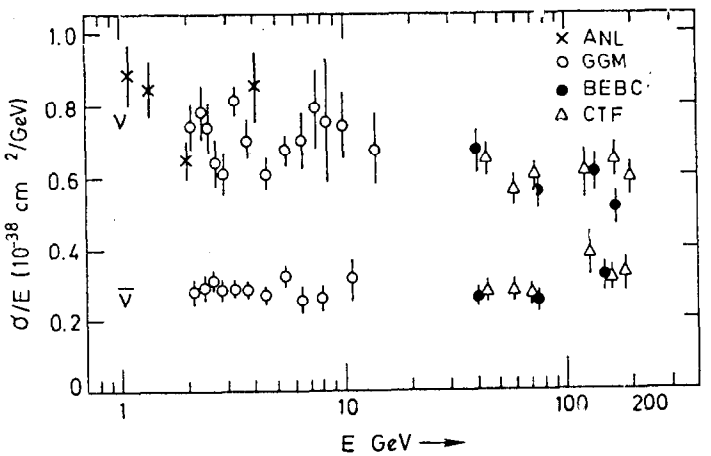

Fig. 13

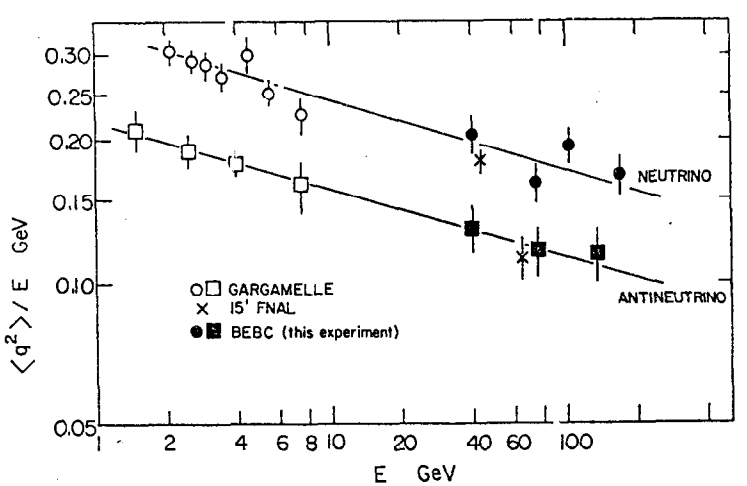

Fig. 14

example is shown in Fig. 14, displaying the value of $\langle q^2/E \rangle = 2M\langle xy \rangle$ as a function of energy. For exact scaling, this quantity should be constant. The straight lines on this graph - corresponding to $\langle q^2/E \rangle \propto E^{-0.14}$ - are from empirical fits to electron and muon data[15] As a third example, we refer to Fig. 11. From this we see that $\bar{Q}$, as measured with neutrinos at low q^2 ($y \sim 0$) is significantly smaller than that for antineutrinos at high q^2 ($y \sim 1$).

To discuss these effects quantitatively, we refer back to equn. (2.2) in which

$$F_i = F_i(x,q^2) \tag{2.26}$$

Thus, if we accept the current-current form of the weak interaction, the structure functions can depend only on the 4-momentum of the exchanged boson, i.e. q^2 and ν, or, equivalently, x and q^2. In principle (2.26) therefore contains all the information on deviations from scaling, and it is therefore more appropriate to consider the q^2 dependence of the cross-sections at fixed x, than energy dependence of y distributions, cross-sections etc.

The first determination of the structure functions $F_i(x,q^2)$ has been made by the ABCLOS collaboration[16], analysing both BEBC Ne/H_2 events obtained in the SPS NB beam (E = 20-200 GeV) and the older GGM events (CF_3Br filling) in a WB PS beam. Their procedure was to evaluate the numbers of events expected for arbitrary values of $F_i(x, q^2)$, by integrating over the known neutrino (antineutrino) fluxes $\phi(E)$ (or $\bar{\phi}(E)$). Thus, in (2.2) if we set $2xF_1 = 1$, $F_2 = xF_3 = 0$ we obtain, in a given bin of $x \to x + \Delta x$, $q^2 \to q^2 + \Delta q^2$

$$N_1(x,q^2) = S\iint \frac{G^2ME}{\pi} \frac{y^2}{2} \phi(E)\,dE\,dy\Big|_{x,q^2}$$

where S = number of nucleons in target. Similarly

$$N_2(x,q^2) = S\iint \frac{G^2ME}{\pi}\left(1-y-\frac{Mxy}{2E}\right)\phi(E)\,dE\,dy\Big|_{x,q^2}$$

$$N_3(x,q^2) = S\iint \frac{G^2ME}{\pi}\left(y-\frac{y^2}{2}\right)\phi(E)\,dE\,dy\Big|_{x,q^2}$$

with similar expressions for antineutrinos. Thus, in the (x,q^2) bin the observed number of events is given by

$$\begin{aligned} N_{obs} &= N_1 \cdot 2xF_1 + N_2 \cdot F_2 + N_3 \cdot xF_3 \\ \bar{N}_{obs} &= \bar{N}_1 \cdot 2xF_1 + \bar{N}_2 \cdot F_2 - \bar{N}_3 \cdot xF_3 \end{aligned} \tag{2.27}$$

Assuming, firstly, that $2xF_1 = F_2$ for all x, q^2, the observed numbers of neutrino and antineutrino events then give values for F_2 and xF_3. The raw event rates have first to be corrected for the finite energy resolution. This was done by generating events via a Monte Carlo program, using as input, the neutrino and antineutrino fluxes and describing the x and y dependence by simple test functions known to reproduce, approximately, the experimental distributions. The effects of energy resolution and losses and nuclear Fermi motion were then applied and the "smearing factors" (ratio of unsmeared to smeared event rates, in a given, x, q^2 bin) evaluated and used to correct the data. The smearing corrections were $\lesssim$10% for $x < 0.6$, and $\lesssim$30% for $x > 0.6$.

The resulting values for $F_2(x,q^2)$ and $xF_3(x,q^2)$ are given in Figs. 15 and 16, with GGM and BEBC data points shown separately. Where the two sets of data overlap, they are in satisfactory agreement. This is a direct demonstration of the validity of the current-current assumption; F_2 depends on x, q^2 and not on E (for which the average values are $\langle E \rangle \sim 4$ GeV for Gargamelle and $\langle E \rangle \sim 90$ GeV for BEBC). Also shown in Fig. 15 are the electron and muon data on $F_2^{ed}(,q^2)$ for experiments in

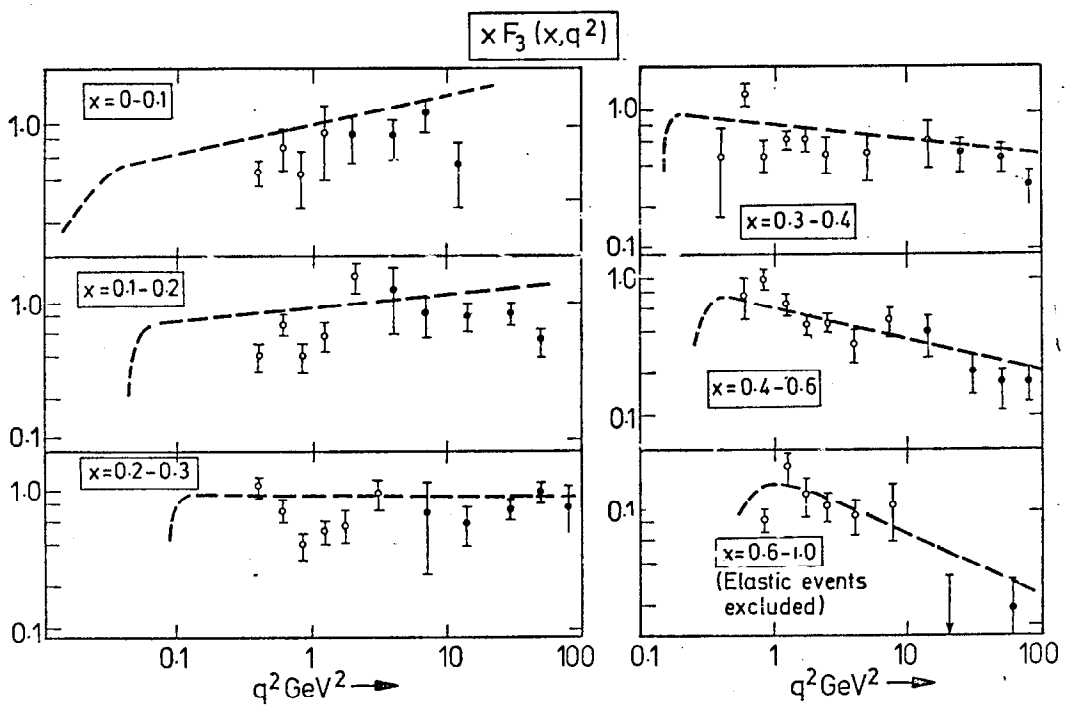
$xF_3(x,q^2)$
x = 0-0.1
x = 0.1-0.2
x = 0.2-0.3
x = 0.3-0.4
x = 0.4-0.6
x = 0.6-1.0
(Elastic events excluded)
1.0
0.1
0.1
1
10
100
q^2 GeV^2

Fig. 16

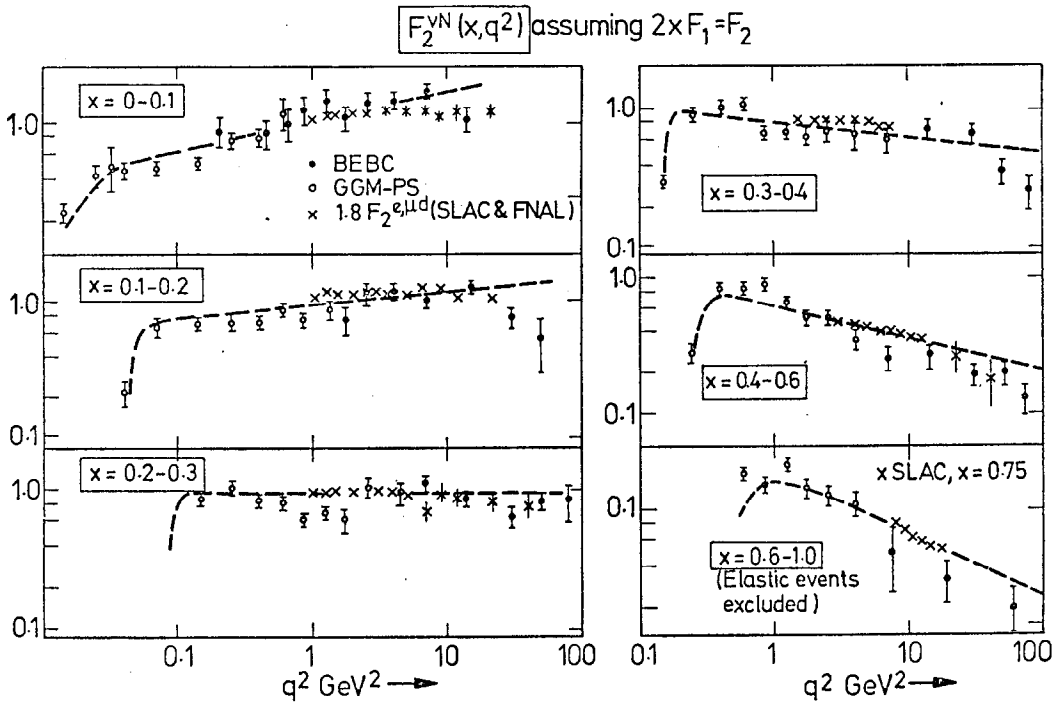
$F_2^{\nu N}(x,q^2)$ assuming $2xF_1=F_2$
x = 0-0.1
x = 0.1-0.2
x = 0.2-0.3
x = 0.3-0.4
x = 0.4-0.6
x = 0.6-1.0
(Elastic events excluded)
• BEBC
○ GGM-PS
× $1.8\,F_2^{e,\mu d}$(SLAC & FNAL)
× SLAC, x = 0.75
1.0
0.1
0.1
1
10
100
q^2 GeV^2

Fig. 15

deuterium at SLAC[17] and FNAL[18]. These have been multiplied by the quark model factor $F_2^{eN}/F_2^{\nu N} = 5/18$ ($= \frac{1}{2} F_2^{ed}/F_2^{\nu N}$). The dashed lines give the slopes of an early empirical fit[15] to the electron/muon data:-

$$F_2(q^2,x) = F_2(q_o^2,x)\left(\frac{q^2}{q_o^2}\right)^{0.25-x} \; ; \; q_o^2 = 3 \text{ GeV}^2 \qquad (2.28)$$

These lines come down to the axis at the pion threshold, $q^2(\text{min}) = m_\pi(2M + m_\pi)x/(1 - x)$. The neutrino data show the same general pattern of scaling deviations as the electron and muon data; namely, a decrease with q^2 for $x > 0.3$, and an increase at small x. It perhaps should be emphasized that the neutrino data have been interpolated to the bin centres in all cases, using (2.28); these centre-of-bin corrections are always quite small in comparison with statistical errors. The two sets of data (ν, and e, μ) are in remarkably good quantitative agreement with the fractional quark charge assignment, even for small x in the dominantly "$q\bar{q}$ sea" region.* The values of $xF_3(q^2,x)$ in Fig. 16 show a similar behaviour to F_2. Note that, for small x, $xF_3 < F_2$, as indicated by the dashed lines, which are the same as in Fig. 15.

Values of $F_2^{\nu N}(q^2, x)$ have also been given recently by the CDHS collaboration[19]; their results are shown in Fig. 17. The trends in the results are similar in form to, but show a somewhat weaker q^2-dependence than, the BEBC data.

All these values for F_2 and xF_3 have been derived from (2.27) under the assumption $A = 2xF_1/F_2 = 1$. To obtain experimental values for A, the y distribution at fixed x,q^2 must be analysed. Referring to (2.2)

* The factor $\frac{18}{5}(1-\frac{1}{2}\sin^2\theta_c) \tilde{\sim} 3.6$ for an SU2 symmetric sea; for an SU3 symmetric sea ($\bar{u} = \bar{d} = \bar{s}$), the factor = 3.0.

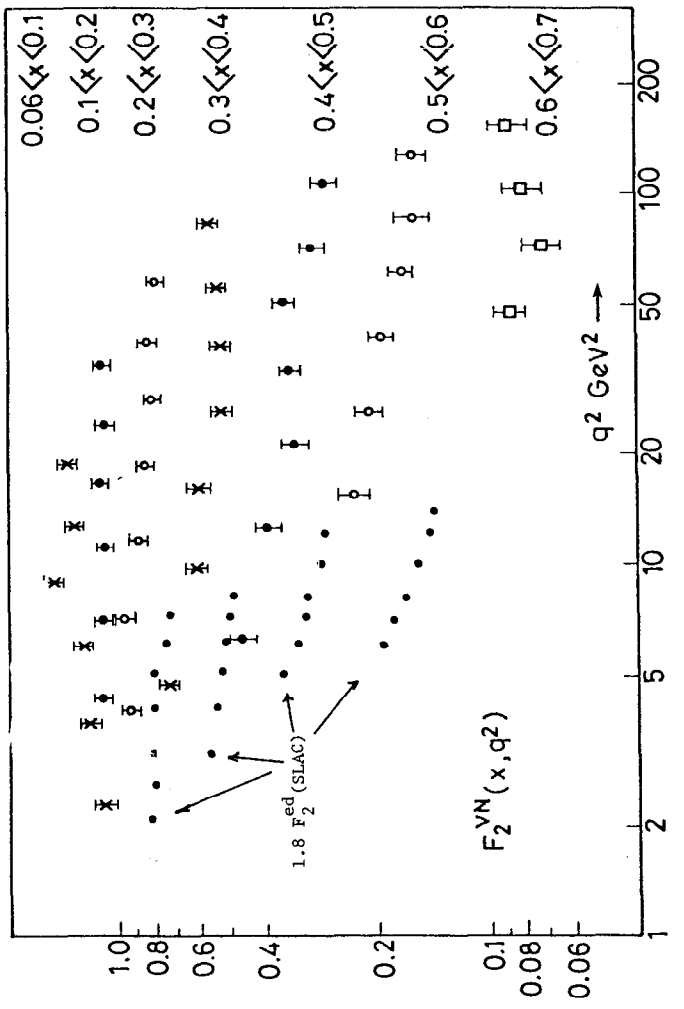

Fig. 17

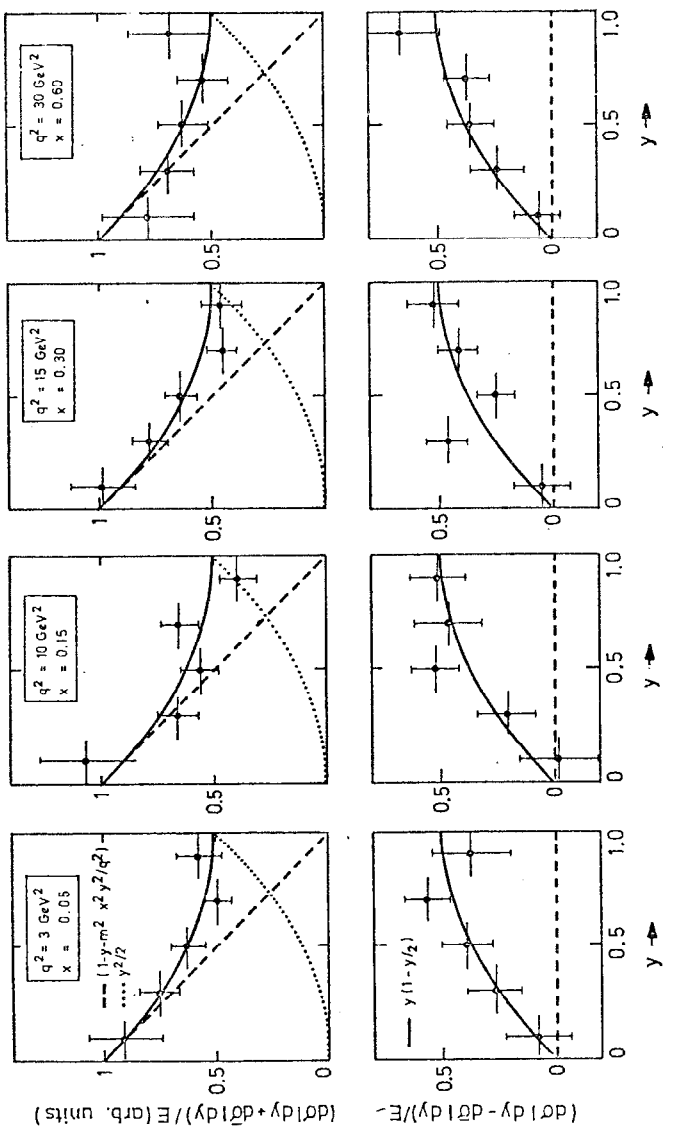

Fig. 18

we note that $(d\sigma/dy + d\bar{\sigma}/dy)/E$ depends on the combination $(1-y)F_2 + (y^2/2)2xF_1$, and $(d\sigma/dy - d\bar{\sigma}/dy)/E$ on $xF_3(y - y^2/2)$. These distributions are given in Fig. 18, from the ABCLOS (BEBC) analysis, for selected values of q^2 and x (the cross-sections again being interpolated to fixed q^2, x). From the shape of the upper distributions, best values of A can be fitted. There is no observable dependence of A on q^2 and x, because the errors are large. The average value observed was

$$\langle A \rangle = 0.89 \pm 0.12\ (.08) \qquad (q^2 > 1) \qquad (2.29)$$

where the figure in brackets represents the possible systematic error (arising from interpolation and flux uncertainties). From this data, any deviations from the asymptotic ($q^2 \to \infty$) Callan-Gross relation A = 1 are below the 20% level. Alternatively the ratio can be recast

$$R = \sigma_S/\sigma_T = (1 + 4M^2x^2/q^2 - A)/A$$

giving

$$\langle R \rangle = 0.15 \pm 0.10\ (.04) \qquad (2.30)$$

The lower plots in Fig. 18 are in excellent agreement with the expected y-dependence of the xF_3 term. Fig. 18 therefore supports our original assumption that the cross-sections (2.2) can be described in terms of just 3 structure functions.

The effect of changes in A, from the value 1.0 assumed in the previous analysis, is fairly small for F_2 and negligible for xF_3. For A = 0.8 for example, F_2 increases from the A = 1 value by between 3 and 10%, while xF_3 decreases by up to 2%.

2.7 Possible Causes of Scaling Deviations

There may be several sources of deviations from Bjorken scaling in the data. Among these could be:

(i) "Trivial" effects

The rise of F_2^{eN} in the low q^2 region ($q^2 < 1$ GeV^2) at small x is expected from conservation of the vector current; in fact $F_2 \propto \frac{q^\mu}{x}(\sigma_T+\sigma_S)$ and must therefore vanish as $q^2 \to 0$ for finite x (or ν). (For neutrino scattering, the axial contribution does not vanish as $q^2 \to 0$, becoming proportional to $\sigma(\pi, N)$ at energy ν). Vector dominance models also predict $F_2(x,q^2)$ rising with q^2 at small x.

(ii) Electromagnetic radiative corrections

The neutrino cross-sections have not been corrected for radiative effects from the charged particles accelerated in the reaction - of which the main contribution comes from the muon. Detailed calculations[20] [21] show that the main effect is to lead to an underestimate of the true cross-sections at large x (the factor being $\sim$ 1-0.2x). However, the q^2-dependence of the correction at fixed x is very weak (<5% for q^2 = 2 → 100 GeV^2). It appears that radiative effects cannot account for the strong q^2-dependence of $F_2^{\nu N}$ for x > 0.3. (In any case, such considerations would not account for the deviations in electron/muon scattering, for which the cross-sections have been radiatively corrected.)

(iii) Threshold effects

The excitation of new quantum numbers (c, b, t ... quarks) would enhance the neutrino cross-sections, predominantly in the "sea region" at small x and large ν. The magnitude of such effects would be expected to be quite a strong function of incident energy, and to be different for electrons and muons, on the one hand, and neutrinos on the other. Yet, the observed dependence of F_2 on q^2 and x seems to be independent of energy and to have a common source for all types of lepton beam. It is difficult to see why threshold excitations should strongly decrease the value of F_2 at large q^2 and large x.

(iv) Failure of the Naive Parton Model

We have already anticipated that, because of the neglect of particle masses and inter-parton interactions, one would not expect Bjorken scaling to hold exactly at finite values of q^2. At the present time, this seems to be the most likely major source of the deviations.

There are two principal sources of scaling deviation associated with the couplings of quark constituents via the gluon field. One source is kinematic in origin, and has to do with the neglect of masses in comparison with q^2. The effect of including masses, as indicated in (2.9), is to modify the scaling variable. This effect was actually investigated empirically a long time ago by Bloom and Gilman[22], who observed that deviations from scaling at low q^2 and low W^2 were reduced by use of $x' = q^2/(2M\nu + M^2) = x(1 - M^2x/q^2 + \ldots)$, with a similar behaviour to that of the ξ parameter, i.e. a correction term $\sim M^2/q^2$. However, we know that mass terms alone cannot account for all the deviations observed,[23] and particularly not those at high x and high q^2 which mainly concern us here.

The other source of deviations from the naive parton model predictions arises from the interactions of the quarks; the inter-quark interaction modifies the naive scaling predictions, based on free, non-interacting constituents. The rest of the section on charged currents is devoted to this topic.

2.8 Predictions on Scaling Deviations from QCD

We begin the discussion with a brief outline of the QCD predictions, already derived in the lectures of John Ellis.

(i) Screening in QED

In quantum electrodynamics, the potential between two charges Q and Q' separated by distance r is modified by virtual pair-production (vacuum polarization) as follows[24, 25]:-

$$V(r) = \frac{QQ'}{r}\left[1+\frac{2\alpha}{3\pi}\int_2^\infty e^{-rz/\lambda_o}\left(1+\frac{2}{z^2}\right)\sqrt{\left(1-\frac{4}{z^2}\right)}\,\frac{dz}{z} + O(\alpha^2)\ldots\right] \qquad (2.31)$$

where α is the (physical) fine-structure constant, $\lambda_o = \hbar/mc$ is the reduced electron Compton wavelength. When $r >> \lambda_o$ the exponential in the integral dominates and the potential follows precisely the Coulomb form* - how else would we define Q and Q'? However, when $r << \lambda_o$, the potential falls progressively relative to the Coulomb value, as r increases:-

$$V(r) = \frac{QQ'}{r}\left[1 + \frac{2\alpha}{3\pi}\left(\ln\frac{\lambda_o}{r} - \frac{5}{6} - 1.781\right) + O(\alpha^2)\ \ldots\right] \qquad (2.32)$$

The screening effect due to virtual pair creation arises

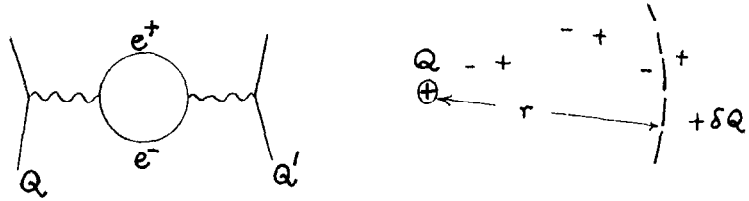

from the resulting polarization of the vacuum, so the effective charge at distance r is Q - δQ. Evaluation of successive terms in (2.32) becomes progressively more complicated - see, for example, the diagrams for the α^3 terms (Fig. 19) involved in computing (g - 2)/2 for the electron/muon (and recall that it took ~15 years to get them right!) To avoid these difficulties, approximations can be made. To lowest order in perturbation theory, the r or q^2- dependence of the effective coupling $\alpha(q^2)$ can be written as

$$\alpha(q^2) = \alpha(\mu^2)\left[1 + \frac{\alpha(\mu^2)}{3\pi}\ln\frac{q^2}{\mu^2}\right] \qquad (2.33)$$

where $q^2 = \mu^2$ is some arbitrary normalization point. In higher orders, one gets terms of the type $\alpha^n(\ln q^2/\mu^2)^r$ with $r \leq n$. If one retains only those terms with r = n - the "leading log approximation" - the series can be summed exactly and one finds

$$\alpha(q^2) = \frac{\alpha(\mu^2)}{\left[1 - \frac{\alpha(\mu^2)}{3\pi}\ln(q^2/\mu^2)\right]} + O(\alpha^2) \qquad (2.34)$$

where terms suppressed by factors of $\ln q^2/\mu^2$, $(\ln q^2/\mu^2)^2$ i.e. by α, α^2... relative to the first term are neglected. To the extent that $\alpha(\mu^2)$ is small, this equation tells us that for $q^2 > \mu^2$ i.e. for a probe of shorter wavelength, the new structure which is revealed in the form of additional vertex corrections etc. as in the second diagram, is equivalent to re-defining the vertex coupling as $\alpha(q^2)$ as in (2.34).

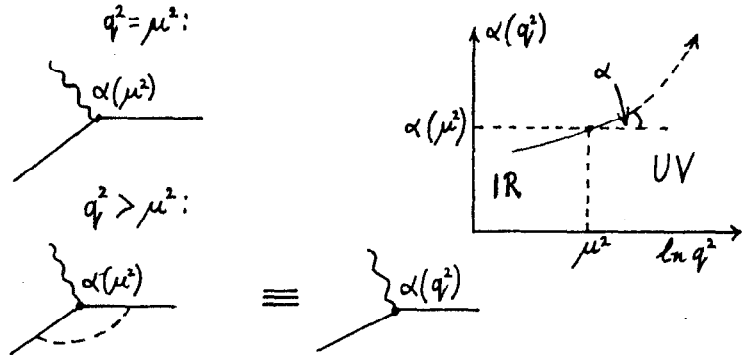

---

* For r large, any possible deviations from the Coulomb potential are measured to be miniscule. For example, limits on a Yukawa-type term $V = e^{-r/R}/r$ are $R > 10^5$ km (photon mass $< 10^{-47}$ gm.) For details (including the inadvertent discovery of Coulomb's (1785) law by B. Franklin in 1755) see the excellent review article by Goldhaber and Nieto[50].

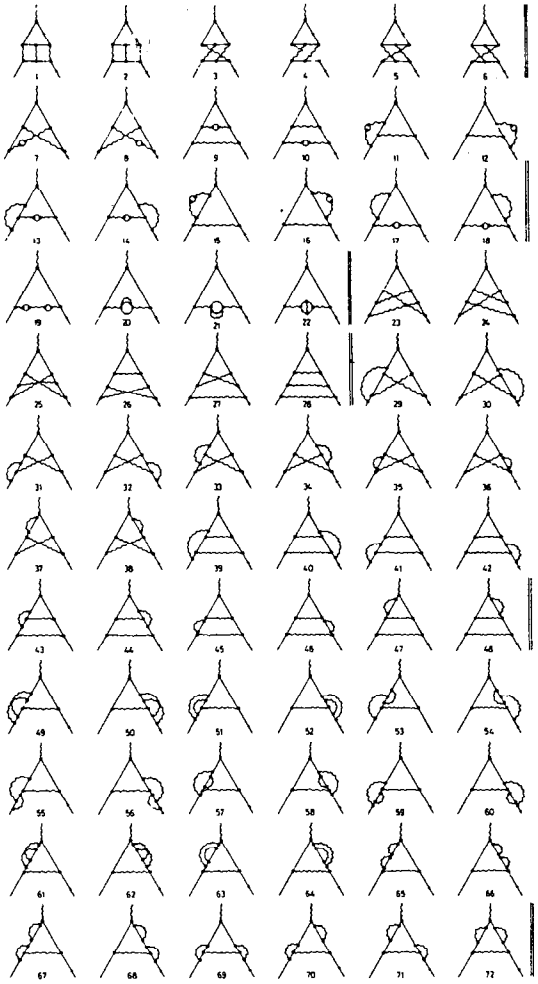

Fig. 19 α^3 contributions to (g-2) of the electron or muon in QED.

The q^2- dependence $\alpha(q^2)$ is indicated in the sketch. In the infra-red region (large r, small q^2) α is well-behaved, while the simple formula (2.34) gives a singularity in the very far ultra-violet, when $q^2 = \mu^2 \exp[3\pi/\alpha(\mu^2)] \sim 10^{56}\mu^2$. Note that the slope of the $\ln q^2$ dependence is small ($\alpha \approx 1/137$).

(ii) Screening in QCD

In quantum chromodynamics the interaction between quarks is mediated by a massless vector field - the gluons - which transmit the strong (colour) forces. QCD, is non-Abelian, the gluons (like the quarks) carrying the colour charges, unlike QED where photons are uncharged. This means virtual gluon pairs as well as $q\bar{q}$ pairs contribute to the vacuum polarization. The coupling constant analogous to (2.33) is given by[26, 27]

$$\alpha_s(q^2) = \alpha_s(\mu^2)\left[1 + \frac{\alpha_s(\mu^2)}{4\pi}.\ln(q^2/\mu^2).(C_1 + C_2 + C_3) + \ldots\right]$$

where $C_1 = 2m/3$ is the $q\bar{q}$ contribution (m is the number of quark flavours) and $C_2 = 5$ is the contribution from transverse gluons. Both lead to screening of the strong charge, as in QED. The third term, $C_3 = -16$ involves longitudinal gluons and gives an antiscreening effect. Thus $C_1 + C_2 + C_3 = -(33-2m)/3$, which is negative for $m \leq 16$. The result analogous to (2.34) is then

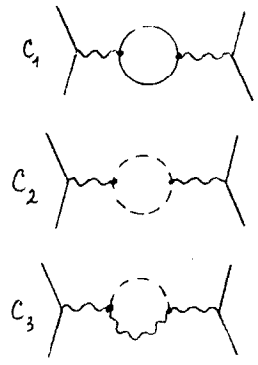

$$\alpha_s(q^2) = \frac{\alpha_s(\mu^2)}{1 + B\alpha_s(\mu^2)\ln(q^2/\mu^2)} \quad ; \quad B = \frac{33-2m}{12\pi} \qquad (2.35)$$

If one defines $\Lambda^2 = \mu^2 \exp[-1/B\alpha_s(\mu^2)]$ then this can be written

$$\frac{\alpha_s(q^2)}{\pi} = \frac{12}{(33-2m)\ln(q^2/\mu^2)} \qquad (2.36)$$

which is a first-order perturbation theory expression for the quark-gluon coupling constant, valid when $\alpha_s(q^2)/\pi << 1$. $\alpha_s(q^2)$ increases with increasing r or decreasing q^2, and the singularity occurs in the IR region rather than the UV. $\alpha_s(q^2) \to 0$ as $q^2 \to \infty$ - hence the term "asymptotic freedom". The low q^2 singularity which appears in the first-order expression for α_s is possibly connected with the phenomenon of quark confinement. It does not seem possible to give an intuitive picture of antiscreening in QCD, but it is as if, in electromagnetism, unlike charges repelled and like charges attracted. Presumably, $\alpha_s(q^2) \sim$ 0.1-1 at $q^2 \sim$ few GeV^2, so that the q^2 dependence should be much larger than in the QED case.

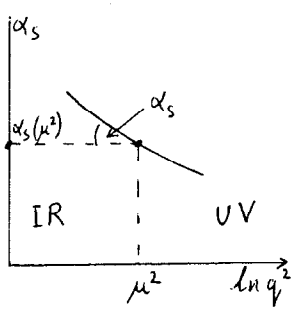

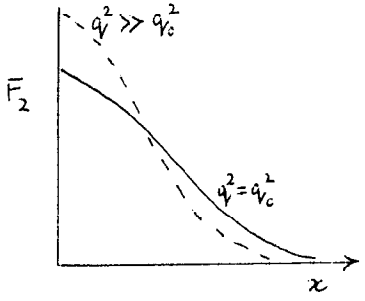

(iii) The structure functions and their moments

The effect of strong radiative corrections on the form of the structure functions, i.e. quark momentum distributions, can be easily understood qualitatively. As q^2 increases, more structure is revealed as the wavelength 1/q of the probe is reduced. For example, a quark at $x = x_1$ at $q^2 = q_0^2$ may resolve, at $q^2 >> q_0^2$, into a quark of momentum $x_2 < x_1$ and a gluon of momentum $(x_1 - x_2)$. As the (electromagnetic or weak) current cannot be absorbed by gluons (which, have by definition, only the strong colour charge), the result is a shrinkage of $F_2(x)$ towards the origin. Since gluons can form $q\bar{q}$ pairs, radiative processes will however increase F_2 at very small x.

The processes taking place can be quantified by writing integro-differential equations for the evolution of the quark and gluon densities. Let $P_{AB}(z)dxdq^2$ be the probability that a parton A emits a parton B with fraction z-z+dz of its momentum, when q^2 is changed to q^2+dq^2. Suppose for simplicity that A and B are valence quarks (as measured in practise by xF_3). The change in the number Q_V of valence quarks in $x \to x + dx$ is then

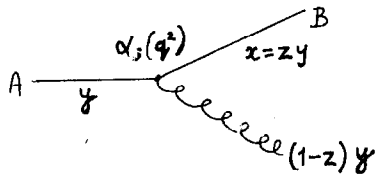

$$q^2\frac{dQ_V}{dq^2}(x,q^2)dx = \frac{\alpha_s(q^2)}{2\pi}\int_{y=x}^{y=1} P_{QQ}(\tfrac{x}{y})\frac{dx}{y}Q_V(y,q^2)dy \qquad (2.37)$$

where $z = x/y$ and $\alpha_s/2\pi$ defines the probability that A radiates a gluon with some fraction (1-z) of the momentum of A. Multiplying both sides of (2.37) by x^{N-1} and integrating:-

$$q^2\frac{d}{dq^2}\int_0^1 x^{N-1}Q_V(x,q^2)dx = \frac{\alpha_s(q^2)}{2\pi}\int_0^1 x^{N-1}dx\int_x^1 Q_V(y,q^2)P_{QQ}(\tfrac{x}{y})\frac{dy}{y}$$

Upon replacing x by yz the RH side becomes

$$\frac{\alpha_s(q^2)}{\pi}\int_0^1\int_0^1 y^{N-1}dy\; Q_V(y,q^2)z^{N-1}P_{QQ}(z)dz$$

where the limits of integration are $z = 0 \to 1$ and $y = 0 \to 1$, as in the

diagram. Defining

$$A = \int_0^1 z^{N-1} P_{QQ}(z)dz$$

$$M(N,q^2) = \int_0^1 x^{N-1} Q_V(x,q^2)dx$$

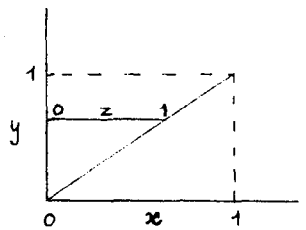

the evolution of the valence quarks is therefore expressed by

$$-\frac{d}{d\ln q^2} M(N,q^2) = \left(\frac{\alpha_s}{2\pi}\right) A\, M(N,q^2) = \frac{A}{2\pi B} \frac{M(N,q^2)}{\ln q^2/\Lambda^2}$$

using (2.35) and (2.36). Hence

$$M(N,q^2) = C/(\ln q^2/\Lambda^2)^d \qquad (2.38)$$

where C = const. and $d = -A/2\pi B$ is the so-called anomalous dimension associated with the valence quark moments. The simple prediction of QCD about structure functions is therefore that their moments should vary as known inverse powers of $\ln q^2/\Lambda^2$. To find the value of A (hence d), we need to know $P_{QQ}(z)$; but this is the same as $P_{QG}(1-z)$, which is known from the Weizsacker-Williams formula for the virtual photon distribution in an electron (with a change in constant, due to colour).

As explained in the lectures of John Ellis, the development of quark, antiquark and gluon distributions with q^2 follows from suitable evolution equations similar to (2.37). Equn. (2.38) deals with the simplest case, applying to the valence quarks (i.e. the moments of xF_3) which are flavour non-singlets. F_2, which measures both valence quarks and sea-quarks (and antiquarks), contains two flavour singlet terms in addition to the non-singlet; there are three terms in the moment expression, each with a different power of $\ln q^2/\Lambda^2$, with three unknown coefficients C_i on top. To find these, one has to experimentally determine the moments of valence quarks, sea-quarks and gluons at some fixed value of q^2 - or, equivalently, the value of the F_2 moment at three values of q^2.

2.9 Moments of the Structure Functions in Neutrino Scattering

The structure function moments with respect to the x variable are defined by the Cornwall-Norton relations

$$M_i(N,q^2) = \int_0^1 x^{N-2} F_i(x,q^2)dx \qquad (2.39)$$

where $F_i = F_2$ or xF_3. Values deduced from the BEBC/GGM data are given in Fig. 20, for N = 2-7. In order to get rid of kinematic effects due to the target (nucleon) mass at finite q^2, however, it is better to use the Nachtmann variable (2.9):-

$$\xi = \frac{2x}{1 + \sqrt{1 + 4m^2x^2/q^2}}. \qquad (2.40)$$

In terms of ξ, the corresponding (Nachtmann) moments have the form

$$M_2(N,q^2) = \int_0^1 \frac{\xi^{N+1}}{x} \frac{F_2(x,q^2)\,[N^2+2N+3+3(N+1)\sqrt{1+4M^2x^2/q^2}+N(N+2)4M^2x^2/q^2]dx}{(N+2)(N+3)}$$

$$M_3(N,q^2) = \int_0^1 \frac{\xi^{N+1}}{x} xF_3(x,q^2) \frac{[1+(N+1)\sqrt{1+4M^2x^2/q^2}]dx}{(N+2)} \qquad (2.41)$$

These are shown in Fig. 21. For $q^2 > 3$ GeV^2, the differences between the Cornwall-Norton and Nachtmann moments are less than the experimental errors.

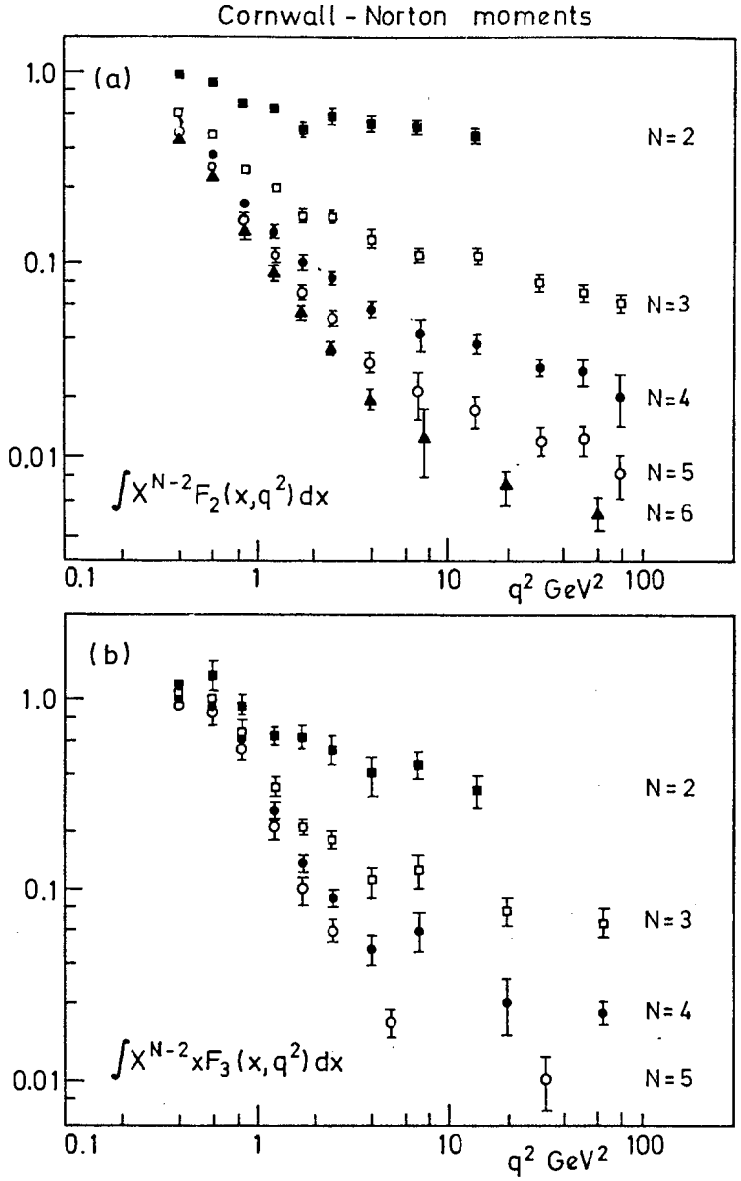
Cornwall - Norton moments
(a)
N=2
N=3
N=4
N=5
N=6
$\int X^{N-2} F_2(x,q^2)\,dx$
1.0
0.1
0.01
0.1
1
10
100
q^2 GeV^2
(b)
N=2
N=3
N=4
N=5
$\int X^{N-2} xF_3(x,q^2)\,dx$
1.0
0.1
0.01
0.1
1
10
100
q^2 GeV^2

Fig. 20

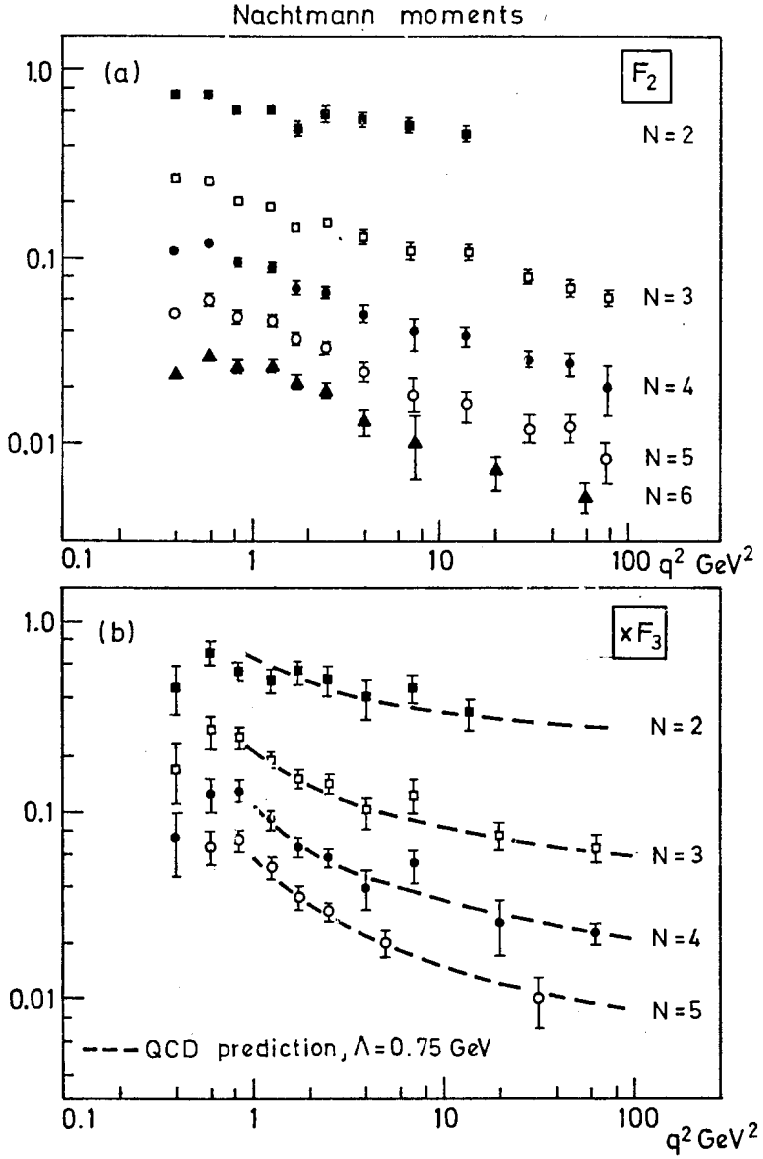
Nachtmann moments
(a)
F_2
N=2
N=3
N=4
N=5
N=6
1.0
0.1
0.01
0.1
1
10
100 q^2 GeV^2
(b)
xF_3
N=2
N=3
N=4
N=5
QCD prediction, $\Lambda = 0.75$ GeV
1.0
0.1
0.01
0.1
1
10
100
q^2 GeV^2

Fig. 21

(i) Moments of the non-singlet function xF_3; first-order analysis

The QCD prediction for the moments of the structure functions in general results in three terms

$$\text{Moment} = \sum_{i=1}^{3} C_i/(\ln q^2/\Lambda^2)^{d_i} \qquad (2.42)$$

corresponding, crudely speaking, to the contributions of the valence quarks, quark-antiquark sea and gluons, respectively. The gluons and sea-quarks are flavour (SU(m)) singlets, while the valence quark term, familiar in the classical unitary symmetry schemes, is a non-singlet. As explained above, the developmental equation for the non-singlet is very simple and the moment has the single-term form

$$M_3(Nq^2) = \text{const.}/(\ln q^2/\Lambda^2)^{d_{NS}} \qquad (2.43)$$

where the anomalous dimension

$$d_{NS} = \frac{4}{(33-2m)}\left[1 - \frac{2}{N(N+1)} + 4\sum_{2}^{N}\frac{1}{j}\right] \qquad (2.44)$$

The term outside the bracket depends on the number of colours and flavours in the gauge symmetry, while the square bracket depends on the nature of the colour field. In particular the last term in this bracket is typical of a vector field. For scalar gluons, this last term would be absent.

The experimental data from the ABCLOS collaboration (BEBC/SPS + GGM/PS data) has been used to test the QCD predictions in various ways. The first prediction, from (2.43) and (2.44) is that the moments for different N values should be related by power laws, i.e. $M(N_2) \propto M(N_1)^{(d_2/d_1)}$. Fig. 22 shows typical experimental results covering the range q^2 = 1-60 GeV^2 and Table 1 a comparison of the best-fit slopes with the predicted coefficients. Note that the predicted ratios (d_2/d_1) depend

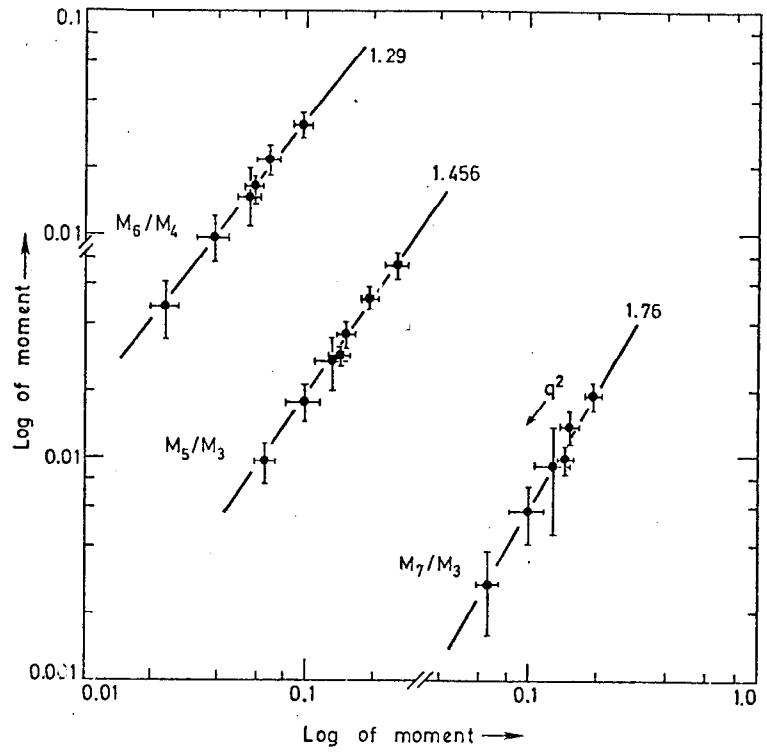

Fig. 22

only on the contents of the square brackets in (2.44), and thus are independent of both Λ (provided $\ln(q^2/\Lambda^2)$ is large) and the numbers of flavours and colours. There is rather spectacular agreement betweeen experiment and QCD theory; scalar gluons, for example, are excluded by the data.

TABLE 1

Moments	Observed Coefficient	QCD (vector gluons)	Scalar Gluons
$N_1 = 4$, $N_2 = 6$	1.29 ± 0.06	1.29	1.06
$N_1 = 3$, $N_2 = 5$	1.50 ± 0.08	1.46	1.12
$N_1 = 3$, $N_2 = 7$	1.84 ± 0.20	1.76	1.16
$N_1 = 2$, $N_2 = 6$	3.00 ± 0.45	2.53	1.43

These results cover the range q^2 = 1-100 GeV^2. They are apparently strong quantitative support for QCD. It is perhaps worth emphasizing that more than one theory of scaling deviations could give the straight-line plots of Fig. 22. For example, a field theory with an ultra-violet fixed point (i.e. $\alpha_s \to$ non-zero constant as $q^2 \to \infty$) would also result in power-law relations for the moments, but with arbitrary slopes. A similar analysis can be made with the moments of $(F_2^{\mu p} - F_2^{\mu n})$ - also a non-singlet measuring the distribution of $(u_v - d_v)$, rather than $(u_v + d_v)$ - as measured in muon and electron scattering.[31] The slopes obtained are also in accord with QCD, over the available range q^2 = 1-22 GeV^2 - see Fig. 26.

Some caution in interpretation is required however, for several reasons:-

(i) the results for N = 3-7 do not test either the small x(<0.1) or large x (>0.8) behaviour. The restriction $N \lesssim 7$ was made to avoid possible errors in smearing corrections at large x, as well as the large statistical errors due to the low event rates in this region.

(ii) The N = 2 moments, when compared with higher moments, give slopes which are about one standard error larger than the QCD prediction. This is also apparent in the muon scattering data. These effects may have nothing to do with QCD, but arise from threshold phenomena (excitation of new quantum numbers) at small x, which would make $M(2, q^2)$ decrease less rapidly with q^2 at large q^2. The small x behaviour is of course suppressed when we take higher moments.

Postponing these and other problems to later discussion, we continue with further analysis of the data in terms of first order QCD predictions. The second test which can be made is of the prediction, from (2.43), that

$$\left[M_3(N,q^2)\right]^{-1/d_{NS}} = \text{const.}(\ln q^2 - \ln\Lambda^2) \qquad (2.45)$$

and is shown in Fig. 23, for even and odd moments. The linear dependence of $M^{-1/d_{NS}}$ on $\ln q^2$ is confirmed (within the large errors) by the data, for $q^2 > 1$ GeV^2. The linearity is a test of the logarithmic q^2-dependence of the QCD moments, which is typical of the asymptotically free gauge theory. A fixed point theory for example would give a stronger dependence on q^2. The intercept of the straight line (2.45) gives an estimate for the parameter Λ. The following table shows values obtained for the N = 3, 5 and 7 moments:-

TABLE 2

FIRST-ORDER FITS TO Λ (GeV) (m = 3)

	$q^2 > 1$	$q^2 > 2$	($q^2 > 1$ No Elastics)
N = 3	0.70 ± .08	0.85 ± .18	0.34 ± 0.11
N = 5	0.77 ± .07	0.70 ± 0.18	0.20 ± 0.13
N = 7	0.75 ± .07	0.95 ± .20	0.01 ± 0.05

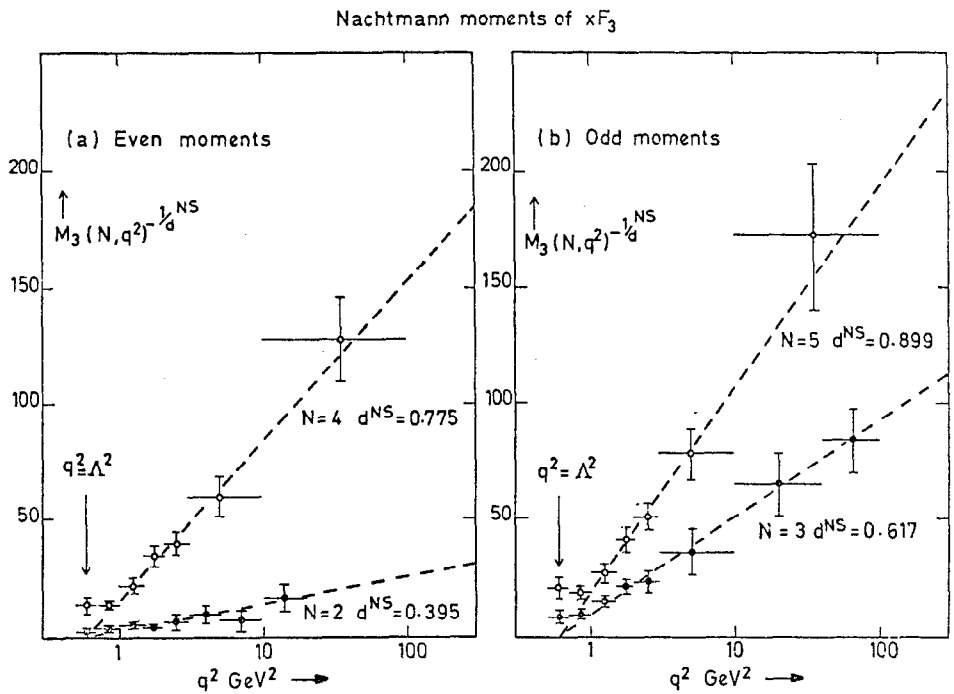

Fig. 23

Thus, averaged over all three moments (taking into account that these are correlated) one obtains

$$\Lambda = 0.74 \pm .05 \text{ GeV} \qquad (q^2 > 1) \tag{2.46}$$

where the error is statistical. Possible systematic errors, from uncertainty in spectrum shape (i.e. the K/π production ratio) corrections etc. are estimated as 0.03 GeV. The choice of the number of flavours (affecting the value of d_{NS}) has a small effect; Λ decreases by 0.04 GeV per added flavour.

It is important to emphasize that elastic events of the type $\nu, \bar{\nu} + N \to \mu^{\pm} + N$ make a substantial contribution to the moments. If these are excluded, the value of Λ is not stable with N or q^2, and the χ^2 of the fit becomes significantly worse.

(ii) Second order corrections; high twist contributions.

The agreement between the experimental data and the linear predictions in Figs. 22 and 23 from lowest-order QCD is somewhat unexpected, since the condition $\alpha_s/\pi \ll 1$ is not fulfilled. Thus, with $\Lambda = 0.74$ GeV, $\alpha_s/\pi = 0.34$ for $q^2 = 2$ GeV^2 and 0.15 for $q^2 = 10$ GeV^2, and α_s^2 terms should therefore be significant.

For the non-singlet function xF_3, the coefficient functions C and the anomalous dimensions d_{NS} have been computed for the α_s^2 terms, by Floratos et al[28] and Buras et al[29]. Unfortunately, there were errors in these calculations and so the α_s^2 corrections computed by the ABCLOS collaboration[16], based on these papers, were incorrect. Meantime, Bardeen et al[30] have re-computed the α_s^2 corrections, and on the basis of these, the most recent analysis gives the numbers shown in Table 3, where, in the first column, data down to $q^2 = 0.7$ GeV^2 is included. The value of Λ is much smaller, and the χ^2 of the fit is slightly better than the first-order fit (Table 2).

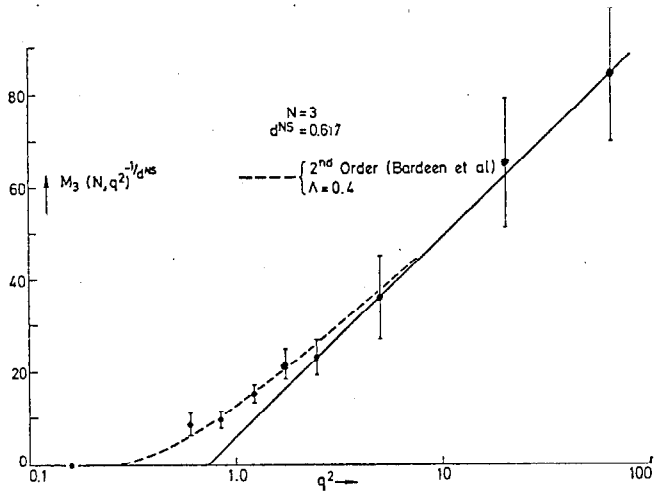

Fig. 24

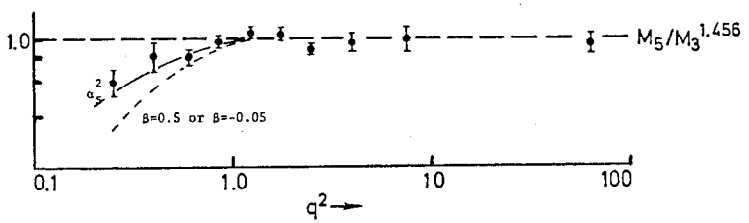

Fig. 25 The ratio of the N=5 moment of xF_3 to the N=3 moment raised to the 1.456 power. First order QCD predicts a constant, independent of q^2. The solid curve shows the effect of second-order corrections; the dashed curve the additional effect of a $(1 + \beta N/q^2)$ term.

TABLE 3

FITS TO Λ INCLUDING α_s^2 CORRECTIONS

	$q^2 > 0.7$	$q^2 > 1.0$	$q^2 > 2.0$	$q^2 > 3.0$
N = 3	0.37 ± .025	0.36 ± .03	0.39 ± .07	0.32 ± 0.14
N = 5	0.43 ± .025	0.43 ± .03	0.42 ± .06	0.32 ± 0.13
N = 7	0.41 ± .025	0.42 ± .035	0.40 ± .07	0.28 ± 0.13

The average over the three moments gives

$$\Lambda = 0.40 \pm .025 \text{ GeV} \quad (q^2 > 1) \qquad (2.47)$$

to be compared with the first-order value (2.46). Despite the drastic change in Λ due to the α_s^2 corrections, the linearity of the logarithmic moment plot (Fig. 22) is virtually unaffected. The revised version of Fig. 23 is shown in Fig. 24.

One cannot of course consider that (2.47) is the value of Λ, since even higher-order corrections (α_s^3 ....) are not included, but presumably the estimate (2.47) is much better than (2.46). There are, in addition other uncertainties of a theoretical nature. These are the so-called "higher-twist" corrections, which are expected to contribute factors of the type

$$F = (1 + \beta N/q^2) \qquad (2.48)$$

with β of the order of the square of the transverse momentum per parton i.e. $\beta \sim 0.1$ GeV^2. However, there is no solid theoretical derivation of (2.45), or of the constants in it.

Fig. 25 shows the ABCLOS data on the moment ratios $M_2/(M_1)^{d_2/d_1}$ against q^2. The solid curves show the QCD predictions, including α_s^2 effects; the dashed curves the additional effects of a term of the type (2.48). The data set a limit $|\beta| < 0.5$ GeV^2.

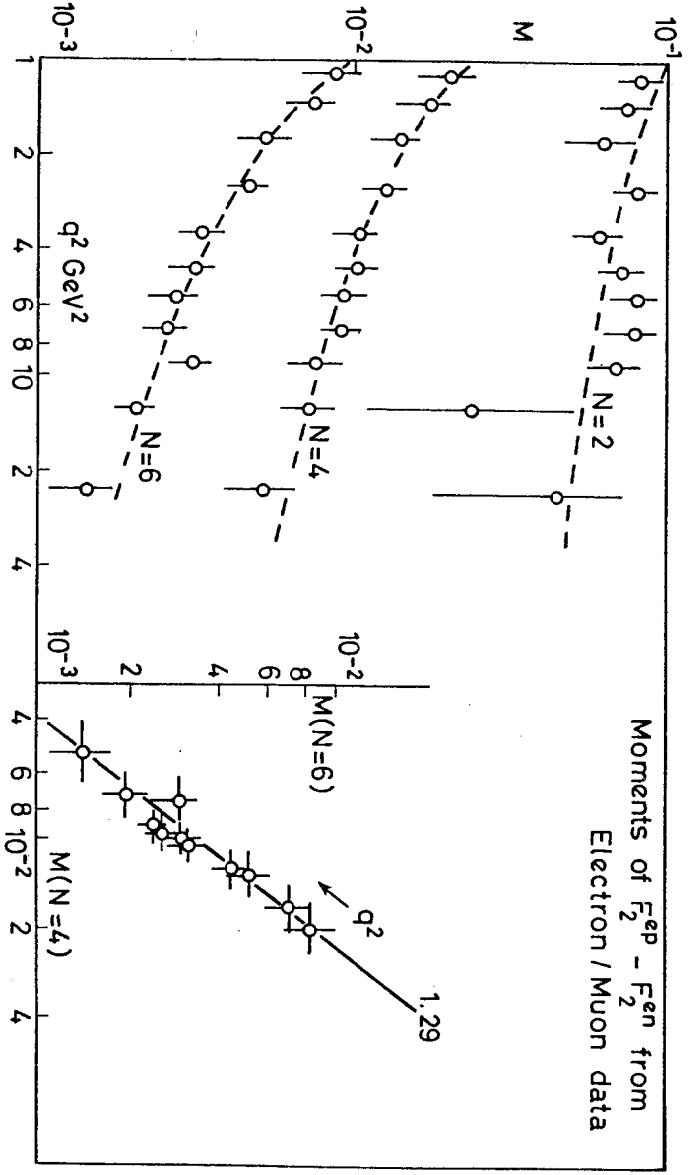
Moments of $F_2^{ep} - F_2^{en}$ from Electron / Muon data
M
q^2 GeV^2
N=6
N=4
N=2
M(N=6)
M(N=4)
q^2
1.29

Fig. 26

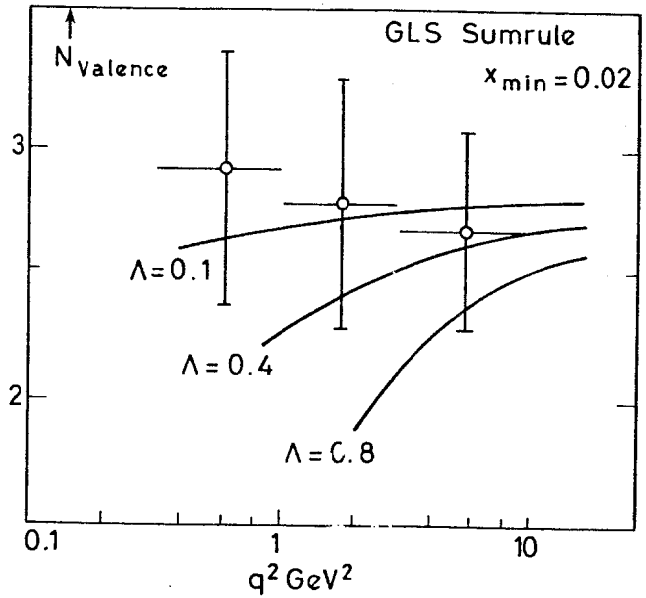
GLS Sumrule
$N_{Valence}$
$x_{min} = 0.02$
$\Lambda = 0.1$
$\Lambda = 0.4$
$\Lambda = 0.8$
q^2 GeV^2

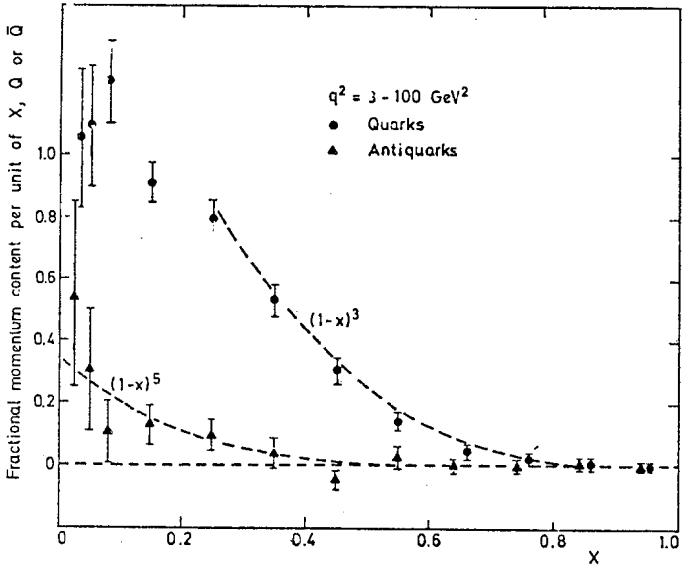
q^2 = 3 - 100 GeV^2
Quarks
Antiquarks
Fractional momentum content per unit of X, Q or $\bar{Q}$
$(1-x)^3$
$(1-x)^5$
X

Fig. 27

(iii) The Gross-Llewellyn Smith sumrule

At finite q^2, the QCD prediction to the GLS sumrule (the N = 1 moment of xF_3) is

$$\int_0^1 x^{-1}.xF_3(x,q^2)dx = 3[1 - \frac{\alpha_s}{\pi} + \ldots] \qquad (2.49)$$

Experimentally, the main difficulty in measuring the integral is that the integral peaks near $x \sim 0$. At fixed q^2, $x_{min} = q^2/2ME_\nu > 0$; so, the measured integral is a lower limit, with x_{min} a function of q^2. Data from a recent analysis by the ABCLOS collaboration is shown in Fig. 27. These results also indicate a rather low value, $\Lambda \approx 0.3$ GeV, for the strong interaction parameter. Note that, for $\Lambda = 0.4$, $\alpha_s/\pi = 0.24$ at $q^2 = 1$ GeV^2. Hence the α_s^2 term in (2.49) is really down at the 5-10% level, as compared with the first term of unity. In this sense, the deviations from the GLS sumrule should give a reliable means of measuring Λ; since, according to (2.48), high twist effects should be smaller at small N, systematic uncertainties on this score should also be minimized.

(iv) Criticism of the analysis

The main criticisms of the above analysis must be that much of the data is in the low q^2 (1-5 GeV^2) region, where

(i) α_s is not very small, so that α_s^2 corrections have dramatic effects

(ii) the value of Λ depends crucially on the contribution from a single exclusive channel - the elastic channel

(iii) $1/q^2$ effects can be important.

Regarding the dominance of the elastic channel, what is the nature of the criticism? One may argue that the primary interaction is between a neutrino and a quark, as described by V-A theory plus QCD; what happens thereafter, for example whether the struck quark, plus the remaining quarks and gluons choose to recoil coherently as a nucleon or other low-lying resonance, is treated as a final-state interaction, (FSI). The FSI can enhance (or depress) the cross-section and hence distort the QCD picture; provided several resonances are averaged over, then duality arguments[22] ensure that the moments will not be affected. However, if the elastic contribution to a particular moment exceeds, say, 25%, these conditions would hardly be fulfilled.

All the above problems can in principal be side-stepped by going to higher q^2. For example for $\Lambda = 0.4$ GeV, $\ln q^2/\Lambda^2$ changes by a factor 3.1 as q^2 varies from 1 to 60 GeV^2; starting from $q^2 = 5$, one would however require an upper value of $q^2 = 7700$ GeV^2 to achieve the same factor. Over the presently accessible range $q^2 = 5$-100 GeV^2, the range of $\ln q^2/\Lambda^2$ would be halved and the experimental precision would therefore have to be doubled. Although the contribution of any $1/q^2$ term, relative to $1/\ln q^2/\Lambda^2$, has decreased, its magnitude relative to the experimental precision has hardly changed; other uncertainties, for example in electromagnetic radiative corrections, have become larger in relation to the experimental errors. So, precision experiments at high q^2 will not be without their problems.

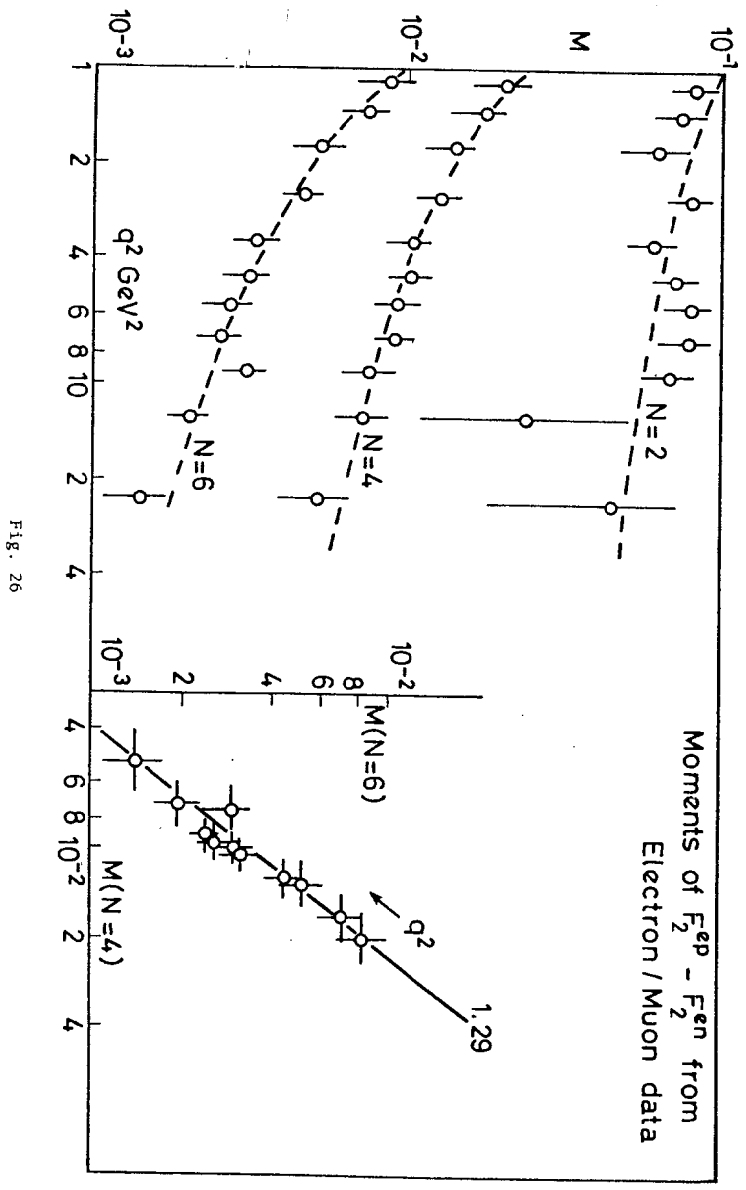
Moments of $F_2^{ep} - F_2^{en}$ from
Electron / Muon data
M
10^{-1}
10^{-2}
10^{-3}
q^2 GeV^2
N=2
N=4
N=6
M(N=6)
M(N=4)
q^2
1.29

Fig. 26

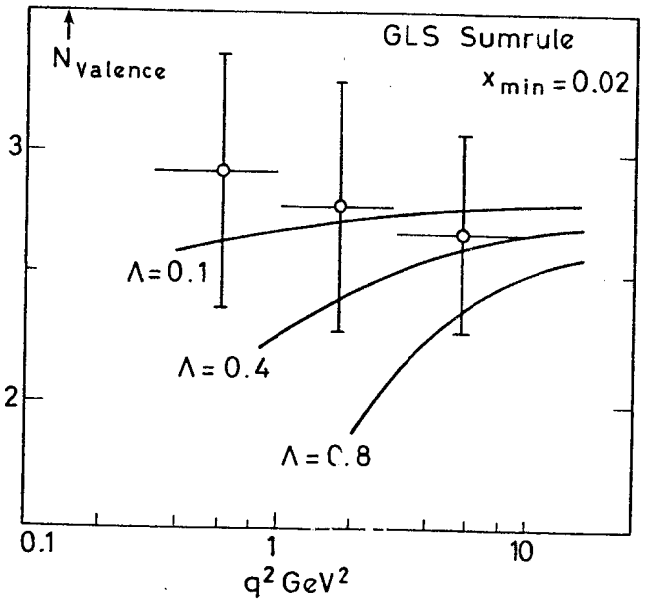
GLS Sumrule
$N_{Valence}$
$x_{min} = 0.02$
$\Lambda = 0.1$
$\Lambda = 0.4$
$\Lambda = 0.8$
q^2 GeV^2

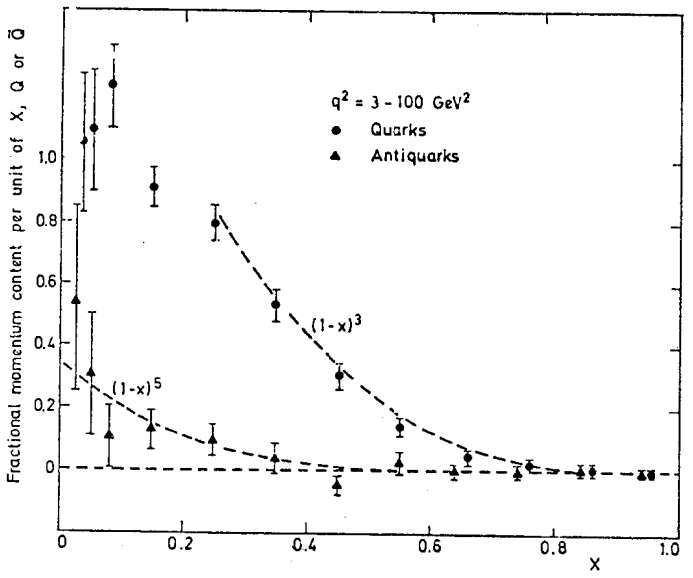
q^2 = 3 - 100 GeV^2
Quarks
Antiquarks
Fractional momentum content per unit of X, Q or $\bar{Q}$
$(1-x)^3$
$(1-x)^5$
X

Fig. 27

(iii) The Gross-Llewellyn Smith sumrule

At finite q^2, the QCD prediction to the GLS sumrule (the N = 1 moment of xF_3) is

$$\int_0^1 x^{-1}.xF_3(x,q^2)dx = 3[1 - \frac{\alpha_s}{\pi} + \ldots] \qquad (2.49)$$

Experimentally, the main difficulty in measuring the integral is that the integral peaks near $x \sim 0$. At fixed q^2, $x_{min} = q^2/2ME_\nu > 0$; so, the measured integral is a lower limit, with x_{min} a function of q^2. Data from a recent analysis by the ABCLOS collaboration is shown in Fig. 27. These results also indicate a rather low value, $\Lambda \simeq 0.3$ GeV, for the strong interaction parameter. Note that, for $\Lambda = 0.4$, $\alpha_s/\pi = 0.24$ at $q^2 = 1$ GeV^2. Hence the α_s^2 term in (2.49) is really down at the 5-10% level, as compared with the first term of unity. In this sense, the deviations from the GLS sumrule should give a reliable means of measuring Λ; since, according to (2.48), high twist effects should be smaller at small N, systematic uncertainties on this score should also be minimized.

(iv) Criticism of the analysis

The main criticisms of the above analysis must be that much of the data is in the low q^2 (1-5 GeV^2) region, where

(i) α_s is not very small, so that α_s^2 corrections have dramatic effects

(ii) the value of Λ depends crucially on the contribution from a single exclusive channel - the elastic channel

(iii) $1/q^2$ effects can be important.

Regarding the dominance of the elastic channel, what is the nature of the criticism? One may argue that the primary interaction is between a neutrino and a quark, as described by V-A theory plus QCD; what happens thereafter, for example whether the struck quark, plus the remaining quarks and gluons choose to recoil coherently as a nucleon or other low-lying resonance, is treated as a final-state interaction, (FSI). The FSI can enhance (or depress) the cross-section and hence distort the QCD picture; provided several resonances are averaged over, then duality arguments[22] ensure that the moments will not be affected. However, if the elastic contribution to a particular moment exceeds, say, 25%, these conditions would hardly be fulfilled.

All the above problems can in principal be side-stepped by going to higher q^2. For example for $\Lambda = 0.4$ GeV, $\ln q^2/\Lambda^2$ changes by a factor 3.1 as q^2 varies from 1 to 60 GeV^2; starting from $q^2 = 5$, one would however require an upper value of $q^2 = 7700$ GeV^2 to achieve the same factor. Over the presently accessible range $q^2 = 5$-100 GeV^2, the range of $\ln q^2/\Lambda^2$ would be halved and the experimental precision would therefore have to be doubled. Although the contribution of any $1/q^2$ term, relative to $1/\ln q^2/\Lambda^2$, has decreased, its magnitude relative to the experimental precision has hardly changed; other uncertainties, for example in electromagnetic radiative corrections, have become larger in relation to the experimental errors. So, precision experiments at high q^2 will not be without their problems.

2.10 Moments of $F_2(x,q^2)$ and the Gluon Distribution

As explained before, the first-order QCD expression for the F_2 moment consists of three terms

$$M_2(N,q^2) = \frac{C_{NS}}{(\ln q^2/\Lambda^2)^{d_{NS}}} + \frac{C_+}{(\ln q^2/\Lambda^2)^{d_+}} + \frac{C_-}{(\ln q^2/\Lambda^2)^{d_-}} \qquad (2.49)$$

where the C's are arbitrary coefficients and the d's are known functions of N. If Q_o, $\bar{Q}_o$ and G_o represent the moments of the quarks, antiquarks and gluons at some reference value $q^2 = q_o^2$, then, for an isoscalar target and with $\theta_c \tilde{\sim} 0$, it can be shown that

$$\frac{C_{NS}}{(\ln q_o^2/\Lambda^2)^{d_{NS}}} = \frac{1}{3}(Q_o + \bar{Q}_o) = \frac{1}{3}M_2(N,q_o^2)$$

$$\frac{C_+}{(\ln q_o^2/\Lambda^2)^{d_+}} = \frac{2}{3}[(1 - A_N)(Q_o + \bar{Q}_o) + B_N G_o] \qquad (2.50)$$

$$\frac{C_-}{(\ln q^2/\Lambda^2)^{d_-}} = \frac{2}{3}[A_N(Q_o + \bar{Q}_o) - B_N G_o]$$

where A_N and B_N are combinations of the d parameters and are given in the paper of Hinchliffe and Llewellyn-Smith.[32] The above equations can be conveniently re-written in the form:

$$YM_2(N,q^2) = M_2(N,q_o^2) + X.G(N,q_o^2) \qquad (2.51)$$

where
$$\frac{1}{Y} = \frac{1}{3}(2x^{d_+} + x^{d_{NS}}) - \frac{2A_N}{3}(x^{d_+} - x^{d_-})$$

$$X = \frac{2}{3}B_N Y(x^{d_+} - x^{d_-})$$

and

$$x = (\ln q_o^2/\Lambda^2)/(\ln q^2/\Lambda^2)$$

Equation (2.51) expresses the q^2 dependence of the N^{th} moment of F_2 in terms of the moment of F_2 at q_o^2 and that of the gluons, G, also at q_o^2, and if we plot YM_2 against x, the slope of the resulting distribution should give $G(N,q_o^2)$ - see Table IV and Fig. 28. The quantities X and Y are known functions of q^2, q_o^2, N and Λ - the last

TABLE IV

GLUON MOMENTS $G(N,q_o^2)$; $q_o^2 = 5$ GeV^2 (ABCLOS Collaboration)

N	$G(N,q_o^2)$	q^2 range	Energy Sumrule	Moment of xF_3
2	0.62 ± .15 (.03)	1-20	0.45 ± .03	0.45 ± .07
3	0.12 ± .05 (.02)	1-100	-	0.12 ± .02
4	0.03 ± .02 (.02)	1-100	-	0.045 ± .01
5	0.02 ± .01 (.02)	1-100	-	0.027 ± .007

being taken from the first-order result (2.46). The errors shown on the gluon moments show the statistical errors (±), and, in brackets, the systematic error arising from the uncertainty in Λ.

The N = 2 moment of the gluon distribution measures their momentum content, which is known independently from energy-momentum conservation: $G(2,q_o^2) = 1 - M_2(2,q_o^2)(1 + \varepsilon)$ where $\varepsilon \sim .03$ takes account of the momentum content of the s, $\bar{s}$ quarks of the sea, and whose contribution to F_2 is suppressed by the Cabibbo factor, $\sin^2\theta_c$. ε is estimated from dimuon data, and discussed in a later section. The two independent measures of $G(2,q_o^2)$ are compatible within about one standard deviation. All the measured gluon moments turn out to be positive, and roughly comparable in magnitude with the moments of the valence quarks (i.e. of xF_3). The positivity of the gluon

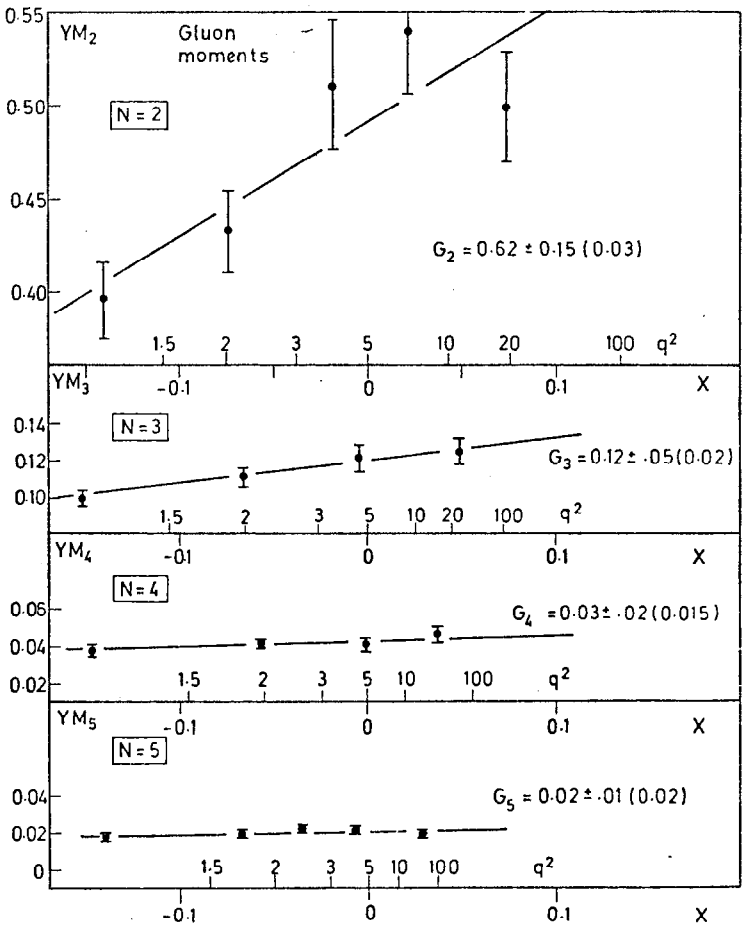

Fig. 28 Moments of the gluon distribution

moments arises because experimentally, the F_2 moments fall of less rapidly with q^2 than do the xF_3 moments; this must be true generally, and not only for the first order analysis described here.

Alternatively, assuming the N = 2 gluon moment $G(2, q_0^2)$ from energy/momentum conservation, eq. (2.51) can be solved to give a value

$$\Lambda = 0.68 \pm 0.10 \text{ GeV} \qquad (2.52)$$

compatible with (2.46).

Finally, we note that conclusions from Table IV depend on the validity of the first-order QCD analysis which is all that is presently theoretically available.

2.10 Distributions of Secondary Hadrons

(i) Fragmentation functions

The description of the process of deep inelastic lepton scattering as elastic scattering off an individual quark, naturally led to a description of the secondary hadrons of the collision as quark fragmentation products. Hadrons travelling forward in the hadron centre of mass (or, more precisely, in the parton Breit frame) were in the "current fragmentation" region, those travelling backward were the result of "target fragmentation". Early electron and neutrino scattering experiments established empirical form of the current fragmentation functions[34, 9] $D_Q^h(z)$ for the probability that a struck quark Q fragments to a hadron h carrying a fraction z of the quark energy, (i.e. $z = E_h/\nu$). For comparable values of the invariant mass W of the hadron system, the form and magnitude of the D-functions for ep, μp, νp and e^+e^- processes are observed to be very similar. Fig. 29 shows examples of the D-functions, averaged over positive and negative hadrons and over u and d quarks. Essentially $z > 0.2$ refers to the current fragmentation region.

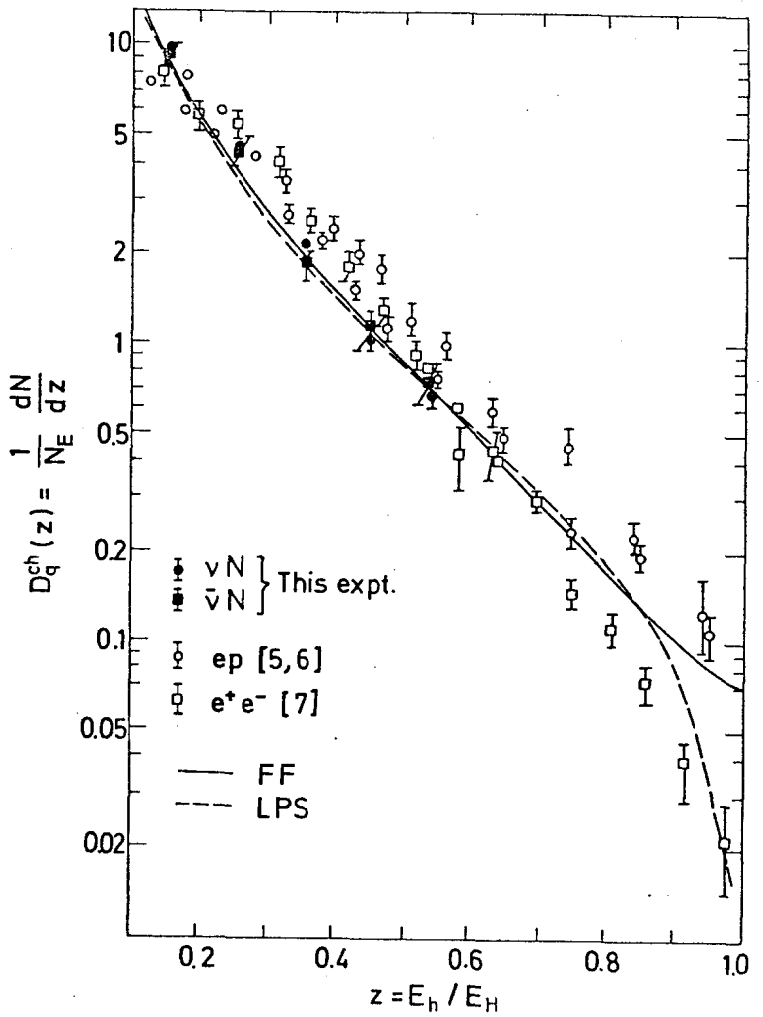

Fig. 29

The most important prediction which QCD makes about the D-functions is that, just like the structure functions F, they should be q^2-dependent, i.e. $D = D(z,q^2)$. This is a clear prediction, since both quarks and gluons fragment into hadrons - with however quite different D-functions - and the relative energy content of the quarks and gluons is q^2-dependent. For example, we expect the non-singlet moment

$$M_H(N,q^2) = \int_{\sim 0}^{1} z^{N-2}\{D^{\pi^+}(z, q^2) - D^{\pi^-}(z,q^2)\}dz \qquad (2.53)$$

to have a q^2-dependence precisely the same as that of xF_3 - see eqn. (2.43).

There is some data from the 15' chamber by the FIMS collaboration[36]. At present, the errors are too big to draw any conclusions about a q^2-dependence. These scaling deviations in the D functions have to be there if QCD is a correct description of strong interactions.

(ii) Angular and transverse momentum distributions

In the approximation of exact Bjorken scaling ($q^2 \to \infty$) the neutrino-nucleon collision is one-dimensional; we can view it in the current-parton Breit frame, in which the current is purely spacelike and the parton momentum is reversed. (see diagram (a)):

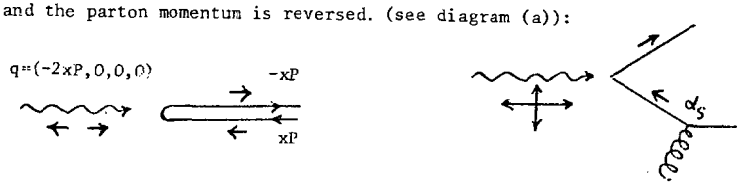

(a) (b)

In the Bjorken limit the parton (quark) has helicity ±1 so that only the current cross-sections σ_L and σ_R are involved. σ_S cannot contibute, and in this situation

$$\lim_{q^2\to\infty} \quad R = \sigma_S/\sigma_T \to 0; \quad A = \frac{2xF_1}{F_2} = \frac{1 + q^2/\nu^2}{1 + R} \to 1 \qquad (2.54)$$

At finite q^2, the quarks have finite interaction and thus an intrinsic transverse momentum, implying that both σ_S and σ_T are finite. On dimensional arguments, one expects the transverse momentum due to the process of hard gluon emission to be given by

$$\langle p_T^2 \rangle \quad \propto q^2/(\ln q^2/\Lambda^2) \qquad (2.55)$$

where the divisor represents the probability, α_s, that the quark emits a gluon. The finiteness of σ_S, σ_L and σ_R has implications for the azimuthal distribution of the hadrons in the current fragmentation region. The azimuthal angle ϕ is measured about the current direction $\vec{p}_H$ and relative to the lepton scattering plane. If three helicity states are present, the current amplitude will be

$$a = a_L + a_R + a_S$$

If we consider secondary pions emitted at azimuth ϕ, the appropriate current amplitude will become

$$a(\phi) = a_L e^{-i\phi} + a_R e^{+i\phi} + a_S$$

and the intensity

$$I = aa^* = A + B\cos\phi + C\cos 2\phi \qquad (2.56)$$

Thus, in principal one can obtain left-right asymmetries ($\langle\cos\phi\rangle \neq 0$) as a result of a_L, a_S or a_R, a_S interference; and also hadron emission preferentially in the scattering plane ($\langle\cos 2\phi\rangle > 0$) as a result of a_L, a_R interference.* These effects result purely from the vector (axial vector) nature of the current, and were pointed out some time ago by Ravndal[37].

---

* A $\cos 2\phi$ effect is well known in Compton scattering of real photons; the scattered photon is emitted preferentially in the plane normal to the E vector of the incident photon.

The first-order QCD contribution to the coefficients of $\cos\phi$ and $\cos 2\phi$ in (2.56) can be computed (B/A and C/A being of order α_s) and their measurement has been proposed as a "clean" test of QCD.[38] Unfortunately, there are non-perturbative contributions corresponding to the intrinsic p_T^Q of the quark constituents, in addition to the calculable effect due to single hard gluon emission; and effects due to the transverse momentum p_T^F of the hadron relative to the fragmenting quark. Thus the non-perturbative terms will give a q^2-independent hadronic p_T of the form

$$p_T^2(\text{hadron}) = z^2(p_T^Q)^2 + (p_T^F)^2 \qquad (2.57)$$

yielding finite values of $\langle\cos\phi\rangle \sim [(p_T^Q)^2/q^2]^{\frac{1}{2}}$ and $\langle\cos 2\phi\rangle \sim (p_T^Q)^2/q^2$, in contrast to the $1/\ln q^2$ dependence of the hard gluon contribution. The data on charged hadrons from the BEBC ABCLOS collaboration[39] are shown in Fig. 30; the errors are so big that we can learn very little; furthermore, the value of $\langle\cos\phi\rangle$ from the first-order QCD calculation depends somewhat on the (unknown) relative fragmentation probabilities of gluons and quarks (denoted by η in the figures).

Investigation of the p_T distributions of the hadrons seems to be slightly more promising. It is however important to eliminate trivial kinematic effects. For example, as shown in Fig. 31, $\langle p_T\rangle$ of a hadron with respect to the resultant hadron vector increases slowly with W, the mass of the hadronic final state.

Since $W^2 = 2MyE + M^2 - q^2$ it follows that W becomes small and $\langle p_T\rangle \to 0$ as $q^2 \to q^2(\max)$, for fixed beam energy, E. Fig. 32 shows the different q^2 dependence of $\langle p_T^2\rangle$ for E < 100 GeV and E > 100 GeV. Fig. 33 shows the component of p_T out of the μ, ν scattering plane (which is experimentally well determined, and free of possible biasses which plague the measurement of p_T in the plane, relative to a resultant hadronic vector which requires

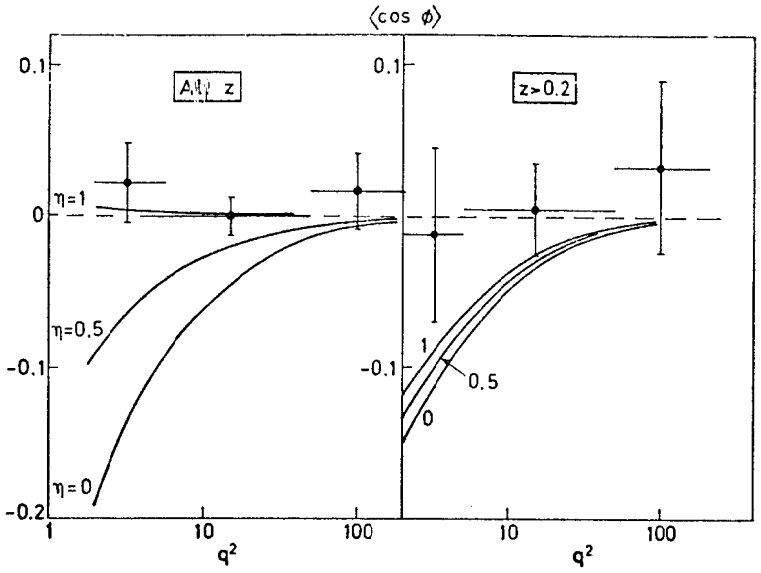

Fig. 30

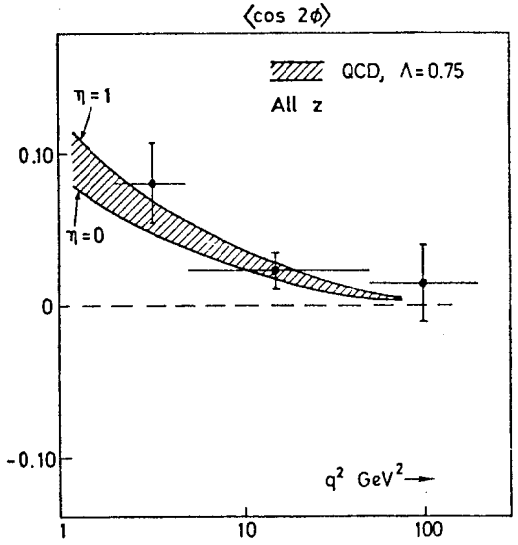

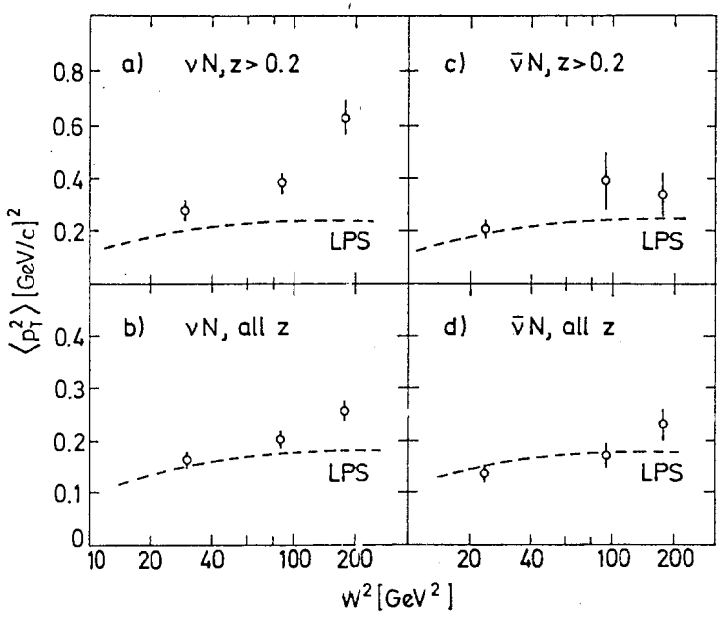

Fig. 31

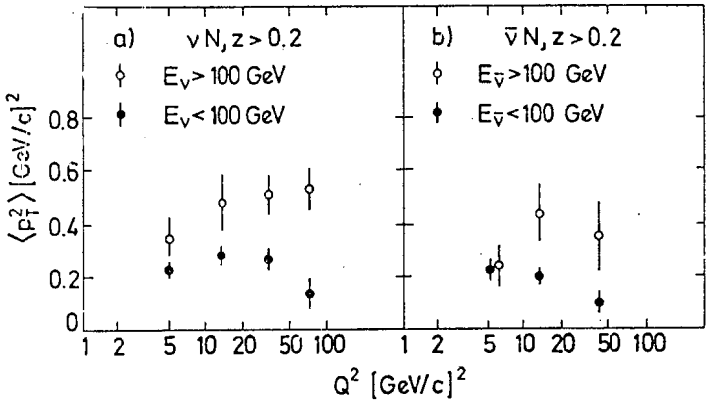

Fig.32

correction for lost energy etc.). Also shown is the prediction from a "limited p_T plus longitudinal phase space" Monte Carlo. There is some evidence for an increase of $\langle p_T^2 \rangle$ with q^2 and the data are not inconsistent with the QCD prediction (40) for the increase $\langle \Delta p_T^2 \rangle$ with q^2 as indicated in (2.55).

The data on hadronic distributions can also be analysed in many other ways - gluon jets, distributions in spherocity, thrust etc. etc. In the naive parton model (i.e. in the limit $q^2 \to \infty$) we expect the intrinsic quark transverse momentum to be negligible and the hadrons from the target and from the current fragmentation processes to appear in the CMS frame, as two oppositely-directed collinear jets of small angular spread. In other words if we define the thrust as

$$T = \frac{2\Sigma p_L^i(\text{forward hemisphere})}{\Sigma p^i} \qquad (2.58)$$

then $T \sim 1$ for 2-jet events. According to first-order QCD, we also expect, at high but finite q^2, a widening of the angular distribution due to gluon bremsstrahlung, and the form of the cross-section[41] is found to be

$$\frac{1}{\sigma}\frac{d\sigma}{dT} = \underset{\text{2-jet}}{\delta(1 - T)} + \frac{2\alpha_s}{3\pi}\left[\frac{2(3T^2 - 3T + 2)}{T(1 - T)} \ln\left(\frac{2T - 1}{1 - T}\right) - \frac{3(3T-2)(2-T)}{(1 - T)}\right] + O(\alpha_s^2)+\ldots \qquad (2.59)$$

Fig. 33 shows that the observed T distribution is much broader than expected according to the lowest-order QCD formula. Again, this demonstrates the importance of the non-perturbative (and non-calculable) contributions to the cross-section.

As a second example, we mention the predictions of Sterman and Weinberg[42] for the angular distributions of jets in e^+e^- annihilation, but which can presumably be carried over to the lepton scattering case. They give a formula for the fraction of events with ε of the total secondary energy

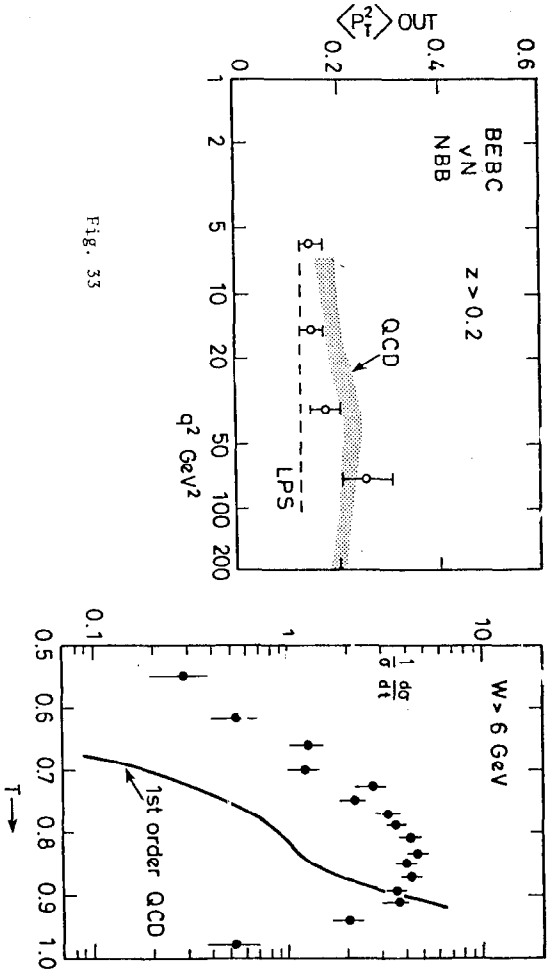

Fig. 33

outside a cone of semi-angle δ, as defined with respect to the current direction in the CMS:-

$$F = 1 - \frac{4\alpha_s}{3\pi} \frac{(3\ln\delta + 4\ln\delta\ln 2\varepsilon + \pi^2/3 - 5/2)}{(1 + \alpha_s/\pi)} \qquad (2.60)$$

which is expected to hold only when $\alpha_s/\pi << 1$ and ε is small, and $F \sim 1$. Basically this is a statement that the typical angle containing the energy flow is of order $\sqrt{\langle p_T^2 \rangle / q^2} \sim 1/(\ln q^2/\Lambda^2)$ i.e. it shrinks logarithmically. The beauty of the Sterman-Weinberg Formula is that it is free of infra-red divergences of the type which plague the calculation of $\langle\cos\phi\rangle$, for example. Equation (2.60) can be re-cast as

$$\frac{1}{(1-F)} = (1 + \frac{\pi}{\alpha_s}) G_1(\delta,\varepsilon)$$

$$= G_2(\delta,\varepsilon)(\ln\frac{q^2}{\Lambda^2} + \frac{12}{33-2m}) \qquad (2.61)$$

so that plotting $1/(1-F)$ against $\ln q^2$ should give a straight line intercepting the x-axis at $q^2 = \Lambda^2 \exp(-12/27)$, for $m = 3$ flavours. This approach does not require a knowledge of the δ and ε dependence of (2.60), only the dependence of F on α_s and hence on $\ln q^2$. Fig. 34 shows typical results from the CERN BEBC experiments.[43] There is a comparatively feeble dependence of $1/(1-F)$ on q^2; for limited p_T jets, one could expect a much stronger q^2 dependence. Again, all that one can say at present is that the data are not in contradiction with QCD, provided q^2 is taken to be large ($q^2 > 10$ GeV^2).

2.11 Conclusions on Charged-Current Interactions

Measurements of neutrino/antineutrino differential cross-sections on nucleons, and the structure functions $F_{1,2,3}$ seem to be in good accord with the analogous measurements of electron and muon scattering. Furthermore, absolute values in the two cases are in excellent agreement with the

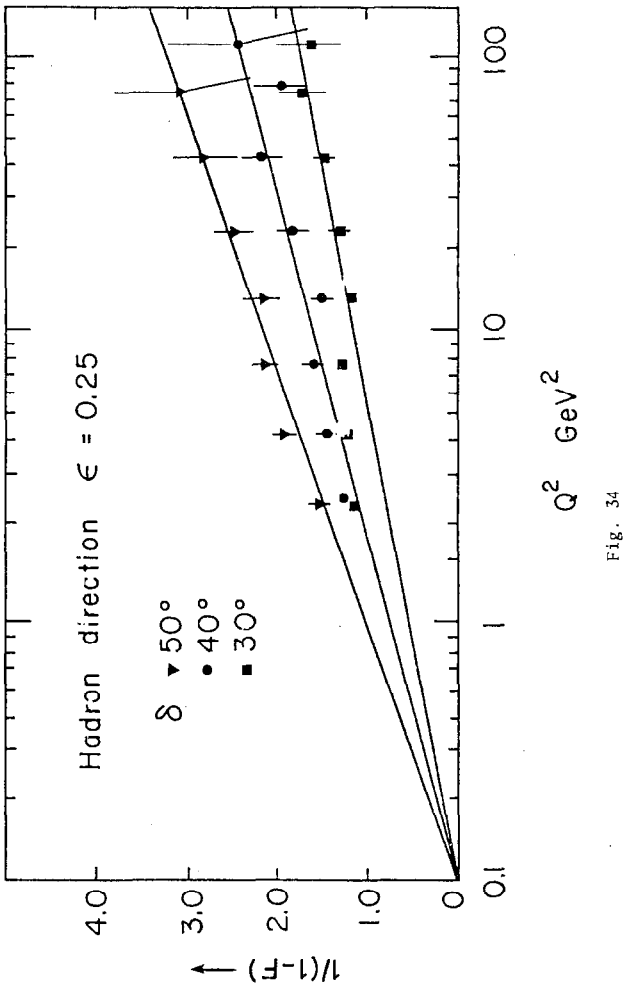

Fig. 34

predictions from the quark charge assignments. Deviations from exact scaling i.e. $F_i = F_i(x,q^2)$ at finite q^2 are also in quantitative agreement with QCD predictions. It is important to emphasize that, for the most part, these are lowest-order (α_s) predictions. More accurate data especially at high q^2 is badly needed, but the preliminary signs are encouraging - one might almost say that things look a bit too good.

Regarding the secondary hadron distributions, the QCD "predictions" are nowhere near as clean and must be considered qualitative. Until more quantitative predictions are forthcoming, it is hard for the experimentalists to know exactly how to analyse their data. In any case, early hopes of dramatic phenomena, such as well-defined "gluon jets" have long since been dashed.

3. WEAK NEUTRAL CURRENTS

Recently there have been a number of excellent reviews on the subject of neutral currents and their connection with gauge theories. On the experimental side, there is a historical review by Scuilli[44], and on the theoretical side I refer you to the lectures of Helen Quinn at this Institute; to the review by Sehgal[45]; and to the monumental works of Sakurai[46]. This means that I can be fairly brief and concentrate on recent experimental aspects of the subject.

Neutral currents were first established in 1973 by observing "muonless events" interpreted as $\nu_\mu + N \to \nu_\mu$ + anything. The analysis of the weak coupling itself was however complicated by the fact a model was required to describe the hadron vertex. As I have tried to explain in the previous section, we can hardly claim that the hadron model is well understood. For these reasons, it is clear that the cleanest analysis of neutral currents rests on experiments on purely leptonic processes - just as the best numbers for charged-current (V-A) coupling came from studies of μ-decay.

3.1 Leptonic Neutral Currents

The only processes of interest in neutrino experiments are those of neutrino-electron scattering, as indicated by the following first-order diagrams .-

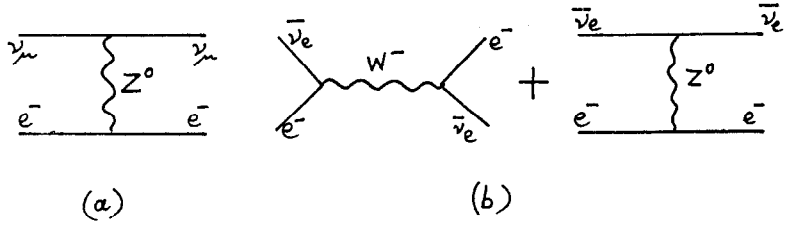

The scattering of ν_e has been studied at a reactor and can proceed via both charged ($W^{\pm}$) and neutral (Z^0) currents, while $\nu_\mu e$ scattering (at accelerators) can proceed only through Z^0 exchange and its existence therefore constitutes an acid test of neutral currents. The cross-sections in both cases are of order $2mEG^2 \sim 10^{-42}$ cm^2/electron at 1 GeV; this is what has made their study very difficult.

The effective Lagrangian describing these pointlike reactions has the form, assuming V, A coupling:-

$$\mathcal{L}_{eff} = \frac{G}{\sqrt{2}} (\bar{\nu}\gamma_\mu(1 + \gamma_5)\nu)(e^-(g_V + \gamma_5 g_A)e) \qquad (3.1)$$

leading to a differential cross-section,

$$\frac{d\sigma}{dy} = \frac{G^2 mE}{2\pi}[A + B(1 - y)^2 - \frac{Cmy}{E}] \qquad (3.2)$$

where E = neutrino energy, m = electron mass, and y measures the recoil electron energy (y = E(electron)/E). The existence of 3 terms follows, as in the nucleon case, from the 3 helicity states for the exchanged vector boson Z^0, $W^{\pm}$. The coefficients A, B and C = $\sqrt{AB}$ are given in terms of the vector/axial-vector coupling constants g_V, g_A in the table, so that neutrino and antineutrino coefficients are related by the sign change $g_A \leftrightarrow -g_A$. Note that, for a given type of neutrino (ν_e or ν_μ), and that if the C term is not measured (i.e. m/E → 0), then there is a

TABLE 3.1

	A	B	C
$\nu_e \to \nu_e$	$(g_V + g_A)^2$	$(g_V - g_A)^2$	$(g_V^2 - g_A^2)$
$\bar{\nu}_e \quad \bar{\nu}_e$	$(gV - g_A)^2$	$(g_V + g_A)^2$	$(g_V^2 - g_A^2)$

4-fold ambiguity, i.e. $d\sigma/dy$ is invariant under the transformation $g_A \leftrightarrow g_V$ and $g_{A,V} \leftrightarrow -g_{A,V}$. It turns out that if one considers $\bar{\nu}_e$ scattering as well as ν_μ and $\bar{\nu}_\mu$, there remains a 2-fold ambiguity.

The theoretical values of the coefficients g_V and g_A depend on the neutral current model. The only model of interest here is the standard SU2 x U1 model proposed first by Glashow in 1961. Recall the Gell-Mann/Nishijima formula for hadrons

$$Q_{hadron} = I_3 + (B + S)/2$$

One can invent, for leptons, a "weak isospin" and "weak hypercharge" so that e, ν appear in an isospin doublet:-

$$Q_{lepton} = \underset{\downarrow}{I_3^{weak}} + \underset{+}{Y^{weak}} \to \begin{array}{lccc} & I_3 & Y & Q \\ \nu & +\tfrac{1}{2} & -\tfrac{1}{2} & 0 \\ e & -\tfrac{1}{2} & -\tfrac{1}{2} & -1 \end{array} \qquad (3.3)$$
$$\text{SU2} \qquad \text{U1}$$

The charge-changing weak current comes from the (x + iy) component of the weak isospin, the neutral current from a combination of the z component of the weak isospin, plus the electromagnetic current. Thus, according to the prescriptions of Bludman, Weinberg, Salam, Ward etc. etc. we write

$$\begin{aligned} J_\lambda^{CC} &= J_\lambda^1 \pm iJ_\lambda^2 = J_\lambda^{\pm} \\ J_\lambda^{NC} &= J_\lambda^3 - J_\lambda^{em}\sin^2\theta_w \qquad (3.4) \\ &= \tfrac{1}{2}(V_\lambda^3 + A_\lambda^3) - J_\lambda^{em}\sin^2\theta_w \end{aligned}$$

where θ_w is an arbitrary angle (usually called the Weinberg angle) and, in the last expression, the first term ($V_\lambda^3 + A_\lambda^3$) corresponds to the vector and axial vector components, coupling to the isospin, while the last term (J_λ^{em}) will couple charge. Hence, with appropriate normalization factors taken care of, one can write for a lepton of type "i":-

$$\begin{aligned} g_V^i &= I_3^i - 2Q^i\sin^2\theta_w \\ g_A^i &= I_3^i \end{aligned} \qquad (3.5)$$

so that for process $\nu_\mu e^- \to \nu_\mu e^-$ we find

$$\left.\begin{aligned} g_V &= -\tfrac{1}{2} + 2\sin^2\theta_w \\ g_A &= -\tfrac{1}{2} \end{aligned}\right\} \quad \nu_\mu e^- \to \nu_\mu e^- \qquad (3.6)$$

while for $\nu_e e^- \to \nu_e e^-$ we have to include a charge-changing contribution ($g_A = g_V = 1$) as indicated in the previous diagram:-

$$\left.\begin{aligned} g_V^1 &= 1 + g_V = \tfrac{1}{2} + 2\sin^2\theta_w \\ g_A^1 &= 1 + g_A = \tfrac{1}{2} \end{aligned}\right\} \quad \nu_e e^- \to \nu_e e^- \qquad (3.7)$$

When (3.6), (3.7) are inserted in Table 3.1 we obtain the predicted cross-sections in terms of $\sin^2\theta_w$, and these are plotted in Fig. 35. Note that the $\bar{\nu}_\mu e^-$ process is sensitive to $\sin^2\theta_w \sim 1$ and $\nu_\mu e^-$, to $\sin^2\theta_w \sim 0$; when $\sin^2\theta_w = 0.25$, $g_V = 0$ and the neutrino and anti-neutrino cross-sections are equal.

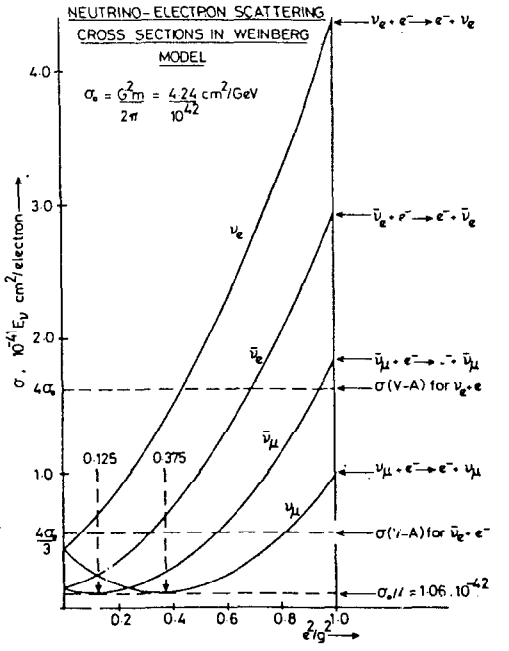

Fig. 35 Neutrino-electron scattering cross-sections in Weinberg model, in terms of $\sin^2\theta_w = e^2/g^2$.

3.2 Early Observations on Leptonic Neutral Currents

The reaction $\bar{\nu}_e + e^- \to \bar{\nu}_e + e^-$ has been observed by Reines et al [47] using antineutrinos from a reactor. The reactor spectrum is very soft, peaking at 0.5 MeV and falling off exponentially by a factor of 10^3 by 8 MeV. To reduce the effect of reactor-associated backgrounds, only the high energy tail of the spectrum (recoil electrons >1.5 MeV) are used, and the effective cross-sections are minute ($\sim 10^{-46}$ cm^2/electron). In two different energy bands the Irvine group obtained the results

$1.5 < E_e < 3$ MeV $\qquad \sigma = (0.87 \pm 0.25)\ \sigma_{V-A}$

$3 < E_e < 4.5$ MeV $\qquad \sigma = (1.70 \pm 0.44)\sigma_{V-A}$

where σ_{V-A} is the charged current cross-section in diagram (b) above.

The reactions $\bar{\nu}_\mu + e^- \to \bar{\nu}_\mu + e^-$, $\nu_\mu + e^- \to \nu_\mu + e^-$ were studied at the CERN PS ($\langle E_\nu \rangle \sim 2$ GeV) by the Gargamelle collaboration [48] and by the Aachen-Padova Group; [49] the results are given in Table VI. The

Aachen-Padova experiment was carried out with Aℓ spark-chambers, without a magnetic field, and consequently the background level is higher than in either the reactor or Gargamelle experiments. Fig. 36 shows the

TABLE VI

CERN PS $\nu_\mu e$, $\bar{\nu}_\mu e$ EXPERIMENTS

Group	Target	Reaction	No of Events	No. of Background Events	$\sigma(\times 10^{42} cm^2/E$ (GeV))
GGM[48]	CF_3Br	$\bar{\nu}_\mu e^-$	3	0.4 ± 0.1	$1.0^{+2.1}_{-0.9}$ } 90% CL
		$\nu_\mu e^-$	1	0.3 ± 0.1	< 3 } 90% CL
Aachen-Padova[49]	Al	$\bar{\nu}_\mu e^-$	17	7 ± 1	2.2 ± 1.1
		$\nu_\mu e^-$	32	21 ± 2	1.1 ± 0.6

Irvine and GGM data on g_A and g_V. Note that, from (3.2), neglecting the C term, one obtains the equation of an ellipse in the g_A/g_V plane:-

$$\frac{\sigma}{E} \propto (g_V + g_A)^2 + \frac{1}{3}(g_V - g_A)^2 \qquad (3.8)$$

The elliptical contours in Fig. 36 correspond to the 90% CL limits on the cross-sections. The two experiments together place g_A and g_V inside the shaded area; in the case of the Weinberg-Salam model, the two experiments give $\sin^2\theta_w \simeq 0.26 \pm 0.06$. The Aachen-Padova experiment, alone, gives a somewhat larger value: $\sin^2\theta_w = 0.35 \pm .08$. However, all three experiments are compatible within the large errors.

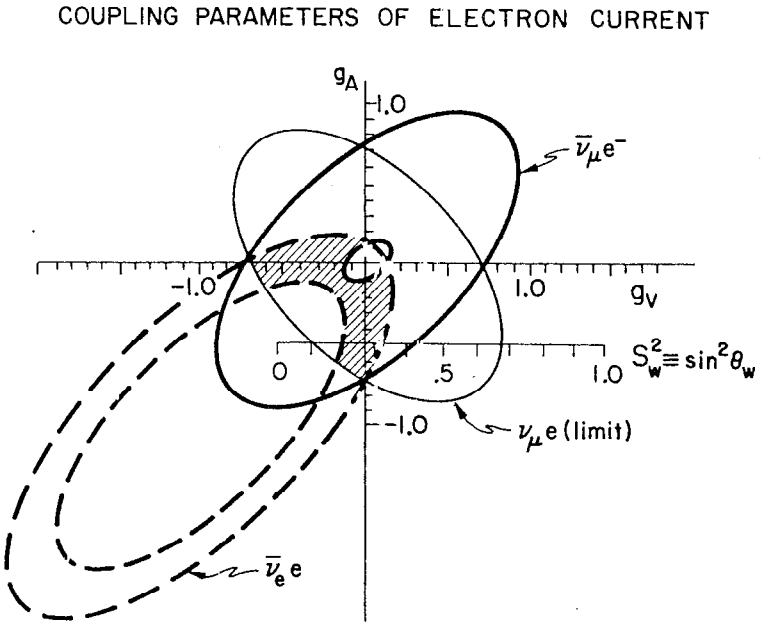

Fig. 36

3.3 Recent Results on Leptonic Neutral Currents

(i) Characteristics and background

At the higher energies at FNAL and the CERN SPS, the backgrounds typical of CERN PS energies (10-30% for GGM, 40-70% for Aachen-Padova) are greatly reduced, and thus much more definitive experiments are possible in principal (i.e. if the experimental resolution is good

enough to exploit the more favourable conditions.)

First, the low cross-section for the purely leptonic processes are to some extent compensated by the nature of the signature, consisting of a single electron projected in the very forward direction. For E >> m, kinematics gives

$$\theta_e = \sqrt{\frac{2m}{E_e} - \frac{2m}{E_\nu}}$$

or

$$E_e \theta_e^2 \leq 2m \qquad (3.9)$$

As previously stated, the cross-section for the reaction

$$\nu_\mu + e^- \rightarrow \nu_\mu + e^- \qquad (3.10)$$

is $\sim 10^{-42} E$ cm^2 GeV. Single high energy electrons may also be produced by the charged current processes on nucleons, e.g.

$$\nu_e + n \rightarrow e^- (+p) \qquad (3.11)$$

$$\nu_e + n \rightarrow e^- (+p + \pi^\circ) \qquad (3.12)$$

where the proton and the γ's from π°-decay are not observed (e.g. the proton track may be too short, or it may be absorbed in the nucleus). The forward cross-sections $d\sigma/dq^2$ for the reactions (3.10), (3.11) and (3.12) are all of order G^2/π. The rates of the last two reactions are suppressed by (i) the requirement that the proton or γ's be unseen (ii) the 100-fold smaller flux of ν_e, as compared with ν_μ. The contributions of both (3.11) and (3.12) can be monitored by observations on the reaction

$$\nu_\mu + n \rightarrow \mu^- (+p, \pi^\circ \ldots) \qquad (3.13)$$

and using the known flux ratio $\phi_{\nu_e}/\phi_{\nu_\mu}$.

A second source of background arises from single γ-rays (from, for example, neutral current π° production) giving Compton electrons or very asymmetric pairs. Since the Compton cross-section, and the probability that the e^+ branch of a pair should be invisible ($E_+ < 5$ MeV), are both proportional to E_γ^{-1}, this is a small background in high energy experiments; it can be computed from the observed number of single γ-rays and the experimentally determined asymmetry probability for γ-rays from normal (charged-current) events.

(ii) The Columbia-Brookhaven experiment[51]

The experiment of Cnops et al was carried out in the 15' FNAL chamber with 64% (atomic) Ne/H_2 mixture (radiation length 0.4m). They observed 11 single e^-, 5 single e^+ and 22 $\gamma \rightarrow e^+e^-$ events of energy E > 2 GeV, $\theta < 3^\circ$, in a total of 134 K pix containing 106K charged current events. Electrons were identified (a) on the basis of associated bremsstrahlung γ-ray conversions or (b) energy loss followed by "spiralisation"; in either case, the negative sign of charge had to be established on the initial section of track. In cases where an early bremsstrahlung conversion made this impossible,

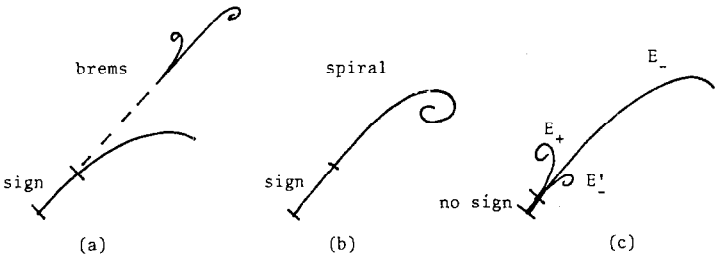

as in (c), the event was still taken as a single electron event if $E_+ < 0.25\ E_-$ and the second negative was energetic enough to exclude a γ-ray on an asymmetric pair. All other possible e^- events were treated as ambiguous with γ's.

From these criteria, and the observed number of single γ-rays, the γ background was calculated as 0.1 events and therefore negligible. From a total of 22 e^-p or $e^-p\pi^0$ events, the background from reactions (3.11) or (3.12) was found to be 0.7 events. The scanning efficiency was rather low, of order 60% per single scan (85% in double scan). Some check on this was obtained from the 5 e^+ events; from the total positron rate, i.e. for $\bar{\nu}_e N \to e^+ X$, (with 108 ± 23 events) a figure of 6 single e^+ events was expected. Fig. 3.7 shows the distribution in $E\theta^2$ for the e^-, e^+ and γ events; the e^+ and γ events have a distribution which is much broader than that of e^-, which is consistent, within the errors, with the limit (3.9). Results on the cross-section are given in Table VII.

(iii) The Gargamelle-SPS experiment[52]

Like the Columbia-Brookhaven experiment, the Gargamelle experiment was carried out in a WB beam. The filling was C_3H_8/CF_3Br (radiation length 0.6m). First results of this Bari-CERN-EP-Milan-Orsay collaboration were published early in 1978 by Alibran et al[52]. They observed 10 e^- events in 128K pix containing 25K events of the type $\nu_\mu N \to \mu^- X$. This is 4 times the rate observed (later) at Columbia/BNL in a similar beam. This very large cross-section implied, on the Salam-Weinberg model, a value $\sin^2\theta_w > 0.74$ at 90% CL, that is incompatible with the value ∿0.25 determined from the semi-leptonic reactions. The relative numbers of e^-, e^+ and γ events of $\theta < 3°$ and E > 2 GeV in the two experiments were however in fair agreement:-

	e^-	e^+	γ
GGM-SPS	8	2	13
BNL-Col.	11	5	22

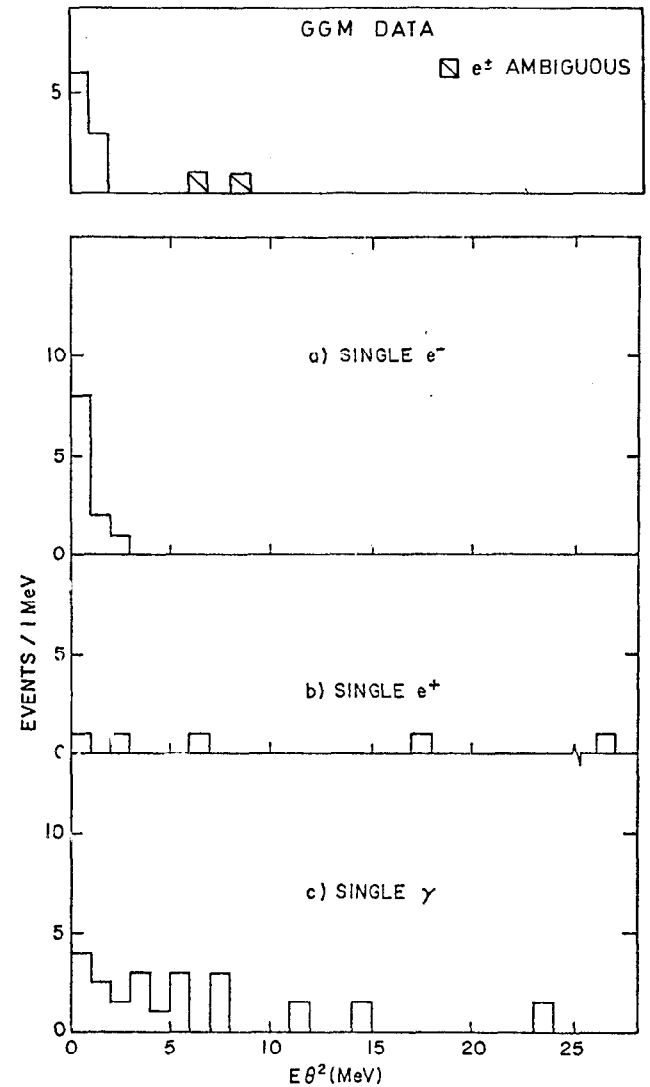

Fig. 37 Distribution in $E\theta^2$ for single electron events in Gargamelle (top) and for electron, positron and gamma events in the 15' chamber (Columbia/BNL)

The reported single-scan efficiency in the GGM experiment (85%) was higher than the BNL-Col. value (60%). It does not seem possible to ascribe the difference in rates to misidentification of γ's as electrons, since the GGM group did very careful measurements of ionization density at the track beginning.

Since the earlier publication, the GGM collaboration have scanned 40% more film and have obtained 1 more e^- event; but, with the use of new e^- identification criteria, have re-classified 2 of the old e^- events as ambiguous. The $E\theta^2$ plot is shown in Fig. 37.

The present situation[54] with regard to e^- scattering at FNAL and the CERN SPS is given in Table VII, which also includes data from

TABLE VII[54]

Beam	ν_μ		$\bar{\nu}_\mu$	
Expt.	GGM-SPS (BCEMO)	15' FNAL (Col/BNL)	BEBC-SPS (BBBERSU)*	15' FNAL (FIMS)**
Filling	C_3H_8/CF_3Br	Ne/H_2	Ne/H_2	Ne/H_2
X_o(m)	0.6	0.4	0.4	0.4
✗ $\nu N \to \mu X$	35K	106K	7.5K	6.3K
✗ e^- events	9	11	≤1	0
✗ background	0.2	0.8	0.4	-
✗ events for $\sin^2\theta = 0.25$	2.4	9	1.5	1.5
σ(units 10^{-42}E)	5 ± 2	1.8 ± 0.8	<3.5 90% CL	<2.9 90% CL

* Bari, Birmingham, Brussels, Ecole Polytechnique, Rutherford, Saclay, UCL.

** FNAL, Moscow, Michigan, Serpukhov.

antineutrino runs. The two antineutrino experiments have not found any sure e^- events; however, if it were true that $\sin^2\theta_W = 0.75$ as suggested by the earlier GGM-SPS result, these two experiments should have seen 20 events (recall that the $\bar{\nu}_\mu$ cross-section is large at large $\sin^2\theta_W$). So, 3 of the 4 SPS/FNAL experiments are consistent with the 2 PS experiments, with a value of $\sin^2\theta_W$ in good accord with the semi-leptonic data. Leaving aside the GGM-SPS result as an incredibly large statistical fluctuation (probability $<10^{-3}$) the values of $\sin^2\theta_W$ from the other experiments are summarized in Table VIII:-

TABLE VIII

VALUES OF $\sin^2\theta_W$ FROM PURE LEPTONIC SCATTERING

Experiment	Beam	$\sin^2\theta_W$
Reines et al.[47, 55]	$\bar{\nu}_e$	0.25 ± 0.05
GGM PS[48]	ν_μ, $\bar{\nu}_\mu$	0.25 ± 0.15
Aachen-Padova[49]	ν_μ, $\bar{\nu}_\mu$	0.35 ± 0.08
Col.-BNL[51]	ν_μ	$0.20^{+0.16}_{-0.08}$ or $(0.57^{+0.07}_{-0.17})$
BEBC-SPS	$\bar{\nu}_\mu$	< 0.45 (90% CL)

3.4 Hadronic Neutral Currents: Inclusive Reactions

In this section we consider inclusive processes of the type

$$\bar{\nu}_\mu, \nu_\mu + N \to \bar{\nu}_\mu, \nu_\mu + X \qquad (3.14)$$

where N denotes an isoscalar target, so that no isospin information is obtained. In principle, we can have V, A, S, T or P operators in the Lagrangian, which are distinguished by the y distributions they generate:-

V,A	1, $(1-y)^2$ combinations
P,S	y^2
T	$(2-y)^2$

The dominance of P and/or S interactions is certainly excluded by the data, which is consistent with a V and A admixture. Indeed, the strength of the S, P couplings relative to V, A is found to be <16% at 95% CL in the CDHS experiments[56] and <6% at 95% CL in the BEBC ABCLOS experiments.[57] However, any V, A combination can always be mimicked by a suitable combination of S, T and P, although this is a very unlikely possibility. In what follows, we assume V,A interactions only, for the very simple reason that at present there is absolutely no evidence for anything else.

If we describe the nulceon targets in (3.14) in terms of the quark-parton model, then in analogy with (3.2) for an electron target

$$\frac{d^2\sigma^{\nu N}}{dxdy} = \frac{G^2ME}{2\pi}\Sigma_i x\Big\{(g_V^i + g_A^i)^2[f^i(x) + \bar{f}^i(x)(1-y)^2] + (g_V^i - g_A^i)^2[f^i(x)(1-y)^2 + \bar{f}^i(x)]\Big\} \tag{3.15}$$

with the antineutrino cross-section obtained by substituting $g_A \leftrightarrow -g_A$. In this expression, $f^i(x)$, $\bar{f}^i(x)$ represent the densities of quarks and antiquarks of type 'i', and g_V^i and g_A^i their couplings. It is usual to express these in terms of the chiral coupling constants for the u, d, s ... quarks i.e. $(g_V^u + g_A^u) = 2U_L$, $(g_V^u - g_A^u) = 2U_R$ etc., and in terms of parameters g^-, g^+ and f:-

$$\begin{aligned} g^- &= U_L^2 + D_L^2 \\ g^+ &= U_R^2 + D_R^2 \\ f &= D_L^2 + D_R^2 \end{aligned} \tag{3.16}$$

here g^- and g^+ measure the strengths of the V-A and V+A couplings, and in the third expression, f denotes the s, $\bar{s}$ quark coupling which, according to the GIM model, will be the same as the d-quark coupling. Thus

$$\left.\frac{d^2\sigma^{\nu N}}{dxdy}\right|_{NC} = \frac{G^2ME}{\pi} x \Big[g^-(u+d+(\bar{u}+\bar{d})(1-y)^2) + g^+((u+d)(1-y)^2 + (u+\bar{d})) + f.2s(1+(1-y)^2)\Big] \tag{3.17}$$

with the antineutrino cross-section obtained by the substitution $g^- \leftrightarrow g^+$. The couplings of the u, d, s quarks in the Weinberg-Salam model are given in Table IX, using (3.5). This model gives for the quantities in (3.16):-

$$\begin{aligned} g^- &= \tfrac{1}{2} + \tfrac{5}{9}\sin^4\theta_w - \sin^2\theta_w \\ g^+ &= \tfrac{5}{9}\sin^4\theta_w \\ f &= \tfrac{1}{4} + \tfrac{2}{9}\sin^4\theta_w - \tfrac{1}{3}\sin^2\theta_w \end{aligned} \tag{3.18}$$

TABLE IX

NC QUARK COUPLINGS IN SW MODEL

$(g_V^i = I_3^i - 2Q^i\sin^2\theta_w;\ g_A^i = I_3^i)$

Quark	I_3^i	Q^i	g_V^i	g_A^i	$(g_V+g_A)^i$	$(g_V-g_A)^i$
u, c	$+\frac{1}{2}$	$+\frac{2}{3}$	$\frac{1}{2} - \frac{4}{3}\sin^2\theta_w$	$\frac{1}{2}$	$\left(1 - \frac{4}{3}\sin^2\theta_w\right)$	$-\frac{4}{3}\sin^2\theta_w$
d, s	$-\frac{1}{2}$	$-\frac{1}{3}$	$-\frac{1}{2} + \frac{2}{3}\sin^2\theta_w$	$-\frac{1}{2}$	$\left(-1 + \frac{2}{3}\sin^2\theta_w\right)$	$+\frac{2}{3}\sin^2\theta_w$

From (3.17) we obtain for the ν-$\bar{\nu}$ cross-section difference

$$\left.\frac{d^2\sigma^{\nu N} - d^2\sigma^{\bar{\nu}N}}{dxdy}\right|_{NC} = \frac{G^2MEx}{\pi}(g^- - g^+)(u + d - \bar{u} - \bar{d})(1 - (1 - y)^2) \tag{3.19}$$

On the other hand, we have for the charged-current cross-sections (with $\theta_c \to 0$)

$$\left.\frac{d^2\sigma^{\nu N}}{dxdy}\right|_{CC} = \frac{G^2MEx}{\pi}(u + d + (\bar{u} + \bar{d})(1 - y)^2)$$

$$\left.\frac{d^2\sigma^{\bar{\nu}N}}{dxdy}\right|_{CC} = \frac{G^2MEx}{\pi}(\bar{u} + \bar{d} + (u + d)(1 - y)^2)$$

hence

$$\left(\frac{d^2\sigma^{\nu N} - d^2\sigma^{\bar{\nu}N}}{dxdy}\right)_{CC} = \frac{G^2MEx}{\pi}(u + d - \bar{u} - \bar{d})(1 - (1 - y)^2) \qquad (3.20)$$

So, (3.18) and (3.19) together give us the important relation

$$\frac{(d\sigma^{\nu N} - d\sigma^{\bar{\nu}N})_{NC}}{(d\sigma^{\nu N} - d\sigma^{\bar{\nu}N})_{CC}} = (g^- - g^+) = (\tfrac{1}{2} - \sin^2\theta_w) \qquad (3.21)$$

which, as pointed out a long time ago (1973) by Paschos and Wolfenstein,[58] is largely independent of the hadron model, and involves only more general hypotheses, (strong isospin invariance).

The traditional analysis of neutral current inclusive cross-sections is based on measuring the ratios of event rates (so as to be flux independent)

$$R = \sigma^{NC}/\sigma^{CC} = (\tfrac{1}{2} - \sin^2\theta_w + \frac{20}{27}\sin^4\theta_w) + \ldots$$
$$\bar{R} = \bar{\sigma}^{NC}/\bar{\sigma}^{CC} = (\tfrac{1}{2} - \sin^2\theta_w + \frac{20}{9}\sin^4\theta_w) + \ldots \qquad (3.22)$$

These relations follow from (3.17)-(3.20), if one neglects $Q\bar{Q}$ sea contributions. Furthermore, it is necessary, experimentally, to impose a minimum hadron energy to eliminate neutron background. Anti-quark contributions, and the effect of the hadron energy cut, modify the relations (3.22), to an extent which clearly depends on quark distribution functions. In practice, since $\sin^2\theta_w \sim 0.25$, then from (3.18) we see that the (V+A) coupling g^+, is small compared with g^- (V-A); hence since comparison is made with the (V-A) charged currents, the effect of cuts, sea contributions etc. is not too severe. All this, of course assumes that one really knows how to describe the charged curret cross-sections in terms of Q, $\bar{Q}$ distributions. Table X lists values of R and $\bar{R}$ and the values of $\sin^2\theta_w$ deduced from them, correcting the raw values for the E_h cuts, and using (3.22) suitably

TABLE X

INCLUSIVE NC/CC CROSS SECTION RATIOS

(corrected for E_h cut)

Experiment	Beam	R	$\bar{R}$	$\sin^2\theta_w$
GGM PS	WB	0.26 ± .04	0.39 ± .06	0.32 ± .04
BNL 7'	WB	0.25 ± .05	-	0.36 ± .09
HPWF	WB	0.30 ± .04	0.33 ± .09	0.23 ± .06
CITF	NB	0.27 ± .02	0.40 ± .08	0.33 ± .07
CDHS	NB	0.28 ± .01	0.35 ± .03	0.24 ± .02
BEBC	NB	0.33 ± .05	0.36 ± .07	0.22 ± .05
BEBC	NB	y distributions	-	0.19 ± .03

modified for Q, $\bar{Q}$ sea contributions. The value of $\sin^2\theta_w$ is determined largely by the value of R, rather than $\bar{R}$, and it is remarkable that 2 experiments (CITF and CDHS) with virtually the same value of R nevertheless come up with quite different values for $\sin^2\theta_w$. In particular, it is certain that the values deduced from the low energy (GGM PS and BNL 7') experiments are strongly suspect, since the analysis involved application of the naive parton model in the region of only a few GeV incident energy.

The very accurate CDHS data[56] is shown in Fig. 38, where R is plotted against hadron energy E_H for different radial distances from the narrowband beam axis (corresponding to different neutrino energies);

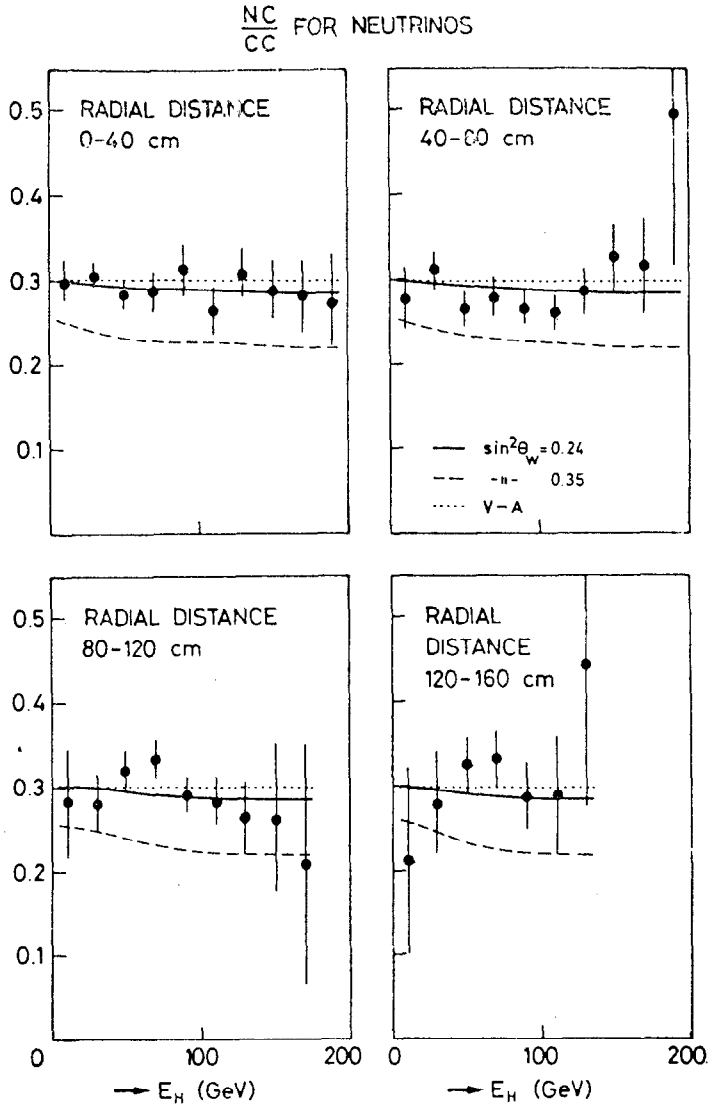

Fig. 38 CDHS data on NC/CC ratios.

one sees that R is independent of E or E_H. The BEBC ABCLOS[57] narrow-band data quotes absolute values of the neutral current cross-sections (subject to the cut $E_H > 15$ GeV) using events within different radial regions and hence in different energy ranges (see Fig. 39). Their result for $\sin^2\theta_w$ comes, not from R and $\bar{R}$ but by measuring the difference ratio (3.21) directly; thus it is much more model-independent than the other determinations.

The cross-sections or rate ratios R, $\bar{R}$ do not utilize all the information available. Recently, the BEBC NB collaboration have fitted the absolute differential cross-sections $d\sigma/dy'$, where y' = (measured hadron energy)/(muon kaon neutrino energy at that radius), to curves computed by a Monte Carlo method, using the Buras-Gaemers[60] quark-antiquark parameterisations, flux data and missing hadron energy distribution (Fig. 9). The results are given in Fig. 40, showing the distribution for CC events (used as a proof of the method) as well as NC events. This analysis[57] gave $\sin^2\theta_w = 0.19 \pm .03$, with a systematic uncertainty (from flux normalization etc.) also of 0.03.

In summary, the most reliable inclusive data on neutral currents seems to be consistent with a unique value of $\sin^2\theta = 0.20 \pm 0.25$. Fig. 41 shows the world average data on g_- and g_+ from Sciulli's review.[44]

3.5 Isospin Analysis

The discussion about the semi-leptonic neutral currents has so far been concerned with inclusive reactions on isoscalar targets. Judging from experience with charged current weak reactions and from neutral current electromagnetic reactions, we expect both isovector (I = 1) and isoscalar (I = 0) currents to be present. Again, there is no evidence for anything exotic, like isotensor (I = 2) currents,

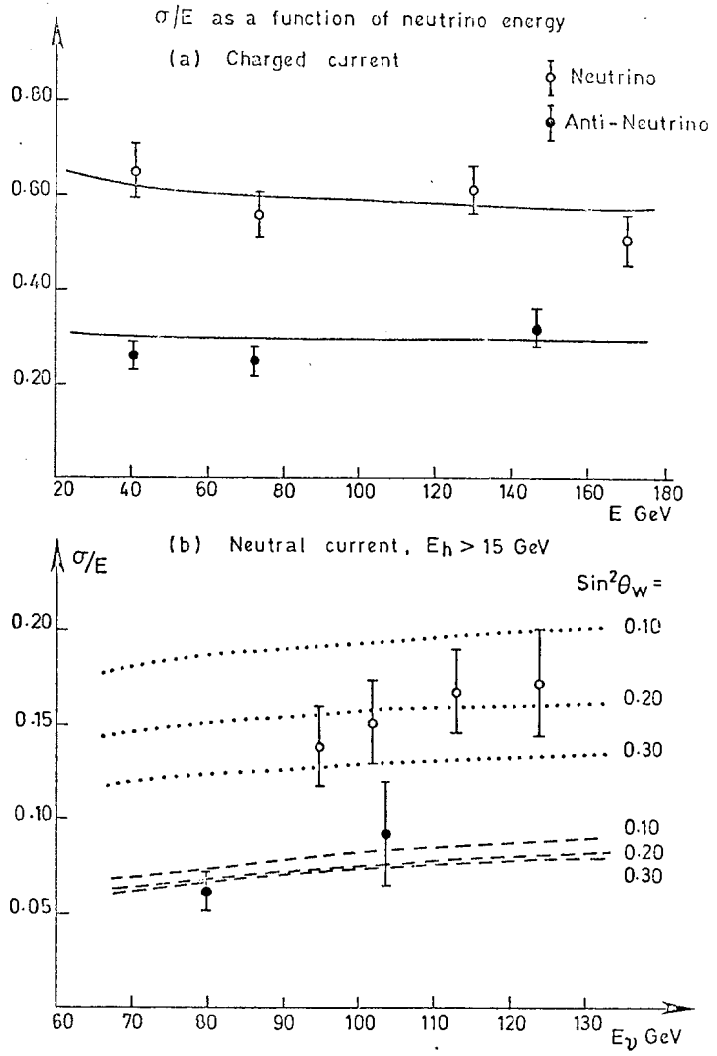
σ/E as a function of neutrino energy
(a) Charged current
Neutrino
Anti-Neutrino
0·60
0·60
0·40
0·20
20
40
60
80
100
120
140
160
180
E GeV
(b) Neutral current, $E_h > 15$ GeV
σ/E
$Sin^2\theta_W$ =
0·20
0·15
0·10
0·05
0·10
0·20
0·30
0·10
0·20
0·30
60
70
80
90
100
110
120
130
E_ν GeV

Fig. 39

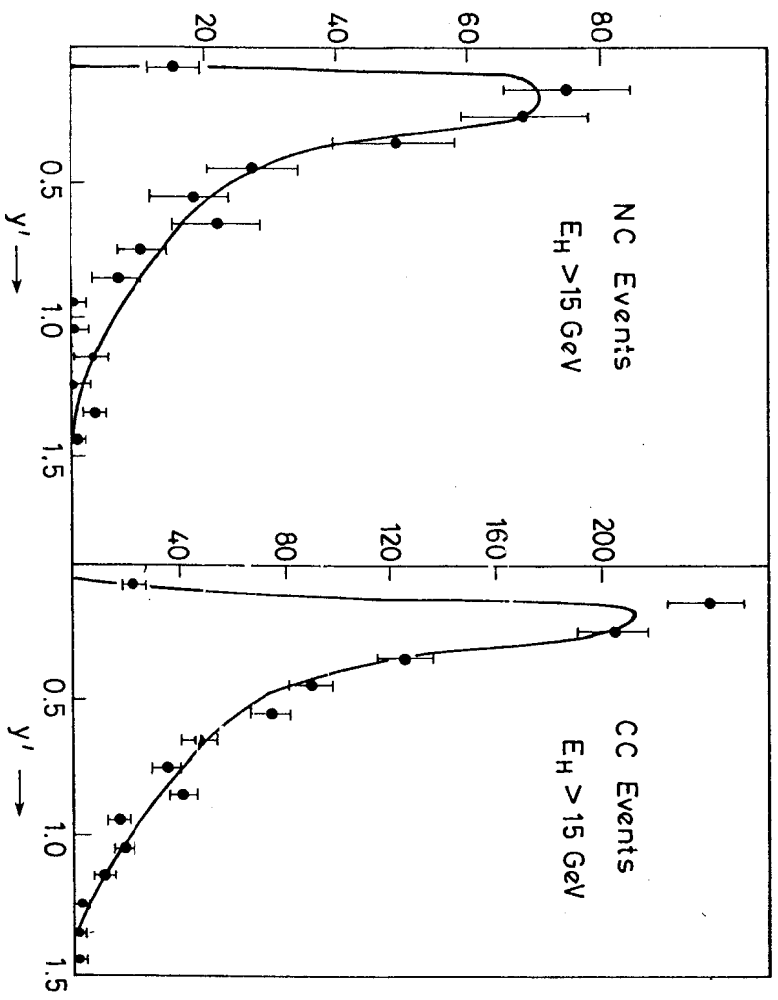
20
40
60
80
y'
0.5
1.0
1.5
NC Events
$E_H > 15$ GeV
40
80
120
160
200
y'
0.5
1.0
1.5
CC Events
$E_H > 15$ GeV

Fig. 40

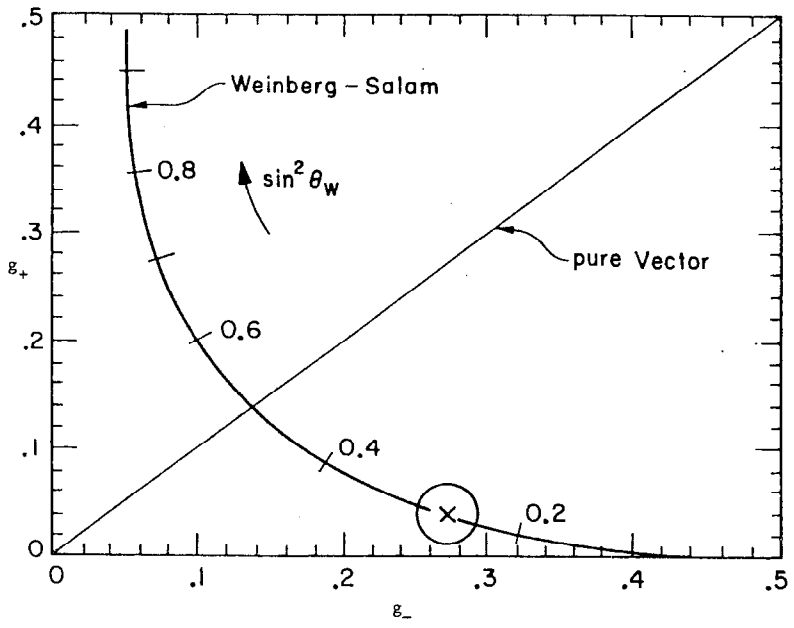

Fig. 41 World average data on g_+ and g_- (after Sciulli)

and we do not consider such possibilities. The assumed V, A and I = 0, 1 structure leads to four amplitudes which we denote in the Sakurai notation[61]

α	V	I = 1
β	A	I = 1
γ	V	I = 0
δ	A	I = 0

In the quark model, terms like $(u\bar{u} - d\bar{d})$ are isovector, while $(u\bar{u} + d\bar{d})$ is isoscalar. The effective interaction Lagrangian can thus be written

$$L_{eff} = \frac{G}{2\sqrt{2}}\left[\bar{\nu}\gamma_\mu(1+\gamma_5)\nu\right]\left[\bar{u}\gamma_\mu(\alpha+\beta\gamma_5)u - \bar{d}\gamma_\mu(\alpha+\beta\gamma_5)d + \bar{u}\gamma_\mu(\gamma+\delta\gamma_5)u + \bar{d}\gamma_\mu(\gamma+\delta\gamma_5)d + \ldots\right] \quad (3.23)$$

where + ... stands for contributions from s, $\bar{s}$ ... quarks. α, β, γ, δ can be expressed in terms of the chiral coupling constants defined previously:-

$$\begin{aligned} U_L &= \tfrac{1}{4}(\alpha+\beta+\gamma+\delta) & D_L &= \tfrac{1}{4}(-\alpha-\beta+\gamma+\delta) \\ U_R &= \tfrac{1}{4}(\alpha-\beta+\gamma-\delta) & D_R &= \tfrac{1}{4}(-\alpha+\beta+\gamma-\delta) \end{aligned} \quad (3.24)$$

For an <u>isoscalar target</u>, we obtain

$$\left(\frac{\sigma^{NC} - \bar{\sigma}^{NC}}{\sigma^{CC} - \bar{\sigma}^{CC}}\right)_{\text{isoscalar}} = g^- - g^+ = (U_L^2 + D_L^2) - (U_R^2 + D_R^2)$$

$$= \tfrac{1}{2}(\underset{\downarrow}{\alpha\beta}_{I=1} + \underset{\downarrow}{\gamma\delta}_{I=0})$$

$$\left(\frac{\sigma^{NC} + \bar{\sigma}^{NC}}{\sigma^{CC} + \bar{\sigma}^{CC}}\right)_{\text{isoscalar}} = \tfrac{1}{4}(\alpha^2+\beta^2+\gamma^2+\delta^2)$$

so that one measures the V/A interference and the overall strength, but obviously not the I = 1/I = 0 interference (i.e. a term of the form $\alpha\gamma + \beta\delta$).

There is now considerable evidence that the neutral current cannot be isospin pure. For example, study of the semi-inclusive process[62]

$$\nu, \bar{\nu} + N \to \nu, \bar{\nu} + \pi^{\pm} + X \qquad (3.25)$$

was made in Gargamelle (CF_3Br filling) for events of $E > 1$ GeV and pions in the "current framgentation region" $0.3 < z < 0.7$. Kluttig et al found

$$(\pi^+/\pi^-)_{\nu} = 0.77 \pm 0.14 \quad (\pi^+/\pi^-)_{\bar{\nu}} = 1.64 \pm 0.36 \qquad (3.26)$$

while a pure I = 0 or I = 1 coupling would predict unity for an isoscalar target. Since n/p = 1.19 in freon, and there could be problems with neutron contamination in the neutral current sample, this result is not cast iron.

However, Gargamelle propane (C_3H_8) results[63] on the cross-sections for the single π° production

$$\frac{\sigma(\nu\pi^\circ p) - \sigma(\nu\pi^\circ n)}{\sigma(\nu\pi^\circ p)} = 0.40 \pm 0.20 \qquad (3.27)$$

seem to establish isoscalar/isovector intereference; in propane, secondary nuclear effects should be much smaller than in freon.

From the inclusive reactions described previously, and a detailed analysis of the semi-inclusive reactions (3.25), Sehgal[64] was able to extract the values of U_L^2, U_R^2, D_L^2, D_R^2. For example, the process $\nu N \to \nu\pi^+ X$ has a cross-section

$$\frac{d\sigma}{d\,xdz}(\nu N \to \nu\pi^+ X) \propto (U_L^2 + \tfrac{1}{3}U_R^2)u(x)D_u^{\pi^+}(z) + (D_L^2 + \tfrac{1}{3}D_R^2)d(x)D_d^{\pi^+}(z) \qquad (3.28)$$

where the fragmentation functions $D_u^{\pi^+}$ etc. can be found from charged-current neutrino data, as well as ep and ed scattering data. So, with different combinations of U_L, U_R, D_L and D_R from equations like (3.28) and (3.17), the chiral coupling constants can be extracted. However, in the future, it will be important to check this analysis with higher-energy data, where the concepts of current fragmentation are more believable than they are at PS neutrino energies.

The determination of the squares of the couplings in (3.24) does not determine α, β, γ and δ unambiguously. In fact, there is a 4-fold ambiguity; the squares of the couplings are invariant under the interchange V $\leftrightarrow$ A, and I = 0 $\leftrightarrow$ I = 1. These correspond to the four solutions A, B, C and D of Hung and Sakurai[61] which are listed in Table XI (with the most recent data included[65]).

TABLE XI

NEUTRAL CURRENT COUPLINGS

Solution	α V, I = 1	β A, I = 1	γ V, I = 0	δ A, I = 0
A	+0.58 ± 0.14	+0.92 ± 0.14	-0.28 ± 0.14	+0.06 ± 0.14
B	+0.92	+0.58	-0.06	-0.28
C	-0.06	+0.28	-0.92	-0.58
D	+0.28	-0.06	-0.58	-0.92

Solutions A and B are isovector-dominant, and are strongly favoured by two pieces of evidence. First, in the GGM propane data[63], a Δ signal is clearly visible, as shown in Fig. 42. Secondly, there is evidence from results on $\nu p \to \nu p$ and $\bar{\nu}p \to \bar{\nu}p$ scattering. The Columbia-Illinois-Rockefeller experiment[66] gives

$$R_p = \frac{\sigma(\nu p \to \nu p)}{\sigma(\nu n \to \mu^- p)} = 0.20 \pm 0.06$$

and of the Harvard-Penn-Wisconsin collaboration,[67]

$$R_p = 0.11 \pm 0.02$$

$$\bar{R}_p = \frac{\sigma(\bar{\nu}p \to \bar{\nu}p)}{\sigma(\bar{\nu}p \to \mu^+ n)} = 0.19 \pm .05$$

The relative magnitudes of R_p and $\bar{R}_p$ turn out to favour solutions A and B.

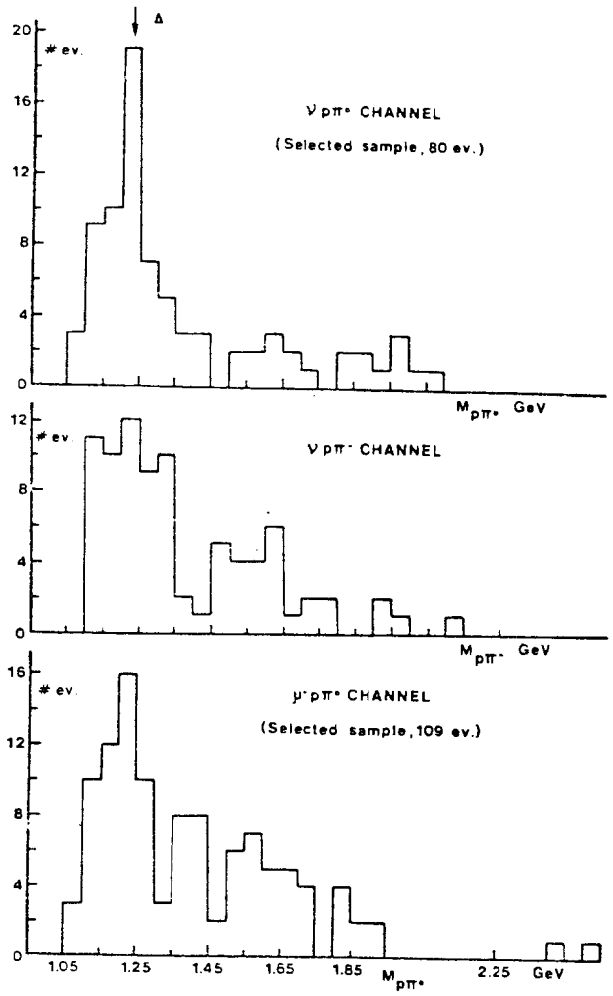

Fig. 42

There are also analyses[68,69] which go further and obtain a unique solution - solution A above - by considering the Gargamelle C_3H_8 data in the light of the Adler model of pion production. However, caution must be exercised in interpretation of pion charge ratios in heavy liquids involving complex nuclei, and further experimental checks are needed.

Solution A is, indeed, exactly what we would expect from the Salam-Weinberg model; from equn. (3.4) we have, decomposing into isoscalar and isovector parts:-

$$J_\lambda^{NC} = \underset{\uparrow}{(V_\lambda^3 + A_\lambda^3)} - 2\sin^2\theta_W . \underset{\uparrow}{J_\lambda^{em}}$$
$$I = 1 \qquad \underset{\uparrow}{(V_\lambda^3} + \underset{\uparrow}{\tfrac{1}{3}V_\lambda^0})$$
$$I = 1 \quad I = 0$$

so that we obtain the following values of α, β, γ, δ, to be compared with Solution A:-

Salam-Weinberg value	$\sin^2\theta_W = 0.22$	Solution A
$\alpha(I = 1,V) = 1-2\sin^2\theta_W$	0.56	0.58 ± 0.14
$\beta(I = 1,A) = 1$	1.0	0.92 ± 0.14
$\gamma(I = 0,V) = -\frac{2}{3}\sin^2\theta_W$	-0.15	-0.28 ± 0.14
$\delta(I = 0,A) = 0$	0	0.06 ± 0.14

3.6 Conclusions

Since they were first observed, some 5 years ago, considerable progress has been made in understanding hadronic neutral weak currents. They consist of V, A and I = 0, I = 1 admixtures, with the couplings α, β, γ and δ closely in agreement with the predictions from the Salam-Weinberg model (with $\sin^2\theta_W = 0.22$). All the most recent inclusive data, including model-independent analyses, are consistent with a unique value of $\sin^2\theta_W = 0.20 - 0.25$.

In the leptonic sector, the very high cross-section for $\nu_\mu e^-$ scattering from a Gargamelle SPS experiment seems to be an unusual statistical fluctuation: the other experiments are very consistent with the Salam-Weinberg model, with the above value of $\sin^2\theta_w$.

4. MULTILEPTON EVENTS AND CHARM PRODUCTION

4.1 Opposite Sign Dileptons in Counter Experiments, and the GIM Scheme

Over the last 2-3 years, of order 10,000 dimuon ($\mu^-\mu^+$) events have been accumulated in counter neutrino experiments, and of order 300 μ^-e^+, μ^+e^-, $\mu^+\mu^-$ events observed in bubble chambers. These events are described by the reactions $\nu_\mu + N \to \mu^- + \ell^+ + X$, $\bar{\nu}_\mu + N \to \mu^+ \ell^- + X$.

All the observed characteristics of the opposite sign dileptons seem to be consistent with the expectations from the standard GIM scheme [70], in which the weak Cabibbo couplings, characterized by the Cabibbo angle θ are described by the quark doublets

$$\begin{pmatrix} u \\ s\sin\theta + d\cos\theta \end{pmatrix} \quad , \quad \begin{pmatrix} c \\ s\cos\theta - d\sin\theta \end{pmatrix} \tag{4.1}$$

resulting in cancellation of the unobserved $\Delta^- = 1$. $\Delta C = 1$ neutral currents. To orient the discussion, we first discuss the predictions of the scheme, regarding single production of charmed hadrons in neutrino (antineutrino) reactions. The typical reactions expected are given in the table below. For neutrino beams, charmed particles can be produced by collisions of both valence and (strange) sea quarks, while for anti-neutrinos, only production of sea quarks is possible. The relative contribution of sea quarks and valence quarks is denoted by ε. In the subsequent disintegration of the charmed hadrons, decay into strange particles is enhanced:

$$\begin{aligned} c &\to s + \bar{d}u \qquad \cos^2\theta \\ &\to d + \bar{d}u \qquad \sin^2\theta \\ &\to s + \ell^+ + \nu \\ \bar{c} &\to \bar{s} + \ell^- + \bar{\nu} \end{aligned} \tag{4.2}$$

Leptonic decay of charmed hadrons is expected to have a branching ratio $B \sim 20\%$.

TABLE XII

CHARM PRODUCTION IN GIM SCHEME

Reaction	ΔC	Quark Target (Valence V, Sea S)	Rate (dσ/dy)
$\nu + d \to \mu^- + u$	0	V	$\cos^2\theta$
$\nu + d \to \mu^- + c$	1	V	$\sin^2\theta$
$\nu + s \to \mu^- + c$ $(+\bar{s})$ $(+\bar{s})$	1	S	$\varepsilon\cos^2\theta$
$\bar{\nu} + u \to \mu^+ + d$	0	V	$\cos^2\theta(1-y)^2$
$\bar{\nu} + \bar{s} \to \mu^+ + \bar{c}$ $(+s)$ $(+s)$	1	S	$\varepsilon\cos^2\theta$

These considerations suggest the following characteristics of dilepton events:-

	Final State		Ratio $(\mu^{\mp}\ell^{\pm}/\mu^{\mp})$	
ν:	$\mu^-\ell^+ + s + ..$	V	$B\tan^2\theta$	
	$\mu^-\ell^+ + s + \bar{s} + ..$	S	$B\varepsilon$	(4.3)
$\bar{\nu}$:	$\mu^+\ell^- + \bar{s} + s + ..$	S	$3B\varepsilon$	

so that the predictions are fairly clear cut:-

(i) Opposite-sign dilepton events should predominate. In all experiments, opposite-sign indeed outnumber same-sign events by at least a factor 10.

(ii) In neutrino reactions, the negative muon, from the lepton vertex, should have a much larger momentum than that of the positive lepton, which should be characteristic of hadron decay; the converse should hold in antineutrino reactions. This is illustrated in Fig. 43, showing the CDHS data.[71]

(iii) Because of transverse momentum conservation between the μ^- and the hadrons, the azimuthal angle (about the beam axis) between

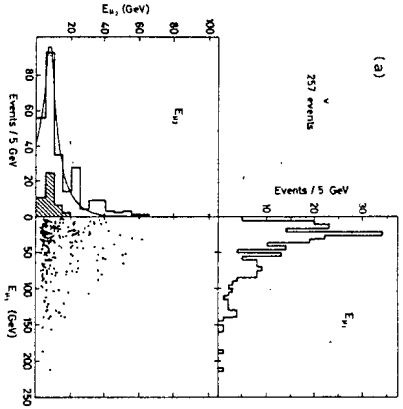

Fig. 43 Plots of the positive (negative) muon momentum vertically, against the negative (positive) momentum horizontally for (a) neutrino (b) antineutrino dimuon events.

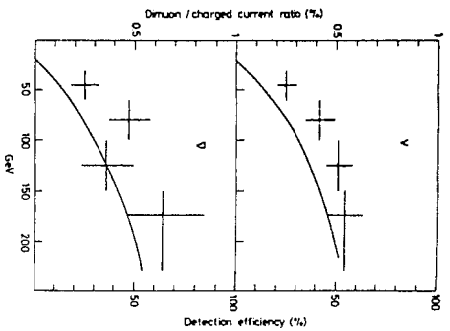

Fig. 44 Dimuon/single muon event rate as a function of neutrino energy. The curves are for the energy dependence of the detection efficiency, computed from the model of Sehgal and Zerwas, and the apparent increase with energy is due entirely to the cut on muon momentum, $p > 4.5$ GeV/c.

the μ^- and ℓ^+ should be large. In the CDHS experiment, $\phi \sim 130^o$, confirming the ℓ^+ as from the hadron, rather than the lepton vertex.

(iv) The x distributions of antineutrino-induced dimuon events should be characteristic of sea quarks (i.e. predominantly at small x-values); that for neutrino events, of a combination of valence and sea quarks, and thus broader. This is confirmed experimentally[71] (Fig.44). As indicated in Table XII, the y distributions for both neutrino and antineutrino dimuon events should be similar, and this is also observed (the flat y distribution expected is in fact modified at finite energies by threshold and acceptance effects).

(v) Experimentally[71] it is observed (Fig.45) that the ratios (dimuon rate)/(single muon rate) are essentially the same for neutrinos and antineutrinos. From 4.3 this implies $\varepsilon \sim /\tan^2\theta = 0.03$ for the strange-particle sea. The curves in Fig.45 show the E-dependence expected[72] purely from acceptance considerations (i.e. both muons were required to have $p_\mu > 4.5$ GeV/c to be identified as muons by their penetration).

Taking account of this, it is seen that the true dimuon/single muon ratio is roughly constant for E > 20 GeV, and ≈ 0.5 - 1% for both neutrino and antineutrino beams. For a muonic branching ratio B/2 ≈ 10%, we expect a $\mu^-\mu^+/\mu^-$ ratio $B(\varepsilon + \tan^2\theta)/2 \approx 1\%$, in good accord with observation.

This brief review of observations and predictions gives great confidence that the vast majority of dimuon events are indeed due to charmed hadron decay. A closer comparison is hardly possible until one has a better understanding of kinematic problems, that is the precise effect of thresholds, momentum cuts, etc., on the scaling distributions

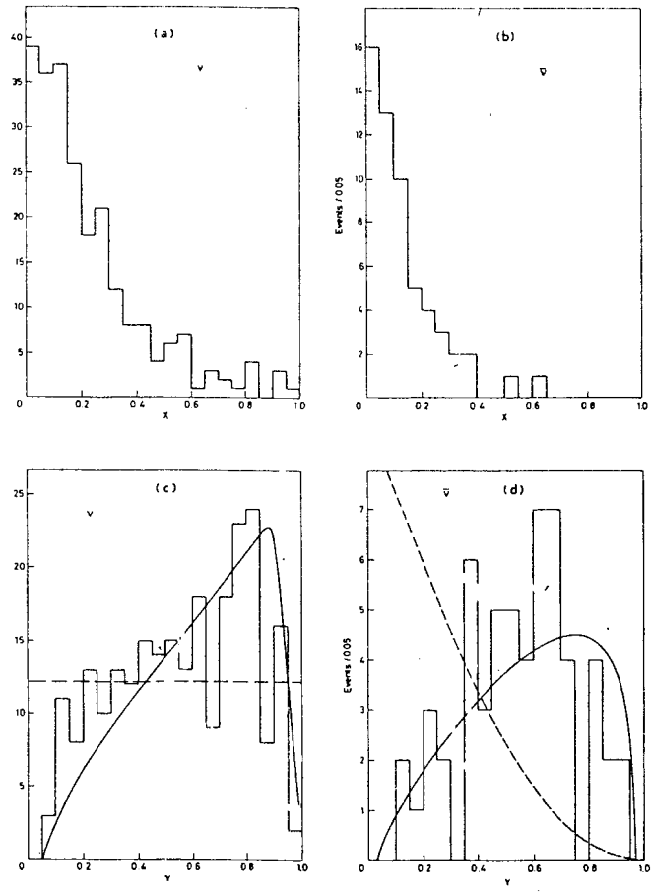

Fig. 45 x distributions of dimuon events produced by (a) neutrinos (b) antineutrinos. In (b) the distribution should be typical of the sea quarks, and in (a) of a combination of sea and valence quarks. y distributions for (c) neutrinos (d) antineutrinos. In both cases one expects a flat distribution, modified by threshold/acceptance factors as indicated by the solid curves.

which are used in computing the expected event rates.

4.2 Dilepton events in Bubble Chambers; Strange Particle Association

To date (July, 1978), a total of 5 neutrino experiments in the 15' FNAL chamber, 2 experiments in BEBC and 1 in Gargamelle (at the SPS) have reported dilepton events. Most of the total of 269 events consist of μ^-e^+; the average value of the ratio $\mu^-e^+X/\mu^-X = 0.5 \pm 0.1\%$. This is not too meaningful, because different minimum momenta ($p_{e^+} > 0.3$ GeV/c or 0.8 GeV/c) have been used in different experiments, but the $\mu^-\mu^+$ and μ^-e^+ rates were measured for the same $p_+(\text{min})$; they were equal (within, however, a large error).

Only 2 experiments, both at FNAL, have quoted rates in antineutrino runs. On a total of 16 dilepton events, the average value $\mu^-e^+X/\mu^+X = 0.22 \pm .06\%$, apparently less than the fractional dimuon rate for neutrinos, in disagreement with the CDHS findings.

The strange-particle (V^o) rates are the quantities of main interest, since they are predicted by the GIM model. In general $K^\pm$, $\Sigma^\pm$ particles are not identified, and we have to rely on the V^o rates (K^o, $\bar{K}^o$, Λ and Σ^o production and decay. Again, in Table XIII all experiments have been averaged.

The first point to make is that the dilepton events have a significantly higher observed V^o rate than the events with a single muon; 23% compared with 6% in the case of neutrinos. Thus the prediction (4.2) of production of charmed hadrons, and their preferential decay into strange particles is verified. More than 80% of the V^o's are due to $K^o_s \to \pi^+\pi^-$ decay. Possible K^o_L decays were not considered here since, even when they are detected, they are likely to be far from the production vertex and cannot always be unambiguously associated with it. Taking this, interactions in flight and the branching ratio for $K^o_s \to \pi^+\pi^-$ into account, the corrected V^o ($=K^o$) rate is given in the final column of the table.

TABLE XIII

V-PARTICLE RATES IN DILEPTON EVENTS

Beam	No. of experiments averaged	# V^o	# $\mu^-\ell^+$	V^o/event
Neutrino	8	74	325	0.70 ±0.1
Antineutrino	2	9	16	1.8 ± 0.7

From the counter data on ϵ in (4.3) the GIM model predicts on average 1.2 strange particles per neutrino dilepton event, and 1.8 per antineutrino dilepton event. Making the plausible assumption that charmed decays to neutral and charged K's are equally probable, it is seen that the predicted and observed rates are quite compatible. The difficulty of identifying K^+ is unfortunate; it means that the expected prevalence of S=-1 (rather than S=+1) products in neutrino dilepton events cannot be verified. There is some evidence that D-meson decays are involved in the dilepton events. Fig. 46 shows the Columbia/BNL data[78] on the $K^o e^+$ mass spectrum in $\mu^- e^+$ events with but a single K^o. It is compatible with that expected from the decay mode $D \to K^o\pi e^+\nu$, which is known to dominate over the decay $D \to K^o e\nu$.

4.3 Evidence for Non-Leptonic Charmed Particle Decay

In summary therefore, the characteristics of the bubble chamber dilepton events provide strong support for the GIM production scheme, with charmed mesons (and possibly baryons) generated in some 10% of neutrino events.

A systematic search for the (more abundant) non-leptonic charmed particle decays has been made by the Columbia/BNL group[78]. In a

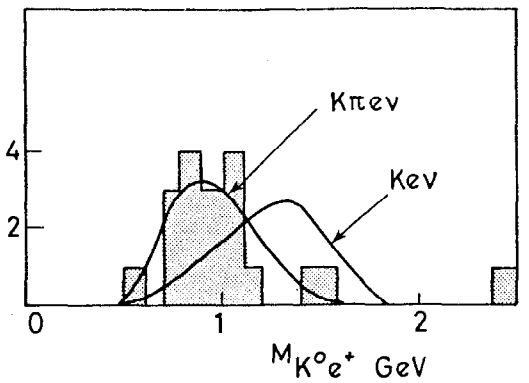

Fig. 46 Distribution in invariant mass of K^0 and positron in dilepton events with single V^0 (Columbia-BNL data). The expected distribution for D→Kπev, the dominant decay mode, is in good accord with the data.

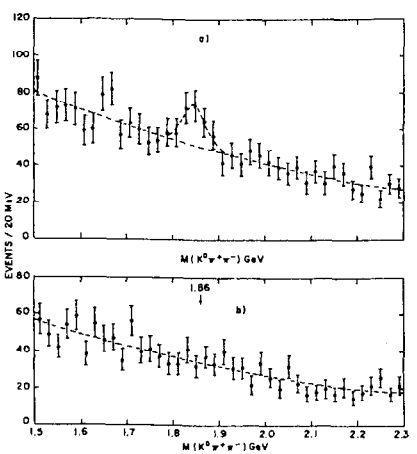

Fig. 47 Invariant mass distributions of $K^0\pi^+\pi^-$ system in (a) charged-current events containing a μ^- of $p > 2$ GeV/c (b) events without a muon (neutral currents). Columbia-BNL data.

total of 50,000 charged-current events in the 15' FNAL chamber(Ne/H_2 filling) they observed 1815 examples of $K^0_s \to \pi^+\pi^-$ and 1367 of $\Lambda^0 \to \pi^-p$, the majority doubtless due to associated production of strange particles. As shown in Fig. 47, the $K^0\pi^+\pi^-$ mass spectrum shows evidence for a peak at the D mass (1.86 GeV/c^2) in events with a negative muon (and none in neutral current events). From the known experimental resolution the group estimates a signal of 55 ± 13 events. Assuming a branching ratio for $D^0 \to K^0\pi^+\pi^-$ of 4% they deduce a D^0 production rate of

$$\frac{\sigma(\nu N \to \mu^- D^0 X)}{\sigma(\nu N \to \mu^- X)} = 7 \pm 3\%$$

which is comparable with the expected rate of about 10% for charmed hadron production (of all types) from Table XII.

4.4 Limits on Single Strange Particle and Charmed Particle Production in Neutral Current Events.

No evidence has been found for flavour-changing neutral currents(i.e. ΔC=1 or ΔS=1). Table XIV lists 90% CL upper limits for such reactions, as

Table XIV

LIMITS ON FLAVOUR-CHANGING NEUTRAL CURRENTS (90% CL)

Experiment	Reaction	E_ν (GeV)	Fraction of total NC cross-section
GGM PS[75]	$\nu N \to \nu X + \Lambda^0, \Sigma^0$	2 - 10	$< 5.10^{-3}$
CDHS NBB[76]	$\nu N \to \nu X + C \to \mu^+$	> 100	$< 26.10^{-3}$
GGM PS[77]	$\nu N \to \nu X + C \to e^+$	2 - 10	$< 13.10^{-3}$
FNAL 15'[78]	$\nu N \to \nu X + C \to e^+$	> 20	$< 80.10^{-3}$
FNAL 15'[79]	$\bar{\nu} N \to \bar{\nu} X + C \to e^+$	> 20	$< 20.10^{-3}$

ratios of the $\Delta C = \Delta S = 0$ reaction cross-sections. Although these limits are only at the few per cent level, and thus not very stringent, they are at least in support of the GIM scheme, in which such neutral currents are forbidden.

4.5 Trimuon Events.

Considerable numbers of trimuon events have been observed in counter experiments by the CDHS[80] group at CERN and by the FHOPRW group[74] at FNAL. As indicated in the table below, the rate is strongly energy-dependent. Identification of the muons depends on their penetration, and this imposes a minimum momentum of 4.5 GeV/c. It turns out that, for all

Table XV

TRIMUON RATES

Experiment	FHOPRW	CDHS
Beam	E_p=400, quad triplet	E_p=350, horn focus
# $\mu^-\mu^-\mu^+$	16	76
# $\mu^-\mu^+\mu^+$	1	4
# background (π,K decay)	~ 1	~ 6
$\mu^-\mu^-\mu^+/\mu^-$ (All E)	$(8 \pm 2).10^{-5}$	$(3\pm0.4).10^{-5}$
$\mu^-\mu^-\mu^+/\mu^-$ (E > 100)	$(17 \pm 6).10^{-5}$	$(11 \pm 3).10^{-5}$

models of trimuon production, the apparent energy dependence (as for the case of dimuons) arises entirely from this acceptance requirement. The results of the two experiments are compatible; however, it should be emphasized that the FNAL quadrupole-triplet beam, with 400 GeV incident protons,is considerably harder than the CERN horn beam, operated with 350 GeV protons (see Fig.4). For neutrino beams, $\mu^-\mu^-\mu^+$ events far outnumber $\mu^-\mu^+\mu^+$ events, all of which can be ascribed to background.

The possible origins of trimuon events have been discussed by a number of authors[59,73]. Three main processes have been considered: (i) decay of heavy leptons, (ii) cascade decay of heavy quarks, (iii) electromagnetic pair production.

We denote the leading μ^- as $\mu1$, the second μ^- as $\mu2$ and the μ^+ as $\mu3$. The leading μ^- is chosen so as to minimize $(p^T_{\mu2} + p^T_{\mu3})$ relative to the vector $\vec{p}_\nu - \vec{p}_{\mu1}$. Referring to the distributions in Figs.46 and 47 for the CDHS data, we consider each possible origin in turn:-

(i) Heavy Lepton $\quad \nu + N \rightarrow L^- + x$

$L^- \rightarrow L^o + \bar{\nu} + \mu^-$

$L^o \rightarrow \nu + \mu^- + \mu^+$

To obtain the correct distribution in invariant mass, M_{123}, M_{L^-} and M_{L^o} are chosen to be 9 GeV and 1.5 GeV respectively. Then, the observed distribution in net transverse momentum, $(p^T_{\mu2} + p^T_{\mu3})$, is found to be peaked to small values, in strong contradiction with the heavy lepton hypothesis (Fig.49). The CDHS group estimate <17% of trimuon events can be due to heavy lepton cascade decay.

(ii) Heavy Quark Cascade $\quad \nu + N \rightarrow \bar{b}(4.5) + \mu^- + X$

$\bar{b} \rightarrow \bar{c} + \nu + \mu^+$

$\bar{c} \rightarrow \bar{s} + \nu + \mu^-$

The leptonic decay chain following b quark production could give rise to trimuon events. However, the distribution in invariant mass M_{23} (Fig.48) is again too peaked to small values. Obviously, possible heavier quarks would give an even larger discrepancy. The CDHS group estimate <10% contribution from such a source.

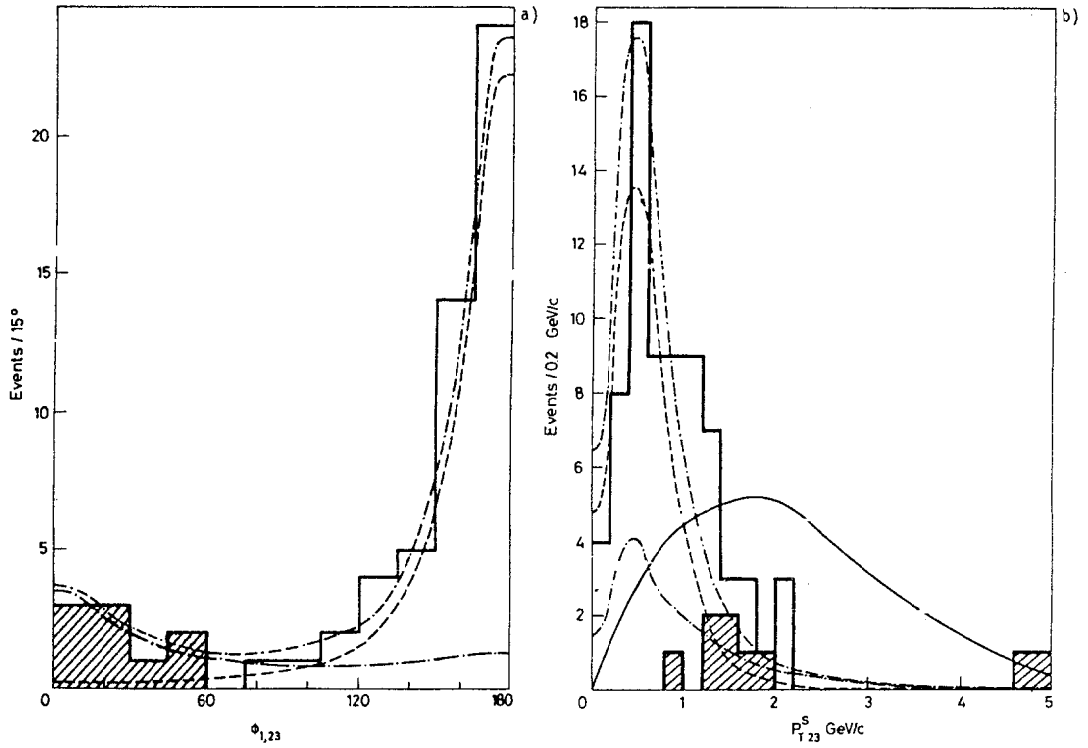
a)
b)
Events / 15°
Events / 02 GeV/c
$\Phi_{1,23}$
$P_{T\,23}^{S}$ GeV/c

Fig. 49

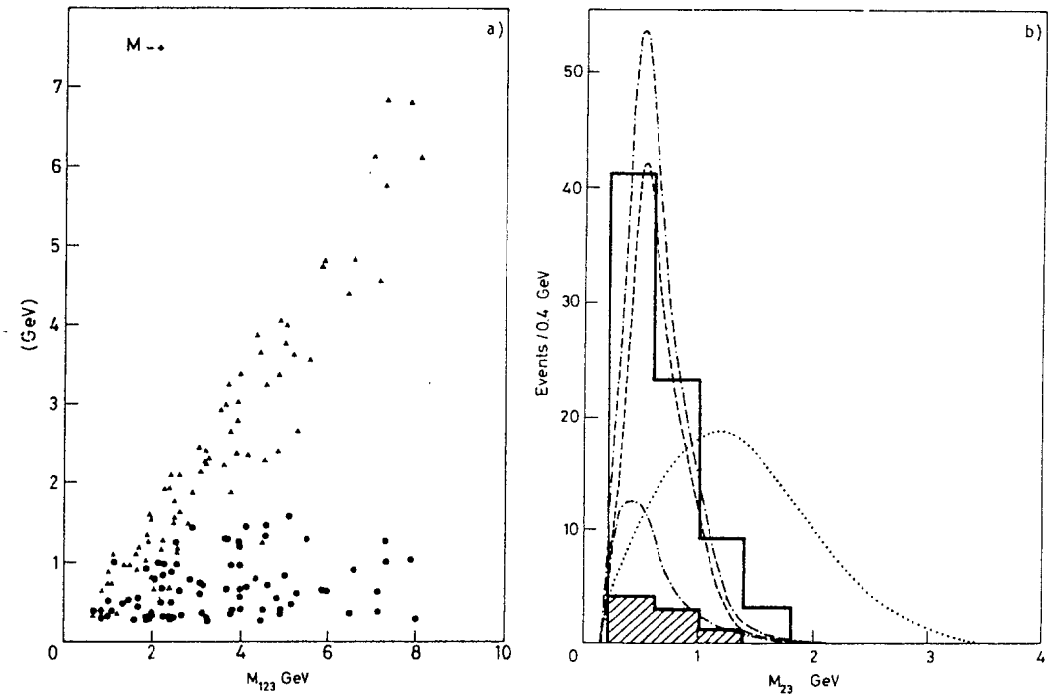
a)
b)
M
(GeV)
Events / 0.4 GeV
M_{123} GeV
M_{23} GeV

Fig. 48

(iii) Electromagnetic pair production

The third possibility considered is that one is dealing with normal one-muon events, in which an extra $\mu^+\mu^-$ pair is produced by either (a) internal bremsstrahlung at the lepton vertex, or (b) by muon pair production from the hadron vertex. The former can be calculated from quantum electrodynamics. Fig.49 shows the distribution in ϕ, the azimuthal angle of $\vec{p}_1$ relative to $\vec{p}_2 + \vec{p}_3$, measured about the beam direction, and it is seen that the absolute rate of trimuons, for $\phi < 60^\circ$, is well accounted for in terms of this bremsstrahlung process.

The hadronic muon pair rate (originating, for example, from $\rho^\circ \to \mu^+\mu^-$, the Drell-Yan process, etc.) has been measured in hadron experiments and, for the range in hadron mass W of the neutrino experiments, one can predict the distribution in ϕ expected. It is compatible, in both shape and magnitude, with the trimuon events of $\phi > 60^\circ$.

The contributions to the $3\mu/1\mu$ ratios from the two sources considered here are $(0.7 \pm 0.1).10^{-5}$ and (2.10^{-5}) respectively - thus in good agreement with the CDHS numbers, although somewhat below those of the FHOPRW collaboration (Table XV).

In addition to the normal trimuons, characterized by one leading muon and two of lower energy, the FHOPRW group have reported two "super trimuons"; in each case E(vis) > 200 GeV, and all three muons have comparable energies (60 - 90 GeV each). There is at present no explanation of these events in terms of known processes.

4.6 Like Sign Dimuons

As stated before, like sign dimuons ($\mu^-\mu^-$) occur at about 1/10 of the rate of the unlike sign ($\mu^-\mu^+$) events.

The FHOPRW group[74] have measured the rate in targets of three different densities; on plotting against the absorption length λ_{abs}, a prompt signal is observed at the 2.5 standard deviation level. The CDHS group do not have data at different λ_{abs}; they can only compare their $\mu^-\mu^-$ rate with the background rate from K,π decay, based on a Monte Carlo program using bubble chamber hadron distributions as input. The calculated background is equal to the signal, within a factor 2.

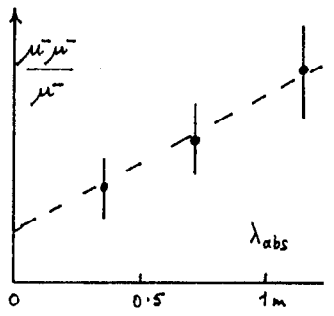

At present, it is not possible to decide if like-sign dimuons exist as a non-trivial phenomenon. Judging from the FHOPRW data on ϕ, $p_\perp$, E_{vis}, $m_{\mu\mu}$ distributions, the characteristics of $\mu^-\mu^-$ events seem to be very similar to those of $\mu^-\mu^+$ - suggesting a hadronic origin.

4.7 Prompt Neutrino Production - Beam Dump Experiments

During the last year, two "beam dump" experiments were carried out, measuring the production of prompt single neutrinos (CERN) or muons (FNAL) in 400 GeV proton-nucleus collisions.

(a) Zero degree experiment

In the CERN experiment, 400 GeV protons, which normally fed the wideband beam, and pointed directly to the detectors, were incident on a copper block of diameter 0.27 m and length 2 m (followed by iron blocks). Conventional sources ($\pi^\pm$, $K^\pm$) of neutrinos were therefore suppressed by a factor f = (interaction length in copper)/(length of decay tunnel) $= 3.10^{-4}$.

The dectectors used were the bubble chambers BEBC[82] (filled with Ne/H_2) and Gargamelle[83] (filled with CF_3Br), and the iron/scintillator array of the CDHS group[84]. The "wideband background" - i.e. the remnant

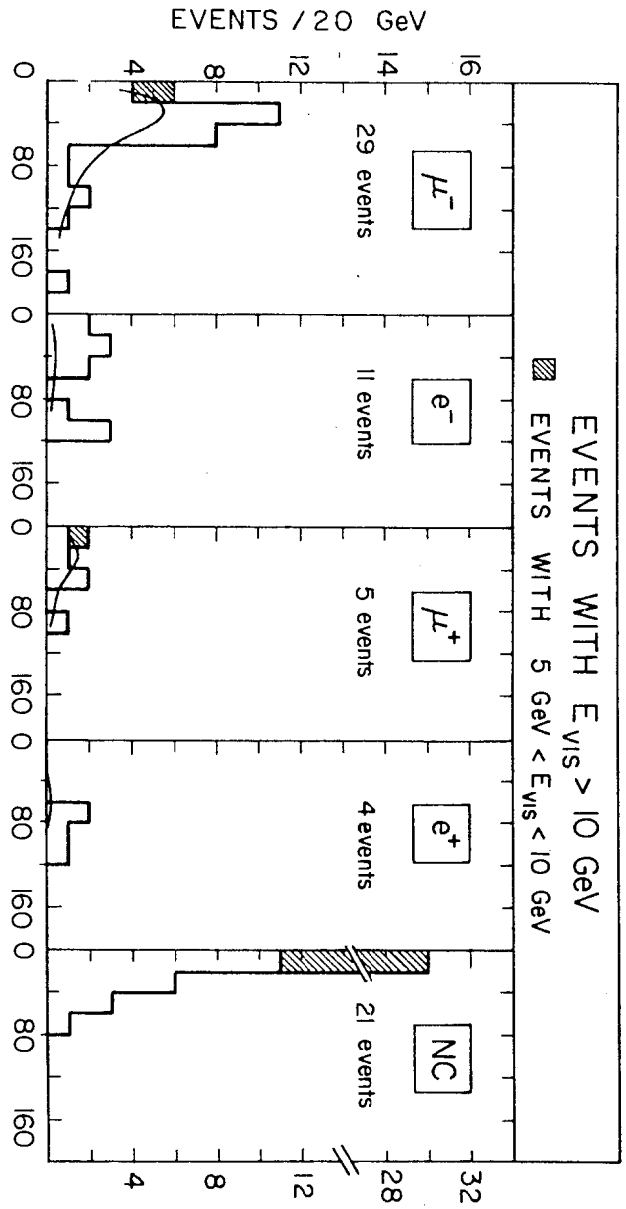

Fig. 50

flux of ν_μ, $\bar{\nu}_\mu$, ν_e and $\bar{\nu}_e$ from normal π and K-decay, was estimated and the calculation checked by measuring the muon fluxes in the shield.

Table XVI shows the salient features of the events observed in the different detectors. In BEBC and Gargamelle, secondary $e^\pm$ could be readily detected*. The observed rate of $e^\pm$, relative to $\mu^\pm$ events is a factor 6 greater than that expected. In the CDHS detector, electron events would appear as muonless events to count as neutral currents, and the observed NC/CC ratio is a factor three times that in normal neutrino running. So, in all the detectors, the results are consistent with a flux of ν_e relative to ν_μ which is much larger than for wideband background; one has to postulate, in addition to such background, an extra, prompt source of neutrinos, in which ν_e and ν_μ are comparable in intensity.

Table XVI: Observed and Expected Event Rates

(brackets indicate event numbers)

Detector	BEBC		Gargamelle	CDHS	
E_{vis}	>10 GeV		>10 GeV	>20 GeV	
	e^-/μ^-	e^+/μ^+	$(e^-+e^+)/(\mu^-/\mu^+)$	NC/CC	μ^+/μ^-
Expected	0.07	0.09	0.07	0.3	0.16
Observed	0.37	0.80	0.56	0.86±.08	0.22±.02
	(11/30)	(4/5)	(9/16)		
ν_e flux per proton per μsr (θ<1.8mr)	$(7.5\pm2).10^{-8}$		$(5\pm2).10^{-8}$	$(1.8\pm0.4).10^{-8}$	

* The sign of charge (e^+ or e^-) was not distinguished in Gargamelle.

The last line in the table shows the computed ν_e flux per incident proton and per microsteradian of solid angle in the forward direction. While the BEBC and Gargamelle data agree, there is a factor 3 discrepancy with the CDHS results, which is not understood. The energy distributions of the various event types in the BEBC experiment are shown in Fig.50, where the curves indicate the calculated wideband contribution (π,K decay in flight in the dump).

Before concluding that the anomalously large ratio of e/μ events signifies a prompt neutrino source, it is necessary to exclude possible effects from proton beam halo. For example, since the ratio of decay modes $K^0_{e3}/K^0_{\mu 3} = 1.5$, a K^0 source could be responsible. This might in principle arise from the proton beam scraping the vacuum pipe, in a region upstream of the dump where the proton beam points to the detectors, and there is enough magnetic bending to sweep out charged kaons (which would give $\phi_{\nu_\mu} >> \phi_{\nu_e}$). The observed rates however require 1% of the proton beam to interact with the vacuum pipe or magnets in this way and this possibility is excluded because no abnormal radioactivity was recorded.

The prompt neutrino fluxes in Table XVI may be compared with prompt muon fluxes measured in other experiments; for this purpose, the neutrino fluxes are divided by the corresponding π^+ fluxes (computed from the Hagedorn-Ranft model) into the same solid angle ($\theta < 1.8$ mrad) subtended by the detector (in this case, BEBC, at the target). The values are given in Fig.51, together with data on prompt muon production. Most of the muons are known to be pair-produced ($\pi^\pm$) and only ~30% are single; thus the single neutrino and single muon rates are very comparable, and it is natural to think of a common origin, namely leptonic decay of a hadron (e.g. $D \to \pi\mu^+\nu_\mu$ or $\pi e^+\nu_e$). A recent CalTech-Stanford experiment[85] was done at FNAL under very similar conditions to the

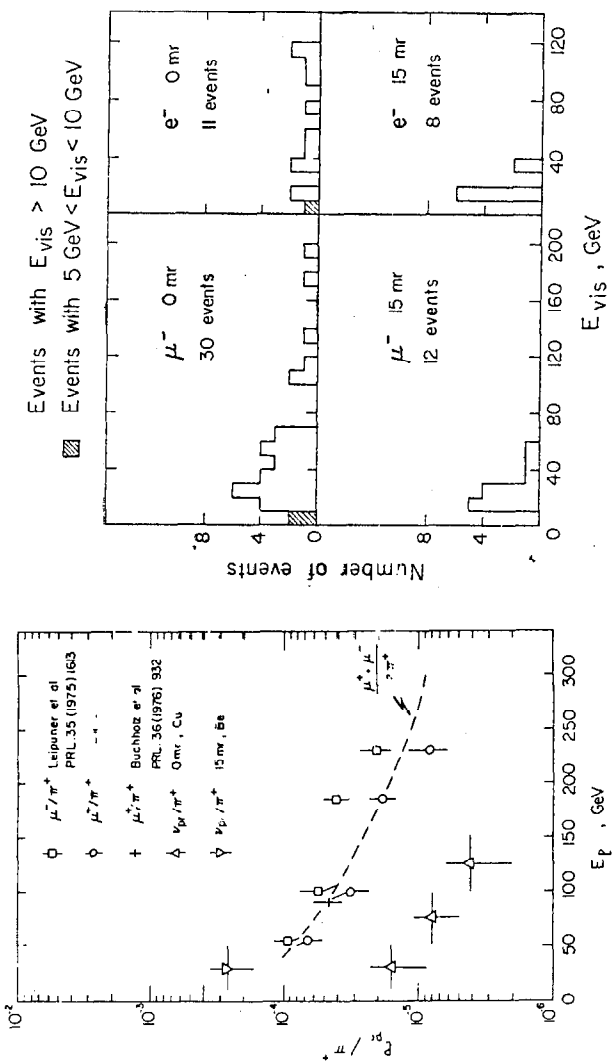

Fig. 51 (left) Ratio of prompt ν_e fluxes to π^+ fluxes in the BEBC beam dump running, at 0 mrad in Cu and at 15 mrad in Be. Data on forward muon fluxes are also indicated.

Fig. 52 (right) Distribution of e^- and μ^- events with visible energy, at 0 mrad and 15 mrad.

CERN experiments. The single muon fluxes per proton were in very close agreement with the single neutrino fluxes quoted above.

(b) 15 mrad beam dump experiment

The data above apply to lepton fluxes generated at the dump target at very small forward angle ($\theta < 1.8$ mrad). During narrowband runs, the 400 GeV protons are incident at 15 mrad to the (wideband) axis on a Be target 1.5 interaction lengths thick and are absorbed also on the narrowband collimators at larger angles (25 mrad) when negative secondaries (π^-,K^-) are selected. Thus, the narrowband runs should record prompt neutrinos emitted at 15 mrad to the forward direction. The distributions of the "wrong sign" μ^- and e^- events in NB antineutrino runs is given in Fig.52, together with the zero degree data. Again, an excess of e^- events is observed; the corresponding ν_e/π^+ production ratio is included in Fig.51. (One should note that the 15 mrad data are for a Be target, while the 0 mrad data were for Cu). The 15 mrad fluxes provide useful constraints when we discuss prompt lepton production mechanisms below.

(c) Interpretation of beam dump results

The prompt neutrino (and muon) fluxes have been interpreted in terms of production and decay of (pairs of) charmed particles in proton-nucleus collisions. The model makes the following assumptions.

(i) The parents of the prompt leptons are $D\bar{D}$ pairs, from which one expects equal fluxes of ν_e, $\bar{\nu}_e$, ν_μ and $\bar{\nu}_\mu$ - consistent with observation.

(ii) The D mesons undergo decays in the dominant mode $D \to K^* e\nu$ (or $D \to K^* \mu\nu$) with 10% branching ratio, as indicated in e^+e^- experiments.

(iii) The invariant cross-section for D production is given by

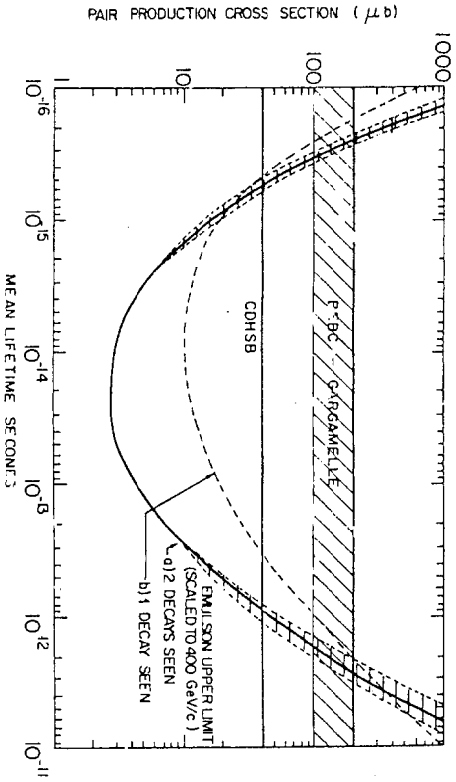

Fig. 53 Charmed particle production cross-sections in pp collisions as measured in the BEBC and CDHS beam dump experiments. The curve shows the upper limit from an emulsion experiment, as a function of the lifetime.

$$Ed^3\sigma/dp^3 = \text{const.}\ (1-x)^n \exp(-bp_T)$$

where $x = x(\text{Feynman}) = p_L/p_L(\text{max})$, p_L is the longitudinal D momentum in the CMS and p_T is its transverse momentum. Judging from results on ψ production by incident protons, we expect $n = 3$ or 4 and $b = 2\ \text{GeV}^{-1}$.

Study of the energy distributions, at 0 and 15 mrad, of the events recorded indicate values of $n = 3 - 5$ and $b \geq 2$. This results in an estimate of a mean multiplicity for D-meson production in proton-nucleus collisions of $\langle n_D \rangle = (3 \to 6).10^{-3}$ per proton.

If we assume 33 mb for the pp inelastic cross-section, and that the D production cross-section on a nucleus of mass number A varies as $A^{2/3}$, this analysis gives

$$\sigma(pp \to D\bar{D} + X) = 100 \to 200\ \mu b$$

If, as seems more likely, the $D\bar{D}$ production varies as A per nucleus, then $\sigma(pp \to D\bar{D}+X) = 25 \to 50\ \mu b$. These cross-section numbers refer to the BEBC and Gargamelle data. As might be expected from Table XVI, the CDHS results give a cross-section estimate which is smaller by a factor 3. But in any case, and irrespective of the exact nature of the x and p_T distributions, the experiment indicates $D\bar{D}$ cross-sections well in excess of 10 μb per nucleon. The muon results yield similar conclusions[85].

(d) Comparison with other data

A large number of counter experiments have been carried out to look for charmed particle production in hadron collisions. They give cross-sections, or, more usually, upper limits, which are not in serious disagreement with the above figures. However, there is a limit of 1.5 μb from an emulsion experiment searching for pair production, and decay, of charmed particles in proton-nucleus collisions[86]. In fact, the limit depends on the lifetime τ assumed; if τ is very small, or very large, the probability of detecting a decay is reduced, as shown in Fig.53. The prompt neutrino (or muon) results and the emulsion result would be compatible if $\tau > 10^{-12}$ or $\tau < 10^{-15}$ sec. The former limit is essentially excluded, since measurable gaps would then be found in bubble-chamber dilepton events. The second limit is hardly reasonable from a theoretical standpoint (i.e. simple application of the Sargent rule of β-decay, could hardly be wrong by a factor 10^3.)

(e) Other conclusions

The beam dump results set interesting limits on other possible processes. Some possibilities can be discarded immediately. For example τ-leptons are not a possible source of the prompt neutrinos observed; the lepton pair production cross-section is known from μ-pair cross-sections and its maximum possible value is at least a factor 10^3 - 10^4 too small. Furthermore, $\tau \to \nu_\tau + \pi$'s would lead to ν_τ interactions, ($\nu_\tau + N \to \tau + X \to \nu_\tau$ + hadrons) and values of NC/CC >1.

A scalar boson called an axion[33,35,81] has been postulated in order to avoid CP violation in strong interactions. Upon interaction in the detector the axions would give neutral current-like events, with however $p_\perp$ balance since there is no secondary lepton. The BEBC group[32] quotes an upper limit of $<2.10^{-67}\ \text{cm}^4$ for the product of axion production and interaction cross-sections, about a factor 50 smaller than that expected for this particle.

In summary, a fraction, perhaps even most, of the beam dump events may be due to leptons from prompt decay of charmed hadrons produced at the target. However, the resulting equality of the excess ν_e, $\bar{\nu}_e$, ν_μ and $\bar{\nu}_\mu$ fluxes is not established and further experiments are required. Quite different sources of the events are also possible, but heavy leptons and axions appear to be excluded.

REFERENCES

1. C. H. Llewellyn-Smith, Phys. Rep. 3C (1972) 261.
2. J. D. Bjorken & E. A. Paschos, Phys. Rev. 185 (1969) 1975.
3. W. Panofsky, Proc. 14th Int. Conf. on High Energy Physics, Vienna (1968)
   G. Miller et al, Phys. Rev. D5 (1972) 528.
4. I. Budagov et al, Phys. Lett. 30B (1969) 364.
5. T. Eichten et al, Phys. Lett 46B (1973) 281.
6. R. P. Feynman, Phys. Rev. Lett. 23 (1969) 1415.
7. O. Nachtmann, Nucl. Phys. B63 (1973) 237; B78 (1974) 455.
8. C. G. Callan & D. G. Gross, Phys. Rev. Lett. 21 (1968) 311.
9. D. H. Perkins, Rep. Prog. Phys. 40 (1977) 410.
10. R. P. Feynmann & M. Gell-Mann, Phys. Rev. 109 (1958) 193.
11. H. Deden et al, Nucl. Phys. B85 (1975) 269.
12. J. T. Friedman & H. W. Kendall, Ann. Rev. Nucl. Sci. 22 (1972) 203.
13. D. J. Gross & C. H. Llewellyn-Smith, Nucl. Phys. B14 (1969) 337.
14. D. J. Fox et al, Phys. Rev. Lett 33 (1974) 1504.
    Y. Watanake et al, Phys. Rev. Lett. 35 (1975) 898.
15. D. H. Perkins, P. Schreiner & W. G. Scott, Phys. Lett. 67B (1977) 347.
16. P. C. Bosetti et al, Oxford Nuclear Physics preprint 16/78.
17. E. M. Riordan et al, SLAC-PUB-1634 (1975).
18. H. L. Anderson et al, Phys. Rev. Lett. 37 (1976) 4; ibid 36 (1976) 1422.
19. M. Holder et al, Proc. SLAC Summer Inst. (1978).
20. J. Kiskis, Phys. Rev. D8 (1973) 2129.
21. R. Barlow & S. Wolfram, Oxford preprint (1978).
22. E. Bloom & F. Gilman, Phys. Rev. Lett. 25 (1970) 1140.
23. R. K. Ellis et al, Phys. Lett. 64B (1976) 97.
    R. Barbien et al, Nucl. Phys. B117 (1976) 50.
    H. Georgi & H. D. Politzer, Phys. Rev. Lett. 36 (1976) 1281.
24. R. Serber, Phys. Rev. 48 (1935) 49.
    A. E. Uehling, Phys. Rev. 48 (1935) 55.
25. M. Gell-Mann & F. E. Low, Phys. Rev. 95 (1954) 1300.
    L. Landau et al, Dokl. Akad. Nauk. USSR, 95 (1954) 1177.
26. D. J. Gross & F. Wilczek, Phys. Rev. D8 (1973) 3633.
27. H. Fritzsch, CERN TH-2483 (1978).
28. I. G. Floratos et al, Nucl. Phys. B129 (1977) 66.
29. A. J. Buras et al, Nucl. Phys. B131 (1977) 308.
30. W. A. Bardeen et al, Fermilab-Pub-78/42 THY.
31. T. Quirk, (private communication).
32. I. Hinchliffe & C. H. Llewellyn-Smith, Nucl. Phys. B128 (1977) 93.
33. F. Wilczek et al, Phys. Rev. Lett. 40 (1978) 279.
34. R. P. Feynmann, "Photon-Hadron Interactions" 1972 (New York: Benjamin).
35. S. Weinberg, Phys. Rev. Lett. 40 (1978) 223.
36. J. Bell et al, UMBC 78-6.
37. F. Ravndal, Phys. Lett. 43B (1973) 301.
38. H. Georgi & H. D. Politzer, Phys. Rev. Lett. 40 (1978) 3.
39. P. C. Bosetti et al, Oxford Nucl. Phys. preprint 58/78.
40. A. Mendez, Oxford Theoretical Phys. preprint 29/78.
41. H. Georgi & M. Machacek, Phys. Rev. Lett. 39 (1977) 1237.
    E. Farhi, Phys. Rev. Lett. 39 (1977) 1587.
42. G. Sterman & S. Weinberg, Phys. Rev. Lett. 39 (1977) 1436.
43. A. Vayaki, Proc. Oxford Conf. Neutrino Phys.(1978 Rutherford Lab).
44. F. Sciulli, CALT-68-639.
45. L. M. Segal, Aachen PITHA-102 (1978).
46. J. J. Sakurai, UCLA-78-TEP-18; Proc. Oxford Conf. Neutrino Physics (1978 Rutherford Lab).
47. F. Reives et al, Phys. Rev. Lett. 37 (1976) 315.
48. F. J. Hasert et al, Phys. Lett. 46B (1973) 121.
    J. Blietschan et al, Nucl. Phys. 114B (1976) 189.
    J. Blietschan et al, Phys. Lett. 73B (1978) 232.
49. H. Faissner et al, Aachen preprint PITHA 100 (1978).
    M. Baldo-Ceolin, Proc. "Neutrino 1978" (Purdue).
50. A. Goldhaber & M. Nieto, Rev. Mod. Phys. 43 (1971) 277.
51. A. M. Cuops et al, Proc. Oxford Conf. Neutrino Phys. (1978, Rutherford Lab).
52. P. Alibran et al, Phys. Lett. 74B (1978) 422.
53. F. Romans, Proc. Oxford Conf. Neutrino Phys. (1978, Rutherford Lab).
54. J. Sacton, IIHE 78.02 (Brussels); Proc. Oxford Conf. Neutrino Phys. (1978, Rutherford Lab).
55. F. T. Avignone & Z. T. Greenwood, Phys. Rev. D16 (1977) 2383.

56. M. Holder et al, Phys. Lett. 72B (1977) 254.

57. P. C. Bosetti et al, Phys. Lett. 76B (1978) 505.
B. Saitta, Proc. Oxford Conf. Neutrino Phys. (1978, Rutherford Lab).

58. E. A. Paschos & L. Wolfenstein, Phys. Rev. D7 (1973) 91.

59. J. Smith et al, Stony Brook preprint ITP-SB 77-66.

60. A. J. Buras & K. J. Gaemers, Nucl. Phys. B132 (1978) 249.

61. P. Q. Hung & J. J. Sakurai, Phys. Lett. 63B (1976) 295.

62. H. Kluttig, J.A. Morfin & W. Van Doninck, Phys. Lett 71B (1977) 446.

63. W. Krenz et al, Nucl. Phys. B135 (1978) 45.

64. L. M. Sehgal, Phys. Lett. 71B (1977) 99.

65. J. J. Sakurai, Proc. Oxford Conf. Neutrino Phys. (1978, Rutherford Lab).

66. W. Lee et al, Phys. Rev. Lett. 37 (1976) 186; and Proc. Oxford Conf.

67. D. Cline et al, Phys. Rev. Lett. 37 (1976) 252; 37 (1976) 648; and Proc. Oxford Conf.

68. L. F. Abbott & R. M. Barnett, Phys. Rev. Lett. 40 (1978) 1303.

69. E. Monsay, ANL-HEP-PR-78-08 (1978).

70. S. Glashow, J. Iliopoulos & L. Maiani, Phys. Rev. D2 (1970) 1285.

71. M. Holder et al, Phys. Lett. 69B (1977) 377.

72. L. M. Sehgal & P. M. Zerwas, Nucl. Phys. B108 (1976) 483.

73. R. M. Barnett et al, private communication;
V. Barger et al, private communication.

74. D. Cline, Proc. Oxford Conf. Neutrino Phys. (]978 Rutherford Lab).

75. J. Blietschan et al, Phys. Lett. 71B (1977) 31.

76. M. Holder et al, Phys. Lett. 74B (1978) 277.

77. H. Deden et al, Phys. Lett. 67B (1977) 474.

78. C. Baltay, Proc. Oxford Conf. Neutrino Phys. (1978, Rutherford Lab).

79. B. Roe, (ibid.).

80. T. Hansl et al, CERN report (submitted to Nucl. Phys. B).

81. J. Ellis & M. K. Gaillard, Phys. Lett. 74B (1978) 374.

82. P. C. Bosetti et al, Phys. Lett. 74B (1978) 143.

83. P. Alibran et al, Phys. Lett. 74B (1978) 134.

84. T. Hansl et al, Phys. Lett. 74 B (1978) 139.

85. M. Shaevitz, Proc. ICTP Trieste Topical Conf. (June 1978).

86. G. Coremans-Bertrand et al, Phys. Lett. 65B (1976) 480.

WEAK INTERACTIONS AT HIGH ENERGIES*

John Ellis

Stanford Linear Accelerator Center
Stanford University, Stanford, California 94305

and

CERN
Geneva, Switzerland

Contents

*Work supported in part by the Department of Energy.

WEAK INTERACTIONS AT HIGH ENERGIES

John Ellis

Stanford Linear Accelerator Center
Stanford University, Stanford, California 94305

and

CERN
Geneva, Switzerland

General Introduction

There is a Yiddish saying "May the Lord preserve you from an interesting life," but we are probably not sorry that life in high energy physics has been quite interesting lately. Indeed we seem to be passing through an archetypal scientific revolution,[1] wherein gathering contradictions dissolve into apparent chaos and confusion, and a new orthodoxy emerges and defines a framework for the next phase of normal accumulative scientific development. It is not yet clear whether the gauge revolution will have any indirect effects outside fundamental physics, but its influence certainly colours the questions we now ask in our high energy experiments. The purpose of these lectures is to review the phenomenological implications of the modern spontaneously broken gauge theories of the weak and electromagnetic interactions,[2] and make some observations about which high energy experiments probe what aspects of gauge theories. It should be emphasized at the outset that the evidence in favour of gauge theories is largely circumstantial--we have yet to find directly incriminating evidence for gauge ideas, and these lectures are presented in the hope that they may furnish useful clues for future detective work. Almost no reference will be made to alternatives to the gauge orthodoxy. This is not because I abhor heresy, but because of a personal feeling that the most fruitful way forward is to take the "standard model" at face value and use it as a paradigm for generating phenomenological questions and experimental tests. And the heretic cause is admirably served by the ingenuity and persistence of Bjorken.[3]

These lectures should be devoted to the weak interactions, but it would be disingenuous to ignore the "standard model" for the strong interactions--quantum chromodynamics or QCD.[4] On a philosophical level, it seems quixotic not to believe that if the gravitational, weak and electromagnetic interactions are described by gauge theories, then so also are the strong interactions--QCD is an unalienable part of the gauge package. On a practical level, many tests of gauge theories of the weak and electromagnetic interactions rely on the quark-parton model[5] for hadrons at large momentum transfers. We surely need some theoretical underpinning for the phenomenological parton model, as a way of exploring its domain of applicability and understanding how it may break down and need modification. On a sentimental level, it would be invidious to exclude the gluon from a shopping list of gauge-theoretical desiderata. Lecture 1 will review some basic QCD phenomenology, including momentum dependent effective quark distributions,[6] the demise of the p_T cutoff,[7] and the search for gluons as sources of hadron jets.[8]

We will then move on to the main business, the phenomenology of weak and electromagnetic interactions at high energies. Lecture 2 will review the status and prospects for the spectroscopy of fundamental fermions (quarks and leptons), and how fermions may be used to probe aspects of

the weak and electromagnetic gauge theory. Lecture 3 will deal with the pursuit, capture and investigation of the anticipated intermediate vector bosons.[9] Lecture 4 discusses miscellaneous possibilities suggested by gauge theories--ranging from the Higgs bosons,[10] which lie at the heart of the spontaneous symmetry breaking mechanism that is supposed to provide the masses of other particles and hence make massive vector boson theories renormalizable, to speculations about proton decay.[11]

The possibilities discussed in these lectures are generally rather conservative and minimal. For example, the simplest $SU(2)_L \times U(1)$ Weinberg-Salam model[12] is often used to illustrate tests of the unified theories of weak and electromagnetic interactions. It has the bare minimum of three massive intermediate vector bosons, one physical Higgs boson, and perhaps as few as six quarks. All other gauge models are more profligate in their generation of new particles and weak interactions. However, we will see that even in this model, the predictable discoveries alone amount to an enticing cornucopia.

1. Will the Strong Interactions be Weak at High Energies?

1.1 Motivation

Since these lectures are supposed to concentrate on the weak interactions, it may be necessary to present some additional apologia for first discussing the strong interactions.

The first reason is that it is difficult to discuss manifestations of weak interactions at high energies without relying on some background theory of the strong interactions. For example, in e^+e^- annihilation we need the parton model of Fig. 1 for total and jet cross sections,[13] for

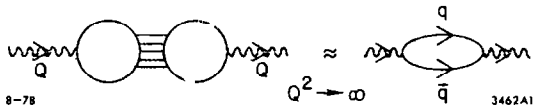

Fig. 1. The quark parton loop diagram for $e^+e^- \to$ hadrons at large Q^2s.

calculating weak/electromagnetic interferences, estimating $W^{\pm}$ and Z^{o} decay rates, and so on. In order for the parton model to be a reliable tool for incorporating hadrons into the calculation of weak amplitudes and cross sections, we need some way of estimating corrections to the naive parton calculations.[5,13] Such a systematic correction procedure can only come from a theory which explains the apparent weakness of strong interactions at high momentum transfers and the basic validity of the parton model in this limit. As another example, consider deep inelastic lepton-hadron scattering (Fig. 2), where Bjorken scaling[14] is a good first order approximation to the systematics of the data,[15] but where deviations from scaling seem to have a coherent pattern. We must seek some understanding of these scaling deviations if we are to disentangle the appearance of new quark thresholds from other effects in deep inelastic lepton-hadron scattering. Another process where it is important to understand whether the parton model of Fig. 3 is applicable is the Drell-Yan[16] process: hadron + hadron → lepton pair + anything. This process is being proposed[9] as a way to produce the intermediate vector bosons and Higgs particles in hadron-hadron collisions. We would like to know whether the naive parton cross section estimates of Fig. 3 should be regarded as reliable, or whether they may acquire large scaling deviations analogous to those observed in deep inelastic scattering.[15] We would also like to know whether the differential cross section might be expected to have a different shape from the naive expectations, for example whether the $\langle p_T \rangle$ of the produced boson should be O(1) GeV as expected in a naive parton model,[5] or might be $O(m_W)$ as some field theories lead you to expect.[7]

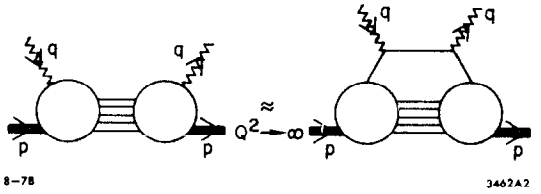

Fig. 2. The quark parton diagram for leptoproduction at large $Q^2=-q^2$.

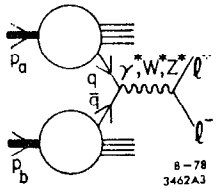

Fig. 3. The quark-antiquark annihilation diagram for hadron + hadron → $\ell^+\ell^-$+X.

Another reason for discussing the strong interactions was mentioned in the general introduction. All strong interaction field theories invoke some sort of bosonic gluon to hold quarks together (e.g., an octet of coloured vector gluons in QCD), and these are constituents of matter as fundamental as the $W^{\pm}$, Z^{o} or photon. The experimental isolation of the gluon and determination of its properties (mass, spin, colour) is therefore of fundamental significance, and it would appear arbitrary and unfair to exclude the gluon from a list of gauge goodies to be studied. Present evidence for the existence and nature of the gluon is generally indirect--there is the classic assignment of the missing fraction of the nucleon momentum to gluon partons which do not interact directly with the lepton probes in deep inelastic scattering.[17] More recently, there has been some evidence from scaling violations in neutrino scattering[15] which also indicates indirectly that gluons are present in the nucleon,[18] and probably have spin 1. This evidence will be discussed later in this lecture, but the interested reader is referred to Don Perkins' lectures at this Summer School for a more detailed analysis. These pieces of evidence are welcome, but it would be nice to see more direct manifestations of gluons as hadronic constituents. One possibility for a gluon search is the conjectured gluon jet,[8] which might show up in a hard (high momentum transfer) process when a gluon is bremsstrahled at large angles as in Fig. 4. Other places to look include the decays $T \to 3$ gluons[19] or 2 gluons + photon[20] which are expected in QCD (see Fig. 5). At the end of this lecture there will be a discussion of the phenomenological prospects of finding gluons in this way.

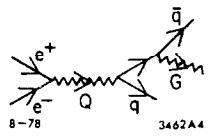

Fig. 4. Gluon bremsstrahlung in e^+e^- annihilation.

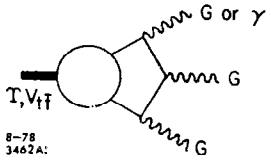

Fig. 5. The 3 gluon and 2 gluon + 1 photon decays of a heavy quark-antiquark vector meson.

There is a final reason for discussing QCD at the outset of these lectures. It is that the author and most other theorists have a strong prejudice that QCD is the correct theory of the strong interactions, and this inevitably colours the way in which we discuss the phenomenology of weak and electromagnetic interactions. The reasons for this consensus are strong but not irresistible. The only[21] field theory which is[22] asymptotically free at high momenta, and hence has a chance of reproducing the gross features of the parton model,[5] is a gauge theory. Also, quarks are apparently not abundant as physical particles in the real world, and QCD is one field theory in which quarks are not obviously unconfined.[23] But as foreshadowed in the general introduction, the best reason for believing in QCD may just be that the gauge principle seems to be a common feature of the other fundamental interactions, and it is philosophically tempting to believe that the gauge principle is universal, although there is no cast-iron motivation for this application of Occam's razor. It should be emphasized that much of the appeal of QCD reflects the lack of a viable alternative, and that conclusive experimental evidence in its favour is still in short supply.[18] Nevertheless, no alternative to QCD will be brooked in these lectures.

The strong interactions result from the QCD lagrangian[4,22,24]

$$\mathscr{L} = -\frac{1}{4} F^a_{\mu\nu} F^{a\mu\nu} + \sum_q \bar{q}\left(i\gamma_\mu D^\mu - m_q\right) q \qquad (1.1)$$

where $F^a_{\mu\nu}$ is the non-Abelian field strength

$$F^a_{\mu\nu} \equiv \partial_\mu A^a_\nu - \partial_\nu A^a_\mu + igf^{abc} A^b_\mu A^c_\nu \qquad (1.2)$$

and D_μ is the gauge-covariant derivative

$$D_\mu \equiv \frac{\partial}{\partial x^\mu} - ig\frac{\lambda^a}{2} A^a_\mu \qquad (1.3)$$

The theory (1.1) is characterized by a unique, unknown coupling constant g to be determined by experiment, and an unknown number of quark flavours q, with their number and masses also undetermined by theory. QCD contains eight gluons A^a_μ which form an adjoint representation of SU(3) acting on the three colours of quark: red, yellow and blue. There are several well known phenomenological motivations for the colour degree of freedom, which include:

--The fact that the lowest-lying baryon octet and decuplet seem to have wave functions which are symmetric s-waves in space and symmetric in spin. For the quarks to have the Fermi statistics appropriate to spin 1/2 particles, they must have an internal degree of freedom wherein the baryon wave function is antisymmetrized. In the colour theory, the baryon wave function contains a factor $\varepsilon_{RYB}\, q^R q^Y q^B$, and the symmetrization problem is solved.[25]

--The decay rate for $\pi^0 \to 2\gamma$. According to current algebra and PCAC, the amplitude for this decay is given by the triangle diagrams of Fig. 6, and is hence proportional to the number of colours.[26] The rate for the decay is calculated to be

$$\Gamma(\pi^0 \to 2\gamma) = \frac{m_\pi^3}{64\pi}\left(\frac{\alpha}{\pi f_\pi}\frac{N}{3}\right)^2 \qquad (1.4)$$

where N is the number of colours. If we take N=3 and f_π = 94 MeV, Eq. (1.4) yields $\Gamma(\pi^0 \to 2\gamma)$ = 7.91 eV, whereas the latest experimental decay rate is 8.04 ± 0.55 eV.[27]

--A related reason for colour is the cancellation of anomalous triangle diagrams like those in Fig. 6 which is required[28] to ensure the renormalizability[29] of a gauge theory of weak and electromagnetic

interactions. In the "standard" $SU(2)_L \times U(1)$ Weinberg-Salam model[12] this cancellation occurs between doublets, each of which contributes an anomaly

$$S = g_A\left(Q_\nu^2 - Q_\ell^2\right) = \frac{1}{2}(0-(-1)^2) = -\frac{1}{2} \qquad (1.5a)$$

and quark doublets, each of which contributes an anomaly

$$S = Ng_A\left(\left(\frac{2}{3}\right)^2 - \left(-\frac{1}{3}\right)^2\right) = \frac{N}{6} \qquad (1.5b)$$

If there were no colour factor of N=3 in Eq. (1.5b) we would need three times as many leptons as quarks, which does not seem to be a good approximation to the experimental situation!

--The cross section ratio for $e^+e^- \to \gamma^* \to$ hadrons relative to $e^+e^- \to \gamma^* \to \mu^+\mu^-$. In the naive parton model[5] this is calculated from the simple quark loops[13] of Fig. 1 and should be

$$R \equiv \frac{(e^+e^- \to \gamma^* \to \text{hadrons})}{(e^+e^- \to \gamma^* \to \mu^+\mu^-)} = N\sum_q Q_q^2 \qquad (1.6)$$

In the absence of colour, this ratio would be 2/3 below charm threshold and 10/9 above. Experimentally, the ratio is about 2-1/2 below charm threshold and about 4-1/2 to 5 above.[30] Allowing for (10 to 20)% systematic experimental errors and the contribution of a heavy lepton above charm threshold, these values are not inconsistent with the values of 2 and 3-1/3 expected for R if N=3.

--A closely related prediction is the ratio of semihadronic decays of the τ relative to purely leptonic decays. We would estimate[31]

$$\Gamma(\tau^- \to \mu^-\bar{\nu}_\mu\nu_\tau):\Gamma(\tau^- \to e^-\bar{\nu}_e\nu_\tau):\Gamma(\tau^- \to \text{hadrons} + \nu_\tau) \approx 1:1:N \qquad (1.7)$$

if the semihadronic decays could be calculated using a naive pointlike coupling of the lepton decay currents to quarks as in Fig. 7. Experimentally, the ratios of these decays are about[32] 1:1:0(4), but we would not expect the pointlike approximation to quark couplings to be exact at the low Q^2 involved in τ decay. The fact that the result (1.7) is even approximately correct indicates that the couplings of the weak current to the low mass hadronic resonances which dominate τ decay[31,32] must somehow average out to look like the pointlike coupling to three colours of quark. It indicates that resonance couplings have some sensitivity to the number of colours.[33]

The above arguments indicate that quarks have a threefold colour degree of freedom. QCD[4] certainly provides colour with something to do, but is there some good reason why gluons should not couple to the flavour group? The simultaneous consideration of strong, weak and electromagnetic interactions provides a possible answer, in that parity and strangeness conservation in $O(\alpha)$ can only be guaranteed[34] if the strong and weak symmetry groups are disjoint and commute. This condition is satisfied by QCD with its couplings to colour rather than flavour. It is an example that nontrivial constraints may be imposed on the theory of the strong interactions by the requirement of consistency with our ideas about gauge theories of the weak interactions.[2,12] Another such interconnection arises from considerations of CP violation,[35] and we will return to it in the fourth lecture. In the meantime we will concentrate on purely strongly strong interaction problems.

1.2 The Parton Model and Corrections in Field Theory

In the naive parton model[5] of Fig. 2, the collision of a virtual photon, Z^0 or $W^\pm$ with a hadron target is viewed in terms of incoherent

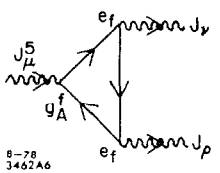

Fig. 6. The fermion triangle diagram which gives anomalies.

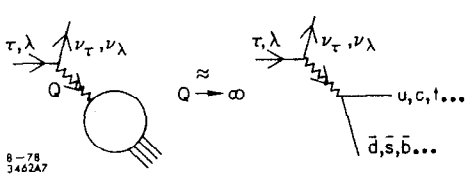

Fig. 7. A parton approximation for semihadronic decays of heavy leptons.

collisions with pointlike parton constituents to be identified as quarks. Because a point has no intrinsic scale, the deep inelastic cross sections would then exhibit naive Bjorken scaling behaviour,[14] and could be simply expressed in terms of quark parton distributions q(x), where $x \equiv -q^2/2p\cdot q$ is the longitudinal momentum fraction of the quark in an infinite momentum frame. Thus we have the usual deep inelastic structure functions

$$W_1^{eN}(\nu,q^2) \to F_1^{eN}(x) = \frac{1}{2}\sum_{q=u,d,\ldots} e_q^2(q(x) + \bar{q}(x))$$

$$\nu W_2^{eN}(\nu,q^2) \to F_2^{eN}(x) = \sum_{q=u,d,\ldots} e_q^2\, x(q(x) + \bar{q}(x))$$

$$\nu W_2^{\nu N}(\nu,q^2) \to F_2^{\nu N}(x) = 2x(d(x) + \bar{u}(x) + \ldots)$$

$$\nu W_3^{\nu N}(\nu,q^2) \to F_3^{\nu N}(x) = 2(\bar{u}(x) - d(x)) + \ldots \qquad (1.8)$$

Notice that in the naive parton model the Callan-Cross relation[36] applies:

$$2xF_1(x) = F_2(x) \qquad (1.9)$$

This relation and the scaling of deep inelastic structure functions apply only because the transverse momenta of the partons are cutoff arbitrarily[5] --probably to 0 (few hundred GeV). It is also supposed that struck partons fragment into final state hadrons with finite transverse momenta, producing jets in the final state,[13] as indicated in Fig. 8. An alternative way of expressing the scaling laws (1.8) is to allow for the possibility that the quark distributions may depend on the momentum transfer $Q^2 \equiv -q^2$ by defining

$$\nu W_2^{eN}(\nu,q^2) \equiv \sum_{q=u,d,\ldots} e_q^2\, x(q(x,Q^2) + \bar{q}(x,Q^2)) \qquad (1.10)$$

and then observing that the laws (1.8) correspond to

$$Q^2 \frac{\partial}{\partial Q^2} q(x,Q^2) = 0 \tag{1.11}$$

We have introduced the logarithmic derivative $Q^2 \frac{\partial}{\partial Q^2}$ in order to keep the left-hand side of Eq. (1.11) dimensionless.

In a renormalizable field theory, the Bjorken scaling predictions (1.8) or (1.11) do not hold,[37] as can be seen by calculating any Feynman diagram. For example, the bremsstrahlung diagrams of Fig. 9(a) and the pair creation diagrams of Fig. 9(b) both depend logarithmically on the Q^2 with which the quark or gluon parton is struck. These diagrams therefore tell us that

$$\begin{aligned} 0 \neq Q^2 \frac{\partial}{\partial Q^2} q(x,Q^2) &= O\left(\frac{\alpha_s}{\pi}\right) + \ldots \\ 0 \neq Q^2 \frac{\partial}{\partial Q^2} G(x,Q^2) &= O\left(\frac{\alpha_s}{\pi}\right) + \ldots \end{aligned} \tag{1.12}$$

where α_s is the strong interaction coupling constant $\alpha_s = g^2/4\pi$ in QCD, $G(x,Q^2)$ is the effective gluon distribution, and the dots in Eq. (1.12) include possible higher order terms from more complicated diagrams. The naive parton model[5] assumes that $\alpha_s/\pi \to 0$ at large Q^2, so that the quarks and gluons can be regarded as essentially free in this kinematic limit. The same assumption underlies the parton calculation of the e^+e^- total cross section in terms of the free quark-parton loop[13] of Fig. 1.

It is easy to deduce some qualitative physical implications[38] from the character of the fundamental processes in Fig. 9. The effect of both bremsstrahlung and pair creation is to generate an increase in the density of partons at small x as the momenta of the parent quark-partons

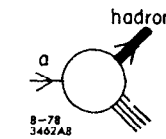

Fig. 8. A quark-parton fragmenting into hadrons.

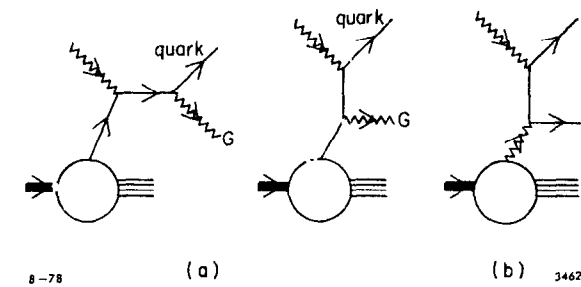

Fig. 9. Strong radiative corrections to leptoproduction cross sections from (a) bremsstrahlung and (b) pair creation.

are degraded. Therefore a typical deep inelastic structure function which is quite broad in x at moderately low Q^2 will move in towards x=0 as $Q^2 \to \infty$, decreasing at large x, and rising towards x=0 as indicated in Fig. 10(a). This process may be envisioned intuitively[39] by thinking of the virtual photon (or Z, or W) probe as a sort of microscope with spatial resolution $\Delta x = O(1/Q)$. Therefore a low Q^2 photon will have poor resolution, while a high Q^2 photon will have better resolution. Perhaps it will resolve a parton seen by the low Q^2 probe into a larger number of smaller constituents, each of which has a smaller longitudinal momentum fraction x, as illustrated in Fig. 11. For example, in $O(\alpha_s)$ in QCD, a quark may be resolved into a quark + gluon (corresponding to the bremsstrahlung of Fig. 9(a)) and a gluon may be resolved into a $q\bar{q}$ or gluon pair (corresponding to the pair creation of Fig. 9(b) in the gluon field of the hadron). The fundamental processes at the root of scaling violation are therefore seen to be radiative corrections analogous to those familiar from high energy electromagnetic showers in QED.

So far we have not made much use of the specific features of QCD--most field theories have some sort of gluon, and the basic Feynman diagrams and resulting qualitative picture (Fig. 10(a)) of scaling violations is common to many field theories.[37,38,39] Thus the observation[15,40] of this general trend as in Fig. 10(b) is not conclusive evidence in favour of QCD rather than any other field theory. However, there is one feature of QCD which is unique, yields a connection with the parton model and enables quantitative predictions as in Fig. 10(c) to be made--the property of asymptotic freedom.[22]

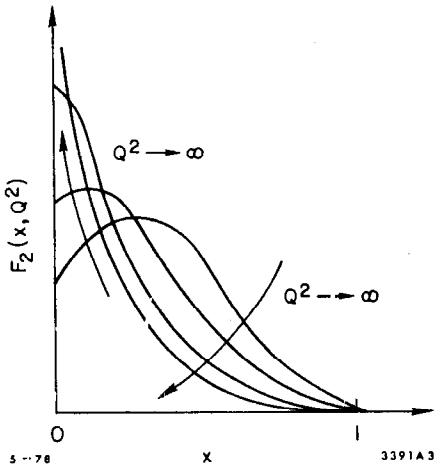

Fig. 10(a). Deviations from scaling in leptoproduction--intuitive expectation.[28,39]

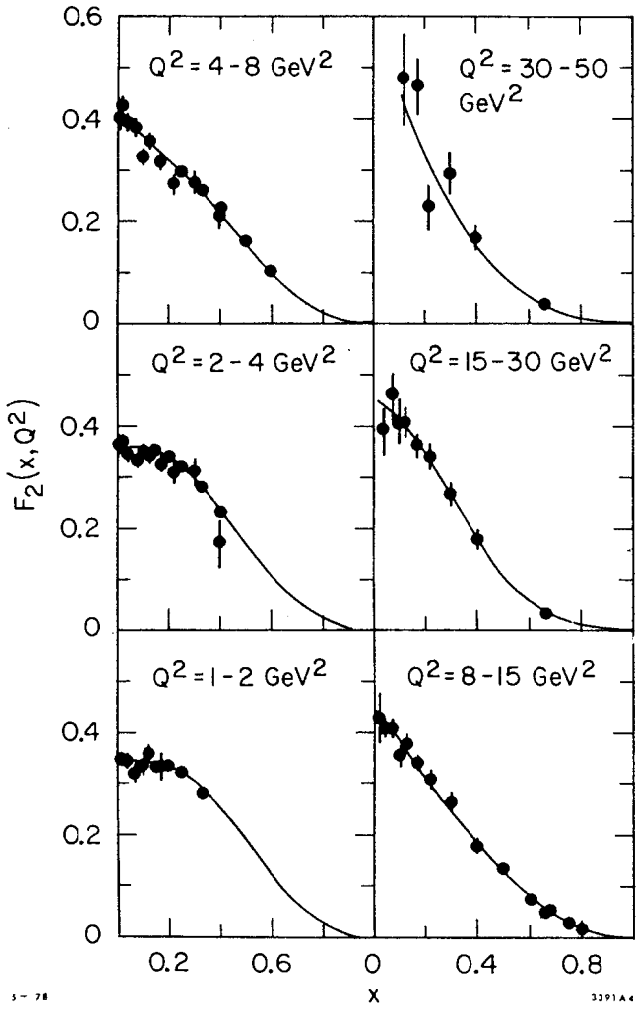

Fig. 10(b). Deviations from scaling in leptoproduction--experimental data.[40]

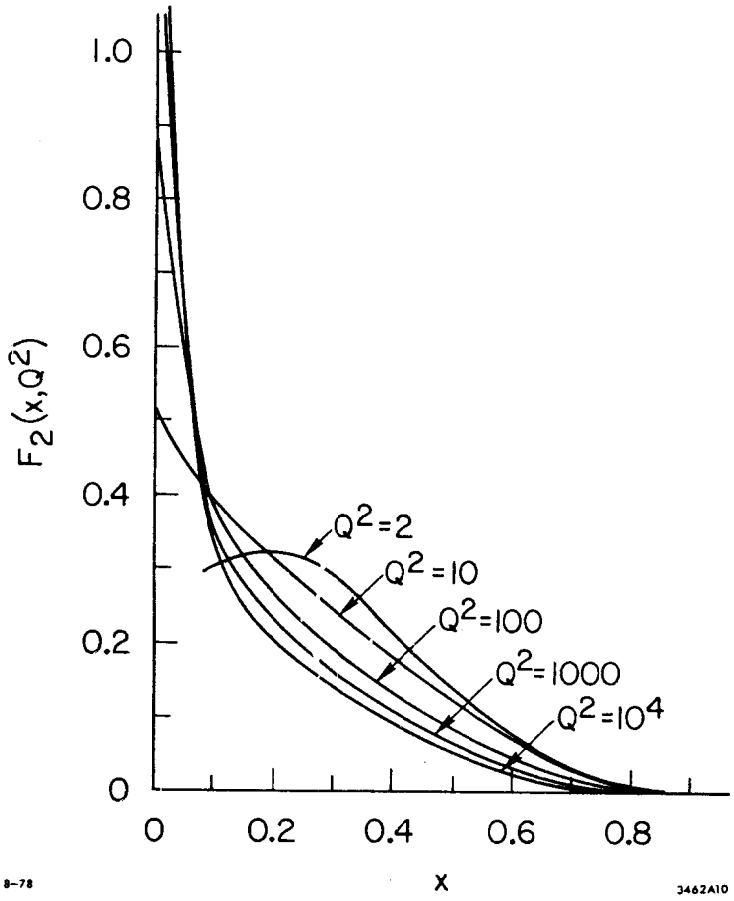

Fig. 10(c). Deviations from scaling in leptoproduction--a typical QCD calculation.

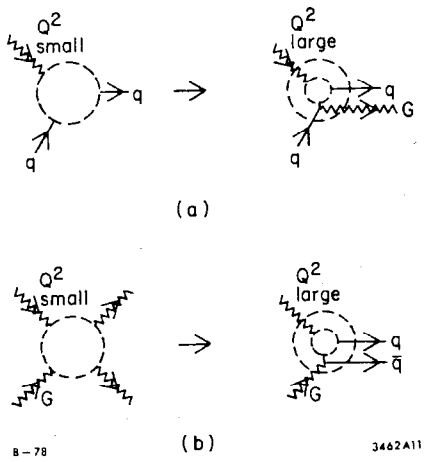

Fig. 11. As Q^2 increases (a) a quark may be resolved into a quark + gluon, (b) a gluon may be resolved into a quark-antiquark pair as the spatial discrimination of the probe increases.

The point is that in a field theory the basic vertex g depends on the momenta q which are fed into it. In perturbation theory as in Fig. 12

$$g \to g + O(g^3 \ln q^2) + O(g^5 \ln^2 q^2) + \ldots \qquad (1.13)$$

Fortunately, in QCD the leading logarithms can be summed exactly and give an effective constant which decreases to zero as $Q^2 = q^2 \to \infty$ (Ref. 22):

$$\alpha_s(Q^2) = \frac{g^2(Q^2)}{4\pi} \underset{Q^2\to\infty}{\approx} \frac{12\pi}{(33-2f)\ln\left(\frac{Q^2}{\Lambda^2}\right)} \qquad (1.14)$$

In formula (1.14) f is the number of quark flavours and Λ^2 is an a priori unknown scale which sets the scale of the Q^2 development of the coupling $\alpha_s(Q^2)$. The complication of a Q^2 dependent coupling does not concern us in QED because the rate of change--$O(\alpha \ln Q^2)$--is very small. In QCD the scale parameter Λ replaces the QED parameter as a way of specifying the strength of the interaction. The derivation[22] of (1.14) will not be discussed in these lectures, though we will see a tantalizing reflection of it later on in this lecture. Instead we will occupy ourselves with exploring the consequences of asymptotic freedom. The general effect will clearly be that perturbation theory for the strong interactions should become evermore applicable as the typical momentum transfer Q^2 of a process $\to \infty$. However, the relatively slow rate of decrease (1.14) of $\alpha_s(Q^2)$ means that one does not always recover the naive scaling expectations of the naive parton model, as we now see.

1.3 Scaling Violations in QCD

In the previous section we saw that naive scaling correspond to $Q^2 \frac{\partial}{\partial Q^2} q(x,Q^2) = 0$, as in the naive parton model, whereas one might expect $Q^2 \frac{\partial}{\partial Q^2} q(x,Q^2) = O\left(\frac{\alpha_s}{\pi}\right) + \ldots$ in an interacting field theory. In QCD where $\alpha_s(Q^2) \to 0$ as $Q^2 \to \infty$, we might hope that the $O\left(\frac{\alpha_s}{\pi}\right)$ approximation to the Q^2 evolution of $q(x,Q^2)$ might be very good. In this order, the only contributions in $O\left(\frac{\alpha_s}{\pi}\right)$ are the basic bremsstrahlung and pair creation processes of Fig. 9, and the rates for them are proportional to $\log Q^2$. The quark parton distribution is characterized by the longitudinal momentum fraction x, and the bremsstrahlung and pair creation probabilities may be written in terms of the longitudinal momentum fraction z carried by the final state parton as in Fig. 13. We therefore specify $P_{A\to B}(z)$ as the probability of parton A emitting a parton B with longitudinal momentum fraction z when Q^2 is changed by dQ^2: by dimensional analysis

$$dP \equiv \left(\frac{\alpha_s}{2\pi}\right) P_{A\to B}(z)\, dz\, \frac{dQ^2}{Q^2} \qquad (1.15)$$

The situation in QCD is analogous to that in QED, where in the Weizsäcker-Williams equivalent photon approximation[41] we talk in terms of the photon density inside an electron being

$$\left(\frac{\alpha}{2\pi}\right)\left(\frac{1 + (1-z)^2}{z}\right) \ln\left(\frac{E}{m_e}\right) \qquad (1.16)$$

corresponding to

$$P_{e\to\gamma} = \left(\frac{1 + (1-z)^2}{z}\right) \qquad (1.17)$$

The density of gluons in a quark is analogous, the only difference being a group theoretical factor from the colour coupling (1.3) of the gluon

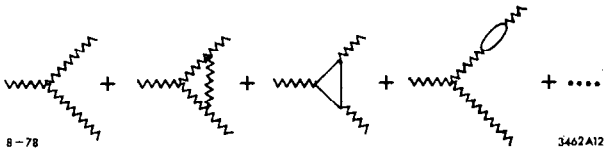

Fig. 12. Some contributions to the 3 gluon vertex g.

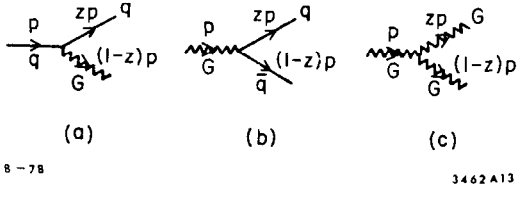

Fig. 13. The basic vertices responsible for the leading order of scaling violations in the evolution equations: (a) $q \to q+G$ (b) $G \to q+\bar{q}$ and (c) $G \to G+G$.

field:

$$\frac{1}{N}\sum_a \left(\frac{\lambda^a}{2}\right)\left(\frac{\lambda^a}{2}\right) = \frac{N^2-1}{2N} = \frac{4}{3} \qquad (1.18)$$

so that the final "splitting function" for q → G of Fig. 13(a) is:

$$P_{q\to G}(z) = \frac{4}{3}\left[\frac{1+(1-z)^2}{z}\right] \qquad (1.19)$$

We can[42] write down the "evolution equations" of the form (1.12) which apply in QCD, just by looking at the basic interactions of Fig. 13:

$$Q^2\frac{\partial}{\partial Q^2}\, q(x,Q^2) = \left(\frac{\alpha_s}{2\pi}\right)\int_x^1 \frac{dy}{y}\left[q(y,Q^2)P_{q\to q}\left(\frac{x}{y}\right) + G(y,Q^2)P_{G\to q}\left(\frac{x}{y}\right)\right] \qquad (1.20)$$

for quarks and

$$Q^2\frac{\partial}{\partial Q^2}\, G(x,Q^2) = \left(\frac{\alpha_s}{2\pi}\right)\int_x^1 \frac{dy}{y}\left[q(y,Q^2)P_{q\to G}\left(\frac{x}{y}\right) + G(y,Q^2)P_{G\to G}\left(\frac{x}{y}\right)\right] \qquad (1.21)$$

for gluons. Because of the slow logarithmic decline (1.14) of $\alpha_s(Q^2)$, the evolution equations (1.20) imply that the parton distributions $q(x,Q^2)$ and $G(x,Q^2)$ do not scale exactly.

The pattern of scaling violation in QCD is well known,[4,22,43] and usually expressed in terms of theoretically precise, but experimentally arcane, numbers called anomalous dimensions. The connection between our physical picture[38,39] and the academic formalism[4,43] is easily made.[42] Let us consider x moments of the structure functions such as

$$M_n^{(2)}(Q^2) = \int_0^1 dx\, x^{n-2}\, F_2(x,Q^2) \qquad (1.22)$$

which is the type of quantity for which rigorous predictions of QCD are usually expressed.[43] QCD makes predictions[43] of logarithmic violations of scaling:

$$M_n^{(2)}(Q^2) \sim (\ln Q^2)^{-d_n} \qquad (1.23)$$

whereas other field theories[21] are expected to violate scaling by powers[38,39] of Q^2. From the parton expression (1.10) we see that generically

$$M_n^{(2)}(Q^2) = \int_0^1 dx\, x^{n-1}\, q(x,Q^2) \qquad (1.24)$$

Let us first consider a flavour nonsinglet combination of quark distributions, such as $u(x,Q^2) - d(x,Q^2)$ which is relevant to the ep-en cross section difference, or $\bar{u}(x,Q^2) - d(x,Q^2)$ which is seen from Eq. (1.8) to be relevant to $F_3^N(x,Q^2)$. The gluon term in the evolution equation (1.20) does not contribute to such a nonsinglet quark distribution $q^{NS}(x,Q^2)$:

$$Q^2\frac{\partial}{\partial Q^2}\, q^{NS}(x,Q^2) = \left(\frac{\alpha_s}{2\pi}\right)\int_x^1 \frac{dy}{y}\, q^{NS}(y,Q^2)\, P_{q\to q}\left(\frac{x}{y}\right) \qquad (1.25)$$

If we take the moment $\int_0^1 dx\, x^{n-1}$ of this equation the left-hand side is $Q^2\frac{\partial}{\partial Q^2} M_n(Q^2)$ and the right-hand side of Eq. (1.25) factorizes neatly:

$$Q^2\frac{\partial}{\partial Q^2} M_n(Q^2) = \frac{\alpha_s}{2\pi} A_n M_n(Q^2) \qquad (1.26)$$

where

$$A_n \equiv \int_0^1 dz\, z^{n-1}\, P_{q\to q}(z) \qquad (1.27)$$

The solution of Eq. (1.26) is quite simple: introducing the notation

$$\alpha_s(Q^2) \approx \frac{1}{b\ln\frac{Q^2}{\Lambda^2}} : b = \frac{33-2f}{12\pi} \qquad (1.28)$$

from Eq. (1.14), we see that Eq. (1.26) implies

$$M_n(Q^2) \approx \bar{M}_n\,(\ln Q^2)^{A_n/2\pi b} \qquad (1.29)$$

Making the comparison with the conventional QCD prediction[4,43] (1.23) it clearly is possible to identify

$$d_n = -\frac{A_n}{2\pi b} \qquad (1.30)$$

so that we are able to calculate the famous anomalous dimensions as soon as we determine the "splitting function" $P_{q\to q}(z)$.[42]

Before doing this, let us just discuss the singlet combinations of parton distributions, which obey somewhat more complicated evolution equations. If we introduce the singlet distribution

$$q^S(x,Q^2) \equiv \sum_{i=1}^{f} \left(q_i(x,Q^2) + \bar{q}_i(x,Q^2)\right) \tag{1.31}$$

it is apparent from Eqs. (1.20) and (1.21) that $q^S(x,Q^2)$ and $G(x,Q^2)$ obey a coupled pair of evolution equations. If we take the moments $\int_0^1 dx\, x^{n-1}$ of these equations we obtain[42] a set of matrix equations

$$Q^2\frac{\partial}{\partial Q^2}\begin{pmatrix} S_n(Q^2) \\ G_n(Q^2)\end{pmatrix} = \left(\frac{\alpha_s}{2\pi}\right)\begin{pmatrix} A_n & 2fB_n \\ C_n & D_n\end{pmatrix}\begin{pmatrix} S_n(Q^2) \\ G_n(Q^2)\end{pmatrix} \tag{1.32}$$

where S_n and G_n are the moments of the singlet quark distribution

$$S_n(Q^2) \equiv \int_0^1 dx\, x^{n-1}\, q^S(x,Q^2) \tag{1.33a}$$

and gluon distribution

$$G_n(Q^2) \equiv \int_0^1 dx\, x^{n-1}\, G(x,Q^2) \tag{1.33b}$$

respectively. On the right-hand side of Eq. (1.32) the matrix elements A_n were defined in Eq. (1.27), while we have introduced

$$B_n \equiv \int_0^1 dz\, z^{n-1}\, P_{G\to q}(z) \qquad C_n \equiv \int_0^1 dz\, z^{n-1}\, P_{q\to G}(z)$$

$$D_n \equiv \int_0^1 dz\, z^{n-1}\, P_{G\to G}(z) \tag{1.34}$$

The solution of the coupled equations (1.32) is quite straightforward. First you must diagonalize the matrices on the right-hand sides

$$\begin{pmatrix} A_n & 2fB_n \\ C_n & D_n\end{pmatrix} \to \begin{pmatrix} A_n^+ & 0 \\ 0 & A_n^-\end{pmatrix} \tag{1.35}$$

which must be done separately for each moment n. Then the eigenvector combinations of $S_n(Q^2)$ and $G_n(Q^2)$ evolve separately, with the result that a singlet moment

$$M_n^S(Q^2) \sim \bar{M}_n^+(\ln Q^2)^{d_n^+} + \bar{M}_n^-(\ln Q^2)^{d_n^-} \tag{1.36}$$

where the singlet anomalous dimensions $d_n^\pm$ are determined similarly to the nonsinglet anomalous dimension

$$d_n^\pm = -\frac{A_n^\pm}{2\pi b} \tag{1.37}$$

Thus the scaling violations in singlet combinations of structure functions (1.36) are somewhat more devious than those in nonsinglet combinations. As an added complication, many physically observable structure functions such as $F_2^{eF}(x,Q^2)$ or $F_2^{\nu N}(x,Q^2)$ are in fact combinations of singlet and nonsinglet structure functions, so that all three terms (1.29) and (1.36) are necessary to fit the data.

1.4 Calculation of the Anomalous Dimensions

We saw in the previous section how the calculation of the anomalous dimensions reduces[42] to the determination of the splitting functions $P_{A\to B}(z)$, and we now proceed to evaluate them. First note that there are certain trivial constraints which must be satisfied by the splitting functions. For example, quark number is conserved in the bremsstrahlung

process, so that

$$\int_0^1 dz\, P_{q\to q}(z) = 0 \qquad (1.38)$$

Also, since it is clear that if you have a quark with momentum fraction z you must have a gluon with momentum fraction (1-z):

$$P_{q\to q}(z) = P_{q\to G}(1-z) \qquad (1.39)$$

The relations (1.38) and (1.39) between them imply that the $P_{q\to q,G}(z)$ obey the momentum conservation condition

$$\int_0^1 dz\, z\left[P_{q\to q}(z) + P_{q\to G}(z)\right] = 0 \qquad (1.40)$$

and there is a corresponding condition for gluon momentum conservation

$$\int_0^1 dz\, z\left[P_{G\to q}(z) + P_{G\to G}(z)\right] = 0 \qquad (1.41)$$

Between them, the momentum conservation conditions (1.40) and (1.41) ensure that the total momentum of the hadron target is conserved:

$$Q^2\frac{\partial}{\partial Q^2}\int_0^1 dx\, x\left[\sum_{i=1}^{f}\left(q_i(x,Q^2)+\bar{q}_i(x,Q^2)\right) + G(x,Q^2)\right] = 0 \qquad (1.42)$$

We will use the conditions (1.38) to (1.41) in a moment to determine the contribution to the splitting functions corresponding to partons which do not interact, corresponding to $\delta(z-1)$ pieces in $P_{q\to q}(z)$ and $P_{q\to q}(z)$.

To determine the $P_{A\to B}(z)$ we first recall the modified Weizsäcker-Williams[41] formula (1.19):

$$P_{q\to G}(z) = \frac{4}{3}\left[\frac{1+(1-z)^2}{z}\right] \quad \text{for } z>0$$

The reciprocity relation (1.39) immediately tells us that

$$P_{q\to q}(z) = \frac{4}{3}\left[\frac{1+z^2}{1-z}\right] \quad \text{for } z<1$$

which unfortunately has a singularity at z=1 which must be regularized. Altarelli and Parisi[42,44] choose to do this by replacing

$$\frac{1}{(1-z)} \to \frac{1}{(1-z)_+}$$

which is defined for f(z) regular at z=1 by

$$\int_0^1 dz\, \frac{f(z)}{(1-z)_+} \equiv \int_0^1 dz\, \frac{f(z)-f(1)}{1-z} \qquad (1.43)$$

The regularized form of $P_{q\to q}(z)$ does not obey the sum rule (1.38) and must be supplemented by a suitably chosen piece $\propto \delta(z-1)$:

$$P_{q\to q}(z) = \frac{4}{3}\left[\frac{1+z^2}{(1-z)_+} + \frac{3}{2}\,\delta(z-1)\right] \qquad (1.44)$$

An elementary calculation[45] of the $q\to q\bar{q}$ pair creation vertex yields

$$P_{G\to q}(z) = \frac{1}{2}\left[z^2 + (1-z)^2\right] \qquad (1.45)$$

which is symmetric between z and (1-z). Finally one can calculate the z<1 part of $P_{G\to G}$ to be

$$P_{G\to G}(z) = 6\left(\frac{z}{1-z} + \frac{1-z}{z} + z(1-z)\right) \quad \text{for } z<1 \qquad (1.46)$$

which regularization and the application of the momentum conservation condition (1.41) cause to become

$$P_{G\to G}(z) = 6\left(\frac{z}{(1-z)_+} + \frac{1-z}{z} + z(1-z) + \left(\frac{11}{12} - \frac{f}{18}\right)\delta(z-1)\right) \qquad (1.47)$$

It should be emphasized at this point that the form of the splitting functions (1.19, 1.44, 1.45, 1.47) depends sensitively on the spin of the

gluon. For example, if we had scalar gluons we would have

$$P^{(S)}_{q\to q} \propto (1-z) - \frac{1}{2}\,\delta(z-1) \tag{1.48}$$

at lowest order in the $q\bar{q}$-scalar gluon coupling. We will see in a moment that the forms (1.44) and (1.48) produce very different anomalous dimensions which can be distinguished experimentally.

We are now in a position to compute the anomalous dimensions by taking the moments of the $P_{A\to B}(z)$ (1.19, 1.44, 1.45, 1.47). We find

$$A_n \equiv \int_0^1 dz\, z^{n-1} P_{q\to q}(z) = \frac{4}{3}\left(-\frac{1}{2} + \frac{1}{n(n+1)} - 2\sum_{j=2}^{n}\frac{1}{j}\right) \tag{1.49a}$$

$$B_n \equiv \int_0^1 dz\, z^{n-1} P_{G\to q}(z) = \frac{1}{2}\left(\frac{2+n+n^2}{n(n+1)(n+2)}\right) \tag{1.49b}$$

$$C_n \equiv \int_0^1 dz\, z^{n-1} P_{q\to G}(z) = \frac{4}{3}\left(\frac{2+n+n^2}{n(n^2-1)}\right) \tag{1.49c}$$

$$D_n \equiv \int_0^1 dz\, z^{n-1} P_{G\to G}(z) = 3\left(-\frac{1}{6} + \frac{2}{n(n-1)} + \frac{2}{(n+1)(n+2)} - 2\sum_{j=2}^{n}\frac{1}{j} - \frac{f}{9}\right) \tag{1.49d}$$

which are the familiar results of more sophisticated field theoretical calculations.[4,43] Hopefully they have been demystified slightly!

How do the predictions of QCD for scaling violations in the moments of the deep inelastic structure functions compare with the experimental data?[15] This question is addressed in more detail by Don Perkins in his lectures, but let us just pick out a few important points here and now. Consider a nonsinglet structure function, such as $F_2^{ep}-F_2^{en}$, or $F_3^{\nu N}$. Then QCD predicts[43] that

$$M_n(Q^2) \sim \bar{M}_n(\ln Q^2)^{-d_n} \tag{1.50}$$

with d_n given by (1.30) and (1.49a). The forms (1.50) imply that

$$\ln M_n(Q^2) \approx -d_n \ln Q^2 + (\text{constant})_n \tag{1.51}$$

If we compare the logarithms of two moments M_n and $M_{n'}$, we shoud find[18] a straight line with slope

$$\frac{d_n}{d_{n'}} = \frac{A_n}{A_{n'}} = \frac{\left(-\frac{1}{2} + \frac{1}{n(n+1)} - 2\sum_{j=2}^{n}\frac{1}{j}\right)}{\left(-\frac{1}{2} + \frac{1}{n'(n'+1)} - 2\sum_{j=2}^{n'}\frac{1}{j}\right)} \tag{1.52}$$

The BEBC[18] data for the n=3,4,5 and 6 moments of $F_3^{\nu N}$ agree very well with the QCD predictions (1.52) as shown in Fig. 14. The best fit values for $d_n/d_{n'}$, obtained from the data are compared with QCD in the table below:

TABLE I

	d_5/d_3	d_7/d_3	d_6/d_4
QCD	1.46	1.76	1.29
Scalar Gluon Theory	1.12	1.16	1.06
Experiment	1.50 ± 0.08	1.84 ± 0.20	1.29 ± 0.06

For comparison, we have also included the "predictions"[46] of a scalar gluon theory. If such a theory were to have a coupling g which went to some small fixed value g* as $Q^2 \to \infty$--the only possible way of fixing to get approximate scaling in such a theory--then the moments would scale approximately as

$$M_n(Q^2) \sim \bar{M}_n(Q^2)^{-\delta_n} \tag{1.53}$$

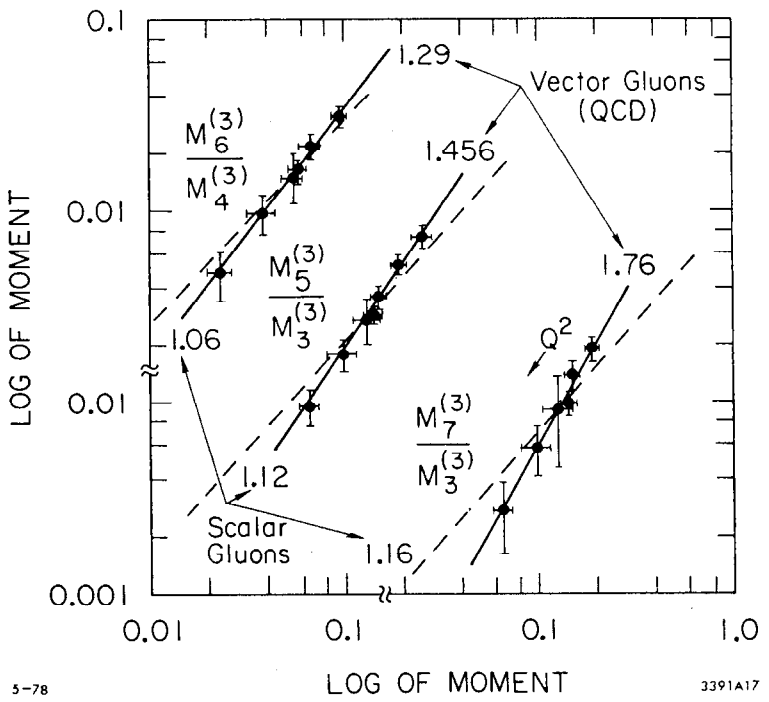

Fig. 14. BEBC[18] data on several moments $M_n^{(3)}(Q^2)$ of the F_3 structure function plotted logarithmically (cf. Eq. (1.51)). Different theories that the data should fall on straight lines with the slopes indicated.

where

$$\delta_n \propto \alpha_n \equiv \int_0^1 dz\, z^{n-1}\, P_{q\to q}^{(S)}(z) \tag{1.54}$$

$$= \left(-\frac{1}{2} + \frac{1}{n(n+1)}\right) \tag{1.55}$$

Plots of the logarithms of the moments should then be straight lines with slopes $\delta_n/\delta_{n'}$, which Eq. (1.55) reveals to be very different from $d_n/d_{n'}$ given by Eq. (1.52). Figure 14 shows that the BEBC[18] data disagree[47] emphatically with the scalar gluon "predictions" (1.55) while agreeing very well with the QCD predictions (1.52). This amounts to a convincing demonstration that the quarks are bremsstrahling vector gluons rather than scalars--the first determination that the gluon spin = 1?

Another important point about the BEBC[18] data is that they indicate a logarithmic, rather than power law variation of the moments with Q^2. If we consider the quantity $M_n(Q^2)^{-1/d_n}$, then QCD (1.50) predicts that it should vary linearly with $\ln Q^2$, and this is consistent with the data shown in Fig. 15. Suppose that the moments had in fact behaved as

$$M_n(Q^2) \sim \bar{M}_n(Q^2)^{-\beta d_n} \tag{1.56}$$

as might have been expected in a (Abelian or non-Abelian) vector gluon theory with a small fixed point coupling g^* as $Q^2 \to \infty$. Then the quantities

$$\ln M_n(Q^2) = -\beta d_n Q^2 + (\text{constant})_n \tag{1.57}$$

as before (1.51), and the theory would also have passed the QCD test in Fig. 14. However

$$\left[M_n(Q^2)\right]^{-1/d_n} \propto (Q^2)^{\beta} \tag{1.58}$$

which fails[47] the test in Fig. 15. Shown for comparison with the straight line QCD fits to the moments are fits of the form (1.58) with the power β chosen[47] so as to give similar scaling violations to the data between Q^2=1 and 10 GeV^2. It is apparent that the data are not well fitted by these curves, and we conclude that such fixed point vector gluon theories are strongly disfavored.

So far we have only looked at nonsinglet combinations of structure functions. When we look at singlet structure functions, we get contributions to the scaling violations which come from the pair creation in the gluon field of Fig. 9(b), as well as the bremsstrahlung of Fig. 9(a). The BEBC[18] group have analyzed the $F_2^{\nu N}$ structure function using the amount of bremsstrahlung indicated by their analysis of $F_3^{\nu N}$. They find strong evidence for an extra contribution coming from pair creation. The amount of it is sensitive to the gluon distribution assumed, and they[18] find that the observed scaling violations are consistent with about $\frac{1}{2}$ the nucleon's momentum being carried by gluons, as found previously by just looking at $\int_0^1 dx\, F_2^{eN,\nu N}(x,Q^2)$.[17] The interested reader is referred to Ref. 18 and the lectures of Perkins for more details.

It seems that the QCD analysis of deep inelastic scaling violations is in very good shape, and probably constitutes the best experimental evidence to date in favour of the theory. Before abandoning completely the topic of deep inelastic scaling violations, it may be worth drawing attention to a few interesting aspects of the evolution equation formalism.

There are some important sum rules for deep inelastic scattering which depend on fundamental properties of the quark model. One example

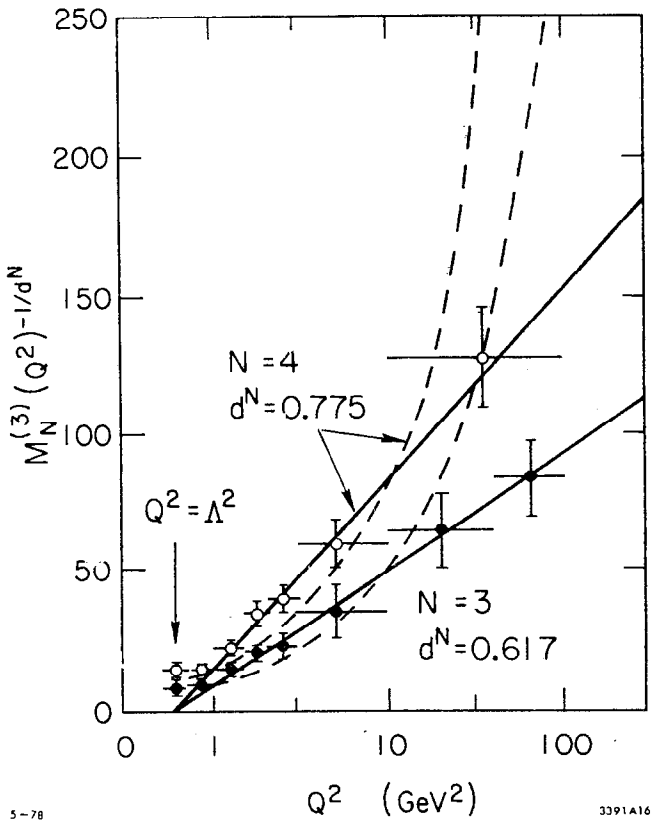

Fig. 15. Suitably chosen powers of $M_n^{(3)}(Q^2)$ [18] which QCD says should vary linearly with ln Q^2 (see text). The curves are attempts to fit the scaling violations with powers of Q^2.

is the Adler sum rule[48]

$$\int_0^1 \frac{dx}{2x}\left(F_2^{\bar{\nu}p} - F_2^{\nu p}\right) = \int_0^1 dx\left[u(x,Q^2) - \bar{u}(x,Q^2) - d(x,Q^2) + \bar{d}(x,Q^2)\right] \tag{1.59}$$

The right-hand side should be 1 at all Q^2. If we compute $Q^2\frac{\partial}{\partial Q^2}$ of the right-hand side we see that it is proportional to $\int_0^1 dz\, P_{q\to q}(z) = 0$, since the right-hand side of (1.59) is the n=1 moment of a nonsinglet combination of quark distributions. Thus the "quark conservation" condition (1.38) ensures the validity of the Adler sum rule at all Q^2. A similar analysis applies to the Gross-Llewellyn Smith[49] sum rule

$$\int_0^1 dx\left(F_3^{\nu p} + F_3^{\bar{\nu}p}\right) = -2\int_0^1 dx\left[u(x,Q^2) + d(x,Q^2) - \bar{u}(x,Q^2) - \bar{d}(x,Q^2)\right] = -6 \tag{1.60}$$

Another interesting sum rule, which is specific to QCD and unobtainable in the naive parton model, is the momentum sum rule.[43] Let us consider the n=2 moment of the F_2 structure function, which corresponds to combinations of $\int_0^1 dx\, x\, q(x,Q^2)$. From Eq. (1.32) we have

$$Q^2\frac{\partial}{\partial Q^2} S_2(Q^2) = \left(\frac{\alpha_s}{2\pi}\right)\left[A_2 S_2(Q^2) + 2f\, B_2 G_2(Q^2)\right] \tag{1.61}$$

Let us look for the possibility that $S_2(Q^2)$, the momentum fraction carried by quarks and antiquarks, is independent of Q^2: this will happen if

$$A_2 S_2(Q^2) + 2f\, B_2 G_2(Q^2) = 0 \tag{1.62}$$

The condition (1.62) can be regarded as a relation for the quark and gluon momentum fractions:

$$\frac{S_2(Q^2)}{G_2(Q^2)} = \frac{-2fB_2}{A_2} = \frac{3f}{16} \tag{1.63}$$

Since momentum conservation (1.42) ensures that $S_2(Q^2) + G_2(Q^2) = 1$, the condition (1.63) is sufficient to ensure that the momentum fractions carried by both quarks and gluons are independent of Q^2. The condition (1.62) amounts to a sort of equilibrium condition that the amount of momentum that quarks lose to gluons by bremsstrahlung is the same as that which gluons give to quarks by pair creation. This equilibrium can be reached as $Q^2\to\infty$, in which limit[43]

$$\int_0^1 dx\, F_2^{eN}(x,Q^2) = \int_0^1 dx\, x \sum_q \left[q(x,Q^2) + \bar{q}(x,Q^2)\right] e_q^2 \underset{Q^2\to\infty}{\longrightarrow} \frac{3f}{16+3f}\left\langle e_q^2\right\rangle \tag{1.64}$$

where the average quark (charge)^2 $\left\langle e_q^2\right\rangle$ is presumably equal to 5/18 because of equal numbers of charge 2/3 and charge -1/3 quarks. The experimental data are consistent with the asymptotic behaviour (1.64) applying for either f=4 or 6. This momentum equilibrium sum rule clearly cannot be derived in the naive parton model,[3] because it relies on the right-hand side of the evolution equation (1.61) being nonzero. In the absence of interactions it is never possible to reach equilibrium. One might wonder what the equilibrium conditions on the higher (n>2) moments of the quark and gluon moment S_n and G_n might be. It is easy to satisfy oneself that there are two independent equations for each such moment which are only satisfied if

$$S_n(Q^2) = G_n(Q^2) = 0 \qquad \text{for all } n > 2 \tag{1.65}$$

The only solutions to the combined equations (1.63) and (1.65) are distributions with singular support at x=0, as suggested by our intuitive reasoning in Section 1.2. The conditions (1.63) and (1.65) are the ultimate fate of all hadrons at large Q^2: the quantum chromodynamic "heat death".

Before leaving the evolution equations[42] (1.20) and (1.21) it may be amusing to point out one intriguing feature of the gluon splitting function $P_{G\to G}(z)$ in Eq. (1.47). The coefficient of the $\delta(z-1)$ piece is directly proportional to the lowest order term in the renormalization of the QCD coupling constant (β function), the coefficient b in Eq. (1.14) or (1.28). Is this a coincidence or a profound truth? I don't know, but it would imply that a gluon--whose "gluon in a gluon" distribution $G(x,Q^2)$ would have a $\delta(x-1)$ piece--would become more "pure"--the $\delta(x-1)$ piece would increase as $Q^2\to\infty$--because of the positive value of the coefficient of $\delta(z-1)$ in $P_{G\to G}(z)$ (1.28) if the number of flavours f is ≤ 16. The increasing "purity" of the gluon wave function is perhaps a harbinger of asymptotic freedom--or perhaps not.

1.5 Search for the Smoking Gluon

So far we have only discussed indirect evidence for the gluon, such as the scaling derivations induced by bremsstrahlung of it and pair production from it. However, the gluon is a constituent of hadronic matter which is as basic as the quark. Therefore we would like to have equally direct evidence for the gluon's existence--from spectroscopy[50] and from jets,[8,13] for example. One effect of the gluons will be to induce scaling violations in the distribution of hadrons within a quark jet. The longitudinal momentum distribution will be softened at large Q^2 by bremsstrahlung and pair creation in a manner analogous to the effects we discussed for the deep inelastic structure functions. For example, if we introduce moments of the inclusive hadron distributions in e^+e^- annihilation

$$\sigma^n(Q^2) \equiv \int_0^1 dz\, z^{n-1} \frac{d\sigma}{dz}(z,Q^2) \tag{1.66}$$

where $z \equiv 2E_{hadron}/Q$, then $\sigma^n(Q^2)$ will exhibit logarithmic violations of scaling just like those (1.29, 1.36) found for deep inelastic leptoproduction, with "anomalous dimensions" simply related[31] to the traditional results (1.40).

Another characteristic of the bremsstrahlung and other field-theoretical processes is their large p_T tail.[7,39] Because the basic field-theoretical vertices have no dimensional scale,

$$\langle p_T^n \rangle \propto O\left(\frac{\alpha_s}{\pi}\right) Q^n \tag{1.67}$$

Of course $\alpha_s \sim 1/b \ln Q^2$ (1.14), but the $\langle p_T \rangle$ coming from (1.67) is much larger than the finite $\langle p_T \rangle = O(300)$ MeV usually observed in hadron-hadron collisions. This means that jets in e^+e^- annihilation or leptoproduction are best[8] described by angular cutoffs rather than field p_T cutoffs. For example, let us suppose in e^+e^- annihilation that the fundamental quanta (q,G) in the final state produce hadrons with finite momenta transverse to their momentum vectors. We can then calculate[52] in perturbation theory from Fig. 4 the probability F_q that a fraction $(1-\varepsilon)$ of the total e^+e^- centre-of-mass energy Q will be contained in some pair of oppositely directed cones of half angle δ:

$$F_q = 1 - \frac{\alpha_s(Q)}{\pi} 4\left\{\ln(2\varepsilon) + \frac{3}{4}\right\} \ln\delta + \text{terms with no logs} \tag{1.68}$$

For sufficiently large energies almost all of the e^+e^- events will fall into two angular jets.[8]

On the other hand, a fraction $O\left(\frac{\alpha_s}{\pi}\right)$ of the events come from hard gluons radiated outside the angular cones. The usual discussion would then suggest that these should show up as three jet final states, the third jet emitting from the metamorphosis of a gluon into hadrons.[8] The cross section for hard gluon bremsstrahlung was easy to calculate:

$$\frac{1}{\sigma_{total}} \frac{d\sigma}{dx_q dx_{\bar{q}}} = \left(\frac{2\alpha_s}{3\pi}\right) \frac{x_q^2 + x_{\bar{q}}^2}{(1-x_q)(1-x_{\bar{q}})} + \text{higher orders} \qquad (1.69)$$

where $x_q = 2E_q/Q$ and similarly for $x_{\bar{q}}$. Such final states would be convincing evidence of the reality of the gluon. A possible strategy[53] for finding such events might run as follows:

--First look for e^+e^- events where the final state hadrons are not highly collimated. This could be done by computing the thrust[54]

$$T \equiv \max \sum_{\text{hadrons}} \frac{|p_h^{\parallel}|}{|p_h|} \qquad (1.70)$$

where the maximization is with respect to the choice of the thrust axis, along which the $p_h^{\parallel}$ are measured. The cross section $\frac{1}{\sigma}\frac{d\sigma}{dT}$ can be calculated reliably[51,54] in QCD perturbation theory, because it does not depend on the details of the infrared properties of the theory which we do not understand[53]:

$$\frac{1}{\sigma}\frac{d\sigma}{dT} \approx \left(\frac{2\alpha_s}{3\pi}\right)\left[\frac{2(3T^2-3T+2)}{T(1-T)} \ln\left(\frac{2T-1}{1-T}\right) - \frac{3(3T-2)(2-T)}{(1-T)}\right] \qquad (1.71)$$

--In such events, find a plane containing the thrust axis which maximizes the sum of the moduli of the hadron momenta out of the plane. Events with only three fundamental quanta $(q,\bar{q},G)$ should define an event plane quite nicely.

--Orient events in the plane by setting $\theta=0^o$ to be along the thrust axis and heading into the hemisphere with smaller $\sum|p_T^h|$. Define the angular range $0<\theta<\pi$ to be the half of the event plane which has the larger amount of hadron energy.

--The events should now be oriented as in Fig. 16, and given any luck there should be a well-defined jet around $\theta=0$, another in the angular range $\frac{\pi}{2}<\theta<\pi$, and another in the range $\pi<\theta<\frac{3\pi}{2}$. To see whether the hadrons really come into three jets, it is first advisable to look at the half-plane $-\frac{\pi}{2}<\theta<\frac{\pi}{2}$, and check that the hadrons there have finite p_T relative to the thrust axis. If so, remove these hadrons and boost[53] the rest by an amount ζ:

$$\text{sh } \zeta = \frac{T}{2\sqrt{1-T}}, \quad \text{ch } \zeta = \frac{2-T}{2\sqrt{1-T}} \qquad (1.72)$$

The remaining hadrons should now have been boosted back to the centre-of-mass of the two putative jets in the half-plane $\frac{\pi}{2}<\theta<\frac{3\pi}{2}$ as in Fig. 17. Given any luck, an axis can be defined for the boosted hadrons relative to which their p_T are finite, and this axis will define the directions of the second and third jets.[55]

It will be interesting to see whether three jet events show up when this analysis is applied. One potential complication is that the $\langle p_T\rangle$ of hadrons in a gluon jet may be larger than the $\langle p_T\rangle$ for a quark jet. As emphasized above, the jets seen so far have a finite $\langle p_T\rangle$ which is not perturbative, and the relevance of the perturbative analysts is not obvious. Nevertheless, one can compute[56] that for a gluon jet the fraction F_G of events with $1-\varepsilon$ of the total energy E inside two oppositely

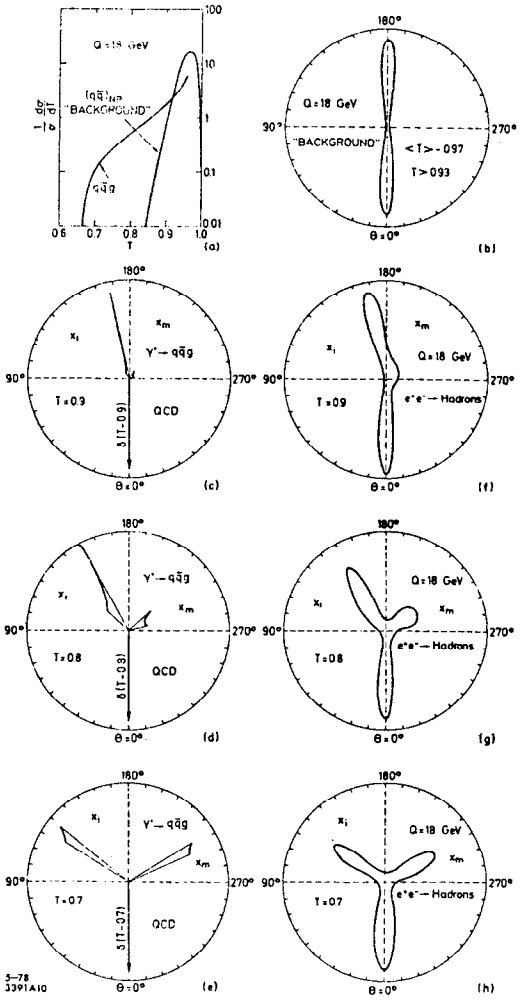

Fig. 16. The distribution of hadronic energy in e^+e^- annihilation expected[53] for different values of the thrust (1.70). (a), (c), (d) and (e) are the results of the perturbative cross section (1.60). (b), (f), (g) and (h) are the results of smearing quark and gluon jets with finite $\langle p_T \rangle$ for the hadrons.

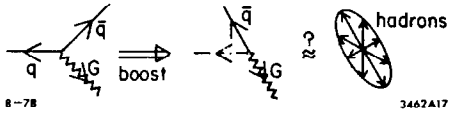

Fig. 17. The effect of the jet boost[53,55] (1.72) which should put the two right-hand jets into their joint centre-of-mass.

directed cones of half angle δ is

$$F_G \approx 1 - \frac{\alpha(E)}{\pi}\left\{12\ln(2\varepsilon) - \left(11 - \frac{2}{3}f\right)\right\}\ln\delta + (\text{finite terms}), \quad (1.73)$$

The perturbative width for small ε and δ is wider than that of (1.68) for a quark jet, but it is not clear whether this is relevant to the gluon jets to be looked for at presently accessible energies. An amusing aspect of the formula (1.73) is that the piece finite as $\varepsilon \to 0$ is again (cf. Eq. (1.47)) proportional to the renormalization (1.14) of the strong coupling constant $\alpha_s(Q^2)$. Coincidence or ...?

Finally, we should note that another good place[19] to look for gluon jets, besides the obvious e^+e^- annihilation and leptoproduction[57] reactions, is in the decay of a heavy quark-antiquark vector resonance such as the T. According to the charmonium model, the dominant decay mode should be into three gluons as in Fig. 5, with a differential cross section[17]

$$\frac{1}{\Gamma_{3G}}\frac{d\Gamma}{dx_1 dx_2} \approx \frac{1}{\pi^2 - 9}\left\{\frac{(1-x_1)^2}{x_2^2 x_3^2} + \frac{(1-x_2)^2}{x_1^2 x_3^2} + \frac{(1-x_3)^2}{x_1^2 x_2^2}\right\} \quad (1.74)$$

This would be an especially pure place to look for gluon jets, using the same jet-finding strategy[53] outlined above. The thrust distribution should be

$$\frac{1}{\Gamma_{3G}}\frac{d\Gamma}{dT} \approx \frac{3}{\pi^2 - 9}\left[\frac{4(1-T)}{T^2(2-T)^3}(5T^2 - 12T + 8)\ln\frac{2-2T}{T} + \frac{2(3T-2)(2-T^2)}{T^3(2-T)^2}\right], \quad (1.75)$$

and orienting events along the thrust axis should give distributions of hadron energy in the event plane like those shown in Fig. 18. Preliminary evidence from DORIS[58] suggests that the final states in T decay are not exactly the same as in the e^+e^- continuum. However, it is premature

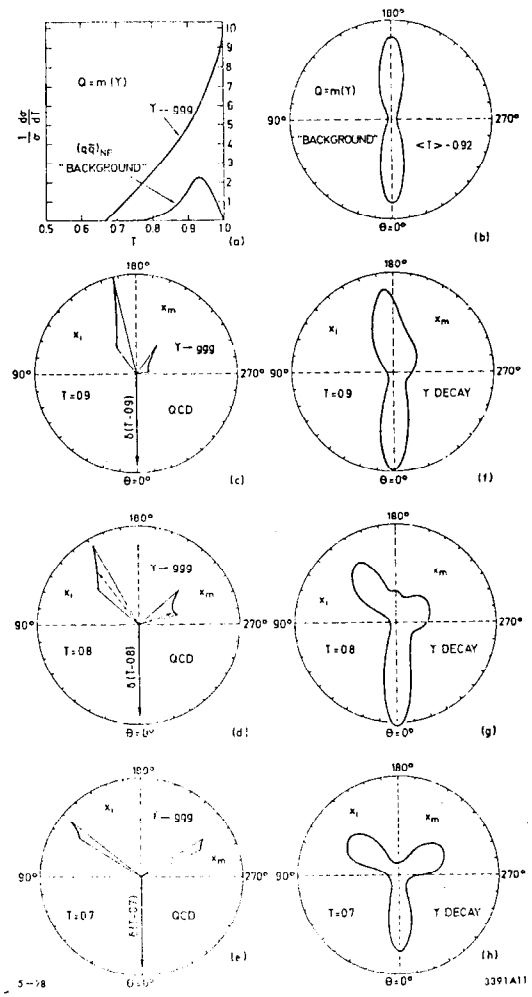

Fig. 18. The distribution of hadronic energy in T decay expected for different values of the thrust (1.70). Cf. Fig. 16.

to think that evidence for the 3-gluon decay yet exists. It will probably be much easier to see gluon jets in the decay of the "topsilon" $t\bar{t}$ vector meson, which presumably has a considerably larger mass $\geq$ 15 GeV, yielding much more phase space for the gluon jets to identify themselves. Other promising ways of looking for gluon jets in onium spectroscopy include $T \to GG\gamma$,[20] and radiative decays to intermediate states which may decay predominantly into 2 gluons.[53,59]

2. Fermions for Fun and Profit

2.1 Weak Interaction Issues

In this first of three lectures devoted to studies of weak interactions at high energies, it seems appropriate to make some introductory suggestions as to what are the important physics issues which one is trying to resolve. Up till now, no one has ever found any deviation from the pointlike four-fermion form of the weak interactions, whether charged or neutral.[60] In the regime where the pointlike approximation is applicable, a generic fermion-fermion scattering cross section will rise linearly with the centre-of-mass invariant s, as in Fig. 19(a):

$$\sigma(f_1 f_2) \sim s \times O\left(\frac{G_F}{\pi}\right) \qquad (2.1)$$

The rise (2.1) cannot continue indefinitely, because there is a unitarity limit of 1 on each partial amplitude. In the case of the naive form (2.1) of cross section this limit will be attained when $\sqrt{s} \sim$ a few hundred GeV.[61] At this juncture, the cross section may either saturate at a constant O(1), or else fall again, as indicated in Fig. 19(b). It is generally supposed that the latter occurs, thanks to the presence of intermediate vector bosons. It is theoretically appealing that the

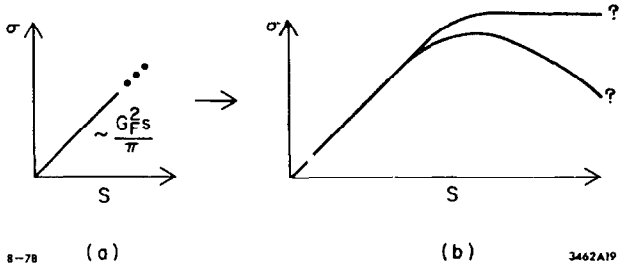

Fig. 19. Weak interaction cross sections (a) rise linearly with s at low energies, but (b) should either flatten out or fall at $\sqrt{s} \geq$ several hundred GeV.

turnover energy $\sqrt{s}$ should be rather smaller than the unitarity limit of a few hundred GeV. This is because it is attractive to unify weak and electromagnetic interactions with couplings which are $O(\alpha)$. In an intermediate vector boson theory,[62] G_F is related to the boson couplings and masses:

$$G_F = O\left(\frac{g^2}{m^2}\right) \tag{2.2}$$

and weak electromagnetic unification suggests

$$m^2 = O\left(e^2 G_F\right) \tag{2.3}$$

and one is naturally led to contemplate vector boson masses of order (50 to 200) GeV. There are empirical reasons for liking intermediate vector bosons, such as the factorization and universality of weak couplings. One of the theoretical reasons for the introduction of intermediate vector bosons is that it helps to make higher order radiative corrections to weak interactions finite and calculable. This happens because such radiative corrections typically involve sums over virtual intermediate states which will diverge if weak cross sections do not fall at high energies roughly as $O\left(\frac{1}{s}\right)$. Unfortunately, just sticking in intermediate vector bosons does not cure all problems. First, it is necessary to include some self-couplings (Fig. 20) between the vector bosons, and it has been shown[63] that essentially the only way of doing this which yields cross sections falling sufficiently fast at high energies is to make these couplings those found in a gauge theory. Such a theory will be based on a non-Abelian gauge group with a charged $W^{\pm}$ or neutral Z^0 boson corresponding to each generator of the group.[64] Fermions (quarks and leptons) must be put into suitably chosen representations of the gauge group. Unfortunately, just using gauge vector bosons with masses acquired in an ad hoc manner does not give a

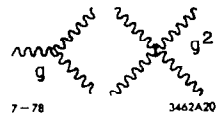

Fig. 20. The 3 and 4 vector boson vertices.

sensible (renormalizable) theory either. The only known way of making such a massive gauge boson theory renormalizable[29] is by breaking the gauge symmetry spontaneously[12] using scalar Higgs fields.[65] A theory of this type seems inevitable to possess at least one physical scalar Higgs boson.

The road to a sensible renormalizable theory[2] of the weak interactions is therefore quite a long one, as indicated in Table 2. Finding an intermediate vector boson is only a small part of establishing the validity of any spontaneously broken unified gauge theory of the weak and electromagnetic interactions such as the Weinberg-Salam[12] model.

TABLE 2. The Road to a Gauge Theory

Physical Input	Experimental Test	Discussed in Lecture
Weak cross sections fall at high energies	Do high energy e^+e^- or ep scattering, look for $W^\pm$, Z^o	3
Interactions described by a gauge theory	Look at 3- and 4-vector boson interactions	3
Choose a gauge group	Look at low energy weak interactions;	2
	Do $W^\pm$, Z^o spectroscopy	3
Choose spectrum of fermions and their group representations	Look for fermions	2
Break gauge symmetry with Higgs fields	Look for Higgs particles	4

The strategy of these remaining lectures will be to survey this road with a view to the experimental confrontation of these theoretical ideas. Finally, at the end of the last lecture 4 we will examine a few speculative possibilities that go beyond this orthodoxy and help keep our lives interesting. We start with fermiology.

2.2 How Much Do We Know Already?

We have so far established[66] unassailably the existence of 10 fundamental fermions:

$$\begin{aligned} &4 \text{ quarks} - u,\ d,\ s,\ c \\ &6 \text{ leptons} - e, \nu_e;\ \mu, \nu_\mu;\ \tau, \nu_\tau \end{aligned} \tag{2.4}$$

and the existence of a fifth quark is not seriously questioned. So far it has only been seen[64,68] bound with its antiquark into the T family of meson resonances. There are some indirect indications that this new heavy quark has charge $-\frac{1}{3}$. They are the smallish coupling of the T to leptons ($\Gamma_{e^+e^-} = (1.3\pm0.4)$ keV [68]), the rumoured small branching ratio of $T \to \mu^+\mu^-$, shaky arguments about the relative production rates of T and T' in hadron-hadron collisions,[69,70] and speculative calculations of the next charge $= -\frac{1}{3}$ quark mass in the context of grand unified gauge theories.[71,72] We will henceforth assume that the fifth quark has charge $-\frac{1}{3}$ and call it b or bottom.[73]

We know quite a lot about some weak interactions of these fermions. The following left-handed charged weak interactions are by now completely classical[66]:

$$\checkmark: \ \begin{pmatrix} u \\ d \end{pmatrix}_L \sim \cos^2\theta_c; \ \begin{pmatrix} u \\ s \end{pmatrix}_L \sim \sin^2\theta_c; \ \begin{pmatrix} \nu_e \\ e^- \end{pmatrix}_L \sim 1; \ \begin{pmatrix} \nu_\mu \\ \mu^- \end{pmatrix}_L \sim 1. \tag{2.5}$$

Recently established but apparently quite reliable are the left-handed charged couplings[21,66,74]

$$\checkmark? \ \begin{pmatrix} c \\ s \end{pmatrix} \text{ large}; \quad 0 < \begin{pmatrix} c \\ d \end{pmatrix}_L << 1; \quad \begin{pmatrix} u \\ b \end{pmatrix}_L << 1; \ \begin{pmatrix} \nu_\tau \\ \tau^- \end{pmatrix}_L \text{ dominant} \tag{2.6}$$

At the present time there is no good evidence for the existence of any right-handed charged currents. The following are excluded at anything approaching unit ($\sim G_F$) strength:

$$\text{x:} \qquad \binom{u}{d}_R ; \quad \binom{u}{s}_R ; \quad \binom{c}{d}_R ; \quad \binom{\nu}{e^-}_R ; \quad \binom{\nu}{e^-}_R \tag{2.7}$$

Plausibly excluded at anything approaching unit strength by observations of charge-changing charm production[74] and of τ decays[32] are

$$\text{x?} \qquad \binom{c}{s}_R ; \quad \binom{\nu}{\tau^-}_R \tag{2.8}$$

There is no time here to discuss in depth the present status of neutral current phenomenology which is admirably reviewed in the talk of Barnett at this Summer Institute.[75] Suffice to say that the following right-handed currents cannot[76] be large:

$$\text{x:} \qquad \binom{u}{b}_R ; \quad \binom{?}{d}_R \tag{2.9}$$

The following current is strongly disfavoured by the recent polarized eD scattering data[77]

$$\text{x?} \qquad \binom{N_e^o}{e^-}_R \tag{2.10}$$

To the best of my knowledge the following left- and right-handed currents are not yet severely constrained by experiment:

$$\binom{c}{b}_{L,R} ; \quad \binom{N_\mu^o}{\mu^-}_R ; \quad \binom{N_\tau^o}{\tau^-}_R \tag{2.11}$$

As far as the neutral currents of the fermions (2.4) are concerned, we only have information at present on those of u, d, e, ν_e and ν_μ all of which seem to agree[75,78] very well with the $SU(2)_L \times U(1)$ Weinberg-Salam[12] model. On the other hand, we have as yet no useful information on the diagonal neutral currents of s, c, b, μ, τ and ν_τ. We do however have information on the off-diagonal neutral current $d \leftrightarrow s$, which is observed[27] to be $O\left(G_F^2\right)$, and we have a constraint[66,79] on the $\Delta C=2$ transition $D^o \leftrightarrow \bar{D}^o$ which is related to the $\Delta C=1$ neutral current $u \leftrightarrow c$, and tells us it is also at most $O\left(G_F^2\right)$. These small couplings are just as expected in the Weinberg-Salam model, and indeed the smallness of the $s \leftrightarrow d$ neutral current was the motivation of Glashow, Iliopoulos and Maiani (GIM)[80] for giving the charmed quark[81] a well-defined role in weak interaction physics, by causing cancellations like that in the diagram of Fig. 21.

With the important exception of certain atomic physics experiments,[82] all present data agree with the Weinberg-Salam model[12] with $\sin^2 \theta_W \sim 0.20$ to 0.25.

It is almost universally expected that there will be at least one more quark, with charge $e = 2/3$ to be called t or top. Some reasons for its existence are as follows:

--Aesthetics: perhaps we should parallel the (so far)

$$\left.\begin{array}{l} \text{three lepton doublets } \binom{\nu_e}{e^-}_L , \binom{\nu_\mu}{\mu^-}_L , \binom{\nu_\tau}{\tau^-}_L \\ \text{with} \\ \text{three quark doublets } \binom{u}{d'}_L , \binom{c}{s'}_L , \binom{t}{b'}_L \end{array}\right\} \tag{2.12}$$

where the primes on the charge $-\frac{1}{3}$ quarks indicates that they are (generalized) Cabibbo mixed, in a manner to be discussed later. It was just such an aesthetic argument that led to the postulation of charm[81] when only three quarks and four leptons were known. It was only much after

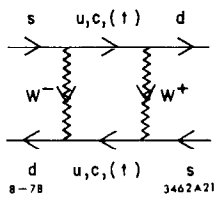

Fig. 21. A box diagram used for calculating the $\Delta S=2$ transition $K^o \leftrightarrow \bar{K}^o$.

this original arbitrary introduction that charm was given[80] a raison d'être in suppressing strangeness-changing neutral currents. Perhaps some similar role will eventually be found for t and b--a possibility is CP violation[35] which will be discussed later in this lecture.

--Anomaly cancellation: The above prescription for constructing a renormalizable gauge theory of the weak interactions is in fact slightly incomplete. The falling high energy cross sections depend on tricky cancellations between different Born diagrams. The relations between these diagrams can be upset[28] by the so-called "anomalies" of perturbation theory which arise from the fermion loops of Fig. 6. The anomalies must be cancelled if the strict renormalizability[29] of the theory is to be preserved. Each triangle diagram makes a contribution $\propto g_A^f e_f^2$. As mentioned in Lecture 1, thanks to colour these anomalies are cancelled if there are equal numbers of left-handed lepton and quark doublets.

$$A_q = \sum_{i=1}^{n} \left(-\frac{1}{2}\right)\left[(-1)^2-(0)^2\right] = -\frac{1}{2}\sum_{i=1}^{n},$$

$$A_q = \sum_{i=1}^{n} 3\left(\frac{1}{2}\right)\left(\left(\frac{2}{3}\right)^2-\left(-\frac{1}{3}\right)^2\right) = +\frac{1}{2}\sum_{i=1}^{n} \qquad (2.13)$$

Nature has so far endowed us with three left-handed lepton doublets: it is natural to want to supplement the b with a t quark so as to get a third left-handed quark doublet to cancel the anomalies. However, other ways of cancelling the anomalies are in principle possible, and it has even been argued[83] that the requirement of anomaly cancellation is not to be taken seriously because it only destroys renormalizability in higher orders of perturbation theory which are not phenomenologically relevant.

--Flavour conservation by neutral currents: As mentioned above, $\Delta S=2$ and $\Delta C=2$ transitions all seem to be suppressed to $O(G_F^2)$. This was explained in the GIM[80] charm model through cancellations involving loop diagrams with charmed quarks (Fig. 21). When more heavy quarks are introduced, the cancellations are no longer automatic whatever the masses and couplings of the new quarks, unless these are chosen to occur in representations of the weak gauge group identical with those of the lighter quarks.[84,71] This would suggest that left-handed quarks should always be in doublets of SU(2), and that right-handed quarks should always be in singlets. Therefore, given a b quark we should need a t quark to partner it.

The above arguments are swasivious, but not rigorous. Nevertheless we will assume that at least one new t quark is yet to be discovered. Unfortunately, I know of no stringent constraint on its mass or guarantee that it will be accessible to the next generation (PETRA/CESR/PEP) of e^+e^- machines.

What constraints are there on the possible existence of other fundamental fermions? We start with the supposedly massless neutrinos. In fact, high energy physics does not even determine them to be massless, but gives upper limits[27]

$$m_{\nu_e} < 60 \text{ eV}, \quad m_{\nu_\mu} < 0.57 \text{ MeV}, \quad m_{\nu_\tau} < 250 \text{ MeV} \tag{2.14}$$

and does not yet seriously restrict the number of "massless" neutrinos. For example the $K^\pm \to \pi^\pm \nu\bar{\nu}$ branching ratio is expected[85] to be

$$B(K^\pm \to \pi^\pm \nu\bar{\nu}) = O(10^{-10}) N_\nu \tag{2.15}$$

whereas the experimental upper limit[27] is 6×10^{-7} corresponding to

$$N_\nu \lesssim 6000 \tag{2.16}$$

In time a better constraint may be available from the decays of heavy $q\bar{q}$ vector mesons.[86] One can estimate

$$\frac{\Gamma(V \to Z^0 \to \nu\bar{\nu})}{\Gamma(V \to \gamma^* \to e^+e^-)} = \frac{G_F^2}{64\pi^2\alpha^2} \frac{m_V^4}{e_q^2} \left(1-4|e_q|\sin^2\theta_W\right)^2 \tag{2.17}$$

$$\approx 0.2 \times 10^{-8} \times m_V^4 \times N_\nu \quad \text{for } e_q = \frac{2}{3} \tag{2.18}$$

For the J/ψ, a guessed limit of 1 on the quantity (2.18) implies that $N_\nu < 5 \times 10^6$. However, the ratio (2.18) is $O(10^{-2})$ for $m_V \approx 30$ GeV, so that a sensitive search for the decay toponium $\to \nu\bar{\nu}$ should be very interesting. One way to do it may be to look for events of the form

$$e^+e^- \to (t\bar{t})' \to (t\bar{t}) + \pi\pi$$
$$\hookrightarrow \text{nothing}$$

There are however much more restrictive constraints[87] on neutrinos than (2.14) and (2.18) if one accepts the standard "big bang" cosmology.[89] Very light neutrinos would have been produced in great profusion during the big bang, and would now have slowed to being nonrelativistic if their masses were not exceedingly small. They would then contribute to the mass density of the Universe and cause its expansion rate to slow down by an experimentally unacceptably large amount unless[87] (see Fig. 22)

$$\sum_\nu m_\nu < 50 \text{ eV} \tag{2.19}$$

which bound can be strengthened to $\lesssim 3$ eV by considering the dynamics of clusters of galaxies. If the neutrino masses obey the constraint (2.19) then they would have been in thermodynamic equilibrium and present in vast numbers at very early stages of the Universe when the temperature

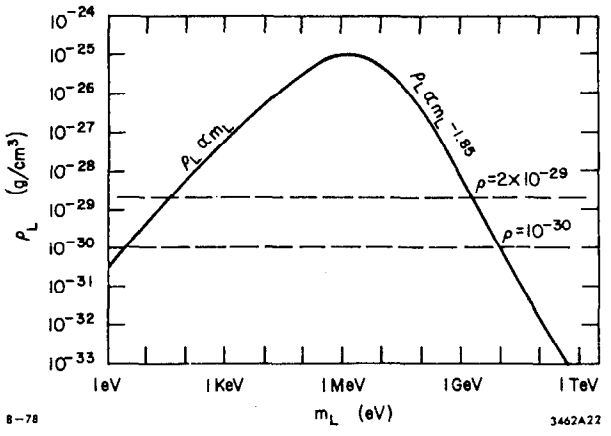

Fig. 22. The mass density of stable neutral leptons expected[87] on the basis of the standard big-bang cosmology[88] compared with the density (2×10^{-29} g/cm^3) required to close the Universe and the density ($\sim 10^{-30}$ g/cm^3) "observed" in the Universe.

$\gtrsim \frac{1}{2}$ MeV. Increasing the number of "massless" neutrinos increases the early Universe's expansion rate, which increases the n/p ratio when the weak interactions drop out of equilibrium, which in turn increases the primordial abundance of Helium. It is currently believed that the primordial Helium abundance was less than 25%, indicating as shown in Fig. 23 that there can be at most one more "massless" neutrino after the ν_τ (an improvement on the limit (2.16)!).

There are also cosmological limits on the possible existence of heavy stable neutral leptons L^o.[89] Figure 22 shows that the upper limit on the mass density of the Universe requires $M_{L^o} > 2$ GeV which can be improved to $\gtrsim 10$ GeV by considering the dynamics of clusters of galaxies. A complete display of the allowed ranges of masses and lifetimes is shown in Fig. 24. The important constraints on semistable L^o production come from upper limits on distortions of the 3°K microwave background, and on the γ-ray background. We see that L^o particles of arbitrary mass are allowed if their lifetimes are $< 5 \times 10^3$ seconds. An L^o with a roughly unit strength weak interaction making it decay would obey this lifetime constraint if its mass were $\gtrsim$ O(1) MeV. Hence the cosmological constraints on massive neutral leptons are not really very useful except in models[90] where some selection rule impedes their decay.

Let us now return to high energy physics to see the constraints it yields on the possible existence of very heavy fermions (either neutral or charged, leptons or quarks). Such objects could have an indirect effect on our low energy phenomenology. One such effect is on the ratio of intermediate vector boson masses.[91,92] In the simplest Weinberg-Salam model with only I=1/2 Higgs doublet fields, there is a zeroth

order prediction:

$$\frac{m_{W^\pm}^2}{m_{Z^o}^2} = \cos^2 \theta_W \qquad (2.20)$$

This prediction gets renormalized by any massive fermion loop to become

$$\frac{m_{W^\pm}^2}{m_{Z^o}^2} \simeq \cos^2 \theta_W \left[1 + \left(\begin{matrix}1\\or\\3\end{matrix}\right) \frac{G_F}{8\sqrt{2}\pi^2} \left(\frac{2m_1^2 m_2^2}{m_1^2 - m_2^2} \ln \frac{m_2^2}{m_1^2} + (m_1^2 + m_2^2) \right)\right] \qquad (2.21)$$

where m_1 and m_2 are the masses of the fermions in the loop, and the factors of 1 and 3 apply to leptons and quarks respectively. Experimentally, low energy neutral to charged current ratios are sensitive to the boson mass ratio:

$$\frac{\sigma(NC)}{\sigma(CC)} \propto \frac{m_W^4}{m_Z^4} \qquad (2.22)$$

The present data agree very well with the naive Weinberg-Salam prediction (2.20): Sehgal[78] finds

$$\frac{m_{W^\pm}^2}{m_{Z^o}^2 \cos^2 \theta_W} = 0.98 \pm 0.05 \qquad (2.23)$$

This apparent success of the I=1/2 Higgs assumption leads to interesting constraints on m_1 and m_2. For example, for a lepton doublet with $m_\nu \sim 0$, the limits (2.23) imply

$$m_L < 400 \text{ GeV} \qquad (2.24)$$

It is possible to imagine possible future experiments with e^+e^- machines[93] which might determine the Z^o mass with an accuracy of 0.1%, in which case Eq. (2.21) would be sensitive to all m_L>100 GeV. In this way future e^+e^- experiments could successfully determine the entire fermion

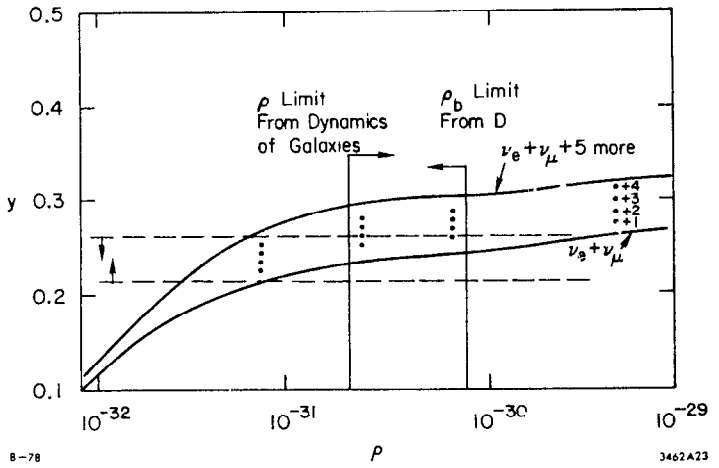

Fig. 23. The Helium abundance Y plotted[87] versus the density of baryons with the limits imposed by galactic dynamics and the Deuterium abundance D. The dashed lines are astrophysical constraints on Y. The curves are the values of Y obtained with different numbers of neutrinos.

mass spectrum, by finding all fermions with mass < 100 GeV and excluding by their indirect effects fermions with larger masses.

In passing, we should note[92] one unaesthetic aspect of very heavy fermions. Since their couplings to Higgs particles in the naive Weinberg-Salam model are

$$g_{\bar{f}fH} = \frac{gm_f}{m_W} \tag{2.25}$$

the Higgs-fermion system becomes strongly interacting if m_f is sufficiently large. Indeed, lowest order perturbation theory violates partial wave unitarity[92] for

$$m_{quark} \sim 550 \text{ GeV}, \qquad m_{lepton} \sim 1.2 \text{ TeV} \tag{2.26}$$

indicating the presence of bound states or other nonperturbative effects. For this reason, one might interpret the values (2.26) as plausible upper bounds on fermion masses, though there is no rigorously logical reason to exclude such strongly-interacting fermions.

2.3 Finding Heavy Leptons

Let us now turn from indirect evidence on heavy fermions to the phenomenological problems of identifying them in future high energy experiments. We start with:

2.3.1 Charged leptons

The principles for locating one of these are strongly suggested by the saga of the discovery of the τ.[94,32,66] The decay modes and branching ratios are well-defined in the framework of conventional weak-electromagnetic and strong (partons, QCD) interaction ideas.[31] Assuming a conventional, sequential (V-A) heavy lepton λ^- with a mass in the range 6 GeV < m_λ < $m_t + m_b \gtrsim 12$ GeV, Tsai[95] has calculated the diagrams of Fig. 7(a) and found the dominant decay modes

$$B(\lambda^- \to e^-\bar{\nu}_e\nu_\lambda):B(\lambda^- \to \mu^-\bar{\nu}_\mu\nu_\lambda):B(\lambda^- \to \tau^-\bar{\nu}_\tau\nu_\lambda):B(\lambda \to d\bar{u}\nu_\lambda):B(\lambda \to s\bar{c}\nu_\lambda)$$
$$\approx 1:1:\left(\frac{1}{2} \text{ to } 1\right):3:(2 \text{ to } 3) \tag{2.27}$$

The leptonic decay modes $\lambda^- \to e^-\bar{\nu}_e\nu_\lambda$ and $\lambda^- \to \mu^-\bar{\nu}_\mu\nu_\lambda$ each have branching ratios $\gtrsim$ 10% and should therefore be identifiable. On the other hand, exclusive semihadronic decay modes such as $\lambda^- \to \pi^-\nu_\lambda$ or $\rho^-\nu_\lambda$ should each have branching ratios <2%, which would therefore be very difficult to detect. In contrast to the τ, the dominant semihadronic decay modes are expected to be multiprong, as exemplified by the last two branching ratios in the set (2.27). For sufficiently heavy heavy leptons with masses $\gtrsim$10 GeV, these multiparticle semihadronic decays should show up as two jets.[96] A possible signature for $\lambda^+\lambda^-$ production--which has the cross section

$$\sigma(e^+e^- \to \lambda^* \to \lambda^+\lambda^-) \approx \beta\left(\frac{3-\beta^2}{2}\right) \cdot \frac{4\pi\alpha^2}{3s} \tag{2.28}$$

would then be a lepton (from one leptonic decay) plus two jets plus missing energy from neutrinos.[96] It seems likely that such an object could be found in e^+e^- collisions if it exists.

2.3.2 Neutral leptons

Heavy neutral leptons are expected in many theories, and even in the Weinberg-Salam[12] model doublets like

$$\begin{pmatrix} E^o \\ e^- \end{pmatrix}, \quad \begin{pmatrix} M^o \\ \mu^- \end{pmatrix} \quad \text{or} \quad \begin{pmatrix} T^o \\ \tau^- \end{pmatrix}$$

cannot yet be excluded.[97] Lower limits on their masses come from the absence of $K^+ \to E^o e^+$ decay, which tells us that $m_{E^o} > 0.4$ Gev. Improved lower limits on $m_{E^o} \sim 1$ GeV come from τ or F decays.[98] An object

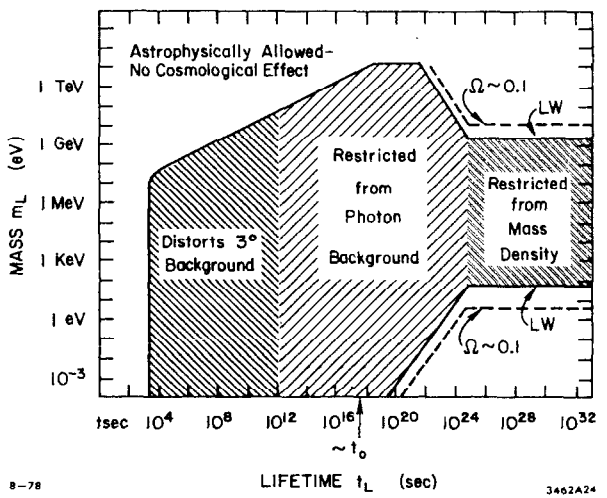

Fig. 24. Cosmologically acceptable and disallowed (the shaded region) ranges of neutral lepton masses and lifetimes.[87]

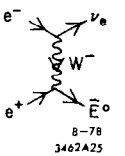

Fig. 25. The process $e^+e^- \to \nu_e \bar{E}^o$ mediated by W^+ exchange.

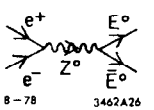

Fig. 26. The process $e^+e^- \to E^o\bar{E}^o$ (or $M^o\bar{M}^o, T^o\bar{T}^o$) mediated by Z^o exchange.

E^o can be produced singly in e^+e^- annihilation by $W^\pm$ exchange as in Fig. 25: $e^+e^- \to \nu_e E^o$, $\bar{\nu}_e E^o$. The total cross sections are calculated[99] to be

$$\sigma(e^+e^- \to \nu_e E^o) \approx \frac{G_F^2}{2\pi}\left(1-\frac{m_{E^o}^2}{s}\right)^2 s\left(1+\frac{s-m_{E^o}^2}{m_W^2}\right)^{-1} \quad \text{for a}$$

$$\text{right-handed } e\text{-}E^o \text{ coupling}$$

$$\approx \frac{G_F^2}{2\pi}\,\frac{s}{3} \quad \text{for } m_{E^o}^2 \ll s \ll m_W^2 \quad \text{and a}$$

$$\text{left-handed } e\text{-}E^o \text{ coupling} \qquad (2.29)$$

One can also produce pairs $E^o\bar{E}^o$ or $M^o\bar{M}^o$ in e^+e^- collisions through a direct channel Z^o as in Fig. 26. In the Weinberg-Salam model, massive left-handed neutral lepton[100] pairs would be produced with cross sections[98]

$$\sigma(e^+e^- \to E^o\bar{E}^o) \approx \frac{G_F^2}{32\pi}\, s\,\beta\left[4\sin^4\theta_W\left(1+\frac{\beta^2}{3}\right)+\left(2\sin^2\theta_W-1\right)^2\left(1-\frac{\beta^2}{3}\right)\right]$$

$$\text{for } s \ll m_Z^2 \qquad (2.30)$$

The cross sections (2.29) and (2.30) exhibit the linear rise with s characteristic of the pointlike four-fermion interaction (2.1). They are rather small for the SPEAR/DORIS generation of e^+e^- machines, but would be substantial at the highest PETRA/PEP energies. Thus one would have

$$\sigma(e^+e^- \to \nu_e\bar{E}^o) = O\left(\frac{1}{10}\right)\sigma(e^+e^- \to \mu^+\mu^-) \qquad (2.31)$$

and

$$\sigma(e^+e^- \to E^o\bar{E}^o) \sim O\left(\frac{1}{100}\right)\sigma(e^+e^- \to \mu^+\mu^-) \qquad (2.32)$$

for beam energies $\sim$ 15 to 20 GeV.[99] At higher energies near and beyond the Z^o pole (or poles) the ratios (2.31) and (2.32) would be O(1). If an M^o exists with a mass of a few GeV, visible cross sections for $\mu p \to M^o + X$ could be expected for FNAL or CERN SPS μ beams. Very substantial cross sections for $ep \to E^o + X$ are found for ep colliding rings with centre-of-mass energies $\sqrt{s} \gtrsim 100$ GeV and $M_{E^o} \lesssim \frac{1}{2}\sqrt{s}$.[101]

As for E^o decays, one might expect[98,99] that for 2 GeV $\lesssim m_{E^o} \lesssim$ 15 GeV the decay branching ratios

$$B\left(E^o \to e^-\begin{pmatrix}e^+\nu_e\\ \mu^+\nu_\mu\\ \tau^+\nu_\tau\end{pmatrix}\right) \gtrsim 10\% \text{ each} \qquad (2.33)$$

with corresponding μ^-X, τ^-X branching ratios for M^o, T^o. Similarly to (2.27) one would also expect

$$B\left(E^o \to e^-\begin{pmatrix}u\bar{d}\\ c\bar{s}\end{pmatrix}\right) \sim 30\% \text{ each} \qquad (2.34)$$

The decay modes (2.33) would have characteristic signatures like $e\mu$ final states with low invariant mass[98]:

$$\langle m_{e^-\mu^+}\rangle \sim \begin{cases}0.5\, m_{E^o} & \text{(left-handed)}\\ 0.6\, m_{E^o} & \text{(right-handed)}\end{cases} \qquad (2.35)$$

The decay modes (2.34) yield the exciting prospect of a peak in an invariant mass distribution $e^- + (\text{hadrons})^+$. Unfortunately, as mentioned earlier heavy heavy leptons probably[95] have very small exclusive semi-hadronic decay modes, so such a peak might be difficult to track down.

Possible signatures[99] for single production $e^+e^- \to \nu_e\bar{E}^o$ would be $(e^+\mu^-)$ final states with the θ_e spectrum having a forward-backward asymmetry, with the $e^+\mu^-$ collinearity collinearity angle peaked towards $\theta \sim 0$, and with low $e^+\mu^-$ invariant masses as mentioned above and as indicated in Fig. 27(a). Possible signatures[99] for double production $e^+e^- \to E^o\bar{E}^o$ events would include events with $e^+\mu^-e^-\mu^+$ and missing energy as in Fig. 27(b), and $e\mu$ + hadrons events with the $e\mu$ collinearity angle

small, so that the pair recoiled against a hadron jet as in Fig. 27(c). In ep collisions[101] one could get events with

$$ep \to (\mu e) + (\text{hadron jet}) \qquad \text{(Fig. 27(d))}$$

or

$$ep \to (e+\text{hadrons}) + (\text{hadron jet}) \qquad \text{(Fig. 27(e))}$$

It seems likely that neutral heavy leptons will have sufficiently distinctive signatures to be discernible in e^+e^- or ep collisions at high energies.

2.4 Heavy Quarks

As was discussed in Section 2.2, we know there is a fifth quark b, and generally assume there will be a sixth quark t. In this section we will discuss some of the possible phenomenology of these quarks and of possible successors. In view of its successes to date, we will assume the Weinberg-Salam model in discussing the weak interactions of the b and t quarks. We therefore have (at least) 3 quark doublets of $SU(2)_L$, which will in general mix:

$$\begin{pmatrix} u \\ d' \end{pmatrix}_L \quad \begin{pmatrix} c \\ s' \end{pmatrix}_L \quad \begin{pmatrix} t \\ b' \end{pmatrix}_L \tag{2.36}$$

The charge-changing weak interactions can be described in terms of an $N_D \times N_D$ unitary-matrix U, where N_D is the

$$J^\mu = (\bar{u},\bar{c},\bar{t},\ldots)\ \gamma_\mu \tfrac{1}{2}(1-\gamma_5)\ U \begin{pmatrix} \bar{d} \\ \bar{s} \\ \bar{b} \\ \vdots \end{pmatrix} \tag{2.37}$$

number of quark doublets. The matrix U would appear to need N_D^2 parameters for its characterization, but $(2N_D-1)$ of these are relative phases between different quark fields, which are unobservable. The matrix U therefore has $(N_D-1)^2$ observable parameters. If N_D were 1, U would have no parameters as is immediately physically obvious. If $N_D=2$, one would

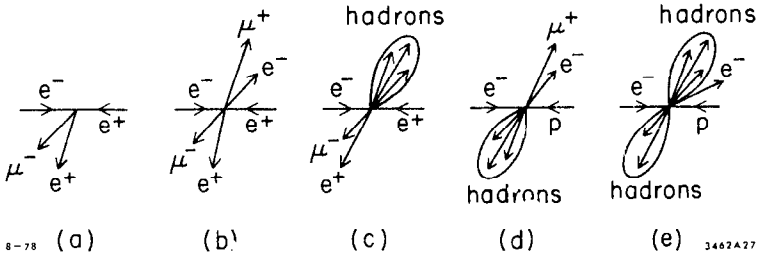

Fig. 27. Possible neutral heavy lepton signatures: (a) $e^+e^- \to \mu^-e^+ +$ nothing from $e^+e^- \to \nu_e\bar{E}^o$, (b) $e^+e^- \to \mu^+e^-\mu^-e^+$ from $e^+e^- \to E^o\bar{E}^o$, (c) $e^+e^- \to \mu^-e^+ +$ hadron jet from $e^+e^- \to E^o\bar{E}^o$, (d) $\bar{e}p \to \mu^+e^- +$ hadron jets from $e^-p \to E^o+X$, and (e) $e^-p \to (e^-+\text{jet}) +$ hadron jets from $e^-p \to E^o+X$.

expect 1 parameter, which is just the Cabibbo angle θ_c:

$$U_2 = \begin{pmatrix} \cos\theta_c & \sin\theta_c \\ -\sin\theta_c & \cos\theta_c \end{pmatrix} \tag{2.38}$$

If $N_D=3$, one has 4 observable parameters.[102] Not all of these can be absorbed as the Euler angles of a 3×3 orthogonal matrix. The unitary matrix U has one extra observable complex phase δ:

$$U_3 = \begin{pmatrix} c_1 & -s_1c_3 & -s_1s_3 \\ s_1c_2 & c_1c_2c_3-s_2s_3e^{i\delta} & c_1c_2s_3+s_2c_3e^{i\delta} \\ s_1s_2 & c_1s_2c_3+c_2s_3e^{i\delta} & c_1s_2s_3-c_2c_3e^{i\delta} \end{pmatrix} \tag{2.39}$$

where the θ_i, i=1,2,3 are generalized Euler-Cabibbo angles, and

$$c_i \equiv \cos\theta_i, \quad s_i \equiv \sin\theta_i, \quad i=1,2,3 \tag{2.40}$$

If the complex phase δ is nonzero, it will generate CP violation, as pointed out by Kobayashi and Maskawa (KM).[102] It is not at all clear whether the observed CP violation in the K^o-$\bar{K}^o$ system comes from this source-another favoured source of CP violation is a complicated, non-minimal Higgs system[105]--but we will return later to review some predictions of the KM mechanism for CP violation.

First we should take account of the phenomenological successes of the Weinberg-Salam model and the GIM[80] mechanism, which tells us that the observed weak interactions are approximately as described by the 2×2 coupling matrix U_2 (2.38). The new mixing angles in (2.39) must obey certain constraints, with

$$\theta_1 \sim \theta_c; \quad c_2, c_3 \sim -1, \quad s_2, s_3 \sim 0 \tag{2.41}$$

The best constraint on θ_3 seems to come[104] from the success of Cabibbo universality for quarks compared to the μ weak coupling. Experiments on nuclear β-decay and hyperon decays indicate that[105]

$$g^2_{\mu\to\nu_\mu} \quad \text{and} \quad g^2_{u\to d} + g^2_{u\to s}$$

differ by $(2.17 \pm 0.27)\%$. However, there should be modifications to universality due to weak radiative corrections. In the standard Weinberg-Salam model these are[106]

$$\frac{\alpha}{2\pi}\left[3\ \ln\left(\frac{m_Z}{m_N}\right) + \ln\left(\frac{m_Z}{m_A}\right)\right] \tag{2.42}$$

If we take $m_Z \sim 94$ GeV, corresponding to $\sin^2\theta_W = 0.20$, and the axial vector form factor parameter $m_A \sim 1.1$ GeV, then Eq. (2.42) gives a violation of μ-quark universality by 2.12%. The net discrepancy between Cabibbo-Weinberg-Salam[12]-GIM[80] theory and experiment is therefore $0.05 \pm 0.27\%$, so that we estimate the "leakage" of the u quark's weak coupling to the b quark to be

$$s_1^2 s_3^2 < 0.003 \tag{2.43}$$

Since $s_1^2 \sim \sin^2\theta_c$, this result gives an upper limit[104] on s_3^2 of

$$s_3^2 < 0.06 \tag{2.44}$$

indicating that s_3 is at most the same order of magnitude as the Cabibbo angle.

The best limit on θ_2 probably[104] comes from the success of calculations[85] of the charmed quark mass from the observed K^o-$\bar{K}^o$ mixing. In the GIM[80] model Gaillard and Lee[85] used the box diagram of Fig. 21 to estimate

$$\frac{\Delta m_K}{m_K} \approx \frac{G_F}{\sqrt{2}} f_K^2 \left(\frac{\alpha}{4\pi}\right)\left(\frac{m_c}{38\ \text{GeV}}\right)^2 \cos^2\theta_c \sin^2\theta_c \tag{2.45}$$

and the experimental ratio of 0.7×10^{-14} suggested $m_c \sim 1.5$ to 2 GeV,

as subsequently confirmed by experiment. If we now include t quarks[104] in the loop the equation (2.45) factor

$$\sin^2\theta_c \cos^2\theta_c\, m_c^2 \to s_1^2 c_1^2 c_3^2 \left[c_2^4 m_c^2 + s_2^4 m_t^2 + \frac{2 s_2^2 c_2^2 m_t^2 m_c^2}{m_t^2 - m_c^2} \ln\left(\frac{m_t^2}{m_c^2}\right)\right] \qquad (2.46)$$

The phenomenological success of the formula (2.45), and the fact that presumably $m_t > 7$ GeV since otherwise toponium would have been seen in the $pp \to \mu^+\mu^- + X$ experiments,[67] gives us a constraint on s_2^2:

$$s_2^2 < 0.1 \quad \text{if} \quad m_t < 7 \text{ GeV} \qquad (2.47)$$

Once again, it seems phenomenologically that this generalized Cabibbo angle cannot be much larger in magnitude than the original Cabibbo angle, though there is no fundamental understanding of this fact.

Armed with the constraints (2.41, 2.44, 2.47) we are now in a position to make some educated guesses about the decay modes expected for bottom and top particles.[69] It is generally felt likely that heavy quarks in new heavy mesons will decay essentially as if they were free into light $qq\bar{q}$ combinations as in Fig. 28. These rates can then be calculated by scaling up the μ-decay formula

$$\Gamma(f \to f_1 f_2 \bar{f}_3) \approx \frac{G_F^2 m_f^2}{192\pi^2} \times \begin{pmatrix}\text{mixing}\\ \text{angle}\\ \text{factor}\end{pmatrix} \times \begin{pmatrix}\text{phase space}\\ \text{suppresion}\\ \text{for } m_{f_i} \neq 0\end{pmatrix} \times \begin{pmatrix}\text{colour}\\ \text{factor}\end{pmatrix} \qquad (2.48)$$

From the weak coupling matrix (2.39) we should anticipate[69]

$$\frac{\Gamma(b \to c+X)}{\Gamma(b \to u+X)} \approx \left(\frac{s_2^2 + s_3^2 + 2 s_2 s_3 \cos\delta}{s_1^2 s_3^2}\right) \times O\left(\frac{1}{3}\right) \qquad (2.49)$$

where we have used $m_b \sim 5$ GeV, $m_c \sim 2$ GeV to estimate the phase space suppression factor $O(1/3)$. Assuming, as is consistent with the

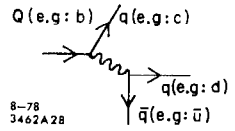

Fig. 28. The class of diagram expected to dominate heavy quark decay.

constraints (2.44) and (2.47), that

$$s_2^2 + s_3^2 + 2s_2s_3 \cos\delta \sim O\left(s_3^2\right)$$

and using $s_1^2 \sim \frac{1}{20}$, we obtain from formula (2.49) the general expectation[69] that

$$\frac{\Gamma(b \to c+X)}{\Gamma(b \to u+X)} \gtrsim O(6) \tag{2.50}$$

Thus the dominant decays of bottom particles should probably be to charmed particles. Analogously to (2.49) we find for top particles that

$$\frac{\Gamma(t \to b+X)}{\Gamma(t \to s+X)} \gtrsim \frac{1}{\left(s_2^2+s_3^2+2s_2s_3 \cos\delta\right)} \times O\left(\frac{1}{3}\right) \tag{2.51}$$

for a randomly guessed $m_t \sim 12$ GeV. With the constraints (2.44) and (2.47) it seems probable that

$$\frac{\Gamma(t \to b+X)}{\Gamma(t \to s+X)} > 1 \tag{2.52}$$

though this may not be the case if m_t is close to its lower limit of 7 GeV.

From the expectations (2.50) and (2.52) it seems very likely that multiple cascades of the form

$$\begin{array}{l} T \to B + X \\ \quad \hookrightarrow C + X \\ \quad\quad \hookrightarrow S + X \end{array} \tag{2.53}$$

could well dominate the decays of heavy quark mesons. At each stage in the cascade, the emitted system X may include an $(e\nu)$ or $(\mu\nu)$ pair, probably each with a branching ratio O(10 to 20)%. (This comes from counting lepton versus coloured quark degrees of freedom, and the belief that nonleptonic decays of heavy quarks are not strongly enhanced.[107,66]) The cascades (2.53) could therefore yield spectacular multilepton signatures in neutrinoproduction or e^+e^- annihilation.

It is also worth thinking what the lifetime of a top or bottom particle might be. Using the standard formula (2.48) and multiplying it by 5 to take account of all the possible semileptonic and nonleptonic decay modes, we find[69]

$$\tau(\text{bottom}) \gtrsim 10^{-14}/\left(s_1^2+s_3^2 + 2s_2s_3 \cos\delta\right) \gtrsim 10^{-13} \text{ sec} \tag{2.54}$$

if we use the bounds (2.44) and (2.47). This suggests that bottom particles may live long enough to leave detectable tracks in emulsions or high resolution spark chambers or bubble chambers. How long could the bottom lifetime be? If the KM mechanism[102] is responsible for the CP violation observed in the K^o-$\bar{K}^o$ system,[104] then as discussed in greater detail later

$$s_2s_3 \sin\delta \sim 10^{-3} \tag{2.55}$$

this gives us a very weak lower bound

$$s_2^2 \text{ or } s_3^2 > 10^{-6} \tag{2.56}$$

which combined with (2.54) suggests that the bottom lifetime should be $\lesssim 10^{-8}$ seconds. On the other hand, the KM mechanism may not lie at the root of the observed CP violation, in which case it becomes interesting to look for longer-lived bottom particles. Indeed, it has been suggested that bottom particles might be absolutely stable (s_3=0).[108] This possibility can probably be excluded now, since two FNAL experiments[109] exclude the existence of any heavy hadrons with $\tau > 5 \times 10^{-8}$ sec and a production cross section as large as that of the T in 400 GeV proton-nucleus collisions, as would be expected for bottom particles. If the bottom lifetime is $\gtrsim 10^{-12}$ sec, as is perfectly consistent with all the constraints mentioned above, then experiments to measure it at e^+e^- machines become imaginable.[110]

What about the production of new heavy quark particles? The three most promising mechanisms would seem to be:

Production in νN collisions. The prospects here are unfortunately not very good,[69] largely because of the severe constraints (2.44) and (2.47) on the mixing angles. These imply that at present energies, where there is a threshold suppression of heavy quark production,[111] one probably has

$$\frac{\sigma(\text{heavy})}{\sigma(\text{total})} \lesssim O(10^{-3}) \tag{2.57}$$

so the total cross section will not show an effect and one must look for distinctive signatures. These might include dilepton events, with one lepton coming from a cascade decay (2.53) and having large p_T because of the large energy release in the decay, or tri- or tetralepton events. Unfortunately, these probably occur--because of (2.57) and the less-than-total acceptances of present neutrino scattering apparatuses--at observable rates

$$\frac{\sigma(3\mu)}{\sigma(\text{total})} \lesssim O(10^{-5}), \quad \frac{\sigma(4\mu)}{\sigma(\text{total})} \lesssim O(10^{-6}) \tag{2.58}$$

Present experiments are perhaps sensitive to the rates (2.58), but most observed 3μ events[112] seem to have a radiative origin, and the two published tetralepton events[113] are difficult to assess.

Production in eN collisions. One expects the production of heavy quarks to be relatively small at low Q^2, but that the sea of heavy $q\bar{q}$ pairs should gradually build up as Q^2 increases, with distributions approaching SU(f) symmetry as $Q^2 \to \infty$. The evolution of the heavy sea can be estimated in QCD using evolution equations of the form (1.20, 1.21)[101] corresponding to Fig. 9(b). Ideally, one should include in these equations the finite mass of the heavy quark.[114] Neglecting it,[101] one finds production cross sections for t and b quarks in high energy ep colliding rings which are several % at low x, being within a factor of 2 or 3 of the SU(f) symmetry predictions.

Production in e^+e^- collisions. The situation here is most favourable, since the production of heavy quarks is expected to be $\sim 3e_q^2 \times \sigma(e^+e^- \to \mu^+\mu^-)$ above threshold, and there may be a threshold enhancement because of an analogue of the ψ(4.03-4.16) just above charm threshold. Unfortunately, even SU(f) symmetry does not give a large increase in the cross section, or large signal-to-background ratio. One finds

$$\left.\begin{aligned} \frac{R_{b\bar{b}}}{R_{\text{total}}} &\approx \frac{\frac{1}{3}}{\frac{10}{3}+\frac{1}{3}} \approx 9\% \\ \frac{R_{t\bar{t}}}{R_{\text{total}}} &\approx \frac{\frac{4}{3}}{\frac{11}{3}+\frac{4}{3}} \approx 27\% \end{aligned}\right\} \tag{2.59}$$

which makes the experimental location of a new threshold nontrivial,[93] and identification of naked top or bottom particles very difficult. Several ways have been proposed for finding distinctive t or b signatures. One of them is suggested[93,53] by the expected dominance of t (or b) → $qq\bar{q}$ decays, which should populate top or bottom meson final states with 3 very embryonic "jets" for each b or t, making a total of 6 embryonic "jets" in an $e^+e^- \to t\bar{t}$ or $b\bar{b}$ final state as in Fig. 29. It is very unlikely that these multiple jets could be disentangled except if one were at extremely high energies and the t quark mass were very large. Close to threshold, one would expect the hadronic final states to be essentially isotropic,[93] rather like phase space. Above threshold

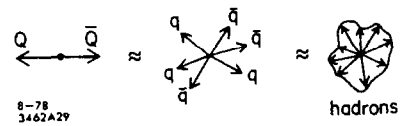

Fig. 29. Heavy quark-antiquark production just above threshold.

one would expect this isotropy to fade away gradually, so that for the thrust[53]

$$\langle 1-T\rangle_{\text{heavy}} \simeq \frac{1}{2}\left(\frac{Q_0^2}{Q^2}\right) \tag{2.60}$$

where Q_0 is the heavy threshold energy as shown in Fig. 30. One could imagine locating a new (t?) threshold by doing a relatively coarse energy scan looking for a jump in the fraction of events with high sphericity which should persist some way above threshold. Once the general location of such a threshold had been found, one could do a more conventional fine scan. A similar idea could be used to enhance the signal-to-background ratio for heavy $q\bar{q}$ final states by making cuts in sphericity or acoplanarity. Suppose you make a standard sphericity[13] analysis of each final state and identify the three eigenvalues λ_i (i=1,2,3) of the sphericity tnesor:

$$\lambda_1 \geq \lambda_2 \geq \lambda_3 \tag{2.61}$$

One may then define quantities

$$Q_i \equiv 1 - \frac{2\lambda_i}{\lambda_1+\lambda_2+\lambda_3} \tag{2.62}$$

for which different classes of events have the following characteristic values:

	Q_1	(Q_3-Q_2)
sphere	$\frac{1}{3}$	0
circular disc	0	0
2 jets	0	1
phase space	$\neq 0$	$\neq 0$

(2.63)

It is apparent from (2.63) that (Q_3-Q_2) is a measure of "jeticity",

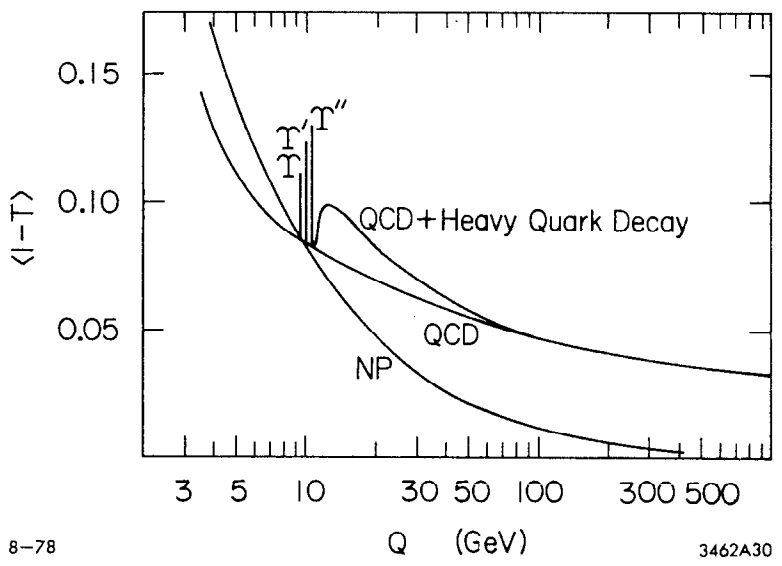

Fig. 30. The quantity <1-T> plotted[53] as a function of centre-of-mass energy as one crosses the $b\bar{b}$ threshold including naive parton nonperturbative contributions, QCD radiative corrections, the narrow resonances T, T' and T'', and the effect of the naked bottom[73] threshold.

while Q_1 is a measure of acoplanarity. One could imagine selecting heavy $q\bar{q}$ events either by making a "jeticity" cut, or by an acoplanarity cut, or by some more sophisticated combination of the two. To see how this procedure might work in practice, I have taken the distributions in Q_3-Q_2 and in Q_1 measured by PLUTO[58] in the e^+e^- continuum close to the T, and compared them with a phase space Monte Carlo[115] to mimic $b\bar{b}$ events in Fig. 31. Clearly the distributions are very different, and it appears that one may make cuts:

$$\text{Jeticity:} \quad Q_3-Q_2 \lesssim \frac{1}{2} : \left\{ \begin{matrix} 7/8 \text{ of } b\bar{b} \\ 1/4 \text{ of 2 jet continuum} \end{matrix} \right\} \begin{matrix} \text{survive} \\ \text{(Fig. 31(a))} \end{matrix} \tag{2.64a}$$

$$\text{Acoplanarity:} \quad Q_1 \gtrsim \frac{1}{18} : \left\{ \begin{matrix} 7/8 \text{ of } b\bar{b} \\ 1/3 \text{ of 2 jet continuum} \end{matrix} \right\} \begin{matrix} \text{survive} \\ \text{(Fig. 31(b))} \end{matrix} \tag{2.64b}$$

Thus it seems that the $b\bar{b}$ signal-to-background ratio may be enhanced by a factor of at least 3 by suitable cuts on the sphericity eigenvalues.

Another tactic may be to select single or multiple prompt lepton events.[32] If one uses the cascades (2.53) one has

$$\frac{R_e\big|_b}{R_e\big|_c} = \frac{1}{2} \; ; \quad \frac{R_{e^+e^-}\big|_b}{R_{e^+e^-}\big|_c} = \frac{1}{2} \tag{2.65}$$

where charm is expected to be the dominant background, while final states with $e^{\pm}e^{\pm}$, or 3 or 4 leptons could only come from $b\bar{b}$ production--until the $t\bar{t}$ threshold is reached. Such triggers suffer from two defects: they knock down the event rate by a factor of 5 to 10 for each semi-leptonic decay, and it is difficult to reconstruct an invariant mass peak when semileptonic decays are involved.

Before leaving the subject of $b\bar{b}$ production, it may be worthwhile to point out some intriguing aspects of b meson decays which would cast

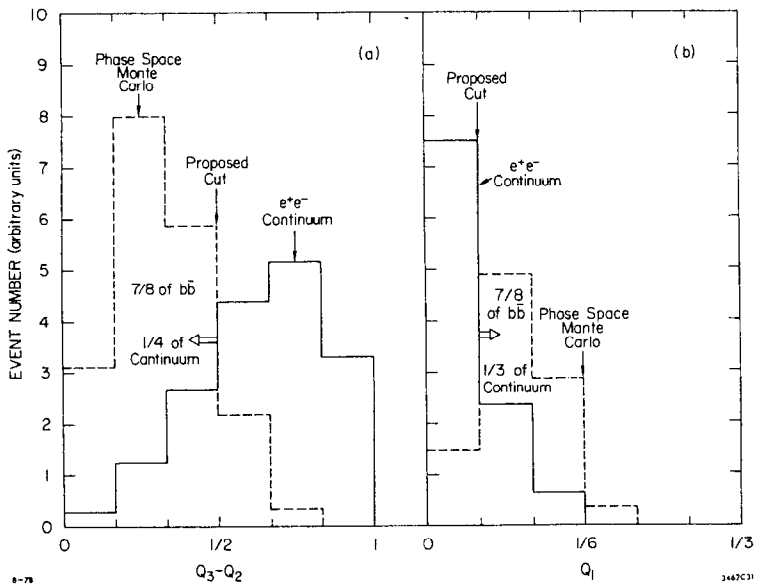

Fig. 31. Distributions (a) in jeticity (see text), and (b) in acoplanarity, comparing PLUTO[58] e^+e^- continuum data with a phase space Monte Carlo[115] expected to mimic heavy $q\bar{q}$ events just above threshold.

strong light on the validity of the KM[102] model and CP violation. These topics are treated in more detail in the talk by M. K. Gaillard[116] at this Summer Institute. The subject of K^o-$\bar{K}^o$ mixing has been touched on already, and is expected to be large in the GIM-KM model, as observed experimentally. It is expected that D^o-$\bar{D}^o$ mixing should be very small $O(10^{-3}$ to $10^{-4})$,[104] since it is sensitive to m_s^2 rather than m_c^2, and comes from diagrams which are Cabibbo disfavoured by comparison with the dominant $c \to s+X$ decays. In the case of $B^o(\equiv b\bar{d})$ - $\bar{B}^o(\equiv \bar{b}d)$ meson mixing, mixing is expected to be intermediate between that in the K^o-$\bar{K}^o$ and D^o-$\bar{D}^o$ systems. The relevant mixing parameter is[69]

$$\left|\frac{\Delta m_B}{\Gamma_B}\right| \approx \frac{m_t^2}{700\ \text{GeV}} \qquad (2.66)$$

where the sensitivity to m_t^2 is intrinsic to the models while the precise number in the denominator is rather uncertain. Since $m_t \geq 7$ GeV, Eq. (2.66) tells us that probably

$$D^o\text{-}\bar{D}^o \text{ mixing} < B^o\text{-}\bar{B}^o \text{ mixing} < K^o\text{-}\bar{K}^o \text{ mixing}$$

and this could be the only route to a phenomenological estimate of m_t before the t is found. Mixing would yield

$$e^+e^- \to B^oB^oX\ , \quad B^oB^+X\ , \quad \bar{B}^oB^-X\ , \quad \bar{B}^o\bar{B}^oX \qquad (2.67)$$

final states, whose primary decay leptons could give like-sign $e^\pm e^\pm$ signatures. Unfortunately, these could also come from cascade decay confusion, though this may be reduced by making a suitable lepton momentum cut[117]: primary leptons should be harder.

Since the KM model has interesting results for CP violation in K decays, it is natural to ask about its implications for bottom meson

systems. In the case of K^o and D^o meson decays, the KM[102] model generally reproduces the predictions of the superweak theory,[69,118] with the usual CP violating parameters

$$|\epsilon_K|, \ |\epsilon_D| \approx O(2s_2s_3 \sin\delta) \approx 2 \times 10^{-3} \tag{2.68}$$

as foreshadowed in Eq. (2.55). The model also predicts a very small neutron electric dipole moment, $\lesssim 10^{-28}$ cm and much smaller than the present experimental limit $\lesssim 3 \times 10^{-24}$ cm.[119] For the B^o-$\bar{B}^o$ system the corresponding CP violating parameter is much larger[69]:

$$|\epsilon_B| \approx \tan 2\delta >> 10^{-3} \tag{2.69}$$

Thus the CP violation could be substantial. A characteristic signature for it would be

$$\sigma(e^+e^+) \neq \sigma(e^-e^-) \tag{2.70}$$

in any region of $e^\pm$ phase space. The expected magnitude of the effect (2.70) is strongly dependent on the values of the mixing angles and m_t,[120] since both $|\epsilon_B|$ (2.69) and $|\Delta m_B/\Gamma_B|$ (2.66) must be large to get large effects.

The bottom may not be "just another quark" but may yield important insight into the great unsolved problem of CP violation. Maybe that is why we need the fifth and sixth quarks, which a fortiori is why we had the third and fourth quarks and the muon!

3. The Intermediate Vector Bosons

3.1 Introduction

We now turn to that most characteristic aspect of gauge theories, the intermediate vector bosons. We will be primarily interested in their spectroscopy and couplings to elementary fermions, but as was emphasized in section 2.1, the study of their interactions among themselves is also very important. This is, after all, the feature that should make them gauge bosons rather than just any old intermediate vector bosons. We will start off by summarizing the masses and widths one expects for charged and neutral vector bosons in a general weak interaction model, but will often use for illustration the Weinberg-Salam model with $\sin^2\theta_W \approx 0.20$. This is the value found in the latest inclusive νN[25] and polarized eD experiments.[77] It leads to rather higher masses and widths for the $W^\pm$ and Z^o than one had previously grown used to contemplating.[9] After reviewing their properties,[93,121,127] we will then move on to discuss how the $W^\pm$ and Z^o may be discovered in hadron-hadron collisions,[9] which seem likely to give our first glimpses of them. We will look at backgrounds as well as cross sections, using as a guide the scale-breaking and differential cross sections expected on the basis of QCD.[123] Then we will study $W^\pm$ and Z^o effects in ep collisions.[101,124] It will transpire that these are not the best way to produce the vector bosons directly, but they allow one to observe weak/electromagnetic interference effects in regions of large Q^2 where they are O(1). One should be able to see clear derivations from the pointlike four-fermion weak interaction, and see the effects of the finite boson masses. Next we will turn to e^+e^- experiments,[93,121,122] discussing in particular the dramatic Z^o peak with its prodigious event rate and the opportunities it affords for precision weak interaction studies and analyses of rare decays. The final section will examine phenomena away from the Z^o peak, including in particular the reaction $e^+e^- \to W^+W^-$,[125,126] which affords a unique opportunity to see the gauge theoretic cancellation

of diagrams at work. The important possibility of seeing the three-point couplings between vector bosons will be mentioned.

It will be clear that while hadron-hadron collisions offer the most immediate prospects for exploratory experiments to find the $W^{\pm}$ and Z^{o}, detailed studies of them will only be possible with $e^{+}e^{-}$ machines.

3.2 Properties of the Vector Bosons

3.2.1 Charged bosons

If we assume that a unique pair of charged vector bosons $W^{\pm}$ is responsible for the observed charge-changing weak interactions, then its decay width to $e^{-}\bar{\nu}_{e}$ is easily calculated[122] to be

$$\Gamma(W^{-} \to e^{-}\bar{\nu}_{e}) \approx \frac{Gm_{W}^{3}}{6\pi\sqrt{2}} \tag{3.1}$$

If we assume that all other fermions occur only in left-handed doublets, their decay rates are simply related to (3.1) by

$$\Gamma(W^{-} \to e^{-}\bar{\nu}_{e}):\Gamma(W^{-} \to \mu^{-}\bar{\nu}_{\mu}):\Gamma(W^{-} \to \tau^{-}\bar{\nu}_{\tau}):$$
$$\Gamma(W^{-} \to d\bar{u}):\Gamma(W^{-} \to s\bar{u}):\Gamma(W^{-} \to d\bar{c}):\Gamma(W^{-} \to s\bar{c}):\Gamma(W^{-} \to b\bar{t})$$
$$\approx 1:1:1:\sim 3\cos^{2}\theta_{c}:\sim 3\sin^{2}\theta_{c}:\sim 3\sin^{2}\theta_{c}:\sim 3\cos^{2}\theta_{c}:\sim 3 \tag{3.2}$$

where the factors of 3 come from colour, and we have neglected the generalized Cabibbo angles θ_{2} and θ_{3}. If there are N_{D} doublets of quarks and leptons, each with the sums of their masses $<m_{W}$ then it is clear that the branching ratio

$$B(W^{-} \to e^{-}\bar{\nu}_{e}) \approx \frac{1}{4N_{D}} \tag{3.3}$$

and the minimal "known" three doublets of everything would imply

$$B(W^{-} \to e^{-}\bar{\nu}_{e}) \approx B(W^{-} \to \mu^{-}\bar{\nu}_{\mu}) \approx \frac{1}{12} \tag{3.4}$$

In order to fix the mass of the $W^{\pm}$ we will assume the Weinberg-Salam model in which

$$m_{W^{\pm}} = \sqrt{\frac{\pi\alpha}{\sqrt{2}\,G}}\,\frac{1}{\sin\theta_{W}} \tag{3.5}$$

If we take the latest experimental value of $\sin^{2}\theta_{W} \approx 0.20$, then we find

$$m_{W^{\pm}} \approx 84 \text{ GeV} \tag{3.6}$$

Armed with this mass estimate we return to Eq. (3.1) to find that

$$\Gamma(W^{-} \to e^{-}\bar{\nu}_{e}) \approx 230 \text{ MeV} \tag{3.7}$$

while Eq. (3.3) implies that

$$\Gamma(W^{-} \to \text{all}) \approx 900\, N_{D} \text{ MeV} \tag{3.8}$$

and the minimal $N_{D}=3$, 6 quark, 6 lepton model would have

$$\Gamma(W^{-} \to \text{all}) \approx 2.7 \text{ GeV} \tag{3.9}$$

This is intriguingly wide so that one begins to wonder whether its width can be measured experimentally in hadron-hadron or $e^{+}e^{-}$ collisions. Notice that according to high energy physics, $\Gamma(W^{-} \to \text{all})$ could be larger because of the paltry limit (2.16) on the number of "massless" neutrinos, and the lack of any other limits on the number of massive fermions in the mass range $\lesssim m_{W}$. Life would indeed be interesting if the W^{-} had too small a leptonic branching mode (3.3) to be detectable!

3.2.2 Neutral bosons

It is by no means universally accepted that a unique Z^{o} boson is responsible for the observed neutral current phenomena,[75] so let us adopt a flexible parametrization[93] of the Z^{o}-f-$\bar{f}$ interaction

$$\mathscr{L}_{Z} = -m_{Z}\left(\frac{G_{F}}{\sqrt{2}}\right)^{1/2} Z^{\mu}\bar{f}\gamma_{\mu}\left(\frac{v_{f}-a_{f}\gamma_{5}}{\sqrt{2}}\right) f \tag{3.10}$$

In terms of the vector (v_f) and axial (a_f) couplings so defined, the Z^0 decay width is just

$$\Gamma(Z^0 \to \text{all}) \approx \frac{Gm_Z^3}{24\sqrt{2}\,\pi}\left[\sum_{\text{leptons}}\left(v_\ell^2+a_\ell^2\right) + 3\sum_{\text{quarks}}\left(v_q^2+a_q^2\right)\right] \tag{3.11}$$

In the Weinberg-Salam model[12] the couplings are specified as follows:

$$\left.\begin{aligned} &a_e = a_\mu = a_\tau = -1, \quad && v_e = v_\mu = v_\tau = -1 + 4\sin^2\theta_W \\ &a_\nu = 1 \quad , && v_\nu = 1 \\ &a_u = a_c = a_t = 1, && v_u = v_c = v_t = 1 - \tfrac{8}{3}\sin^2\theta_W \\ &a_d = a_s = a_b = -1, && v_d = v_s = v_b = -1 + \tfrac{4}{3}\sin^2\theta_W \end{aligned}\right\} \tag{3.12}$$

Inserting these couplings into Eq. (3.11) we find the following total Z^0 decay rate:

$$\begin{aligned}\Gamma(Z^0 \to \text{all}) \sim \frac{Gm_Z^3}{24\sqrt{2}\,\pi}\Big\{&\left(1 + \left(1 - 4\sin^2\theta_W\right)^2\right) N_{\ell^-} + 2N_\nu \\ &+ 3\left(1 + \left(1 - \tfrac{8}{3}\sin^2\theta_W\right)^2\right) N_{2/3} \\ &+ 3\left(1 + \left(1 - \tfrac{4}{3}\sin^2\theta_W\right)^2\right) N_{-1/3}\Big\}\end{aligned} \tag{3.13}$$

where we have been agnostic about the numbers of particles of each type. If we assume $\sin^2\theta_W \approx 0.20$ as before, we find the relative decay rates

$$\Gamma(Z^0 \to \nu\bar{\nu}):\Gamma(Z^0 \to \ell^+\ell^-):\Gamma(Z^0 \to u\bar{u}):\Gamma(Z^0 \to d\bar{d})$$

$$2:1.04:3.63:4.67 \tag{3.14}$$

To go further, we need to estimate m_{Z^0}. If the Weinberg-Salam model only has I=1/2 Higgs multiplets, then as discussed in Lecture 2[127]

$$\frac{m_Z}{m_W} \approx \frac{1}{\cos\theta_W} \tag{3.15}$$

and present data on neutral current cross sections suggest[78] that the mass formula (3.15) is correct to within $(1 \pm 2\tfrac{1}{2})\%$. Taking $\sin^2\theta_W \approx 0.20$ as before then yields

$$m_Z \approx 94 \text{ GeV} \tag{3.16}$$

which is rather higher than the traditional guess[9,93] of 80 GeV. We then see from Eq. (3.13) that

$$\Gamma(Z^0 \to e^+e^-) \approx 82 \text{ MeV} \tag{3.17}$$

and from Eq. (3.14)

$$B(Z^0 \to e^+e^-) \approx \frac{1}{11N_D} \tag{3.18}$$

Correspondingly the total Z^0 decay width

$$\Gamma(Z^0 \to \text{all}) \approx 900\, N_D \text{ MeV} \tag{3.19}$$

and if there are the traditional minimal 3 doublets then

$$B(Z^0 \to e^+e^-) \approx 3\% \,, \quad \Gamma(Z^0 \to \text{all}) \approx 2.7 \text{ GeV} \tag{3.20}$$

Notice that in this case we really do have to worry about the number of "massless" neutrinos since the Z^0 will decay indiscriminately into all of them. If the cosmological bound[87] is disastrously wrong, the observable e^+e^- decay mode could have an embarrassingly small branching ratio.

Before leaving this section, it should be mentioned what general, model-independent bounds exist on the masses of the $W^\pm$ and Z^0. Bjorken[128] was able to show on reasonably general gauge theoretical assumptions that $m_{W^\pm}$ should be within about 20% of the Weinberg-Salam value (3.6), while m_{Z^0} was only constrained to be <200 GeV unless more stringent assumptions were made. Gauge theories generally seem to like to have their vector boson masses in the range up to 200 GeV. To my knowledge, the only indication that they really should have this mass scale comes from the

calculation[105] of radiative corrections to μ-quark universality (2.42), which would come somewhat unstuck if the boson masses were as high as the unitarity limit. It seems that a conservative hadron-hadron experiment to search out vector bosons should have sensitivity up to $m_{W^\pm}$, $m_{Z^0} \sim 200$ GeV. On the other hand, the phenomenological successes and aesthetic economy of the basic Weinberg-Salam make a gamble on a "Z^0 factory" e^+e^- machine with 50 or 60 GeV energy per beam look like a reasonable bet.

3.3 Production in Hadron-Hadron Collisions

To estimate the cross sections for $W^\pm$ and Z^0 production in hadron-hadron collisions we will use a cautious approach. First we will derive conservative "lower bounds" from the CVC and scaling hypotheses, then calculate the cross section using a naive parton Drell-Yan[9] mechanism which incorporates these two assumptions. Finally, we will use QCD to estimate the effects of scaling violations,[129] and the p_T distributions which are expected to be rather broader than in the naive parton model.

In order to produce a $W^\pm$ or Z^0 it is necessary to bring together to a point a quark and an antiquark. But the same mechanism is needed to produce a γ^* and hence a massive $\mu^+\mu^-$ (or e^+e^-) pair, so one should be able to relate the cross sections. The $W^\pm$ may be produced by vector or axial currents, so

$$\sigma_W = [\sigma_W]_V + [\sigma_W]_A \geq [\sigma_W]_V \tag{3.21}$$

If one neglects s, c and heavier quarks, then the $W^\pm$ are produced by the I=1 current $\bar{u}d$, and one can use CVC in Eq. (3.21) to obtain

$$\langle\sigma_W\rangle \equiv \frac{1}{4}\left[\sigma_{W^+}(pp) + \sigma_{W^-}(pp) + \sigma_{W^+}(pn) + \sigma_{W^-}(pn)\right]$$

$$\geq \frac{3G\cos^2\theta_c}{4\alpha^2\sqrt{2}}\, m_W^4 \left[\frac{d\sigma}{dM^2}(pp \to \ell^+\ell^- X) + \frac{d\sigma}{dM^2}(pn \to \ell^+\ell^- X)\right]_{I=1} \tag{3.22}$$

Hence the W and $\ell^+\ell^-$ continuum cross sections are related by the "conditional lower bound":

$$\langle\sigma_W\rangle \geq 0.22\ \text{GeV}^{-2}\, m_W^4 \left\langle \frac{d\sigma}{dM^2}(\ell^+\ell^-)\right\rangle_{I=1} \tag{3.23}$$

To use the bound (3.13) we must make a large extrapolation, because there are experimental data on $pN \to \ell^+\ell^- X$ only at low values of s and M^2. But if the $\ell^+\ell^-$ continuum is produced in a pointlike manner, the scaling law

$$M^4 \frac{1}{dM^2} = f\left(\tau \equiv \frac{M^2}{s}\right) \tag{3.24}$$

applies. Using the scaling law in the bound (3.23) and neglecting possible I=0 contributions one finally obtains

$$\left\langle \sigma_W\left(\frac{m_W^2}{s} = \tau\right)\right\rangle \geq 0.22\ \text{GeV}^{-2}\, f(\tau) \tag{3.25}$$

As an example, let us take $\sqrt{s} = 540$ GeV, $m_W = 84$ GeV in which case experimental data on $pN \to \ell^+\ell^- + X$ at $\sqrt{s} = 27$ GeV suggest

$$\left\langle \sigma_W\left(\frac{m_W^2}{s} = 0.024\right)\right\rangle \geq 2 \times 10^{-34}\ \text{cm}^2 \tag{3.26}$$

The above estimate is not very satisfactory, since it depends on assumptions about the neglect of I=0 contributions to the cross sections, and neglects production by axial currents. To go further, we use the

naive parton model which enables these contributions to be calculated, as well as obeying the CVC and scaling assumptions. The simple Drell-Yan[16] collision mechanism of Fig. 3 yields[9]

$$\frac{d\sigma}{dx}(a+b \to W+X) = G\pi\sqrt{2}\, H(\tau,x) \tag{3.27}$$

where $x \equiv 2p_{\parallel}^{W}/\sqrt{s}$, $\tau \equiv m_W^2/s$ and

$$H(\tau,x) \equiv \frac{x_a x_b}{\sqrt{x^2+4\tau}} W_{ab}^{\pm}(x_a,x_b) \tag{3.28}$$

where $W_{ab}^{\pm}(x_a,x_b)$ is the $q\bar{q}$ annihilation luminosity in ab collisions:

$$W_{ab}^{+}(x_a,x_b) \equiv \frac{1}{3}\left(u_a(x_a)\bar{d}_b(x_b) + \bar{d}_a(x_a)u_b(x_b)\right)\cos^2\theta_c + [s,c,\ldots] \text{ contributions} \tag{3.29}$$

and $W_{ab}^{-}(x_a,x_b)$ is defined similarly to (3.29) by interchanging quarks and antiquarks. If one puts reasonable distributions of sea antiquarks into the formulae (3.27, 3.28, 3.29) one finds that for $m_W = 84$ GeV and $\sqrt{s} \sim 540$ to 800 GeV (see Fig. 32)

$$\begin{aligned}\sigma(pp \to W^{+}+X) &\sim 2 \times 10^{-33}\ \text{cm}^2\\ \sigma(pp \to W^{-}+X) &\sim 1 \times 10^{-33}\ \text{cm}^2\\ \sigma(pp \to W^{\pm}+X) &\sim 3 \times 10^{-33}\ \text{cm}^2\end{aligned} \tag{3.30}$$

In assessing the observability of the cross sections (3.30), one should not forget to fold in the branching ratio into a detectable final state such as $e^{-}\bar{\nu}_e$ or $\mu^{-}\bar{\nu}_{\mu}$, which the lower bound of 3 lepton and quark doublets implies will be $\lesssim 8\%$.

A precisely analogous calculation to the above can be done for Z^{o} production to yield

$$\sigma(pp \to Z^{o}+X) \sim 1 \times 10^{-33}\ \text{cm}^2$$

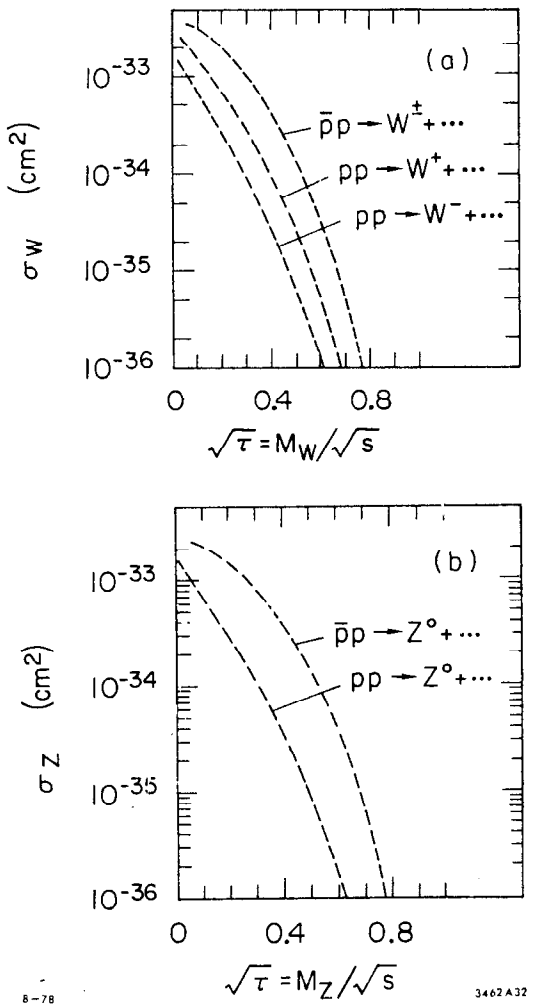

Fig. 32. Cross sections for (a) $W^{\pm}$ and (b) Z^{o} production in pp and $\bar{p}p$ collisions as functions of m^2/s, taken from Quigg.[9]

$$\sigma(\bar{p}p \to Z^0+X) \sim 2 \times 10^{-33} \text{ cm}^2 \qquad (3.31)$$

in the centre-of-mass energy $\sqrt{s} \sim 540$ to 800 GeV. The cross sections (3.31) are somewhat smaller than for the $W^\pm$ (3.30), and the observable leptonic decay modes $Z^0 \to e^+e^-, \mu^+\mu^-$ are expected to have somewhat smaller branching ratios, $\lesssim 3\%$ for $\gtrsim 3$ lepton and quark doublets.

The naive parton model makes predictions for the differential cross sections as well as the total. Distributions for the decays $W^\pm \to \mu^\pm(+\nu)$ or $W^\pm \to$ hadron jets are also easy to calculate because the polarization state of the $W^\pm$ is known. Representative calculations from the paper of Quigg[9] are shown in Fig. 33. We see that there is a large charge symmetry violating forward-backward asymmetry in the distributions of leptons from $W^\pm$ produced in $\bar{p}p$ collisions. Unfortunately, this effect is likely to be very small in Z^0 production which may lead the sceptic to question how one knows that the "weak" Z^0 is being produced, rather than just any "strong" vector meson V. Paradoxically, the cross section for such an hadron V is expected to be much smaller than that for a Z^0 of comparable mass, since the "charmonium" Zweig rule is expected to suppress $\Gamma(V \to \text{hadrons})$ to a few dozen keV, while $\Gamma(Z^0 \to \text{hadrons})$ is O(1) GeV, and the production rates are probably roughly proportional to the hadronic decay widths.[130] A characteristic of the naive parton model[5] is its p_T cutoff for partons, and hence the expected low $\langle p_T \rangle$ for the produced $W^\pm$ and Z^0.[16] This prediction is presumably wrong, since the p_T of observed $\ell^+\ell^-$ pairs in hadron-hadron collisions seems to increase[131] with M^2 if $\tau \equiv m^2/s$ is held fixed. Such behaviour is expected in QCD (or any other field theory) where the pointlike nature of the fundamental interactions implies $\langle p_T \rangle = O(M) \times \text{logs}$.[7,38,39] Field theories

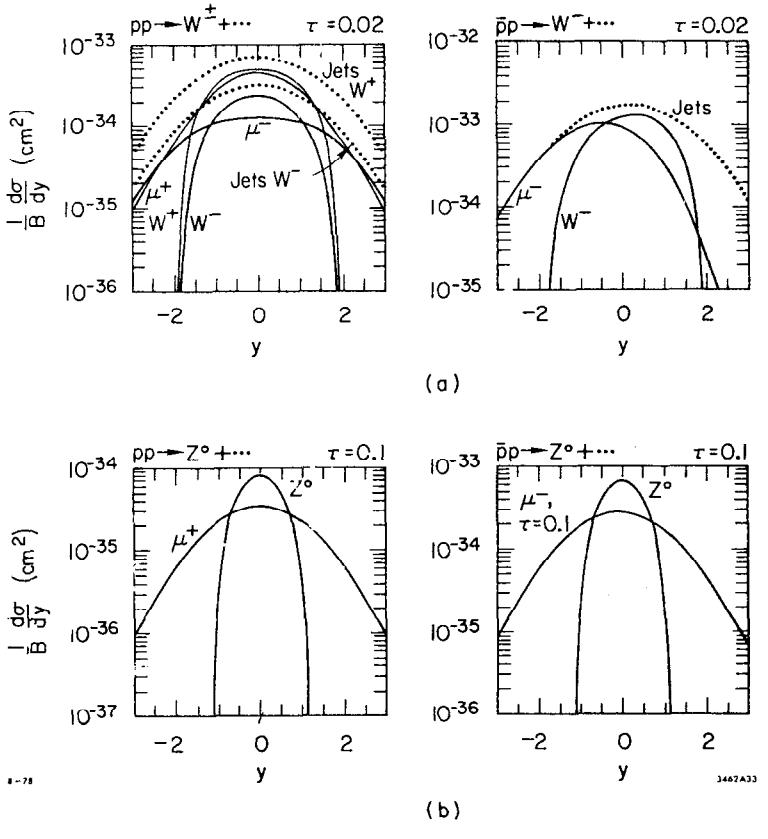

Fig. 33. Differential cross sections in rapidity for decay products of (a) $W^\pm$ and (b) Z^0 with $\sin^2\theta_W = 0.3$, taken from Quigg.[9]

also expect scaling violations in the cross sections, analogous to those predicted and observed (Fig. 10) in deep inelastic leptoproduction. Surely we would not expect scaling in $pp \to \ell^+\ell^- + X$ to be sacrosanct if it is violated in $\ell p \to \ell + X$.[19]

In QCD, modifications to the naive parton cross section formulae come from radiative corrections to the fundamental $q\bar{q}$ annihilation process, and from new processes such as $q\bar{q} \to W+q$, $G+q \to W+q$, etc. as in Fig. 34. The important changes in the $W^\pm$ or Z^0 cross section are threefold. First, in the $q\bar{q}$ annihilation luminosity (3.29) one should use[132,133] the Q^2 dependent effective parton distributions[42] introduced in Lecture 1. Analysis of the logarithms of perturbation theory[51,132] shows that the leading Q^2 (or $M^2_{\ell^+\ell^-}$) evolution of the Drell-Yan cross section is correctly taken up by this substitution:

$$W^+_{ab}(x_a,x_b) \to \frac{1}{3}\left[u_a\left(x_a,M^2\right)d_b\left(x_b,M^2\right) + \bar{d}_a\left(x_a,M^2\right)u_b\left(x_b,M^2\right)\right]\cos^2\theta_c + \left[s,c,\ldots(M^2)\right] \text{ contributions} \qquad (3.32)$$

with $u_a\left(x_a,M^2\right)$, etc. obeying Eqs. (1.20, 1.21). There are also radiative corrections to the basic cross section formula (3.28) relating $H(\tau,x)$ to $W^\pm_{ab}(x_a,x_b)$. These will be $O(\alpha_s/\pi)$ and not very important relative to the effect of going from (3.29) to (3.32). More important is the third effect, which is to add to the $q\bar{q}$ annihilation subprocess essentially new subprocesses such as $q+G \to q+W$ as in Fig. 34. The cross section for these reactions will be superficially $O(\alpha_s/\pi)$ or $O(\alpha_s/\pi)^2$, but the effective luminosities analogous to (3.29) may be considerably larger, at least in pp collisions.[134] In this case the density of $\bar{q}$ is rather small, $O\left(\frac{1}{10}\right)$ of the valence quarks, which can compensate for the (α_s/π)

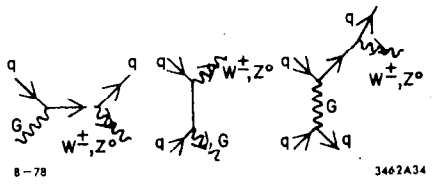

Fig. 34. Subdominant QCD subprocesses for vector boson production.

suppression of other subprocess cross sections. In $\bar{p}p$ collisions both the q and $\bar{q}$ in (3.32) can be valence, so that the expected effect of these extra subprocesses is relatively smaller.

Figure 35 shows a typical QCD calculation[133] of the corrections to the naive parton formulae (3.27, 3.28, 3.29) due to the effective $q(M^2)$ substitution (3.32). It transpires that the effects on the expected $W^{\pm}$ or Z^0 cross sections (3.30) and (3.31) are relatively small, because for the likely range of m_W^2/s there is a cross-over in the QCD scaling violation effects. This reflects the behavior of the QCD calculations of $F_2^{eN}(x,Q^2)$ shown in Fig. 10 (see also the experimental data), which indicate that for foreseeable values of Q^2 the structure function does not change much in the neighborhood of $x \approx 0.15$. On the other hand, the effects of QCD scaling violations are potentially rather serious at larger values of m^2/s. This may pose problems for the production of gauge bosons much more massive than 200 GeV in the presently discussed generation of $\bar{p}p$ and pp colliding ring machines, and is one reason why a low energy ($\sqrt{s} \lesssim 300$ GeV) pp collider was somewhat unappetizing. As mentioned above, the other QCD corrections to the formulae (3.27, 3.28, 3.32) are expected not to be very important in $\bar{p}p$ collisions. This is reflected in Fig. 36[133] which shows a calculation of the fractional modification of the cross section (3.27, 3.28, 3.32) expected in both $\bar{p}p$ and pp collisions. We notice that in the likely range of interest for $m^2/s \sim 0.01$ to 0.1 the modifications to the $q\bar{q}$ annihilation formulae are not even very big in pp collisions, though the effects at large m^2/s are again embarrassingly suppressive.

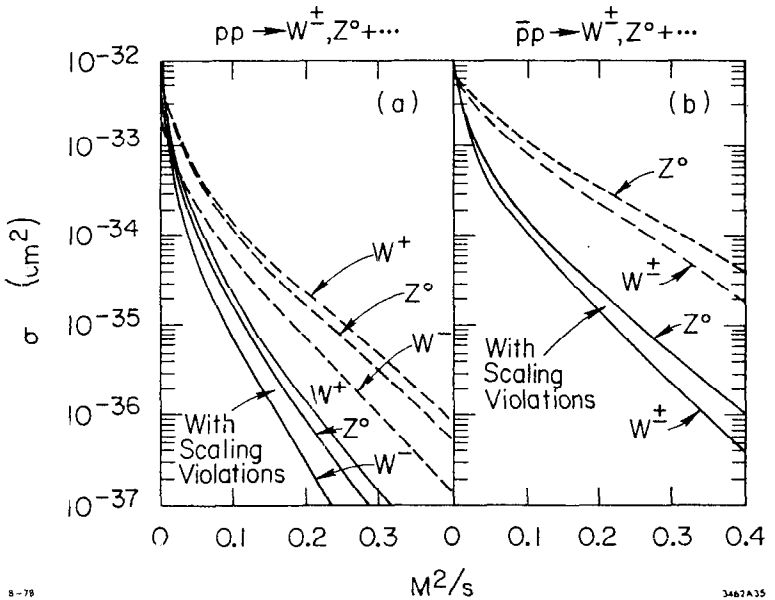

Fig. 35. Estimates[129] of the effects of QCD scaling violations in the quark distributions (3.34) on the vector boson production cross sections in (a) pp, (b) $\bar{p}p$ collisions.

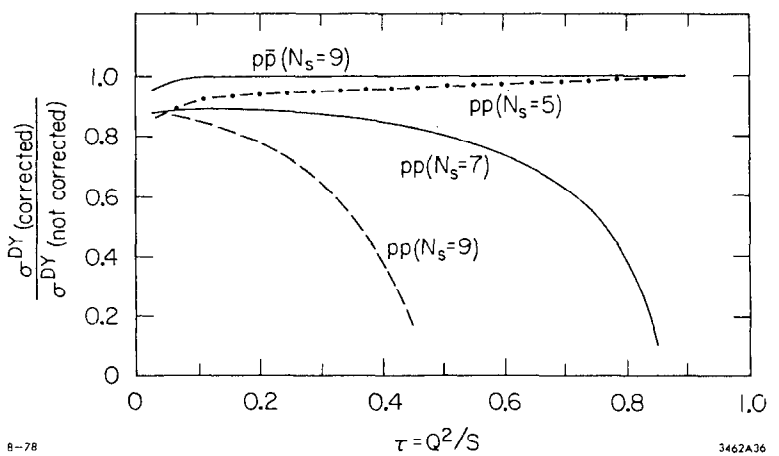

Fig. 36. Estimates[133] of the QCD modifications to the $q\bar{q}$ annihilation cross section contribution (3.32) for $q\bar{q}$ sea distributions $1/x\ (1-x)^{N_S}$.

As mentioned earlier, it is expected that $\langle p_T \rangle$ should be large for vector bosons produced in QCD. Generally one expects a typically bremsstrahlung cross section with

$$\langle p_T^n \rangle = O\left(\frac{\alpha_s}{\pi}\right) \quad M_{W,Z}^n$$

A typical calculation[123] of $\langle p_T^2 \rangle$ is shown in Fig. 37. However, it should be emphasized that there is no solid indication yet that the p_T distributions of Drell-Yan lepton pairs seen so far are well described by QCD. In line with the discussion of growing $\langle p_T \rangle$ and jets in section 1.5, one would expect that $W^\pm$ or Z^o production events with large p_T would be accompanied by an opposite side gluon or quark jet.[135]

So far we have said relatively little about how one might look for vector bosons in hadron-hadron collisions. The best prospects are apparently provided by $Z^o \to e^+e^-$ or $\mu^+\mu^-$ decay, where one has an invariant mass peak to find superimposed on a continuum background which is expected to be very small. The large $\langle p_T \rangle$ of the Z^o should not disturb us, as long as we have a detector with sufficiently large lepton acceptance. The next most likely signature would appear to be $W^\pm \to \ell^\pm(\nu)$ decay. Here there is no invariant mass peak to be found, but the kinematics of $W^\pm$ decay give the $\ell^\pm$ spectrum quite a well-defined Jacobian peak in p_T as long as the $\langle p_T \rangle$ of the $W^\pm$ is not too large. Figure 38 shows a calculation[123] of the spread of the $W^\pm$ Jacobian peaks expected in QCD. The smearing is not disastrous, despite the relatively large p_T (3.33) expected in QCD. The reason is apparently the characteristic bremsstrahlung shape of the spectrum, which keeps a sharp peak at $p_T \sim 0$. Also shown in Fig. 38 is a calculation[123] of the lepton background expected in QCD which is two or three orders of magnitude below the peak. However, it should be noticed that no experiment has ever found such a

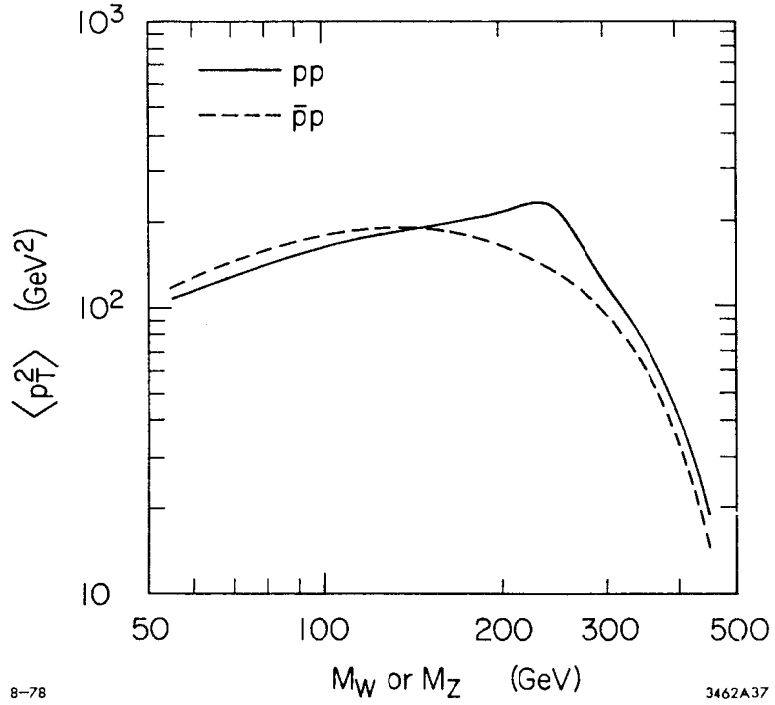

Fig. 37. A calculation[123] of $\langle p_T^2 \rangle$ for different values of the boson mass in pp and $\bar{p}p$ collisions at $\sqrt{s}$ = 540 GeV.

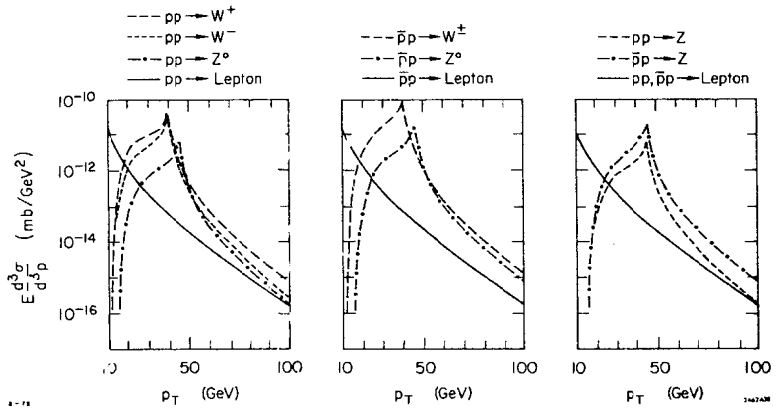

Fig. 38. A calculation[123] of the Jacobian peak with QCD calculations of the p_T smearing and likely lepton backgrounds, using $\sin^2 \theta_W$ = 0.21 and $\sqrt{s}$ = 540 GeV.

nice Jacobian peak, and one could certainly imagine ways in which the neat pictures of Fig. 38 could be diluted.[136] For example $W^{\pm} \to \tau^{\pm}(\nu)$ would give prompt leptons which could start filling in the holes at p_T=O(20) GeV, or there could be large numbers of prompt leptons coming from heavy quark decays to push up the background levels. There are of course features of the W decay leptons which could be used to suppress background contamination. For one thing, the missing unobserved neutrino will cause lots of p_T to be missing, and this could be noticed by a detector with sufficiently large acceptance. For another thing, plausible backgrounds would not have the charge-symmetry violating forward-backward asymmetry of W decay leptons in $\bar{p}p$ collisions shown in Fig. 33. It therefore seems likely that the $W \to e\nu$ or $\mu\nu$ decays could also be seen in hadron-hadron collision experiments.

Much more difficulty will be experienced with hadronic decays of the vector bosons. These should give two jets with an invariant mass of 84 or 94 (?) GeV, but the background expected from QCD is very large. The fundamental q-q, q-G and G-G scattering processes in QCD give a p_T^{-4} hadron background,[137] which will mainly be in the form of pairs of jets with a continuous mass distribution at a level considerably above the $W^{\pm}$ and Z^o production rates. Figure 39 shows a calculation[123] of the $pp \to$ jet+X QCD background. (It also features guesses at the prompt γ and μ spectrum which are useful in estimating backgrounds to the search for leptonic decays of the vector bosons.) In the absence of a cunning trick for suppressing the QCD background, it seems to me unlikely that the vector bosons will be easy to find in their hadronic decay modes.

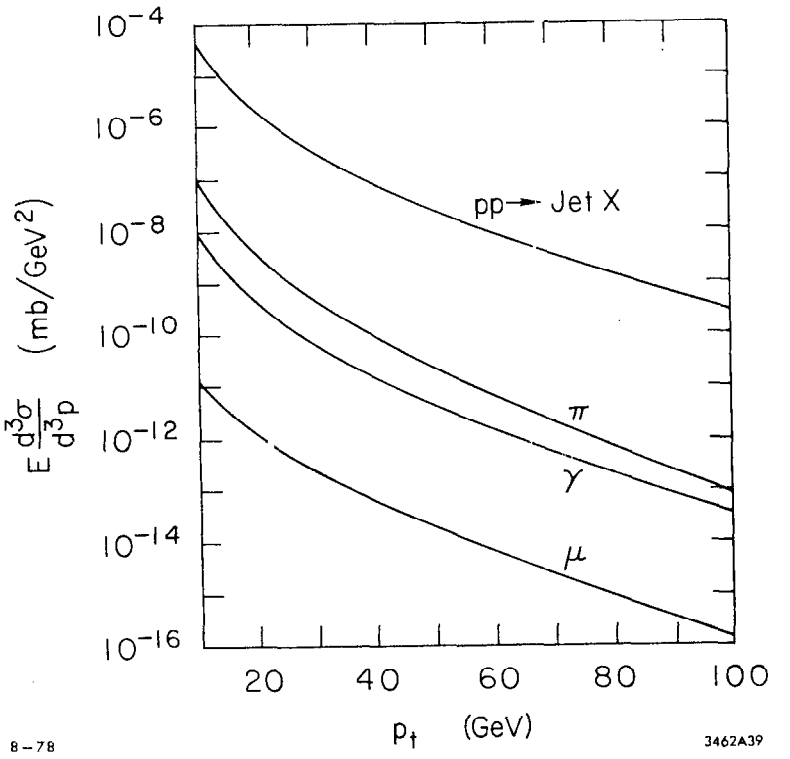

Fig. 39. QCD calculations[123] of jet, π, γ and muon cross sections in pp collisions at $\sqrt{s}$ = 540 GeV.

Before leaving the topic of vector boson production in hadron-hadron collisions, it may be worthwhile to remember[138] that the production of W^+W^- or Z^oZ^o pairs is not totally negligible:

$$\frac{\sigma(pp \to W^+W^-X)}{\sigma(pp \to W^-X)} = O\left(\frac{\alpha}{\pi}\right) \tag{3.34}$$

Some relevant graphs are shown in Fig. 40, and the results of a naive parton cross section calculation are[138] shown in Fig. 41. It seems that for pp collisions at $\sqrt{s} \sim 800$ GeV one might expect cross sections

$$\begin{aligned} \sigma(pp \to W^+W^-X) &\sim 10^{-36}\ \text{cm}^2 \\ \sigma(pp \to Z^oZ^oX) &\sim 10^{-37}\ \text{cm}^2 \end{aligned} \tag{3.35}$$

Given the luminosity $O(10^{33}\ \text{cm}^{-2}\ \text{sec}^{-1})$ expected at Isabelle, it should be possible to detect the processes (3.35). It is apparent from Fig. 40 that the W^+W^- production process is sensitive to the 3-boson vertex. However the measurement of it in this reaction seems much more tricky than in e^+e^- collisions because of the large backgrounds in hadron-hadron collisions.

3.4 Effects in ep Collisions

Let us first consider[101,124] the direct production of $W^\pm$ and Z^o in ep collisions. The most important Feynman diagrams are those shown in Fig. 42. Production from the lepton vertex is generally larger than that from the hadron vertex because the hadron momentum is shared out between a number of quarks and gluons, only one of which can participate in any given reaction. Forms for the cross sections are rather complicated and not of intrinsic interest, so they will not be exhibited here.[101,124] In Fig. 43 are plotted the cross sections for $ep \to \nu WX$ and $ep \to eZX$. We see that for immediately foreseeable centre-of-mass energies for ep

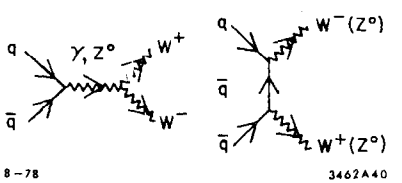

Fig. 40. Diagrams used in calculating $pp \to W^+W^-X$ and Z^oZ^oX .

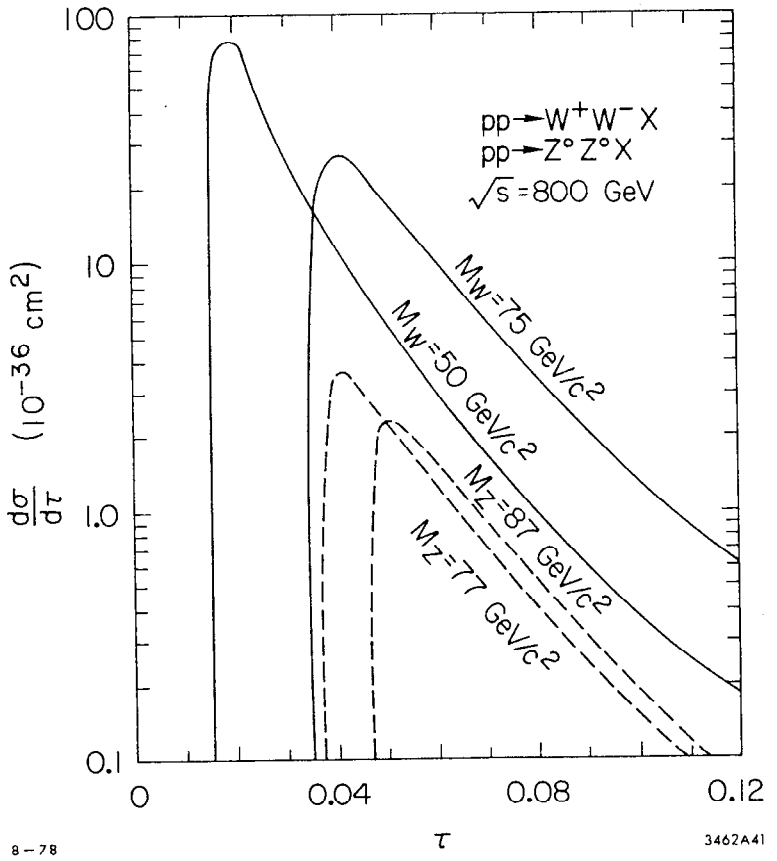

Fig. 41. Cross sections[138] for $pp \to W^+W^-+X$ and Z^oZ^o+X at $\sqrt{s}$ = 800 GeV.

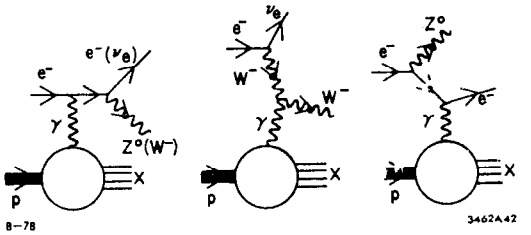

Fig. 42. Diagrams for $e^-p \to \nu W^-+X$ and $e^-p \to e^-Z^o+X$ involving the lepton vertex.

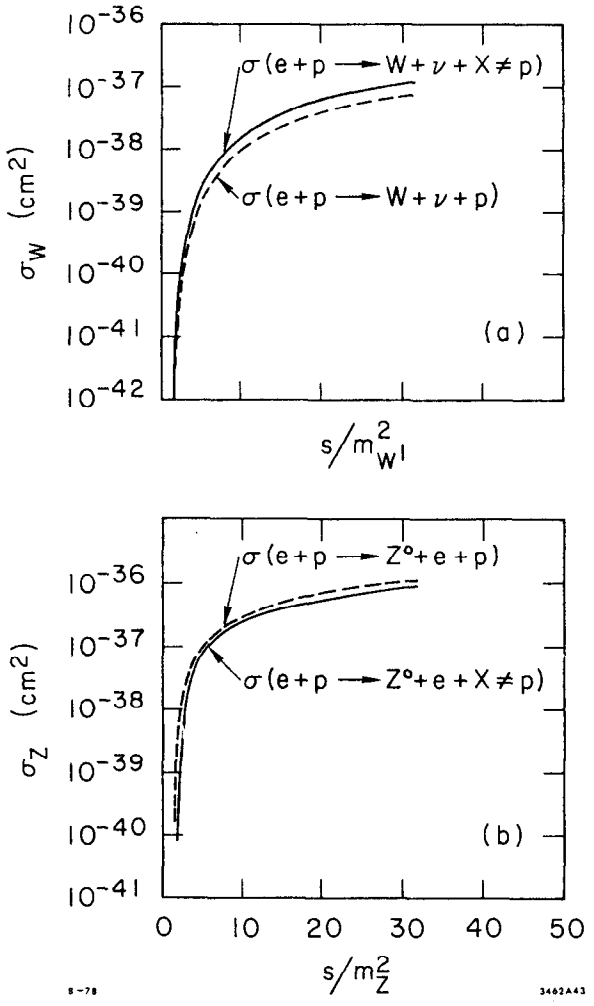

Fig. 43. The cross sections[101,124] for $e^-p \rightarrow \nu W^- + X$ and $e^-p \rightarrow e^-Z^o + X$ as functions of m^2/s.

colliding rings ($E_e \sim 20$ to 30 GeV, $E_p \sim 250$ to 400 GeV, $\sqrt{s} \sim 150$ to 200 GeV) and reasonable $W^\pm$ and Z^o masses the orders of magnitude of the cross sections are

$$\sigma(ep \rightarrow \nu WX) \sim 10^{-38}\ \text{cm}^2$$
$$\sigma(ep \rightarrow eZX) \sim 10^{-37}\ \text{cm}^2 \qquad (3.36)$$

so that with the projected[101] luminosities $O(10^{32}\ \text{cm}^{-2}\ \text{sec}^{-1})$ we are talking about very marginal event rates O(1) per week or day at best. One asset of these reactions is that they are potentially very clean, with the final hadronic state X being a single proton about $\frac{1}{2}$ the time, and otherwise having a tendency to be a lightweight hadronic system, by the general standards of such a machine. However, it must be admitted that presently conceivable ep machines offer bleak prospects for detecting or studying intermediate vector bosons.

Much more interesting for this class of machines[101,124] is the study of indirect effects of the $W^\pm$ and Z^o from their exchanges, and interference with γ exchange in the case of the Z^o. The Q^2 accessible with such a machine range up to $O(10^4)$ GeV^2, where γ and Z^o exchanges are of equal order of magnitude, and one can expect O(1) charge asymmetries or parity violations, to be compared with the $O(10^{-4})$ effects detected in present experiments. *Detailed formulae for the effects are given in the* CHEEP report[101]: some representative calculations are shown in Fig. 44. Figure 44(a) shows the charge asymmetry

$$\frac{\sigma(e^-p)}{\sigma(e^+p)} \neq 1 \qquad (3.37)$$

expected in ep collisions at x=0.25, s=27,000 GeV^2 and varying values of Y. The $SU(2)_L \times U(1)$ Weinberg-Salam model (A,B), $SU(2)_L \times SU(2)_R \times U(1)$ model (C)

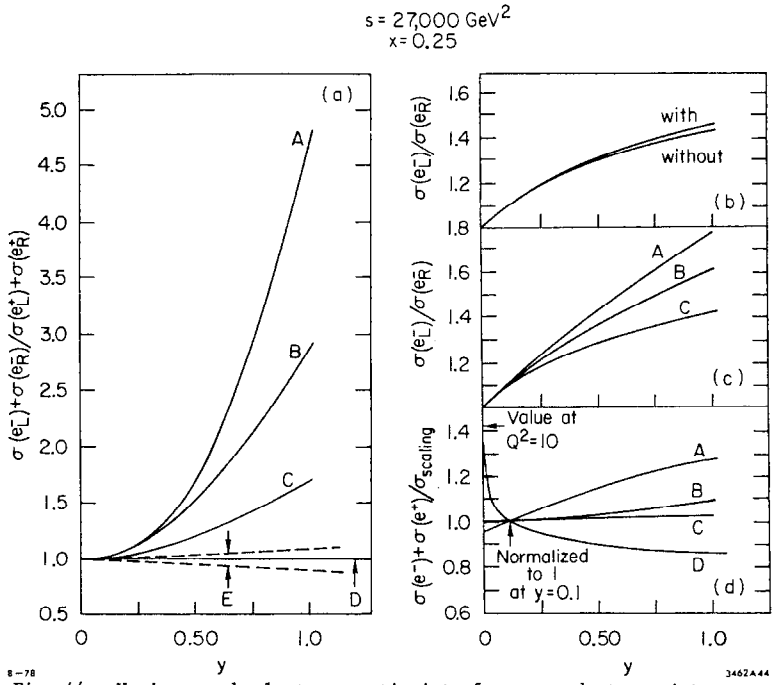

Fig. 44. Various weak electromagnetic interference and strong interaction scaling violation effects[101] in ep → e+X. (a) Charge asymmetries in $\sigma(e^-p)/\sigma(e^+p)$: A--Weinberg-Salam model with m_Z arbitrarily increased to 150 GeV; B--Weinberg-Salam model with m_Z = 86 GeV; C--$SU(2)_L \times SU(2)_R \times U(1)$ model; D--Hybrid model with $\begin{pmatrix} E^o \\ e^- \end{pmatrix}_R$ doublet; E--estimated uncertainty due to 2γ contributions. (b) Parity violating asymmetry for the Weinberg-Salam model with and without QCD scaling violations. (c) Parity violation in $\sigma(e_L^-p)/\sigma(e_R^-p)$: A--Weinberg-Salam couplings with m_Z taken to ∞; B--Weinberg-Salam with m_Z = 150 GeV; C--Weinberg-Salam with m_Z = 86 GeV. (d) Apparent scaling violations in $\sigma(e^-p) + \sigma(e^+p)$ coming from strong and weak interaction sources: A--$\begin{pmatrix} E^o \\ e^- \end{pmatrix}_R$ doublet; B--Weinberg-Salam model; C--$SU(2)_L \times SU(2)_R \times U(1)$ model; D--Asymptotic freedom.

and model with an $\begin{pmatrix} E^o \\ e^- \end{pmatrix}_R$ doublet (D) can clearly be easily distinguished. We also see considerable sensitivity to the mass of the Z^o, which can be measured indirectly in this way. Figure 44(b) shows the parity violating effect

$$\frac{\sigma(e_L^-p)}{\sigma(e_R^-p)} \neq 1 \qquad (3.38)$$

which can be expected for similar values of the kinematic variables. All calculations are in the Weinberg-Salam model, but with m_Z adjusted arbitrarily while keeping identical neutral current cross sections near Q^2=0. You might wonder to what extent these calculations are independent of the strong interaction model used, which was the naive parton model. Figure 44(c) shows the effect on the parity-violating asymmetry (3.38) of including asymptotic freedom effects[101] which modify the quark distributions as discussed in Lecture 1. We see that the changes are minimal, indicating that strong effects do not confuse the weak effects. Figure 44(d) shows a comparison[101] of the scaling violations expected from asymptotic freedom compared with the apparent deviations from a point-like electromagnetic cross sections which would be exhibited by weak interference effects on $\sigma(e^-p) + \sigma(e^+p)$ in a variety of models. We see that strong scaling deviations are expected to be small in the range of large Q^2 where weak interferences are large. Conversely, the strong scaling violations are big when $Q^2 \lesssim 0(1000)$ GeV^2 where the weak interference effects are relatively small. It seems that QCD and weak gauge theory effects can plausibly be disentangled in the reaction ep → e+X.

Figure 45 shows the effect on the charged current reaction ep → ν+X of asymptotic freedom and/or the finite mass of the $W^{\pm}$.[124] There is

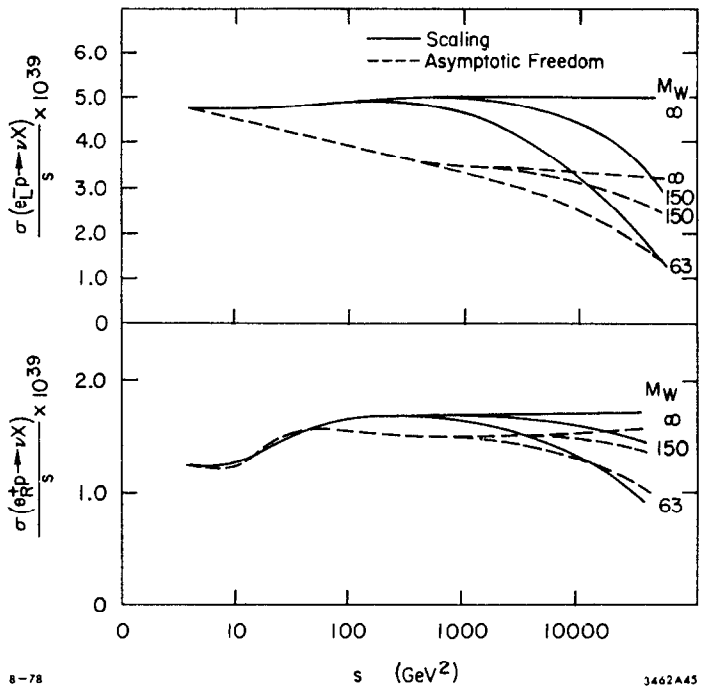

Fig. 45. The effects[69,101,124] on (a) $\sigma(e^- p \to \nu_e + X)$ and (b) $\sigma(e^+ p \to \bar{\nu}_e + X)$ cross sections of finite boson masses and QCD scaling violations.

clearly great sensitivity to deviations from the pointlike four-fermion interaction. With a luminosity of 10^{32} cm^{-2} sec^{-1} one would obtain several hundred events a day even in the most pessimistic case of a low $W^{\pm}$ mass.

3.5 The Z^0 Peak in e^+e^- Annihilation

Clearly the cleanest and most dramatic place to study the Z^0 is in e^+e^- collisions,[93,121,122] where it is produced alone and with a high rate. For comparison, let us normalize the cross sections of this and the subsequent section to

$$\sigma_{pt} \equiv \sigma(e^+e^- \to \gamma^* \to \mu^+\mu^-) = \frac{4\pi\alpha^2}{3s} \tag{3.39}$$

At the centre-of-mass energy of order 94 GeV which we are interested in, $\sigma_{pt} \sim 10^{-2}$ nb corresponding to an event rate of 3.6 events per hour if the projected luminosity of 10^{32} cm^{-2} sec^{-1} is attained. The analysis of section 3.2.2 suggested that we should be prepared for a total Z^0 decay width of order 2 to 3 GeV. This is much wider then the e^+e^- beam energy evolution which is expected to be $O(10^{-3})$ of the beam energy itself, giving a an energy resolution O(100) MeV. We can therefore discuss the Z^0 peak under the assumption

$$\Gamma(Z^0 \to \text{all}) >> \Delta E_{\text{beam}} \tag{3.40}$$

whereas the reverse situation applies to the J/ψ and T hadronic resonances. At the peak of the resonance, the condition (3.40) means that

$$\frac{\sigma(e^+e^- \to Z^0 \to \text{all})}{\sigma_{pt}} \simeq \frac{9}{\alpha^2} B(Z^0 \to e^+e^-) \tag{3.41}$$

Putting in $B(Z^o \to e^+e^-) \sim 3\%$ as suggested in Eq. (3.20), we find

$$\frac{\sigma(e^+e^- \to Z^o \to \text{all})}{\sigma_{pt}} \approx 5000 \tag{3.42}$$

corresponding to O(5) Z^o decays/second.[139] It should be emphasized that this rate is sensitive to the existence of unsuspected decays of the Z^o (many neutrinos?) which could suppress $B(Z^o \to e^+e^-)$ and the size of the peak. Nevertheless, experiments with $O(10^7)$ Z^o decays become imaginable. This gives us many possibilities for precision measurements and/or studies of rare Z^o decays.

Let us first discuss the shape[93] of total $e^+e^- \to f\bar{f}$ cross sections in the neighborhood of the Z^o peak. The quantity

$$R_f \equiv \frac{(e^+e^- \to \gamma^*, Z^o \to f\bar{f})}{\sigma_{pt}}$$

$$= Q_f^2 - \frac{2s\rho Q_f v_e v_f}{\left(\left(\frac{s}{m_Z^2} - 1\right) + \frac{\Gamma_Z^2}{s-m_Z^2}\right)} + \frac{s^2\rho^2\left(v_e^2+a_e^2\right)\left(v_f^2+a_f^2\right)}{\left(\left(\frac{s}{m_Z^2} - 1\right)^2 + \frac{\Gamma_Z^2}{m_Z^2}\right)} \tag{3.43}$$

where the vector and axial couplings v_e and v_f were defined in Eq. (3.10), and the Weinberg-Salam values are tabulated in Eq. (3.12). The quantity ρ appearing in Eq. (3.43) is defined by

$$\rho \equiv \frac{G_F}{8\sqrt{2}\,\pi\alpha} \tag{3.44}$$

and sets the scale for the magnitude of weak interference effects. In the special case that $f\bar{f}=\mu^+\mu^-$, we have

$$R_\mu \approx 1 + 2v^2\chi + (v^2+a^2)^2\,\chi^2 \tag{3.45}$$

if we neglect Γ_Z, and assume e-μ universality

$$v_e = v_\mu \equiv v, \qquad a_e = a_\mu \equiv a \tag{3.46}$$

In Eq. (3.45), χ is defined by

$$\chi \equiv \rho m_Z^2 \frac{s}{s-m_Z^2} \tag{3.47}$$

In the special case of m_Z = 94 GeV corresponding to $\sin^2\theta_W = 0.20$, the expression (3.44) implies that $m_Z^2\rho \approx 0.39$. The cross section ratio (3.45) goes through a minimum when

$$\frac{s}{m_Z^2} = \left(\frac{1}{m_Z^2\rho}\right)\frac{v^2}{(v^2+a^2)^2} \tag{3.48}$$

In the Weinberg-Salam model with $\sin^2\theta_W = 0.20$ this occurs at $\sqrt{s}$ = 29 GeV. The value of R_μ at the minimum is

$$R_\mu = 1 - \frac{v^4}{(v^2+a^2)^2} \tag{3.49}$$

Unfortunately, if $\sin^2\theta_W = 0.20$ so that v=0.2, the minimum value of R_μ is 0.9985, which might be difficult to disentangle from 1. However, Eqs. (3.45), (3.48) and (3.49) show that the shape R_μ of the cross section is in principle sensitive to the ratio $|v/a|$. Figure 46 shows the behaviour of R_μ for some representative values[93] of the vector and axial couplings. The Weinberg-Salam model with $\begin{pmatrix} E^o \\ e^- \end{pmatrix}_R$ and $\begin{pmatrix} M^o \\ \mu^- \end{pmatrix}_R$ doublets would have a=0, which would certainly make the R_μ plot interesting!

Another measurement of interest is the charge violating forward backward asymmetry. In general one has, neglecting Γ_Z,

$$\frac{d\sigma(e^+e^- \to f\bar{f})}{d\cos\theta} \simeq \frac{\pi\alpha^2}{2s}\left\{Q_f^2(1+\cos^2\theta) - 2Q_f\chi\left[v_e v_f(1+\cos^2\theta) + 2a_e a_f\cos\theta\right]\right.$$
$$\left. + \chi^2\left[\left(v_e^2+a_e^2\right)\left(v_f^2+a_f^2\right)(1+\cos^2\theta) + 8v_e a_e v_f a_f\cos\theta\right]\right\} \tag{3.50}$$

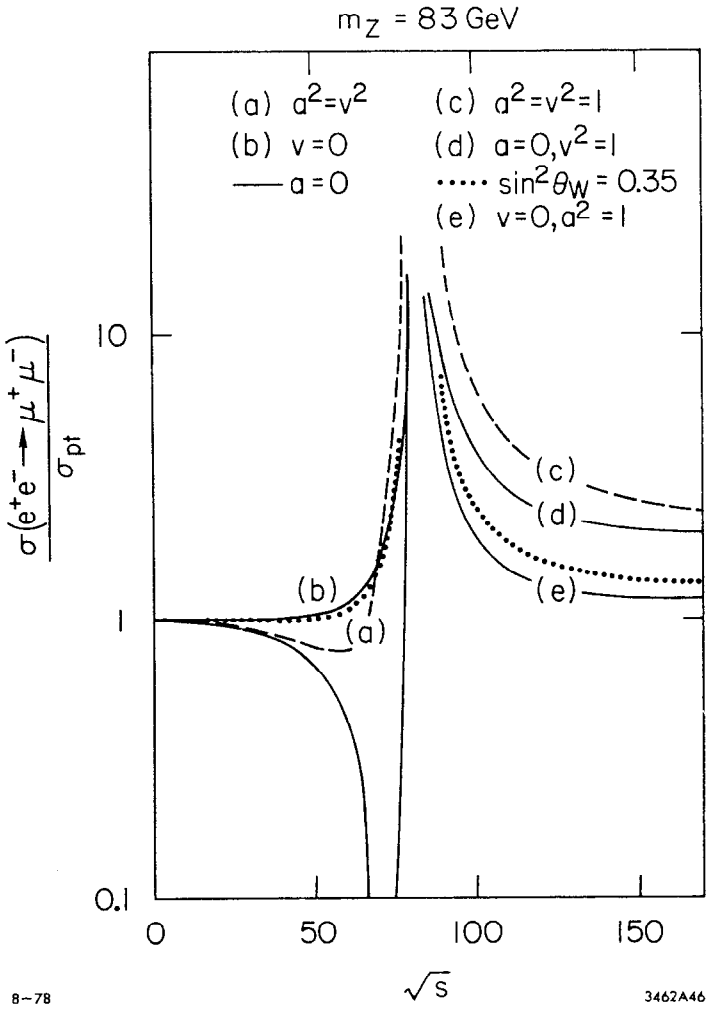

Fig. 46. The shape[93] of the $e^+e^- \to \mu^+\mu^-$ cross section near the Z^0 pole.

where χ was previously defined in Eq. (3.47). The integrated asymmetry

$$A_f \equiv \frac{\int_0^1 d\sigma_f - \int_{-1}^0 d\sigma_f}{\int_0^1 d\sigma_f + \int_{-1}^0 d\sigma_f} \tag{3.51}$$

is readily calculated from Eq. (3.50) to be

$$A_f = \frac{\frac{3}{2}\chi\left(-Q_f a_e a_f + 2v_e a_e v_f a_f \chi\right)}{\left[Q_f^2 - 2Q_f \chi v_e v_f + \chi^2\left(v_e^2+a_e^2\right)\left(v_f^2+a_f^2\right)\right]} \tag{3.52}$$

There is bound on A_f from the combination of L_Z=0 and 1 initial states:

$$|A_f| \leq \frac{3}{4} \tag{3.53}$$

and a nonvanishing effect clearly requires a_e, $a_f \neq 0$. If we first specialize to the low energy case where only the term linear in χ is retained:

$$A_f \approx -\frac{\frac{3}{2}\chi\, a_e a_f}{Q_f} \tag{3.54}$$

Since $|a_e| = |a_f| = 1$ for all fermions in the Weinberg-Salam model (3.12), if we set

$$\chi = \rho m_Z^2 \frac{s}{s-m_Z^2} \approx 0.07 \tag{3.55}$$

corresponding an e^+e^- centre-of-mass energy around 40 GeV, we see from (3.54) that

$$|A_\mu| \approx 10\% \ , \quad |A_{u,c,t}| \approx 7\% \ , \quad |A_{d,s,b}| \approx 14\% \tag{3.56}$$

with the differences being generated by the differences in the quark charges. This type of asymmetry measurement may be a good way of getting at the weak couplings of the s,c,... quarks which were not accessible in

neutral current experiments to data (c.f. section 2.2). The asymmetries get more exciting closer to the Z^0 pole. Specializing to $\mu^+\mu^-$ we have from Eq. (3.52)

$$A_\mu = \frac{3}{2}\chi \frac{(a^2 + 2v^2a^2\chi)}{\left(1+2\chi v^2 + \chi^2(v^2+a^2)^2\right)} \tag{3.56}$$

which goes through a minimum at

$$\frac{s}{m_Z^2} = \frac{1}{1 + \left(\rho m_Z^2\right)(a^2+3v^2)} \tag{3.57}$$

where it attains the value

$$A_\mu = -\frac{3}{4}\frac{1}{\left(1 + \frac{2v^2}{a^2}\right)} \tag{3.58}$$

For comparison, the value at the peak of the resonance is approximately

$$A_\mu \approx \frac{3v^2a^2}{(v^2+a^2)^2} \tag{3.59}$$

while the asymmetry is a maximum at

$$\frac{s}{m_Z^2} = \frac{1}{1 - \left(\rho m_Z^2\right)(a^2-v^2)} \tag{3.60}$$

where it attains the maximum value

$$A_\mu = +\frac{3}{4} \tag{3.61}$$

For orientation purposes, the values and positions of the asymmetries (3.57) to (3.60) have the following values in the Weinberg-Salam model with $\sin^2\theta_W \simeq 0.20$:

$$A_\mu^{min} = -0.69 \quad \text{at} \quad \sqrt{s} = 78 \text{ GeV}$$

$$A_\mu^{peak} = +0.11 \quad \text{at} \quad \sqrt{s} = 94 \text{ GeV}$$

$$A_\mu^{max} = +0.75 \quad \text{at} \quad \sqrt{s} = 118 \text{ GeV} \tag{3.62}$$

In Fig. 47 we plotted[93] generic curves of the asymmetry A_μ (3.56) for a fixed $m_Z = 83$ GeV and an interesting collection of v and a couplings.

A third class of interesting measurements at and near the Z^0 pole concerns polarization and helicity-dependent effects. If we first consider the case of unpolarized e^+e^- beams, the dependence of the cross section on the helicity of the final state fermion is of the form:

$$\frac{d\sigma_f}{d\cos\theta} = \sigma_1 + h_f\sigma_2 \tag{3.63}$$

where $\sigma_1 = \frac{1}{2}\frac{d\sigma(e^+e^- \to f\bar{f})}{d\cos\theta}$ (cf. Eq. (3.50)) and

$$\sigma_2 \equiv \frac{\pi\alpha^2}{2s}\chi\Big\{Q_f\left[v_e a_f(1+\cos^2\theta) + 2a_e v_f\cos\theta\right] - \chi\left[v_f a_f\left(a_e^2+v_e^2\right)(1+\cos^2\theta) + 2a_e v_e\left(a_f^2+v_f^2\right)\cos\theta\right]\Big\} \tag{3.64}$$

with the mean fermion helicity

$$\langle h_f\rangle = -\langle h_{\bar{f}}\rangle = \frac{\sigma_2}{\sigma_1} \equiv H_f(\theta,s) \tag{3.65}$$

The dependence on initial $e^\pm$ beam helicity $h^\pm$ is

$$\frac{d\sigma_f(h^+,h^-)}{d\cos\theta} = (1-h^+h^-)\sigma_1 + (h^- - h^+)\bar{\sigma}_2 = \sigma_1\left[(1-h^+h^-) + (h^- - h^+)\bar{H}_f(\theta,s)\right] \tag{3.66}$$

where $\bar{\sigma}_2$ and $\bar{H}_f$ are obtained from σ_2 and H_f respectively by the substitutions $(a_e,v_e) \leftrightarrow (a_f,v_f)$. The integrated average final state fermion

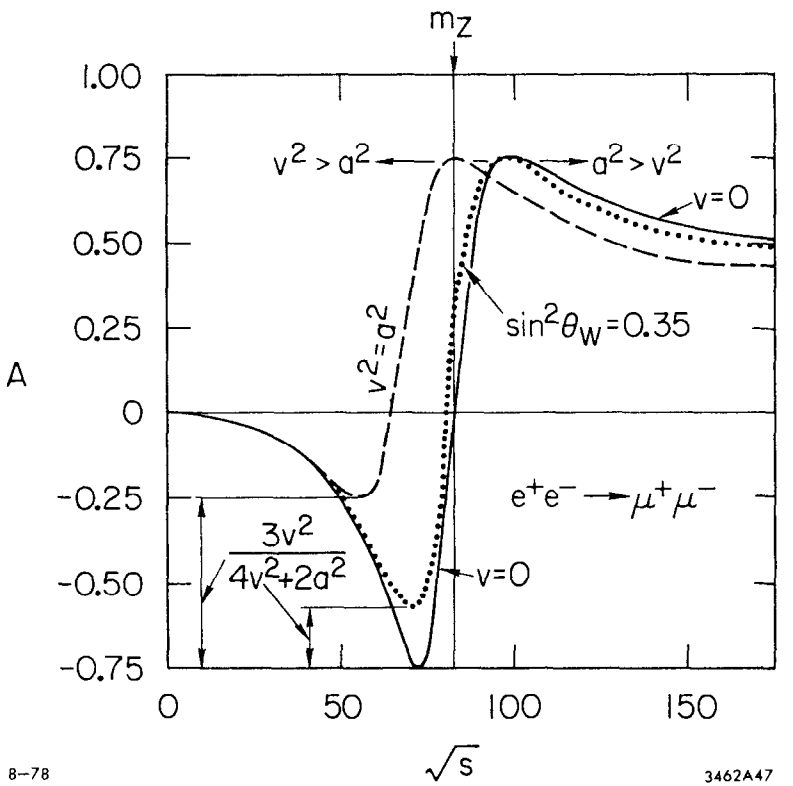

Fig. 47. The shape[93] of the $e^+e^- \to \mu^+\mu^-$ forward-backward asymmetry near the Z^o pole.

helicities from unpolarized beams are

$$H^f(s) = -H^{\bar{f}}(s) = \frac{\int_{-1}^{1} \sigma_2 \, d\cos\theta}{\int_{-1}^{1} \sigma_1 \, d\cos\theta}$$

$$= \frac{2\chi a_f \left[Q_f v_e - \chi v_f \left(a_e^2+v_e^2\right)\right]}{Q_f^2 - 2Q_f \chi v_e v_f + \chi^2 \left(a_e^2+v_e^2\right)\left(a_f^2+v_f^2\right)} \qquad (3.67)$$

It is clear the final state fermion helicity is sensitive to the product $a_f v_e$ at low energies, and $a_f v_f$ close to the Z^o pole. A sample plot of (3.67) for the mean μ (or τ helicity) is shown in Fig. 48.[93] Unfortunately, if the Weinberg-Salam model with $\sin^2\theta_W \approx 0.20$ is correct, the average helicity is rather small. For example, if we specialize to the forward direction $\cos\theta = +1$ to maximize the effect,

$$H^{\mu^-} \text{ or } \tau^-(s,\cos\theta=+1) = \frac{4\chi \, av\left[1 + \chi(a^2+v^2)\right]}{\left[1 + 2\chi(v^2+a^2) + \chi^2\left[(a^2+v^2)^2 + 4a^2v^2\right]\right]} \qquad (3.68)$$

which becomes 0.13 on the resonance peak. There is a similar effect on the cross sections of the initial state electron helicity, which is dependent on $a_e v_f$ at low energies and $a_e v_e$ near the Z^o pole. Since the v_f are not necessarily small in the Weinberg-Salam model with $\sin^2\theta_W \approx 0.20$, unlike v_e, measurements of the dependence of cross sections on the e^+e^- helicity may perhaps be most interesting away from the Z^o peak itself.

One reaction we have not discussed up to now is $e^+e^- \to e^+e^-$, where there are crossed channel exchanges as well as the direct channel γ and Z^o diagrams. We are used to the differential cross section for this reaction being sharply peaked forward-backward because of the crossed

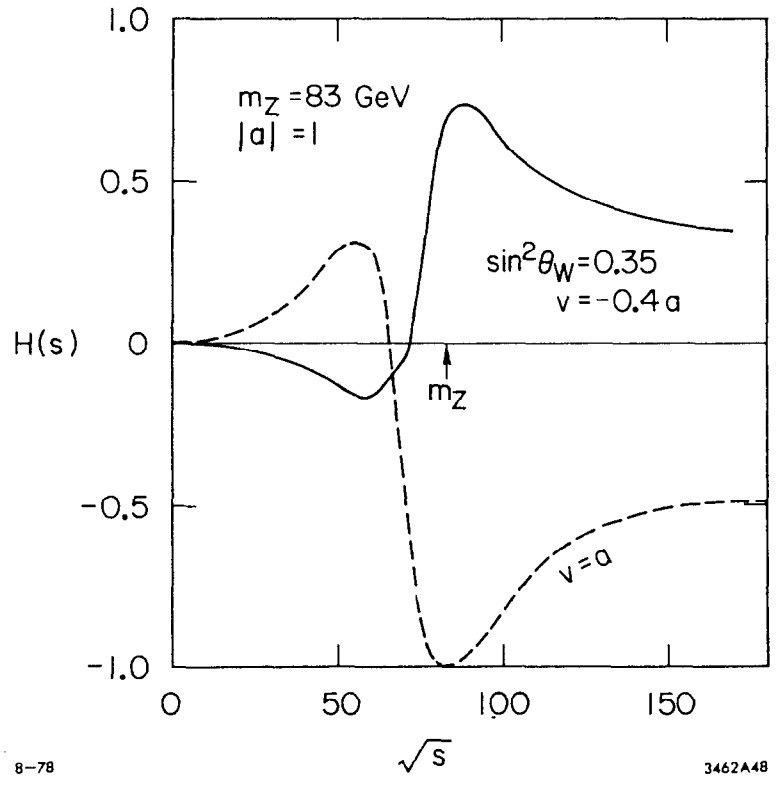

Fig. 48. The average μ (or τ) helicity[93] in $e^+e^- \to \mu^+\mu^-$ (or $\tau^+\tau^-$) near the Z^o pole.

channel γ exchange. In the neighborhood of the Z^o resonance this asymmetry may be sharply reduced. More details can be found in section 3 of the CERN e^+e^- report.[93]

Detailed measurements of the Z^o peak will be useful for several things besides measuring $\sin^2\theta_W$ to 3 decimal places. For example, a detailed measurements of m_{Z^o} enables us to exclude very massive fermions,[91,92] as discussed in section 2.2. On the other hand, a precise measurement of the width of the Z^o peak or of the height (3.41), combined with a determined search for massive fermions with masses $< m_{Z/2}$, can tell us how many unobserved neutrinos there are. We should therefore be able to clear up fermion spectroscopy as well as boson spectroscopy. The possibility of precise measurements with 10^7 Z^o decays should enable us to probe weak radiative corrections, which might for example give us a look at the effects of very massive Higgs systems.[140] As for rare Z^o decays, one interesting possibility is $Z^o \to$ Higgs + ($\mu^+\mu^-$ or e^+e^-), which looks to be a promising way of scanning for neutral Higgs particles with masses up to O(50) GeV as will be discussed in Lecture 4. One might hope that the decay $Z^o \to W^\pm e^\mp \nu$ or $\mu^\mp \nu$ would be a good way of looking for single $W^\pm$ production below the W^+W^- threshold. Unfortunately, the decay rate[125]

$$\Gamma(Z^o \to W^- e^+ \nu) \lesssim 10^{-7} \text{ GeV} \tag{3.69}$$

which makes the prospects look bleak, even with 10^7 Z^o decay experiments. Even above resonance the $e^+e^- \to We\nu$ cross section is unappetizingly small, being

$$(e^+e^- \to W^- e^+ \nu) = O(10^{-37} \text{ to } 10^{-36}) \text{cm}^2 \quad \text{for } \sqrt{s} \sim 110 \text{ to } 200 \text{ GeV} \tag{3.70}$$

It seems that the best prospects for $W^{\pm}$ production will be above the pair production threshold, to which we turn in the next section. For the moment, we just note that e^+e^- experiments are a source of Z^o production and decays which enables studies many orders of magnitude more precise than any other machine.

3.6 e^+e^- Annihilation Beyond the Z^o Pole

The next most obviously interesting reaction beyond the Z^o pole is W^+W^- pair production.[125,126] This reaction is a showcase for gauge theories, since it enables one to search for, and hopefully observe, the cancellations between different crossed and direct channel exchanges which are needed[63] for the renormalizability of the theory. The diagrams involved should be the direct channel γ and Z^o, and the crossed channel neutrino and possible heavy lepton exchanges in Fig. 49. In particular, one would like to see evidence for the archetypical 3 boson interaction, either in the form of the γW^+W^- vertex which should have a specific value for the anomalous magnetic moment, or in the form of the $Z^oW^+W^-$ vertex itself. A useful study of the $e^+e^- \to W^+W^-$ reaction has been made by Alles, Boyer and Barras,[125] who emphasize that the gauge theory cancellations are important even quite close to threshold.

Let us consider the Weinberg-Salam model,[141] where the differential cross section can be written in the form

$$\frac{d\sigma(e^+e^- \to W^+W^-)}{d\Omega} = \frac{\alpha^2}{32 \sin^4 \theta_W} \frac{\beta}{s} \sum_{i,j} M_{ij} \qquad (3.71)$$

where the M_{ij} are the distinct interferences and cross sections. They take the forms

$$M_{\nu\nu} = F_1(\theta,s) \qquad M_{\gamma\gamma} = \sin^4 \theta_W F_2(\theta,s)$$

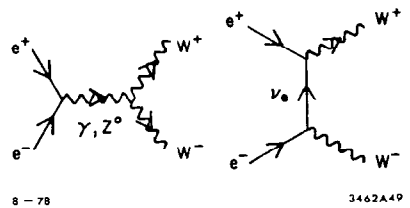

Fig. 49. Diagrams contributing to $e^+e^- \to W^+W^-$.

$$M_{ZZ} = \left(\sin^4\theta_W - \frac{1}{2}\sin^2\theta_W + \frac{1}{8}\right)\frac{s^2}{\left(s-m_Z^2\right)^2}\,F_2(\theta,s)$$

$$M_{Z\gamma} = 2\sin^2\theta_W\left(\frac{1}{4} - \sin^2\theta_W\right)\frac{s}{s-m_Z^2}\,F_2(\theta,s)$$

$$M_{\nu Z} = \left(\sin^2\theta_W - \frac{1}{2}\right)\frac{s}{s-m_Z^2}\,F_3(\theta,\epsilon)$$

$$M_{\gamma\nu} = -\sin^2\theta_W\,F_3(\theta,s) \qquad (3.72)$$

where the F_i are useful kinematic combinations

$$F_1(\theta,s) \equiv \frac{2}{a} + \frac{\sin^2\theta}{2}\left\{\left(\frac{s}{K^2}\right)^2 + \frac{1}{4a^2}\right\}\beta^2$$

$$F_2(\theta,s) \equiv \beta^2\left(\frac{16}{a} + \left(\frac{1}{a^2} - \frac{4}{a} + 12\right)\sin^2\theta\right)$$

$$F_3(\theta,s) \equiv 16\left(1 + \frac{m_W^2}{K^2}\right) + 8\beta^2/a + \beta^2\,\frac{\sin^2\theta}{2}\left(\frac{1}{a^2} - \frac{2}{a} + \frac{4s}{K^2}\right) \qquad (3.73)$$

The definitions of various quantities appearing in Eqs. (3.72) and (3.73) are

$$a = \frac{m_W^2}{s}\,, \quad \beta = \sqrt{1-4a}\,, \quad L = \ln\left|\frac{1+\beta}{1-\beta}\right|\,, \quad K^2 = m_W^2 - \frac{s}{2} + \frac{s}{2}\beta\cos\theta \qquad (3.74)$$

Meditation will reveal that $M_{\nu\nu}$ is sharply peaked forward-backward, while γ and Z exchanges are relatively isotopic. When we integrate (3.71) over the solid angle Ω to get the total cross section we find

$$\sigma(e^+e^- \to W^+W^-) = \frac{\pi\alpha^2}{8\sin^4\theta_W}\,\frac{\beta}{s}\sum_{ij}\bar{\sigma}_{ij} = \sum_{ij}\sigma_{ij} \qquad (3.75)$$

where corresponding to Eq. (3.72):

$$\bar{\sigma}_{\nu\nu} = \bar{\sigma}_1 \qquad \bar{\sigma}_{\gamma\gamma} = \sin^4\theta_W\,\bar{\sigma}_2$$

$$\bar{\sigma}_{ZZ} = \left(\sin^4\theta_W - \frac{1}{2}\sin^2\theta_W + \frac{1}{8}\right)\frac{s^2}{\left(s-m_Z^2\right)^2}\,\bar{\sigma}_2$$

$$\bar{\sigma}_{Z\gamma} = 2\left(\frac{1}{4} - \sin^2\theta_W\right)\sin^2\theta_W\,\frac{s}{s-m_Z^2}\,\bar{\sigma}_2$$

$$\bar{\sigma}_{\nu Z} = \left(\sin^2\theta_W - \frac{1}{2}\right)\frac{s}{s-m_Z^2}\,\bar{\sigma}_3$$

$$\bar{\sigma}_{\gamma\nu} = -\sin^2\theta_W\,\bar{\sigma}_3 \qquad (3.76)$$

with

$$\bar{\sigma}_1 = \frac{2}{a} + \frac{1}{12a^2}\beta^2 + 4\left\{(1-2a)\,\frac{L}{\beta} - 1\right\}$$

$$\bar{\sigma}_2 = \frac{16}{a}\beta^2 + \frac{2}{3}\beta^2\left(\frac{1}{2} - \frac{4}{a} + 12\right)$$

$$\bar{\sigma}_3 = 16 - 32\,\frac{La}{\beta} + 8\,\frac{\beta^2}{a} + \frac{\beta^2}{3a^2}(1-2a) + 4(1-2a) - \frac{16La^2}{\beta} \qquad (3.77)$$

Getting it all together we finish up with

$$\sigma(e^+e^- \to W^+W^-) = \frac{\pi\alpha^2\beta}{2\sin^4\theta_W s}\left\{(1+2a+2a^2)\,\frac{L}{\beta} - \frac{5}{4}\right.$$
$$+ \frac{m_Z^2\left(1-2\sin^2\theta_W\right)}{s-m_Z^2}\left[2a^2\left(1+\frac{2}{a}\right)\frac{L}{\beta} - \frac{1}{12a} - \frac{5}{3} - a\right]$$
$$\left. + \frac{m_Z^4\left(8\sin^4\theta_W - 4\sin^2\theta_W + 1\right)}{48\left(s-m_Z^2\right)^2}\,\frac{\beta^2}{a^2}\,(1+20a+12a^2)\right\} \qquad (3.78)$$

In Fig. 50 we have plotted[125] $\sigma(e^+e^- \to W^+W^-)$ from Eq. (3.78) for some (rather large) values of $\sin^2\theta_W$ and (rather small) values of $m_{W^\pm}$. We see that the cross section has a rather neat peak about 40 GeV above

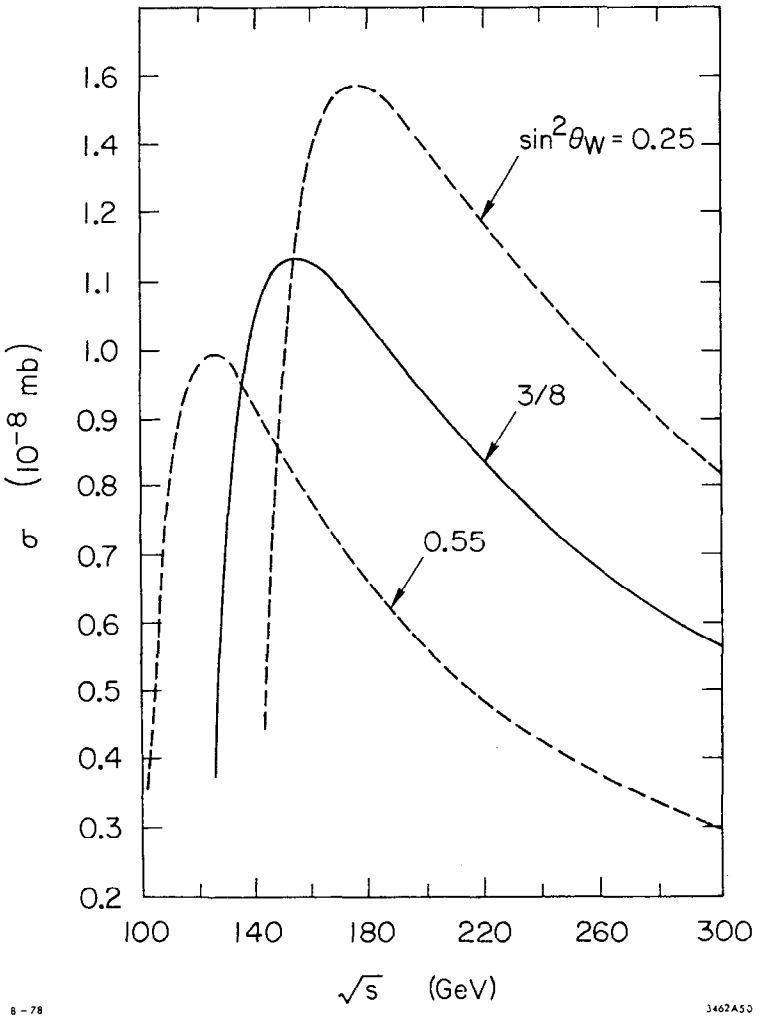

Fig. 50. The total cross section[125] for $e^+e^- \to W^+W^-$ as a function of the centre-of-mass energy and $\sin^2\theta_W$.

threshold, of height $O(10^{-35})$ cm^2 which could be observable given a luminosity of 10^{32} cm^{-2} sec^{-1}, followed by a sharply falling cross section at higher energies which is a few times σ_{pt} (3.39). The diagrammatic cancellations are exhibited[125] in Fig. 51, and are very significant even quite close to threshold. Therefore we may hope to see the famous gauge theory cancellations even at low centre-of-mass energies $\sqrt{s} \leq 200$ GeV. The neutrino exchanges cause the W^+W^- angular distribution to be sharply peaked forward-backward even relatively close to threshold.[125] On the other hand, it is difficult[141] to disentangle the γ and Z^0 exchange effects because they are required by gauge theory to have similar structure, but even the determination of the γW^+W^- vertex would be an interesting nontrivial check of gauge theory ideas.

Another interesting reaction is the process $e^+e^- \to Z^0$ + Higgs,[10] which may be a good way of producing Higgs particles with masses above 50 GeV, and is more background-free than the $Z^0 \to$ Higgs + $\ell^+\ell^-$ decay mode mentioned earlier. This reaction will be discussed in more detail in Lecture 4.

Mention should be made of the reaction $e^+e^- \to Z^0Z^0$.[138] In the standard model, this only proceeds by lepton exchange in the crossed channel. It is therefore less interesting than $e^+e^- \to W^+W^-$, since it does not give us a window on the 3-boson vertex. However, the cross section is quite big close to threshold (see Fig. 52), quite likely being as large as for $e^+e^- \to W^+W^-$ around $\sqrt{s}$ = 200 GeV. Is this reaction useful for something?

It would be nice to measure the 4-boson vertex, perhaps in the two-photon process $e^+e^- \to e^+e^-W^+W^-$, but... .

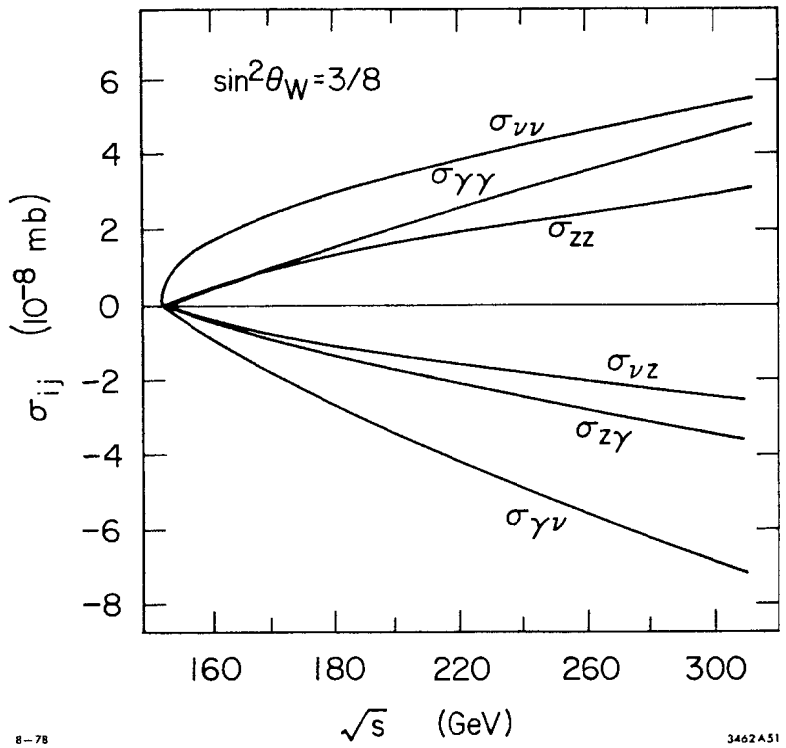

Fig. 51. The relative magnitudes[125] of different diagrams and their interferences in $e^+e^- \to W^+W^-$.

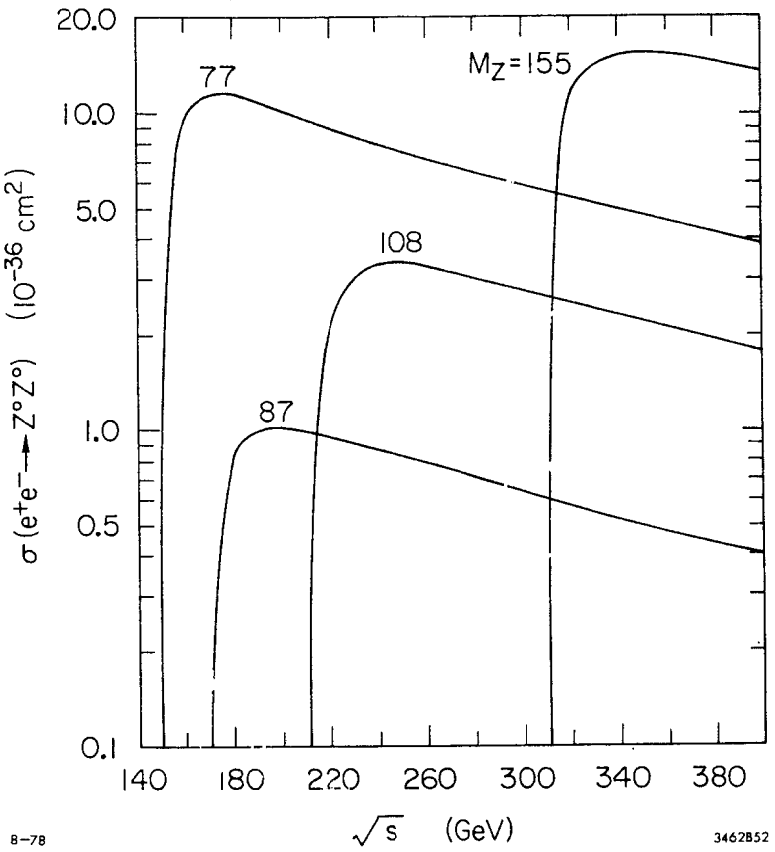

Fig. 52. The cross section[138] for $e^+e^- \to Z^oZ^o$.

4. The Funny Farm

4.1 Introduction

This last lecture will be concerned with various aspects of gauge theories which are more controversial than the topics discussed so far. Most of the lecture will be devoted to Higgs bosons in some form or another. As was emphasized in the introduction to Lecture 2, the renormalizability of present gauge theories of the weak interactions[2,63] depends on the masses of particles being generated by spontaneous symmetry breaking. No fully satisfactory way has ever been found of generating masses by some dynamical mechanism which does not invoke elementary Higgs fields. Furthermore, all realistic spontaneously broken weak interaction models have at least one Higgs boson remaining in the physical spectrum. For example, the simplest $SU(2)_L \times U(1)$ Weinberg-Salam model has just one physical neutral Higgs boson if the symmetry is broken by just one $I=\frac{1}{2}$ multiplet, and there are additional charged and neutral bosons if more than one multiplet is used. It therefore seems very important to do experimental searches for Higgs particles.[10] Either they will be found, in which case the spontaneously broken gauge theory picture will finally be confirmed, or if they do not exist theorists will have to totally rethink their ideas. Much of the lecture will discuss empirical and theoretical constraints on the simplest Higgs system in the Weinberg-Salam model, and possible ways of doing experimental searches for neutral Higgs particles.

There will also be some discussion of more complicated Higgs systems, including possible charged bosons. One possible modification[142] of the Higgs system which has attracted much interest recently implies the existence of a very light pseudoscalar Higgs boson, the axion,[143] which would play a role in preventing QCD from having a strong source of CP violation. In its simplest form, the axion would be very light with a mass $\leq$ O(1) MeV, but this possibility now seems to be phenomenologically excluded.[144,145,146] However, a more sophisticated, massive, axion could still exist. A search for it then becomes rather like the search for a neutral Higgs boson discussed earlier.

The last parts of the lecture will be concerned with much more speculative aspects of gauge theories. One possibility present in some gauge theories was the existence of a magnetic monopole,[147] with a mass O(1) TeV. The phenomenology of monopoles is rather amusing. Unfortunately, they are not present in the Weinberg-Salam model, which is just as well since there are cosmological arguments[148] that exclude monopoles of the simplest type, as found[147] for example in the Georgi-Glashow model.[149] The Weinberg-Salam may possess other types of "extended" structures on a scale of 1 TeV or more, but they would not be strictly (topologically) stable. These include rotating dumb-bells[150] and vortex-like[151] solutions of the field equations. It is not at all clear whether such things do exist, or if they are stable even if they do exist, or if they are observable even if they are stable. But their existence would certainly make life interesting.

In the rest of the lectures, we have been relatively conservative in our theoretical models, only considering models that unify weak and electromagnetic interactions. However, we should clearly keep in mind the possibility of unifying them with strong interactions. The last part of this lecture will discuss this inspirational topic,[152,153]

focusing in particular on phenomenological tests of this grand unification concept. For example, the proton is generally unstable in grand unified theories, and may have a lifetime within a few orders of magnitude of the present experimental limit of 2×10^{30} years.[154,72] While not strictly speaking a weak interaction at high energies, an experiment to refine the limit on this fundamental quantity seems an encouragingly offbeat note on which to finish these lectures.

4.2 Higgs in the Weinberg-Salam Model

As was mentioned before, gauge theories[2] need Higgs bosons if they are to incorporate masses and remain renormalizable. Indeed, it has been shown that from analyses[63] of the Born diagrams that Higgs particles must not only be present, but must have interactions with fermions, bosons and each other which are essentially those specified in a spontaneously broken gauge theory. In the Weinberg-Salam theory one needs at least one $I=\frac{1}{2}$ Higgs multiplet $H \equiv \begin{pmatrix} H^+ \\ H^o \end{pmatrix}$ to give masses to the fermions through couplings of the form

$$\mathscr{L}_H \ni \bar{f}_R H^+ f_L \tag{4.1}$$

(recall that right-handed fermions are SU(2) singlets, while left-handed fermions are SU(2) doublets[2]). As emphasized in Lecture 2, the apparent success[25,78] of the neutral current rate predictions resulting from the relation (2.20) strongly suggests that the vector bosons also get most of their masses from $I=\frac{1}{2}$ Higgs. We are therefore led to contemplate spontaneous symmetry breaking by $I=\frac{1}{2}$ Higgs alone, and the simplest possibility is to use just one multiplet. In this case the Higgs system has just 4 degrees of freedom

$$\underset{\sim}{H} \equiv \begin{pmatrix} H^+ \\ H^o \end{pmatrix}, \qquad \underset{\sim}{H}^+ \equiv \begin{pmatrix} -H^{o*} \\ H^- \end{pmatrix} \tag{4.2}$$

When the neutral Higgs acquires a vacuum expectation value v:

$$H^o = \frac{1}{\sqrt{2}} (v + H + i\tilde{H}) \tag{4.3}$$

from the minimum (Fig. 53(a)) of a Higgs potential of the form

$$V(H) = \mu^2 H^+H + \lambda (H^+H)^2 \quad : \quad \begin{matrix} \mu^2 < 0 \\ \lambda > 0 \end{matrix} \tag{4.4}$$

3 of the Higgs degrees of freedom (4.2), namely H^+, H^- and $\tilde{H}$, are eaten by the W^+, W^- and Z^o respectively to become their longitudinal polarization states, while one degree of freedom H is left over as a physical, neutral Higgs particle.[10] The magnitude of v reflects the masses of the vector bosons:

$$v^2 = \frac{1}{\sqrt{2}\, G} \tag{4.5}$$

with

$$m_W^2 = \frac{g^2 v^2}{4}, \qquad m_Z^2 = \frac{g^2 v^2}{4 \cos^2 \theta_W} \tag{4.6}$$

where g is the non-Abelian SU(2) semiweak coupling constant. The W^+W^-H and Z^oZ^oH couplings are fixed to be large:

$$g_{W^+W^-H} = \frac{2m_W^2}{v}, \qquad g_{Z^oZ^oH} = \frac{2m_Z^2}{v} \tag{4.7}$$

On the other hand, the $f\bar{f}H$ couplings are generally small

$$\mathscr{L}_H \ni (H^o + v)\, \bar{f} f\, g_{f\bar{f}H} \tag{4.8}$$

implying that

$$g_{f\bar{f}H} = \frac{m_f}{v} = \left(2^{\frac{1}{4}} G^{\frac{1}{2}}\right) m_f \tag{4.9}$$

which is small as long as m_f is in the range of presently known fermion masses. Some of the implications of fermions with very large masses[91,92] were discussed in section 2.2.

The parameters of the potential (4.4) are simply related to the value of v:

$$\lambda v^2 = -\mu \tag{4.10}$$

and the resulting physical Higgs mass is

$$m_H^2 = -2\mu^2 \tag{4.11}$$

It is apparent that none of the formulae (4.4 to 4.11) give us any way of fixing m_H, which is a priori totally unknown. Is it $O(m_f) << m_W$? or $O(m_W)$ like other bosons? or $>> m_W$?

There are some theoretical considerations on the Higgs boson mass which come from considering radiative corrections[154] to the Higgs potential (4.4). Effectively, they give a lower bound to the interaction term, which by an analogue of Eq. (4.10) for the simple interaction gives in turn a lower bound[155] on the Higgs mass. The extra potential term has the form

$$\Delta V_1(\underset{\sim}{H}) = \frac{1}{64\pi^2 v^4}\left[3\sum_{W,Z} m_V^4\right](\underset{\sim}{H}^+\cdot\underset{\sim}{H})^2 \ln\left(\frac{\underset{\sim}{H}^+\cdot\underset{\sim}{H}}{M_0^2}\right) \tag{4.12}$$

and demanding that the gauge symmetry break spontaneously to the minimum value of the combined potential (4.4), (4.12) as in Fig. 53(b) yields the bound:

$$m_H^2 \gtrsim \frac{3\sqrt{2}\,G}{16\pi^2}\left[2m_W^4 + m_Z^4\right] \tag{4.13}$$

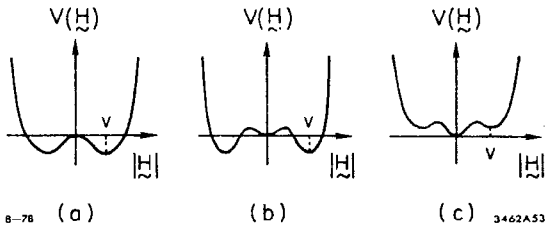

Fig. 53. The Higgs potential (a) in tree approximation, with radiative corrections and the Universe in (b) a stable vacuum, and (c) an unstable vacuum.

where we have neglected the fermion contribution in Eqs. (4.12 and 4.13) implying

$$m_H^2 \gtrsim \frac{3\alpha^2\left(2 + \sec^4 \theta_W\right)}{16\sqrt{2}\, G \sin^4 \theta_W} \tag{4.14}$$

which for $\sin^2 \theta_W \approx 0.20$ is

$$m_H \geq 7.1 \text{ GeV} \tag{4.15}$$

This bound is interestingly nontrivial, but some cautionary remarks should be made. The first is that the bound disappears[10] if there is any fermion with mass $O(m_W)$, because the fermions contribute to (4.13) with a minus sign. The second comment is that it is not strictly necessary that the Universe must lie in the lowest possible vacuum.[156] If one allows for the Universe to have chosen a nonminimal value of the Higgs potential as in Fig. 53(c), and demands only that the lifetime for quantum-mechanical tunnelling to the lowest vacuum be greater than the age of the Universe $\sim 10^{10}$ years, the bound (4.15) is greatly relaxed,[157] to

$$m_H > 260 \text{ MeV} \tag{4.16}$$

for $\sin^2 \theta_W \simeq 0.33$, somewhat higher for $\sin^2 \theta_W \approx 0.20$. However, it has been argued[157] that the nonminimal vacuum could only be chosen and the bound (4.16) attained only if the early Universe initially had enormous lepton number $L \gtrsim 10^8 B$. If there were no such large asymmetry, one would recover a bound of the same order as (4.14). It therefore seems that observation of a low-mass Higgs boson with a mass in the range between (4.16) and (4.15) would be cosmologically fascinating! Before leaving the subject of the radiative correction bound (4.13), it should be emphasized that if there are more than one $I=\frac{1}{2}$ Higgs multiplet, while the bound (4.13) would apply to one of the neutral Higgs particles, some of the others could have lower masses.[158]

In view of the above remarks, it seems reasonable to ask for empirical constraints on the existence of low-mass Higgs bosons. The most substantial phenomenological bounds are 3 independent arguments[10] that $m_H > 0$ (15 to 20) MeV. One is the absence of light scalar Higgs bosons produced in $0^+ \to 0^+$ nuclear transitions, which exclude $m_H < 18$ MeV. Another is the absence of Higgs exchange effects in neutron-nucleus scattering, which suggest that m_H is probably >13 MeV. The third is muonic atom X-rays, which at one time showed anomalies which could be explained by the effects of exchanging a Higgs with mass 0 (10-20) MeV, but which have now become completely canonical.

The three empirical constraints above all come from nuclear physics, and reflect characteristic nuclear energy scales. One might expect some more stringent restrictions on the mass of the Higgs to come from high energy physics, but this does not seem to be the case. The closest high energy physics comes seems to be in K decay, where the branching ratio

$$B(K^+ \to \pi^+ + H) \sim O(10^{-7}) \tag{4.17}$$

was estimated[10] for $m_H \simeq O(m_\pi)$, and there is an experimental upper limit

$$B(K^+ \to \pi^+ + H)\, B(H \to e^+e^-) < 0.4 \times 10^{-7} \tag{4.18}$$

for 140 MeV $< m_H <$ 340 MeV. Only Higgs particles in the mass range up to 210 MeV are expected to have a substantial ($\geq 10\%$) branching ratio into e^+e^- (see the next section), but it seems that the bound (4.18) is not even sufficient to rule out 140 MeV $< m_H < 2m_\mu$.

There are some theoretical arguments[140,159,160] against the existence of a very heavy Higgs boson which, while not rigorously excluding the possibility, emphasize the problems involved. As in the case of massive fermions discussed in section 2.2, the point is that Higgs particles become strongly interacting if they are very massive, as is seen immediately from Eqs. (4.10) and (4.11). Veltman[140] in particular has suggested that the Higgs mass should be less than the value which makes perturbation theory break down. This would require

$$\frac{g^2}{4\pi}\,\frac{m_H^2}{m_W^2} \lesssim 1 \qquad (4.19)$$

or $m \lesssim 300$ GeV. Lee, Quigg and Thacker[160] have done a detailed partial wave analysis for WW, ZZ and HH scattering and conclude that partial wave unitarity is violated by the Born diagrams unless

$$m_H^2 \lesssim \frac{8\pi\sqrt{2}}{3G} \approx 1\ (\text{TeV})^2 \qquad (4.20)$$

If the Higgs mass tried to exceed this value, presumably perturbation theory would not be applicable, but probably some sort of complicated bound state would drop out on a mass scale $\lesssim 1$ TeV. One might expect that the strong interactions of the Higgs particles would have some dramatic lower energy manifestations. Unfortunately, no example of this has yet been found, because the Higgs effects are always shielded by the relatively small $f\bar{f}H$ or WWH couplings.

In view of all these inconclusive remarks about the mass of the Higgs boson, even in the relatively tightly constrained Weinberg-Salam model, it behooves us to consider almost any possible mass, and look for the Higgs in many different places. We therefore turn to possible future experimental probes.

4.3 Higgs Phenomenology

4.3.1 Decays

Before discussing experiments to find a Higgs boson, perhaps we should first think about what we should look for.[10] The decay modes of relatively light Higgs are simple to deduce from Eq. (4.9). In general, the favoured decay mode for a Higgs with mass $<2m_W$ will be into the heaviest available fermion pair as in Fig. 54(a):

$$\Gamma(H \to f\bar{f}) \approx \frac{Gm_f^2}{4\sqrt{2}\,\pi}\, m_H \left[1 - \frac{4m_f^2}{m_H^2}\right]^{3/2} \begin{pmatrix}\times 3 \text{ for} \\ \text{colour}\end{pmatrix} \qquad (4.21)$$

Thus $c\bar{c}$ decays should dominate H decays in the mass range 4 GeV $< m_H <$ 10 GeV, with $\tau^+\tau^-$ decays suppressed by a colour factor of 3. Between the top and bottom thresholds, $b\bar{b}$ decays should dominate by a factor of $O(10)$ compared with $c\bar{c}$ decays, and so on. The situation is less clear for light Higgs particles, because the quark-parton model cannot be used to estimate the hadronic decays. But estimates support the naive guess that strange particles will dominate H decays in the mass range of 1 to 4 GeV, while $\pi\pi$ final states should dominate for $2m_\pi < m_H < 1$ GeV, and $\mu^+\mu^-$ decays for $2m_\mu < m_H < 2m_\pi$. Higgs masses below the $\mu^+\mu^-$ threshold may be somewhat academic in view of the remarks of section 4.3, but it is possible that $H \to \gamma\gamma$ through virtual fermion and boson loops as in Fig. 54(b) could be important for $m_H \gtrsim 30$ MeV, with $H \to e^+e^-$ otherwise dominating when $m_H > 2m_e$. A compendium[10] of likely Higgs branching modes for 1 MeV $< m_H <$ 100 GeV is shown in Fig. 55. Heavy Higgs bosons would[160]

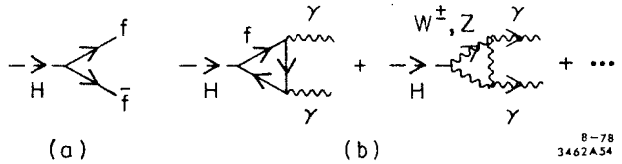

Fig. 54. Higgs decays (a) into $f\bar{f}$, and (b) into $\gamma\gamma$ through virtual fermion and vector boson loops.

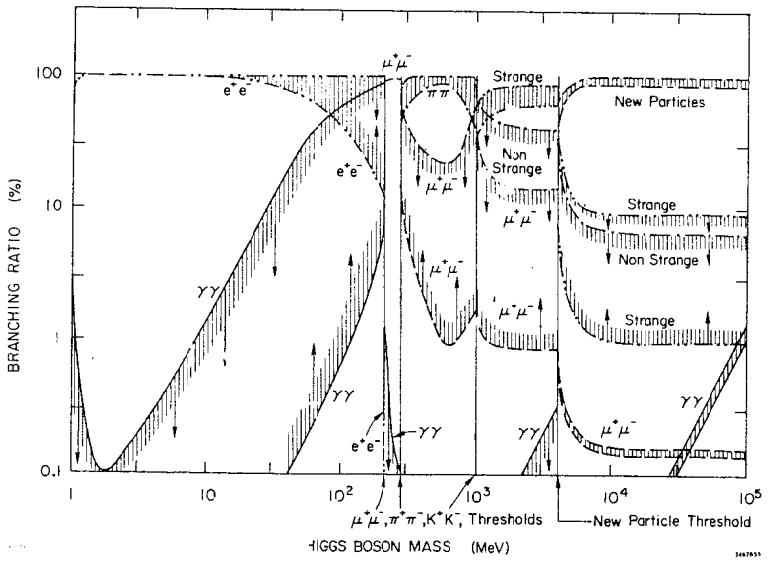

Fig. 55. A compendium[10] of Higgs decay branching ratios for different values of m_H.

decay into W^+W^- or Z^oZ^o pairs:

$$\left.\begin{matrix}\frac{\Gamma(H \to W^+W^-)}{m_H} \\ \frac{\Gamma(H \to Z^oZ^o)}{m_H}\end{matrix}\right\} = \left\{\begin{matrix}2\\1\end{matrix}\right\} \frac{Gm_W^2}{16\pi\sqrt{2}} \frac{\sqrt{1-x}}{x}(3x^2-4x+4) \qquad (4.22)$$

where $x \equiv 4m_W^2/m_H^2$ or $4m_Z^2/m_H^2$ respectively.

The lifetimes for Higgs particles which result from these available decay modes are portrayed[10] in Fig. 56, becoming unobservably short 10^{-15} sec $> \tau_H > 10^{-21}$ sec for $2m_\pi < m_H < 100$ GeV. The dominant boson pair decays (4.22) of heavier Higgs bosons push up their decay rates to become comparable with their masses when $m_H \sim 1$ TeV. This corresponds to the strong interaction "bound" (4.20).

4.3.2 Production

We now run through a selection of possible Higgs production mechanisms.

Vector meson → H+γ

The radiative decay (Fig. 57) of a heavy $q\bar{q}$ vector meson, say $T(b\bar{b})$ or the forthcoming toponium $t\bar{t}$ into a Higgs particle has a substantial[161] branching ratio:

$$\frac{\Gamma(V \to H+\gamma)}{\Gamma(V \to \mu^+\mu^-)} \approx \frac{Gm_V^2}{4\sqrt{2}\,\pi\alpha}\left(1-\frac{m_H^2}{2m_V^2}\right)F\left(\frac{m_H^2}{m_V^2}\right) \qquad (4.23)$$

where $F\left(m_H^2/m_V^2\right)$ is a known function[162] which is quite well approximated by

$$F\left(\frac{m_H^2}{m_V^2}\right) \approx \left(1-\frac{m_H^2}{2m_V^2}\right) \qquad (4.24)$$

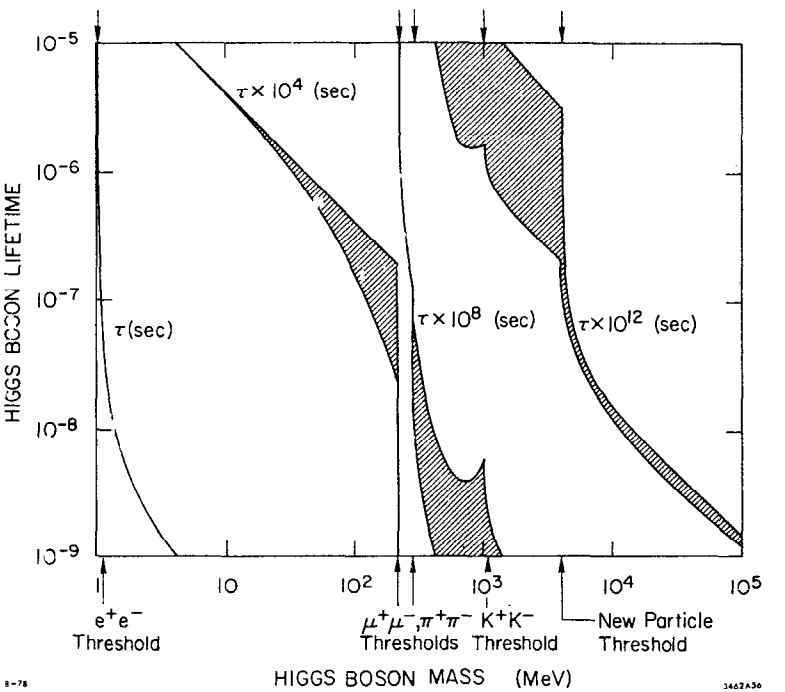

Fig. 56. The Higgs boson lifetime[10] as a function of its mass.

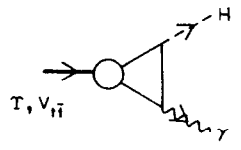

Fig. 57. The decay V → H+γ.

For $m_H \sim \frac{1}{2}m_V$ the formulae (4.23, 4.24) yield

$$\frac{\Gamma(V \to H+\gamma)}{\Gamma(V \to \mu^+\mu^-)} \approx \begin{cases} 3 \times 10^{-3} & \text{for T} \\ 3 \times 10^{-2} & \text{for } t\bar{t} \text{ if } m_t = 15 \text{ GeV} \end{cases} \tag{4.25}$$

Putting in the expected branching ratios

$$B(T \to \mu^+\mu^-) \sim 3\% , \qquad B(t\bar{t} \to \mu^+\mu^-) \sim 8\% \tag{4.26}$$

we find the final branching ratios

$$B(V \to H+\gamma) \approx \begin{cases} 10^{-4} & \text{for T} \\ 2 \times 10^{-3} & \text{for } t\bar{t} \text{ if } m_t = 15 \text{ GeV} \end{cases} \tag{4.27}$$

These branching ratios (4.27) are quite promising, and suggest that the decay V → H+γ may be a good way of looking for Higgs bosons with masses up to the as yet unknown mass of the $t\bar{t}$ bound state.

$Z \to H + \ell^+\ell^-$

This can proceed through the diagram shown in Fig. 58, where the $\mu^+\mu^-$ pair are produced by a virtual Z, and the relatively large Z^oZ^oH coupling (4.7) is being exploited to get a reasonable branching ratio. Bjorken[122] has calculated the decay rate

$$\frac{1}{\Gamma(Z^o \to \mu^+\mu^-)} \frac{d\Gamma(Z^o \to H\mu^+\mu^-)}{dx} = \frac{\alpha}{4\sin^2\theta_W \cos^2\theta_W} \frac{\left[1-x+\frac{x^2}{12}+\frac{2}{3}\frac{m_H^2}{m_Z^2}\right]\left[x^2-\frac{4m_H^2}{m_Z^2}\right]^{\frac{1}{2}}}{\left(x-\frac{m_H^2}{m_Z^2}\right)^2} \tag{4.28}$$

where $x \equiv 2E_H/m_Z$. In Fig. 59 is shown $\frac{\Gamma(Z^o \to H\mu^+\mu^-)}{\Gamma(Z^o \to \mu^+\mu^-)}$ as a function of m_H for $\sin^2\theta_W = 1/3$. We see that the relative decay rate is $\geq 3 \times 10^{-5}$ for $m_H \leq 40$ GeV. Taking the branching ratio for $Z^o \to \mu^+\mu^-$ to be 3% gives a

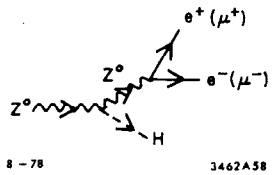

Fig. 58. The decay $Z^o \to H + \mu^+\mu^-$.

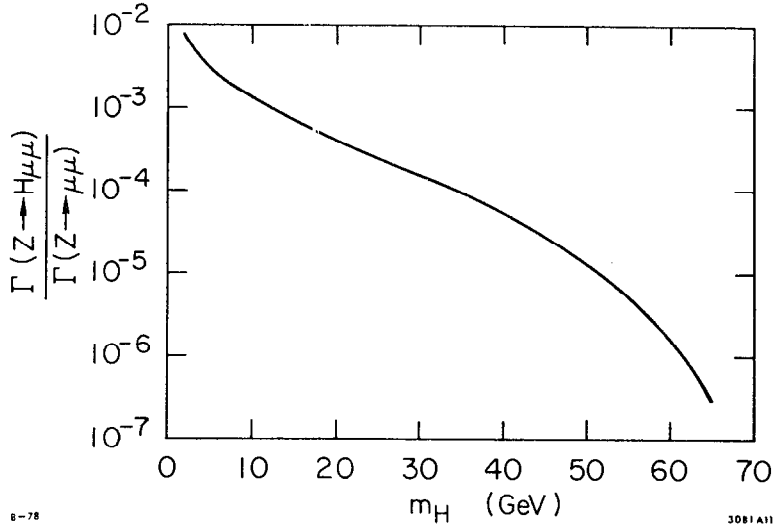

Fig. 59. The rate $\Gamma(Z^o \to H\mu^+\mu^-)/\Gamma(Z^o \to \mu^+\mu^-)$ as a function of m_H.[122]

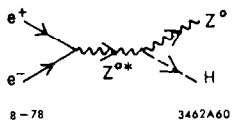

Fig. 60. The process $e^+e^- \to Z^{o*} \to Z^o+H$.

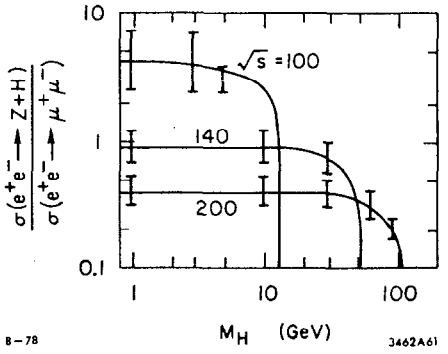

Fig. 61. Calculations[164] of $\sigma(e^+e^- \to Z^o+H)/\sigma_{pt}$ for different values of $\sqrt{s}$, m_H and $\sin^2\theta_W$.

total branching ratio

$$B(Z^o \to H\mu^+\mu^-) \geq 10^{-6} \quad \text{or } He^+e^- \tag{4.29}$$

for $m_H < 40$ GeV. This should be accessible if one really can do experiments with $O(10^7)$ Z^o decays, as seemed possible (section 3.5) with a Z^o factory.

Another decay which may yield Higgs at a rate comparable to (4.29) is $Z^o \to H+\gamma$, which would proceed via virtual fermion and $W^\pm$ loops. An order of magnitude calculation suggests that $B(Z^o \to H+\gamma) \sim 10^{-6}$ also.

$\underline{e^+e^- \to Z^o+H}$

This is the complement of the $Z^o \to H+\mu^+\mu^-$ reaction. Again one uses the large Z^oZ^oH coupling (4.7) to bremsstrahl a Higgs. The only difference is that the process is now $Z^* \to Z+H$ instead of $Z \to Z^*+H$ as in Fig. 60. The cross section is[163]

$$\sigma(e^+e^- \to Z^o+H) = \frac{\pi\alpha^2}{24}\left(\frac{2K}{\sqrt{s}}\right)\left(\frac{K^2+3m_Z^2}{(s-m_Z^2)^2}\right)\frac{(1-4\sin^2\theta_W+8\sin^4\theta_W)}{\sin^2\theta_W(1-\sin^2\theta_W)^2} \tag{4.30}$$

where K is the centre-of-mass momentum of the Z^o or H.

The cross section for $e^+e^- \to Z^o+H$ relative to the QED $\sigma(e^+e^- \to \mu^+\mu^-) \equiv \sigma_{pt}$ (3.39) is plotted[164] in Fig. 61 for a range of centre-of-mass energies $\sqrt{s}$, and values of m_H. The "error bars" on the theoretical curves represent the uncertainty in varying $\sin^2\theta_W$ from 0.22 to 0.29. We see that at $\sqrt{s} \sim 200$ GeV even a Higgs of mass close to 100 GeV could be produced with a cross section $\geq 10^{-37}$ cm^2, corresponding to 1 event/day at a luminosity of 10^{32} cm^{-2} sec^{-1}. Furthermore, the event will be relatively "clean" and easy to pick out using a Z^o trigger.

pp → H+X

Three possible Higgs production mechanisms have been proposed for high energy hadron-hadron collisions. First there is a simple pp → H+X, where the dominant production mechanism is probably via gluon-gluon collisions,[165] and the Higgs-GG coupling is estimated using virtual quark loops.[161] Calculations (see Fig. 62) indicate that

$$\sigma(pp \to H+X) \gtrsim 10^{-35}\ \text{cm}^2 \quad \text{for } m_H \leq 30\ \text{GeV}, \quad \sqrt{s} \geq 400\ \text{GeV} \tag{4.31}$$

depending somewhat how many quarks are put into the loops. This cross section certainly yields a sizeable event rate at a machine like Isabelle. Unfortunately, it is difficult to think of a signature which would enable the Higgs events to be separated from the less interesting events. One possible way of solving this problem is to look for pp → Q+$\bar{Q}$+H+X, where Q is some heavy quark, and the Higgs is bremsstrahled from the heavy quark line. A naive order of magnitude estimate[166] suggests that the cross section for pp → b+$\bar{b}$+H+X might be comparable to (4.31), and the presence of heavy quark particles in the final state might serve as a useful signature. A still better signature would come from the reaction[167,164] pp (or $\bar{p}p$) → $W^{\pm}$ or Z^o+H+X. Calculations[164] (see Fig. 63) indicate that

$$\frac{\sigma(p\,p \to W^{\pm} \text{ or } Z^o + H + X)}{\sigma(p\,p \to W^{\pm} \text{ or } Z^o + X)} \sim 10^{-4} \tag{4.32}$$

for $m_H \sim 30$ GeV and pp collisions at $\sqrt{s}$ = 800 GeV or $\bar{p}p$ collisions at $\sqrt{s}$ = 540 GeV. The cross section (4.33) might well be accessible at Isabelle, and the $W^{\pm}$ or Z^o could provide a signature through decay leptons.

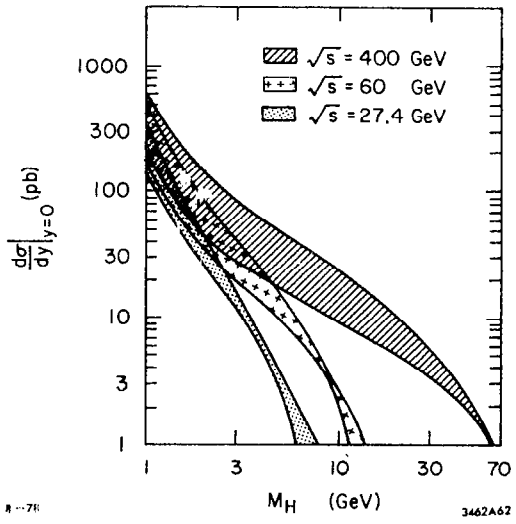

Fig. 62. Calculations[165] of pp → H+X as functions of m_H and $\sqrt{s}$.

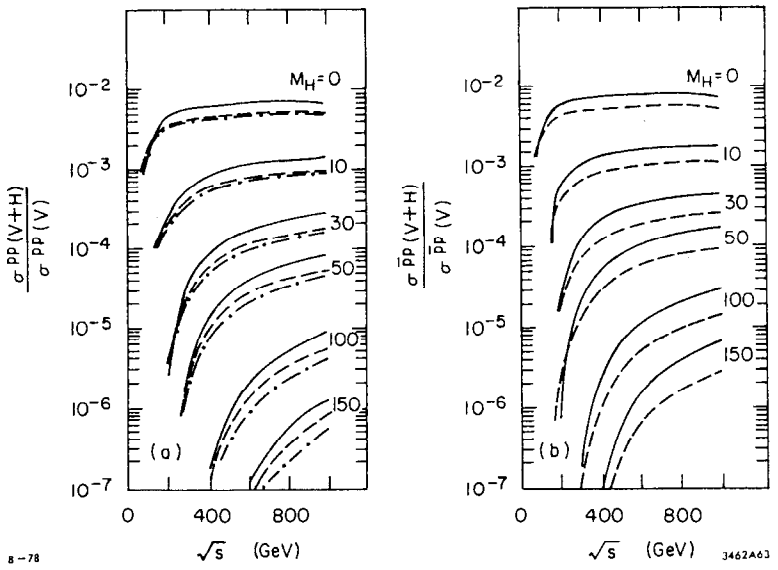

Fig. 63. Calculations[164] of pp or $\bar{p}p \to W^{\pm}$ or Z^0 +H+X as functions of m_H at $\sqrt{s}$ = 800 GeV. In (a) the solid/dashed/dot-dashed lines refer to $\sigma(W^+ + H)/\sigma(W^+)$, $\sigma(W^- + H)/\sigma(W^-)$ and $\sigma(Z+H)/\sigma(Z)$ respectively; in (b) the solid/dashed lines refer to $\sigma(W^{\pm}+H)/\sigma(W^{\pm})$ and $\sigma(Z+H)/\sigma(Z)$ respectively.

$\nu+N \to \mu+H+X$

In this reaction the dominant diagram is likely to be that where the Higgs is bremsstrahled from the exchanged W line[10,168] as in Fig. 64. For light Higgs and neutrino energies which are not so large that $W^{\pm}$ propagator effects are important,

$$\frac{\sigma(\nu+N \to \mu+H+X)}{\sigma(\nu+N \to \mu+X)} \sim 3 \times 10^{-8} \times E_{\nu}(\text{GeV}) \qquad (4.33)$$

The cross section ratio (4.34) is probably too low to be usable, given the absence of a distinctive Higgs decay signature. The same remarks apply to high energy ep colliding rings,[101] where the Higgs cross section is plausibly $O(10^{-38})$ cm^2, compared with a possible luminosity of $O(10^{32})$ cm^{-2} sec^{-1}.

To summarize the above discussion, it seems that the most promising sources of the basic neutral Weinberg-Salam Higgs boson may be (in order of increasing m_H): T decays, toponium decays, Z^0 decays, $e^+e^- \to Z^0+H$, with $pp \to W^{\pm}$ or Z^0 + H as the least unpromising alternative to e^+e^- colliding beam experiments.

4.4 More Complicated Higgs Systems

4.4.1 Charged Higgs particles

If the Weinberg-Salam model is modified very slightly to include more than one I=½ Higgs multiplet, then only one combination of the charged Higgs fields ($\phi_1^+, \phi_2^+, \ldots$) can be eaten by the W^+, and the remaining combination or combinations will show up as physical charged scalars. There is considerable freedom to adjust parameters, but one would expect a general correlation of the Higgs couplings with the masses of the fermions. Thus important decays of H^+ might be[169] $H^+ \to \tau^+\nu_\tau$, $c\bar{s}$, $t\bar{b}$, etc., depending on the mass of the H^+. An invariant mass peak in a

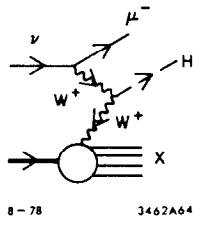

Fig. 64. The dominant diagram[10] for $\nu+N \to \mu^-+H+X$.

combination $(DK)^+$ would be interesting! The cross section for producing H^+H^- pairs in e^+e^- collisions is just

$$\frac{\sigma(e^+e^- \to \gamma^* \to H^+H^-)}{\sigma_{pt}} = \frac{1}{4}\left(1 - \frac{4m_{H^+}^2}{s}\right)^{3/2} \tag{4.34}$$

Such a charged Higgs would therefore not have a big threshold in e^+e^- collisions. However, if the H^+ were sufficiently massive, H^+H^- events would probably have high sphericity and acoplanarity close to threshold, and the sort of sphericity scan advocated in Lecture 2 for finding heavy quarks would also find an H^+H^- threshold. The H^+H^- threshold would then be distinguished by its pointlike structureless nature and the absence of resonances below threshol'. If m_t (or m_b) and m_{H^+} are in the right relationship, decays like $t \to H^+ + b$ or $b \to H^- + c$ become kinematically accessible.[170] Bearing in mind the expected generic correlation of H^+ couplings with quark mass, one might expect

$$\Gamma(Q \to H^+ + q) \approx \frac{G_F m_Q^3}{32\pi} \times \left(\begin{matrix}\text{angle}\\ \text{factors}\end{matrix}\right) \times \left(\begin{matrix}\text{phase}\\ \text{space}\end{matrix}\right) \tag{4.35}$$

for a heavy quark Q to decay into H^+ and a lighter quark q. In the case of Q=b a (generalized) Cabibbo angle factor might be present, so that

$$\Gamma(b \to H^+ + c) \approx 10^{-5}\ (\sin^2\theta)\ \text{GeV}$$
$$\approx 1\ \text{keV}\ ? \tag{4.36}$$

This decay rate would certainly dominate conventional weak decays of b: it would even be a significant decay mode of $T = b\bar{b}$,[171] giving final states $T \to H^+B\bar{C}X$! It should soon be possible to exclude such decays at the level of a branching O(1)%, which would militate against an H^+ with mass < 2 GeV, and similar searches could be made in the decays of mesons

made of heavier quarks. One can easily add decays like H^o or $Z^o \to H^+H^-$ to the list of possible places to look, but these are somewhat more distant prospects.

4.4.2 The axion

The axion[143] is a special type of neutral Higgs particle which was proposed as a way of solving certain problems concerning CP violation in QCD.[142,172] These are that when nonperturbative topological aspects of QCD are taken to account, it turns out that there may be an extra term

$$\mathscr{L}_\theta \equiv \frac{\theta}{32\pi^2}\,\varepsilon_{\mu\nu\rho\sigma}\,F^a_{\mu\nu}F^a_{\rho\sigma} \tag{4.37}$$

to be included in the QCD Lagrangian with θ an a priori unknown parameter. You can see from the form of $\mathscr{L}_\theta$ (4.32) that it has C even and P odd, and hence violates CP. In the real world, CP violation due to the strong interactions is extremely small. The best limit on it comes from the neutron electric dipole moment $\frac{D}{e}$, which is known experimentally[27] to be

$$\frac{D}{e} \lesssim 3 \times 10^{-24}\ \text{cm} \tag{4.38}$$

This quantity violates CP and would be proportional to θ if it were nonzero but small. One calculation[173] gives

$$\frac{D}{e} \approx 4 \times 10^{-16}\ \theta\ \text{cm} \tag{4.39}$$

so allowing for uncertainties in the theoretical calculation, θ must be $< 10^{-8}$. It would be nice to ensure that $\theta=0$ automatically. This could be done[142] by giving the world's Lagrangian an extra U(1) symmetry with an associated current J^5_μ. Similar anomalies to the ones we discussed in Lectures 1 and 2 cause the divergence of this current to be nonzero:

$$\partial^\mu J^S_\mu = \frac{\varepsilon_{\mu\nu\rho\sigma}}{16\pi^2}\,F^a_{\mu\nu}F^a_{\rho\sigma} \tag{4.40}$$

By making a chiral transformation of the J^5_μ type, one changes the Lagrangian by an amount proportional to $\partial^\mu J^5_\mu$ (4.40), and so may remove any possible term $\mathscr{L}_\theta$ (4.37) from the QCD Lagrangian. The next problem is to find a way of giving the Lagrangian this U(1) symmetry. One way would be if one of the quarks--probably the u quark--had zero mass. But this hypothesis, while not completely excluded, looks to be in bad shape when one looks at meson and baryon mass differences.[174] An alternative way of getting a U(1) symmetry is to introduce a pseudoscalar boson which is essentially massless. This can be done by extending the simplest Weinberg-Salam model to two or more Higgs multiplets, and restricting their interactions so that the combined QCD-modified Weinberg-Salam theory has the requisite U(1) symmetry. The low mass pseudoscalar boson introduced in this way is the axion (a).[143] Its mass is not strictly zero because of strong interaction symmetry breaking effects, which cause its mass to be generically of order

$$m_a \approx \sqrt{G_F} \times \mu^2 \tag{4.41}$$

where μ is some typical strong interaction scale--O(300) MeV?--so that one might expect $m_a = O(10^{2\pm1})$ keV. Being a Higgs particle, one would expect the couplings g_{aff} to be $O\left(gm_f/m_W\right)$, as for the basic Higgs boson (4.9).

To proceed further, we will turn to the simplest axion model,[143] which has just two $I=\frac{1}{2}$ Higgs multiplets. The theory is then characterized

by a free parameter

$$\frac{v_1}{v_2} = \frac{\langle 0|H_1^o|0\rangle}{\langle 0|H_2^o|0\rangle} = \tan\alpha \tag{4.42}$$

where in order to get the $W^{\pm}$ mass correct

$$v_1^2 + v_2^2 = \frac{1}{\sqrt{2}\,G} \tag{4.43}$$

which should be compared with the single Higgs formula (4.5). In this model, the coupling to heavy quarks has a form analogous to (4.8):

$$\mathscr{L}_{aq} = 2^{\frac{1}{4}} G^{\frac{1}{2}} a\left[m_c \bar{c}\gamma_5 c \tan\alpha + m_b \bar{b}\gamma_5 b \cot\alpha + \ldots\right] + m_t \bar{t}\gamma_5 t \tan\alpha + \ldots \tag{4.44}$$

On the other hand, the axion coupling to light quark systems goes predominantly through mixing with the π^o and η which have the same quantum numbers (C=+1, P=-1) as the axion. The mixing is specified by parameters

$$\xi_\pi = \xi\left[\left(\frac{3m_d - m_u}{m_d + m_u}\right)\tan\alpha - \left(\frac{3m_u - m_d}{m_u + m_d}\right)\cot\alpha\right]$$
$$\xi_\eta = \xi\left[\sqrt{3}\tan\alpha + \frac{1}{\sqrt{3}}\cot\alpha\right] \tag{4.45}$$

where $\xi \equiv 2^{-5/4} G^{1/2} f_\pi \approx 1.9 \times 10^{-4}$, and the axion mass in this simplest model is approximately

$$m_a \approx \frac{f \times m_\pi f_\pi}{\sqrt{2}(m_u + m_d)^{\frac{1}{2}}}\left[\frac{m_u m_d m_s}{m_u m_d + m_d m_s + m_s m_u}\right]\frac{2^{1/4} G^{1/2}}{\sin 2\alpha}$$
$$\approx \frac{23 \times f}{\sin 2\alpha}\ \text{keV} \tag{4.46}$$

where f is the number of quark flavours, as usual. The simplest axion described by the formulae (4.42) to (4.46) would presumably be lighter than $2m_e$ and so decay mainly into 2γ with a lifetime $\geq 10^{-4}$ sec. The mixings (4.45) would allow the axion to be produced at rates $O(10^{-7})$ of π^o or η production in any hadronic process. The couplings (4.44) ensure its production in heavy vector meson decays[143,161] $V \to a+\gamma$ at a rate $\tan^2\alpha$ (or $\cot^2\alpha$) times the $V \to H+\gamma$ rate (4.23).

Can the axion exist? Probably not in the simplest form discussed above, but this is not totally excluded. Evidence against it comes from several sources.

Beam dump experiments

In experiments[175,176] at CERN, a proton beam has been dumped into a hadron target which absorbed hadronic secondaries before most of them decayed, and searches were made for events in neutrino experiment detectors downstream which could have been generated by neutral penetrating particles such as neutrinos or the axion as in Fig. 65. Axion-induced events would have shown up as apparent neutral current events with small missing p_T in the hadronic final state. It has been estimated[144] that

$$\frac{\sigma(p+p \to a+X)}{\sigma(p+p \to \pi^o+X)} \approx \xi_\pi^2 + \tfrac{1}{3}\xi_\eta^2, \qquad \frac{\sigma(a+p \to X)}{\sigma(\pi^o+p \to X)} \approx \xi_\pi^2 + \tfrac{2}{3}\xi_\eta^2 \tag{4.47}$$

implying a product of axion production and interaction cross sections

$$\sigma(p+p \to a+X)\sigma(a+p \to X) \approx \left(\xi_\pi^2 + \tfrac{1}{3}\xi_\eta^2\right)\left(\xi_\pi^2 + \tfrac{2}{3}\xi_\eta^2\right) \times 2 \times 10^{-31}\ \text{cm}^4$$
$$\geq 9 \times 10^{-66}\ \text{cm}^4 \tag{4.48}$$

where the lower bound comes from the fact that ξ_η (4.45) cannot be switched off, even though ξ_π can be zero for uncooperative values of m_d/m_u and $\tan\alpha$. Various experimental limits on axion production in the CERN beam dump experiments[175,176] are $O(10^{-67})$ cm^4, indicating that the bound (4.48) is violated by about two orders of magnitude,[145] so that an axion with

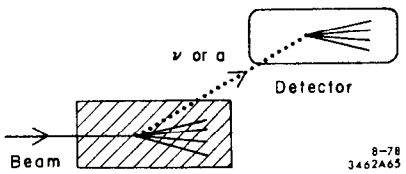

Fig. 65. A schematic sketch of a beam dump experiment.

mass $\lesssim$ 2 MeV cannot exist. An analysis[146] has also been made of a SLAC beam dump experiment which also finds an upper limit of an axion-induced events about two orders of magnitude less than would have been expected in the simple model discussed above.

Reactor neutrino experiments

Axions could show up in these experiments by being produced in nuclear transitions and then decaying into $\gamma\gamma$, or undergoing Compton scattering $a+e \to \gamma+e$, or by causing deuteron disintegration $a+d \to n+p$.[143] Unfortunately, theoretical estimates of axion production rates by nuclei are rather unreliable. Nevertheless, it has been conservatively[146] estimated that

$$N_{a\to 2\gamma} \simeq 10^3 \left(\frac{m_a}{100\ \text{keV}}\right)^6 \tag{4.49}$$

axion $\to \gamma\gamma$ decays should have been seen per day, compared with an experimental limit of (-160 ± 260) γ events/day. Also

$$N_{a+e\to\gamma+e} \sim \frac{10^3}{\tan^2 \alpha} \tag{4.50}$$

would have been expected. The deuteron disintegration rate is naively calculated to be $O(10^3)$ larger than the experimental limit, though this calculation is particularly sensitive to unreliable details of nuclear calculations. Despite the uncertainties[143,146] in the nuclear calculations, it seems likely that reactor neutrino experiments also rule out the simplest form of axion.

Cosmology and astrophysics

The best restriction on the axion from these sources comes from considerations on the evolution of red giant stars. It is apparently[177] required that $m_a > 200$ keV, but this is not inconsistent with the mass estimate (4.46).

$K^+ \to \pi^+ + a$

We believe that this decay rate should be comparable with that estimated[101,178] for $K^+ \to \pi^+ + H \sim O(10^{-7})$ (4.17). The relevant experimental limit is that on $K^+ \to \pi^+ \nu\bar{\nu} < 6 \times 10^{-7}$. We conclude that K decays do not yet exclude the axion's existence.

The preponderance of the above evidence is against the existence of an axion in the simple form given by Eqs. (4.42) to (4.46). However, the existence of an axion cannot be totally excluded.[179] For example, the parameter α (4.42) could be very small for some reason which may seem unnatural in the context of this model, but might be made to look less unreasonable in a more complicated model with more Higgs multiplets and/or vector bosons.[179] When α is sufficiently small the axion decays mainly into e^+e^-, which it does too quickly to show up in beam dump or reactor experiments. Its phenomenology would then resemble that of the very light Higgs bosons discussed in sections 4.2 and 4.3, with the exception that being a pseudoscalar, the various nuclear constraints that $m_H >$ (15 to 20) MeV would not apply to the axion.

What if there is no axion? No other totally satisfactory method of ensuring $\theta=0$ has yet been proposed. Even if $\theta=0$ for the strong interactions alone, the possibility exists that it may be renormalized by the weak interactions and become unacceptably large. In the simplest Weinberg-Salam model with one Higgs multiplet, if one sets $\theta=0$ for the strong interactions, the renormalization of θ due the CP violation in the weak interactions generated by the Kobayashi-Maskawa model (2.39) is zero in $O(\alpha)$, but nonzero and $O(10^{-16})$ in $O(\alpha^2)$.[180] There is another popular model of CP violation which uses multiple Higgs multiplets,[103] which has a larger renormalization of θ than allowed by experiment (4.38). There is[181] another multi-Higgs model with θ renormalization which is finite and $O(10^{-6}$ to $10^{-7})$, which is on the outskirts of phenomenological acceptability.[180] It seems that the problem of CP violation in QCD and weak electromagnetic gauge theories is still very little understood, and in particular we lack any good reason why θ should be zero or small before weak renormalization.

4.5 Monopoles, etc.

We are now at the stage of the lectures where fantasy begins to take over, and we examine some more speculative possibilities suggested by gauge theories. In this section we would look into the possible existence of heavy particles arising from extended solutions of the non-Abelian field equations. The first example will be the monopole,[147] which is a sort of topological knot tied in the Higgs system of a spontaneously broken gauge theory. So far (cf. Eq. (4.5)) we have always discussed situations where the Higgs vacuum expectation value was independent of x as in Fig. 66(a):

$$\langle 0|H^0(x)|0\rangle = v \tag{4.51}$$

but it could happen that $\langle 0|H^0(x)|0\rangle$ was x-dependent as illustrated in Fig. 66(b). This could happen if there were an isotriplet of Higgs particles:

$$\langle 0|H^i(x)|0\rangle \to v\left(\frac{x^i}{|\underline{x}|}\right) \tag{4.52}$$

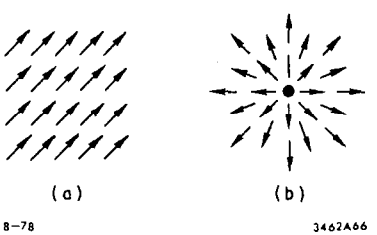

Fig. 66. The spontaneous symmetry breaking Higgs vacuum expectation value (a) independent of $\underset{\sim}{x}$ as usual, and (b) in the presence of a monopole.

as $|\underset{\sim}{x}| \to \infty$ in all 3-space directions. Solutions like (4.52) exist in some gauge theories like the (phenomenologically defunct) Georgi-Glashow model,[152] but not in the Weinberg-Salam model with its $I=\frac{1}{2}$ Higgs multiplets.

Nothing daunted, the generic properties of such monopoles are that they have masses

$$m_M \gtrsim \frac{1}{\sqrt{\alpha}} m_{W,Z} \sim 1 \text{ TeV} \tag{4.53}$$

Their couplings to weak and electromagnetic fields are characteristically strong:

$$\frac{g_M^2}{4\pi} = O\left(\frac{1}{\alpha}\right) \tag{4.54}$$

and they presumably interact strongly with each other. Monopoles are guaranteed by their topological properties to be absolutely stable. Above the threshold $2m_M$, one would expect monopoles to be produced in pairs as in Fig. 67(a), but not by a single photon. The pair production cross section should be $O(1)$ because of the strong coupling (4.54). The monopole pair could also annihilate into many photons and/or vector bosons as in Fig. 67(b). This process might be particularly important close to threshold, and have a dramatic signature in the form of very large γ showers. The motion of a monopole in a magnetic field is characteristically bizarre--its momentum tends to align itself parallel to any magnetic field as in Fig. 67(c). It should also be remembered that the monopole would find it very easy to lose energy by radiating photons (and W's and Z's)[101] as in Fig. 67(d).

Can monopoles exist? No one has ever been able to confirm seeing one. If one accepts the standard big-bang cosmology for the early

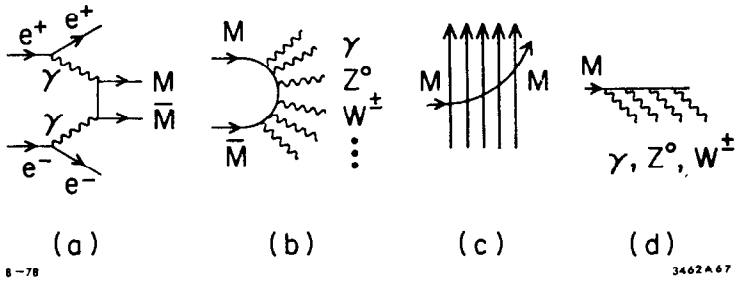

Fig. 67. Monopoles[147] (a) being produced, (b) annihilating to give many γ's, (c) aligning parallel to a magnetic field, and (d) losing energy by radiation.

Universe, one can estimate[148] the density of monopoles which should have been formed then. The calculation of the monopole density today depends on how one believes the production model and estimates of the probability of mutual annihilation of the primordial monopoles. But it seems that monopoles with the properties (4.53, 4.54) should probably have been $O(10^6)$ more abundant than the experimental upper limit. But surely someone can come up with a theory containing more massive monopoles which would be cosmologically rarer and hence acceptable.

It was mentioned above that the Weinberg-Salam model does not have monopoles. Does it have any other sort of extended, heavy object? It has been proposed[150] that there may be quasi-stable string-like objects which somewhat resemble dumb-bells with a sort of monopole at each end as in Fig. 68(a). These would form Regge trajectories with an intercept and Regge slope of order 1 TeV^2. High spin "particles" on the leading trajectory--corresponding to rapidly rotating dumb-bells--would possibly be somewhat stable because of the angular momentum barrier. However, these objects would not be guaranteed stable by any topological conservation law, and their lifetimes are difficult to estimate. If these string-like solutions exist, so probably do other string configurations such as closed loops[151] which loosely resemble smoke rings or vortices as in Fig. 68(b). They would also have Regge trajectories, which would correspond to the Pomeron in normal Regge lore, and also have a mass-scale O(1 TeV).

Unfortunately, it is not clear whether these string-like objects really exist in the Weinberg-Salam model, and if so how stable they are. Even if they do exist and are stable, it is not clear what their

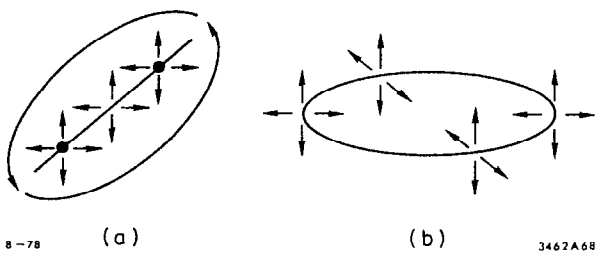

Fig. 68. Illustrations of possible extended objects in the Weinberg-Salam model: (a) a dumb-bell,[150] and (b) a flux loop.[151]

production cross section is, except that it is probably very small. They are in some sense coherent extended field configurations containing $O\left(\frac{1}{\alpha}\right)$ vector bosons, and the overlap with the O(1) vector boson state produced, say, by e^+e^- collisions is probably very small.

The prospects for finding anything like a monopole in presently conceivable weak interaction experiments seem rather dim. However, the subject is still rather uncertain, and it is hoped that these remarks may stimulate more serious theoretical thoughts, because objects of this type would be very interesting if they exist.

4.6 Grand Unification Phenomenology

Up till now, we have been treating the strong and weak electromagnetic interactions rather separately. With the exception of the discussion of CP violation and the axion, which was not brilliantly successful, we have not really addressed the theoretical interrelationship between the different interactions. However, since we rather complacently believe we have found the correct theory of the strong interactions, namely QCD,[4] and think we are on the track of the right spontaneously broken gauge theory of the weak interactions[2]--very possibly the Weinberg-Salam model[16]--it is clearly high time to speculate on the next phase of unification.[152,153] In the process of this grand unification, we may hope first to find certain consistency conditions that must be imposed on the individual strong, weak and electromagnetic interactions before they can be unified. We may also hope to predict dramatic new types of interaction, such as those violating baryon and lepton number and causing the proton to decay.

Let us consider the type[152] of theory where a large group G is postulated which has a unique coupling constant, and which is broken somehow into component parts

$$G \to SU(3) \times SU(2)_L \times U(1) \times ? \tag{4.55}$$

for the different interactions. Clearly the grand unification symmetry[152] must be considerably broken, because the observed strong and weak coupling strengths are very different. However, after Lecture 1 and Eq. (1.14) we are used to the idea that coupling strengths depend on the scale at which they are measured. We believe that the strong interactions get weak at high momenta, so perhaps it is not[182] inconceivable that the strong and weak/electromagnetic coupling strengths may come together at some sufficiently high Q^2 as in Fig. 69(a). In the Weinberg-Salam model the $SU(2)_L$ and U(1) couplings g and g' are independent, and the ratio

$$\sin^2 \theta_W = \frac{g'^2}{(g^2+g'^2)} \tag{4.56}$$

is a number to be determined by experiment. A symmetry group G would make a prediction for g^2/g'^2, and hence for $\sin^2 \theta_W$. In the same way as the ratio α_s/α, the ratio g^2/g'^2 will be renormalized[182] if the G symmetry is only exact at very high momenta.

The simplest grand unification model is the SU(5) model of Georgi and Glashow,[152] which breaks down into exactly QCD × Weinberg-Salam. Simple application of the QCD evolution formula (1.14) for $\alpha_s(Q^2)$ shows that it will be $O(\alpha)$ only at very high Q^2. In fact, the best estimate of the momentum at which grand unification takes place in SU(5) is[72,183]

$$m_{GUM} = O(10^{15} \text{ to } 10^{16}) \text{ GeV} \tag{4.57}$$

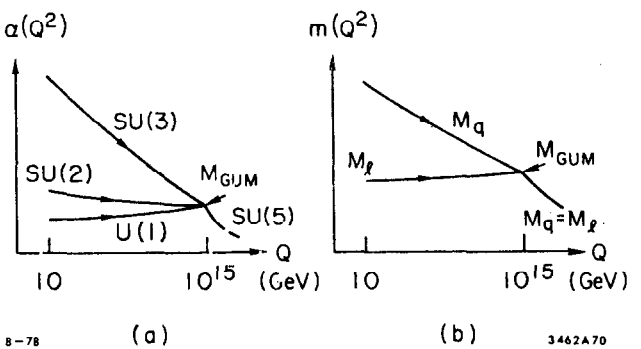

Fig. 69. Qualitative sketches (a) of the present greatly different weak and strong coupling constants becoming unified at very high energies, and (b) of quark and lepton masses which are equal when measured on the grand unification mass scale becoming different at low Q^2.

Using this value, one can estimate the renormalization of $\sin^2\theta_W$, which is 3/8 in the symmetry limit, to[72]

$$\sin^2\theta_W \approx 0.20 \tag{4.58}$$

which is not in disagreement with the latest experiments. It is characteristic of grand unification models that they put quarks and leptons into the same multiplet of the grand unification symmetry group G. For example in SU(5)[152] there are multiplets

$$(\bar{d}_R,\bar{d}_Y,\bar{d}_B;\ e^-,\nu_e)_L;\ (\bar{s}_R,\bar{s}_Y,\bar{s}_B;\ \bar{\mu},\nu_\mu)_L;\ (\bar{b}_R,\bar{b}_Y,\bar{b}_B;\ \bar{\tau},\nu_\tau)_L \tag{4.59}$$

which put meat on the often-discussed concept of quark-lepton universality that was discussed in section 2.2. Because of the large symmetry-breaking (4.57) inherent to this type of model, the quark-lepton symmetry will not be exact. But analogously to (4.58), the renormalizations of symmetry predictions may sometimes be calculable. Possible examples are quark and lepton masses.[71,72] The simplest SU(5) representation of Higgs fields which can provide fermion masses is 5 dimensional, and it reduces to the usual $I=\frac{1}{2}$ doublet of Weinberg-Salam. The multiplet assignments (4.59) imply that in the symmetry limit

$$m_d=m_e;\qquad m_s=m_\mu;\qquad m_b=m_\tau \tag{4.60}$$

Just as $\alpha_s(Q^2) > \alpha$ at present Q^2, so we also find that (4.60) gets renormalized to give $m_q > m_\ell$ as in Fig. 69(b). In fact one finds, using m_μ and m_τ as inputs, that[72,184]

$$m_s \sim 0.5\ \text{GeV},\qquad m_b \sim (5 \text{ to } 5\tfrac{1}{2})\ \text{GeV} \tag{4.61}$$

where these masses are to be interpreted as approximately the masses of the lightest strange or bottom pseudoscalars respectively. (It is not possible to calculate m_d very reliably, but it does seem to be too small by comparison with the usual current algebra estimates of m_d/m_s.) The predictions (4.58) and (4.61) of the SU(5) model are quite encouraging: it is unfortunate that in this model the masses of the charge 2/3 quarks cannot be calculated, so that there is no prediction for m_t. It should be mentioned that while the calculation of $\sin^2\theta_W$ (4.58) is insensitive to the number of quark flavours, the quark mass calculations (4.61) depend crucially[72,184] on the number of quarks, and increase substantially if there are 8 or more quarks.

In view of the failure of this simplest type of grand unified model to have totally disastrous phenomenology, it is reasonable to continue speculating and think about baryon number-violating forces.[182] There is nothing sacred about baryon number conservation: it is believed to be violated by black holes[185] and by nonperturbative weak effects.[186] Baryon number is almost always violated in grand unified models. Indeed we see from the multiplet structure (4.59) that gauge bosons changing quarks into leptons must be present in the SU(5) model.[152] When the multiplets involving charge 2/3 quarks are added to (4.59), one finds transitions of the general form $q+q \to \ell+\bar{q}$ (Fig. 70) which are described by an effective low-energy four-fermi interaction (α,β,γ are colour indices, $u_L = \frac{1}{2}(1-\gamma_5)u$, etc.):

$$2\sqrt{2}\ G_{GUM}\left[\left(\varepsilon_{\alpha\beta\gamma}\bar{u}^c_{\alpha_L}\gamma_\mu u_{\beta_L}\right)\left(\bar{e}^+\gamma^\mu\gamma_5 d_\gamma\right)+\left(\varepsilon_{\alpha\beta\gamma}\bar{u}^c_{\gamma_L}\gamma_\mu d_{\beta_L}\right)\left(-\bar{e}^+_L\gamma^\mu u_{\alpha_L}+\bar{\nu}^c_{e_R}\gamma^\mu d_{\alpha_R}\right)\right]$$

$$+\ \text{Hermitian conjugate} \tag{4.62}$$

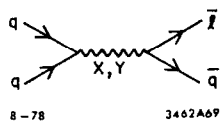

Fig. 70. A typical baryon number violating interaction.

where $m_{GUM} \approx m_{X,Y}$ the masses of the baryon-number violating vector bosons and

$$G_{GUM} \equiv \frac{g^2}{8m_X^2} \approx \frac{g^2}{8m_Y^2} \tag{4.63}$$

The interaction (4.62) can give proton decays of the form

$$p \to e^+ + \pi^o, \quad \to \bar{\nu}\pi^+ + \pi^o, \quad \to \mu^+ + \pi^o, \quad \to \ldots \tag{4.64}$$

It is easy to see from the form of the interaction (4.62, 463) that the decay rate[182] for $p \to$ anything

$$\Gamma(p \to \text{all}) \propto \frac{1}{m_{GUM}^4} \tag{4.65}$$

More detailed calculations[72] suggest that

$$\tau(\text{proton}) \sim 10^{30}\left(\frac{m_{GUM}}{10^{14}\ \text{GeV}}\right)^4 \text{ years} \tag{4.66}$$

The present lower limit on the proton lifetime is[187]

$$\tau(\text{proton}) \gtrsim 2 \times 10^{30} \text{ years} \tag{4.67}$$

Comparing this limit with the estimate (4.57) of the grand unification mass and Eq. (4.66) we see that the SU(5) model makes the proton sufficiently stable.

Clearly the estimates (4.57) and (4.66) are very uncertain, even given the speculative nature of the grand unification ideas, and the remote possibility that the specific SU(5) model has anything to do with reality. Nevertheless these results may be generic, and suggest that experiments to improve the lower bound (4.67) by a few orders of magnitude may be worthwhile. The limit (4.67) was obtained by looking at 20 tons of scintillator underground for about a year, and looking for

electrons with energies of a few hundred MeV, which might come from the decays of muons produced in proton decay. A present-day experiment cannot run for much more than a year, so an improved version would need much more matter to observe decaying. On the other hand, perhaps one could lengthen the time-base by looking in a smaller quantity of matter exposed over a geological epoch for fossil tracks of one of the types (4.64) produced in proton decay.

Regardless of the theoretical ideas discussed here, any experiment to improve the limit on the proton lifetime is of fundamental interest and importance.

Acknowledgements

I would like to thank J. D. Bjorken, D. V. Nanopoulos and particularly M. K. Gaillard for many discussions about the topics discussed in these lectures. I also thank I. Karliner for her helpful comments on the manuscript. Thanks also go to the SLAC theory group for its kind hospitality.

References

1. T. S. Kuhn, The Structure of Scientific Revolutions (University of Chicago Press, Chicago, 1970).

2. E. S. Abers and B. W. Lee, Phys. Reports 9C, 1 (1973); J. C. Taylor, Gauge Theories of Weak Interactions (Cambridge University Press, 1976); J. Iliopoulos, "An Introduction to Gauge Theories," CERN Yellow Report 76-11 (1976). For a review and references, see H. Quinn, Lectures at this Summer Institute.

3. J. D. Bjorken, Stanford Linear Accelerator Center preprints SLAC-PUB-2062 (1977), SLAC-PUB-2133, -2134 (1978).

4. H. D. Politzer, Phys. Reports 14C, 129 (1974); W. Marciano and H. Pagels, Phys. Reports 36C, 137 (1978).

5. J. D. Bjorken and E. A. Paschos, Phys. Rev. 158, 1975 (1969); S. D. Drell, D. J. Levy and T.-M. Yan, Phys. Rev. D 1, 1617 (1970); R. P. Feynman, Photon-Hadron Interactions (Benjamin, Reading, 1972).

6. For reviews and references see G. Altarelli, 1977 Gif-sur-Yvette Summer School Lectures, Rome preprint INFN-ROME-701 (1978); C. H. Llewellyn Smith, 1978 Schladming Winter School Lectures, Oxford University preprint 47/78 (1978).

7. It has long been folklore that this is a general feature of renormalizable field theories, hence the need for p_T butchery in the naive parton model, Ref. 5. For a discussion in the context of QCD, see H. D. Politzer, Phys. Lett. 70B, 430 (1977).

8. J. Ellis, M. K. Gaillard and G. G. Ross, Nucl. Phys. B111, 253 (1976); T. A. DeGrand, Y. J. Ng and S.-H. H. Tye, Phys. Rev. D 16, 3251 (1977).

9. For reviews and references see C. Quigg, Rev. Mod. Phys. 49, 297 (1977); R. F. Peierls, T. L. Trueman and L.-L. Wang, Phys. Rev. D 16, 1397 (1977); L. B. Okun and M. B. Voloshin, Nucl. Phys. B120, 459 (1977).

10. J. Ellis, M. K. Gaillard and D. V. Nanopoulos, Nucl. Phys. B106, 292 (1976); for a recent review see M. K. Gaillard, CERN preprint TH 2461, to be published in Comments on Nuclear and Particle Physics.

11. See for example, H. Georgi and S. L. Glashow, Phys. Rev. Lett. 32, 438 (1974); H. Georgi, H. R. Quinn and S. Weinberg, Phys. Rev. Lett. 33, 451 (1974).

12. S. Weinberg, Phys. Rev. Lett. 19, 1264 (1967); A. Salam, Proceedings of the 8th Nobel Symposium, ed. by N. Svartholm (Almquist and Wiksell, Stockholm, 1968), p. 367.

13. S. D. Drell, D. J. Levy and T.-M. Yan, Phys. Rev. 187, 2159 (1969) and D 1, 1617 (1970); N. Cabibbo, G. Parisi and M. Testa, Lett. al Nuovo Cim. 4, 35 (1970); J. D. Bjorken and S. J. Brodsky, Phys. Rev. D 1, 1416 (1970).

14. J. D. Bjorken, Phys. Rev. 179, 1547 (1969).

15. D. H. Perkins, Lectures at this Summer Institute. See also R. E. Taylor, Proc. 1975 Int. Symp. on Lepton and Photon Interactions at High Energies, Stanford, ed. by W. T. Kirk (Stanford Linear Accelerator Center, Stanford, 1975); Y. Watanabe et al., Phys. Rev. Lett. 35, 898, 901 (1975); H. L. Anderson et al., Phys. Rev. Lett. 37, 4 (1976) and 38, 1450 (1977).

16. S. D. Drell and T.-M. Yan, Phys. Rev. Lett. 25, 316 (1970).

17. D. H. Perkins, Proc. 16th Int. Conf. on High Energy Physics, Chicago -Batavia, 1972 (NAL, Batavia, 1972), p. 189.

18. P. C. Bosetti et al., Oxford University preprint "Analysis of Nucleon Structure Functions in CERN Bubble Chamber Neutrino Experiments" (1978).

19. T. A. DeGrand, Y. J. Ng and S.-H. H. Tye, Ref. 8; K. Koller and T. F. Walsh, Phys. Lett. 72B, 227 (1977), E 73B, 504 (1978); H. Fritzsch and K.-H. Streng, Phys. Lett. 74B, 90 (1978); K. Hagiwara, Nucl. Phys. B137, 164 (1978).

20. S. J. Brodsky, D. G. Coyne, T. A. DeGrand and R. R. Horgan, Phys. Lett. 73B, 203 (1978).

21. A. Zee, Phys. Rev. D 7, 3630 (1973); S. Coleman and D. J. Cross, Phys. Rev. Lett. 31, 851 (1973).

22. D. J. Gross and F. A. Wilczek, Phys. Rev. Lett. 30, 1343 (1973); H. D. Politzer, Phys. Rev. Lett. 30, 1346 (1973).

23. See for example A. M. Polyakov, Nucl. Phys. B121, 429 (1977); C. G. Callan, R. Dashen and D. J. Gross, Phys. Rev. D 17, 2717 (1978).

24. H. Fritzsch, M. Gell-Mann and H. Leutwyler, Phys. Lett. 47B, 365 (1972); D. J. Gross and F. Wilczek, Phys. Rev. D 8, 3633 (1973); S. Weinberg, Phys. Rev. Lett. 31, 494 (1973).

25. J.J.J. Kokkedee, The Quark Model (Benjamin, Reading, 1969).

26. S. L. Adler, Lectures on Elementary Particles and Quantum Field Theory, 1970, ed. by S. Deser, M. Grisaru and H. Pendleton (MIT Press, Cambridge, 1971). K. G. Wilson, Phys. Rev. 179, 1499 (1969).

27. Particle Data Group, Phys. Lett. 75B, 1 (1978).

28. C. Bouchiat, J. Iliopoulos and Ph. Meyer, Phys. Lett. 38B, 519 (1972); D. J. Gross and R. Jackiw, Phys. Rev. D 6, 477 (1972).

29. G. 't Hooft, Nucl. Phys. B35, 167 (1971).

30. R. Brandelik et al., Phys. Lett. 76B, 361 (1978).

31. G. Alexander et al., DESY preprint 78/30 (1978) and references therein.

32. M. L. Perl, Stanford Linear Accelerator Center preprint SLAC-PUB-2153 (1978) and references therein; J. Kirkby, Talk at this Summer Institute.

33. See for example P.G.O. Freund and S. Nandi, Phys. Rev. Lett. 32, 181 (1974).

34. S. Weinberg, Ref. 24 and Phys. Rev. D 8, 4482 (1973); D. V. Nanopoulos, Lett. al Nuovo Cim. 8, 873 (1973).

35. C. G. Callan, R. Dashen and D. J. Gross, Phys. Lett. 63B, 334 (1976); R. D. Peccei and H. R. Quinn, Phys. Rev. Lett. 38, 1440 (1977) and Phys. Rev. D 16, 1791 (1977).

36. C. G. Callan and D. J. Gross, Phys. Rev. Lett. 22, 156 (1969).

37. See for example Ref. 5, and K. G. Wilson, Ref. 26.

38. A. M. Polyakov, Soviet Phys. JETP 32, 296 (1971), 33, 850 (1971), Proceedings of the 1975 Int. Symp. on Lepton and Photon Interactions at High Energies, Stanford, ed. by W. T. Kirk (Stanford Linear Accelerator Center, Stanford, 1975), p. 855.

39. J. Kogut and L. Susskind, Phys. Rev. D 9, 697, 3391 (1974).

40. See Y. Watanabe et al. and H. L. Anderson et al., Ref. 15; also H. L. Anderson, H. S. Mathis and L. C. Myrianthopoulos, Phys. Rev. Lett. 40, 1061 (1978); and T. Quirk, private communication.

41. C. F. von Weizsäcker, Z. Phys. 88, 612 (1934); E. J. Williams, Phys. Rev. 45, 729 (1934).

42. G. Altarelli and G. Parisi, Nucl. Phys. B126, 298 (1977).

43. D. J. Gross and F. A. Wilczek, Phys. Rev. D 8, 3633 (1973) and D 9, 980 (1974); H. Georgi and H. D. Politzer, Phys. Rev. D 9, 416 (1974).

44. An alternative means of regularizing $P_{q\to q}(z)$ is to subtract from it $\delta(z-1)\int_\varepsilon^1 dy\, P_{q\to q}(y)$. The subtracted function $P_{q\to q}(z)$ has finite moments in the limit $\varepsilon\to 0$, which are identical to those obtained with the regularization (1.43).

45. These calculations are easily done in old-fashioned perturbation theory, keeping initial and final particles on mass-shell, and conserving 3-momentum but not energy.

46. D. Bailin and A. Love, Nucl. Phys. B75, 159 (1974); M. Glück and E. Reya, Phys. Rev. D 16, 3242 (1977).

47. J. Ellis, "Applications of QCD," Stanford Linear Accelerator Center preprint SLAC-PUB-2121, to appear in Current Trends in the Theory of Fields, to be published by the APS. For previous analyses showing that deep inelastic data favour QCD over other field theories, see V. Baluni and E. Eichten, Phys. Rev. Lett. 37, 1181 (1976) and Phys. Rev. D 14, 3045 (1976); and M. Glück and E. Reya, Ref. 46.

48. S. L. Adler, Phys. Rev. 143, 1144 (1965).

49. D. J. Gross and C. H. Llewellyn Smith, Nucl. Phys. B14, 337 (1969).

50. D. Robson, Nucl. Phys. B130, 328 (1977) and references therein.

51. D. K. Choudhury and L.G.F. Vanryckeghem, Phys. Rev. D 17, 1766 (1978); H. Georgi and H. D. Politzer, Nucl. Phys. B136, 445 (1978); J. F. Owens, Florida State University preprint 78-02-06 (1978).

52. G. Sterman and S. Weinberg, Phys. Rev. Lett. 39, 1436 (1977); see also J. Ellis, M. K. Gaillard and G. G. Ross, Ref. 8. For a recent commentary, see P. M. Stevenson, Imperial College, London preprint ICTP/77-78/25 (1978).

53. A. DeRújula, J. Ellis, E. G. Floratos and M. K. Gaillard, Nucl. Phys. B138, 387 (1978).

54. E. Farhi, Phys. Rev. Lett. 39, 1587 (1977); see also H. Georgi and M. Machacek, Phys. Rev. Lett. 39, 1237 (1977): Earlier variables such as sphericity[13] are not suitable for computation in perturbative QCD because they are sensitive to the infrared cutoff.

55. A more detailed analysis of this technique has been made by J. Ellis and I. Karliner, Stanford Linear Accelerator Center preprint SLAC-PUB-2191 (1978).

56. K. Shizuya and S.-H. H. Tye, Fermilab preprint Pub-78/54-THY (1978); M. B. Einhorn and B. G. Weeks, Stanford Linear Accelerator Center preprint SLAC-PUB-2164 (1978).

57. See for example E. G. Floratos, Nuovo Cim. 43A, 241 (1978); K. H. Craig and C. H. Llewellyn Smith, Phys. Lett. 72B, 349 (1978); H. Georgi and H. D. Politzer, Phys. Rev. Lett. 40, 3 (1978); G. Altarelli and M. Martinelli, Phys. Lett. 76B, 89 (1978); A. Mendez, Oxford University preprint 29/78 (1978).

58. See the talk by H. Meyer at this Summer Institute, and read between the lines.

59. M. Krammer and H. Krasemann, Phys. Lett. 73B, 58 (1978).

60. R. P. Feynman and M. Gell-Mann, Phys. Rev. 109, 193 (1958); E.G.C. Sudarshan and R. E. Marshak, Phys. Rev. 109, 1860 (1958).

61. T. D. Lee and C. N. Yang, Phys. Rev. Lett. 4, 307 (1960); B. L. Ioffe, L. B. Okun and A. Rudik, Zh. Eksperim. Teor. Fiz. 47, 1905 (1964) (Soviet Phys. JETP Lett. 20, 1281 (1965)).

62. Lower limits on $m_{W^\pm}$ of the order of 20 to 30 GeV come from deep inelastic neutrinoproduction experiments. For general gauge theory bounds on $m_{W^\pm}$, m_{Z^0} see J. D. Bjorken, Phys. Rev. D 15, 1330 (1977).

63. C. H. Llewellyn Smith, Phys. Lett. 46B, 233 (1973); J. S. Bell, Nucl. Phys. B60, 427 (1973); J. M. Cornwall, D. N. Levin and G. Tiktopoulos, Phys. Rev. Lett. 30, 1268 (1973) and Phys. Rev. D 10, 1145 (1974).

64. C. N. Yang and R. Mills, Phys. Rev. 96, 191 (1954).

65. P. Higgs, Phys. Lett. 12, 132 (1964); T. Kibble, Phys. Rev. Lett. 13, 585 (1964).

66. See the lectures by S. Wojcicki at this Summer Institute.

67. S. Herb et al., Phys. Rev. Lett. 39, 252 (1977); W. R. Innes et al., Phys. Rev. Lett. 39, 1240 (1977); J. K. Yoh et al., Fermilab preprint Pub-78/52-EXP (1978).

68. C. H. Berger et al., Phys. Lett. 76B, 243 (1978); C. W. Darden et al., Phys. Lett. 76B, 246 (1978).

69. J. Ellis, M. K. Gaillard, D. V. Nanopoulos and S. Rudaz, Nucl. Phys. B131, 285 (1977).

70. C. E. Carlson and R. Suaya, Phys. Rev. Lett. 39, 908 (1977); T. Hagiwara, Y. Kazama and E. Takasugi, Phys. Rev. Lett. 40, 76 (1978); D. B. Lichtenberg, J. G. Wills and J. T. Kiehl, Phys. Rev. Lett. 39, 1592 (1977); S. S. Gershtein et al., Serpukhov preprint IFVE 77-11 (1977).

71. M. S. Chanowitz, J. Ellis and M. K. Gaillard, Nucl. Phys. B128, 506 (1977).

72. A. J. Buras, J. Ellis, M. K. Gaillard and D. V. Nanopoulos, Nucl. Phys. B135, 66 (1978).

73. Some physicists have expressed unease about this nomenclature. Similar unease was once felt by the Board of Supervisors of San Francisco, who forbade the display of advertisements containing certain dubious words. This led to the bowdlerization of some signs, so that the North Beach area had a proliferation of "ottomless" bars. Perhaps we should refer to the b and t as the "ottom" and "op" quarks respectively. The San Francisco ordinance has now fallen into disuse.

74. M. Holder et al., Phys. Lett. 69B, 377 (1977). See also the lectures by M. Holder and D. Perkins at this Summer Institute.

75. R. M. Barnett, talk at this Summer Institute. See also L. F. Abbott and R. M. Barnett, Phys. Rev. Lett. 40, 1303 (1978).

76. M. Holder et al., Phys. Rev. Lett. 39, 433 (1977).

77. C. Prescott et al., Stanford Linear Accelerator Center preprint SLAC-PUB-2148 (1978).

78. L. M. Sehgal, Aachen preprint PITHA-102 (1978); see also L. F. Abbott and R. M. Barnett, Ref. 75.

79. For $\Delta S=1$ neutral currents and $\Delta S=2$ K^o-$\bar{K}^o$ mixing, see Ref. 27. For $\Delta C=2$ transitions, see G. J. Feldman, 1977 SLAC Summer Institute lectures.

80. S. L. Glashow, J. Iliopoulos and L. Maiani, Phys. Rev. D 2, 1285 (1970).

81. Y. Hara, Phys. Rev. 134, B701 (1964); Z. Maki and Y. Ohnuki, Progr. Theor. Phys. 32, 144 (1964); D. Amati, H. Bacry, J. Nuyts and J. Prentki, Phys. Lett. 11, 190 (1964) and Nuovo Cim. 34, 1732 (1964); B. J. Bjørken and S. L. Glashow, Phys. Lett. 11, 255 (1964).

82. See the talk by N. Fortson at this Summer Institute.

83. This point of view is not universal. In particular, J. D. Bjorken stresses that the observable effects of "anomalies" at present energies are negligible. The issue is rather one of principle.

84. S. L. Glashow and S. Weinberg, Phys. Rev. D 15, 1958 (1977); E. A. Paschos, Phys. Rev. D 15, 1966 (1977); M. S. Chanowitz et al., Ref. 71.

85. M. K. Gaillard and B. W. Lee, Phys. Rev. D 10, 897 (1974).

86. J. Rich and D. R. Winn, Phys. Rev. D 14, 1283 (1976). A promising related process: $e^+e^- \to \gamma\nu\bar{\nu}$ is discussed by E. Ma and J. Okada, Phys. Rev. Lett. 41, 287 (1978).

87. For reviews see D. N. Schramm, AIP Conf. Proceedings, APS Div. of Particles and Fields (1978), and Fermi Institute preprint 78-25 (1978).

88. S. Weinberg, Gravitation and Cosmology (J. Wiley and Sons, New York, 1972).

89. B. W. Lee and S. Weinberg, Phys. Rev. Lett. 39, 165 (1977); J. E. Gunn, B. W. Lee, I. Lerche, D. N. Schramm and G. Steigman, Astrophysical Journal, in press (1978).

90. B. W. Lee and S. Weinberg, Phys. Rev. Lett. 38, 1237 (1977).

91. M. Veltman, Nucl. Phys. B123, 39 (1977).

92. M. S. Chanowitz, M. Furman and I. Hinchliffe, Lawrence Berkeley Laboratory preprint LBL-7903 (1978).

93. L. Camilleri et al., CERN Yellow Report 76-18 (1976); particularly section 2.

94. M. L. Perl et al., Phys. Rev. Lett. 35, 1489 (1975).

95. Y. S. Tsai, Stanford Linear Accelerator Center preprint SLAC-PUB-2105 (1978).

96. J.A.M. Vermaseren, Purdue University preprint "Signals for Very Heavy Leptons in e^+e^- Annihilation" (1978).

97. Notice however that the eD parity violation data of Ref. 77 almost exclude an $\begin{pmatrix} E^o \\ e^- \end{pmatrix}_R$ doublet: no direct evidence against $\begin{pmatrix} M^o \\ \mu^- \end{pmatrix}_R$ or $\begin{pmatrix} T^o \\ \tau^- \end{pmatrix}_R$ doublets is yet available. The direct channel production mechanism (2.30) could also be used to produce M^o or T^o pairs. Their decay modes would be similar to those of an E^o, with e^- replaced by μ^- or τ^-.

98. J. L. Rosner, Nucl. Phys. B126, 124 (1977).

99. F. Bletzacker and H. T. Nieh, Phys. Rev. D 16, 2115 (1977).

100. B. W. Lee, S. Pakvasa, R. E. Shrock and H. Sugawara, Phys. Rev. Lett. 38, 937 (1977), 38, 1230 (E) (1977).

101. CHEEP--An ep Facility in the SPS, ed. by J. Ellis, B. H. Wiik and K. Hübner, CERN Yellow Report 78-02 (1978).

102. M. Kobayashi and K. Maskawa, Progr. Theor. Phys. 49, 652 (1973).

103. S. Weinberg, Phys. Rev. Lett. 37, 657 (1976).

104. J. Ellis, M. K. Gaillard and D. V. Nanopoulos, Nucl. Phys. B109, 213 (1976). Though calculated using a free quark model, the formula (2.46) is probably not grossly altered by QCD corrections.

105. L. Ryder, Phys. Reports 34C, 55 (1977).

106. A. Sirlin, Nucl. Phys. B71, 29 (1974) and B100, 291 (1974); W. Angerson, Nucl. Phys. B69, 493 (1974). The analysis in these lectures (see also Ref. 104) may underestimate the uncertainties due to nuclear physics effects, strong interaction effects in (2.42) and so on. However, comparable limits on $S_{\frac{1}{2}}^2$ and $S_{\frac{1}{3}}^2$ come from the negative results of searches for heavy quarks in neutrinoproduction--see the talk of M. Holder at this Summer Institute.

107. J. Ellis, M. K. Gaillard and D. V. Nanopoulos, Nucl. Phys. B100, 313 (1975).

108. R. N. Cahn, Phys. Rev. Lett. 40, 80 (1978); R. N. Mohapatra and D. P. Sidhu, Phys. Rev. D 17, 1876 (1978); and B. W. Lee and S. Weinberg, Ref. 90.

109. D. Cutts et al., Phys. Rev. Lett. 41, 363 (1978); R. Vidal et al., Fermilab preprint "A Search for New Massive Particles" (1978); S. Wolfram, Oxford University preprint "Abundances of Stable Particles Produced in the Early Universe" (1978) argues that the standard "big bang" cosmology would generate more stable fermions of mass $\leq$16 GeV than are allowed by observation.

110. J. Jaros, private communication. I thank M. Perl for interesting discussions about this idea.

111. R. M. Barnett, Phys. Rev. Lett. 36, 1163 (1976).

112. M. Holder et al., Phys. Lett. 77B, 114 (1978) and CERN preprint "Characteristics of Trimuon Events Observed in High Energy Neutrino Interactions" (1978); see also the talk by M. Holder at this Summer Insitute.

113. M. Holder et al., Phys. Lett. 73B, 105 (1978); R. J. Loveless et al., University of Wisconsin preprint COO-088-29 (1978).

114. An approach to this problem which combines finite mass effects and the Altarelli-Parisi formalism[42] is being developed by R. C. Brower, A. J. Buras, D. Duke and J. Ellis.

115. The results of this were kindly provided by T. Schalk and A. Seiden.

116. M. K. Gaillard, talk presented at this Summer Institute.

117. A. Ali, CERN preprint TH 2411 (1977).

118. S. Pakvasa and H. Sugawara, Phys. Rev. D 14, 305 (1976); L. Maiani, Phys. Lett. 62B, 183 (1976); C. Quigg and J. L. Rosner, Lawrence Berkeley Laboratory preprint LBL-7961 (1978).

119. For a recent discussion of the theoretical value of this quantity in the KM model see J. Ellis and M. K. Gaillard, Fermilab preprint 78/66-THY (1978). Previous calculations--Refs. 104, 118 and E. P. Shabalin, ITEP preprint ITEP-31 (1978) neglected perturbative strong interaction effects and got results which were too low. Ellis and Gaillard also estimate the nonperturbative strong interaction contribution to the neutron electric dipole moment coming from renormalization of the strong interaction θ vacuum parameter by weak interactions in the KM[102] model. They find the nonperturbative contribution to be smaller than the perturbative contribution.

120. For a discussion of different models, see A. Ali and Z. Z. Aydin, DESY preprint 78/11 (1978).

121. B. L. Ioffe and V. A. Khoze, Leningrad preprint LINP-274 (1976).

122. J. D. Bjorken, 1976 SLAC Summer Institute Lectures, Stanford Linear Accelerator Center report SLAC-198 (1976) or preprint SLAC-PUB-1866 (1977).

123. F. Halzen and D. M. Scott, University of Wisconsin preprint COO-881-41 (1978).

124. C. H. Llewellyn Smith and B. H. Wiik, DESY preprint 77/38 (1977).

125. O. P. Sushkov, V. V. Flambaum and I. B. Khriplovich, Sov. J. Nucl. Phys. 20, 537 (1975); W. Alles, Ch. Boyer and A. J. Buras, Nucl. Phys. B119, 125 (1977).

126. F. Bletzacker and H. T. Nieh, Nucl. Phys. B124, 511 (1977).

127. D. A. Ross and M. Veltman, Phys. Rev. B95, 135 (1975).

128. J. D. Bjorken, Phys. Rev. D 15, 1330 (1977).

129. I. Hinchliffe and C. H. Llewellyn Smith, Nucl. Phys. B128, 93 (1977); J. Kogut and J. Shigemitsu, Nucl. Phys. B129, 461 (1977).

130. J. D. Bjorken, Proc. of the 1977 Int. Symp. on Lepton and Photon Interactions at High Energies, Hamburg, 1977, ed. by F. Gutbrod (DESY, Hamburg, 1977), p. 960.

131. J. K. Yoh et al., Ref. 67.

132. Yu. L. Dokshitser, D. I. D'yakonov and S. I. Troyan, "Inelastic Processes in Quantum Chromodynamics," Materials of the 13th Winter School of the Leningrad B. P. Konstantinov Institute of Nuclear Physics, Leningrad, 1978, p. 1: available in translation as SLAC TRANS-183 (1978); R. K. Ellis, H. Georgi, M. Machacek, H. D. Politzer and G. G. Ross, MIT preprint CTP-718 (1978); A. H. Mueller, Columbia University preprint CU-TP-125 (1978).

133. G. Altarelli, R. K. Ellis and G. Martinelli, MIT preprint CTP-723 (1978).

134. H. Georgi, Harvard University preprint HUTP 77/A090 (1977).

135. See C. H. Llewellyn Smith, Ref. 6, and references 123, 132 and 134.

136. J. Thaler emphasized this point to me.

137. This oft-used conjecture--see for example B. Combridge, J. Kripfganz and J. Ranft, Phys. Lett. 70B, 234 (1977); R. Cutler and D. Sivers, Phys. Rev. D 17, 196 (1978); R. D. Field, Phys. Rev. Lett. 40, 997 (1978)--has recently been justified in QCD. See C. T. Sachrajda, Phys. Lett. 76B, 100 (1978). W. Furmanski, Jagiellonian University, Kraków preprints 10, 11, 12/78 (1978).

138. R. W. Brown and K. O. Mikaelian, Fermilab preprint Pub-78/49-THY (1978).

139. Radiative corrections reduce this rate by a factor of O(2)--J. D. Bjorken (private communication). A complete programme of calculating weak radiative corrections to e^+e^- processes at these high energies is being undertaken by M. Veltman.

140. M. Veltman, Acta Physica Polonica B8, 475 (1977).

141. P. Darriulat and M. K. Gaillard, LEP physics note "Comments on the Feasibility of Studying the $Z^oW^+W^-$ Vertex in High Energy e^+e^- Collisions" (1978).

142. R. D. Peccei and H. R. Quinn, Ref. 35.

143. S. Weinberg, Phys. Rev. Lett. 40, 223 (1978); F. Wilczek, Phys. Rev. Lett. 40, 279 (1978).

144. J. Ellis and M. K. Gaillard, Phys. Lett. 74B, 374 (1978).

145. E. Bellotti, E. Fiorini and L. Zanotti, Phys. Lett. 76B, 223 (1978).

146. T. W. Donnelly, S. J. Freedman, R. S. Lytel, R. D. Peccei and M. Schwartz, Stanford University preprint ITP-598 (1978).

147. G. 't Hooft, Nucl. Phys. B79, 276 (1974); A. M. Polyakov, Zh. Eksp. Teor. Fiz. Pis'ma 20, 430 (1974) (JETP Lett. 20, 194 (1974)).

148. J. Richet, private communication from M. J. Perry (1978).

149. H. Georgi and S. L. Glashow, Phys. Rev. Lett. 28, 1494 (1972).

150. Y. Nambu, Nucl. Phys. B130, 505 (1977).

151. M. B. Einhorn and R. S. Savit, University of Michigan preprint UM HE 78-18 (1978).

152. H. Georgi and S. L. Glashow, Ref. 11.

153. For an alternative approach to grand unified gauge theories, see J. C. Pati and A. Salam, Phys. Rev. D 8, 1240 (1973) and Phys. Rev. D 10, 275 (1974).

154. S. Coleman and E. Weinberg, Phys. Rev. D 7, 1888 (1973).

155. S. Weinberg, Phys. Rev. Lett. 36, 294 (1976); A. D. Linde, Zh. Eksp. Teor. Fiz. Pis'ma Red 23, 73 (1976) (JETP Lett. 23, 64 (1976)).

156. P. H. Frampton, Phys. Rev. Lett. 37, 1378 (1976).

157 A. D. Linde, Phys. Lett. 70B, 306 (1977).

158. E. Gildener and S. Weinberg, Phys. Rev. D 13, 3333 (1976) and references therein.

159. C. E. Vayonakis, Lett. al Nuovo Cim. 17, 383 (1976) and Athens University preprint "New Threshold of Weak Interactions" (1978).

160. B. W. Lee, C. Quigg and H. B. Thacker, Phys. Rev. Lett. 38, 883 (1977) and Phys. Rev. D 16, 1519 (1977). See also D. A. Dicus and V. S. Mathur, Phys. Rev. D 7, 3111 (1973).

161. F. Wilczek, Phys. Rev. Lett. 39, 1304 (1977).

162. P. H. Frampton and W. W. Wada, Ohio State University preprint COO-1595-235 (1978).

163. This process was discussed in Ref. 10 and a cross section given for $e^+e^- \to Z^oH$ for light Higgs close to threshold: see also Refs. 121, 122. The exact formula (4.31) is given by B. W. Lee, C. Quigg and H. B. Thacker, Ref. 160. See also Ref. 164. A related process is discussed by K.J.F. Gaemers and G. J. Gounaris, CERN preprint TH 2502 (1978).

164. S. L. Glashow, D. V. Nanopoulos and A. Yildiz, Harvard University preprint HUTP-78/A012 (1978).

165. H. M. Georgi, S. L. Glashow, M. E. Machacek and D. V. Nanopoulos, Phys. Rev. Lett. 40, 692 (1978).

166. W. W. Wada, private communication (1978).

167. C. Rubbia, CERN $\bar{p}p$ physics note and private communication (1977).

168. J. Lo Secco, Phys. Rev. D 14, 1352 (1976).

169. J. E. Kim and G Segré, Phys. Lett. B to be published; Y. Tomozawa, University of Michigan preprint UM 77-22 (1977); J. Grifols, Stanford Linear Accelerator Center preprint SLAC-PUB-2108 (1978); L. N. Chang and J. E. Kim, University of Pennsylvania preprint UPR-0097-T (1978); J. F. Donoghue and L.-F. Li, Carnegie-Mellon preprint COO-3066-113 (1978).

170. E. Golowich and T. C. Yang, University of Massachusetts preprint "Charged Higgs Bosons and Decays of Heavy Flavoured Mesons" (1978).

171. This process was suggested to me by R. N. Cahn during the Summer Institute.

172. See Ref. 35, J. Ellis and M. K. Gaillard, Ref. 119, and Ref. 144.

173. V. Baluni, MIT preprint CTP-726 (1978).

174. A. Zepeda, Phys. Rev. Lett. 41, 139 (1978); P. Langacker and H. Pagels, Princeton preprint "Light Quark Mass Spectrum in Quantum Chromodynamics" (1978).

175. H. Faissner et al., Phys. Lett. 60B, 401 (1976). See also A. F. Rothenberg, Stanford Linear Accelerator Center report SLAC-147 (1972) and Ref. 146.

176. P. Alibran et al., Phys. Lett. 74B, 134 (1978); T. Hansl et al., Phys. Lett. 74B, 139 (1978); P. C. Bosetti et al., Phys. Lett. 74B, 143 (1978).

177. D. A. Dicus, E. W. Kolb, V. L. Teplitz and R. V. Wagoner, University of Texas preprint ORD-3992-337 (1978).

178. For $K^+ \to \pi^+ + a$ see also T. Goldman and C. M. Hoffman, Phys. Rev. Lett. 40, 220 (1978).

179. See for example T. C. Yang, Phys. Rev. Lett. 41, 523 (1978); H. R. Quinn, private communication (1978); P. Ramond and G. G. Ross, Caltech preprint CALT-68-674 (1978).

180. J. Ellis and M. K. Gaillard, Ref. 119. This analysis supersedes that of Ref. 144. For related remarks see S. Weinberg, unpublished note (1978).

181. H. Georgi, Harvard University preprint 78/A010 (1978); M.A.B. Bég and H.-S. Tsao, Phys. Rev. Lett. 41, 278 (1978).

182. H. Georgi, H. R. Quinn and S. Weinberg, Ref. 71: see also Ref. 71.

183. D. A. Ross, CERN preprint TH 2469 (1978).

184. D.V. Nanopoulos and D. A. Ross, CERN preprint in preparation. For a recent review see D. V. Nanopoulos, CERN preprint TH 2534 (1978).

185. M. J. Perry, Talk at the Ben Lee Memorial Conference (1977).

186. G. 't Hooft, Phys. Rev. Lett. 37, 8 (1976).

187. F. Reines and M. F. Crouch, Phys. Rev. Lett. 32, 493 (1974).

ADDENDA AND CORRIGENDA

There are the following errors in formulae in the text:

Equations (3.7):	230 MeV	→	260 MeV
(3.8):	900 N_D MeV	→	1000 N_D MeV
(3.9):	2.7 GeV	→	3 GeV
(3.17):	32 MeV	→	90 MeV
(3.19):	900 N_D MeV	→	1000 N_D MeV
(3.20):	2.7 GeV	→	3 GeV
(3.56):	7%	→	14%
	14%	→	28%

I have so far found one misprint:

p. 83: Barras should read Buras

Some useful additional references:

Add to 72: More recent estimates of the baryon lifetime in SU(5) are lower than those in this paper by a factor O(10): C. Jarlskog and F. J. Yndurain, CERN preprint TH 2556 (1978).

Add to 86: For a critique of this suggestion and an extension to higher centre-of-mass energies, see K.J.F. Gaemers, R. Gastmans and F. Renard, ECFA/LEP note 45 (1978) and for a general discussion of neutrino counting see J. Ellis, M. K. Gaillard and C. H. Llewellyn Smith, ECFA/LEP note in preparation (1978).

Add to 125: For the inclusion of effects due to beam and $W^{\pm}$ polarization, and an investigation of non gauge theory vertices, see K.J.F. Gaemers and G. J. Gounaris, CERN preprint TH 2548 (1978).

GAUGE THEORIES OF THE WEAK INTERACTIONS*

H. Quinn

Stanford Linear Accelerator Center
Stanford University, Stanford, California 94305

Lecture I

Nowadays it seems almost unnecessary to motivate a discussion of gauge theories of the weak interactions--they are fast becoming the accepted dogma. Furthermore one particular version, the Weinberg-Salam version,[1] or (more specifically in the context of charm) the Weinberg-Salam-Glashow-Iliopoulos-Maiani[2] version seems to be able to explain most of the relevant data, though some areas are still unclear, especially the question of parity violation in atomic physics. My lectures will focus on this model. I will try to leave you with some feeling for how it is put together, which along the way will allow comment on some possible variations, many of which exist in the literature.

In spite of my first disclaimer let me begin with a short discussion of the improvement afforded by gauge theories over their predecessor, the four fermi theory of weak interactions. That theory was successful in describing the phenomenology of low energy weak interactions (such as angular and energy distributions of product particles in β-decay) but was not completely satisfactory for two (closely related) reasons: At sufficiently high energy ($\sim$ 300 GeV) the predictions violate unitarity, and any attempt to perform higher order calculations is plagued by infinities which cannot be removed by renormalization. We needed a theory which could remove these two problems without changing

*Work supported by the Department of Energy.

the low energy predictions--gauge theories provide such a theory. In addition, each gauge model one writes down makes a host of new and testable predictions. Weinberg in 1967 wrote down "a theory of leptons" as a first simple example of such a theory. This model, extended to incorporate hadronic weak interactions by inserting the quarks by analogy to the leptons, gives a remarkably successful phenomenology.

When Weinberg wrote his model he hoped it would solve the above mentioned problems of renormalizability and unitarity--that it did indeed do so was shown somewhat later.[3] In a four-fermi or current-current theory we start with a weak charge-changing current, empirically determined to be of the V-A type, for example for leptons

$$j_\alpha = \bar{\mu}\gamma_\alpha \frac{(1-\gamma_5)}{2}\nu_\mu + \bar{e}\gamma_\alpha \frac{(1-\gamma_5)}{2}\nu_e \qquad (I.1)$$

(I shall use Bjorken and Drell conventions throughout, and notice that V-A = $1-\gamma_5$ with my definitions. Also I will often write particle names to stand for the Dirac spinor for that particle.) The weak interaction amplitude is then

$$\frac{4G}{\sqrt{2}} j_\alpha j^{\alpha\dagger} \qquad (I.2)$$

(The factor of 4 may look strange, it compensates for the fact that I have written j_μ with $(1-\gamma_5)/2$ rather than the old-fashioned $(1-\gamma_5)$. This definition will be convenient to maintain when we get to gauge theories since $(1-\gamma_5)/2$ is the correct projection operator for left-handed fermions, in fact one usually sees the shorthand μ_L for $((1-\gamma_5)/2)\mu$ in gauge theory papers.)

The interaction (I.2) can be represented diagramatically, for example, the process shown in Fig. 1 is part of the cross term between the electron and muon pieces of the current. The idea of introducing an intermediate vector boson to try to damp the high energy growth of this amplitude predates its gauge theory realization by some time. Naively one might hope the diagram of Fig. 2 for which the amplitude is given by

$$A = g^2 j_\alpha D^{\alpha\beta} j_\beta^\dagger \qquad (I.3)$$

would give a suppression of $m_W^2/(s-m_W^2)$ for large s when g^2/m_W^2 is adjusted to give the correct low energy strength. Clearly this requires m_W^2 to be large enough that at present energies the propagator is effectively a constant, in order to maintain the good results of the current-current theory. That is easily enough achieved, however in this simple form the idea does not work for all possible processes. In this process $e^-\bar{\nu}_e \to \mu^-\bar{\nu}_\mu$ it provides the necessary suppression, but when looking at other processes, for example, $e^+e^- \to W^+W^-$ and even $e^+e^- \to W^+W^-\gamma$ one finds again problems with unitarity. The problem is that the propagator for a massive vector particle has the form

$$D_{\alpha\beta}(q) = -i\left(g_{\alpha\beta} - \frac{q_\alpha q_\beta}{m^2}\right)/(q^2-m^2) \qquad (I.4)$$

The term proportional to $g_{\alpha\beta}$ has indeed the desired behavior in all cases but the $q_\alpha q_\beta/m^2$ term in some processes can give terms of order q^2/m^2 which cancel out any large q^2 suppression from the denominator.

After gauge theories had been found to be a workable way to circumvent this problem several people asked the question "Are they the only way?" in the following form: Suppose I start with the vectors and

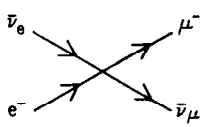

Fig. 1. Typical process in four-fermi theory.

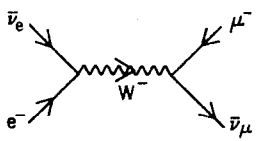

Fig. 2. Introduction of an intermediate vector boson to modify the amplitude shown in Fig. 1.

quarks coupled as in the process (I.3) and allow in addition neutral vector and scalar particles in the theory with arbitrary masses and coupling constants. Now I require tree graph unitarity,[4] this is that the partial wave amplitudes generated by the sum of tree graph diagrams for a given process should not grow more rapidly than s^{2-m} for $2 \to m$ particle processes. Imposing this condition on a sufficiently large set of amplitudes gives relationships among the masses and coupling constants (Yukawa couplings and vector-scalar couplings as well as vector-vector couplings). In every case the set of couplings so determined are a set which one could derive by building a gauge theory with the same particle content!

Having come so far, let me now explain how to build a gauge theory. The recipe is simple[5]

I. Choose a gauge group.

II Choose fermion representation content.

III. Choose Higgs scalar representation content.

IV. Arrange for spontaneous symmetry breaking to give a non-vanishing vacuum expectation value for some scalar or set of scalars.

Of course all this needs some further explanation to be meaningful—and some cleverness in following the steps to arrive at a possible theory of the weak and electromagnetic interactions--there are many theories I could write following steps I to IV which would not be viable for this purpose--for example it is trivial to arrange that only one massless vector survives after the spontaneous symmetry breaking but it is somewhat more complicated to arrange that that vector has the correct couplings to be a photon.

Let us start with step I. What do I do when I choose a gauge group. In a gauge theory the vector mesons are always in the adjoint representation of the group, so choosing a group tells me how many vector mesons I have, and defines the way they couple to one another. In less group theoretic language "in the adjoint representation" means there is one vector meson for each independent structure matrix λ^α. In SU(2) the structure matrices are the set of traceless unitary 2 × 2 matrices, the familiar Pauli σ-matrices, of which there are three ((2×2)-1) so SU(2) means three vectors. A product of groups such as SU(2) × U(1) has as many vectors as needed for each factor group separately so SU(2) × U(1) has four vectors, SU(3) has eight ((3×3)-1), etc.

In deriving vector couplings it is convenient to define the matrix

$$A_\mu = A_\mu^\alpha \lambda^\alpha \quad . \tag{I.5}$$

Since every term in the Hamiltonian (or Lagrangian) must be a scalar (singlet) under the gauge group we can readily construct possible terms from the objects (I.5) by taking traces, for example

$$TR\ (A_\mu A_\nu A_e) = if^{\alpha\beta\gamma}\ A_\mu^\alpha A_\nu^\beta A_e^\gamma \tag{I.6}$$

is a group singlet three-vector term. The structure function $f^{\alpha\beta\gamma}$ is defined by

$$\left[\lambda^\alpha, \alpha^\beta\right] = if^{\alpha\beta\gamma}\ \lambda^\gamma \quad . \tag{I.7}$$

Of course the Lorentz indices in (I.6) must also be contracted in some way to give it the correct Lorentz invariance properties.

Now we come to step II, choosing the representation content of the fermions. Let us discuss this and subsequent steps in the context of SU(2) × U(1) in order to give concrete examples. Choosing representation content simply means choosing which multiplets of fermions we are to introduce. The Weinberg SU(2) is often called weak isospin, a priori we may choose fermions as weak isospin singlets, doublets, triplets, etc. In doing this one treats the left- and right-handed components of the fermions completely separately. The choice we make is guided by experiment. Let us start by examing Weinberg's choices for the leptons. He chose left-handed doublets

$$\begin{pmatrix}\nu_e\\ e\end{pmatrix}_L \quad \begin{pmatrix}\nu_\mu\\ \mu\end{pmatrix}_L \tag{I.8}$$

and right-handed singlets e_R, μ_R and the standard Weinberg-Salam model extends this choice to quarks

$$\begin{pmatrix}u\\ d_c\end{pmatrix}_L \quad \begin{pmatrix}c\\ s_c\end{pmatrix}_L \cdots \quad u_R,\ d_R,\ s_R,\ c_R \cdots \tag{I.9}$$

where

$$d_c = d\cos\theta_c + s\sin\theta_c \quad \text{and} \quad s_c = -d\sin\theta_c + s\cos\theta_c$$

Why these choices? For the leptons they are clearly the simplest possible choice, which allows us to couple to the SU(2) vectors, to left-handed fermions. Using the group singlet quantity

$$\left(\nu_e e\right)_L^\dagger \gamma_0\gamma^\mu \left(A_\mu^\alpha \cdot \sigma^\alpha\right)\begin{pmatrix}\nu_e\\ e\end{pmatrix}_L \tag{I.10}$$

while the U(1) vector can couple to both left- and right-handed fermions

$$\left(\nu_e e\right)_L^\dagger \gamma_0\gamma^\mu\ B_\mu \cdot I \begin{pmatrix}\nu_e\\ e\end{pmatrix}_L \quad \text{and} \quad e_R^\dagger \gamma_0\gamma^\mu\ B_\mu e_R \tag{I.11}$$

All I am doing here is constructing group singlet objects of the form

$$\sum_{a,b} \bar{\psi}_a \gamma^\mu \left(A_\mu^\alpha, M^\alpha\right)_{ab} \psi_b$$

Clearly if my fermions are in triplets the matrices M_{ab} must be the 3×3 representations of SU(2) and so on.

It is immediately clear from (I.10) why Weinberg did not stop at SU(2). If we write out this expression we have

$$\frac{g}{\sqrt{2}} \left(A_\mu^+ \bar{\nu}_L \gamma^\mu e_L + A_\mu^- \bar{e}_L \gamma^\mu \nu_L\right)$$

$$+ \frac{g}{2} A_\mu^o \left(\bar{\nu}_L \gamma_\mu \nu_L - \bar{e}_L \gamma_\mu e_L\right) \qquad \text{(I.12)}$$

The charge-carrying vectors A^+ and A^- have been constructed to couple to the correct weak currents of (I.4), but the neutral particle is not a good photon candidate, it couples to the electron with a V-A coupling, and it also couples to the neutrino. Weinberg added the U(1) factor, thus introducing an additional neutral vector B. Now by astutely choosing the relative strengths of the left- and right-handed couplings of the B it can be arranged that there is a linear combination of A^o and B which has pure vector coupling to the electron and which does not couple to the neutrino--thus this linear combination is a candidate photon. However there is then inevitably another (orthogonal) linear combination of A^o and B, call it the Z, which couples with some well defined set of couplings, a mixture of vector and axial, to both neutrinos and electrons. It is only a matter of algebra to find it out. I recommend that you should carry through this exercise, starting from (I.10) and (I.11). Defining g as the coupling of the SU(2) vectors to the fermion doublet and g'/2 for the B-coupling to the left-handed doublet coupling one finds the relationship

$$e = gg'/(g^2 + g'^2)^{1/2} \qquad \text{(I.13)}$$

One free parameter is left, it is usually written as

$$\sin \theta_W = g'/(g^2 + g'^2)^{1/2} \qquad \text{(I.14)}$$

Now to the quarks, or even the muon; what determines that I should make the same assignments for them, especially for the right-handed parts, since clearly I have enough right-handed quarks to put some or all of them in nontrivial multiplets too. The answer is phenomenology; the following points are important:

(i) Cabibbo universality

The relationship between μ-decay and β-decay is most readily achieved by the choice (I.9). For example if I put the u and d quarks as neighboring members of a triplet then their coupling to the W^+ would have a factor of $\sqrt{2}$ relative to the muon and electron couplings (simply a Clebsch Gordon coefficient which is different for different isotopic spin assignments.)

(ii) The u and d couplings are left-handed, at least at present energies. Thus if u_R or d_R are members of nontrivial multiplets of the SU(2) they must be in different multiplets, paired with heavier quarks. As we will see later presently existing data from ν-scattering does not allow a doublet right-handed assignments for u and d with quarks of mass less than about 5 GeV.

(iii) The repetition of the $(u,d_c)_L$ by the $(c,s_c)_L$ is a manifestation of the Glashow-Iliopoulous-Maiani mechanism to avoid strangeness changing neutral currents. That must be such an old story around here

these days that it scarcely needs to be mentioned. What may not be so well known is that naive generalizations to further flavors such as $(t,b)_L$, t_R, b_R avoids all flavor changing neutral currents--the rule is that I must assign all left-handed quarks of the same charge to the same multiplet (position and type) and similarly for the right-handed quarks to avoid the generation of flavor changing neutral currents.[6] So far we have little experimental evidence on the subject, but the theoretical literature is heavily biased in this direction.

I am trying to make clear the ad hoc nature of the construction. Within the basic recipe many variations are possible, even once I complete step I there are many choices at step II, etc. The beauty of the game is that each choice gives many predictions. The history of the field is a tribute to the experimentalists, who seem to be able to eliminate models almost as fast as the theorists can cook them up (following the recipe). Of course, the more that is known the harder the game of cooking becomes--there are more and more constraints that a model must satisfy before it is even worth discussing. More remarkable yet, the one model which seems to be doing best is the original $SU(2) \times U(1)$. There are some murky points, about which we will no doubt hear much more in the next week or so. In particular, in atomic physics parity violations and $\bar{\nu}_\mu e$ scattering experiments differ, but there is possible conflict with the models. However the model is doing well enough that I will continue to treat it here as the prime candidate theory.

Let us then proceed to steps III and IV of the recipe which introduce the Higgs sector. Why put in Higgs at all? The question can be asked at various levels of sophistication. Let me begin by proceeding naively, which in this context really means perturbatively. From the unitarity arguments given earlier, in particular one finds the scalars are needed if the W and Z are assumed to be massive. From a theorists viewpoint it is a question of writing a Lagrangian with a given non-Abelian gauge invariance, which a priori means massless vectors, and in addition a chiral invariance which means also massless fermions. Now we want a way to introduce vector and fermion masses without destroying the renormalizability of that theory. The only way to do this which gives perturbatively calculable predictions is to introduce elementary scalars which couple gauge-invariantly to the vectors and via Yukawa couplings to the fermions. The "Higgs" trick involves arranging the mass (ϕ^2) and self-interaction (ϕ^4) parameters of these scalars so that a nonvanishing vacuum expectation appears for some scalar--this is called spontaneous symmetry breaking, despite the fact that it is about as spontaneous as the appearance of a horse in a corral. (I first build the corral and herd the horses if I wish to have the effect occur.)

What does a nonvanishing vacuum expectation value for a field mean? It means that quanta of the theory, to which I can give a particle interpretation, are simply quantum fluctuations about zero of the variable

$$\rho = \phi - v \tag{I.15}$$

where $v = \langle\phi\rangle$ is the vacuum expectation value, as opposed to fluctuations of ϕ itself about zero. Hence it is convenient to change variables and rewrite the Lagrangian in terms of ρ. I can represent this process diagrammatically by writing

v = ---x

for any term v which appears. For example a Yukawa coupling term is shown in Fig. 3. Clearly

$$Y\bar{\psi}\phi\psi = Y\bar{\psi}\rho\psi + (Yv)\bar{\psi}\psi \tag{I.16}$$

and we see that a quark mass term (Yv) has appeared. Similarly the terms

$$g^2\phi^2 A_\mu^\alpha A^{\alpha\ \mu}$$

gives a gluon mass term as shown in Fig. 4 with

$$m^2 \propto g^2 v^2 \tag{I.17}$$

How do I achieve a nonvanishing vacuum expectation value? Everyone by now must have seen the picture many times. I want a potential $V(\phi)$ which has the form shown in Fig. 5. Since we are talking about breaking a continuous symmetry, the phase symmetry of $\phi \to e^{i\theta}\phi$, the picture is three-dimensional--the Mexican hat potential. In a scalar field theory

$$V(\phi) = \mu^2\phi^2 + \lambda\phi^4 \tag{I.18}$$

where μ and λ are the parameters appearing in the Lagrangian. Obviously, negative values of μ^2 give the desired shape. Notice that although μ^2 looks like a mass parameter when we change variables there are additional scalar mass terms proportional to λv^2, so that there is no problem of negative $(\text{mass})^2$ for physical scalar particles.

Before I get too far from this picture let me comment on another obvious feature of it. The choice of the direction of vacuum expectation value in the (ϕ_{Re}, ϕ_{Im}) space is arbitrary, no phase is preferred. This means that for any value I choose there is one mode of oscillation about that value which has zero frequency, it is along the minimum of the potential. This is the Goldstone phenomenon which happens whenever

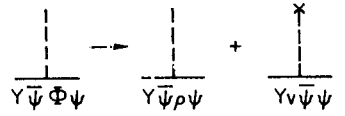

Fig. 3. Diagramatic representation of the change of variables $\Phi = \rho+v$.

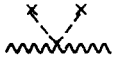

8-78 3454A2

Fig. 4. Effective gluon mass term generated by vacuum expectation value v.

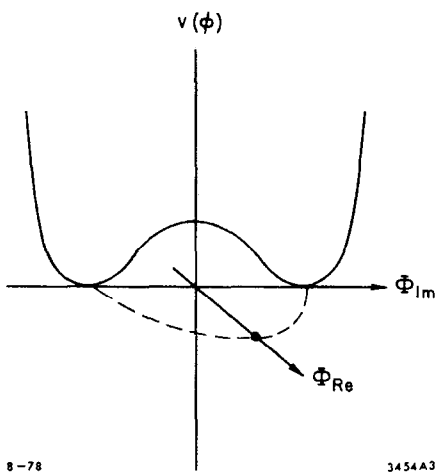

Fig. 5. Typical scalar potential for theory with spontaneous symmetry breaking.

a continuous symmetry is spontaneously broken. There is a zero mass particle associated with such a zero frequency mode. The trick of the Higgs scheme is that this zero mass scalar (one degree of freedom) can be eaten up by the zero mass vector (two degrees of freedom) to give a massive vector (three = 2 + 1 degrees of freedom). Since there do not appear to be any real zero mass scalars in the world we must arrange our Higgs sector in such a way that every such Goldstone boson corresponds to a symmetry which is gauged, and hence that there is a vector available to eat it up. (The pseudo-Goldstone[7] boson is a possible evasion of this rule, it may happen that there is a symmetry of Higgs Lagrangian which is not a symmetry of the full Lagrangian. If such a symmetry is spontaneously broken it will appear in a lowest order calculation of the type just discussed that there is a massless scalar, but keeping higher order effects from the vector mesons will give this particle a mass.)[8]

After all these preliminaries we are ready to perform steps III and IV. In SU(2) × U(1) with the fermion assignments which we have just made we need at least one Higgs doublet. Yukawa couplings are of the form

$$\Upsilon\bar{\psi}_R\phi^*\psi_{\ell} + \text{hermitian conjugate} \qquad \text{(I.19)}$$

The right-handed electron is in an SU(2) singlet and the left-handed electron is in a doublet. The only scalar representation choice which allows such a coupling is a doublet. Here is yet another reason for making quark multiplet assignments mirror fermion assignments: it allows one to be economical in the Higgs sector. Suppose I were to choose to put the right-handed up quark in a high isospin multiplet. First I would have to introduce peculiar new quarks (charges other than -1/3 or

2/3) to fill up the multiplet, and then I would need additional Higgs content to contrive to give the up quark and the rest of its new cousins their masses. Such games usually rapidly proliferate in particles and in ugliness.

With standard SU(2) × U(1) assignments I can get by with only Higgs doublets of the form

$$\phi = \begin{pmatrix} \phi^o \\ \phi^- \end{pmatrix} \tag{I.20}$$

The charge conjugate doublet

$$\tilde{\phi} = \begin{pmatrix} \phi^+ \\ -\phi^{o*} \end{pmatrix} \tag{I.21}$$

is then also present. Up-type quarks get mass from Yukawa terms of the type $\bar{u}_R \phi^* \begin{pmatrix} u \\ d \end{pmatrix}_L$, and down quarks (like electrons) need $\bar{d}_R \phi^* \begin{pmatrix} u \\ d \end{pmatrix}_L$ couplings.

I have defined the ϕ charges in relationship to my previously defined photon. That photon can only stay massless if only the neutral part of ϕ has a nonvanishing vacuum expectation value. (Remember the photon was defined simply as that linear combination of the A^o and B particles which coupled to the electron with a vector coupling and decoupled from the neutrino.) The U(1) factor is a hypercharge, in general this photon couples to electric charge, defined as

$$Q = T_3 + Y/2 \tag{I.22}$$

and we can arrange the hypercharge to get the standard quark charges, and the charges defined above for the scalars.

In my next lecture I will write out the Lagrangian to show how all this works. A few more comments can be made without doing so. I have said we need at least one complex Higgs doublet, for most of the rest of my lectures I will talk as if there is only one doublet. The existence of additional scalar doublets does not change the phenomenology of the lepton quarks and vector mesons very much, though it becomes important when finer points such as CP invariance and of course scalar particle phenomenology are discussed--John Ellis will talk about these things later in the school. However the matter of whether there are in addition to the doublet other scalar representations such as triplets does indeed affect the phenomenology. We will shortly see that assuming only Higgs doublets leads to the mass relationship

$$m_W/m_Z = \cos\theta_W \tag{I.23}$$

Adding a Higgs triplet with a nonvanishing vacuum expectation value for its neutral member would change this relationship, allowing the Z-mass to be increased arbitrarily, thus weakening the effective strength of the low energy ($s << m_Z^2$) neutral current effects. Using only doublets the SU(2) × U(1) theory predicts the curve shown in Fig. 6 for the ratio of neutral current to charge current total cross sections for neutrinos and for antineutrinos. Each point on the curve corresponds to a value for $\sin^2\theta_W$. As the figure shows the experimental values[9] are consistent with this prediction for a value

$$\sin^2\theta_W \sim .2 - .3 \tag{I.24}$$

so apparently we do not need to add any triplet Higgs. To do so would relax the prediction of the model, instead of the line we could adjust parameters to yield any point in the cone enclosed by the two dotted lines and the Weinberg-Salam prediction.

All this is just a brief introduction to the rules of the game of model building. The main points I want to stress in this lecture are

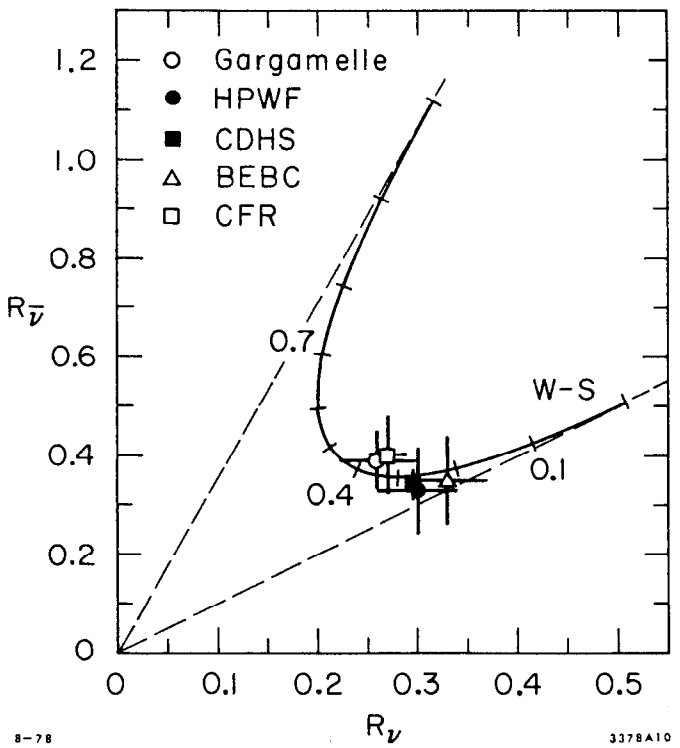

Fig. 6. The ratio of neutral-current to charged-current total cross sections for neutrinos (R_ν) and antineutrinos ($R_{\bar{\nu}}$) scattering of equal numbers of neutrons and protons. The solid line is the standard model prediction for various $\sin^2\theta$ values. The dashed lines enclose the area allowed by adding a triplet of Higgs bosons.

that the idea of a gauge theory of the weak interactions is very general and allows many specific realizations, of which the standard SU(2) × U(1) model is only one. The structure is very rich and flexible, but flexibility is usually obtained at the price of introducing more and more particles. The beauty of Weinberg-Salam-GIM is that so far it has fit a lot of data while being quite economical in particle content. If it survives the parity violation test[10] (which means if either the Novosibirsk experiment and the theoretical atomic physics calculations, or the Oxford and both the Washington experiments, are wrong) we will have a remarkable candidate weak interaction theory. If not then the theorists must go back to work to produce a model which can fit the SLAC results for parity violation in polarized electron scattering and the atomic physics--no doubt several people are already working on such models.

As John Ellis will discuss next week there is at least one area where the predictions of these theories remain virtually untested--the Higgs sector. So far no one has seen any direct effect of these particles. They have been introduced in a somewhat arbitrary fashion to allow us to write a renormalizable theory with vector and fermion masses; one with which we can perform perturbative calculations. There is a school of thought among theorists which says that elementary scalars are ugly, perhaps the same effects can occur dynamically from formation of boundstates in the scalar channels. The problem is that we cannot do much more than suggest the possibility, the idea takes us beyond the realm of perturbation theory and hence, for the most part, beyond the range of our ability to calculate.

One could go even further and add that we have no direct evidence for the vector sector. (Again John Ellis will discuss the phenomenology of this sector later this week.) Bj[11] for one, has tried to introduce a note of caution into the general bandwagon acceptance of gauge theories as dogma by discussing how much of the phenomenology can be obtained by making weaker assumptions--such as symmetry properties without necessarily assuming gauge realizations of them--and he concludes that nothing in the present data compels us to accept the gauge theory picture. However neither does anything preclude us from doing so, so for the next week we will continue to ignore all alternatives and discuss, as the title of this lecture series states, only the gauge alternatives.

Lecture II

Yesterday I managed to be very general and avoided writing any detailed algebra. Today's lecture will be much more detailed, as we investigate all those generalities in the context of the Weinberg-Salam SU(2) × U(1) and see how one arrives at specific experimental predictions, a few of which I have already mentioned.

There are two types of exercise which we must pursue. The first is, once I have told all there is to tell about gauge group and particle content, to read off from that whatever we can about the physical couplings and mass relationships. The second is, given the couplings, to compute cross sections.

I will write down the full Weinberg-Salam theory and then we will investigate it piece by piece to see the phenomena discussed yesterday at work.

Let me define

$$F^{\alpha}_{\mu\nu} = \partial_\mu A^{\alpha}_{\nu} + \partial_\nu A^{\alpha}_{\mu} + g f^{\alpha\beta\gamma} A^{\beta}_{\mu} A^{\gamma}_{\nu} \quad \text{for the SU(2) vectors} \tag{II.1}$$

and

$$G_{\mu\nu} = \partial_\mu B_\nu + \partial_\nu B_\mu \quad \text{for the U(1) vector .} \tag{II.2}$$

Further let

$$\psi^{i}_{L} = \begin{pmatrix} a^{i}_{L} \\ b^{i}_{L} \end{pmatrix} \tag{II.3}$$

where i runs over both leptons and quarks. Then

$$\begin{aligned}
\mathcal{L} = & -\frac{1}{4} F^{\alpha}_{\mu\nu} F^{\alpha,\mu\nu} - \frac{1}{4} G_{\mu\nu} G^{\mu\nu} \\
& + \sum_{k} \left| \left(\partial_\mu - i g A^{\alpha}_{\mu} \sigma^{\alpha} + i \frac{g'}{2} I_{\mu} \right) \phi_k \right|^2 \\
& + \sum_{i} \left\{ \bar{\psi}^{i}_{L} \gamma^{\mu} \left(\partial_\mu - i g A^{\alpha}_{\mu} \sigma^{\alpha} - i \frac{g'}{2} \alpha_i B_\mu \right) \psi^{i}_{L} \right. \\
& \left. + \bar{a}^{i}_{R} \gamma_\mu \left(\partial_\mu - i \frac{g'}{2} \beta_i B_\mu \right) a^{i}_{R} + \bar{b}^{i}_{R} \gamma_\mu \left(\partial_\mu - i \frac{g'}{2} \delta_i B_\mu \right) b^{i}_{R} \right\} \\
& + \sum_{ijk} \left[Y_{ijk} \bar{a}^{i}_{R} \phi^{*}_{k} \psi^{j}_{L} + \tilde{Y}_{ijk} b^{i}_{R} \tilde{\phi}^{*}_{k} \psi^{j}_{L} + \text{h.c.} \right] + V(\phi_k)
\end{aligned} \tag{II.4}$$

Now we shall proceed through a set of trivial exercises in algebra with this Lagrangian, assuming the Higgs potential is such that the vacuum expectation value

$$\left\langle \sum_{k} \phi_k \right\rangle_{\text{vac}} = \begin{pmatrix} v \\ 0 \end{pmatrix} \tag{II.5}$$

For simplicity we will carry out these exercises as if there is only one term in this sum, that is as if there is only one doublet. If there are many doublets we can simply define that (normalized) linear combination which gets a nonvanishing vacuum expectation value to be ϕ_1 and then the

following discussion is valid for k=1.

Exercise I. What are the vector mass terms? We have in the Lagrangian

$$\left|\left(g\vec{A}\cdot\vec{\sigma} + \frac{g'}{2} BI\right)\begin{pmatrix}\phi^0\\ \phi^-\end{pmatrix}_{vac}\right|^2$$

$$= \left|\left(\frac{g}{2}\begin{bmatrix} A_0 & \sqrt{2}A^+\\ \sqrt{2}A^- & -A_0\end{bmatrix} + \frac{g'}{2}\begin{bmatrix} B & 0\\ 0 & B\end{bmatrix}\right)\begin{pmatrix} v\\ 0\end{pmatrix}\right|^2 \qquad (II.6)$$

$$= \left|\begin{pmatrix}\frac{1}{2}(gA_0+g'B)v\\ \frac{g}{\sqrt{2}}A^-v\end{pmatrix}\right|^2 = \frac{1}{2}g^2v^2A^+A^- + \frac{1}{4}(g^2+g'^2)v^2\left[\frac{gA_0+g'B}{(g^2+g'^2)^{\frac{1}{2}}}\right]^2$$

Thus, identifying the massive neutral state as Z, we have

$$Z = \frac{gA_0 + g'B}{(g^2+g'^2)^{\frac{1}{2}}} = \cos\theta_W A_0 + \sin\theta_W B \qquad (II.7)$$

we can read off the masses from (II.6)

$$m_Z = \frac{1}{\sqrt{2}}(g^2+g'^2)^{\frac{1}{2}}v \qquad m_W = \frac{1}{\sqrt{2}}gv$$

This gives the advertized ratio $m_W/m_Z = \cos\theta_W$ and the orthogonal combination to the Z, the photon,

$$A = -\sin\theta_W A_0 + \cos\theta_W B \qquad (II.9)$$

clearly has zero mass, by construction.

Here we have defined a photon as the linear combination of A_0 and B which gets no mass. Now for Exercise II we can go back and check how to choose α_i, β_i and δ_i so that this particle has pure vector couplings with the right coefficients, that is

$$q = \begin{cases} -1 \text{ for electron, muon, tau, etc.}\\ 2/3 \text{ for u quark, c quark, etc.}\\ -1/3 \text{ for d quark, s quark, etc.}\end{cases} \qquad (II.10)$$

To do this we start by simply rewriting the relevant terms in terms of $\mathscr{L}$ and using

$$A_0 = Z\cos\theta_W - A\sin\theta_W, \qquad B = Z\sin\theta + \gamma\cos\theta$$

We find the fermion couplings to neutral vectors are

$$-\bar{a}_i\gamma^\mu\left\{\left(\frac{g}{2}A_{0\mu} + \frac{g'}{2}\alpha_i B_\mu\right)\left(\frac{1-\gamma_5}{2}\right) + \frac{g'\beta_i}{2}B_\mu\left(\frac{1+\gamma_5}{2}\right)\right\}a_i$$

$$-\bar{b}_i\gamma^\mu\left\{\left(\frac{-g}{2}A_{0\mu} + \frac{g'}{2}\alpha_i B_\mu\right)\left(\frac{1-\gamma_5}{2}\right) + \frac{g'\delta_i}{2}B_\mu\left(\frac{1+\gamma_5}{2}\right)\right\}b_i$$

$$= -\frac{(g^2+g'^2)^{\frac{1}{2}}}{2}\left\{\bar{a}\gamma^\mu\left[\left(\cos^2\theta_W + \sin^2\theta_W\alpha_i\right)\left(\frac{1-\gamma_5}{2}\right) + \sin^2\theta_W\beta_i\left(\frac{1+\gamma_5}{2}\right)\right]Z_\mu a_i\right.$$

$$+ \bar{a}_i\gamma^\mu(\sin\theta_W\cos\theta_W)\left[(-1+\alpha_i)\left(\frac{1-\gamma_5}{2}\right) + \beta_i\left(\frac{1+\gamma_5}{2}\right)\right]A_\mu a_i$$

$$+ \bar{b}_i\gamma^\mu\left[\left(-\cos^2\theta_W + \sin^2\theta_W\alpha_i\right)\left(\frac{1-\gamma_5}{2}\right) + \sin^2\theta_W\delta_i\left(\frac{1+\gamma_5}{2}\right)\right]Z_\mu b_i$$

$$\left. + \bar{b}_i\gamma^\mu(\sin\theta_W\cos\theta_W)\left[(1+\alpha_i)\left(\frac{1-\gamma_5}{2}\right) + \delta_i\left(\frac{1+\gamma_5}{2}\right)\right]A_\mu b_i\right\} \qquad (II.1)$$

The requirement of absence of γ_5 couplings for the photon immediately gives

$$\beta_i = -1 + \alpha_i \qquad \text{and} \qquad \delta_i = 1 + \alpha_i \qquad (II.12)$$

The charges of a_i and b_i are then given by

$$eq_a = \frac{gg'}{(g^2+g'^2)^{\frac{1}{2}}}\left(\frac{1-\alpha_i}{2}\right) = \frac{gg'}{(g^2+g'^2)^{\frac{1}{2}}}\left(T_3 - \frac{\alpha_i}{2}\right) \qquad (II.13)$$

$$eq_b = \frac{gg'}{(g^2+g'^2)^{\frac{1}{2}}}\ \frac{-1-\alpha_i}{2}$$

where T_3 is the weak isospin assignment of the left-handed fermion. Hence we can identify the coupling of the photon

$$e = \frac{gg'}{(g^2+g'^2)^{\frac{1}{2}}} \qquad \text{(II.14)}$$

My parameter α_i is the negative of the hypercharge. We arrive at the right charge assignment for leptons with $\alpha_i=1$ giving $q_a=0$ and $q_b=-1$. (Notice that this gives $\beta_i=0$ as it must since there is no right-handed neutrino to form a β type coupling with the B.) For quarks we set $\alpha_i = \frac{-1}{3}$ giving $q_a = \frac{2}{3}$ and $q_b = \frac{-1}{3}$. Furthermore we have now specified the Z-couplings which with a little further algebra we can rewrite as

$$-(g^2+g'^2)^{\frac{1}{2}}\left\{T_3\left(\frac{1-\gamma_5}{2}\right) - Q\sin^2\theta_W\right\} \qquad \text{(II.15)}$$

Clearly the couplings of the Z are in general a mixture of V and A although a peculiar accident may happen to remove the V part, for example the negative leptons e, μ, etc. would have pure axial coupling to the Z if $\sin^2\theta_W = 0.25$. (Experimentally we will find the preferred value of $\sin^2\theta_W$ is not very far from this value.) I could at this point proceed to the next set of terms--the Yukawa coupling terms, and carry out exercise III, which is to find the quark and lepton mass matrices. I will not do more than make a few comments on this exercise--carry it out as a homework problem if you wish. I remark that the Y_{ijk} and $\tilde{Y}_{ijk}$ do not require that i=j--this has the consequence that the mass eigenstates, the quarks, u,c... and d,s... may be linear combinations of the a^i and b^i respectively. This phenomenon has already been mentioned, we find Cabibbo combinations

$$\begin{aligned} b_1 &= \cos\theta_c d + \sin\theta_c s \\ b_2 &= -\sin\theta_c d + \cos\theta_c s \end{aligned} \qquad \text{(II.16)}$$

are the weak eigenstates. If we introduce further quarks with the same charges then they could, in principle, also mix with the d and s. Experimentally the success of Cabibbo universality tells us that the amount b in the doublet with u must be small, as Stan Wojcicki discussed in Monday's lecture. The Yukawa couplings must then be arranged so that this is so.

Just a few more comments on the rules for putting together theories of the Weinberg-Salam type and then on to real physics--that is to cross section calculations. One of the advertized virtues of gauge theories compared to the old four fermi theory is renormalizability. In fact the Weinberg-Salam theory as I have written it is not necessarily renormalizable--because of anomalies, which means processes involving the triangle of Fig. 7. One can take the attitude that this does not much matter. We have to go to such high order before there is any problem that we might be being unreasonably optimistic to hope that our present theory is valid to that accuracy. However the dogma says we must get rid of these anomalies; that is to say we must have a renormalizable theory. We can arrange to do so by having a number of such triangle diagrams with their sum vanishing identically. In general this is achieved by requiring the sum of the fermion charges to vanish. In Weinberg-Salam, with SU(3) color, this happens if one has as many flavors of quark doublet as there are lepton doublets, e.g.,

$$\begin{pmatrix}\nu_e\\ e\end{pmatrix}\quad\begin{pmatrix}\nu_\mu\\ \mu\end{pmatrix}\quad\begin{pmatrix}\nu_\tau\\ \tau\end{pmatrix}$$

$$\begin{pmatrix}u\\ d_c\end{pmatrix}\quad\begin{pmatrix}c\\ s_c\end{pmatrix}\quad\begin{pmatrix}t\\ b\end{pmatrix}$$

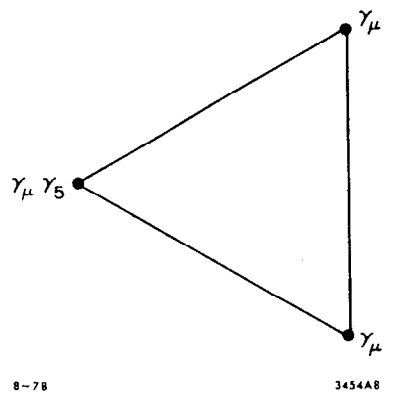

Fig. 7. The anomalous triangle graph.

For each pair of doublets $\Sigma q = (0 + -1)$ for leptons + $n_c \times\left(\frac{2}{3} + -\frac{1}{3}\right)$ where n_c is the number of colors of each quark flavor. For color SU(3), n_c=3 and Σq=0 with this arrangement.

As I stressed yesterday there is no a priori reason for the continuing replication of similar multiplets. Assuming such replication leads to a prediction that there are no flavor changing neutral currents. In the context of this theory the masses of the various fermions are achieved quite arbitrarily by adjusting Yukawa couplings.

We have now written a model which tells us everything there is to know about the weak interactions of leptons and of quarks. For leptons the rest is completely straightforward, we can simply calculate any process we choose. For hadron physics we need something more to relate this model to experiment--we need to know how the quarks are put together to make hadrons. That we do not really know, so we are left somewhat up in the air by our beautiful theory of the weak interactions. However there is a great deal we can do, in the framework of the quark-parton model. We define a set of functions called the structure functions which describe at least part of what we need to know--they are a description, at least in the high energy limit, of hadron composition in terms of quarks. We can then calculate cross sections for a number of processes in terms of these same functions, and hence test the theory by the consistency between the various rates--testing whether all experiments can be fit with the same set of structure functions.

Let us therefore discuss the familiar example of deep inelastic scattering. For sufficiently high energy and momentum transfer we can neglect lepton and quark masses, though clearly if we come to a new

quark threshold that rule will be in abeyance for a while. This means we only have to do very few calculations, since the interactions γ_μ and $\gamma_\mu\gamma_5$ each preserve helicity up to corrections of order m/E. The calculations are simple enough. I will not go through them here; I will simply state the results for deep inelastic scattering. I define the usual set of variables for the process shown in Fig. 8.

$$\nu = q\cdot p \qquad x = \frac{-q^2}{2\nu} \qquad y = p.q/p\cdot k \tag{II.17}$$

In terms of the quark-parton model the cross sections for various deep-inelastic processes can be obtained by assuming incoherent scattering off the individual quark constituents of the target and defining structure functions $f_q(x)$ which, in the high energy limit, represent the probability of finding a quark of type q carrying a fraction x of the proton's momentum in a frame in which the proton is moving with very large momentum. This parton picture interpretation of the structure function is of course frame dependent, but the cross sections which we write down are functions of the invariants and hence are not. In a more general picture one finds that the structure functions could in fact be functions of q^2 as well as x, the fact that to a first approximation they should be q^2 independent was first suggested by Bj and hence is known as Bjorken scaling.[12] In the context of a specific model of the strong interactions, namely QCD, one can obtain more detailed predictions about these functions and their q^2 dependence[13]--these predictions will be discussed tomorrow by John Ellis. For the moment however let us take the naive parton model point of view and treat these as functions of x alone. Neglecting lepton and quark masses one obtains a very simple set

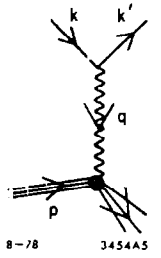

Fig. 8. Labeling of momenta in deep inelastic scattering processes.

of predictions, namely scattering left-handed fermion on left-handed fermion or right on right gives

$$\frac{d\sigma}{dxdy} \propto xf(x) \tag{II.18}$$

scattering left-handed on right-handed gives

$$\frac{d\sigma}{dxdy} \propto xf(x)\ (1-y)^2 \tag{II.19}$$

Let us look at this for $\nu(\bar{\nu})$ nucleon $\to \mu^-$ (μ^+) anything. The charged weak current sees only left-handed quarks and thus only right-handed antiquarks, so the above rule gives the familiar predictions

$$\begin{aligned}\frac{d\sigma^{\nu}}{dxdy} &= \frac{G^2ME}{\pi}\, 2x \sum_q \left[f_q(x) + f_{\bar{q}}(x)(1-y)^2\right] \\ \frac{d\sigma^{\bar{\nu}}}{dxdy} &= \frac{G^2ME}{\pi}\, 2x \sum_q \left[f_q(x)(1-y)^2 + f_{\bar{q}}(x)\right]\end{aligned} \tag{II.20}$$

with

$$G^2 = \frac{1}{8}\left(\frac{g^2}{2m_W^2}\right)^2 = \frac{1}{8v^2} \tag{II.21}$$

in Weinberg-Salam.

The same calculations can be made for the deep inelastic neutral current neutrino scattering. To do so it is convenient to write the Z couplings as

$$-(g^2+g'^2)^{\frac{1}{2}}\left\{\frac{\varepsilon_L^i(1-\gamma_5)}{2} + \frac{\varepsilon_R^i(1+\gamma_5)}{2}\right\} \tag{II.22}$$

For SU(2) × U(1) theories we find

$$\begin{aligned}\varepsilon_L^i &= T_{3L}^i - q^i \sin^2\theta_W \\ \varepsilon_R^i &= T_{3R}^i - q^i \sin^2\theta_W\end{aligned} \tag{II.23}$$

In the standard version we had $T_{3R}^i = 0$ for all fermion types. We notice that these formulae apply either for quarks or antiquarks, and imply the relationships

$$\varepsilon_L^q = -\varepsilon_R^{\bar{q}}\ ; \qquad \varepsilon_R^q = -\varepsilon_L^{\bar{q}} \tag{II.24}$$

The strength of the neutral current processes can be compared to those of charged currents. For charged currents the amplitude is proportional to $g^2/2m_W^2 = 1/v^2$ whereas for neutral currents the comparable factor is $(g^2+g'^2)\ \varepsilon^a\varepsilon^b/m_q^2 = 2\varepsilon^a\varepsilon^b/v^2$. Thus for example we obtain for neutrino deep inelastic scattering, using (II.24),

$$\begin{aligned}\frac{d\sigma^{\nu\to\nu}}{dxdy} = \frac{G^2ME}{\pi}\, 8x \sum_q \Big\{&\left(\varepsilon_L^q\right)^2\left[f_q(x) + f_{\bar{q}}(x)(1-y)^2\right] \\ &+ \left(\varepsilon_R^q\right)^2\left[f_q(x)(1-y)^2 + f_{\bar{q}}(x)\right]\Big\}\end{aligned} \tag{II.25}$$

and similarly

$$\begin{aligned}\frac{d\sigma^{\nu\to\nu}}{dxdy} = \frac{G^2ME}{\pi}\, 8x \sum_q \Big\{&\left(\varepsilon_L^q\right)^2\left[f_q(x)(1-y)^2 + f_{\bar{q}}(x)\right] \\ &+ \left(\varepsilon_R^q\right)^2\left[f_q(x) + f_{\bar{q}}(x)(1-y)^2\right]\Big\}\end{aligned} \tag{II.26}$$

(An obvious note, if the target contains neutrons and protons then

$$f_q^{\text{target}}(x) = N_P f_q^P(x) + N_N f_q^N(x) \tag{II.27}$$

where N_P (N_N) is the number of protons (neutrons) in the target. Isospin invariance tells us that

$$\begin{aligned}f_u^P(x) &= f_d^N(x) \\ f_d^P(x) &= f_u^N(x)\end{aligned}$$

$$f_s^p(x) = f_s^N(x) \qquad \text{(II.28)}$$

and similarly for antiquarks.)

I can treat photon exchange in this same formalism, the photon couplings can be written in analogy to the Z-couplings as

$$e\beta_L^i \frac{(1-\gamma_5)}{2} + e\beta_R^i \frac{(1+\gamma_5)}{2} \qquad \text{(II.29)}$$

where obviously

$$\beta_L^i = \beta_R^i = q^i \qquad \text{(II.30)}$$

The strength factor $g^2/2m_W^2$ is replaced by e^2/q^2.

For deep inelastic electron scattering I can treat the left- and right-handed parts of the electron incoherently, but I must remember that photon and Z exchanges add coherently. Thus I have

$$\frac{d\sigma}{dxdy} = \frac{d\sigma^L}{dxdy} + \frac{d\sigma^R}{dxdy} \qquad \text{(II.31)}$$

and

$$\frac{d\sigma^L}{dxdy} = \frac{e^4 ME}{4\pi} \times \sum_i \left\{ \left[\frac{-Q^i}{q^2} + \frac{\epsilon_L^e \epsilon_L^{q_i}}{\sin^2\theta_W \cos^2\theta_W (q^2 - m_Z^2)} \right]^2 \left[f_{q_i}(x) + f_{\bar{q}_i}(x)(1-y)^2 \right] \right.$$
$$\left. + \left[\frac{-Q^i}{q^2} + \frac{\epsilon_L^e \epsilon_R^{q_i}}{\sin^2\theta_W \cos^2\theta_W (q^2 - m_Z^2)} \right]^2 \left[f_{q_i}(x)(1-y)^2 + f_{\bar{q}_i}(x) \right] \right\} \qquad \text{(II.32)}$$

For $d\sigma^R/dxdy$ one simply makes the replacements

$$\epsilon_L^e \to \epsilon_R^e \; ; \qquad \epsilon_L^{q_i} \leftrightarrow \epsilon_R^{q_i} \qquad \text{(II.33)}$$

in (II.32).

Lecture III

Note for the reader--this lecture followed after Lecture I by John Ellis.

I want to start this lecture with some comments on what we have discussed so far. In my first lecture I told you how to build a gauge theory model. I remind you that it is an extremely ad hoc process, good and bad models are distinguished by experimental tests, not by theoretical reasoning. Even when a model can be constructed to fit all present data it makes no definite prediction about how many heavier quarks there might be, and there is similarly much arbitrariness the predictions about the scalar sector. These things will be discussed further by John Ellis in subsequent lectures, and by Mary Kay Gaillard in the topical conference.

In the second lecture I told you how to calculate: Given a model, one can read off W and Z masses and couplings and from them proceed directly to predictions for deep inelastic scattering processes. These calculations are valid in the naive form only when it is reasonable to neglect both the lepton and the quark masses. Near a threshold, for example, where charm production begins to enter in the allowed final states, the model is not capable of giving clear predictions. There exist a number of slightly different suggestions for including quark mass corrections in the near threshold region. They all interpolate smoothly between the scaling prediction below threshold and the new scaling prediction sufficiently far above. They differ somewhat in how rapidly the new value is achieved--in other words in how far above threshold is sufficiently far. I will not go into this discussion here. The quantity y plotted as a function of energy for $\bar{\nu}$ scattering has been used in the

literature as a particularly sensitive test for the appearance of a threshold corresponding to a right-handed coupling of a u or d quark to a heavier quark. The reason for the choice is obvious enough. With only left-handed couplings the valence quark contribution to antineutrino scattering is proportional to $(1-y)^2$, so a right-handed coupling, giving a term proportional to 1 would give a marked increase in <y>. However the scaling corrections discussed yesterday by John Ellis also tend to increase <y> with increasing energy. The reason for this is that the contribution of antiquarks in the target increases, due to the glue → quark-antiquark terms which John discussed, giving also an increasing contribution of y independent cross section. I think it is now generally agreed that these corrections are sufficient to account for the observed variation of <y> with energy, thus excluding right-handed coupling of the u or d quarks to any quark with mass less than about 5 GeV.

For the theorists in the audience I want to add one warning (it is obvious to the experimenters)--every experiment makes certain cuts in the data for purely experimental reasons. In comparing experiment with theory one must know about these cuts and take them into account. We theorists have a bad habit of trying to extract numbers from the experiments to compare directly with the simplest theoretical calculations. What should be done is the other way around, one extracts numbers from the theory (if necessary via Monte Carlo calculations) to compare directly with what has actually been measured.

Let me now go on to discuss further predictions which can be obtained from a gauge theory model, as before continuing to use Weinberg-Salam SU(2) × U(1) as the sample model. Obviously purely leptonic processes such as $\nu_\mu e$ scattering can be calculated by the same rules as deep inelastic, simply replacing structure functions by a delta-function at x=1. For $\bar{\nu}_e e$ or $\bar{\nu}_\mu \mu$ scattering one must remember that there is a direct channel W-exchange diagram to include as well as the t-channel Z-exchange. The predictions are usually given in terms of g_V and g_A, in terms of the previously defined Z-couplings

$$\left.\begin{aligned} g_V &= \varepsilon_L^e + \varepsilon_R^e \to -\frac{1}{2} + 2\sin^2\theta_W \\ g_A &= \varepsilon_L^e - \varepsilon_R^e \to -\frac{1}{2} \end{aligned}\right\} \text{ for standard Weinberg-Salam.} \qquad \text{(III.1)}$$

The experimental situation is shown in Fig. 9. There is one further result from Gargamelle which is in conflict with the other experiments, and with the Weinberg-Salam prediction, however, it appears that the analysis of the second half of the data will significantly change the result, so I do not include it here.

The next area where the theory can be tested is in elastic νp scattering experiments. One new unknown function enters--the axial form factor of the proton. However, one can make a reasonable model for this, in parallel to the behavior of the vector form factor. In the context of such a model the Weinberg-Salam prediction is in good agreement with the measurements,[15] for $\sin^2\theta_W$ in the range .2 to .3.

Recently Mike Barnett and Larry Abbott[16] have made a very nice systematic study of predictions of neutral current process, including semi-inclusive processes. They find this gives them a good tool for distinguishing between gauge theory models. Mike will be talking about this in the topical conference, so I will not discuss it further here.

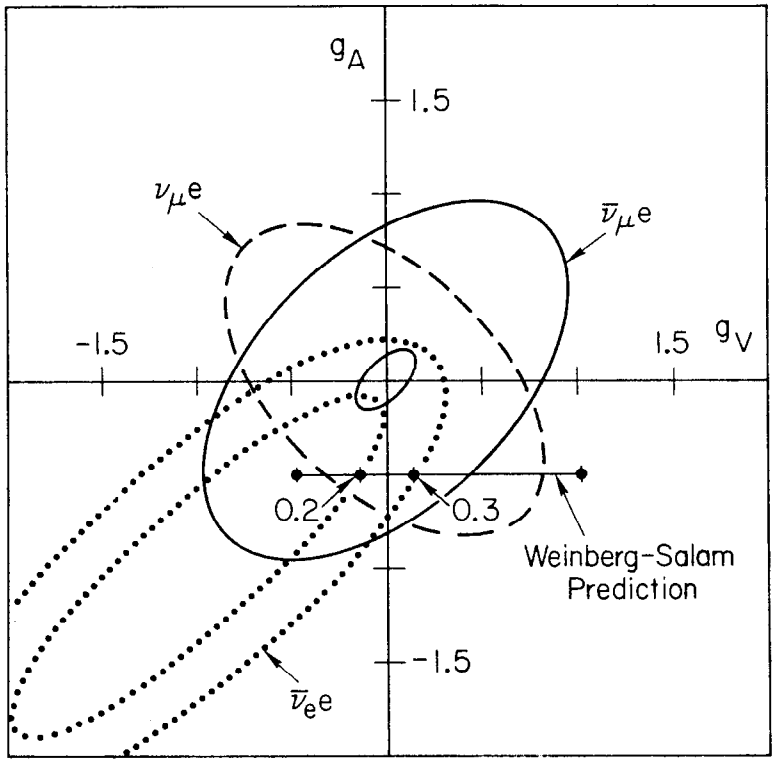

Fig. 9. Experimental constraints on g_V and g_A from lepton scattering data.[19]

Now we come to the topic of the first morning of the topical conference, parity violations. Let me start with the easy cases first. I refer you to a paper by Bob Cahn and Fred Gilman[17] for the details of the calculations. Using the deep inelastic scattering formulae given in Lecture II one arrives at the following predictions

$$A(x,y) = \left(\frac{d\sigma^L}{dxdy} - \frac{d\sigma^R}{dxdy}\right) / \left(\frac{d\sigma^L}{dxdy} + \frac{d\sigma^R}{dxdy}\right) \qquad \text{(III.2)}$$

For deuterium, keeping only valence quark contributions

$$A_{ed} = \frac{-Gq^2}{2\sqrt{2}\,\pi\alpha} \cdot \frac{9}{10} \cdot \left[\left(1 + 2T^e_{3R}\right)\left(1 - \frac{20}{9}\sin^2\theta_W + \frac{4}{3}T^u_{3R} - \frac{2}{3}T^d_{3R}\right)\right.$$
$$\left. + \left(1-4\sin^2\theta_W - 2T^e_{3R}\right)\left(1 - \frac{4}{3}T^u_{3R} + \frac{2}{3}T^d_{3R}\right)\left(1-(1-y)^2\right) / \left(1+(1-y)^2\right)\right] \qquad \text{(III.3)}$$

Notice A is x independent. For any target

$$f_u(x) = N_P f^P_u(x) + N_N f^P_d(x)$$
$$f_d(x) = N_P f^P_d(x) + N_N f^P_u(x) \qquad \text{(III.4)}$$

Thus we see that if $N_P = N_N$ then $f_u = f_d$ and hence f(x) cancels out in the ratio A. I remark also that with right-handed singlet assignment for all quarks and leptons the prediction becomes y-independent for $\sin^2\theta_W = .25$, or slowly varying with y for $\sin^2\theta_W$ near that value; and the present best values are quite close to .25. This is in marked contrast to some other models, for example, models with nontrivial T_{3R}. Models such as $SU(2)_L \times SU(2)_R \times U(1)$ (Ref. 18) have also been constructed to reproduce the standard Weinberg-Salam predictions for deep inelastic ν-scattering, but can give quite different predictions for parity violating effects, in particular for the atomic physics experiments they predict no effect. The result of the SLAC-Yale experiment[19]

along with the predictions of Weinberg-Salam and of a theory with the right-handed electron in a doublet is shown in Fig. 10. This result is also in conflict with the version of $SU(2)_L \times SU(2)_R \times U(1)$ which gives no atomic physics parity violations. Further information, in particular on the relative u and d couplings is gained from data on hydrogen.[19] The SLAC-Yale collaboration intends to make further measurements for smaller y. The results of such measurements, if they can be made with errors comparable to those of the existing measurement, will provide very interesting further information.

Cahn and Gilman have also calculated predictions for asymmetries for elastic ep and ep → ℓΔ(1236). These predictions, like those for elastic νp total cross sections, depend on some assumptions about form factors, but one could obtain some further tests of the model by measuring these quantities.

Now we come to the "Mares Nest" for Weinberg-Salam, the question of parity violations in atomic physics. These are of course tests of some of the same parameters in the model as occur in ep and ed scattering at y=0. (One needs both ep and ed to be able to test up and down quark couplings separately.) In the atomic physics experiments what is measured is the optical rotation of light in a laser induced atomic transition. This effect is proportional to the matrix element for the mixing of a "wrong parity" state due to the axial coupling of the Z to an electron. In Weinberg-Salam $g_A^e = -1/2$. At the nucleus we need a g_V

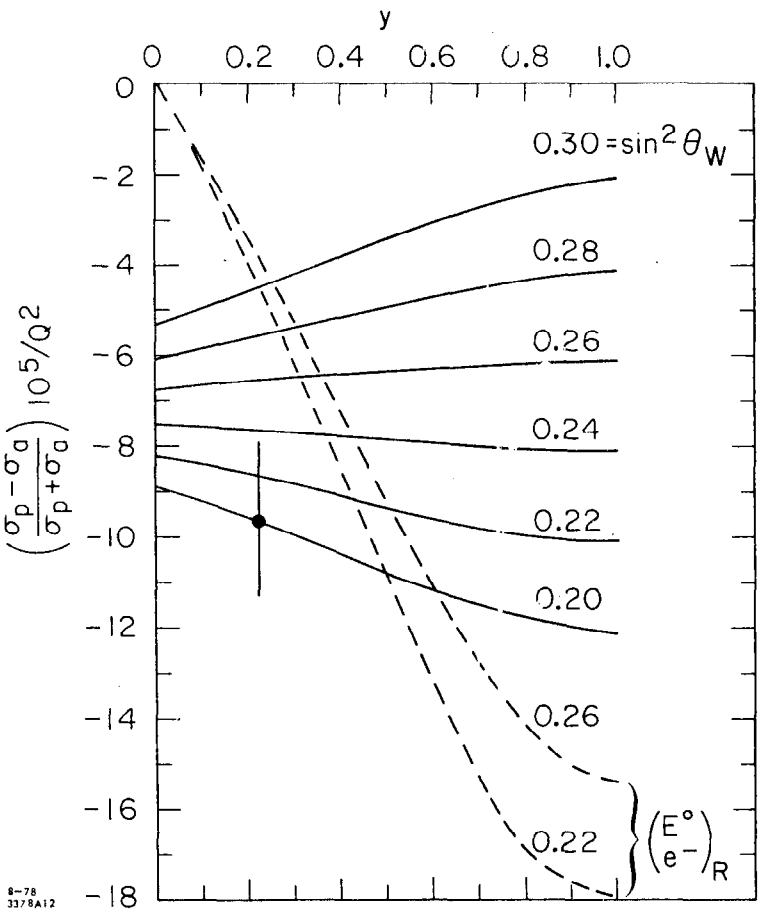

Fig. 10. Comparison of SLAC-Yale ed asymmetry measurement with predictions of Weinberg-Salam and a model with the right-handed electron in a doublet.

coupling, which is given by

$$N_u\left(\frac{1}{2} - \frac{4}{3}\sin^2\theta_W\right) + N_d\left(-\frac{1}{2} + \frac{2}{3}\sin^2\theta_W\right)$$

$$= (2N_P+N_N)\left(\frac{1}{2} - \frac{4}{3}\sin^2\theta_W\right) + (2N_N+N_P)\left(-\frac{1}{2} + \frac{2}{3}\sin^2\theta_W\right)$$

$$= -Z\left(\sin^2\theta_W + \frac{A-2Z}{2Z}\right) \qquad \text{(III.5)}$$

However this is the easy part of the calculation, the hard part is the constant of proportionality, which is to say the calculation of the atomic physics matrix elements

$$\phi = \left(\begin{matrix}\text{known}\\ \text{coefficient}\end{matrix}\right) \sum_n \left\{ \frac{\langle f|D|n\rangle\langle n|\bar{e}\gamma_\mu\gamma_5 e|i\rangle}{E_i - E_n} + \frac{\langle f|\bar{e}\gamma_\mu\gamma_5 e|n\rangle\langle n|D|i\rangle}{E_f - E_n} \right\} \qquad \text{(III.6)}$$

where D is an electric dipole operator. To calculate this one needs to know the energy levels and the relevant wave functions for the atom in question, which is Bismuth in all experiments carried out to this date.

The energy levels are well measured, but the wave functions are not as easily obtained. One makes models for them, and the models are tested by their ability to reproduce certain measured results, such as energy levels. I display in Table I as an example a table from a paper by Henley, Kaplisch and Wilets.[20] CI in this table means "configuration interaction." The point of the paper is that the original calculations by Henley and Wilets of the expected parity violating effect used a Hartree-Fock independent-particle model, including the configuration interaction corrections changes the predicted effect by as much as 0.65. You may judge for yourselves from the table the extent to which the energy levels confirm these corrections.

There are independent calculations by Novikov, Sushkov, and Khriplovich[21] which take what they call a semi-empirical approach. This means

TABLE I. Some energy levels in Bi I of $J = \frac{3}{2}$ (in inverse centimeters).

Level	Without CI	CI including 7s	CI including 6s	Expt.[a]
$6p_{3/2}^2(2)6p_{1/2}$	11 658	11 598	11 770	11 419
$6p_{3/2}^3$	34 903	34 694	33 364	33 164
$6p_{1/2}6p_{3/2}(1)7s$	42 674	42 710		44 865
$6p_{1/2}6p_{3/2}(2)7s$	49 696	49 595		49 456
$6s6p_{1/2}^2 6p_{3/2}^2$	81 299		84 828	

[a] C. E. Moore, *Atomic Energy Levels*, National Bureau of Standards Circular No. 467 (U.S. GPO, Washington, D. C., 1958), Vol. III.

that adjustments are made in the model to correct certain predictions to match measured values. Unfortunately some corrections have to be made based on measurements in Thallium rather than Bismuth, since the relevant measurement is not available for Bi. The relevant quantity is

$$\rho_6 = \int dr\ r^3\ R_{6s}R_{6p_{3/2}} \qquad \text{(III.6)}$$

where R is the radial part of relevant wave function. For Thallium the model predicts

$$\rho_6 = -2.9\ a_0$$

and photoionization measurements give $|\rho_0| = 1.8\ a_0$. Hence the effect of a 6s → 6p electron transition in Bismuth is corrected by a factor (1.8/2.9) from the theoretical prediction. There are other relevant contributions coming from 6p → 7s and 6p → (higher states including continuum) for which the estimates are made similarly, but with reference to tests in Bi. In calculating the total predicted effect the relative signs of these various contributions are very important. (The above discussion was given, with some further detail, in a talk by Peter Rosen at the Workshop on Weak Interactions at Ames, Iowa last month.) [22]

Where does all this leave us--after all corrections have been applied the best value for the predicted effect, for either the 876 or 648 nm line is of order -10×10^{-8} using $\sin^2\theta_W = .2 - .25$. The experimental situation will be discussed in detail at the Topical Conference next week. There are now four experiments, two from Seattle, one from Oxford and one from Novosibirsk. Of these, three including the second generation Seattle experiment, give an upper limit about an order of magnitude below the prediction while the fourth, from Novosibirsk finds an effect in agreement with the predicted value. Obviously not everyone is right--there are several options, among them

1. Novosibirsk, Atomic Theory and Weinberg-Salam are right and Oxford and Seattle are wrong.
2. Novosibirsk and Atomic Theory are wrong and Weinberg-Salam, Oxford, and Seattle are right.
3. Novosibirsk and Weinberg-Salam are wrong and Atomic Physics, Oxford, and Seattle are right.
4. Everyone is wrong.

I do not intend my previous discussion to be a judgment on the atomic physics theory. I have not studied it carefully enough to make such a judgment. Clearly there are some uncertainties, but the question is whether they are at the factor of 2 level or as much as an order of magnitude. One must also look very carefully at the experiments to try to understand what might possibly be going wrong in any one of them, since they disagree. These are difficult measurements but I do not know of any telling point which has been raised against any one of them, all I can say is the discussion next Wednesday promises to be interesting. The situation may also be resolved by further experiments. An experiment in Thallium is being worked on at Berkeley, which has the virtue that certain cross-checks of the model can be made at the same time. From the theorists point of view the ideal experiment is of course in hydrogen. This will come; groups at Michigan, Seattle, and Yale are working on it. Results are not expected for some time. (Predictions vary from a few months to more than a year.)

For the most part the composite quark picture of hadrons, together with a gauge theory of the weak interactions, gives us a good description of the observed weak interactions. Let me list some salient points:

We do not see second class currents.[23] (Their existence would be a serious problem, if not a disaster for these theories.)

Deep inelastic neutrino scattering data is for the most part well fit by the model; we do not need to invoke scalar component, which would give a term proportional to (1-y) in $d\sigma/dxdy$, though such a contribution is also not excluded by the present data. One outstanding problem here is the ratio σ_L/σ_T which is found in electron scattering which, even including higher order gluon effects, is predicted to be somewhat smaller than the measured value.[24] This quantity must be dominated by terms involving mass corrections, terms dropped in all the standard asymptotic (scaling) treatments. Various attempts[25] have been made to estimate such effects, it is a pretty grubby business. From a pragmatic point of view it is fair to keep the magnitude of σ_L/σ_T in mind as a measure of the order of magnitude of possible corrections to the quark model plus QCD treatment which we have discussed.

There are some areas where the theory ceases to be useful. It is a theory of the weak interactions of quarks and not of physical hadrons. In deep inelastic scattering we could absorb our ignorance of the hadron wave functions into a few structure functions and then compare experiments. For explaining hyperon decays however we need to know more. Certain absolute rules like $\Delta Q = \Delta S$ arise as a natural consequence of the structure of the quark currents. However the $\Delta I = 1/2$ enhancement, which Stan Wojciki discussed on Monday, is a detailed property of the hadronic matrix elements of two quark currents. There are both $\Delta I = 1/2$ and $\Delta I = 3/2$ operators formed from these currents. Empirically we find the $\Delta I = 1/2$ parts dominated by a factor of 50-100. Keeping higher order gluon corrections, anomalous dimensions as discussed in the context of scaling violations by John Ellis, gives some $\Delta I = 1/2$ enhancement,[26] but it is my judgment that with reasonable values of the parameters involved it is not enough to fit the data, it is more like a factor of 5 than the factor experimentally observed. That does not mean the theory is wrong, simply that the effect is dominated by the part which we cannot calculate, the long distance part, rather than by the short distance part for which this calculation can be made. If we really understood hadrons as quark bound states we should be able to explain the effect, but that of course is a strong interaction problem, gauge theories of the weak interactions can at present only make useful predictions where such problems can be avoided.[27]

There is another area of weak phenomenology which I have barely mentioned--the area of CP violation. As Stan Wojcicki told you on Monday a six quark version of Weinberg-Salam in general has some CP violating phase in the quark-mixing matrix which defines weak eigenstates in terms of mass-eigenstates (or vice versa). Adding more than one Higgs doublet can also introduce CP violating effects. John Ellis will tell you more about how these things work. I just want to comment that these theories naturally incorporate CP violating effects without having to add anything radically new. The simplest Weinberg-Salam theory with just four quark flavors and one complex Higgs doublet does not have CP-violations, but experimental results are already pushing us beyond that model anyway.

A complicated Higgs sector can lead to CP violations of the milliweak type, with a predicted value for the neutron dipole moment not much below the present experimental upper bound.[28] The CP violations coming from phases in the quark sector are typically superweak in character. The CP violating phase in this case, like everything else coming from the Yukawa coupling terms, is a free parameter in the model.

I have tried in these lectures to give you some feeling for the generality of the gauge theory idea, as well as of the status of the "standard model". There clearly are some questions yet to be settled, but in the last year much progress has been made. A year ago there were many candidate models to discuss--now there is just one, and that is a very economical one. A viable model must at least reproduce the neutrino phenomenology of the Weinberg-Salam model. There is a large class of models of the type SU(2) × U(1) × G which do so;[29] the parity violation situation may force us to extend the model in this way. There are many areas yet to be explored. I have focused on what we know now, leaving John Ellis with the problem of spending his next three lectures talking about things we know practically nothing about, at least experimentally speaking.

References

1. S. Weinberg, Phys. Rev. Letters 19, 1264 (1967); A. Salam in Elementary Particle Theory, ed. by N. Svartholm (Almquist and Wiksell, Stockholm, 1969), p. 367.

2. S. Glashow, J. Iliopoulos and L. Maiani, Phys. Rev. D 2, 1285 (1970).

3. G. 't Hooft, Nucl. Phys. B33, 173 (1971), B35, 167 (1971); B. W. Lee and J. Zinn-Justin, Phys. Rev. D 5, 3121 (1972), 5, 3137 (1972), 5, 3155 (1972) and 7, 1049 (1973).

4. J. Cornwall, D. Levin and G. Tiktopoulos, Phys. Rev. D 10, 1145 (1974), also Phys. Rev. Letters 30, 1268 (1973) and 31, 572 (1973); C.H. Llewellyn Smith, Phys. Letters 46B, 233 (1973).

5. J. Bjorken and C. H. Llewellyn Smith, Phys. Rev. D 7, 887 (1973).

6. S. L. Glashow and S. Weinberg, Phys. Rev. D 15, 1958 (1977); E. A. Paschos, Phys. Rev. D 15, 1966 (1977).

7. S. Weinberg, Phys. Rev. Letters 29, 1698 (1972).

8. This discussion is presented in the language of the unitary gauge. For calculational convenience it is often better to work in one of the manifestly renormalizable gauges for an introduction to such gauges; see E. S. Abers and B. W. Lee, Physics Reports 9C (1973).

9. M. Holder et al. (CDHS), Phys. Letters 72B 254 (1977); J. Blietschau et al. (Gargammelie), Nucl. Phys. B118, 218 (1977); A. Benvenuti et al. (HPWF), Phys. Rev. Letters 37, 1039 (1976); P. Wanderer et al. (HPWF), Phys. Rev. D 17, 1679 (1978); F. S. Merritt et al. (CF), Phys. Rev. D 17, 2199 (1978); K. Schultze (BEBC), in Proc. 1977 Int. Symp. on Lepton and Photon Interactions at High Energies, edited by F. Gutbrod (DESY, Hamburg, 1977), p. 359; and P. C. Bosetti et al., Report no. Oxford-NP-20/78 (1978).

10. See talks by Fortson and Commins in these proceedings and references contained therein. For published experimental results see Nature 264, 528 (1976).

11. J. D. Bjorken, "Alternatives to Gauge Theories," talk given at the Ben Lee Memorial Conference, Fermilab, September 1977 (SLAC-PUB-2133 and 2134). See also earlier work by P. Hung and J. J. Sakurai, (1976).

12. J. D. Bjorken, Phys. Rev. 179, 1547 (1969).

13. G. Parisi, Phys. Letters 43B, 207 (1973), 50B, 367 (1974); H. P. Politzer, Physics Reports 14C, #4 (1974); G. Altarelli and G. Parisi, Nucl. Phys. B126, 198 (1974).

14. This picture is taken from L. Abbott and M. Barnett, "Quark and Lepton Couplings in the Weak Interactions," Stanford Linear Accelerator Center preprint SLAC-PUB-2136 (see also Ref. 16). The data used are P. Alibran et al. (Gargamelle P.S. $\nu_\mu e$), Phys. Letters 74B, 422 (1978); J. Bleitschau et al. (Gargamelle P.S. $\bar{\nu}_\mu e$), Nucl. Phys. B114, 189 (1976); F. Reines et al. ($\bar{\nu}_e e$), Phys. Rev. Letters 37, 315 (1976); M. Baldo-Ceolin (Aachen-Padua $\nu_\mu e$ and $\bar{\nu}_\mu e$) to appear in Proceedings of Neutrinos 78 Conference, Purdue, April 28-May 2, 1978. Recent data from C. Baltay et al. on $\nu_\mu e$ (Fermilab report) are in agreement with the 90% confidence limits shown. A recent result from the Gargamelle S.P.S. P. Alibran et al., CERN/EP/PHYS 78-6 (1978) does not agree with these results, but the group have stated that analysis of further data changes the result, so this measurement is not included here.

15. L. Sulak, Harvard report to appear in the Proceedings of the Neutrinos 78 Conference, Purdue, April 28-May 2, 1978. J. B. Strait and W. Kozanecki, Harvard University Ph.D. Theses (1978); D. Cline et al., Phys. Rev. Letters 37, 252, 648 (1976).

16. L. F. Abbot and R. M. Barnett, Phys. Rev. Letters 40, 1305 (1978) and SLAC-PUB-2136. See also talk by R. M. Barnett in these proceedings.

17. R. N. Cahn and F. J. Gilman, Phys. Rev. D 17, 1313 (1978).

18. J. Pati and A. Salam, Phys. Rev. D 10, 275 (1974). The particular version to which I refer here was discussed by A. DeRujula, H. Georgi and S. L. Glashow, Ann. Phys. 109, 242, 258 (1977).

19. C. Prescott et al., "Parity Non-Conservation in Inelastic Electron Scattering," Stanford Linear Accelerator Center preprint SLAC-PUB-2148 (July 1978). See also the talk by D. Sherden in these proceedings.

20. E. M. Henley, M. Klapisch and L. Wilets, Phys. Rev. Letters 39, 994 (1977).

21. V. N. Novikov, O. P. Sushkov and I. B. Khriplovich, Zh. Eksp. Teor. Fiz. 71, 1665 (1976) Sov. Phys. J.E.T.P. 44, 872 (1976) .

22. P. Rosen, Proceedings of the Workshop on Weak Interactions, Iowa State University, Ames, Iowa (June 1978).

23. H. Braende, L. Grenacs, J. Lang, L. P. Roesch, V. L. Telegdi, P. Truttmann, A. Weiss, A. Zehnder, and Villigen Sin, Phys. Rev. Letters 40, 306 (1978).

24. A. De Rujula, H. Georgi, and H. D. Politzer, Ann. Phys. (N.Y.) 103, 315 (1977).

25. R. Barbieri, J. Ellis, M. K. Gaillard, and G. G. Ross, Nucl. Phys. B117, 50 (1976).

26. M. K. Gaillard and B. W. Lee, Phys. Rev. Letters 33, 108 (1974); G. Altarelli and L. Maiani, Phys. Letters 52B, 351 (1974).

27. For a "state of the art" discussion of this subject see the talk by M. K. Gaillard in these proceedings.

28. S. Weinberg, Phys. Rev. Letters 37, 657 (1976).

29. H. Georgi and S. Weinberg, Phys. Rev. D 17, 275 (1978).

TABLE OF CONTENTS

WEAK DECAYS

Stanley Wojcicki
Stanford University

I. Introduction

These lectures will attempt to cover a subject of weak decays from the phenomenological point of view. Clearly, a subject this wide cannot hope to cover all of the possible material in 3 lectures, and thus a choice needs to be made as to what should be included and what excluded. In making this choice I have been guided by the following considerations:

a) the last few years have witnessed a whole spectrum of new theoretical and experimental successes and thus it appears reasonable to emphasize these new results and ideas.

b) In the same last few years there has been a profound change in our ideas as to the number of "elementary"quark and lepton fields. Accordingly, I would like to emphasize the relation of the recent results to this new "standard" theoretical model.

c) Some of the burning questions of five years ago appear to have been settled experimentally in the last few years. Accordingly, as far as the "old" physics is concerned I would like to limit myself to the discussion of those topics that either have received recent experimental attention or else are relevant to the "new" physics being pursued more recently. For more detail on this subject I refer the interested reader to the lectures on this topic at the SLAC Summer Institute of 1972[1] or to several other more recent reviews in the intervening time.[2]

These lectures will thus divide themselves naturally into the following topics:

a) Introduction, discussing the general framework within which we view the weak decays, some of the relevant fundamental questions and the standard model against whose predictions the new results on new particles can hopefully be tested in the near future.

b) Discussion of the weak decays of "old" (i.e. noncharmed) hadrons.

c) Discussion of the decays of heavier leptons, i.e. μ and τ decays with the emphasis on new results.

d) Discussion of the decays of charmed particles.

I shall start out the introductory discussion by reviewing very briefly some of the sacred tenets of the weak interaction theory. The general Lagrangian thought to be responsible for the weak interactions in general (and hence weak decays in particular) is

$$\mathcal{L}_{\text{eff}} = \frac{G}{\sqrt{2}} J_\lambda^\dagger J_\lambda$$

where G is the weak interaction coupling constant and J_λ is the current which can be decomposed into the hadronic and leptonic parts, i.e.

$$J_\lambda = J_\lambda^{(h)} + J_\lambda^{(\ell)}$$

The individual components of the current are written in terms of the fundamental fields, i.e. quarks and leptons, based on the belief that the subsequent "dressing" of the quark fields into physically observable hadrons will not obscure the basic features of the fundamental weak interactions.

Thus to understand the full structure of the relevant currents one has to understand the full spectrum of quarks and leptons. It is here, that there has been a very profound revolution in the last few years and I would like to briefly summarize what is our current understanding of this topic. One might start out with some general features that appear to be emerging from both the theoretical and experimental work.

a) $SU(2) \times U(1)$[3] appears to be an important gauge theory group. The spectacular recent successes[4] supporting the Weinberg-Salam model strongly suggest that this group must play an important part in the ultimate theory of weak interactions.

b) Charged weak currents have a lefthanded nature.

c) Leptons and quarks appear in doublets. Some of the empirical evidence for τ lepton not being a singlet will be discussed in Part 3.

d) An "elegant" theory demands an equal number of quark and lepton doublets to cancel the divergences in the triangle graphs (Adler anomalies).

e) Quark mass eigenstate doublets are different from the doublets diagonalizing the weak interactions. The natural question arises here whether the same statement holds true for the leptons.

f) The discovery of the τ[5,6] and the rapidly growing evidence confirming the leptonic nature of the τ suggest that a six quark, six lepton picture is the most economical one that can accommodate all of the known particles.

I would like to end this introduction by elaborating more fully on these last two points. It has been known for a long time that the up (or p) quark couples both with the down and strange quark, the latter coupling leading to the observable effects of strangeness violation. In the

conventional language this has been known as the Cabibbo mixing,[7] where the relative strengths of the $\Delta S=0$ and $\Delta S=1$ transitions were given by $\cos^2\theta_c$ and $\sin^2\theta_c$. The observed strong suppression of the strangeness changing neutral current transitions[8] as evidenced by the absence of the decays $K_L^o \to \mu^+\mu^-$ and $K^+ \to \pi^+\nu\nu$, coupled with the observation at CERN,[9] and later at Fermilab,[10] of the strangeness conserving neutral currents in neutrino interactions, led to the hypothesis of the fourth quark and the so called GIM model.[11] This model provided a natural, up to second order, suppresion of these phenomena, and the spectacular verification of its many predictions, culminating in the discovery of the bare charm[12] led to the acceptance of this 4-quark picture.

The ideas described above can be recast and generalized in an n-quark formalism where the bare quarks can be placed in mass eigenstate doublets $(P_i N_i)$ with the charges of the two members given by $Q_P = 2/3$ and $Q_N = -1/3$. On the other hand the lower members of the doublets that diagonalize the weak interactions are now given by

$$d_i = A_{ik} N_k \qquad i,k = 1, \ldots n$$

and A_{ik} is an n x n unitary matrix. Because of arbitrary phases of the quark fields and the one overall arbitrary phase, one has $(n-1)^2$ free parameters in the A matrix. In the conventional 4 quark picture, we have n=2, and hence 1 free parameter, traditionally called the Cabibbo angle, θ_c. This leads to the A matrix given by

$$A = \begin{pmatrix} \cos\theta_c & \sin\theta_c \\ -\sin\theta_c & \cos\theta_c \end{pmatrix},$$

which relates the traditional bare quark doublets (p n) and (c λ), to the Q=-1/3 members of the weak interaction doublets i.e.

$$n_w = n\cos\theta_c + \lambda \sin\theta_c$$
$$\lambda_w = -n \sin\theta_c + \lambda \cos\theta_c$$

These ideas have been generalized to the 3 doublet picture by Kobayashi and Maskawa.[13] The 4 free parameters are now 3 "Euler angles" and 1 phase, and the whole matrix can be written as

$$A = \left(\begin{array}{c|c|c} C_1 & -S_1C_3 & -S_1S_3 \\ \hline S_1C_2 & C_1C_2C_3 - S_2S_3e^{i\delta} & C_1C_2S_3 + S_2C_3e^{i\delta} \\ \hline S_1S_2 & C_1S_2C_3 + C_2S_3e^{i\delta} & C_1S_2S_3 - C_2C_3e^{i\delta} \end{array}\right)$$

where $S_i = \sin\theta_i$ and $C_i = \cos\theta_i$.

Clearly, if S_2 and S_3 are small, as appears to be indicated by the data,[14] (see below) one recovers all of the standard 4 quark phenomenology, with only small couplings for the potential new (t, b) doublet with the other 2 old doublets. The other attractive feature of the K-M model is the natural appearance of a small amount of CP violation without the necessity of introducing a very small, i.e. $\sim 10^{-3}$, parameter characterizing the CP violation.

The obvious question, and one that can only be answered experimentally, is whether this dichotomy between the mass eigenstates and the weak interaction eigenstates is also present in the lepton sector. If so, then we can expect transitions between different lepton doublets, leading to expectations of possible $\mu \to e\gamma$ decay mode. We shall say more about this in the chapter on lepton decays.

Finally one must pose the fundamental question, i.e. can we say anything about maximum potential proliferation of quark and lepton doublets. The

theory says very little here and the number of flavors in principle is unlimited. However there have been recently put forth cosmological arguments,[15] based on the big bang theory and the relative abundance of helium in the universe. This argument is summarized in Fig. 1, which shows that with the present measurement of the helium abundance, the number of additional lepton doublets cannot exceed 2 or 3.

Another limit, albeit far less stringent, can be obtained from the limits on the partial widths of the bound heavy quark states, i.e. ψ,T,etc. into neutrinos, as pointed out by J. Ellis in a parallel series of lectures.[16] In principle, those states have to decay via

$$\psi \to \nu\bar{\nu} \ , \quad T \to \nu\bar{\nu}$$

and existence of more lepton doublets will provide more open channels, leading to a larger width. Experimentally, this decay mode could be observed[17] in a step reaction

$$\psi' \to \psi \, \pi^+\pi^- \ , \ \psi \to \nu\bar{\nu}.$$

Finally, more recently Ma and Okada[18] have suggested measuring the rate for $e^+e^- \to \gamma\nu\bar{\nu}$ as a means of obtaining total number of possible lepton flavors.

II. "Old" Hadronic Decays

In this section we shall discuss several topics dealing with the weak decays of "old" i.e. noncharmed hadrons. Specifically the 5 distinct questions we shall address are:

a) Status of the Cabibbo theory

b) Form factors in the semileptonic decays

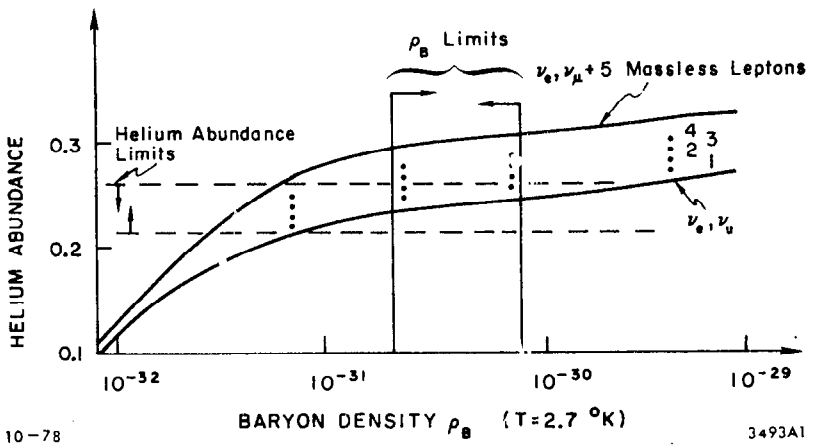

Fig. 1 Helium abundance in the universe versus baryon density as a function of number of neutrino types.

c) $\Delta I=1/2$ rule in hadronic decays

d) Status of the CP violation

e) Status of the $\Delta S=1$ neutral current decays.

In each case we shall emphasize both the most recent results, as well as the relevance of those ideas to our extended "standard" model of six quarks.

a) Cabibbo Theory. The Cabibbo theory was able to extend the basic ideas of Feynman and Gell-Mann's CVC theory to strangeness changing currents by applying the symmetry ideas embodied in SU_3. More specifically the theory firstly provided an elegant framework which incorporated many of the observed regularities in the semileptonic decays of the hadrons, i.e.

1 - Suppression of the hyperon leptonic decays with respect to the nuclear β decays

2 - The $\Delta S=\Delta Q$ rule

3 - $\Delta I=1/2$ rule in semileptonic decays

4 - Absence of $\Delta S=2$ transitions.

Furthermore, however, the theory had a considerable predictive power and its predictions were readily subjected to the experimental tests in the immediate future. We shall start out this section with a brief outline of the basic ideas of the Cabibbo theory, followed by a discussion of the comparison of the experimental results with the predictions of the theory.

The CVC theory incorporated the strangeness conserving charged weak current as a member of an isotopic spin triplet, whose neutral member was the vector part of the electromagnetic current. The Cabibbo theory extended these ideas to strangeness changing currents by postulating that all currents have transformation properties of members of an octet under SU_3. Since we have not only vector weak currents, but also axial weak currents, two distinct SU_3 octets are necessary to incorporate all the possible currents.

To be more specific, the construction of the actual currents can be seen by considering the direct product of two octets, i.e. a baryon and antibaryon one where the baryon octet is given by

$$B = \begin{pmatrix} \frac{1}{\sqrt{2}}(\Sigma^o + \frac{1}{\sqrt{3}}\Lambda) & \Sigma^+ & p \\ \Sigma^- & \frac{1}{\sqrt{2}}(-\Sigma^o + \frac{1}{\sqrt{3}}\Lambda) & n \\ \Xi^- & \Xi^o & -\frac{2}{\sqrt{6}}\Lambda \end{pmatrix}$$

and there is a comparable octet for the antibaryons. The direct product of 2 octets can be decomposed as follows:

$$8 \otimes 8 = 27 + 10 + \overline{10} + 8 + 8 + 1$$

Thus we see that there are 2 possible octets in the final sum, i.e. 2 possible ways to couple 2 octets to give us an octet. These are traditionally decomposed into the symmetric coupling (D coupling) and antisymmetric coupling (F coupling). Thus the most general formulation of the weak currents would involve two terms (and thus two arbitrary coupling strengths) for both the axial and vector currents, i.e. we could write symbolically :

for the vector current: $D_V\, 8_S + F_V 8_A$

and for the axial current $D_A\ 8_S + F_A\ 8_A$

where the D_V, D_A, F_V, F_A are the coupling constants and the 8_S and 8_A, the symmetric and antisymmetric couplings of the baryon antibaryon octets. The requirement that CVC be incorporated automatically into the Cabibbo scheme imposes some constraints however. These can be seen most readily if we examine the exact nature of the $\Delta S=0$ coupling for both the symmetric and antisymmetric case.

For the symmetric case we have

$$\frac{2\ \bar{\Lambda}\Sigma^+}{\sqrt{6}} + 2\ \frac{\overline{\Sigma^-}\Lambda}{\sqrt{6}} + \bar{n}p + \overline{\Xi^-}\Xi^0$$

and for the antisymmetric case

$$\sqrt{2}\ \overline{\Sigma^-}\Sigma^0 + \sqrt{2}\ \Sigma^0\Sigma^+ - \overline{\Xi^-}\Xi^0 + \bar{n}p$$

Thus we see that the symmetric coupling generates a transition between members of different isotopic spin multiplets i.e. $\Sigma \to \Lambda$, a transition that is contrary to the CVC hypothesis. The only way to reconcile the CVC requirement is to demand that this particular coupling vanish, i.e. $D_V=0$ (note that no corresponding requirement exists for the axial currents). Furthermore, by the CVC hypothesis, the strength of the other vector coupling is now completely determined.

The additional Cabibbo hypothesis involves the idea that there is a mixing between the $\Delta S=0$ and $\Delta S=1$ parts of the hadronic current. This mixing is parametrized by one number θ_c, in such a way that the strength of the $\Delta S=0$ transitions is given by $\cos^2\theta_c$ and of the $\Delta S=1$ transitions by $\sin^2\theta_c$. Thus we have 3 free parameters in the theory, D_A, F_A, and θ_c. In principle, the mixing angle could be different for the axial and vector currents giving rise to an additional free parameter. In practice, however, the overall global fit to all of the data is not improved if we allow this extra degree of freedom, so for the purpose of subsequent discussion we shall deal with but one Cabibbo angle.

We have to ask next how do we relate these parameters to the actual observables that we measure in the laboratory. As the bulk of the information comes from the baryonic semi-leptonic decays we shall consider them in some detail. The matrix elements for the vector and axial transitions can be written as

$$\mathcal{M}_V^{\lambda} \propto \begin{pmatrix}\cos\theta_c\\ \sin\theta_c\end{pmatrix} \bar{u}_i \left[f_1(q^2)\gamma^{\lambda} + i\ f_2(q^2)\sigma^{\lambda\rho}\ q_\rho + f_3(q^2)q^{\lambda}\right] u_j$$

$$\mathcal{M}_A^{\lambda} \propto \begin{pmatrix}\cos\theta_c\\ \sin\theta_c\end{pmatrix} \bar{u}_i \left[g_1(q^2)\gamma^{\lambda}\gamma^5 + i g_2(q^2)\sigma^{\lambda\rho}\gamma^5 q_\rho + g_3(q^2)\gamma^5 q^{\lambda}\right] u_j$$

where $\cos\theta_c$ ($\sin\theta_c$) is the multiplicative factor appropriate for the $\Delta S=0$ ($\Delta S=1$) transition, u_i and u_j are the baryon spinors and f_i and g_i the form factors that by Lorentz invariance can depend only on the 4 momentum transfer between the two baryons.

We can now make some assumptions that simplify the whole situation considerably. Firstly, as q^2 is quite low in all the "old" baryon weak decays, we assume that the form factors are constant in the physical region. Secondly, since the contribution of g_3 is multiplied by m_i^2, that term is irrelevant for the electronic decays. Thirdly, f_3 and g_2 are forbidden if second class currents are absent, so we also neglect them. Finally, the contribution of f_2 is small, so it is customary to assume for it the theoretical value.

The form of the symmetric and antisymmetric couplings discussed above

yields then the following values for f_1 and g_1 expressed in terms of D and F axial coupling strengths for the baryonic semileptonic decays accessible to the experimental study:

Table I. Cabibbo expressions for form factors.

Decay	f_1	g_1	f_2/f_1	Mixing Multiplier
$n \to pe^-\nu$	1	D+F	$\mu_p - \mu_n$	$\cos\theta_c$
$\Sigma^\pm \to \Lambda \ell^\pm \nu$	0	$\sqrt{2/3}$ D	$-3/2\mu_n/D^*$	$\cos\theta_c$
$\Sigma^- \to n\ell^-\nu$	-1	D-F	$\mu_p + 2\mu_n$	$\sin\theta_c$
$\Lambda \to p\ell^-\nu$	$-3/\sqrt{6}$	$-\frac{1}{\sqrt{6}}$ (D+3F)	μ_p	$\sin\theta_c$
$\Xi^- \to \Lambda\ell^-\nu$	$-3/\sqrt{6}$	$-\frac{1}{\sqrt{6}}$ (D-3F)	$\mu_p + \mu_n$	$\sin\theta_c$

* f_2/g_1 for this decay only

Thus a measurement of g_1 constitutes a measurement of a specific linear combination of D and F coupling constants, and once θ_c is known, this measurement determines a straight line in the D-F space. The prediction of the Cabibbo theory is that there exists an angle θ_c for which all of these lines will intersect at a point (within the approximation of the theory and the experimental errors). The position of this point will determine the D and F coupling constants.

It remains accordingly to discuss the kinds of measurements that allow us to determine f_1 and g_1. These can be divided into five categories and are summarized briefly below:

1 - Decay rate (i.e. branching ratio combined with the lifetime) is proportional to $|f_1|^2 + 3|g_1|^2$.

2 - Measurement of the recoil spectrum of the nucleon (identical to measuring the angle between ℓ and ν, i.e. $\theta_{\ell\nu}$). More specifically we must have

$$\frac{d\sigma}{d\cos\theta_{\ell\nu}} = \frac{1}{2}(1 + \alpha_{\ell\nu}\cos\theta_{\ell\nu}) \text{ with } \alpha_{\ell\nu} = \frac{|f_1|^2 - |g_1|^2}{|f_1|^2 + 3|g_1|^2}$$

3 - Shape of the lepton spectrum.

4 - Decay asymmetry (if the initial baryon is polarized).

5 - Polarization of the final state baryon.

At the present time the available experimental input can be grouped into 9 different kinds of experiments. Some of these reactions must yield the same answer independent of the Cabibbo theory, as a "more fundamental" symmetry principle is also operative. In these cases the two reactions are grouped together, as they contribute only one independent piece of data to the overall Cabibbo fit. The individual experiments are listed below in Table II.

Table II

Different experiments entering into the Cabibbo fit

Reaction	Type of Measurement	Comment
1) $n \to pe^-\nu$	Overall decay	---
2) $\Lambda \to pe^-\nu^-$ $\Lambda \to p\mu^-\nu$	Decay rate	Connected by the μ-e universality
3) $\Sigma^- \to ne^-\nu$	e-ν correlation	---
4) $\Sigma^- \to ne^-\nu$ $\Sigma^- \to n\mu^-\nu$	Decay rate	Connected by the μ-e universality
5) $\Lambda \to pe^-\nu$	Decay asymmetry	---
6) $\Sigma^- \to \Lambda e^-\nu$ $\Sigma^+ \to \Lambda e^+\nu$	Decay rate	Connected by charge symmetry
7) $\Xi^- \to \Lambda e^-\nu$	Decay rate	---
8) $\Sigma^- \to ne^-\nu$	Decay asymmetry	Measures sign of g_1/f_1. Two measurements disagree.
9) $\Sigma^- \to \Lambda e^-\nu$ $\Sigma^+ \to \Lambda e^+\nu$	Decay chain	Tests CVC. Does not effect the parameters resulting from the Cabibbo fit.

The main part of the original work on hyperon semileptonic decays comes primarily from low energy K^-p bubble chamber work and electronic low energy associated production experiments. The last few years have seen the experimental innovation of hyperon beams and the bulk of the recent information on this topic has come from primary beam hyperon decays.

There have been two new high statistics experiments measuring the neutron spectrum in the $\Sigma^- \to ne^-\nu$ decays, which disagree however with each other at the level of three standard deviations. The Yale-NAL-BNL experiment at the Brookhaven AGS[19] obtained for the ratio of form factors $|g_1|f_1| = 0.435 \pm 0.035$ while the Orsay-Ecole Polytechnique group[20] quotes $|g_1|f_1| = 0.17^{+0.07}_{-0.09}$ based on their work at the CERN PS. The overall situation on the Σ decay is summarized in the accompanying table.

Table III

$\Sigma^- \to ne^-\bar{\nu}_e$ Form Factor Measurements

Group	Method	Events	$\|g_1\|f_1\|$
Maryland	Dalitz plot and (e,ν) Correlation	49	0.23 ± 0.16
Heidelberg		33	$0.37^{+0.26}_{-0.19}$
Columbia - Stony Brook		36	$0.29^{+0.28}_{-0.29}$
Yale - NAL - BNL	Neutron Spectrum	3507	0.435 ± 0.035
Orsay-Ecole Polytechnique		519	$0.17^{+0.07}_{-0.09}$
Heidelberg	Lepton Spectrum		(+) 0.20 ± 0.28
Berkeley	Electron asymmetry with polarized Σ^-	61	(-) $0.19^{+017}_{-0.20}$
BNL, Mass, Yale		63	(+) $0.33^{+0.85}_{-0.30}$
Oxford et al.		43	(+) $0.40^{+1.5}_{-0.52}$

Two new pieces of experimental information on the decay $\Sigma^- \to \Lambda e^-\nu$ from the Σ beam work have been published in the last few years. The Yale-NAL-BNL group has performed an analysis of their 55 reconstructed $\Sigma^- \to \Lambda e^-\nu$ events to obtain $f_1|g_1 = -0.17\pm0.35$ based on the assumption that the weak magnetic form factor is given by the theory. The Pittsburgh-BNL group has measured[21] the branching ratio for that decay mode to be $(0.60\pm0.06)\times10^{-4}$.

Finally, in the same experiment, the Pittsburgh-BNL group has measured the branching ratio for the decay $\Xi^- \to \Lambda e^-\nu$ as $(0.31\pm0.11) \times 10^{-3}$ and obtained a preliminary upper limit[22] for the mode $\Xi^- \to \Sigma^0 e\nu$ of 1.3×10^{-4}.

As yet, there are no new results from the work on the neutral hyperon beams, although there is in progress at this time an extensive high statistics study of lambda beta decay by the UMass-BNL group[23] involving some 150,000 examples of this decay.

Regarding the overall fit of all the baryon data to the Cabibbo theory one can probably say that the fit is quite good but the numerical values of the parameters (especially of the D and F coupling constants) are uncertain due to the confusion regarding the $\Sigma^- \to ne^-\nu$ situation. As an example the fit by Roos[24] to all the data in 1971 (i.e. before the hyperon beam data were available) gave

$$\theta_c = 0.239 \pm 0.003$$

$$\alpha = \frac{D}{D+F} = 0.638 \pm 0.009$$

That fit utilized the world average value of $|g_1|f_1|$ of that time of 0.23 ± 0.10 and a negative sign i.e. in agreement with the Berkeley result.

On the other hand, a subsequent fit performed by the Yale group[19] which included their new Σ^- data and a value

$$\left|\frac{g_1}{f_1}\right| = 0.413 \pm 0.033$$

gave for the values of the parameters

$$\theta_c = 0.232 \pm 0.003$$

$$\alpha = 0.651 \pm 0.008$$

Clearly the CERN result is closer to the old average of $|g_1|f_1|$ but an average of the different experiments is probably not meaningful because of the large discrepancy between the two measurements. The other recent results quoted above are consistent with the predictions for the overall fit and their inclusion would not change the value of the fit significantly. In overall summary one might say that the two sets of values quoted above probably represent a reasonable estimate of the systematic uncertainty on these parameters, due to possible systematic uncertainties in some of the measurements.

For completeness, one should summarize here the results obtained for the Cabibbo angle θ_c from other data.

a) from the rates for $K^+ \to \mu^+\nu$ and $\pi^+ \to \mu^+\nu$ one obtains

$$\frac{f_K}{f_\pi} \tan\theta_c = 0.2755 \pm 0.0007$$

In the limit of perfect SU_3 symmetry, i.e. $f_K = f_\pi$, one obtains $\theta_c = 0.269$.

b) from the K_{e_3} rate and form factor analysis one obtains

$$f_+(0) \sin\theta_c = 0.220 \pm 0.002$$

Again, if one takes $f_+(0)=1$, since SU_3 symmetry breaking effects should be here of second order, one obtains the results $\theta_c = 0.222 \pm 0.002$.

c) finally a comparison of μ decay with nuclear β decay transitions yields[25] after inclusion of the radiative corrections

$$\cos^2\theta_c = 0.948 \pm 0.004$$

One might combine this last result with the value of $\sin\theta_c$ from the baryonic decays to obtain (using $\sin\theta_c = 0.235 \pm 0.004$)

$$\sin^2\theta_c + \cos^2\theta_c = 1.003 \pm 0.004.$$

This last comparison is very interesting in the framework of the heavy quark phenomenology. In the Kobayashi-Maskawa picture this sum becomes

$$\cos^2\theta_1 + \cos^2\theta_3 \sin^2\theta_1 = 1.003 \pm 0.004$$

and thus the difference of this sum away from unity is a measure of $\sin^2\theta_1 \sin^2\theta_3$. Thus at the 95% confidence limit we obtain the result that

$$\sin^2\theta_1 \sin^2\theta_3 < 0.005$$

or

$$\sin^2\theta_3 < 0.09$$

giving us an upper limit on the strength of the possible coupling of the p quark to the b quark.

b) Form factors in K semileptonic decays. This topic has been a subject of considerable experimental controversy as recently as 5 years ago and also appeared to be one area where the theoretical ideas of current algebra might be in some disagreement with the data. In the last several years, however, considerably improved experiments appear to have converged upon a common answer, one that appears to be in good agreement with the theoretical predictions. In this section I shall attempt briefly to summarize some of the recent work on this subject.

I start out by reviewing briefly the formalism used in the form factor analysis. The general V-A matrix element in $K_{\ell 3}$ decays is

$$\mathcal{M} = \frac{G}{\sqrt{2}} \sin\theta_c \left[f_+(q^2)(p_K+p_\pi)^\lambda + f_-(q^2)(p_K-p_\pi)^\lambda \right] J_\lambda^\ell$$

where $\sin\theta_c$ is the sine of the Cabibbo angle, and f_+ and f_- the two form factors describing the decay. It is convenient to define two other form factors, i.e.

$$\xi(q^2) \equiv f_-(q^2)/f_+(q^2)$$

and $$f_o(q^2) \equiv f_+(q^2) + \frac{q^2 f_-(q^2)}{m_K^2 - m_\pi^2}$$

and since the range of q^2 in the region of interest (i.e. physically accessible region) is relatively small, we might hope that a linear expansion of the form factors is justified, i.e.

$$f_+(q^2) = f_+(0)\ (1 + \lambda_+\ q^2/m_\pi^2)$$

$$f_o(q^2) = f_o(0)\ (1 + \lambda_o\ q^2/m_\pi^2)$$

It is conventional to use here $f_o(q^2)$ rather than $f_-(q^2)$ since this is the form factor that is more meaningful from the theoretical point of view.

Traditionally, the $K_{\ell 3}$ studies have provided a rich testing ground for some of the theoretical ideas that form the cornerstones of the weak interaction theory. More specifically one can test here:

1) General V-A nature of the decay (i.e. absence of S, P, and T interactions).
2) $\Delta I = 1/2$ rule, which predicts that the form factors for the K^o and $K^\pm$ must be the same.
3) μ-e universality, which states that λ_+ as derived from K_{e_3} and $K_{\mu 3}$ must agree with each other (contribution of $f_-(q^2)$ to K_{e_3} decay is negligible). In addition, under this hypothesis the K_{μ_3}/K_{e_3} branching ratio must be entirely determined by λ_+ and λ_o.
4) SU_3 breaking effects. In the limit of perfect SU_3, $\xi(q^2)=0$; furthermore up to second order in SU_3 breaking effects, $f_+(0)=1$.
5) Current algebra, i.e. Callan-Treiman prediction.[26] Specifically, it states

$$\frac{f_o(m_K^2)}{f_+(0)} = \frac{f_K}{f_\pi f_+(0)}$$

which gives $f_o(m_k^2) = 1.26\ f_+(0)$. The test of this prediction involves extrapolation to the unphysical region, since the physical region extends only to about $q^2 \approx \frac{m_K^2}{2}$. Assuming linear extrapolation, as motivated partly by the Dashen-Weinstein theorem,[27] this prediction yields $\lambda_o \approx 0.021$.

6) $K^*(890)$ dominance of the $f_+(q^2)$ form factor. Assuming this pole form, and fitting to a linear variation of the form factor, one obtains $\lambda_+ = 0.029$.

It was mainly on these last three points that there appeared for a long time to be a serious confrontation both between different experiments, and also between the experiment and theory. Before discussing the situation in detail, one must enumerate three kinds of experiments that can provide information on f_+ and f_o form factors.

1) Measurement of the Dalitz plot population yields λ_+ from a study of K_{e_3} decays and λ_+ and λ_o from a study of $K_{\mu 3}$ decays.
2) Direction of polarization of the muon in K_{μ_3} decay gives the value of $\xi(q^2)$, and thus of $f_o(q^2)$ if $f_+(q^2)$ is known.
3) K_{e_3}/K_{μ_3} branching ratio gives a quadratic relationship between λ_+ and λ_o.

There are several general experimental comments that one can make about these experiments, that, at least in my mind, help to understand some of the potential difficulties in obtaining and understanding some of these results available in the literature.

1) The branching ratios for the K^+ decay modes are rather low (10^{-2}-10^{-1}).

Thus the sample of $K^+_{\mu 3}$ decays can be easily contaminated by the process $K^+ \to \pi^+\pi^o$, followed by $\pi^+ \to \mu^+\nu$ decay in flight.

2) A 2-fold ambiguity in reconstructing the K^o decay provides some confusion on an event by event basis.

3) It is important for the polarization measurements to have the capability both to precess the μ's and to reconstruct the position on the Dalitz plot. This technique allows one to measure directly the direction of the polarization vector rather than its magnitude along some direction. The relative sensitivity to the level of understanding of the Monte Carlo, polarimeter, etc. is considerably reduced in this kind of arrangement.

4) At low q^2, the sensitivity to variations in $f_o(q^2)$ is considerably poorer than at high q^2. This is true both for the Dalitz plot and polarization measurements (see Fig. 2).

5) Partly as a result of the spinoff from CP violation studies, there has been in the last few years a considerable statistical improvement in the K^o Dalitz plot studies.

Having made these rather general comments, I would like now to summarize the experimental status of the $K\ell_3$ form factor situation. Rather than quoting world averages, a job that is done much better by the Particle Data Group, I limit myself to a personal assessment of the present status.

Regarding the λ_+ situation, I feel that a world average is probably meaningful for $K^+_{e_3}$ decay since these experiments are relatively bias free. On the other hand, the $K^+_{\mu 3}$ experiments are much more bias prone, and the existing experiments do not really allow one to disentangle the strong correlation between λ_+ and λ_o. Thus a simple average is probably not very significant

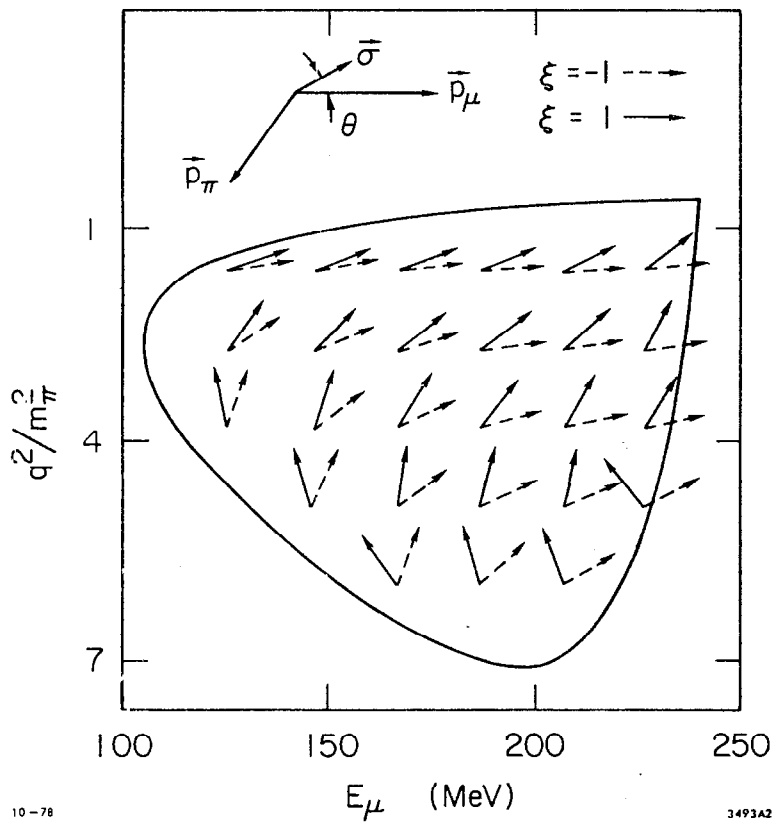

Fig. 2 Muon polarization as a function of Dalitz plot position for Re $\xi = \pm 1$, Im $\xi = 0$. The orientation of the momentum vector is shown at the top of the figure.

in this case. Finally, the situation regarding $K^o_{\mu_3}$ and $K^o_{e_3}$ is entirely dominated by the recent two high statistics experiments,[28,29] and I think it is more meaningful to just quote those two results. In Table IV I display the averages for the two K^+ decays from the Particle Data Group compilation[30] and the values for K^o decays from the two high statistics experiments. As can be seen, the agreement is excellent even for the most suspect average, i.e. $K^+_{\mu_3}$. Furthermore, the values agree with the $K^*(890)$ dominance prediction.

Table IV. λ_+ status in $K\ell_3$ decays

Decay	λ_+	Reference
$K^+\to e^+\pi^o\nu$	0.0285±.0043	30
$K^+\to\mu^+\pi^o\nu$	0.026 ±.008	30
$K^o\to e^\pm\pi^\mp\nu$	0.0312±.0025	28
$K^o\to\mu^\pm\pi^\mp\nu$	0.030 ±.003	29
K^+ dominance prediction	0.029	

As far as the status of the λ_o is concerned, I choose to be even more arbitrary in quoting the relevant results. I quote only the 2 recent high statistics polarization results[31,32] from experiments that both precess the muons and reconstruct the event; the world average[30] for $K^+_{\mu 3}$; Donaldson et al.[27] value for $K^o_{\mu_3}$; the world averages for the λ_o from K^+ and K^o branching ratios, but also separately the one from the most recent experiment[33] measuring the $K^+_{\mu_3}/K^+_{e3}$ relative branching ratio. For reasons mentioned above, the K^+ world average values are probably the most suspect ones. All the values mentioned above are summarized in Table V. Even though the agreement is far from excellent, there appears to be no reason to doubt the validity of the Callan-Treiman prediction, especially if the two suspect averages are partially deemphasized.

Table V. λ_o status in $K\ell_3$ decay

Experiment		λ_o	Reference
$K^+\to\mu^+\pi^o\nu$	Polarization	0.008±0.021	32
$K^o\to\mu^\pm\pi^\mp\nu$	Polarization	0.044±0.009	31
$K^+\to\mu^+\pi^o\nu$	Dalitz Plot	-0.003±0.007	30
$K^-\to\mu^\pm\pi^\mp\nu$	Dalitz Plot	0.019±0.004	29
$K^+_{\mu_3}/K^+_{e_3}$	BR	0.014±0.012	30
$K^+_{\mu_3}/K^+_{e_3}$	BR	0.019±0.010	33
$K^o_{\mu_3}/K^o_{e_3}$	BR	0.037±0.011	30

I would like to end the discussion of form factors with a few comments about $K\ell_4$ decays. In the last few years a Geneva-Saclay experiment[34] studied a sample of 30000 K_{e_4} decays, attaining a considerable statistical improvement over the previously published data. Their overall results can be briefly summarized as follows:

a) the form factors are in fair agreement (∿25% level) with the current algebra predictions.

b) π-π phase shifts obtained from this analysis of $K\ell_4$ decays are consistent with those obtained from the π-π scattering experiments.

c) scattering length is consistent with the PCAC prediction.

d) there is no evidence[35] for $\Delta S/\Delta Q$ forbidden decay $K^+\to\pi^+\pi^+e^-\nu$. The obtained 95% C.L. upper limit is

$$\Gamma(K^+_{e_4}(e^-))/\Gamma(K^+e_4(e^+)) < 3.4 \times 10^{-4}$$

c) $\Delta I=1/2$ rule in hadronic decays. We examine here very briefly the general theoretical framework in which this rule has to be viewed, its main experimental implications, and the present experimental status regarding the validity of this rule.

We can start out with two very simple minded ideas. Firstly, if we look at a 4 quark coupling e.g. $(s\bar{p})(n\bar{p})$ that is presumably responsible for the strange particle decay, then we see that a priori the effective Hamiltonian can involve either $\Delta I=1/2$ or $\Delta I=3/2$ in this transition. On the other hand, experimentally the $\Delta I=3/2$ transitions appear to be relatively suppressed. The assumption that $\Delta I=3/2$ transition is identically zero leads to several quantitative predictions; alternatively we can say that the deviation of the experiment from these predictions will allow one to estimate the size of this amplitude. The wide range of the kinds of predictions that are obtained under the assumption of the vanishing of the $\Delta I=3/2$ amplitude are illustrated below:

1) Branching ratios: $\Lambda\to p\pi^-/\Lambda\to n\pi^o=2 \quad K_s^o\to\pi^+\pi^-/K_s^o\to\pi^o\pi^o=2$

2) Lifetimes: $\tau_{\Xi^o} = 2\,\tau_{\Xi^-}$

3) Decay asymmetries: $\alpha(\Xi^o) = \alpha(\Xi^-) \quad \alpha(\Lambda\to p\pi^-)= \alpha(\Lambda\to n\pi^o)$

4) Suppression of decay modes: $K^+ \not\to \pi^+\pi^o$

5) Dalitz plot population: $G_1 = G_2 = 0$

where $G_1 = g_{+-o} - g_{+oo}$

$$G_2 = g_{++-} + \frac{1}{2} g_{+-o}$$

and g is the coefficient in front of the T_{π^o} term (or odd T_π term) in the expression for Dalitz plot density for $K \to 3\pi$.

It should be added that the above predictions must be corrected for the obvious electromagnetic effects, e.g. mass differences.

The second observation (which may or may not be related to the question of $\Delta I=1/2$ rule) has to do with the apparent enhancement of the decays $\Lambda\to p\pi^-$ (i.e. purely hadronic decays) with respect to the semi-leptonic decays (e.g. $\Lambda\to pe^-\nu$). In a simple quark picture the two types of decay proceed via the processes illustrated in Fig. 3. If the coupling of the W boson to quark antiquark system is of the same strength as to the $\ell\nu$ system, as indicated by universality, then the relative strength of these diagrams (for a single color state in the case of the quark diagram) should be equal except for phase space arguments. This simple minded picture predicts that the electronic decay of the Λ would be of the order of 20% times phase space correction, a prediction that appears too high by at least an order of magnitude Other more complicated possible diagrams, however, would upset this simple prediction.

Are these two observations related? The answer would be yes if for some reason the $\Delta I=1/2$ part of the purely hadronic weak Hamiltonian were "enhanced" with respect to the naive prediction.

This is basically the origin of the idea of octet enhancement. If the Hamiltonian is of the current-current form, each current being a member of an octet, then their direct product can be written as

$$8 \times 8 = 27 \oplus 10 \oplus \overline{10} \oplus 8 \oplus 8 \oplus 1$$

The $\Delta I=3/2$ part (which is contained only in the 27 representation) would be suppressed if the effective Hamiltonian itself also transformed like an octet, i.e. the octet part in the sum were enhanced.

How valid are these simple minded arguments? This is certainly a complex question and we shall limit ourselves here to two statements. Firstly, the theoretical situation[36] is not very clear and it is not obvious how big a special dynamical enhancement is really necessary here.

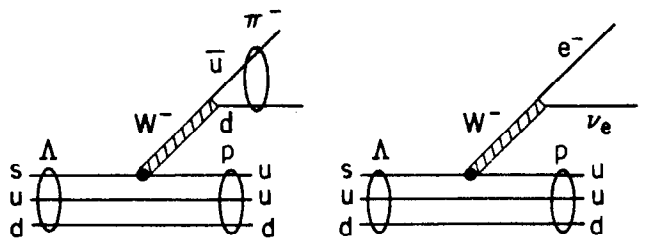

10-78 3493A3

Fig. 3 Simple quark picture for Λ hadronic and beta decays.

Conceivably, a test of $\Delta I=1/2$ rule in a system involving another SU_3 multiplet, e.g. Ω^- decay, might shed some light here. Secondly, these ideas and questions can be extrapolated to the higher group of SU_4 that we have to deal with when we discuss the question of charm non leptonic decays. We shall return to this specific point in the last chapter on charm decays.

We might briefly end this section with a short summary of the experimental situation on the status of the $\Delta I=1/2$ rule. In general, it appears that there does exist a finite $\Delta I=3/2$ amplitude, above and beyond purely electromagnetic corrections, whose magnitude is of the order of few percent of $\Delta I=1/2$ amplitude. Furthermore, in decays where such amplitudes could a priori contribute (e.g. $K\to 3\pi$) there appears to be no need for $\Delta I=5/2$ or $7/2$ at the level of 1% of the dominant amplitude.

As an example we quote several illustrative, and thus by no means exhaustive, examples of the relative magnitudes of the $\Delta I=3/2$ and $\Delta I=1/2$ amplitudes:

1) $A_{3/2}/A_{1/2}$ in $K \to 2\pi$ decay[36] $= 0.0448 \pm 0.0002$

2) $S_{3/2}/S_{1/2}$ in Λ decay[37] $= 0.027 \pm 0.008$

3) $S_{3/2}/S_{1/2}$ in Ξ decay[38] $= 0.041 \pm 0.015$

In addition, the analysis of the decay rates and the slopes of the various charge states for the $K \to 3\pi$ also indicate[39] clear violation of the $\Delta I=1/2$ rule.

d) CP violation. The observation in 1964 by Christenson et al.[40] of the apparent decay process $K_L^o \to \pi^+\pi^-$ has led during the next few years to a burst of experimental and theoretical activity. This activity appears

to have culminated after a decade of hard work in the conclusion that no presently experimentally accessible CP violation effects exist outside of the K^o system and that the superweak model of Wolfenstein[41] appears to adequately explain all the data. The question of CP violation received recently renewed theoretical interest, by virtue of its possible manifestation[42] in the weak decays of the anticipated heavy quark states. In this section we briefly review the experimental situation that led to the conclusions stated above.

The fact that the process observed by Christenson et al. was indeed due to CP violation and not to some other strange phenomena was established shortly after the initial discovery. Possible effects due to cosmological forces[43] were soon excluded by lack of any energy dependance in the branching ratio[44] and the possibility that the observed process is really due to the decay of some new particle was killed by an interference observed between the K_L^o and the regenerated K_S^o component.[45] The spectacular difference that can be seen in more recent experiments, between the no interference and interference hypothesis is illustrated in Fig. 4, taken from the latest high statistics work at BNL.[46]

To discuss the experimental work on CP violation in the K^o-$\overline{K^o}$ system one must define a minimum amount of formalism:

$$\text{Defining } |K_1^o> = \frac{|K^o> + |\overline{K^o}>}{\sqrt{2}} \quad \text{and} \quad |K_2^o> = \frac{|K^o> - |\overline{K^o}>}{\sqrt{2}}$$

$$\text{and} \quad |K_L^o> = \frac{|K_2^o> + \varepsilon|K_1^o>}{\sqrt{1 + |\varepsilon|^2}} \quad |K_S^o> = \frac{|K_1^o> + \varepsilon\ |K_2^o>}{\sqrt{1 + |\varepsilon|^2}}$$

$$\text{leads to } <K_L^o|K_S^o> = 2\ \text{Re}\ \varepsilon$$

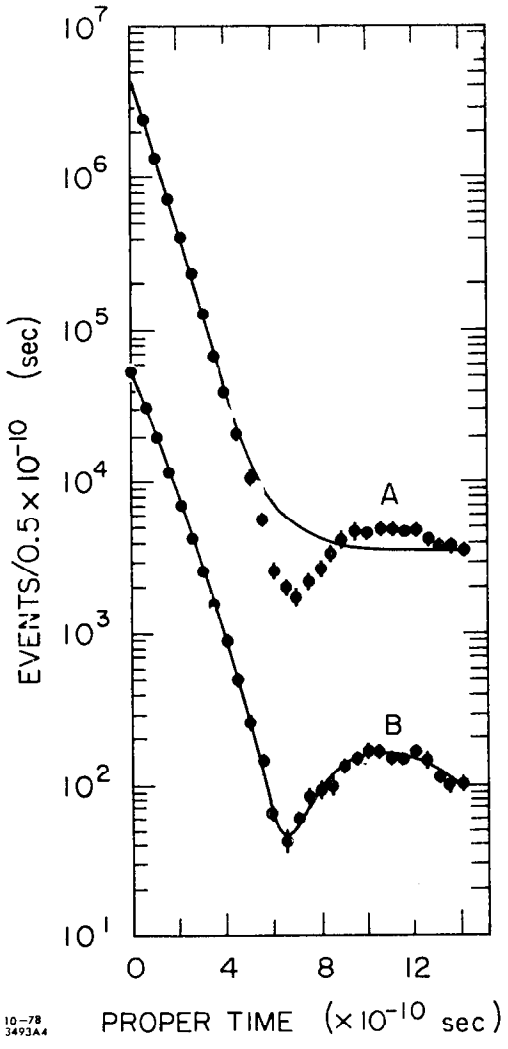

Fig. 4 Time distribution of $K^o \to \pi^+\pi^-$ events behind a regenerator. Curve A is the best fit obtained under the assumption of no interference between K_L^o and K_S^o; curve B is the fit with interference effects.

i.e. ϵ is just a measure of CP violation in the mass matrix. In addition, CP violation effects can exhibit themselves also through a violation in the $K\to 2\pi$ decay amplitude itself.

We define $A_{0,2}$ as the amplitude for $K\to 2\pi$ decay leading to the 2π system in T=0(2) state. Taking A_0 to be real, we define

$$\epsilon' = \frac{i}{\sqrt{2}}\, e^{i(\delta_2-\delta_0)}\ \mathrm{Im}\, A_2/A_0$$

where $\delta_{0,2}$ are the $\pi-\pi$ scattering phase shifts in the T=0(2) state. Thus CP violation in the decay amplitude simply means a non zero phase between the T=0 and T=2 amplitudes.

We can furthermore define two "experimental" parameters that are related more closely to the actual empirical observations:

$$\eta_{+-} = \frac{A(K_L^o\to\pi^+\pi^-)}{A(K_S^o\to\pi^+\pi^-)} \qquad \eta_{oo} = \frac{A(K_L^o\to\pi^o\pi^o)}{A(K_S^o\to\pi^o\pi^o)}$$

These two sets of complex amplitudes are related by

$$\eta_{+-} = \epsilon + \epsilon' \qquad \eta_{oo} = \epsilon - 2\,\epsilon'$$

We should next mention the different types of experiments that can provide some of the information about these parameters

1) Measurement of $K_L^o\to\pi^+\pi^-$ determines $|\eta_{+-}|^2$
2) Measurement of $K_L^o\to\pi^o\pi^o$ determines $|\eta_{oo}|^2$
3) Interference between $K_L^o\to\pi^+\pi^-$ and $K_S^o\to\pi^+\pi^-$ gives phase of η_{+-}.
4) Interference between $K_L^o\to\pi^o\pi^o$ and $K_S^o\to\pi^o\pi^o$ gives phase of η_{oo}.
5) Charge asymmetry in $K\ell_3$ decays yields Re ϵ.

In addition two other pieces of information can be obtained from the data from non-CP experiments.

6) $\pi-\pi$ phase shifts measurement (from $\pi-\pi$ scattering or $K\ell_4$ decays) yields phase of ϵ'.
7) From the unitarity condition one obtains the relation

$$-i(m_L-m_S) + \frac{\gamma_L+\gamma_S}{2}\ \langle K_L^o|K_S^o\rangle = \sum_f \langle f|T|K_L^o\rangle^*\langle f|T|K_S^o\rangle$$

Because of $\Delta I=1/2$ rule and very low decay rate of K_S^o into any other than 2π channel, only important state $|f\rangle$ is $|2\pi$'s in T=0 state$\rangle$. The right hand side can then be simplified to $\gamma_S\epsilon^*$ and we obtain the relation

$$\tan\arg\epsilon = \frac{2(m_L-m_S)}{\gamma_S} \qquad \text{since } \gamma_S \gg \gamma_L.$$

A graphical way to summarize these data has been suggested by Wu and Yang[47] and is schematically illustrated in Fig. 5.

The statistical and systematic precision of the recent experiments is extremely high and the parameters of the CP violation discussed above can now be determined with very high accuracy.[2] We enumerate here briefly some of those results as compiled by Kleinknecht,[2] and compare them with the predictions of superweak theory (which demands $\epsilon'=0$).

Experimentally we have

$$\Phi_{+-} = 44.9 \pm 1.3^o$$

$$\Phi_{oo} = 48.0 \pm 13.1^o$$

to be compared with the superweak prediction for both of these of

$$\tan^{-1}\frac{2(m_L-m_S)}{\gamma_S} = 43.8 \pm 0.2^o$$

For the ratio of amplitudes we have experimentally

$$|\eta_{oo}|/|\eta_{+-}| = 1.008 \pm 0.041$$

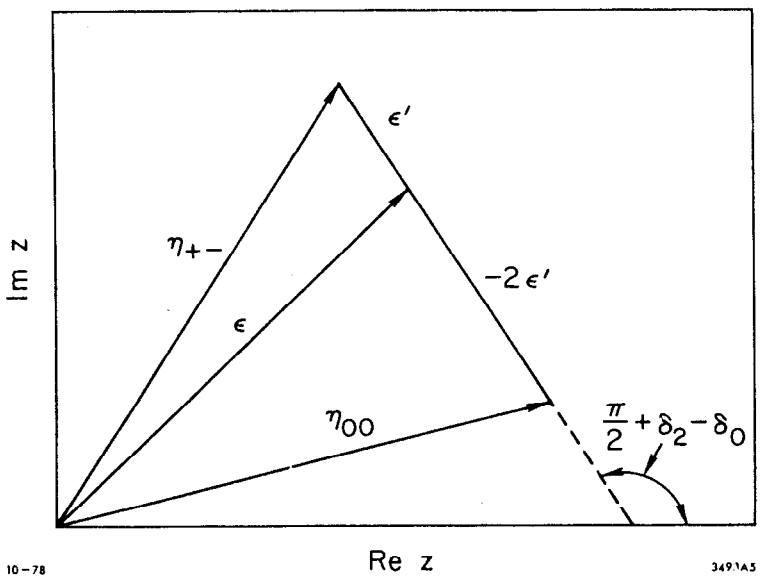

Fig. 5 A schematic representation of the Wu-Yang triangle.

to be compared with unity in superweak theory.

And finally, from charge asymmetry experiments

$$2 \text{ Re } \epsilon/|\eta_{+-}| = 1.448 \pm 0.055$$

to be compared with the prediction of

$$2 \cos (43.8 \pm .2^{o}) = 1.443 \pm 0.005.$$

Clearly the agreement of the data from the K^{o}-$\overline{K^{o}}$ system with the superweak theory is excellent. The results are displayed graphically in Fig. 6 in terms of a Wu-Yang triangle.

For the sake of completeness one should mention that no statistically significant CP (or T) violation has been seen in any other system. The other kinds of experiments looking for those effects included a whole variety of diverse phenomena, such as detailed balancing in nuclear and particle reactions, η and η' charge asymmetry, T violation in $\Delta Q=-\Delta S$ $K\ell_3$ decays, transverse polarization in $K_{\mu 3}$, charge asymmetries in $\bar{p}p$ annihilations, hyperon decays, etc.

By far the most promising place to look for T violating effects appears to be the neutron electric dipole moment which must vanish if either parity or time invariance are good, i.e. absolutely conserved. The present experimental limit[48] i.e. $D_n=(0.4 \pm 1.1) \times 10^{-24}$ e cm, where D_n is the neutron electric dipole moment, appears to exclude all but superweak models from among the "conventional" models of CP violation.

One can ask to what extent the Kobayashi-Maskawa[13] model, with its natural small CP violation, is compatible with all of these experimental results. The answer is that the predicted effects would be far smaller than the existing limits and thus within the present experimental uncertainties, the superweak model and the K-M model are undistinguishable.[42]

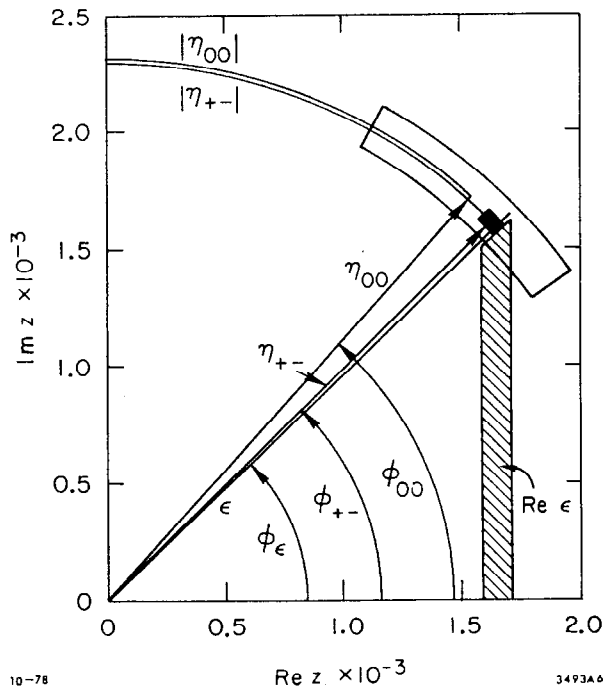

Fig. 6 The K^o CP violation data displayed on the Wu-Yang triangle. The values come from the compilation by Kleinknecht (Ref. 2).

For example, one would expect a finite electric dipole moment for the neutron due to contributions of diagrams illustrated in Fig. 7, but anticipated order of magnitude is only about 10^{-28}-10^{-31} e cm. One does however expect in this model potentially observable effects in the decays of new particles composed of heavy (i.e. b and t) quarks.

e) Status of the $\Delta S=1$ neutral current decays. It was the apparent absence of the $\Delta S=1$ neutral current decays, demonstrated most dramatically in the processes

$$K_L^o \to \mu^+\mu^-$$

and $K^+ \to \pi^+\nu\bar{\nu}$

that led to the formulation of the GIM mechanism. In addition, however, the original search by Clark et al.[8] for the decay mode $K_L^o \to \mu^+\mu^-$ set an upper limit for this process that was significantly lower than the so called unitarity limit due to the 2γ intermediate state (see Fig. 8). Since that time, however, three different groups[49,50,51] have studied this process, and all obtained mutually consistent results that were also slightly above the unitarity limit. The original Berkeley result has been recently revised slightly upward,[52] taking into account a new value of $|\eta_{+-}|$ that was used in the flux determination, and correcting small errors in the original Monte Carlo calculation. It still remains however significantly below the unitarity limit. The overall situation is summarized in Table VI.

For completeness, we should mention that the $\Delta S=0$ counterpart of the $K_L^o \to \mu^+\mu^-$ decay, i.e. $\pi^o \to e^+e^-$ process, has now been observed[53] with a branching ratio of $(2.23^{+2.4}_{-1.1}) \times 10^{-7}$ (90% C.L.). This number should be

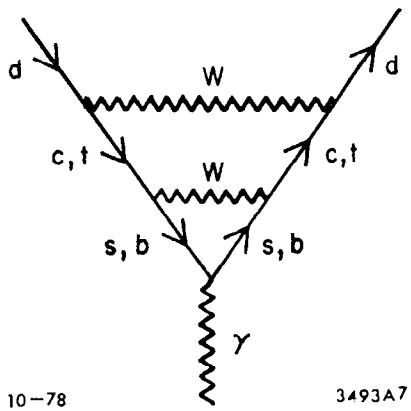

Fig. 7 Typical diagrams involving heavy quarks that give rise to a finite neutron electric dipole moment.

compared with the unitarity limit of 4.75×10^{-8}, and is in fair agreement with the calculations for the second order electromagnetic process by vector mesons.

Table VI

Status of $K_L^o \to \mu^+\mu^-$ branching ratio measurements*

Group	Value($\times 10^{-7}$)	Reference
Berkeley	<3.1(90% C.L.)	52
Columbia - BNL	12^{+8}_{-4}	49
Princeton - U. Mass	$8.8^{+10.7}_{-5.5}$	50
Chicago-Argonne	$9.4^{+2.8}_{-1.8}$	51
Unitarity Limit	6	

* All measurements have been adjusted to the value of 0.21% for $K_L^o \to \pi^+\pi^-/K_L^o \to$ all.

We finally end with some comments about the decay $K^+ \to \pi^+ \nu\bar{\nu}$. The experiment[8] of J. H. Klems et al. designed to search for this mode set a 90% C.L. limit of 1.4×10^{-6} on its branching ratio by looking for energetic π's unaccompanied by any other particle. Thus this apparatus would have been also sensitive to the possible decay:

$$K^+ \to \pi^+ h$$

where h is any light, non-interacting particle. Because of the two body nature of this decay, the sensitivity of the experiment to this mode is even higher and one can interpret the result as setting a branching ratio limit for this mode[54] of 2.7×10^{-7} (90% C.L.). The importance of this result stems from the fact that the existence of a low-mass isoscalar pseudoscalar meson (referred to as axion or higglet) is very attractive

from the theoretical point of view[55] since it prevents the appearance of strong interaction CP violating effects in QCD and gauge theories of weak interactions. If the axion exists, the theory gives a branching ratio[54,55] for the decay $K^+ \to \pi^+ h$ comparable (within an order of magnitude or so) to the upper limit quoted above.

III. Lepton Decays

We divide this chapter into three sections:

a) discussion of μ decay with special emphasis on the new results on exotic decay modes of the muon

b) few brief comments about neutrinos

c) our present understanding of the τ lepton.

Clearly in the spirit of trying to emphasize the newest results, the large fraction of this chapter shall deal with the τ.

a) μ decay. For a long time the muon decay

$$\mu^{\pm} \to e^{\pm} \nu_e \nu_\mu$$

was the unique accessible purely leptonic process. Accordingly, it was a good testing ground for the theory of weak interactions, insofar that this transition is unencumbered by the difficulties associated with the presence of hadrons. This uniqueness aspect of μ decay has disappeared in the last few years as technological improvements and new discoveries have provided us with several new laboratories of pure leptonic interactions. For example, in neutrino interactions we can study the processes

$$\nu e \to \nu e$$

$$\nu e \to \nu \mu \quad \text{(i.e. inverse } \mu \text{ decay)}$$

$$\nu Z \to \ell^+ \ell^- \nu Z \text{ (in the field of the nucleus)}$$

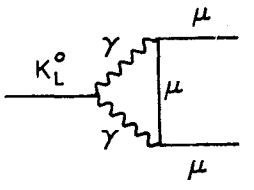

Fig. 8 The diagram for the $K_L^o \to \mu^+ \mu^-$ decay via a two photon intermediate state.

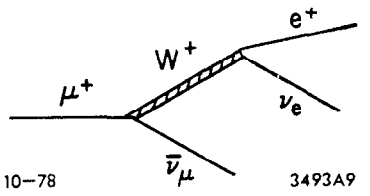

Fig. 9 Conventional diagram for $\mu^+ \to e^+ \nu_e \bar{\nu}_\mu$ decay.

and in the colliding beams

$$\tau \to e\nu\nu$$

$$\tau \to \mu\nu\nu$$

$e^+e^- \to \mu^+\mu^-$ (or $\tau^+\tau^-$) for weak-electromagnetic interference.

The historical importance of the muon is still there, however. Furthermore, the μ decay provides an opportunity to do very high statistics experiments, albeit in the low q^2 region, and thus test the weak interaction models to a high degree of accuracy.

It is important to remember that to a very high accuracy the muon is a point particle without any anomalous interactions. This conclusion is reached on the basis of the remarkable agreement between the theory and experiment in a variety of experiments involving the muon, i.e. the hyperfine structure of the muonium,[56] the g-2 of the muon,[57] and the production cross section of muon pairs in high energy e^+e^- collisions.[58] Thus we can have great confidence that the μ decay does test solely the weak interaction diagram illustrated in Fig. 9.

We shall commence our discussion by seeing how well do the μ decay data agree with the standard model of weak interaction,[59] i.e. a model incorporating universality in the framework of the Cabibbo theory and a V-A interaction. Rather than looking at the most general complete theoretical expression for the μ decay, we shall examine it piece by piece in such a way as to be able to compare specific experimental measurements with the predictions of various models. It is conventional in this kind of comparison to look at 6 different experimental parameters.

1) The decay rate i.e. the lifetime of the muon. This is the test of μ-e universality and of the Cabibbo theory, since the integrated muon decay rate measures weak interaction constant squared G^2, and nuclear β decay $G^2\cos^2\theta_c$. We have already previously discussed Cabibbo theory universality in a slightly different context. Here we merely restate the result as

$$\sin^2\theta_c + \cos^2\theta_c = 1.003 \pm 0.004$$

i.e. an excellent agreement with Cabibbo universality.

2) Overall spectrum of the decay electron. If we define a parameter x

$$x = E_e/E_e^{max}$$

and integrate over all the other variables, then we obtain the expression for the electron energy spectrum

$$N(x)\,dx \alpha x^2\left[1 - x + \frac{2}{9}\rho\,(4x-3)\right]dx$$

In general, i.e. for an arbitrary mixture of S, P, T, A, and V interactions, we have the restrictions

$$0 \le \rho \le 1$$

whereas V-A demands $\rho = 0.75$.

The experimental value is 0.752 ± 0.003.

3) Decay asymmetry parameter (averaged over all x). Defining as θ the angle between the direction of the μ spin orientation and the momentum vector of the decay electron, the most general distribution in the variable cos θ is

$$N(\cos\theta)\,d\cos\theta\ \alpha(1 + P\,\frac{\xi}{3}\cos\theta)\,d\cos\theta$$

For the most general case, the restrictions on ξ are

$$0 \le |\xi| \le 3 - \frac{8}{3}\rho$$

whereas V-A dictates $\xi = 1$

The experimental value is $\xi = 0.972 \pm 0.013$.

4) The decay asymmetry parameter is in general a function of x, and thus can vary in magnitude (or even change sign) as the energy of the decay electron is varied. This variation is described by a parameter conventionally called δ, and the double distribution is given by

$$N(x,\cos\theta)dxd\cos\theta \propto x^2\left\{\left[1-x+\frac{2\rho}{9}(4x-3)\right] \mp \frac{\xi}{3}\cos\theta\left[1-x+2\delta(4x-3)\right]\right\} dxd\cos\theta$$

The most general restriction is

$$|\xi\delta| \leq \rho$$

and the V-A predicts $\delta = 0.75$

The experiment gives $\delta = 0.755 \pm 0.009$.

5) Helicity of the decay electrons. In general, since parity is violated in μ decay, the decay electrons will be longitudinally polarized along their direction of flight in the muon rest frame, i.e. have a non-zero helicity.

The general requirement on the helicity h is

$$0 \leq |h| \leq 1$$

whereas V-A demands $h_+ = +1$, $h_- = -1$

and the experiment gives:

$$h_+ = 1.03 \pm 0.13$$

$$h_- = -0.89 \pm 0.28$$

6) The low end of the electron energy spectrum. That end of the energy spectrum is influenced by a parameter η, as the general formula for the spectrum contains the term

$$N(x)dx \propto x^2\left[\ldots\ldots + \frac{m_e}{m_\mu}\frac{(1-x)}{x}\eta\right]dx$$

The most general restriction on η is

$$0 \leq |\eta| < 1$$

whereas V-A predicts that $\eta = 0$

The experimental value is $\eta = -0.12 \pm 0.21$.

In conclusion we can say that the μ decay studies are in excellent agreement with the V-A theory. However one can still pose several important questions relevant to this decay. The remainder of this section shall be devoted to the study of those points.

1) How good are the limits on possible admixtures of other possible interactions and how well is the V-A phase determined? In spite of the excellent agreement of the data with a pure V-A theory, there is a surprisingly great deal of room for admixtures of other couplings. We quote here the results of a review by Derenzo[60]

$$|g_S| \leq 0.33\ |g_V|$$
$$|g_T| \leq 0.28\ |g_V|$$
$$|g_P| \leq 0.33\ |g_V|$$

where g_S, g_T, etc. are the strengths of the S, T, etc. couplings. The V-A phase ϕ is measured to be

$$\phi = 180 \pm 15^\circ$$

2) Are the neutrinos really massless? Assuming that the electron neutrino in μ decay is identical to the one in β decay and the muon neutrino identical to that in $\pi \to \mu\nu$ decay we can quote the following upper limits on their masses

$$m_{\nu_e} < 60\ eV^{61)}$$
$$m_{\nu_\mu} < 550\ KeV^{62)}$$

However, there is a considerably better limit on these two neutrino's mass difference from the neutrino oscillations. We shall return to this point in our discussion about neutrinos.

3) What is the exact nature of the 2 neutrinos emitted in the μ decay? More specifically, can we have a multiplicative conservation law operative, where we conserve $L_e + L_\mu$ and $(-1)^{L\mu}$ but not L_e and L_μ separately.[63] Such a law would allow a process

$$\mu^+ \to e^+ \bar{\nu}_e \nu_\mu$$

in addition to $\mu^+ \to e^+ \nu_e \bar{\nu}_\mu$

The present data do not exclude completely this situation even though this would be a rather inelegant theory from the point of view of universality. To discuss this question quantitatively we define the ratio r by

$$r \equiv \frac{BR(\mu^+ \to e^+ \nu_e \bar{\nu}_\mu)}{\mu^+ \to \text{all}}$$

Then r will be 1.0 or 0.5 for additive and multiplicative laws respectively. The results from the recent Gargamelle exposure to the PS ν beam yield:

from the neutrino exposure: $r = 0.9 \pm 0.3$ (from excess of e^+ events)

$r = 1.0 \pm 0.6$ (from lack of e^- events)

and from the antineutrino exposure:

$r = 0.8 \pm 0.2$ (from excess of e^- events)

$r = 1.3 \pm 0.6$ (from lack of e^+ events)

Clearly the data show no evidence for violation of the additive law but are not able to put a very significant limit on the contribution from the multiplicative law. I understand, however, that an experiment currently in progress at the Los Alamos Scientific Laboratory will soon be able to improve on these numbers by almost an order of magnitude.

4) Are there μ-e transitions at any level, or are the L_e and L_μ quantum numbers conserved rigorously? Specifically are the processes

$$\mu^+ \to e^+ \gamma$$
$$\mu^+ \to e\gamma\gamma$$
$$\mu^+ \to e^+ e^+ e^-$$
$$\mu^- Z \to e^- Z$$

totally forbidden? This is the question that has received a great deal of experimental and theoretical attention in the last couple of years and we shall conclude the discussion of μ decay by giving a summary of the present status on this point.

The upper limits given on these exotic processes by the recent experiments are summarized in Table VII.

Table VII

Experimental upper limits on various possible μ-e transitions			
Process	Upper limit (90% C.L.)	Accelerator and Group	Reference
$\mu^+ \to e^+ \gamma$	3.6×10^{-9}	TRIUMF Montreal-UBC-Victoria-TRIUMF-Melbourne	64
	1.1×10^{-9}	SIN ETH-Zurich-SIN	65
	2.0×10^{-10}	LASL LASL-Chicago-Stanford	66
$\mu^+ \to e^+ \gamma\gamma$	5×10^{-8}	Theory + μ→eγ limits	67
μ^- + Sulfur → e^- + Sulfur	4×10^{-10}	SIN Berne	68
$\mu^+ \to e^+ e^+ e^-$	1.9×10^{-9}	Dubna	69

These limits, although representing a significant improvement over what was known several years ago, still allow a wide range of theories with a finite rate for μ-e transitions (see discussion below). Accordingly, one might ask how much further one could push the existing limits, and what are the fundamental background and/or flux limitations on improving these numbers. To be specific we shall consider the decay $\mu \to e\gamma$.

The two serious backgrounds appear to be:

a) simultaneous μ decays, one ordinary decay with an electron near the tip of the spectrum, the other a radiative decay with the γ energy being almost half of the muon mass. Alternatively, the electron from the other decay could give an energetic externally radiated γ ray (for example in the stopping target).

b) $\mu \to e\,\nu\nu\gamma$ process with the two neutrinos almost at rest.

We can estimate very roughly the limitation imposed by each of these potential backgrounds. To avoid the accidental problem, we would want to look at individual μ's, 1 at a time, i.e. μ's should stop in a target with a time interval between different μ's that is long compared to μ lifetime, e.g. 10 μsec. That would give us about 10^{10} μ's a day, and assuming a run of 100 days a potential branching ratio limit of 10^{-12} with a 100% detection efficiency. 10% is probably more reasonable, but on the other hand the spatial extent of the stopping target can be made large enough so that there is no ambiguity problem between μ's stopping in different parts of the target. That factor can probably gain us the loss due to detection efficiency, so that 10^{-12} appears to be an achievable limit.

The background due to radiative decays can be reduced only by improving spatial and energy resolution of the detector. The expression for the branching ratio for $\mu \to e\nu\nu\gamma$ with e and γ going off at 180° with respect to each other is

$$B_{rad}\,(180^{\circ}) = \frac{\alpha}{2\pi}\left[(1-x)^2 + 4(1-x)(1-y)\right] y\,dy\,dx\,d\cos\theta_{e\nu}$$

where we have defined

$$x \equiv E_e/E_e^{max} \qquad y \equiv E_\gamma/E_\gamma^{max}$$

The radiative decay will look like a $\mu \to e\gamma$ decay if within the resolution of our detector all the kinematical variables will be consistent with the 2 body decay. Defining our normalized energy resolution parameters as

$$r_e = \Delta E_e/E_e^{max} \qquad r_\gamma = \Delta E_\gamma/E_\gamma^{max}$$

we obtain[70] the achievable branching ratio limit as

$$\sqrt{B_{rad}} \approx 2.4 \times 10^{-2}\, r_e\, r_\gamma\, \delta\theta$$

where $\delta\theta$ is the error on the e-γ angle.

To give an idea of what has been achieved already, one can quote the relevant parameters for the Stanford-Chicago-LASL experiment

$$r_e = 3.6\% \qquad r_\gamma = 3.3\% \qquad \theta_\gamma = 1.9^{\circ}$$

These set a limit on achievable branching ratio of about 10^{-12}. One can probably improve the resolution on each of these parameters by at least 50%, leading to an order of magnitude improvement on the rate limit. We conclude accordingly that the accidentals probably present the most serious

limitation on the quality of the potential upper limit measurement, and that this limit is somewhere in the vicinity of 10^{-12}.

We turn next to some of the theoretical arguments for the importance of searching for μ-e transitions. The basic point is that in general in gauge theories μ-e transitions can occur at levels that conceivably could be as high as 10^{-9} of the total decay rate. The experimental limits on these exotic processes discussed above can thus put stringent limits on determining which of many possible gauge theories are still viable. We shall briefly enumerate some of the possible models predicting finite rate for μ→e transition.

a) standard model with a heavy neutral lepton (Fig. 10a). If the neutral lepton accompanying the τ is massive[71] then in general there will be mixing among the neutral leptons, and weak interaction eigenstates will not be eigenstates of mass matrix in a manner comparable to the quark situation. The limit on the amount of the mixing is given by the available data on hadron-lepton universality, μ-e universality and nonorthoganality between ν_e and ν_μ. For BR $\gtrsim 10^{-9}$ one needs $m_{L^o} \gtrsim$ 12-30 GeV (the branching ratio is preportional to $(m_{L^o}/m_w)^4$ where m_w is the mass of the intermediate vector boson.

b) Presence of right handed doublets, i.e.[72]

$$\binom{N_e}{e}_R, \binom{N_\mu}{\mu}_R, \cdots$$

with massive neutral partners N_e, N_μ, in addition to the conventional left handed doublets (see Fig. 10b). The transition rate here will be proportional to $\left[\cos\phi \sin\phi \,(m_{N_e}^2 - m_{N_\mu}^2)/m_W^2\right]^2$ where ϕ is the mixing angle and will yield branching ratios $\sim 10^{-10}$ for a mass difference squared

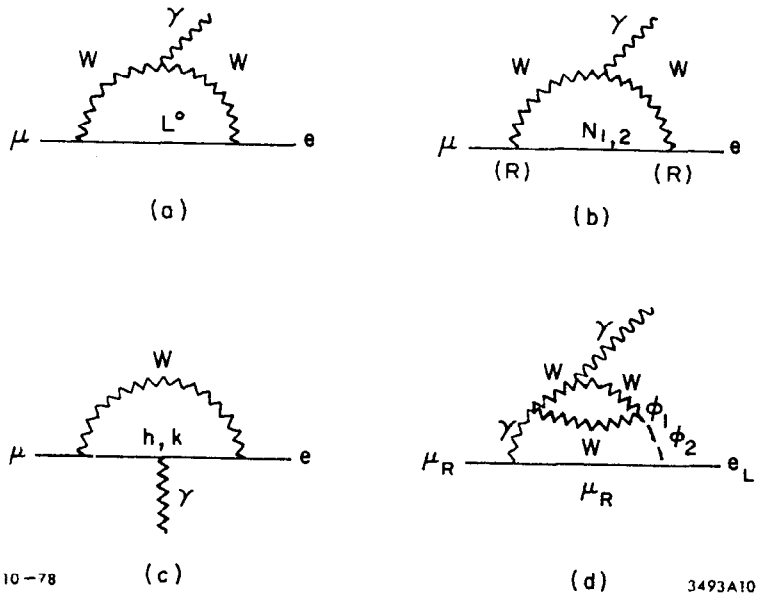

Fig. 10 Examples of possible diagrams generating μ → eγ transitions. h, k in (c) are postulated doubly charged leptons; Φ in (d) is the Higgs boson.

of 1 GeV^2.

c) Left handed lepton triplets, with the third member of the triplet being doubly charged.[73] The doubly charged leptons (called heptons by the authors) mix with a mixing angle ϕ and thus give rise to μ-e transitions (Fig. 10c). The transition rate has a similar dependance on the parameters of the theory as the theory with the right handed doublets.

d) Existence of several scalar bosons[74] (Higgs particles). The dominant contribution in this case to a μ-e transition is via two-loop diagrams, with the scalar boson coupling once to leptons and the second time to some intermediate heavy particle (e.g. Z^o, $W^{\pm}$, or the Higgs boson itself). An example of one of these diagrams is illustrated in Fig. 10d. The order of magnitude of the branching ratio for μ→eγ transition is $(\alpha/\pi)^3$.

Clearly, there can be constructed a variety of other models involving larger gauge groups that can also generate μ-e transitions. The discussion above is by no means meant to be comprehensive but rather illustrate the order of magnitude of various effects that can be expected within the framework of recently popular models.

Finally, one should say a few words about the relative sensitivity of the various "forbidden" processes involving μ-e transition. Clearly a detailed answer can be only given in the framework of a specific model. In general, however, the decay μ→3e is suppressed with respect to the decay μ→eγ by a factor comparable to α/π which one might expect a priori. The exception is the triplet model[73] where the μ→3e process can occur by virtue of non-zero transition charge radius and where this rate can actually be larger than the μ→eγ rate. The nuclear capture process,

$$\mu^- Z \rightarrow e^- Z$$

turns out to be generally the most sensitive probe of potential effects generating μe transitions.[74] The reasons are quite general and stem from the fact that this process can occur coherently on all the nucleons in constrast to the "allowed" μ^- capture in nuclei:

$$\mu^- Z \rightarrow \nu_\mu (Z-1).$$

There is an additional enhancement factor, as large as an order of magnitude for copper, originating from the Pauli principle suppression of the allowed process. The μ-e capture process, leaving the capture nucleus unchanged, is not subject to the same suppression factor and thus is relatively enhanced. There are,however, models where the $\mu \rightarrow e\gamma$ experiment is predicted to be more fruitful. For illustrative purposes we present in Fig. 11 the relative rates calculated by Altarelli et al.[75] for three of the forbidden processes as a function of neutral τ lepton mass assuming standard 6 lepton model and maximum mixing compatible with the data.

b) Neutrino decays and oscillations. In this section we briefly discuss the available limits on neutrino decays and make a few remarks about neutrino oscillations, a topic that has received renewed interest recently in light of the enlarged family of leptons.

If neutrinos have a finite mass, then in principle it is possible for them to decay, the natural mode being

$$\nu \rightarrow X + \gamma$$

where X is some lower lying state. As an example, if $m_{\nu_\mu} > m_{\nu_e}$ and lepton number is not rigorously conserved, then we could have

$$\nu_\mu \rightarrow \nu_e + \gamma$$

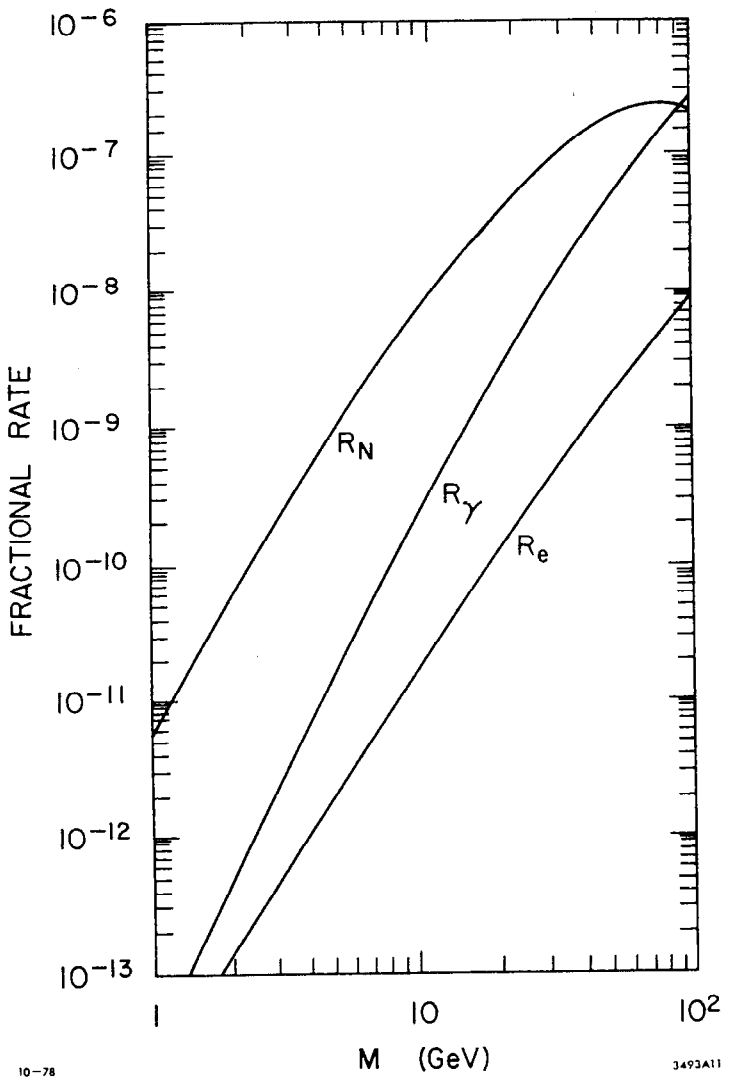

Fig. 11 The fractional rates for μ capture (R_μ), $\mu \to e\gamma$ decay (R_γ), and $\mu \to eee$ decay (R_e) as a function of τ neutrino mass according to the calculation in Ref. 75.

In the exposures of large bubble chambers to the accelerator beams of neutrinos a considerable neutrino path length has been accumulated, the appropriate measurement scale being of the order of light years (2.3 light years for the Argonne experiment).[76] If the general decay mode mentioned above exists, then one should see in the bubble chamber e^+e^- pairs pointing along the ν beam direction, and having a typical energy of the order of half of the neutrino energy. Since this technique measures the decay rate in the lab, that is related to the more fundamental quantities by

$$\Gamma_{LAB} = m_\nu \Gamma / E_\nu^{LAB},$$

one can set limits only on the product of $m_\nu \Gamma$, Γ being the decay rate in the neutrino rest frame. The upper limits obtained by different experiments are enumerated below in Table VIII.

Table VIII.

Experimental Limits on $m_\nu \Gamma$

Type of Neutrino	Limit (90% C.L.)	Experiment	Reference
ν_μ	4.6×10^{-4} MeV/sec	ANL 12' B.C. Argonne-Purdue	76, 77
ν_μ	1.4×10^{-4} MeV/sec	Gargamelle B.C. Milano	78
$\bar{\nu}_\mu$	2×10^{-5} MeV/sec	Gargamelle B.C. Milano	78
$\bar{\nu}_e$	0.8×10^{-8} MeV/sec	Reactor U.C. Irvine	79

One might ask about the significance of these numbers in the content of general gauge theories, by comparing this limit with the limit on $\mu \to e\gamma$ results discussed previously. The latter corresponds to a partial rate of $\sim 1 \times 10^{-4}$ sec^{-1}. We would expect the decay to be proportional to $(m_{lepton})^5$. Thus if we take the existing experimental upper limit for m_{ν_μ}, we obtain a crude theoretical limit on $m_{\nu_\mu} \Gamma_{\nu_\mu} < 1 \times 10^{-16}$ MeV/sec on the assumption

that the same mechanism contributes to the decay $\mu \to e\gamma$ as to $\nu_\mu \to \nu_e\gamma$. Clearly, the existing experimental limits do not approach anywhere near this number.

The neutrino mixing idea has been introduced by Pontecorvo[80] some time ago who observed that if ν_e and ν_μ are not both massless and non degenerate, then the observed states (ν_μ, ν_e) will be different from the mass eigenstates N_1, N_2.[81] Specifically they will appear as linear combinations of N_1 and N_2, characterized by one parameter θ_ν, i.e.

$$\nu_\mu = N_1 \cos\theta_\nu + N_2 \sin\theta_\nu$$

$$\nu_e = -N_1 \sin\theta_\nu + N_2 \cos\theta_\nu$$

Thus in analogy with the K^o-$\overline{K^o}$ system, a beam, composed initially only of ν_μ, can give rise to ν_e after traversing a certain distance ℓ. This probability for effective $\nu_\mu \to \nu_e$ transition is a function of the mixing angle and difference of squares of individual masses, i.e.

$$P = \sin^2(2\theta_\nu) \sin^2\left(\frac{m_1^2 - m_2^2}{4} \frac{\ell}{pc}\right)$$

The present limit on this effect allows us to set a limit[78] on the difference of squares of masses

$$(m_1^2 - m_2^2) < 1 \text{ ev}^2$$

on the assumption that mixing is maximal (i.e. $\theta_\nu = \pi/4$). This is considerably smaller than the limit on individual neutrino masses obtained from direct measurements.

Just as it is with the quark mixing, the situation here also becomes more complex as the number of different leptons increases. The situation for the 3 neutral lepton case has been discussed recently by Cabibbo[82] who showed that in that case phase factors will occur in the mixing matrix, just as for the 6 quark case, which will give rise to time reversal and CP violation effects.

c) Status of the τ lepton. The initial observation[83] of 2 prong $e\mu$ events in e^+e^- annihilations at SPEAR was accompanied by a conjecture that these events are due to the production and subsequent decay of a pair of new particles, denoted initially by U (for unknown) i.e.

$$e^+e^- \to U^+ U^- \quad \begin{cases} \to e^\mp + \ldots \\ \to \mu^\pm + \ldots \end{cases}$$

The absence of any other visible particles besides the $e\mu$ pair led to the natural speculation that one or more neutrinos are emitted in the decay together with the charged leptons.

This hypothesis of production of new particles had to overcome two potentially serious objections, namely:

1) Are these events genuine or could they be misidentified hadrons? One must remember here that the probability of misidentifying hadrons as leptons in this initial experiment was close to 20%.

2) If these events are indeed real, could they be somehow associated with charm production? This question was relevant since the apparent threshold for $U\bar{U}$ production appeared to be the same (within the experimental uncertainty of 100 MeV or so) as that for the charm production.

The first of these questions was soon answered[84] by the PLUTO group at DESY who confirmed the SPEAR results with a much better lepton-hadron discrimination. The unambiguous dissociation of U particles from the charm phenomena was achieved by the observation of 2 prong $e\mu$ events below charm threshold; at the ψ' by the DASP group[85] and at several other energies by the DELCO group.[86] These data dispelled the last remaining objections against the existence of a new phenomena, and the proposed hypothesis of a new

lepton, henceforth referred to as τ, became well accepted.

In the following, I shall try to discuss the evidence leading to the point of view that the τ is most likely another sequential lepton, which together with its own neutrino forms a third doublet of leptons and appears to satisfy e-μ-τ universality. The outline of the discussion will follow the following steps:

1) The τ is apparently a spin 1/2 lepton (i.e. a point particle).

2) The τ needs to have its <u>own</u> neutrino, i.e. the economy model of 5 leptons appears excluded.

3) The τ is unlikely an ortholepton or paralepton.

4) The τ appears to couple to the standard weak interaction current with the standard V-A coupling.

The arguments for the τ being a spin 1/2 lepton have been recently summarized by Tsai.[87] These are by no means unique arguments and a great deal of additional data support this point of view. They do, however, form a rather brief but cogent argument in support of this thesis and we shall summarize them briefly below.

The τ cannot be a baryon (assuming baryon conservation) since if it were a baryon decay, its decay products would have to include a baryon. On the other hand, the missing neutral(s) in the decay

$$\tau \to e\nu + \text{neutral(s)}$$

has been shown to have a mass well below the mass of a proton.[88]

The τ also cannot be a boson, since the τ production threshold clearly exhibits s wave behavior.[86] (see Fig. 12). Since a boson and its antiboson have opposite parity, we cannot have a $\tau^+\tau^-$ production in an s state from an initial J^P state of 1^-. The only possibility is the production process

$$e^+e^- \to \tau\tau^*$$

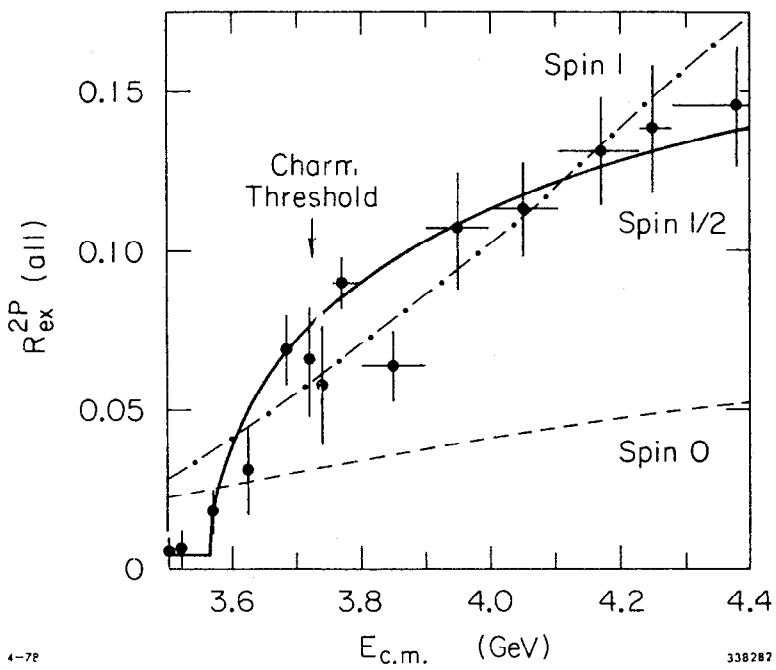

Fig. 12 τ production cross section near threshold as measured in the DELCO experiment. The curves indicate the expected threshold behavior for a pair of spin 0 (dashed), spin 1/2 (solid) and spin 1 particles (dash-dot).

where τ^* is some excited state of the hypothetical τ meson that has opposite parity. In that case the decay mode of τ^* would be expected to be

$$\tau^* \to \tau + \pi^0 \quad \text{or} \quad \tau^* \to \tau \to \gamma$$

leading in either case to a large number of γ rays associated with the $e\mu$ events. Experimentally, this is not observed and the only possible out is to require the τ^*-τ mass difference to be small enough so that the photons would be below the experimental detection threshold.

Finally, the spin of a point particle τ could not be greater or equal to 3/2, since that threshold behavior is much more divergent. That point is dramatically illustrated in Fig. 13, taken from Ref. 87. One is thus led to the conclusion that the τ is most likely a spin 1/2 lepton. The arguments made further on in this section will only reinforce that conclusion.

We consider next the question whether τ could be a lepton singlet, or do the data require it to have its own neutrino? Clearly, the τ would be stable in the former case (contradicting the data), unless there is μ-e-τ mixing. We need to see, therefore, to what extent other available data set limits on the amount of possible μ-e-τ mixing, and what do those limits in turn tell us about the τ properties. This point has been considered in detail by several authors[89] with a conclusion that the singlet possibility is excluded. We review briefly the relevant arguments.

The SU(2) x U(1) classification of the leptons in this case would consist of two lefthanded doublets and one left handed singlet, i.e.

$$\begin{pmatrix} \nu_e \\ E \end{pmatrix}_L, \quad \begin{pmatrix} \nu_\mu \\ M \end{pmatrix}_L, \quad S_L$$

where E, M, and S are linear orthogonal combinations of e,μ, and τ.

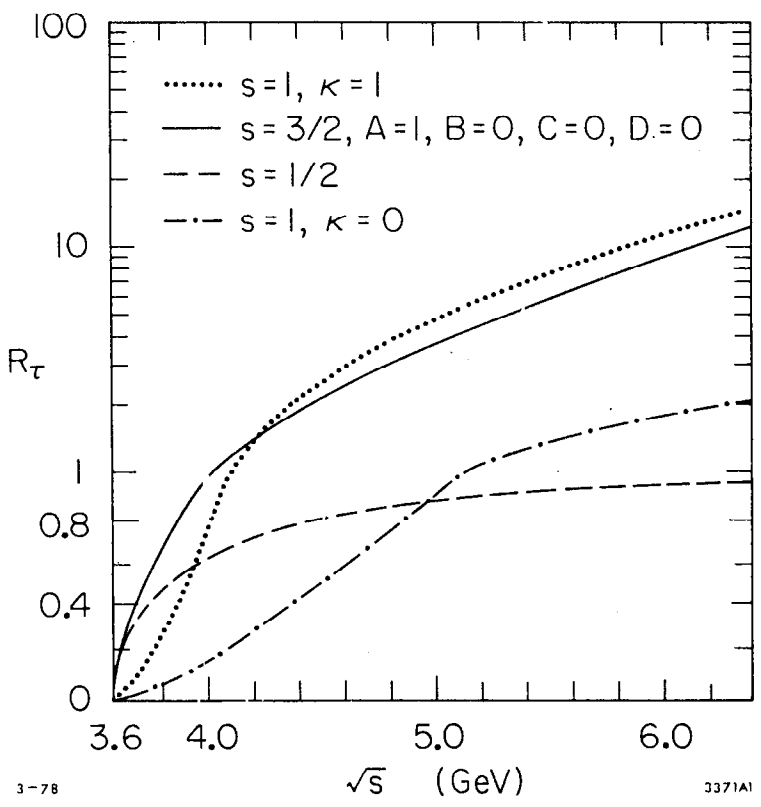

Fig. 13 Expected threshold behavior for a pair of particles with different spins. K, A, B, C, D represent constants related to the gyromagnetic ratio and multipole values of the produced particles (see Ref. 87 for details). Note that the scale of the ordinate is linear up to 1, logarithmic above 1.

The mixing is defined in terms of two real parameters, called γ and β. One can now impose the following limits[90] on γ and β. From the limit on the process

$$\mu^- + Cu \to e^- + Cu$$

one obtains $\beta^2\gamma^2 \leq 5.3 \times 10^{-9}$

and from the limit on the lifetime of the τ, and hence its total decay rate: $\beta^2 + \gamma^2 > 1.0 \times 10^{-1}$.

The only way to make these two limits compatible with each other is by requiring imbalance between β^2 and γ^2, i.e. $\beta^2 >> \gamma^2$ or $\gamma^2 >> \beta^2$. There are, however, two sets of experimental consequences, violated by the data, which are demanded by this imbalance:

1 - the ratio $R_{\mu e} \equiv \Gamma(\tau \to \mu\nu\nu)/\Gamma(\tau \to e\nu\nu)$ must be very close to either 1/2 or 2. The experimental value is very close to unity.[91]

2 - there would have to be an appreciable decay rate into 3 leptons, i.e. of the order of 2-3%. The experimental limits at the 90% confidence limit are better than 1%.[92]

Accordingly one concludes that the economy model of a τ singlet is excluded. We turn now to the possibility that τ is a paralepton,[93] i.e. either a paraelectron meaning that the lepton number assignment for τ^+ is identical to e^-, or a paramuon, which would assign to τ^+ identical lepton numbers as to μ^-. The basic argument which excluded this assignment has to do again with the value of $R_{\mu e}$ defined above. A paraelectron τ^+ could decay either via

$$\tau^+ \to \mu^+ + \nu_\mu + \nu_e \quad \text{(2 distinct neutrinos)}$$

or

$$\tau^+ \to e^+ + \nu_e + \nu_e \quad \text{(2 identical neutrinos)} .$$

Because of the Pauli exclusion principle the rate for the second process would be twice as large as for the first one. Thus for a paralepton assignment, $R_{\mu e} = 2$ or $R_{\mu e} = 1/2$. It has been pointed out however recently by Rosen[94] that this result strictly holds only for a pure V-A assignment for the decay process, which does appear to be favored experimentally (see discussion below). For a more general interaction one could have $R_{\mu e} = 1$ for a paralepton assignment.

An experiment that is relevant to the paralepton question is the search for electrons unaccompanied by muons produced by interactions of predominantly ν_μ beams. Such events could be potential signatures of the process

$$\nu_\mu + Z \to \tau^- + \ldots$$
$$\hookrightarrow e^- + \ldots$$

and similarly for τ^+. These events were looked for by the Columbia-BNL group in the FNAL 15' bubble chamber filled with neon[95]. All the events of this nature which were found were consistent with being produced by the ν_e (or $\bar{\nu}_e$) contamination in the beam, allowing one to set a limit on the production cross section times branching ratio for a paramuon of an arbitrary mass. These upper limits could then be compared with the theoretical production rate for such a heavy muon assuming a V-A coupling of standard strength (see Fig. 14). This result can be interpreted in several ways. It excludes a simple paramuon hypothesis for the τ; if the τ does have a muon lepton number then the strength of ν_μ-τ coupling must be only 2.5% of the ν_μ-μ coupling. Finally, for a mixing model, it limits the mixing angle to $\tan^2\theta < 0.025$.

Another kind of a possible lepton is an ortholepton, i.e. a lepton with identical charge and lepton number as the electron or the muon but with a heavier mass. Thus a possible decay mode for a τ orthoelectron

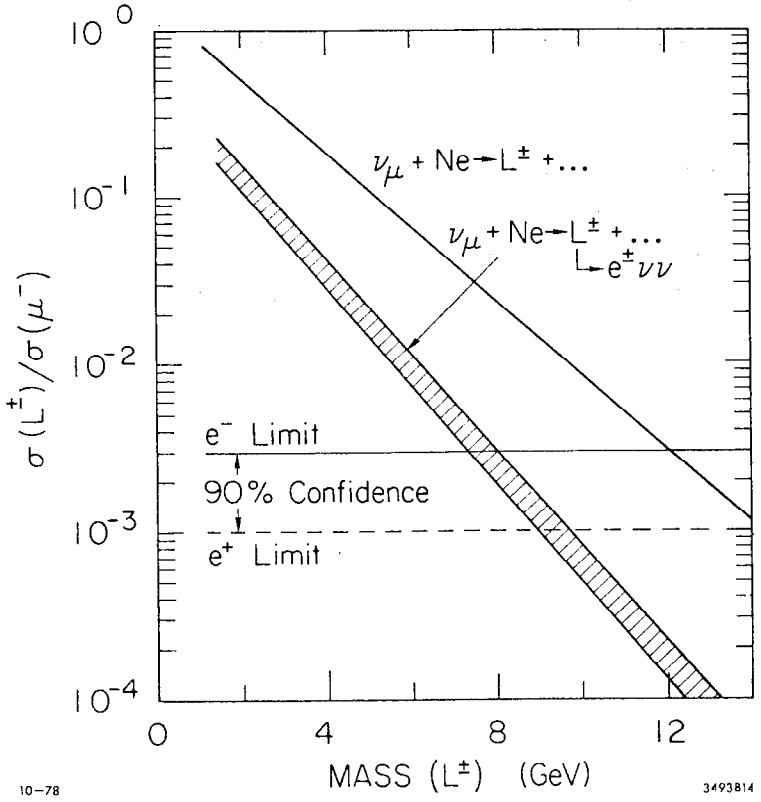

Fig. 14 The expected ratio of heavy lepton to muon production in the Columbia-BNL experiment as a function of the heavy lepton mass together with the experimental 90% confidence limits.

would be

$$\tau^+ \rightarrow e^+ + \gamma$$

and similarly for the orthomuon possibility.

The standard orthomuon picture is again excluded by the bubble chamber experiment discussed above, since that would require again a full strength coupling between ν_μ and τ. The orthoelectron possibility is rather unlikely in light of the low reported branching ratio[96] for $\tau \rightarrow e\gamma$, i.e. $\Gamma(\tau \rightarrow e\gamma)/\Gamma(\tau \rightarrow \text{all}) \leq 2.6\%$ (90% C.L.).

We conclude accordingly that the possibilities other than that of sequential lepton appear to be highly unlikely for the τ, and the most reasonable possibility is that τ forms a new lepton doublet $(\tau\ \nu_\tau)$. The typical decays of the τ might thus be expected to proceed via diagrams illustrated in Fig. 15. The subsequent discussion then naturally will break up into 2 parts; firstly, is the current to which τ couples the standard weak interaction current, i.e. we examine the right hand side of the diagrams of Fig 15; and, secondly, how do the τ and ν_τ couple to this current, i.e. the nature of the left hand side of the vertex.

The first question is answered by studying the different decay modes of the τ and comparing them with the predictions based on the assumption that we are dealing here with the standard current.[97]

1 - equality of electronic and muonic branching ratios. The various measurements relevant here and available as of April, 1978, have been summarized by Feldman.[91] His overall fit to all the data gives $R_{\mu e} = 1.07 \pm 0.17$ to be compared with the theoretical prediction of 0.97. Clearly the agreement is excellent.

2 - absolute value of e,μ branching ratios. The theoretical numbers are here less certain because of the uncertainly associated with the rate into

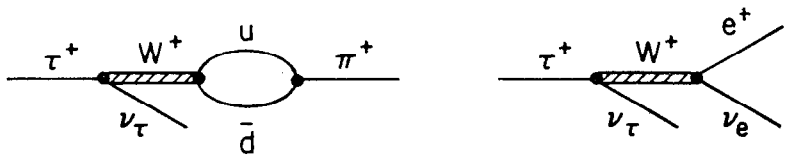

10−78 3493A15

Fig. 15 The standard diagrams for the decay τ→πν and τ→eνν.

multipion final states. The best theoretical estimates are 16.4% for the eνν mode and 16.0 for the μνν mode. These numbers should be compared with Feldman's fit yielding 17.4 ± 2.1% and 18.7 ± 2.0% for the electronic and muonic decay modes respectively, and a recent number for the μνν decay mode from the DELCO experiment[98] of 21±5%.

3 - πν decay mode. The theoretical estimate for this decay rate is on very firm ground, insofar as the calculation relies solely on the π→μν decay rate and the assumption that we are dealing in τ decay with a standard weak current. Accordingly, the early low value for the branching ratio for this mode reported by the DASP group,[99] 2.4 ± 3.0% to be compared with the theoretical 9.8% gave rise to serious doubts as to whether the τ does indeed fit into the standard weak decay picture. Subsequently, however, 3 different experiments have yielded results in very good agreement with the theory, so the issue of the πν decay also appears to be settled in favor of the standard model.

The most direct observation of this mode has been made by the DELCO group[100] who used a hadron filter to identify π's and the Cerenkov counter to identify electrons and thus were able to isolate a sample of the events of the type

$$e^+e^- \to \tau^\pm \tau^\mp \quad \tau^\mp \to \pi^\mp \nu_\tau \quad \tau^\mp \to e^\mp \nu_e \nu_\tau$$

and quote a branching ratio of 8.0 ± 3.2 ± 1.3%, where the first error is statistical and second systematic. The spectrum of π's and μ's (from μνν decay) shown in Fig. 16 agrees very well with the Monte Carlo calculation, supporting the hypothesis of correct identification of the events.

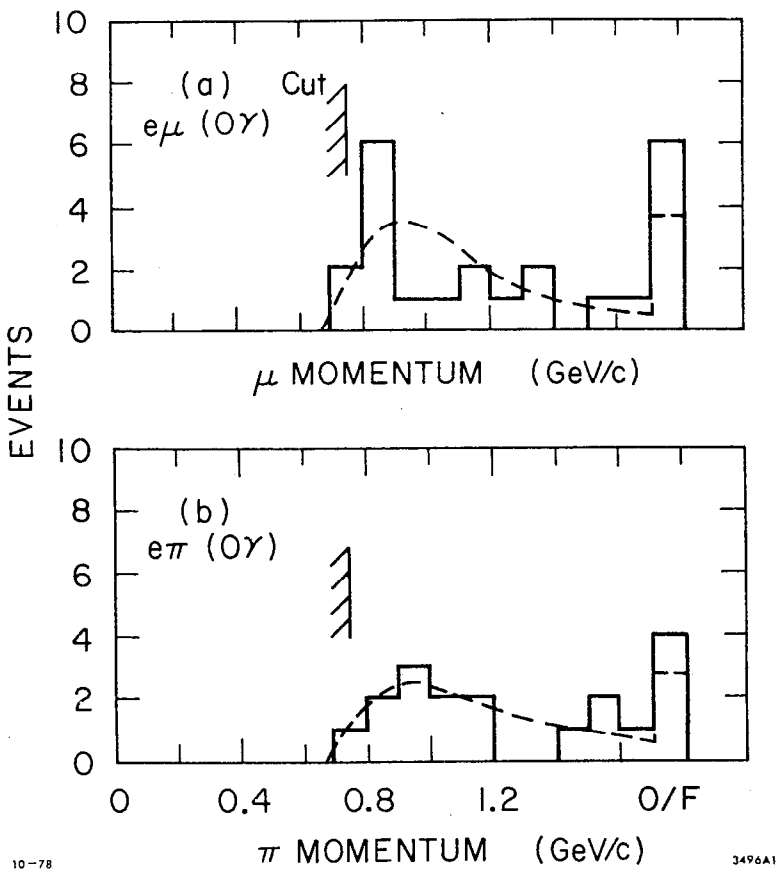

Fig. 16 Momentum spectrum of the μ in eμ events (a) and of the π in eπ, 0γ events (b). The dashed lines indicate the predicted shapes expected from the τ decays. The data is from DELCO.

The SLAC-LBL group used a more indirect method[101] by looking for 2 prong events with an energetic pion and no detected γ rays. A clear excess (Fig. 17) is observed over what one would expect if no $\tau \to \pi\nu$ mode were present. Estimating the hadronic background on the basis of a jet model, they calculate the πν branching fraction to be 9.3 ± 3.9%.

More recently, the PLUTO group[102] has looked for 2 prong events with an identified hadron and no photons to obtain a branching rate for this mode of 9.0 ± 2.9%.

4 - Kν decay mode. This should be the Cabibbo suppressed mode and the theoretical expectation is 0.62%. The only experimental input here is by the DASP group who find[99] BR (Kν) < 1.6% (90% C.L.).

5 - ρν decay mode. This should be one of the major decay modes, with the standard model predicting 23%. To my knowledge the only information available on this subject is the preliminary data presented by the DASP group at the Hamburg meeting[95] who quote 24±9%. Their evidence rests on the observation of the channel

$$e^+e^- \to \pi^\pm \pi^0 + 1 \text{ charged track}$$

where the $\pi^\pm\pi^0$ mass spectrum, and the momentum of the $\pi^+\pi^0$ system (Fig. 18) is consistent with those events coming from the process

$$e^+e^- \to \tau^\pm \tau^\mp \quad \tau^\mp \to \rho^\mp \nu \to \pi^\mp \pi^0, \quad \tau^\pm \to 1 \text{ charged track} + \ldots$$

6 - Multiprong decay modes and their composition. The rates for these decay modes, as well as their composition can be calculated from the e^+e^- annihilations in the appropriate energy range since the isovector electromagnetic current is believed to be directly related to the weak hadronic

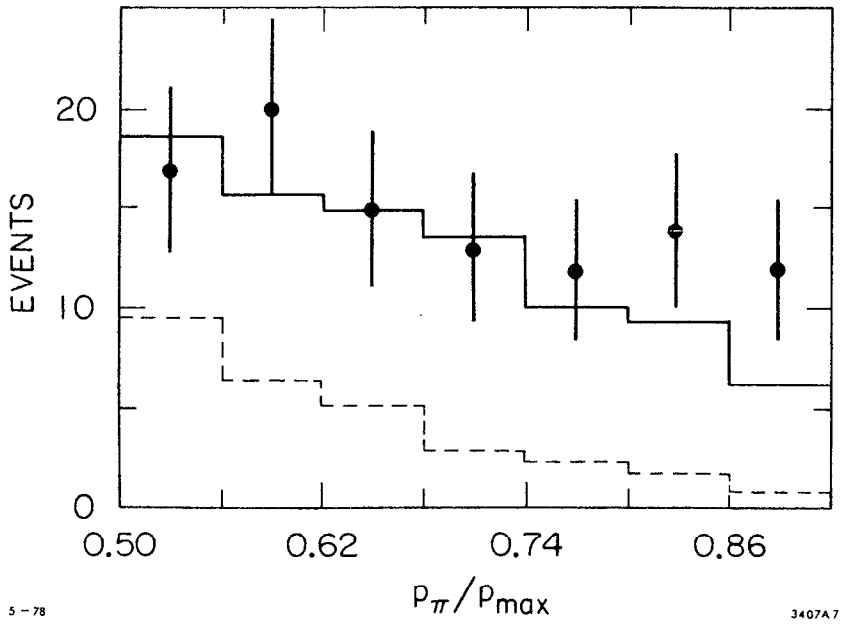

Fig. 17 The ratio of the pion momentum to its maximum value for τ decay for the SLAC-LBL events with a pion, another charged particle, and no detected photons. The solid curve is the expected distribution if the τ decays normally; the dashed curve if πν decay is absent.

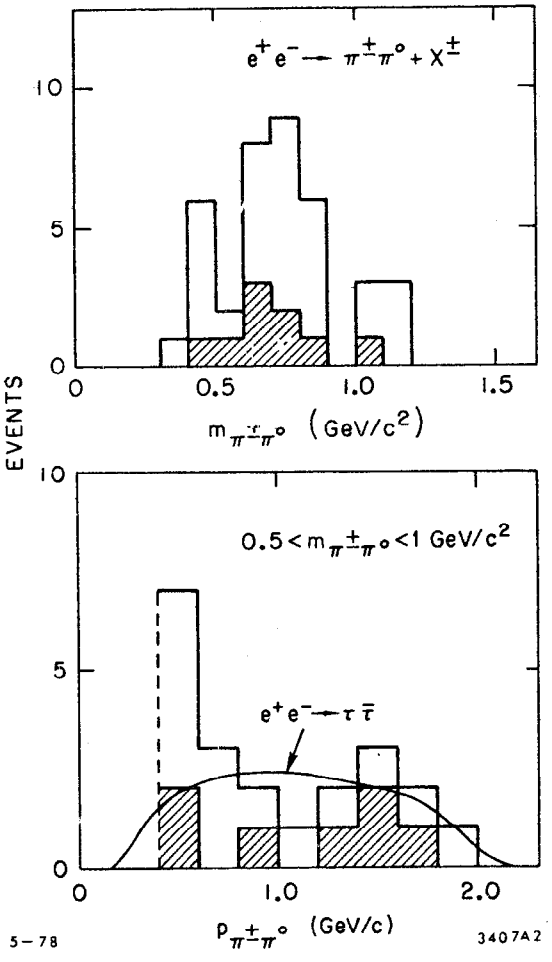

Fig. 18 The DASP invariant mass distribution of the $\pi^\pm\pi^0$ system (a) and the momentum distribution of the $\pi^+\pi^0$ system for the events in the ρ mass band (b). The shaded events have the second charged particle identified as electron.

current.[103] The results of the standard model are listed in Table IX.

Table IX

τ branching ratios into various multibody channels

Mode	Predicted branching ratio
$A_1 \nu_\tau$	9.3%*
$Q\ \nu_\tau$	0.4%
$\nu_\tau + \bar{u}d$ ($M_{\bar{\mu}d} > 1.1$ GeV)	21.3%
$\nu_\tau + \bar{u}s$ ($M_{\bar{\mu}s} > 1.1$ GeV)	1.5%

*half of this mode will go into single prong topology.

The experimental situation is in good agreement with the theory, although there is room for considerably more work here on the experimental side. We attempt to summarize the experimental situation very briefly. The PLUTO collaboration[104] has reported a branching fraction of $5 \pm 1.5\%$ for the decay mode $\tau^+ \to \nu\ \rho^0\pi^+$. They argue that the mass spectrum of the 3π system is consistent with coming from an A_1 (see Fig. 19). A similar measurement has been performed[105] by the SLAC-LBL collaboration, who however do not claim to be able to separate out the events with extra π^0's. Accordingly, they choose to quote a total rate for $\tau^\pm \to \nu\pi^+\pi^-\pi^\pm(n\pi^0\text{'s})$ as $18 \pm 6.5\%$. Again, there is some enhancement in the data in the 3π mass spectrum around the A_1 mass, as demonstrated in Fig. 20.

The total branching ratio into multiprongs has been measured by several groups. The DELCO group has obtained a branching fraction of $32 \pm 5\%$ in 2 different ways, i.e. by measuring[86] the rate for eX events which yields $2b_e(1 - b_e - b_{mp})$ and by plotting[106] the ratio of the observed multiprong events with an electron to the eX events as a function of minimum electron momentum cutoff. The asymptotic value of this ratio will be free of charm

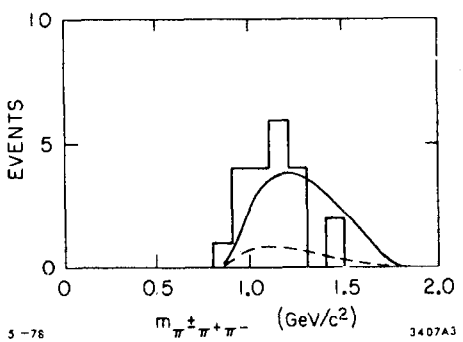

Fig. 19 The PLUTO invariant mass distribution of $\rho^0\pi^\pm$ combinations in events with electron and 3 π's, compatible with $\tau^+\tau^-$ hypothesis. The solid curve represents a nonresonant $\rho^0\pi^\pm$ spectrum from τ decay; the dashed line is an estimate of the background.

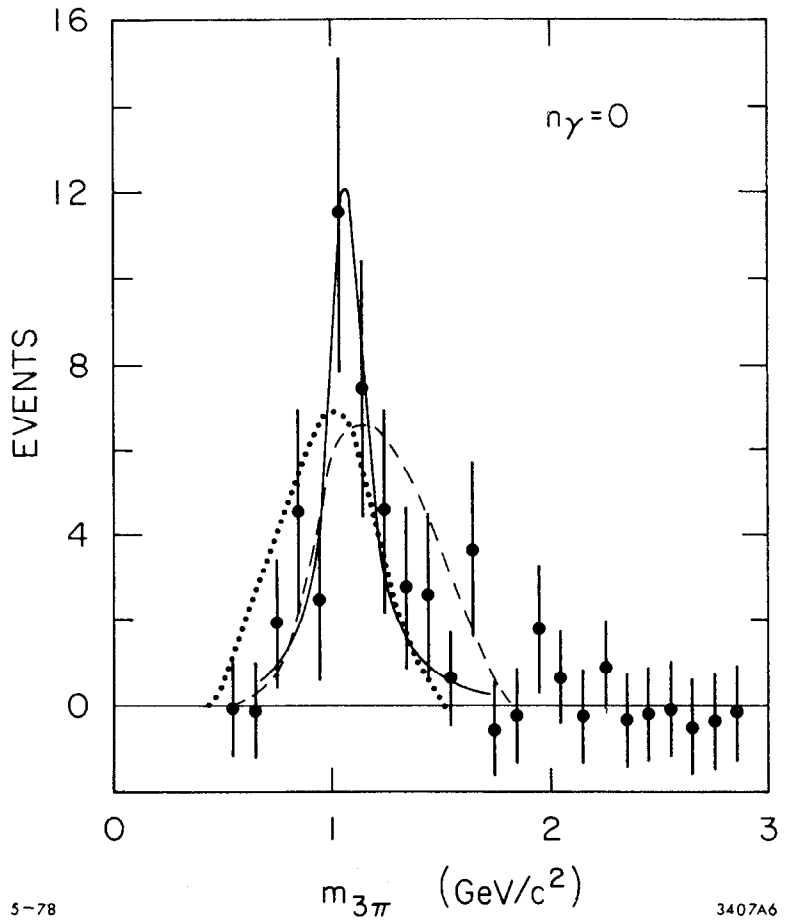

Fig. 20 SLAC-LBL mass spectrum of 3 π's from events with a μ, 3 charged π's, and no detected γ's. The dotted line represents $\tau \to \pi^{\pm}\pi^{+}\pi^{-}\pi^{o}\nu$ hypothesis, the dashed line non resonant $\tau \to \pi^{\pm}\pi^{+}\pi^{-}\nu$, and the solid line $\tau \to A_1\nu$, with mass and width of A_1 being 1.1 GeV/c^2 and 200 MeV/c^2 respectively.

contamination and thus measures the ratio of multiprongs to 1 prong non-electron decays (corrected for slightly different detection efficiencies) in τ decays. These data are displayed in Fig. 21.

The DASP group has measured[85] the same quantity utilizing the relationship $b_{mp} = 1 - b_e - b_{ns}$ where b_{ns} is the branching ratio into a non-showering single charged prong. They obtain 35 $\pm$ 11% for the multiprong mode. Finally the PLUTO group[107] has obtained 30 $\pm$ 12% for this rate by looking at multiprong events associated with a muon.

7 - Rare decay modes. The standard current model predicts that there should not be any exotic decay modes, besides those discussed above. This is indeed the case experimentally, as can be seen from Table X reproduced from the Hamburg Conference proceedings.

Table X

Upper Limits on τ Rare Decay Modes

Experimental Group or Detector	Mode	Upper Limit on Branching Ratio	C.L.	Ref.
PLUTO Group	$\tau^- \to$ (3 charged particles)$^-$	0.01	95%	108
PLUTO Group	$\tau^- \to$ (3 charged particles)$^-$	0.01	95%	108
SLAC-LBL Magnetic Detector	$\tau^- \to$ (3 charged particles)$^-$	0.006	90%	92
SLAC-LBL Magmetic Detector	$\tau^- \to \rho^- + \pi^o$	0.024	90%	109
PLUTO Group	$\tau^- \to e^- + \gamma$ $\tau^- \to \mu^- + \gamma$	0.12	90%	108
LBL-SLAC Lead Glass Wall	$\tau^- \to e^- + \gamma$	0.026	90%	96
LBL-SLAC Lead Glass Wall	$\tau^- \to \mu^- + \gamma$	0.013	90%	96

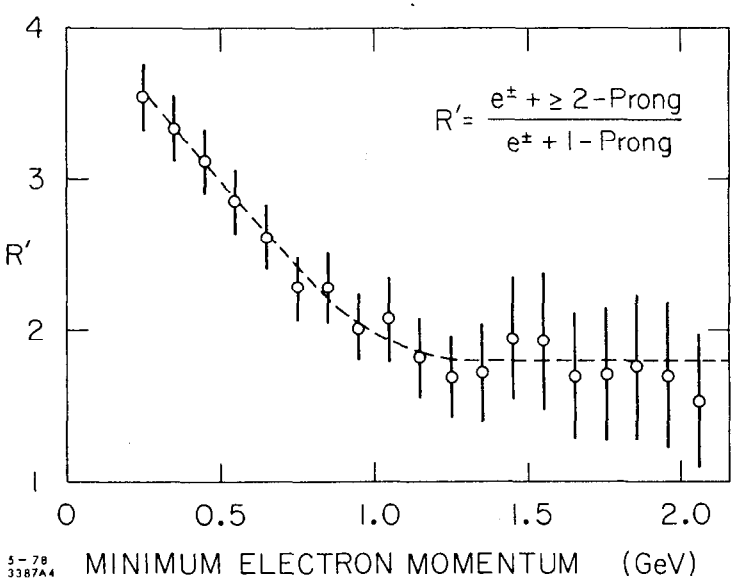

Fig. 21 The ratio of observed multiprong electron events to the observed two prong electron events at electron momenta above the value indicated on the horizontal axis. The dashed curve is drawn to guide the eye. Note the suppressed zero on the vertical scale. The data is from DELCO.

In summary, we conclude that the branching ratios of the τ lepton are in excellent agreement with the standard model predictions and thus the evidence is very strong that the τ couples to the same weak interaction current that appears to be responsible for all the other hitherto observed weak processes.

We can now turn to the other vertex and discuss what we know about the τ-ν_τ-W vertex. We first consider the electron spectrum which can distinguish between the V-A and V+A couplings. One can characterize the spectrum by the Michel parameter, ρ, which takes on the value of 0 for V+A hypothesis and results in a spectrum peaked near the center of possible electron energies, or the value of 0.75 for V-A which gives an electron energy distribution peaked at the maximum possible value. These two distributions, illustrated roughly in Fig. 22, become less distinguishable as we go from the τ rest frame to the laboratory system because of Lorentz smearing. The radiative corrections[110] effect significantly the lower part of the spectrum and have the phenomenological effect of reducing the expected ρ value for each hypothesis by about 0.1.

The experimental data is in good agreement with the V-A and appears to exclude the V+A hypothesis. The most powerful data statistically comes from the DELCO experiment[111] and is displayed in Fig. 23, both for all the energies and the energies near threshold, where the statistics are poorer but the sensitivity considerably higher. The preliminary result quoted by the DELCO group is $\rho = 0.66 \pm 0.13$.

The overall τ decay rate, i.e. its lifetime, measures the strength of the τ-ν_τ-W coupling. In the standard model, i.e. assuming universality and no lepton mixing, the expected decay rate is 3.3×10^{12} sec^{-1} yielding

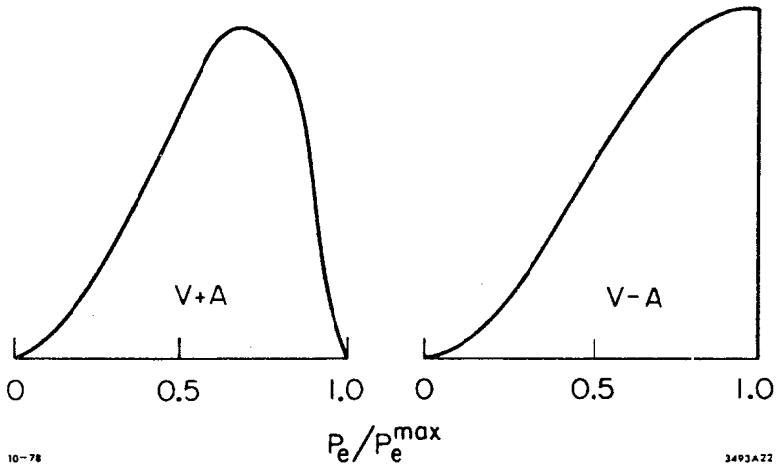

Fig. 22 Rough sketch of the expected electron momentum from τ decay for V+A and V-A hypotheses.

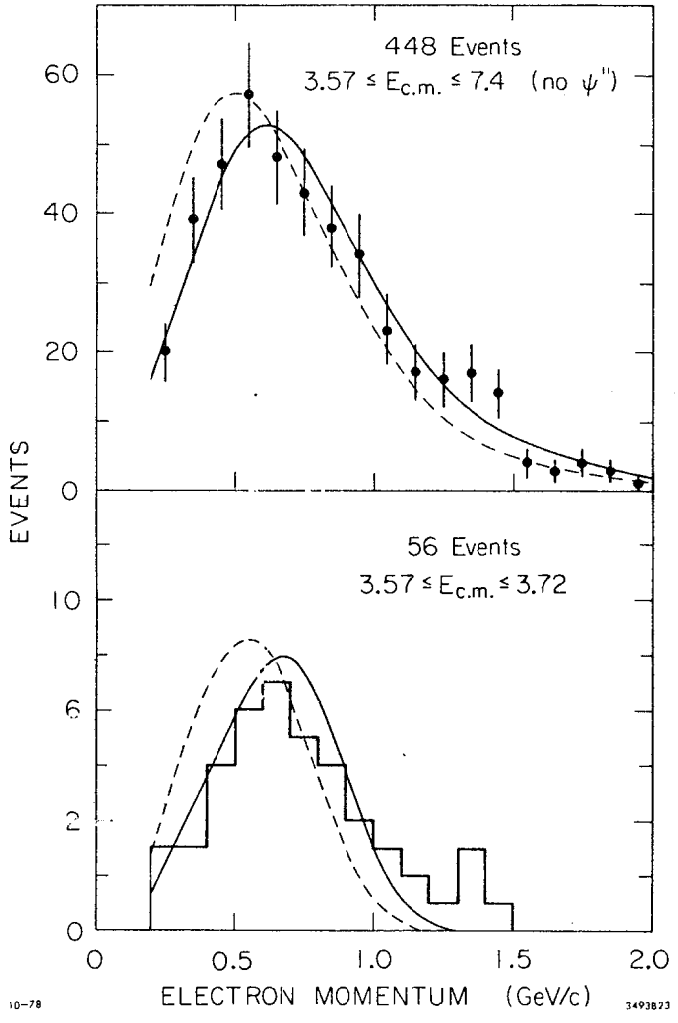

Fig. 23 The preliminary electron momentum spectrum for eX events from DELCO. The solid line is the V-A prediction, the dashed line V+A prediction. (a) all events; (b) events below charm threshold.

a lifetime of 3.0×10^{-13} sec. Such a value appears to be below the capability of the present measurements, but an upper limit would nevertheless be useful in putting a severe constraint on the various models incorporating lepton mixing. The best limits came from the DELCO[111] and PLUTO[112] groups who quote $\tau_\tau < 3 \times 10^{-12}$ sec and $\tau_\tau < 3.5 \times 10^{-12}$ sec respectively, obtained by looking for a finite distance between the annihilation point of e^+e^- and τ decay point.

The final question has to do with the nature of the neutrino associated with the τ. On the assumption that it is indeed the τ neutrino that is emitted in τ decay we have the following most recent experimental limits on its mass:

from the DASP group[85] $m_{\nu_\tau} < 0.74$ GeV (90% C.L.) for V-A

$m_{\nu_\tau} < 0.54$ GeV (90% C.L.) for V+A

from the PLUTO group[113] $m_{\nu_\tau} < 0.36$ GeV (90% C.L.)

and from the DELCO group[88] $m_{\nu_\tau} < 0.25$ GeV (90% C.L.) } for V-A

On the other hand there exists the possibility that $m_{\nu_\tau} > m_\tau$,[114] and τ decays via a non zero mixing angle between ν_τ and ν_μ and ν_e. In that case we observe either the electron or muon neutrino in the decay and those experimental limits are meaningless. One should point out, however, that this possibility is probably already ruled out experimentally.[81]
The mixing in the six lepton picture involves two parameters, a and b, which are bounded from below by the limit on the τ lifetime, i.e.

$$a^2 + b^2 > 1.0 \times 10^{-1}$$

for $\tau_\tau \leq 3 \times 10^{-12}$ sec. On the other hand, the relative rates for $\pi \to e\nu$ and $\pi \to \mu\nu$ put limits on $b^2 - a^2$. Specifically there is a 1.5σ difference[115] in the ratio of these 2 rates from what one expects from theory giving

$$b^2 - a^2 = (3 \pm 2) \times 10^{-2}.$$

Thus this inequality may be interpreted as setting a bound on the value of $|b^2 - a^2|$, i.e.

$$|b^2 - a^2| < 7 \times 10^{-2}$$

within 95% confidence limits.

Finally, in the framework of this model there will be a finite probability for the muon neutrinos to turn themselves into electron neutrinos. Experimentally, this would allow a neutrino beam, that is initially a pure ν_μ beam to produce electrons unaccompanied by muons. This rate is given by

$$\frac{\nu_\mu + N \to e^- + \ldots}{\nu_\mu + N \to \mu^- + \ldots} = a^2 b^2$$

and the experimental 95% confidence limit bound obtained from the Gargamelle experiment of J. Blietschau et al.,[63] is

$$a^2 b^2 < 1.2 \times 10^{-3}$$

Interpreting these last two numbers literally, we obtain an upper bound on the higher of a^2, b^2, i.e.

$$\text{Max } (a^2, b^2) < 8.3 \times 10^{-2}$$

The value of the smaller parameter corresponding to this limit would then be 1.3×10^{-2}, thus barely disagreeing with the limit on $b^2 + a^2$ and ruling out the hypothesis of a heavy neutral τ lepton.

A similar conclusion can be reached in a slightly more direct way by considering the Cabibbo universality, i.e. comparison of muon decay with the nuclear β decay. In Chapter I we have shown that

$$\sin^2\theta_c + \cos^2\theta_c = 1.003 \pm 0.004$$

i.e. at a 95% confidence limit the violation of universality is less than 1.1%. In terms of a^2 and b^2, this limit can be written as

$$b^2 < 1.1 \times 10^{-2}$$

in the approximation that terms $O(\sin^2\theta_c)$ can be ignored. Combining this with the data from the $\pi \to e\nu/\pi \to \mu\nu$ ratio we obtain a clear contradiction

with the lower limit on $a^2 + b^2$ from the lifetime limit, thus ruling out the heavy τ neutrino hypothesis.

One can conclude this section with a summary of what we know today about the τ.

1 - It appears to be a sequential spin 1/2 lepton with its own neutrino.

2 - Mass of the τ neutrino is probably low, and a mixing scheme with $m_{\nu_\tau} > m_\tau$ appears to be ruled out by the data.

3 - The three precise measurements of the τ mass are in good agreement and are listed in Table XI.

Table XI

τ Mass Determinations

Group	Value (GeV)	Reference
DASP	1.807 ± 0.020	85
DELCO	$1.782 \, {}^{+\,0.002}_{-\,0.007}$	86
Heidelberg	$1.787 \, {}^{+\,0.010}_{-\,0.018}$	116

4 - Branching ratios are in good agreement with the standard model

5 - Coupling appears to be of the V-A form.

6 - Decay rate consistent with universality but within rather large limits, however.

On the other hand, one would still like to obtain better information on the following points:

1 - how exact is the e-μ-τ universality.

2 - what is the nature of ν_τ? Is it massless? If no, what is the mixing with the ν_μ and ν_e.

3 - better branching ratio measurements in the multibody sector.

Unless these last three questions will be answered in a surprising and unexpected way, we can assume that most likely τ is a standard sequential lepton. If so, and the mass of its neutrino is zero, then unfortunately we shall not see any of the exciting experimental possibilities like neutrino oscillations, CP violation in the lepton sector, and μ-e transitions due to mixing phenomena. One has to regretfully conclude that the standard model is a dull model.

IV. Charm Decays

In this chapter we shall discuss the available experimental information on charm decays and compare it with the standard charm model. As shall be hopefully apparent from this discussion, there is still a lot to be learned on this topic and many questions remain unanswered. This can be contrasted with the question of τ decays, where we appear to be much closer to the ultimate understanding.

We shall discuss in this chapter the following topics:

a) expected charm spectroscopy

b) evidence for weak decays

c) comparison with GIM predictions

d) semileptonic decays

e) pure hadronic decays

f) D^o-$\overline{D^o}$ mixing

g) F meson and charmed baryons

h) the status on the lifetime of D meson.

a) expected charm spectroscopy. We shall review here very briefly some of the fundamental ideas put forth for the first time in great detail by

Gaillard, Lee, and Rosner.[117] Their classic paper is remarkable in its great predictive power and in the good accuracy of their quantitative predictions.

In the quark picture the mesons are bound states of a $q\bar{q}$ system. Before the introduction of charm, different mesons could be obtained by allowing the general $q\bar{q}$ system to be a different combination of the u, d, and s quarks and the $\bar{u}$, $\bar{d}$, and $\bar{s}$ antiquarks. The introduction of the new quark, the c quark, will allow one to create new meson states by forming systems composed of a c quark plus an antiquark. Thus the expected mesonic states with c=1 quantum numbers are:

$$\left.\begin{array}{ll} c\bar{d} \Rightarrow D^+ & \\ c\bar{u} \Rightarrow D^\circ & T = 1/2 \\ c\bar{s} \Rightarrow F^+ & T = 0 \end{array}\right\} \text{ and their antiparticles}$$

We also indicate above the isotopic spin multiplets and the conventionally assigned names to the new quark states. Fig. 24 exhibits the expected mesonic states (old and new) displayed in the 3-dimensional space defined by the C, Y, and I_3 (Y is the hypercharge).

Clearly, if the charm quantum number is to be conserved by the strong and electromagnetic interactions in analogy with strangeness, then at least one of the 3 new meson states should be stable against those interactions and thus have to decay weakly. In the conventional picture, all three: D^+, D°, and F, were predicted to decay weakly, since the electromagnetic splitting is expected to be less than a pion mass and the predicted masses of the quarks were such that the transition $F \to D + K$ would be energetically forbidden.

The baryons are qqq states and thus we can form charmed baryonic states with charm quantum number equal to 1 by replacing one of the old

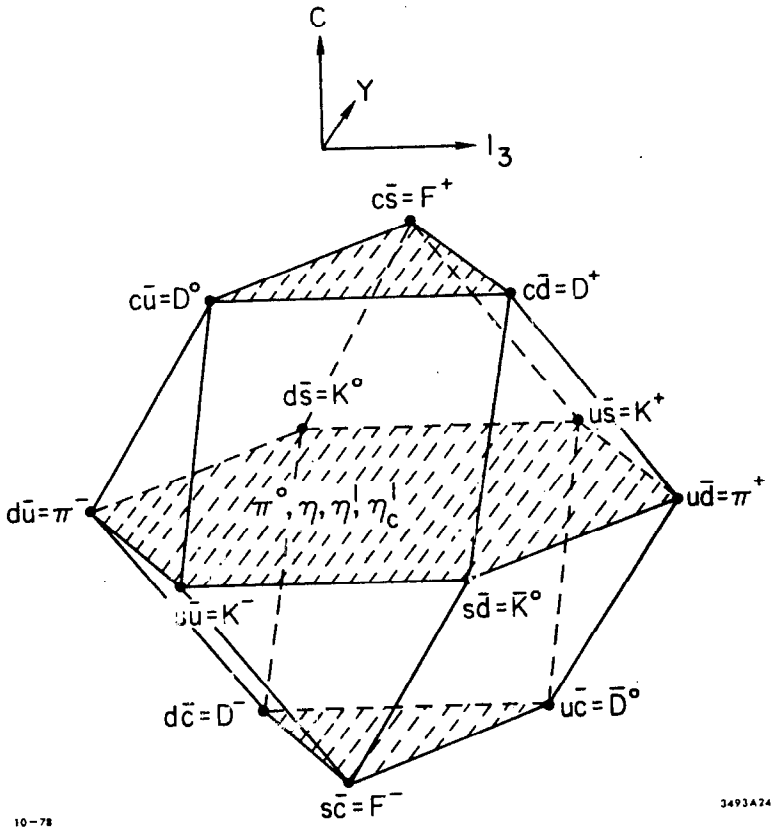

Fig. 24 The predicted meson spectrum in the charm scheme.

quarks with a c quark, or equal to 2 by using 2 charmed quarks. The three c quark state would be expected to be a 3/2+ state in analogy with Ω^-. Accordingly, we can expect to have:

9 C = 1 states i.e. S = 0 triplet and singlet

S = -1 two doublets

S = -2 singlet

and 3 C = 2 states i.e. ccu, ccd } T = 1/2, S = 0

ccs T = 0, S = -1

Together with the 1/2+ ground state octet of the old baryons, they will form a 20 representation of SU_4 which is displayed in Fig. 25 in the 3 dimensional C, Y, I_3 space. The figure is a truncated tetrahedran and each of the 4 large sides represents an SU_3 octet composed with a different set of 3 out of the 4 quarks.

Considering the charmed baryonic decays in general, we have 2 distinct possibilities, i.e.

1 - $B^{charmed} \rightarrow B^{old} + M^{charmed}$, i.e. strong decay

2 - $B^{charmed} \rightarrow B^{old} + M^{old}$, i.e. weak decay.

Whether the first process goes is strictly a kinematical question, i.e. is it energetically allowed. If the answer is yes, then we would see no weak charmed baryon decays. That is the possibility that appeared more plausible to Gaillard, Lee, and Rosner. The nature, however, appears to have chosen the second possibility as we shall discuss towards the end of this chapter.

b) evidence for weak decays. We would like to consider next two points that appear to confirm the theoretical prejudice that the D decays proceed via weak interactions, i.e. their narrow width and the existence of parity violation in the decay process.

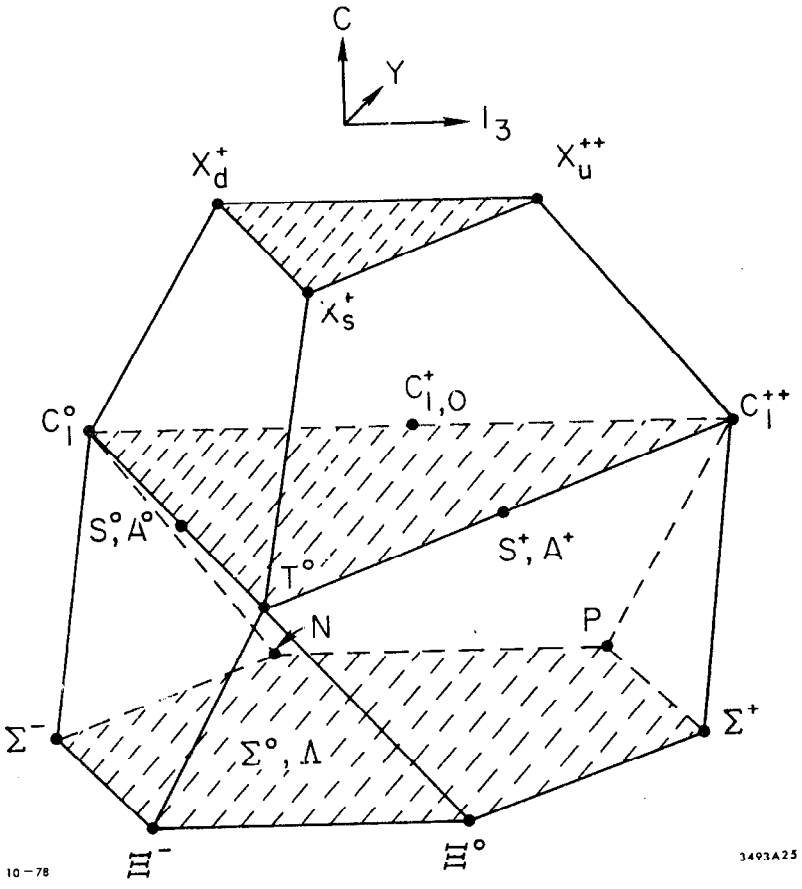

Fig. 25 The predicted baryon spectrum in the charm scheme.

In spite of the relatively large Q value released in most charm decays, their mass can be measured experimentally in e^+e^- collisions quite accurately, leading to a stringent upper limit on the natural $D^o(D^\pm)$ width. To see this we can consider the process

$$e^+e^- \to D\bar{D}$$

near threshold. In general, we have for the mass of the D squared

$$M^2 = \Sigma E_i^2 - \Sigma \vec{p}_i^{\,2}$$

where the summation is over all the D decay products.

$$\delta M^2 = \Sigma 2E_i \delta E_i - \Sigma 2\, \vec{p}_i\, \delta \vec{p}_i$$

$$= 2\, E_{tot}\, \delta E_{tot} + 2|\vec{p}_{tot}|\, \delta P_{tot}$$

where the last sum implies that the proper correlations between δE_{tot} and δP_{tot} are taken into account. Now usually near threshold $\vec{p}_{tot} \approx 0$ i.e. $E_{tot} >> P_{tot}$, and thus the first term tends to dominate the error. But in e^+e^- collisions $E_{tot} = E_{beam}$ which is known very well, and thus δE_{tot} and hence δM^2 is indeed very small.

This technique is especially useful in the case of the $D\bar{D}$ system because of the presence of ψ'' just past the $D\bar{D}$ threshold [118], resulting in an appreciable rate (about 1 R unit) for the $D\bar{D}$ production. The narrow peaks seen at the D mass [119] are exhibited in Fig. 26, with a typical $\Gamma_{exp}^{FWHM} \leq 10$ MeV. Parenthetically, one might add that the circumstances discussed above allow one to measure the D mass with a very high accuracy, yielding [120]

$$m_{D^o} = 1863.3 \pm 0.9 \quad MeV/c^2$$

$$m_{D^+} = 1868.4 \pm 0.9 \quad MeV/c^2$$

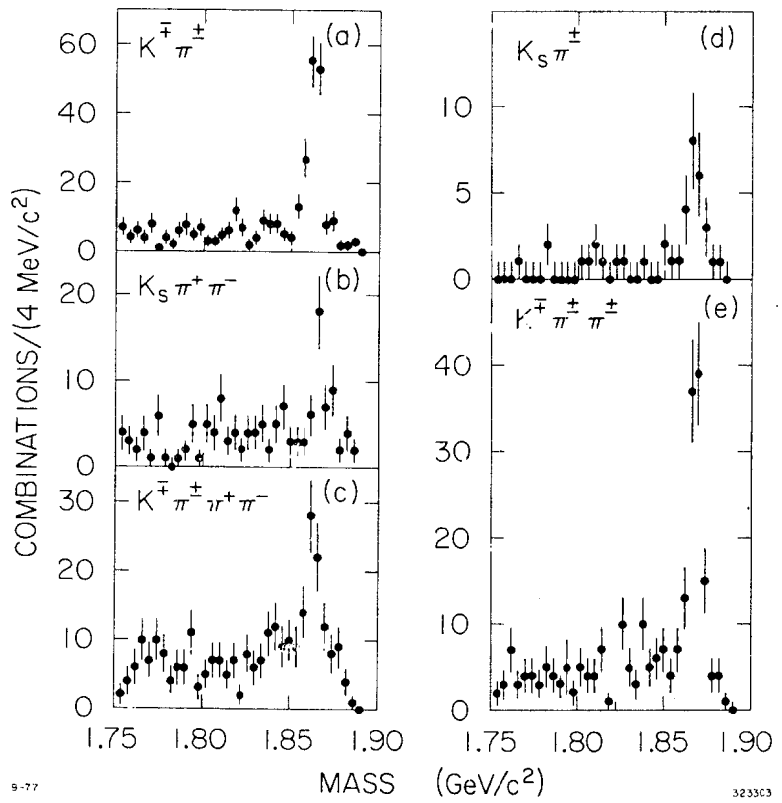

Fig. 26 The mass spectra for different neutral and exotic Knπ combinations. The data is from the SLAC-LBL collaboration.

The evidence for parity violation parallels very closely the arguments relevant to the old τ-θ puzzle. We recall that in the days before the discovery of the parity violation, the two distinct decay modes of the K meson

$$\theta^+ \to \pi^+\pi^o \quad \text{and} \quad \tau^+ \to \pi^+\pi^-\pi^+$$

were believed to have to have been two distinct mesons since the parity of the two final states had to be different for the same value of angular momentum.

The experimental situation in the case of the D is very similar. A sharp enhancement around 1870 MeV is observed both in[120] the $K^o_s \pi^\pm$ and in the $K^\mp \pi^\pm \pi^\pm$ spectrum[119] (see Fig.26d and e). The identical value of the mass for both of these cases leads one to believe that these are two decay modes of the same particle.

Considering now spin-parity assignments for the 2 decay modes, we note that $K^o\pi^\pm$ is a system of 2 0^- mesons. Accordingly, its J^P assignment has to have natural spin parity, namely $P = (-1)^J$ i.e. 0^+, 1^-, 2^+, 3^-.... On the other hand, the $K\pi\pi$ system is composed of 3 0^- mesons and as such has to have a vanishing population at the boundaries[121] for natural spin-parity assignments. This is not the case, as illustrated by the data[122] shown in Fig. 27. The symmetrized Dalitz plot shows no depopulation around the boundaries for the resonant $K^\mp\pi^\pm\pi^\pm$ events (Fig. 27a). For comparison we also show the non-resonant $K^\pm\pi^\mp\pi^\mp$ events in the same mass region.

For low values of the spin, the argument can be made even more quantitative. We consider the J^P assignments of 0^+, 1^-, 2^+. The first state is absolutely forbidden for 3 0^- mesons. The 1^- assignment would

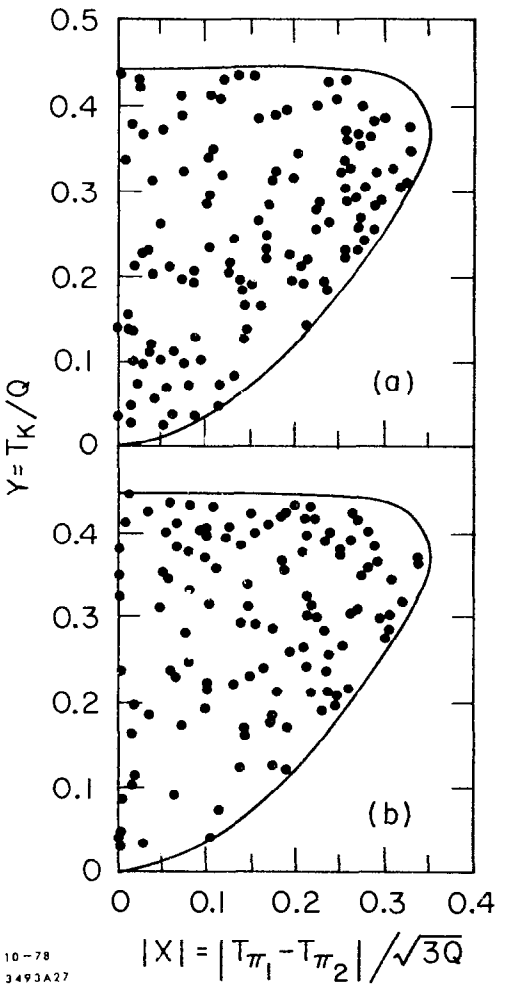

Fig. 27 Symmetrized Dalitz plots for the $K\pi\pi$ system in the mass region of 1.86-1.92 GeV/c^2. (a) Exotic combinations $K^\mp\pi^\pm\pi^\pm$; (b) Non-exotic combinations $K^\pm\pi^+\pi^-$. Q is the sum of the kinetic energies of the 3 final state mesons. The data is from the SLAC-LBL collaboration.

predict an additional zero at the symmetry axis and the 2^+ on additional zero at the top of the Dalitz plot.[121] Accordingly we can now consider the size of the enhancement in the $K^{\mp}\pi^{\pm}\pi^{\pm}$ mass spectrum for both the allowed and forbidden regions of the Dalitz plot under the hypothesis that the J^P assignment is either 1^- or 2^+. The dividing line on the Dalitz plots was chosen in such a way that for a 0^- assignment (i.e. a flat Dalitz plot population) the two peaks would be equal. As is clear from Fig.28, the two enhancements are equal within statistics (the ratio of the enhancement in the allowed to the forbidden regions would be 8.2 and 5.6 for the 1^- and 2^+ assignments respectively) excluding the natural spin parity assignments. Accordingly, we must conclude that the parity is not conserved in this process.

c) Comparison with the GIM predictions. We have already seen how the central prediction of the GIM model, i.e. existence of narrow states characterized by the new quantum number charm has been verified experimentally. In this section we shall consider how well does the data agree with the other predictions of the GIM model.

The GIM model requires that the final state of the decay products of $D^{\pm}$ have exotic quantum numbers, i.e. quantum numbers that can not be possessed by any $q\bar{q}$ combination. This is because in terms of quark transitions, the D decay corresponds to

$$c \to s + W^+$$

and thus the final physical state can have quantum numbers $S=-1$, $Q=1$ (for D^+ the quark composition of the initial state is $c\bar{d}$) which are inaccessible to any $q\bar{q}$ pair.

Thus, more specifically, we have the prediction that

$$D^+ \to K^-\pi^+\pi^+$$

should be an allowed decay whereas

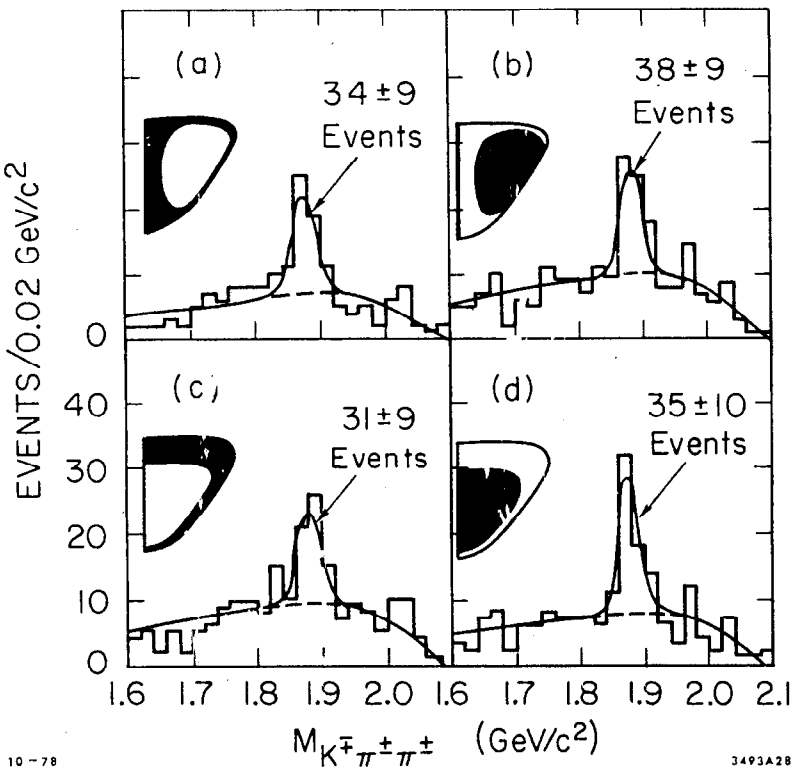

Fig. 28 Mass plot for the exotic $K\pi\pi$ system. Forbidden (a) and allowed (b) regions for 1^- matrix element and forbidden (c) and allowed (d) regions for 2^+ matrix element. The data is from SLAC-LBL callaboration.

$$D^+ \not\to K^+\pi^+\pi^-$$

should be forbidden. This prediction was confirmed in the first observation[123] of a bump in the $K\pi\pi$ state by Peruzzi et al. whose data is displayed in Fig. 29. The sharp enhancement present at 1.876 GeV/c^2 in the exotic combination is totally absent in the nonexotic channel.

The second quantitative prediction of the GIM model has to do with the Cabibbo favored nature of the $c \to s$ transition, and hence the Cabibbo suppressed nature of the $c \to d$ transition. Thus the former decays should be enhanced by a factor of $\tan^2\theta$ as compared to the decays into non strange final states. This prediction will be somewhat modified by the phase space factor that will enhance the non-strange decays by ≈ 2 and by possible dynamical effects. The experimental data at 4.028 GeV for both 2 and 3 body decays[124] is summarized in Table XII.

Table XII

Comparison of Cabibbo suppressed and forbidden decays

	σB for $K^{\mp}\pi^{\pm}(K^{\mp}\pi^{\pm}\pi^{\pm})$	σB for $\pi^+\pi^-(\pi^+\pi^-\pi^{\pm})$	σB for K^+K^-
2 body	0.57 ± 0.11 mb	< 0.04 mb	< 0.04 mb
3 body	0.40 ± 0.10 mb	< 0.03 mb	

Even though the Cabibbo suppressed decays have not yet been observed, the data does indicate strongsuppression of $\Delta S=0$ transitions á la GIM model.

Finally we can ask what is the measured number of K's associated with the D production, since the GIM model predicts this number to be very close to 2. Experimentally, one looks at multihadron events with an electron, on the hypothesis that those events represent associated production of $D\bar{D}$ pair, followed by a semileptonic D decay, and measures the $K^{\pm}$ content in those

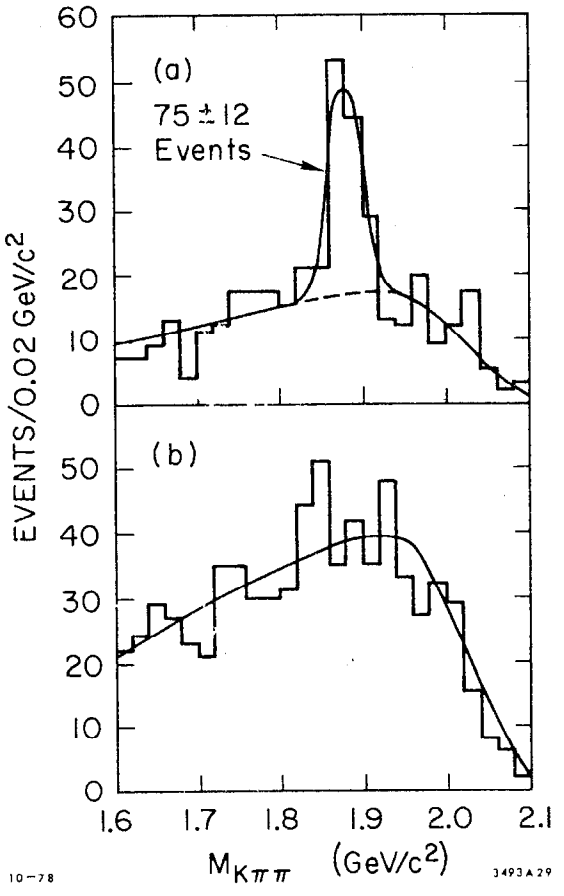

Fig. 29 The $K\pi\pi$ mass distribution with the cuts designed to enhance the signal to background ratio: E_{CM}= 3.90-4.25 GeV and M_{rec}=1.96-2.04 GeV/c^2. (a) Exotic combinations; (b) non-exotic combinations. The data is from the SLAC-LBL collaboration.

events. The result is 0.90 ± 0.18 $K^{\pm}$/electron event, in excellent agreement with GIM if one doubles this number for possible K^{o}'s.

d) (Semi) leptonic decays. We shall start by making some comments about purely leptonic decays of the charmed mesons. In general for the decay

$$M \to \ell \nu$$

where M is a 0^- meson, we have

$$\Gamma = \frac{G^2}{8\pi} f_M^2 \left(\begin{matrix}\cos^2\theta \\ \sin^2\theta\end{matrix}\right) m_\ell^2 \left(1 - \frac{m_\ell^2}{m_M^2}\right) m_M$$

where f_M is the coupling constant that in the limit of perfect SU_4 would be equal to f_π, and $\cos^2\theta$ ($\sin^2\theta$) is used for the Cabibbo favored (suppressed) decays. We now make some general observations:

1 - electronic decays are totally negligible

2 - F leptonic decays will be enhanced over D leptonic decays by roughly a factor of $\tan^2\theta$. Specifically, we expect

$$\Gamma (D \to \mu^+\nu) \approx 2 \times 10^8 \text{ sec}^{-1}$$

$$\Gamma (F \to \mu^+\nu) \approx 3.6 \times 10^9 \text{ sec}^{-1}$$

Compared to a total estimated[126] semileptonic rate of the F of $\approx 10^{12}$ sec^{-1}.

3 - expected decay rate for

$$F^+ \to \tau^+\nu$$

should be about 16 times larger than the $F \to \mu\nu$ rate.

Not surprisingly, none of these decays have been observed as yet.

We turn next to the question of semileptonic decay modes of charmed mesons. The first interesting problem here is the total semileptonic branching ratio. That number tells us right away whether there exists in the charm decays an enhancement of the purely hadronic decays analogous to the situation in strangeness violating decays (see our previous discussion of $\Delta I = 1/2$ rule).

Very crudely we can estimate the total D semileptonic decay rate by assuming that it proceeds via the fundamental process

$$c \to s + \ell + \nu$$

and then the rate can be related easily to the total muon decay rate via

$$\Gamma^{tot}_{D\to e\nu x} = \Gamma^{tot}_{D\to \mu\nu x} = \left(\frac{m_D}{m_\mu}\right)^5 \Gamma^{tot}_{\mu}$$

This kind of calculation gives $\sim 3 \times 10^{12}$ sec^{-1} for the total semileptonic rate into $e\nu$ + hadrons (or $\mu\nu$ + hadrons). In this simple picture, the total hadronic decay rate would then be given by

$$c \to s + u + \bar{d}$$

resulting in a comparable rate times the appropriate hadronic enhancement factor.

There appears to be some theoretical disagreement whether the mechanisms believed responsible[127] for the octet enhancement in "old" particle decays will be relevant when carried over to the case of charm decays. More specifically the quantitative estimates for semileptonic branching ratios range from a low[126] of about 1%, corresponding to an enhancement equivalent to one found in strange particle decays to about 25%, corresponding to essentially no enhancement at all.[126] We shall say more about the details of hadronic enhancement when we discuss the nonleptonic decays, but in the meanwhile we turn to see what do the semileptonic decay data have to say about this question.

There are now several independent measurements of the total semileptonic rate, obtained by means of slightly different primary measurements.

One can measure the total semileptonic rate by comparing $R_e(R_\mu)$ i.e. cross section for production of hadrons associated with an electron (muon) expressed in terms of point cross section, with R_{charm} i.e. total charm contribution to R. We have then

$$BR(e) = 2\ R_e/R_{charm}.$$

We should note that this procedure gives the branching ratio for all charmed ground states (i.e. states decaying weakly) weighed by their production rate, i.e.

$$2\ R_e/R_{charm} = \sum_i \sigma_i\ BR_i/\Sigma\sigma_i$$

Alternatively one can compare the rise in R_e vs. the rise in R at ψ''. This has the fundamental simplicity of measuring effectively an average branching ratio for D^o and D^+ since their production rates there are almost equal (except for phase space factors).

Finally, the branching ratio can be extracted by a comparison of R_{2e} with R_e (R_{2e} is the total rate of hadronic events accompanied by 2 electrons). The last 2 measurements together can in principle disentangle any possible difference between the D^o and D^+ branching ratios.

We shall discuss first the experimental measurements at low energies:

1 - The lead glass wall (LGW) collaboration[129] has measured the D^o-$D^\pm$ B.R. into $e\nu X$ at the ψ'' (3.77) to be 7.2 ± 2.6% by looking at the total number of eX events. The result is mildly dependent through the detection efficiency on the assumption that the two dominant decay modes $Ke\nu$ and $K^*(890)e\nu$ are equal.

2 - The DELCO group[130] has measured the same branching ratio at the ψ'' by comparing the relative sizes of the Breit-Wigner peaks in both R_e and R (see Fig. 30). They obtained 11 ± 2%.

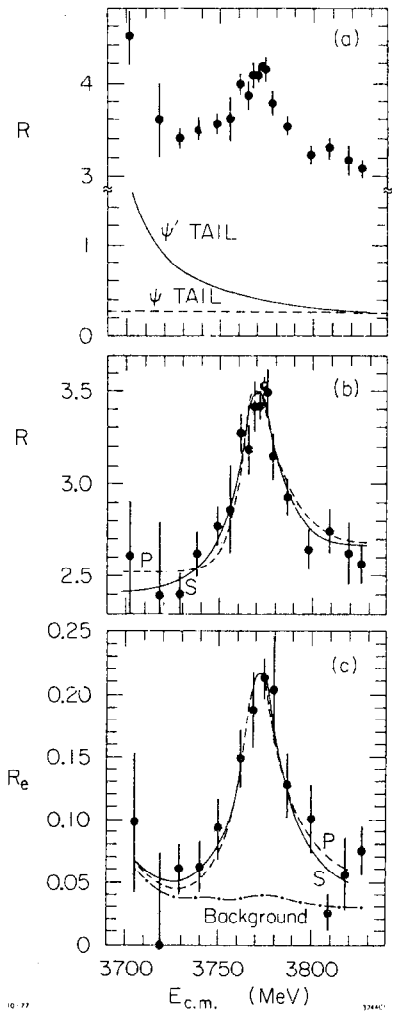

Fig. 30 DELCO data used in extracting the D semileptonic branching ratio at the ψ''. (a) raw R plot, (b) R plot after subtracting the ψ and ψ' tails and (c) R_e plot. The curves are P wave and S wave fits to the resonance.

3 - The DASP group[131] has obtained 11 ± 3% for the eX branching ratio overaged over a wide energy range. The majority of their data however comes from 4.03 GeV total energy point, and thus should reflect mainly D^o and $D^{\pm}$ contributions.

As we can see, all the experiments are consistent with a number $BR_e \approx 10\%$, indicating that the hadronic enhancement discussed above is probably not very important in the charm decays.

The lead glass wall collaboration[132] has also published their determination of BR_e as a function of energy. Their average value, 8.2 ± 1.9% is consistent with the DASP value quoted above and with the low energy (3.77 GeV) measurements. Taken at face value, that implies either that there is very little F and charmed baryon production or that the F and the charmed baryons have a semileptonic rate comparable to that of the D mesons. As seen from Fig. 31, however, the experimental errors are large enough so as yet no strong statement on this point can be made from the published data.

We should finally mention two values for the electronic branching ratio obtained from the comparison of R_{2e} and R_e, i.e. 16 ± 6% from the DASP collaboration[131] and a preliminary value from DELCO of 16 ± 4%.[133] The experimental uncertainties are too high to be able to conclude anything meaningful at this time about the possible difference of $D^{\pm}$ and D^o semileptonic branching ratios.

We turn next to the question of specific exclusive channels responsible for the D semileptonic decay rate. The most likely candidates are the Kev and $K^*(890)ev$ final states, the $K^*(1400)ev$ final state being suppressed by phase space, and the $Kev(n\pi)$ channels expected to be negligible by virtue of the soft pion theorems.[117,134] One rough theoretical estimate[126]

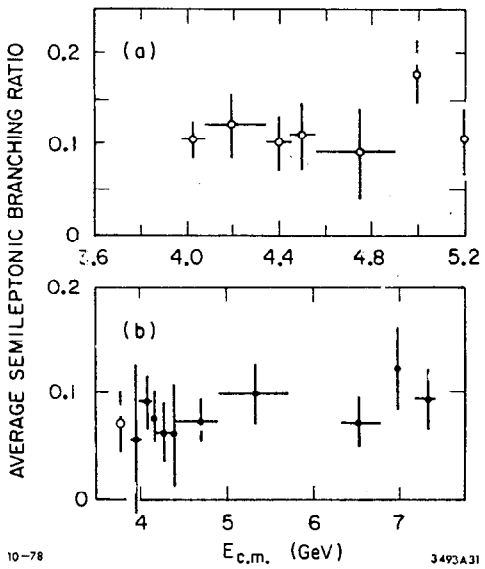

Fig. 31 The average branching ratio for charmed particle decay into an electron plus additional particles vs. the center of mass energy (a) DASP data; (b) LGW data.

indicates that the Kεν rate should form about 30% of the total semileptonic rate.

Experimentally, the electron momentum spectrum appears to be the most sensitive way to extract this information from the e^+e^- annihilation data. The two expected spectra, however, i.e. for Kεν and K^*εν decay modes, do not differ very much[134,135] and one has to exercise considerable care in understanding the experimental backgrounds and detection efficiencies to be able to draw correct conclusions. Some of the relevant backgrounds are:

1 - hadrons misidentified as electrons

2 - τ multibody decays

3 - Cabibbo suppressed decays.

The first source would tend to enhance the lower end of the spectrum, the latter two the higher end. The experimental situation at the present time is inconclusive, appearing to favor sizable contributions from both the Kεν and $K^*(890)$εν modes. Figs 32 and 33 display the published DASP[131] and LGW[132] data together with some curves giving an estimate of the expected spectral shapes for the two hypotheses as well as the shape of the backgrounds. The DASP collaboration quotes 35 ± 30% as the fraction of Kεν in the total semileptonic rate. The preliminary data from DELCO[136] is shown in Fig. 34. A 50-50 mixture of Kεν and K^*εν gives an adequate fit to the data. This problem can probably be best settled by looking at $D\bar{D}$ events at 3.77 GeV where one D is tagged by its hadronic mode and then doing kinematical reconstruction on the remaining particles.

A slightly more indirect information on this question can be obtained from the study of $D^{\pm} \to K^{\mp} + X$ inclusive rate. The hadronic rates contributing to this process would be $K^-\pi^+\pi^+$, $K^-\pi^+\pi^+\pi^o$, and other final states involving 4 or more pions. Furthermore, the Kεν state cannot contribute

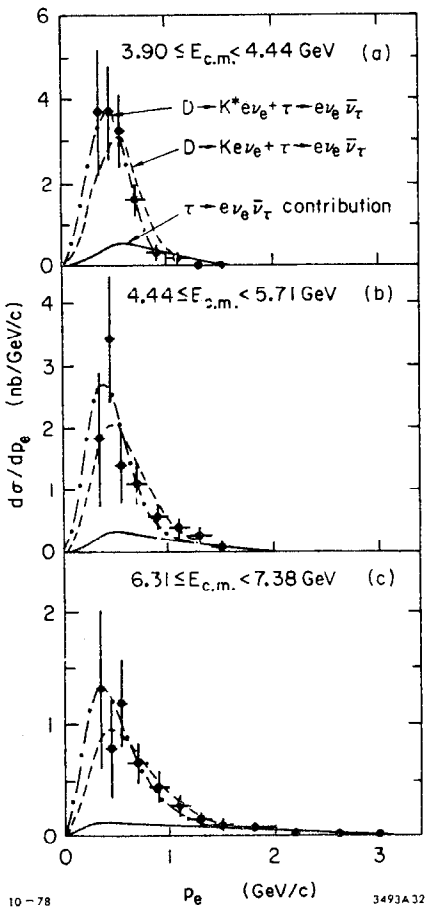

Fig. 32 The electron momentum spectrum from the electron multi-prong events from the LGW experiment for the 3 different center of mass energies.

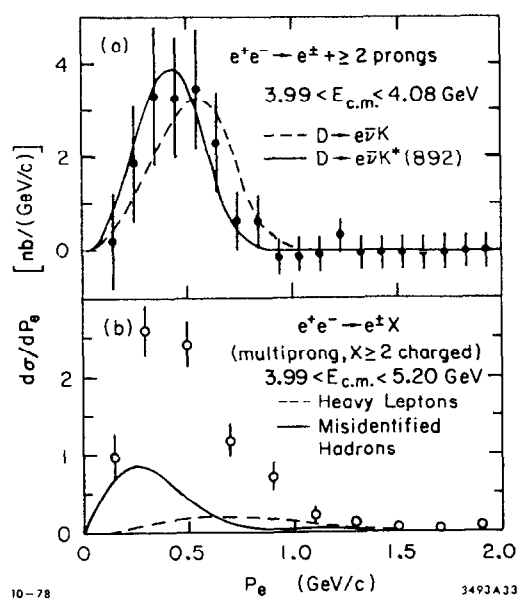

Fig. 33 The electron momentum spectrum from electron-multi prong events from the DASP experiment for the 4 GeV E_{CM} region (a) and all the data (b).

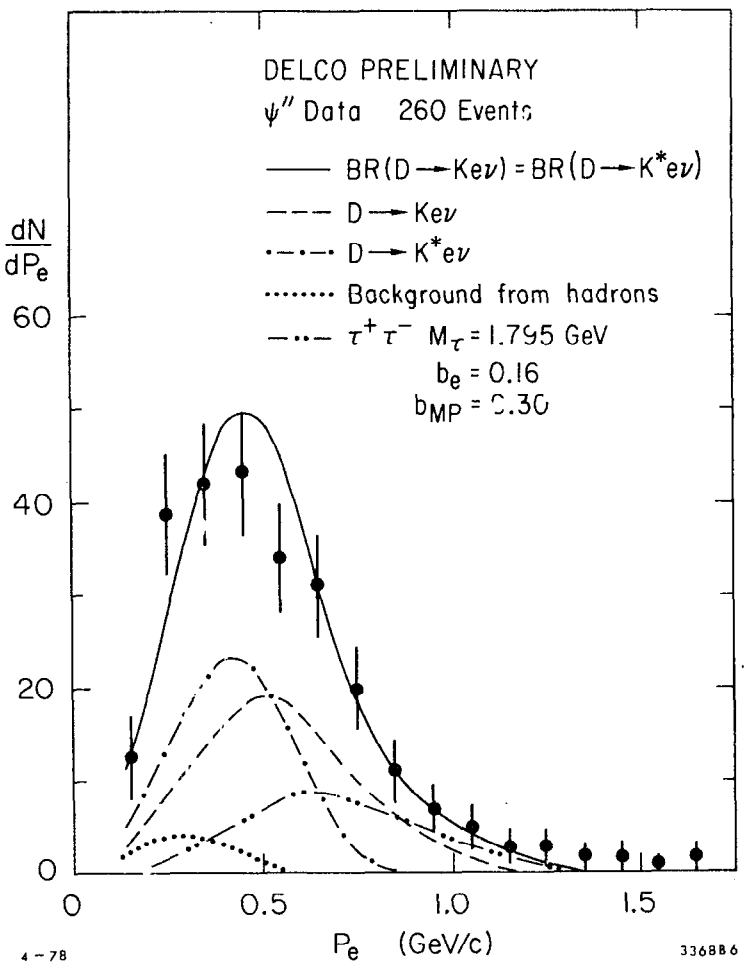

Fig. 34 The preliminary electron momentum spectrum from the electron multi-prong events from the DELCO experiment.

here (final state is $K^o e^+ \nu$) but 2/3 of the $K^{*o} e^+ \nu$ state will decay via $K^- \pi^+ e^+ \nu$. Thus we can see whether the purely hadronic states already saturate the experimental inclusive rate, or is there still room for some $K^* e\nu$ and $K^* \mu\nu$ decay.

The published experimental number from the SLAC-LBL collaboration[137] for the inclusive rate is 10 ± 7% to be compared with the $K^- \pi^+ \pi^+$ rate of 3.5 ± 0.9% and the expected contribution of the 4 and 5 body hadronic states with a charged K of about 20-25% according to the statistical model of Quigg and Rosner.[138] A 100% $K^* e\nu$ contribution to the semileptonic rate would add another 13% to this rate (assuming 10% BR each for e and μ semileptonic rate of $D^\pm$). Thus the room for an appreciable amount of $K^* e\nu$ appears limited.

Some information on the $Ke\nu/K^* e\nu$ ratio question is also available from the high energy ν-Ne interactions at FERMILAB. The Columbia-BNL group has observed both the $\mu^- e^+$ events[139] and the process[140]

$$\nu_\mu + Ne \to \mu^- + D^o + ... \quad \hookrightarrow K^o \pi^+ \pi^-$$

(see Fig. 35). Thus, at least some fraction of the $\mu^- e^+$ events must be due to

$$\nu_\mu + Ne \to \mu^- + D^o + ... \quad \hookrightarrow e^+ + ...$$

and therefore study of μe events with a K^o, and specifically of the $K^o e^+$ and $K^o \pi^-$ mass spectra should provide some information about the relative strenths of the $D^o \to Ke\nu$ and $D^o \to K^* e\nu$ decay modes.

The experimental situation[141] on these points is far from clear for the following reasons:

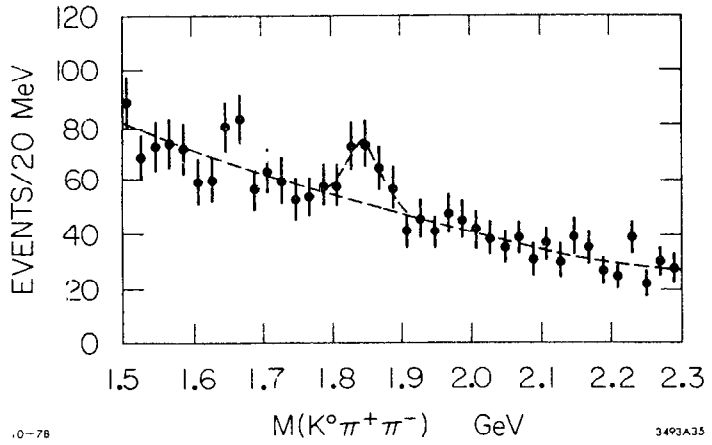

Fig. 35 $K^o \pi^+ \pi^-$ mass spectrum for events with a μ^- from the Columbia-BNL ν-Ne experiment.

1 - Presumably some of the $\mu^- e^+$ events come from semileptonic decays of charmed particles other than D^o, i.e. D^+, F, charmed baryons, etc. Thus, we should have the inequality

$$\frac{\mu^- e^+}{\mu^- (K^o\pi^+\pi^-)_{D^o}} \geq \frac{BR(D^o \to e^+ + \ldots)}{BR(D^o \to K^o\pi^+\pi^-)}$$

where the left hand side represents the number of events of each type from the Columbia-BNL experiment and the right hand side can be obtained from e^+e^- annihilation measurements on the assumption that the D^o and D^+ semileptonic decay rates are equal. Using the data of ref. 140 and the LGW data on branching ratios, the inequality reduces to

$$(0.7 \pm 0.3) \geq (1.8 \pm 0.9)$$

Use of the DELCO or DASP numbers would raise 1.8 on the right hand side to 2.7. Maybe even more importantly, if one also uses the DELCO and DASP data, the error on the right hand side becomes essentially the fractional error on $K^o\pi^+\pi^-$ branching ratio, i.e. $\gtrsim$ 30%. Thus there appears to be a discrepancy here, possible explanations of which are:

a) statistical fluctuation
b) BR $(D^+ \to e^+) >>$ BR $(D^o \to e^+)$
c) an error in one of the data inputs.

2 - The mass spectrum of the $K^o_s e^+$ system (Fig. 36) appears to favor the $K^* e\nu$ decay hypothesis rather than the $Ke\nu$ hypothesis. It must be remembered, however, that if it is the D^o's that are dominantly produced here, then the 3 body semileptonic decay mode would not give a K^o (since $D^o \to K^- e^+ \nu$). The majority of the K^o's that are observed would then be produced directly rather than come from the D decay (i.e. we have charm production from the sea s quarks).

3 - There appears to be no significant enhancement in the $K^o\pi^-$ spectrum at 890 MeV for those events where $m(K^o\pi^- e^+) < 1900$ MeV, i.e. $K^o\pi^-$ combinations compatible with having originated from a D^o decay (see Fig. 36a).

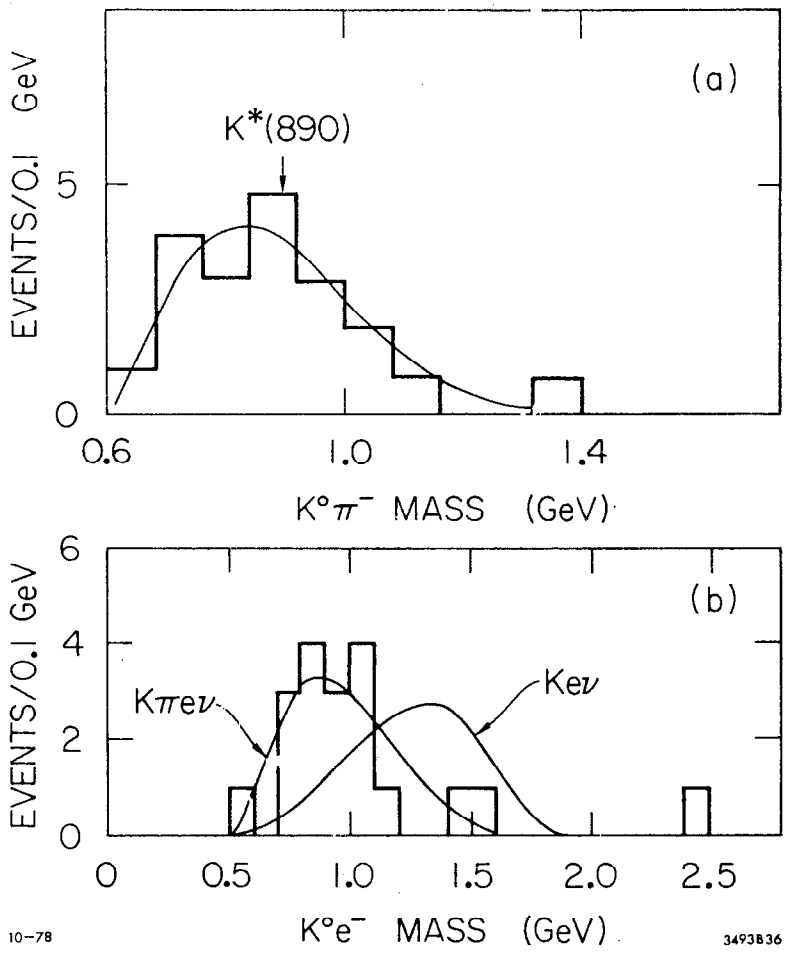

Fig. 36 (a) $K^o\pi^-$ mass spectrum for Columbia-BNL events of the type $\nu_\mu + Ne \to \mu^- K^o e^+ \pi^- + \ldots$ with $M(K^o e^+ \pi^-) < M_D$.
(b) $K^o e^+$ mass spectrum for events of the type $\nu_\mu + Ne \to \mu^- + K^o e^+ + \ldots$.
Only single V events have been included.

Clearly, no conclusion can be drawn here and the resolution of some of these experimental discrepancies must await further data.

e) Hadronic decays of the D mesons. We start by reviewing briefly the theoretical ideas leading to the possible extension to the SU_4 of the octet enhancement concept in SU_3. Consider a product of 2 hadronic currents i.e. $(\bar{u}d)(\bar{s}u)$; its transformation properties will be those of a $\pi^- K^+$ system and thus the isotopic spin decomposition will give

$$\sqrt{\frac{2}{3}} \mid 1/2, -1/2 > - \frac{1}{\sqrt{3}} \mid 3/2, -1/2 >$$

i.e., both T=1/2 and T=3/2 pieces. Experimentally, we have the $\Delta I=1/2$ rule which appears to work to a few percent; theoretically[127,128] it is attractive to explain it through the idea of octet enhancement. The Hamiltonian in general can have transformation properties of an octet or a 27 representation; it is only the latter that contains a T=3/2 pieces and thus enhancing the 8 will automatically generate the approximate $\Delta I=1/2$ rule.

In SU_4, the 8 is replaced by the 15, so again if our Hamiltonian is to be of the current form, i.e.

$$H_w = JJ^+ + h.c.$$

then we must decompose 15 x 15. If we limit ourselves to the symmetric terms since H_w is symmetric, then we are left with $1 \oplus 15 \oplus 20 \oplus 84$. The presence of charm and strangeness changing transistions excludes the singlet, and the 15 does not occur for the GIM current.[142] We can now consider the SU_3 decomposition of the two remaining representations, i.e. 20 and 84. The charm conserving SU_3 multiplet in the 20 is the 8; in the 84 we have 1, 8, and 27. Thus it is clear that to eliminate the 27 in SU_3 one should eliminate the 84 in SU_4, and the SU_4 equivalent of octet enhancement in the 20-plet enhancement.

To consider the experimental ramifications of this ansatz we decompose the 20 into SU_3 multiplets i.e.

$$20 = 6 \oplus 8 \oplus 6^*$$

where the 8 gives us the charm conserving transitions, and 6 and 6^* $\Delta C=+1$ and $\Delta C=-1$ transitions respectively. The sextet dominance reduces the number of parameters needed to describe the $\Delta C=\pm 1$ transitions and thus leads to some rather stringent relations between different possible decay modes. Specifically, all 26 charm changing decays of a pseudoscalar meson into two pseudoscalar mesons can be represented in terms of one common parameter.[143] As mentioned before, there have been arguments put forth[126] to the effect that the 20 enhancement in SU_4 will be minimal, a point of view at least partially supported by the semileptonic total branching ratios. What we want to emphasize here, however, is that the enhancement hypothesis is subject to a rather direct experimental test.

Experimentally, the most significant pieces of information have to do with the measured branching ratio for $D^+ \to \bar{K}^0 \pi^+$, $D^0 \to K^-\pi^+$, and $D^0 \to K^-\pi^+\pi^0$. The interest in the two body decays stems from the fact that in the sextet dominance model we have the prediction,

$$\Gamma(D^+ \to \bar{K}^0\pi^+) = 0 \qquad \Gamma(D^0 \to K^-\pi^+) \neq 0$$

On the other hand, the experimental branching ratios for these two decay modes are comparable, i.e.[120]

$$BR(D^+ \to \bar{K}^0\pi^+) = 1.5 \pm .6\%$$

$$BR(D^0 \to K^-\pi^+) = 2.2 \pm .6\% \ .$$

To reconcile the data with the prediction of the sextet dominance we have to require that the D^+ lifetime be significantly larger than the D^0 lifetime. We can define ratio R by

$$R \equiv \Gamma_{TOT}(D^+)/\Gamma_{TOT}(D^0) \ .$$

The model would be in good shape if R were small. Accordingly, we shall consider next the general theoretical considerations regarding the value of R.

If the Hamiltonian for the charm charging decays is of the current current form then it must be mainly of the $\Delta T=1$ type. This can be seen easily if we consider the relevant transition in the quark picture, i.e. $c \to s\ u\ \bar{d}$. This has the implication that in D^+ decays the final state can be only $T = 3/2$; in the D^o decays however, it can be a mixture of both $T = 3/2$ and $T = 1/2$ (to see that consider for example $D^+ \to K^-\pi^+\pi^+$ and $D^o \to \overline{K^o}\pi^+\pi^-$). This difference leads to bounds on R, i.e.

$$0 \leq R \leq 3$$

as first pointed out by Peshkin and Rosner[144] and independently by Pais and Treiman[143];

We consider next the experimental information on the $D \to K\pi\pi$ channels that has a bearing on this question.

The experimental facts are the following:

1 - The two relevant branching ratios are

$$BR(D^+ \to K^-\pi^+\pi^+) = 3.9 \pm 1\%\ ^{120)}$$

$$BR(D^o \to K^-\pi^+\pi^o) = 12 \pm 6\%\ ^{146)}$$

2 - The Dalitz plot population for the $K^-\pi^+\pi^+$ decay mode is consistent with being flat[122] i.e. there is no evidence for any $K\rho$ or $K^*\pi$ contribution.

In addition, from the consideration of the $\Delta T=1$ rule in this decay, we have a theoretical prediction

$$\Gamma(D^+ \to K^-\pi^+\pi^+) = 4\ \Gamma(K^-\pi^+\pi^o)$$

which is valid for the case of no important intermediate state (i.e. flat Dalitz plot).

Combining the experimental information with the theoretical prediction one obtains $R=12 \pm 6$. The errors on this number are still large, but should this result hold up with better statistics, it would be a serious problem as emphasized by Rosen.[148] The least painful way to get out of it would be to accept important contributions due to $K^*\pi$ and/or $K\rho$ which, in light of limited statistics at the present time, might still be compatible with the data.

We see thus the fundamental contradicting demands made on R; the 2 body data requires R to be significantly less than 1, the 3 body data wants R as large as possible. One should emphasize here that the $K\pi\pi$ problem is independant of the idea of sextet dominance; even if we abandon the sextet enhancement, on much more general grounds we have the requirement that $R \leq 3$. Parenthetically, we should remind the reader that a small R would also solve the apparent discrepancy discussed previously between the νNe data and the D branching ratios.

In principle, at least, the question discussed above can be resolved by extracting the separate semileptonic branching ratios for D^o and D^+, since the absolute rates for these decays have to be equal.[149] That question should be answered soon, either by comparing the R_{2e}/R_e rates or by comparing the D branching ratio numbers extracted at 3.77 and at 4.03 where the relative production rates for D^o and $D^\pm$ are significantly different.

We finally say a few words about some more general treatments of hadronic decays of charmed particles. Quigg and Rosner[138] have used a statistical model to estimate the relative branching ratios. That kind of model would be expected to be very good in the limit of very high mass of the parent particle and large multiplicity. On the other hand, for decays involving only 2 or 3 particles special dynamical effects might become important. The general predictions of this model are illustrated in Fig. 37, for both the D^o and $D^\pm$ decays. The predicted branching ratios

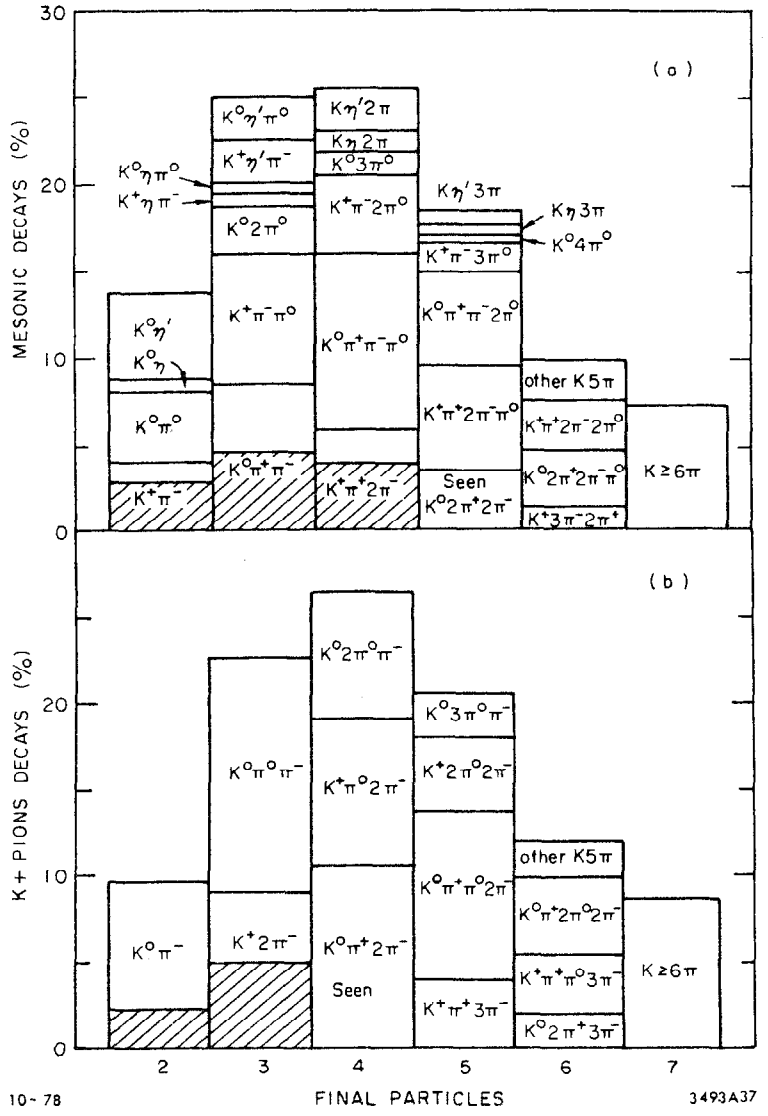

Fig. 37 Predictions of the statistical model for (a) D^0 hadronic decays and (b) $D^{\pm}$ hadronic decays. The shaded areas are the experimental results from the LGW collaboration.

have been renormalized to take account of the fact that the model does not calculate the semileptonic decays (or decays involving η's for $D^{\pm}$). The shaded regions represent the experimental measurements.

In general, as can be seen from Table XIII the model predicts a higher charged multiplicity than is observed experimentally.

Table XIII

Comparison of statistical model predictions with experiment

	$\langle n_c \rangle_{D^0}$	$\langle n_c \rangle_{D^+}$
Model predictions	3.0	3.1
Experiment (Ref. 137)	2.3±0.3	2.3±0.3

S. Kaptanoglu has adopted a different approach,[151] namely one utilizing PCAC with an extrapolation to physical region that takes final state interactions into account. He also explicitly requires the validity of $\Delta T=1$. He finds that final state interactions without requiring a specific resonant state contributions, can give significant enhancements for some of the decay modes. We should also mention that L. Maiani[152] has calculated the two body decay rates of charmed particles using the parton model. He gets a good agreement with the experiment for the ratio of the branching fractions for $D^0 \to K^-\pi^+$ and $D^+ \to K^0\pi^+$.

In summary, we can say that the situation of the hadronic decays of D mesons is far from understood. As can be seen from Fig. 37, the experimental data is very scanty, and some of these questions probably will not be answered until more information is forthcoming.

f) $D^o - \overline{D^o}$ mixing. We expect here an analogous situation with the K^o-$\overline{K^o}$ system, i.e. physical states will be

$$\psi = \frac{1}{\sqrt{2}} (D^o \pm \overline{D^o})$$

where ψ is a state characterized by a definite mass and lifetime. In other words just as we have second order transitions, i.e.

$$K^o \leftrightarrow i \leftrightarrow \overline{K^o}$$

where i is some intermediate state that can communicate both with the K^o and $\overline{K^o}$ system via lst order weak interaction so we expect also to have

$$D^o \leftrightarrow i \leftrightarrow \overline{D^o}$$

There is, however, an important difference here: whereas in the K^o, $\overline{K^o}$ system one of the intermediate states could have been $|\pi^+\pi^->$, i.e. the dominant decay mode, here the allowed intermediate states are the Cabibbo suppressed states i.e. $|n\pi's>$ since the states with non zero strangeness cannot communicate with both D^o and $\overline{D^o}$. Thus, whereas for K^o-$\overline{K^o}$ system we have $\Gamma_s \approx \Delta m$, in the charmed system the ratio of the off-diagonal to diagonal terms is expected to be $\approx \tan^4\theta_c$ i.e. $\approx 10^{-3}$. The experimental ramification is that D^o(or $\overline{D^o}$) will not live long enough to transform itself into the state of opposite charm and mixing effects will be negligible. In addition, as pointed out by Kingsley et al.[143] in the limit of exact SU_3, the mixing would vanish altogether, and thus the effects could be considerably smaller than 10^{-3}.

On the other hand, one could have[153] first order $|\Delta C|=2$ neutral currents which would create D^o-$\overline{D^o}$ mixings effects on a time scale of the order of D^o lifetime. This interaction then would manifest itself as a 50% mixing effect. The experimental data exclude the latter hypothesis but is far too poor in sensitivity to approach the standard model prediction.

In the $3.9 < E_{CM} < 4.6$ GeV region in e^+e^- annihilations a search has been performed[154] for charm events exhibiting apparent strangeness violation. The absence of such events allows one to put a limit of 18% (90% C.L.) on this kind of a process.

A search[155] in the $5 < E_{CM} < 7.8$ GeV region for the process

$$D^{*+} \rightarrow \pi^+ D^o \quad (D^o \rightarrow K^+\pi^-)$$

has yielded a 90% C.L. of 16% for this process. This decay chain, representing a $\Delta C=-\Delta S$ transition, would also have to result from some sort of D^o-$\overline{D^o}$ mixing mechanism. A better limit on this mixing parameter should be soon forthcoming from the DELCO experiment, from the search for 2 electron hadronic events, where the 2 electrons have the same charge.

The D^o-$\overline{D^o}$ mixing phenomena can also give rise to observable CP violating effects in analogy to the K^o-$\overline{K^o}$ system. Since these effects are expected to be small, however, and as yet no experimental data is available on this subject, we refer the interested reader to the extensive literature on this topic.[156]

g) Status of the F and charmed baryons. The experimental situation on these two topics is very scanty. Let us first summarize the totality of relevant experimental data on the subject of charmed baryons.

1 - One famous event[157] of the type

$$\nu_\mu p \rightarrow \mu^- \Lambda \pi^+\pi^+\pi^+\pi^-$$

has been observed in a BNL 7' bubble chamber exposure. None of the other possible interpretations are stated to have a probability in excess of 3×10^{-5} and thus the event is most likely an example of

$\Delta Q = -\Delta S$ which could be understood as a production and decay of a charmed baryon. The effective mass of the $\Lambda 4\pi$ system is 2426 ± 12 Mev.

2 - A narrow peak has been observed[158] in a photoproduction experiment at Fermilab in the $\bar{\Lambda}\pi^+\pi^-\pi^-$ system with a mass of 2.26 ± 0.01 GeV/c^2. (see Fig. 38) The quantum numbers are consistent with the state being a charmed baryon. In addition the experimental width of the state is consistent with the resolution and thus compatible with a weak decay. One should note that one of the 3 possible $\Lambda\pi^+\pi^+\pi^-$ combinations in the BNL event has a mass of 2.26 GeV/c^2.

3 - The inclusive $p(\bar{p})$ cross section (expressed in terms of the point cross section) is reported to have a step[159] around 5 GeV center of mass energy. (see Fig. 39) To a lesser extent a similar behavior is seen in the $\Lambda(\bar{\Lambda})$ cross section, but the statistics there are much less significant.

4 - There appears no significant step in the inclusive antiproton cross section in the preliminary DASP data[160] as evidenced by Fig. 40. Note, however, that this plot is in terms of absolute cross section.

5 - There is some weak evidence[161] from the UCLA-SLAC collaboration for a rise in the $\bar{\Sigma}^{\pm}$ production in e^+e^- annihilations at 7 GeV as compared to 4 GeV. The evidence comes from a presence of a significant peak in the $\bar{n}\pi^{\pm}$ mass spectrum at the mass of $\Sigma^{\pm}$ at 7 GeV, whereas no such peak is seen at 4 GeV (Fig. 41).

Clearly the data are very scanty and some of the results quoted above may not hold up with better statistics. One can however draw some tentative conclusions accepting on face value the main features of the results quoted above.

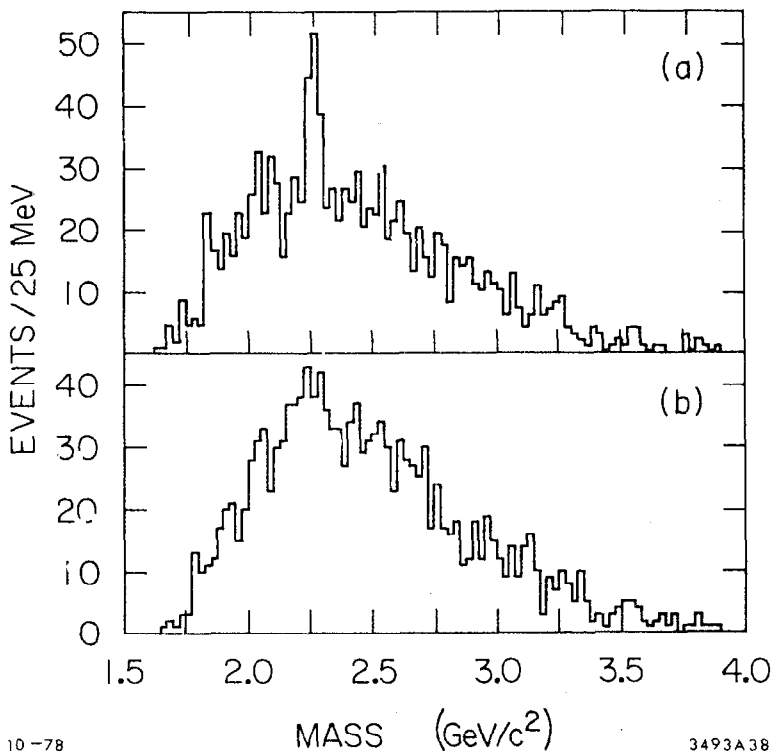

Fig. 38 Mass distribution for (a) $\bar{\Lambda}\pi^+\pi^-\pi^-$ events and (b) $\bar{\Lambda}\pi^+\pi^+\pi^-$ events from the photoproduction experiment at Fermilab.

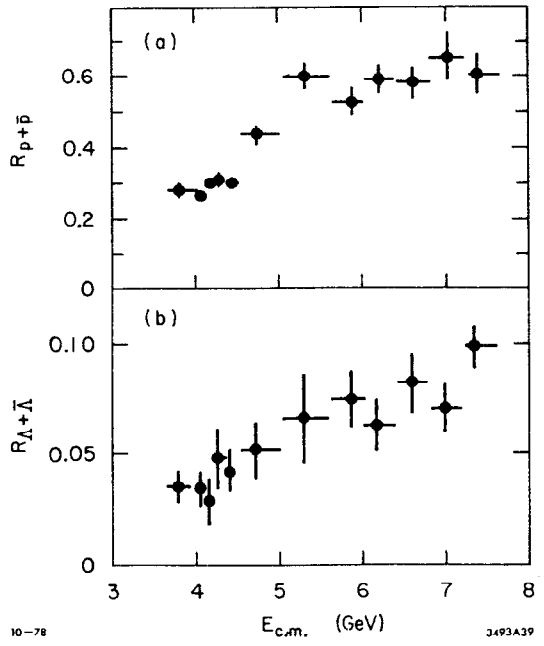

Fig. 39 Plot of the R value for (a) $\bar{p}p$ production and (b) $\bar{\Lambda}\Lambda$ production as a function of the center of mass energy. The data is from the SLAC-LBL collaboration.

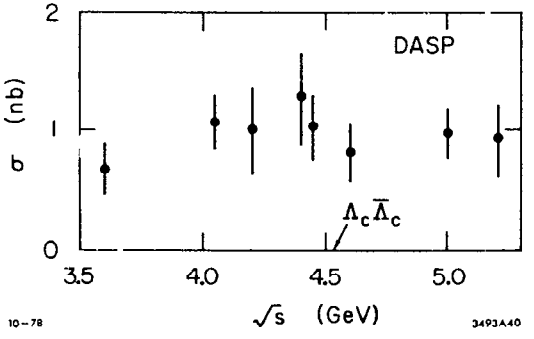

Fig. 40 The cross section for $\bar{p}p$ production as a function of center of mass energy from the DASP experiment. The data shown is preliminary and includes only events with momenta above 500 MeV/c.

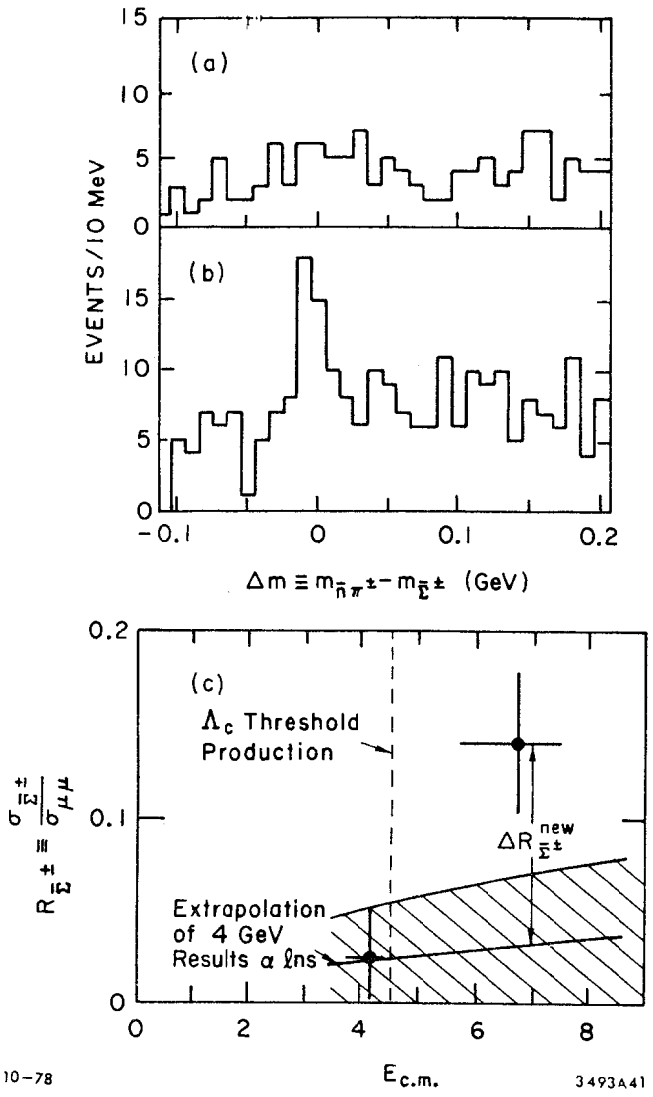

Fig. 41 The $\bar{\Sigma}^{+}$ data from the UCLA-Mark I collaboration. In (a) is displayed the difference between the mass of the $\bar{n}\pi^{\pm}$ system and the $\bar{\Sigma}^{\mp}$ mass at 4 GeV, and in (b) the same quantity at 7 GeV. The corresponding R_{Σ} value at these two energies is shown in (c).

1 - The mass of the ground state of charmed baryon spectrum is low enough (2.26 GeV/c^2) so that it decays weakly.

2 - The production of charmed baryons in e^+e^- annihilations bears the same ratio to non-charmed baryons as charmed mesons to non charmed mesons (assuming that the rise in $R_{p,\bar{p}}$ is due entirely to charmed baryon production).

3 - The observed larger rise in the $p\bar{p}$ system than in the $\Lambda\bar{\Lambda}$ system would argue that a $\bar{K}N$ ($n\pi$'s) decay modes are relatively more important than the hyperon modes.

The experimental situation with respect to the F's is almost as scanty. The F being a $c\bar{s}$ combination, the searches have concentrated on particle systems containing either an η or a $K\bar{K}$ combination (η has some $s\bar{s}$ content). Again we summarize the overall situation:

1 - The DASP collaboration[162] finds evidence for an enhanced production of η's associated with a soft photon at 4.4 GeV. One possible mechanism explaining such an observation would be

$$e^+e^- \to F^* + \ldots$$
$$\hookrightarrow F + \gamma$$
$$\hookrightarrow \eta + \ldots$$

The relevant data are displayed in Fig. 42.

2 - The same group[163] also found evidence for enhanced η production at 4.16 GeV when no soft photon requirement was made (Fig. 43). The detailed $m_{\gamma\gamma}$ spectra in the region of these two enhancements (4.16 and 4.4 GeV) are shown in Fig. 44.

3 - The same group has also looked at specific events[162,163] to see whether any 2γ + soft γ+ π events at this energy gave an acceptable fit either to the hypothesis

$$e^+e^- \to F + (F + \gamma_{soft})$$
$$\hookrightarrow \pi + \eta$$
$$\hookrightarrow \gamma + \gamma$$

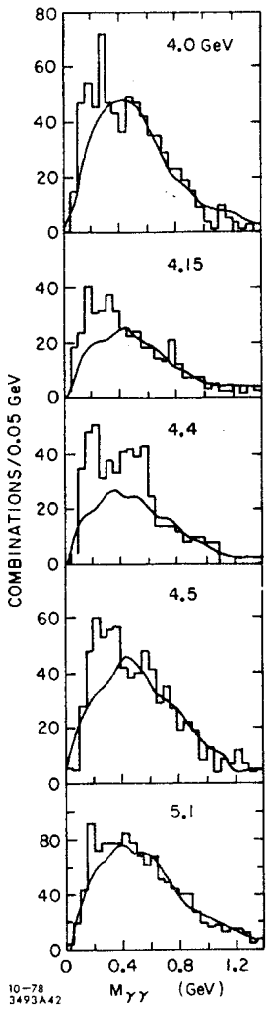

Fig. 42 Distribution of $m_{\gamma\gamma}$ for events having an additional low energy photon (E_γ < 140 MeV). The solid lines are estimates of uncorrelated photon background. The data is from DASP.

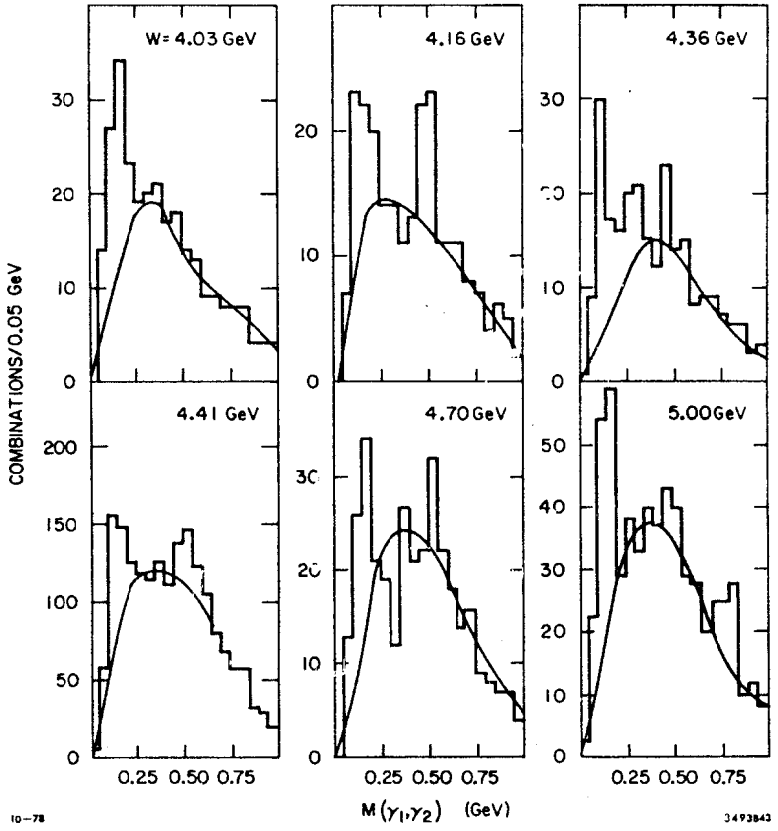

Fig. 43 Distribution of $m_{\gamma\gamma}$ without requiring the low energy photon. The data is from the DASP experiment.

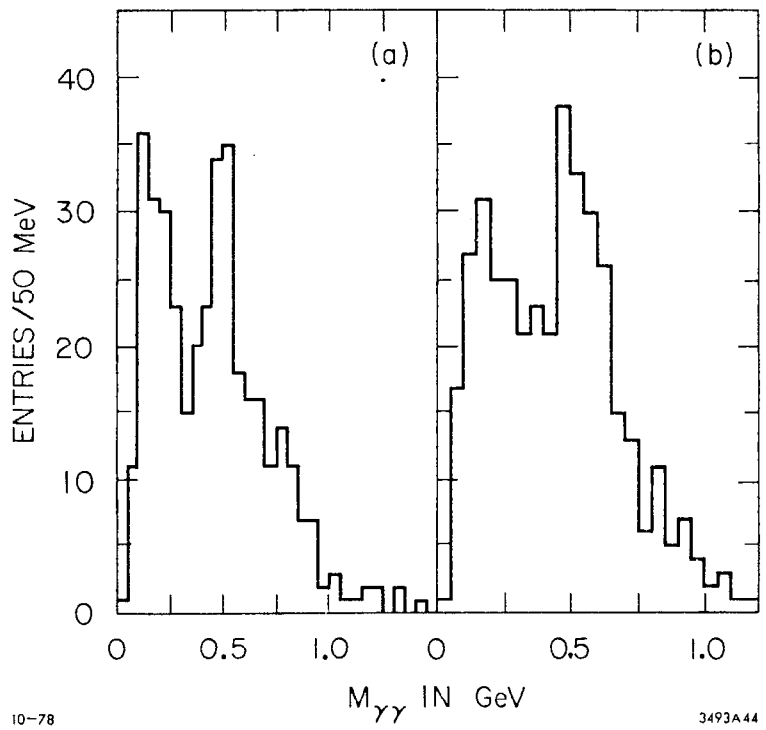

Fig. 44 Distribution of $m_{\gamma\gamma}$ for (a) E_{CM} between 4.10 and 4.22 GeV without soft photon requirement, and (b) at 4.4 GeV with the soft photon requirement. The data is from the DASP experiment.

or $e^+e^- \to F^* + F^*$

$\hookrightarrow F + \gamma_{soft}$

$\hookrightarrow \pi + \eta$

$\hookrightarrow \gamma + \gamma$

For each event the mass of the F (or F^*) were allowed to be a free parameter but the mass was forced to be the same for the 2F's (or F^*'s) in any given event. The events fitting one hypothesis generally also gave a satisfactory χ^2 for the second one with slightly different mass values. The events satisfying the first hypothesis are displayed in Fig. 45. The cluster in the upper right hand corner is interpreted as coming from the FF^* production giving m_F = 2030±60 MeV and m_{F^*} = 2140 ± 60 MeV.

4 - The SLAC-LBL collaboration[164] has studied the $K\bar{K}$ ($n\pi$) combinations at the E_{CM} energy of 4.161 GeV. Their preliminary data analyzed on the hypothesis of $e^+e^- \to F\bar{F}$ is shown in Fig. 46 indicating a possible F with a mass of 2039.5 ± 1.0 MeV. The channels into which the F is forbidden to decay according to the GIM scheme, show no such enhancement.

Again, to summarize the situation, we can say that there appears now to be a reasonably good and self consistent evidence for the existence of an F meson with a mass in the appropriate range. Its apparent weak decays support the conventional charm picture.

h) Charmed particle lifetime. We shall finally discuss the theoretical and experimental situation on the D lifetime. As we saw above, only crude hand waving arguments can be made about the total decay rate; on the other hand, one can estimate the $D \to K\ell\nu$ rather reliably, since presumably one knows the matrix elements reasonably well, and the only uncertainty comes

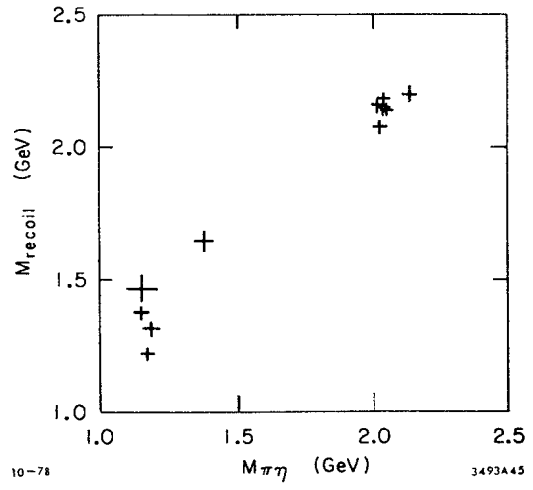

Fig. 45 Scatter plot of events that fit the reaction $e^+e^- \to FF^*$, $F \to \eta\pi$, $F^* \to \gamma_{soft}\, F$. The data is from the DASP experiment.

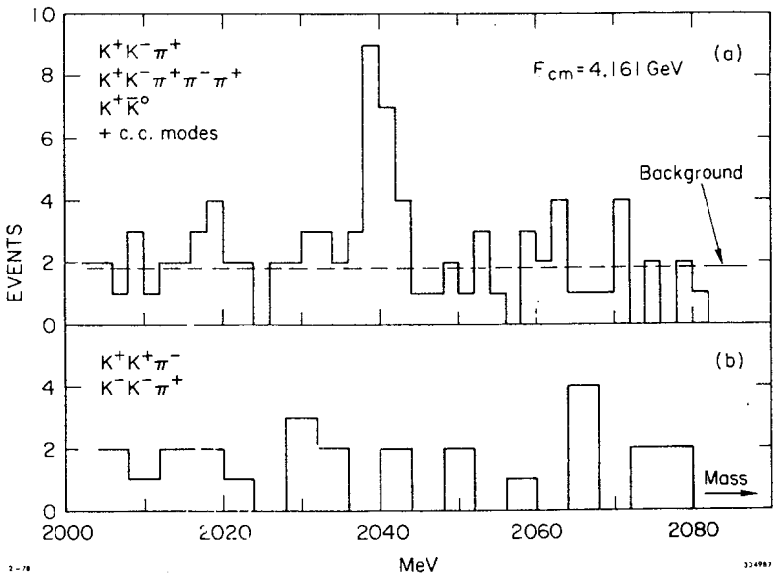

Fig. 46 Preliminary invariant mass spectra at 4.161 for (a) $K^+K^-\pi^+$, $K^+K^-\pi^+\pi^-\pi^+$, $K^+\bar{K}^0$ combinations and their charge conjugate states and (b) $K^+K^+\pi^-$ and $K^-K^-\pi^+$ combinations. The results are from the SLAC-LBL collaboration.

from the value of the form factor f_+ (the other form factor, f_-, will not contribute to the Kev decay). If $K\ell_3$ data can be our guide, then one can probably assume that $f_+(0)=1$ and pole dominance (F^* in this case) are reasonable assumptions.

The calculations for constant form factors give[165] $\Gamma(D \to K\ell\nu) \approx 1.1 \times 10^{11}$ sec^{-1}; inclusion of form factor dependance raises this to 1.4×10^{11} sec^{-1}. The less reliable calculations[165),147] for $\Gamma(D \to K^*\ell\nu)$ and $\Gamma(D \to K\pi\ell\nu)$ give 0.8 and 0.5×10^{11} sec^{-1} respectively. This is in good agreement with qualitative indications from DELCO that Kev is responsible for 50% of total electronic decay rate of the D. These arguments give us $\tau \gtrsim 3 \times 10^{-13}$ sec for the D lifetime, and a pretty rigorous limit of $\tau_D \geq 9 \times 10^{-13}$ sec, on the assumption of constant form factors and no K^*ev or $K\pi ev$ contribution.

There is indirect experimental evidence on the question of D lifetime through measurements of lifetime dependent limits on charm production on one hand, and positive results which can be interpreted as observation of charm production in hadronic interactions on the other hand. We shall end these lectures with the discussion of these experiments and comparison with the numbers discussed above obtained through theoretical arguments.

In principle, the most stringent limits on charm production in hadronic interactions come from the emulsion exposures at Fermilab. These experiments look for short tracks emenating from a proton interaction, and to avoid backgrounds require two such tracks (i.e. associated production of charm) to classify an event as a charm producing one. The two most sensitive experiments by G. Goremans-Bertrend et al.[166] and by W. Bozzoli et al.[167] have comparable sensitivity, insofar as the latter experiment looks at a smaller sample of events but accepts a larger field of view. Neither experiment sees any double decay events, but the limit that corresponds to it is very highly lifetime dependent since the efficiency for detecting two decays varies strongly as a function of lifetime (see Fig. 47).

Three CERN experiments have recently reported evidence for excess of electron neutrino events coming from the beam dump. Both the Gargamelle[168] and BEBC[169] collaborations have been able to identify the individual electron neutrino events; the CDHSB collaboration[170] has seen an excess of apparent neutral current events whose characteristics were such that they are most readily interpretable as the ν_e events. The details of the three experiments have been summarized by Wachsmuth[171] and his comparison of expected and observed event rates is reproduced below in Table XIV.

If one interprets these data as due to the process

$$p + \text{nucleon} \to D\bar{D} + \text{anything}$$

followed by semileptonic decay of the D then one obtains the following pp cross sections, on the assumption of $A^{2/3}$ dependance

BEBC, Gargamelle	100-200 μb
CDHSB	40 μb

A linear A dependance, which might be a more reasonable assumption on the basis of the ψ production data[172] would give cross sections a factor of smaller. We can make several comments about these data:

1 - For the purpose of subsequent comparison with the emulsion data the A dependance question is irrelevant since the value of A in emulsion and the beam dump experiment (which used copper) is very comparable.

2 - The CERN experiments do not contradict the most stringent lifetime independent experimental limit on charm production in this energy range[173]

Table XIV

Observed and expected relative event rates

	BEBC		CDHSB			GARGAMELLE
	e^-/μ^-	e^+/μ^+	$NC/CC^{\pm}$	μ^+/μ^-		$(e^-+e^+)/(\mu^-+\mu^+)$ (*)
	E_{vis}>10 GeV		E_H>20 GeV	E_{vis}>20	E_{vis}>50 GeV	E_{vis}>10 GeV
Expected ratio ± 10% 0 mr	0.07(1.4/21)	0.09(0.3/3.4)	0.3	0.16	0.12	0.07
Expected ratio ± 10% 15 mr	0.16(1.3/8)					
Observed 0 mr	0.37(11/30)	0.80(4/5)	0.86±0.08	0.22±0.02	0.19±0.02	0.56 (9/16)
Observed 15 mr	0.67(8/12)	not analysed				absent

(*) Due to the short radiation length in Gargamelle (11 cm) e^+ and e^- could not be distinguished.

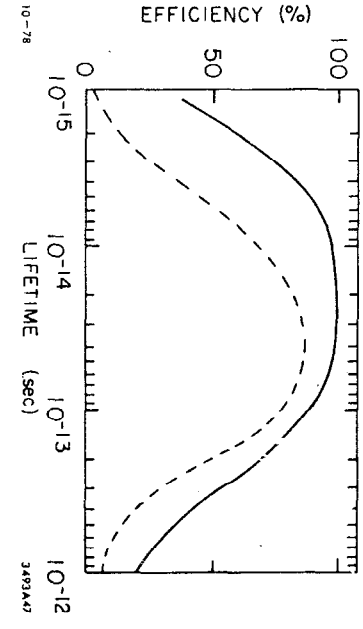

Fig. 47 Detection efficiency for the observation at 300 GeV of the decay of one (solid line) or two (dashed line) charmed particles plotted as function of charmed particle lifetime. The curves are relevant for experiment of Ref. 167.

obtained by looking for $D^o \to K^{\mp} + \pi^{\pm}$ decay. With some assumptions about y dependance their limit is about 25μb for D^o and $\overline{D^o}$ production. It thus should be multiplied by at least a factor of 2 (to allow for $D^{\mp}$, F's, charmed baryons) for comparison with the CERN beam dump experiments. Clearly the A dependance assumption is important here.

3 - There is clearly an internal inconsistency between the bubble chamber experiments and the CDHSB experiment. The data relevant to the 3 detectors has been summarized by Wachsmuth[171] and is reproduced in Table XV. The origin of the discrepancy is not understood at the present time.

Table XV

Comparison of the signal in the three detectors

	BEBC		CDHSB	GARGAMELLE
	0 mr	15 mr*	0 mr	0 mr
mass (t)	13	12	580	10.5
solid angle (μsr)	10	9	10.8	1.8
length (m)	∿3		9.3	4.6
interacting protons (10^{17})	3.5	3.7	4	3.5
distance from target (m)	820		890	950
neutrino flux dilution	1.0		0.85	0.75
μ^- events (E_{vis} > 20 GeV) predicted	17	4.5	790	10
observed	26	7	850	∿11
excess e^+ and e^- events (E_{vis}>20 GeV)	11.3	1.7	236	7.3
normalized to BEBC (0 mr)	1	.16	.48	1.1
<E> of excess events (E_{vis}>20 GeV)	71	30	85	73
ν_e flux per proton and μsr, derived from excess e^+, e^- events (E_{vis}>20 GeV)	5×10^{-8}	2.1×10^{-8}	1.8×10^{-8}	5×10^{-8}

* 15 mr data were obtained with a Be (rather than Cu) target

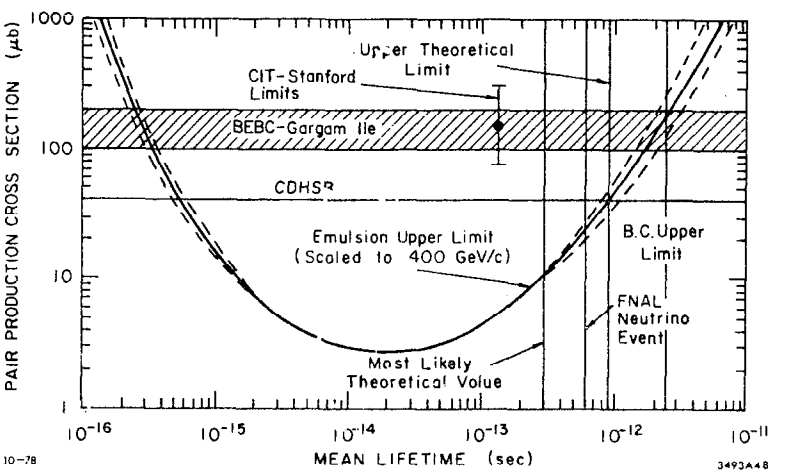

Fig. 48 The relevant data that has a bearing on the production cross section and lifetime of charmed particles. For ease of comparison all the experiments on nuclear targets have been converted to the nucleon cross sections by assuming $A^{2/3}$ dependence.

Recently the Cal Tech-Stanford collaboration has presented results[174] indicating the production of single prompt μ's in p-Fe collisions. Their preliminary analysis indicates that the observed rate, if interpreted as due to production and semileptonic decay rate of D mesons, would correspond to a cross section of about 40 μb (uncertain to a factor of 2) if one assumes linear A dependance.

There are a couple of final experimental comments to be made about the D lifetime. The Fermilab neutrino emulsion event,[175] interpreted as a possible charm condidate, had an observed lifetime of 6×10^{-13} sec. Furthermore, the analysis of 2μ events in the ν bubble chamber exposures appear to exclude lifetimes longer than $2\text{-}3 \times 10^{-12}$ sec.[176]

The experimental data and theoretical considerations discussed above are displayed in Fig. 48. The translation of the emulsion limits to a curve in the $\sigma_{D\bar{D}} - \tau_D$ space has been taken from the analysis of Crennell et al.[177] There is probably a narrow window i.e.

$$5 \times 10^{-13} < \tau_D < 10^{-12}$$

with which all the pieces of information can be made compatible. Whether this is indeed the case, or whether this topic contains some deeper mysteries, will be hopefully answered in the future with more experimental results.

The lifetime range quoted above, coupled with a $\gamma \approx 10$ gives a typical mean decay path of the order of one millimeter. These distances unfortunately fall into the awkward region of being too short for a bubble chamber or electronic detectors, but unconveniently long for the emulsion experiments. The newly developed high resolution steamer chamber[178] should however be able to cover well this lifetime range.

References

1) Experimental Phenomenology, M. Schwartz and S. Wojcicki, Proceedings of Stanford Summer Institute on Particle Physics, July 9-28, 1973, p. 23, vol. II.

2) Konrad Kleinknecht, CP violation and K^0 decays, Ann. Rev. of Nucl. Sc. p.1, vol. 26, 1976; Lee G. Pondrom, Weak Decay Processes, Proceedings of the Annual Meeting of the American Physical Scoiety, Division of Particles and Fields, BNL, October 6-8, 1976, p. C1.

3) A. Salam, in "Elementary Particle Physics", ed. by N. Svartholm (Almquist and Wiskells, Stockholm, 1968); S. Weinberg, Phys. Rev. Lett. 19, 1264 (1967).

4) see for example the results presented at the XIX International Conference on High Energy Physics in Tokyo, Japan, August 23-30, 1978.

5) S. W. Herb et al., Phys. Rev. Lett. 29, 252 (1977).

6) C. H. Berger et al., Phys. Lett. 76B, 243 (1978); C. W. Darden et al., Phys. Lett. 76B, 246 (1978).

7) N. Cabibbo, Phys. Rev. Lett. 10, 531 (1963).

8) A. R. Clark et al., Phys. Rev. Lett. 26, 1667 (1971); J. H. Klems, R. H. Hildebrand, and R. Stiening, Phys. Rev. D4, 66 (1971).

9) F. J. Hasert et al., Phys. Lett. 46B, 138 (1973).

10) A. Benvenuti et al., Phys. Rev. Lett. 32, 1025 (1974).

11) S. L. Glashow, J. Iliopoulos, and L. Maiani, Phys. Rev. D2, 1285 (1970); B. J. Bjorken and S. L. Glashow, Phys. Lett. 11, 255 (1964).

12) G. Goldhaber et al., Phys. Rev. Lett. 37, 255 (1976).

13) M. Kobayashi and K. Maskawa, Progr. Theor. Phys. 49, 652 (1973).

14) J. Ellis, M. K. Gaillard, D. V. Nanopoulos, and S. Rudez, Nucl. Phys. B131, 285 (1978).

15) For a recent review of these ideas see David N. Schramm, Cosmology and New Particles, Proceedings of the 1977 Annual Meeting of the Division of Particles and Fields, Argonne, Ill., October 6-8, 1977, p.87.

16) J. Ellis, Lectures at this Institute.

17) For a detailed discussion of a possible experimental arrangement see J. Rich and D. R. Winn, Phys. Rev. D14, 1283 (1976).

18) E. Ma and J. Okada, Phys. Rev. Lett. 41, 287 (1978).

19) W. Tanenbaum et al., Phys. Rev. D12, 1871 (1975).

20) D. Décamp et al., The ratio $|g_A|g_v|$ in the decay $\Sigma^- \to ne^-\nu$, Orsay preprint.

21) M. L. Herbert et al., Phys. Rev. Lett. 40, 1230 (1978).

22) W. E. Cleland et al., Bull. Am. Ph. Soc., 23 (1978), paper DL6.

23) J. Wise et al., Bull. Am. Ph. Soc., 23 (1978), paper DL10.

24) M. Roos, Phys. Lett. 36B, 130 (1971).

25) M. M. Nagels et al., Nucl. Phys. B109, 1 (1976).

26) C. Callan and S. Treiman, Phys. Rev. Lett. 16, 153 (1966).

27) R. Dashen and M. Weinstein, Phys. Rev. Lett. 22, 1337 (1969).

28) S. Gjesdal et al., Nucl. Phys. B109, 118 (1976).

29) G. Donaldson et al., Phys. Rev. D9, 2960 (1974).

30) C. Bricman et al., Phys. Lett. 75B, 1 (1978).

31) A. R. Clark et al., Phys. Rev. D15, 553 (1977).

32) G. D. Law, Determination of the $K\mu_3^+$ Form Factor, $\xi(q^2)$ From the Muon Polarization, U. of Michigan Ph. D. thesis; W. G. Wilke, U . of Wisconsin Ph.D. Thesis.

33) J. Heintze et al., Phys. Lett. 70B, 482 (1977).

34) L. Rosselet et al., Phys. Rev. D15, 574 (1977).

35) P. Bloch et al., Phys. Lett. 60B, 393 (1976).

36) T. J. Devlin and J. O. Dickey, Weak Hadronic Decays: K↦2π and K↦3π, U. of Rutgers preprint, RU 78-79.

37) O. E. Overseth, Appendix II in Ref. 30.

38) G. Bunce et al., A New Measurement of the Λ Helicity in the Decay $\Xi^0 \to \Lambda\pi^0$, submitted to Phys. Rev. D, BNL preprint 24047.

39) see Appendix I in Ref. 30 for the most recent summary; also ref. 36.

40) J. H. Christenson et al., Phys. Rev. Lett. 13, 138 (1964).

41) L. Wolfenstein, Phys. Rev. Lett. 13, 562 (1964).

42) J. Ellis, M. K. Gaillard, and D. V. Nanopoulos, Nucl. Phys. B109, 213 (1976); see also H. Harari, SLAC Summer Institute 1977, SLAC-204.

43) J. S. Bell and J. K. Perring, Phys. Rev. Lett. 13, 348 (1964); J. Bernstein, N. Cabibbo and T. D Lee, Phys. Lett. 12, 146 (1964).

44) X. De Bouard et al., Phys. Lett. 15, 58 (1965); W. Galbraith et al., Phys. Rev. Lett. 14, 383 (1965).

45) V. L. Fitch et al., Phys. Rev. Lett. 15, 73 (1965), C. Alff-Steinberger et al., Phys. Lett. 20, 207 (1966).

46) W. C. Carithers et al., Phys. Rev. Lett. 34, 1244 (1975).

47) T. T. Wu and C. N. Yang, Phys. Rev. Lett. 13, 380 (1964).

48) N. F. Ramsey, Bull-Am. Phys. Soc. 21, 61 (1976).

49) W. C. Carithers et al., Phys. Rev. Lett. 30, 1336 (1973) and 31, 1025 (1973).

50) Y. Fukushima et al., Phys. Rev. Lett. 36, 348 (1976).

51) M. J. Shochet et al., Phys. Rev. Lett. 39, 59 (1977).

52) R. C. Field, Revision of Bevatron Branching Ratio Results on $K_L^0 \to \mu^+\mu^-$ and $K_L^0 \to \pi^+\pi^-$, SLAC-PUB-1498, October 1974.

53) J. Fischer et al., Phys. Lett. 73B, 364 (1978).

54) T. Goldman and C. M. Hoffman, Phys. Rev. Lett. 40, 220 (1978).

55) S. Weinberg, Phys. Rev. Lett. 40, 223 (1978); F. Wilchek, to be published; see also R. D. Peccei and H. R. Quinn, Phys. Rev. Lett. 38, 1440 (1977).

56) R. DeVoe et al., Phys. Rev. Lett. 25, 1779 (1970).

57) J. Bailey et al., Phys. Lett. 68B, 191 (1977).

58) B. L. Beron et al., Phys. Rev. D11, 2839 (1978).

59) For a detailed discussion of μ decay see for example A. M. Sachs and A. Sirlin, in Muon Physics, Vol. II, p.49, ed. by V. W. Hughes and C. S. Wu or E. D. Commins, Weak Interactions, McGraw Hill, 1973.

60) S. Berenzo, Phys. Rev. 181, 1854 (1969).

61) E. T. Tretyakov et al., paper presented at the XVIIIth International Conference on High Energy Physics, Tbilisi, 1976.

62) M. Daum et al., Phys. Lett. 74B, 126 (1978).

63) G. Feinberg and S. Weinberg, Phys. Rev. Lett. 6, 38 (1966); for experimental results quoted see J. Blietschau et al., Nucl. Phys. B133, 205 (1978).

64) P. Depommier et al., Phys. Rev. Lett. 39, 1113 (1977).

65) H. P. Povel et al., Phys. Lett. 72B, 183 (1977).

66) C. M. Hoffman et al., LASL report LA-UR 78-1686; also paper presented at this institute.

67) J. D. Bowman et al., Phys. Rev. Lett. 41, 442 (1978).

68) A. Bodertscher et al., Phys. Rev. Lett. 39, 1385 (1977).

69) S. M. Korenchenko et al., Sov. Phys. JETP 43, 1 (1976).

70) S. Frankel, in Muon Physics, Vol. II p.86, ed. by V. W. Hughes and C. S. Wu.

71) B. W. Lee et al., Phys. Rev. Lett. 38, 937 (1977).

72) T. P. Cheng and Ling-Fong Li, Phys. Rev. Lett. 38, 381 (1977).

73) F. Wilczek and A. Zee, Phys. Rev. Lett. 38, 531 (1977).

74) J. D. Bjorken and S. Weinberg, Phys. Rev. Lett. 38, 622 (1977).

75) For a detailed discussion of predictions by different models see W. J. Marciano and A. I. Sanda, Phys. Rev. Lett. 38, 1512, (1977) and G. Altarelli et al., Nucl. Phys. B125, 285 (1977).

76) V. E. Barnes et al., Phys. Rev. Lett. 38, 1049 (1977).

77) V. E. Barnes, Phys. Lett. 65B, 174 (1976).

78) E, Bellotti et al., Lett. Nuovo Cim. 17, 553 (1976); J. Blietschau et al., Nucl. Phys. B133, 205 (1978).

79) F. Reines et al., Phys. Rev. Lett. 32, 180 (1974).

80) B. Pontecorvo, Soviet Physics JETP 53, 1717 (1967).

81) For a more detailed review of neutrino mixing phenomenology and its present status see N. Cabibbo, Quark and Lepton Mixing, Lectures given at the XV Ettore Majorana School for subnuclear physics, Erice 1977, and B. Pontecorvo, Lepton Charges and Lepton Mixing, rapporteur talk given at the European Conference on Particle Physics, Budapest, Hungary 4-9 July, 1977.

82) N. Cabibbo, Phys. Lett. 72B, 333 (1978).

83) M. L. Perl et al., Phys. Rev. Lett. 35, 1489 (1975).

84) J. Burmester et al., Phys. Lett. 68B, 297 and 301 (1977).

85) R. Brandelik et al., Phys. Lett. 73B, 109, (1978).

86) W. Bacino et al., Phys. Rev. Lett. 41, 13 (1978).

87) Y. S. Tsai, Evidence for τ being a spin 1/2 lepton, SLAC-PUB-2105.

88) The present best limits on the mass of the missing neutral X in the decay $\tau \to e\nu X$ come from the DELCO and PLUTO groups who quote limits of 0.25 GeV (Ref.100) and 0.36 GeV (Ref.113) respectively.

89) D. Horn and G. G. Ross, Phys. Lett. 67B, 460 (1977); G. Altarelli, N. Cabibbo, L. Maiani, and R. Petronzio, Phys. Lett. 67B, 463 (1977).

90) We quote the numbers here from G. Altarelli et al., ref. 89, who have actually used some older and less stringent experimental limits for μ^- capture than presently available. Clearly, the argument becomes stronger if one used the more recent data.

91) R. Brandelik et al.(ref. 85) quote 0.92±0.32 for this number. See also G. Feldman, invited talk at the Neutrino 78 Conference in Purdue SLAC-PUB-2138, for a summary of other measurements; see also Ref. 86 and W. Bacino et al., ref. 98.

92) G. Feldman, private communication, quoted by M. Perl, review talk given at the 1977 International Symposium on Lepton and Photon Interactions at High Energies, Hamburg, West Germany.

93) J. D. Bjorken and C. H. Llewellyn-Smith, Phys. Rev. D7, 887 (1973).

94) S. P. Rosen, Phys. Rev. Lett. 40, 1057 (1978).

95) A. M. Cnops et al., Phys. Rev. Lett. 40, 144 (1978).

96) J. Jaros, private communication, quoted by M. Perl at the 1977 Hamburg conference.

97) Y. S. Tsai, Phys. Rev. D4, 2821 (1971). The more up to date numbers for these branching ratios can be found in ref. 87.

98) W. Bacino et al., Measurement of the Branching Ratios for $\tau \to \pi \nu_\tau$ and $\tau \to \mu \nu_\mu \nu_\tau$, submitted to Phys. Rev. Lett., SLAC-PUB-2223.

99) S. Yamada, invited talk at the 1977 International Symposium on Lepton and Photon Interactions at High Energies, Hamburg, West Germany.

100) See W. Bacino et al., ref. 98. The preliminary results of this work were presented by J. Kirkby in an invited talk at the International Conference on Neutrino Physics and Neutrino Astrophysics, Purdue University, SLAC-PUB-2127.

101) G. Hanson, unpublished analysis, quoted by G. Feldman, Ref. 91.

102) G. Alexander et al., Phys. Lett. 78B, 162 (1978).

103) see Y. S. Tsai, ref. 87 and 97; F. J. Gilman and D. H. Miller, Phys. Rev. D17, 1846 (1978); N. Kawamoto and A. I. Sanda, DESY preprint 78/14 (1978).

104) G. Alexander et al., Phys. Lett. 73B, 99 (1978).

105) J. A. Jaros et al., Phys. Rev. Lett. 40, 1120 (1978).

106) J. Kirkby, ref. 100.

107) J. Burmester et al., Phys. Lett. 68B, 297 (1977).

108) G. Flugge in Proceedings of the 1977 Experimental Meson Spectroscopy Conference at Northeastern University, Boston, 1977.

109) H. K. Nguyen, private communication, quoted by M. Perl at the 1977 Hamburg conference.

110) A. Ali and Z. Z. Aydin, Nuov. Cim. 42A, 270 (1978).

111) J. Kirkby, talk presented at this summer institute; see also J. Kirkby, Ref.100 and A.M.Diamant-Berger, Ref.136, for discussion of ρ parameter.

112) J. Burger, invited talk at the XIII Rencontre de Moriand, Les Ares (1978).

113) G. Knies, Sixth Trieste Conference on Particle Physics, Trieste, June, 1978.

114) D. A. Bryman and C. Picciotto, Phys. Rev. D11, 1337 (1975).

115) H. Fritzsch, Phys. Lett. 67B, 451 (1977).

116) W. Bartel et al., A Precise Determination of the τ-Mass, Heidelberg University preprint.

117) M. K. Gaillard, B. W. Lee and J. L. Rosner, Rev. Mod. Ph. 47, 277 (1975).

118) P. Rapidis et al., Phys. Rev. Lett. 39, 526 (1977).

119) G. Goldhaber et al., Phys. Rev. Lett. 37, 255 (1976).

120) Lead-glass Wall Collaboration, reported by A Litke in Proceedings of the 1977 European Conference on Particle Physics, Budapest, Hungary, 4-9 July, 1977, p. 687; I. Peruzzi et al., Phys. Rev. Lett.39, 1301(1977).

121) C. Zemach, Phys. Rev. B133, 1201 (1964).

122) J. E. Wiss et al., Phys. Rev. Lett. 37, 1531 (1976).

123) I. Peruzzi et al., Phys. Rev. Lett. 37, 569 (1976).

124) G. J. Feldman, Properties of the D mesons, Proceedings of the SLAC Summer Institute 1977, p. 241.

125) R. Brandelik et al., Phys. Lett. 70B, 125 (1977); see also V. Luth et al., Phys. Lett. 70B, 120 (1977).

126) J. Ellis, M. K. Gaillard, D. V. Nanopoulos, Nucl. Phys. B100, 313(1975).

127) M. K. Gaillard and B. W. Lee, Phys. Rev. Lett. 33, 108 (1974); G. Altarelli and L. Maiani, Phys. Lett. 52B, 351 (1974).

128) G. Altarelli, N. Cabibbo, L. Maiani, Nucl. Phys. B88, 285 (1975).

129) J. M. Feller et al., Phys. Rev. Lett. 40, 274 (1978).

130) W. Bacino et al., Phys. Rev. Lett. 40, 671 (1978).

131) R. Brandelik et al., Phys. Lett. 70B, 387(1977).

132) J. M. Feller et al., Phys. Rev. Lett. 40, 1677 (1978).

133) J. Kirkby, invited talk at the 1977 International Symposium on Lepton and Photon Interactions at High Energies, Hamburg, West Germany.

134) I. Hinchliffe and C. Llewellyn Smith, Nucl. Phys. B114, 45 (1976).

135) F. Bletzacker, H. T. Nieh and A. Soni, Phys. Rev. D16, 732 (1977); A. Ali and T. C. Yang, Phys. Lett. 65B, 275 (1976).

136) A-M. Diamant-Berger, in Proceedings of the XIII Rencontre de Moriand at Les Arcs, 1978.

137) V. Vuillemin et al., Inclusive Studies of D Meson Decays at the $\psi(3772)$, Phys. Rev. Lett. 41, 1149 (1978).

138) C. Quigg and J. L. Rosner, Hadronic Decays of Charmed Mesons, FERMILAB-Pub-77/60 THY (1977).

139) C. Baltay et al., Phys. Rev. Lett. 39, 62 (1977).

140) C. Baltay et al., Phys. Rev. Lett. 41, 73 (1978).

141) C. Baltay, et al., Recent Results from Neutrino Interactions in Heavy Neon, paper presented to Neutrinos-78 Conference, Purdue U., BNL-24663; A. M. Cnops et al., Lepton and Charm Production in the 15 foot FNAL Bubble Chamber, paper presented at the XIIIth Rencontre de Moriond Conference by Robert B. Palmer, BNL-24536.

142) M. B. Einhorn and C. Quigg, Phys. Rev. D12, 2015 (1975).

143) R. L. Kingsley et al., Phys. Rev. D11, 1919 (1975).

144) M. Peshkin and J. L. Rosner, Nucl. Phys. B122 144 (1977).

145) A. Pais and S. B. Treiman, Phys. Rev. D15, 2529 (1977).

146) D. L. Scharre et al., Phys. Rev. Lett. 40, 74 (1978).

147) M. Matsuda et al , Prog. Theor. Phys. 58, 1502 (1977).

148) S. P. Rosen, Phys. Rev. Lett. 41, 3 (1978).

149) see for example M. Katuya and Y. Koide, Is the total D^+ Width Much Smaller than the Total D^0 Width?, SH-78-05, preprint, July 1978.

150) A. Barbaro-Galtieri, Proceedings of the 1977 International Symposium on Lepton and Photon Interactions at High Energy in Hamburg, West Germany, p.21.

151) Sinan Kaptanoglu, Non-leptonic Charm Decays, SLAC-PUB-2072, January 1978.

152) L. Maiani, Two Body Decays of Charmed Particles, Ecole Normale preprint.

153) S. L. Glashow and S. Weinberg, Phys. Rev. D15, 1958 (1977); E. A. Paschos, Phys. Rev. D15, 1966 (1977).

154) G. Goldhaber, Bull. Am. Phys. Soc. 22, 20(T) (1977); also G. Goldhaber, invited talk given at the European Conference on Particle Physics, Budapest, Hungary, July 1977, p. 509.

155) G. J. Feldman et al., Phys. Rev. Lett. 23, 1313 (1977).

156) R. L. Kingsley, Phys. Lett. 63B, 329 (1976); A. Pais and S. B. Treiman, Phys. Rev. D12, 2744 (1975); M. Goldhaber and J. L. Rosner, Phys. Rev. D15, 1254 (1977); L. B. Okun, V. I. Zakharov, and B. M. Pontecorvo, Lett. Nuov. Cim. 13, 218 (1975).

157) E. G. Cazzoli et al., Phys. Rev. Lett. 34, 1125 (1975).

158) B. Knapp et al., Phys. Rev. Lett 37, 882 (1976).

159) M. Piccolo et al., Phys. Rev. Lett. 39, 1503 (1977).

160) W. de Boer, Recent Results from Doris, invited talk given at the SLAC Summer Institute on Particle Physics, p. 270.

161) H. F. W. Sadrozinski, Proceedings of the 1977 International Symposium on Lepton and Photon Interactions at High Energy in Hamburg, West Germany, p. 59.

162) R. Brandelik et al., Phys. Lett. 70B, 132 (1977); see also G. Weber, Recent e^+e^- Results from Doris, DESY 78/35, July 1978.

163) H. Meyer, Results on e^+e^- Annihilation Studies at Doris, Particles and Fields - 1977 (APS-DPF, Argonne) p. 413.

164) D. Lüke, e^+e^- Production of Charmed Particles at the Spear Magnetic Detector, Particles and Fields - 1977 (APS-DPF, Argonne) p. 441.

165) D. Fakirov and B. Stech, Nucl. Phys. B133, 315 (1978); see also ref.147.

166) G. Goremans-Bertrand et al., Phys. Lett. 65B, 480 (1976).

167) W. Bozzoli et al., Lett. Nuov. Cim. 19, 32 (1977).

168) P. Alibran et al., Phys. Lett. 74B, 134 (1978).

169) P. C. Bosetti et al., Phys. Lett. 74B, 143 (1978).

170) T. Hansl et al., Phys. Lett. 74B, 139 (1978).

171) H. Wachsmuth, 400 GeV proton induced prompt neutrinos at 0 and 15 milliradians, invited talk given at the Topical Conference on Neutrino Physics, Oxford, July 1978, CERN/EP/PHYS 78-29.

172) A. Bamberger et al., Nucl. Phys. B134, 1, (1978).

173) W. R. Ditzler et al., Phys. Lett. 71B, 451 (1977).

174) K. W. Brown et al., talk presented by M. H. Shaevitz at the 3rd International Conference at Vanderbilt on New Results in High Energy Physics, Nashville, Tenn., March 6-8, 1978.

175) A. L. Read et al., Fermilab PUB-78-56 Exp. (1978).

176) Aachen-Bonn-CERN-London-Munich-Oxford-Saclay Collaboration, talk presented by L. Pape at the Topical Conference on Neutrino Physics, Oxford, July 2-7, 1978, CERN/EP/PHYS 78-25.

177) D. J. Crennell, C. M. Fisher and R. L. Sekulin, Understanding Hadronic Charm Production Data and Particle Lifetime, Rutherford Laboratory preprint, RL-78-051/A; also Phys. Lett. 78B, 171 (1978).

178) T. Cardello et al., Search for Short-Lived Particles Using a High Resolution Streamer Chamber, May 1977, Fermilab Proposal #490.

OBSERVATION OF PARITY VIOLATION IN POLARIZED ELECTRON SCATTERING

David J. Sherden
Stanford Linear Accelerator Center

I. INTRODUCTION

I am going to discuss an experiment (1) performed at SLAC to measure a parity non-conserving asymmetry in the deep inelastic scattering of electrons from deuterium. The participants in the experiment, and their institutions, are listed in Table I. The reaction measured is

$$e \text{ (polarized)} + d \rightarrow e' + X \qquad (1)$$

in which only the scattered electron is detected. The asymmetry sought is given by

$$A = \frac{\sigma^R - \sigma^L}{\sigma^R + \sigma^L} \qquad (2)$$

in which σ is the differential cross section $d^4\sigma/d\Omega dE'$, and the superscripts R and L designate the helicity of the incident electron as right-handed and left-handed, respectively.

TABLE I
Participants

SLAC
- C.Y. Prescott
- W.B. Atwood
- R.L.A. Cottrell
- H. DeStaebler
- E.L. Garwin
- A. Gonidec
- R.H. Miller
- L.S. Rochester
- T. Sato
- D.J. Sherden
- C.K. Sinclair
- S. Stein
- R.E. Taylor

Yale
- J.E. Clendenin
- V.W. Hughes
- N. Sasao
- K.P. Schuler

CERN
- M.G. Borghini

Aachen
- K. Lubelsmeyer

Hamburg
- W. Jentschke

Because the asymmetry given by eq. 2 violates parity conservation, and one does not expect such a violation in purely electrodynamic processes, measurement of such an asymmetry provides a unique opportunity to observe interference effects between the weak and electromagnetic amplitudes. Furthermore, because recent gauge theoretical models provide specific predictions for the asymmetry (2), its measurement can test current theory at a rather fundamental level.

In virtually any weak/electromagnetic theory the asymmetry is expected to be of the form

$$A = \frac{GQ^2}{4\pi\alpha} f(\text{model}) \simeq 10^{-4} Q^2 f, \qquad (3)$$

where G is the Fermi coupling constant, α is the electromagnetic coupling constant, Q^2 is the square of the momentum transfer (in GeV^2), and f is some model dependent function $\lesssim 1$ (3). Consequently one expects the size of the asymmetry to be $\lesssim 10^{-4} Q^2$. Specific calculations from a number of theoretical models give predictions in accord with these simple arguments. The prime difficulty of the experiment then becomes the measurement of such a small asymmetry.

The major elements of the experiment are shown schematically in fig. 1. Polarized electrons whose helicity could rapidly be reversed were produced from an intense gallium arsenide source and injected into the SLAC accelerator. An extensive beam monitoring system was used to stabilize the accelerated beam and to verify the absence of systematic effects due to

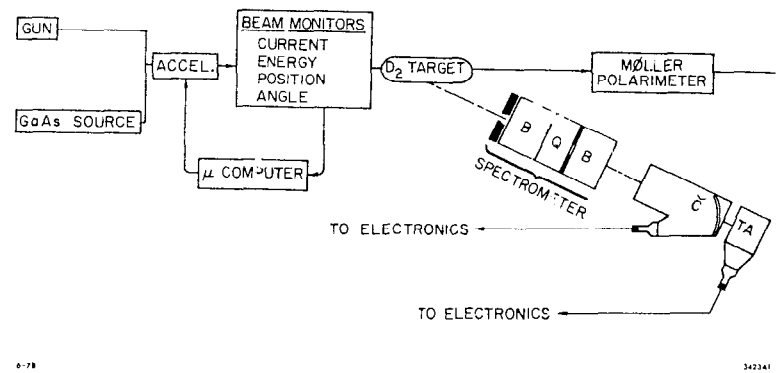

Fig. 1. Schematic illustration of the experiment.

asymmetries in beam parameters. Electrons inelastically scattered from a deuterium target were momentum analyzed by a three element magnetic spectrometer and detected in a gas Cerenkov counter and a lead glass shower counter. Because of the high rates required by the experiment, the detectors were instrumented to measure the scattered electron flux rather than to count individual scattered electrons. The polarization of the incident electron beam was measured after acceleration using Moller scattering from a longitudinally magnetized supermendur foil.

II. POLARIZED ELECTRON SOURCE

The high statistical precision of the experiment required the development of an intense source of polarized electrons. Furthermore, the minimization of systematic effects placed stringent requirements upon the source. In particular, it was important that the beam helicity be rapidly reversible, and that changes in the beam parameters upon helicity reversal should be negligibly small.

The source utilized optical pumping by circularly polarized light of electrons in a gallium arsenide crystal from the J=3/2 valence band to the J=1/2 conduction band (4), as (hopefully) can be understood from fig. 2. The circularly polarized light has a well defined spin component along the incident direction (z). Hence for a given photon helicity (+/- 1), simple consideration of Clebsch-Gordan coefficients indicates that the ratio of ($J_z = \mp 3/2 \rightarrow \pm 1/2$) to

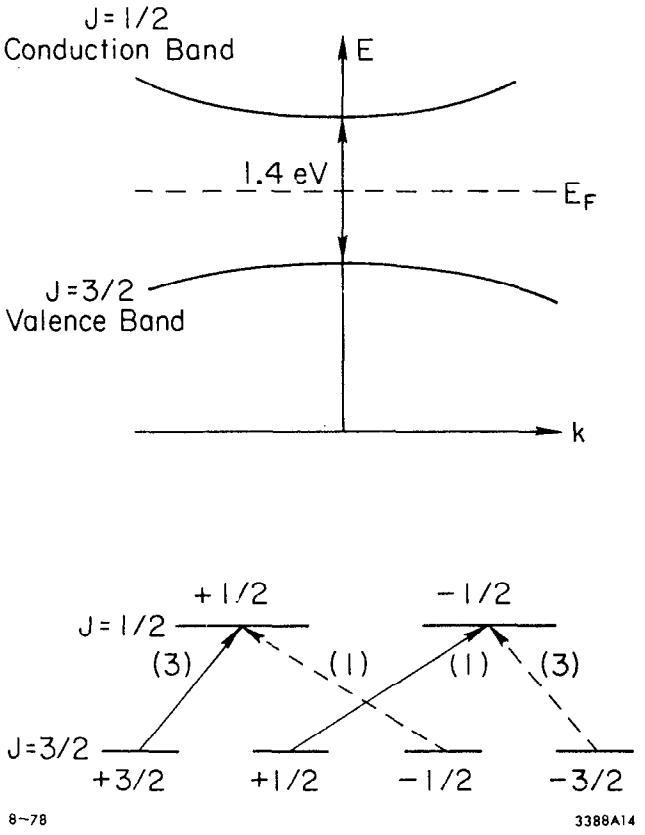

Fig. 2. Schematic illustration of the electron spin structure for the valence and conduction bands of gallium arsenide crystal.

$J_z = \mp 1/2 \rightarrow \pm 1/2$) transitions should be 3 to 1, thus giving a polarization of 50% for the conduction band electrons. The surface of the crystal can be treated with cesium and oxygen to produce a negative affinity surface, allowing the conduction band electrons to escape from the crystal.

The source apparatus is shown schematically in fig. 3. A pulsed dye laser was used to produce light of ≈7100Å which passed through an optical polarizing system to produce the circular polarization. The circularly polarized light incident on the GaAs crystal caused the emission of longitudinally polarized electrons. These were accelerated through a 65 kV potential in a structure very similar to that of the unpolarized thermionic electron sources normally used at SLAC. The polarized electrons were then magnetically deflected by 90° and injected into the accelerator.

Beam intensities of 3×10^{12} electrons per 1.5μ sec long pulse (matched to the accelerator duty cycle) before injection were achieved, resulting in beams of $1\text{-}4 \times 10^{11}$ electrons per pulse after acceleration. The average beam polarization obtained was 37%.

The optical polarizing system by which the beam helicity was reversed is shown schematically in fig. 4. Because the helicity of the electron beam is determined by the sense of circular polarization of the incident light, the objective is to produce a circularly polarized light source whose sense of polarization can be rapidly reversed with minimal changes in

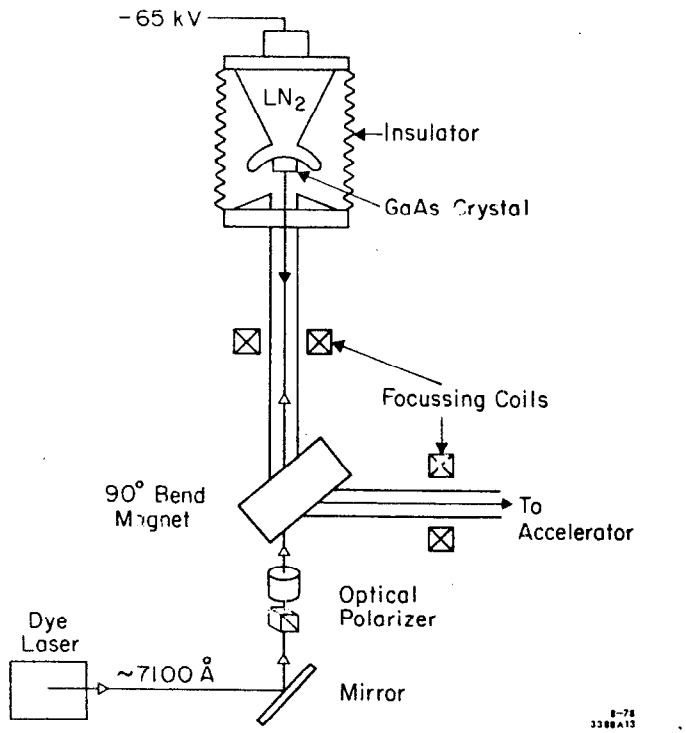

Fig. 3. Schematic illustration of the polarized source.

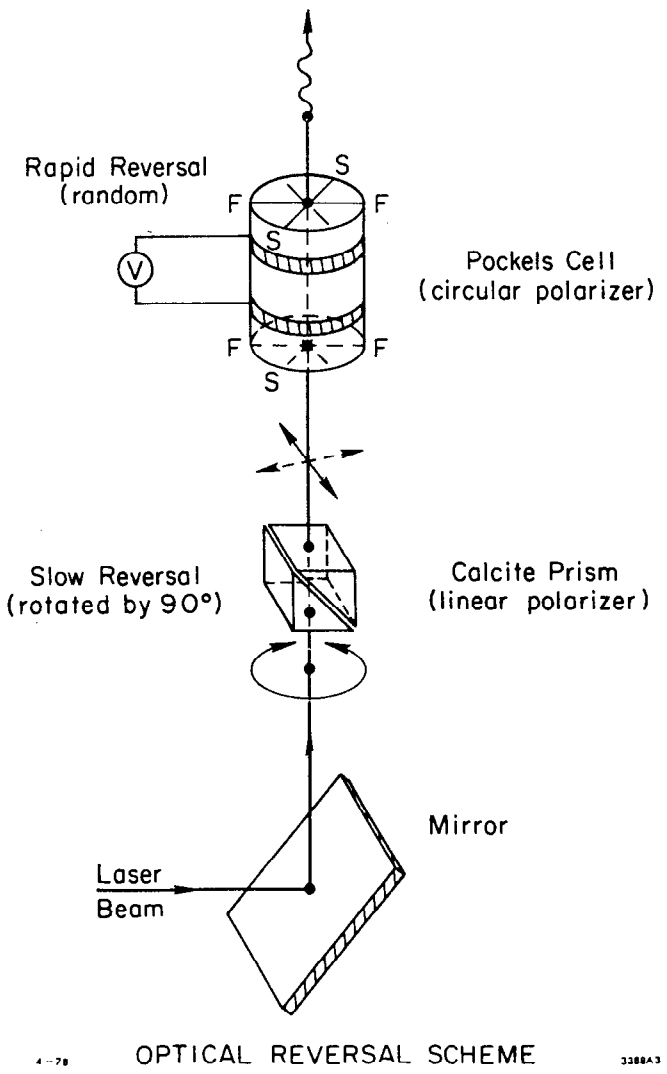

Fig. 4. Schematic illustration of the source optical polarizing system.

other parameters. Light from the laser was first linearly polarized using a calcite (Glan) prism. The linearly polarized light was then circularly polarized using a Pockels cell, which may be thought of as an electrically driven fractional wave plate whose retardation is proportional to the applied electric field. Application of a voltage of ~2 kV resulted in a quarter-wave plate, producing the required circular polarization. The retardation in the Pockels cell is reversible with voltage, so that changing the sign of the applied voltage reversed the sense of circular polarization. Thus the only change required to reverse the beam helicity was the reversal of the sign of the voltage applied to the Pockels cell. In particular, no mechanical motion was required, and no changing magnetic fields were involved.

The Pockels cell voltage could easily be reversed within the 8.3 msec between beam pulses, so that the beam helicity could be reversed on a pulse to pulse basis. This ability to obtain many reversals was important in eliminating the effect of long-term drifts in the source, accelerator, and detection system. Rather than using a fixed pattern of helicity changes, the helicity for each beam pulse was chosen randomly in order to avoid accidental correlations between helicity and any periodic patterns which might be present in the acceleator beam parameters. The random helicity selection was obtained using the number of disintegrations detected from a pair of radioactive sources.

III. MEASUREMENT OF THE BEAM POLARIZATION

The polarization of the beam was measured after acceleratic using Moller (elastic electron-electron) scattering from a magnetized supermendur foil as shown schematically in fig. 5. The foil was tilted at 20° with respect to the beam axis in order to provide a large longitudinal polarization, and was magnetized using a Helmholtz coil. Electrons elastically scattered in the horizontal plane at 90° in the center of mass were momentum analyzed in the vertical plane by a septum magnet and detected in a proportional wire chamber placed behind 4 radiation lengths of tungsten to enhance the electron signal. The wires of the chamber were spaced horizontally to provide an angular distribution. Because of the high counting rates involved, the wire chambers could not resolve individual scattered electrons. Instead, the outputs from the chamber were integrated over each beam pulse to provide a signal which, when normalized to the incident beam for that pulse, was proportional to the cross section.

The asymmetry measured, calculable from quantum electrodynamics, is the asymmetry in the differential cross section for longitudinally polarized incident and target electron spins parallel vs. anti-parallel:

$$A_{Moll} = \frac{\sigma_p - \sigma_a}{\sigma_p + \sigma_a} = -\frac{7}{9} \text{ at } 90^\circ \text{ in c.m.} \qquad (4)$$

When the finite target polarization, the non-Moller backgrounds, and the angle of target magnetization with

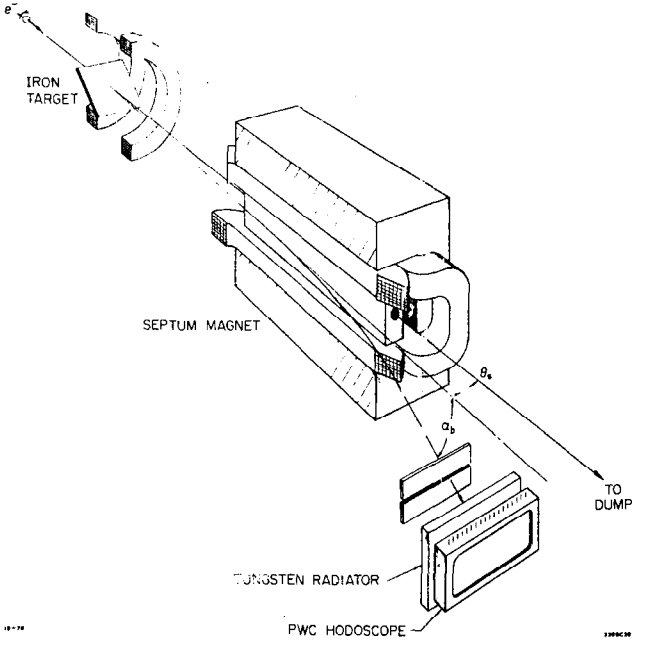

Fig. 5. Schematic illustration of the Moller scattering apparatus.

respect to the beam axis are taken into account, one obtains an experimentally observed asymmetry of

$$A_{Moll}^{exp} \simeq 0.05 P_e \qquad (5)$$

where P_e is the polarization of the electron beam.

Sample results of the angular distributions obtained are shown in fig. 6. The Moller peak is clearly visible in both the cross section and in the measured asymmetry. The background is principally due to the radiative tail from scattering off nuclei. The finite asymmetry at small angles is due to the radiative tail of Moller scattering.

Because of the high counting rate available, the beam polarization could be measured with good statistical precision ($\delta P_e / P_e \simeq 3\%$) in approximately 20 minutes. Systematic errors are estimated to be $\delta P_e / P_e \simeq 5\%$, principally due to uncertainty in the background subtraction. The beam polarization was measured roughly once every eight hours.

IV. SPECTROMETER

Because of the factor Q^2 in eq. (3), one might be tempted to perform the measurement at very large Q^2. However, the relative statistical precision of the experiment is proportional to $A^{\frac{1}{2}}$, and the cross section falls faster than Q^4. Consequently, one does not gain statistically by increasing Q^2, and we content ourselves with $Q^2 \sim 1$ GeV. In

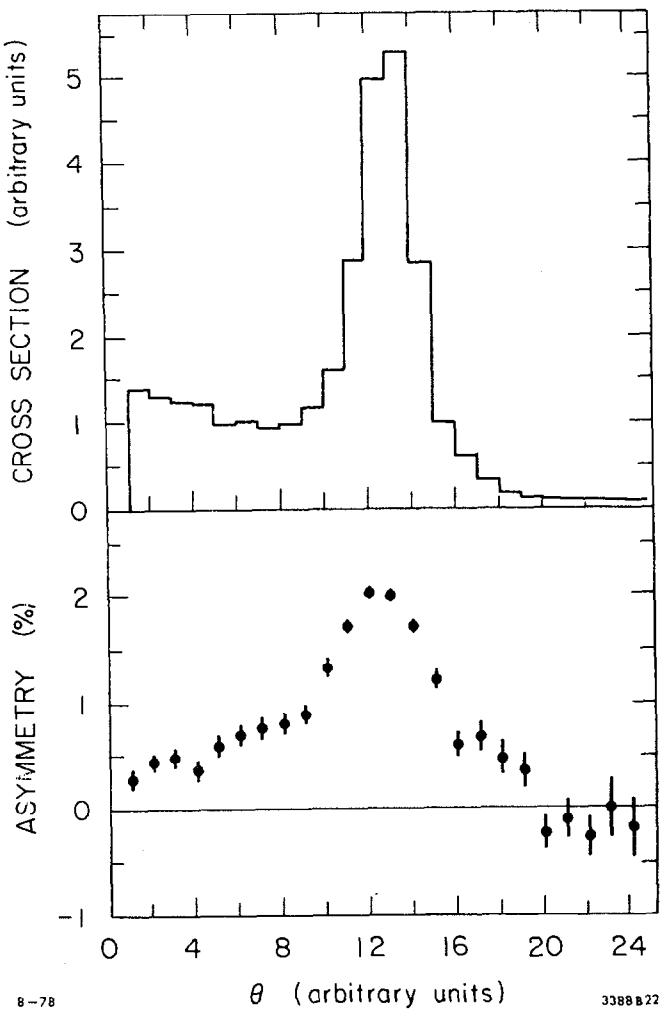

Fig. 6. Angular distributions from Moller scattering: a). cross section; b). asymmetry.

order to maximize the detected scattered electron rate, a spectrometer was constructed which, at least by End Station A standards, had a very large acceptance. As shown in fig. 1 the spectrometer consisted of two bending magnets and one quadrupole. Electrons were scattered from the 30 cm liquid deuterium target at 4° in the vertical plane, and momentum analyzed in the horizontal plane. The quadrupole was horizontally focussing in order to provide momentum resolution within the spectrometer acceptance, although this feature was not used by the present experiment. (To the extent that the target may be considered a point source in the vertical plane, vertical focussing is not necessary to obtain angular resolution.)

Most of the data were taken with a beam energy of 19.4 GeV and a spectrometer momentum of 14.5 GeV/c. Fig. 7 shows the cross section at 19.4 GeV for electrons and pions as a function of momentum, together with the spectrometer acceptance. As can be seen from the figure, the momentum acceptance is sufficiently broad to have some acceptance in the elastic and resonance region. For beam energies above 19 GeV, however, the elastic and resonance cross sections contribute only a few percent to the total yield.

It should also be noted that the pion rejection of the detectors was rather poor. Pion backgrounds were kept to a few percent of the electron signal by the simple expedient of operating in a kinematic region where the pion to electron ratio is very small.

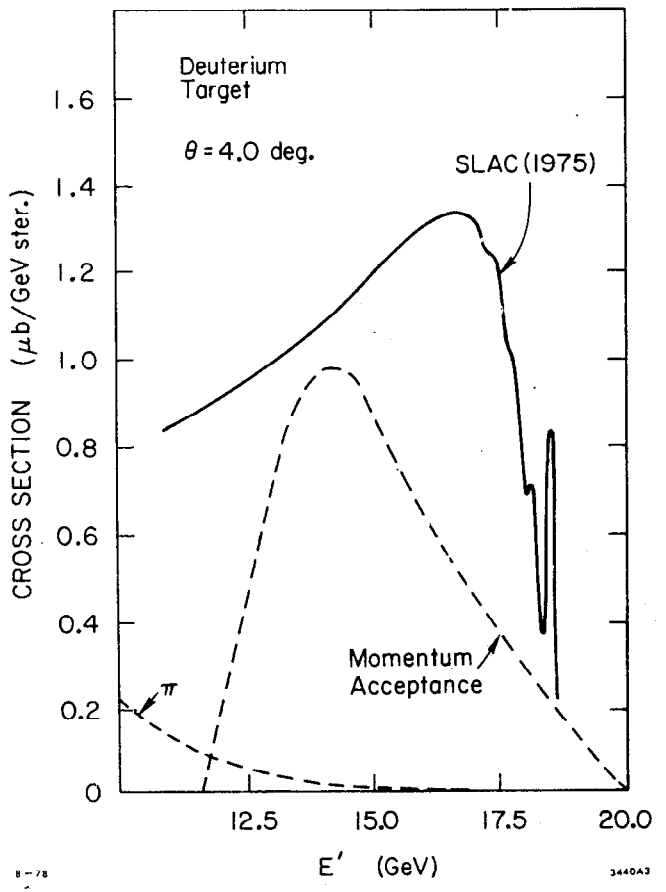

Fig. 7. Spectrometer acceptance and electron and pion cross sections from deuterium as a function of momentum for a beam energy of 19.4 GeV and scattering angle of 4°.

7. ELECTRON DETECTORS

The small size of the expected asymmetry presents a serious problem even in the simple consideration of counting statistics. Considering that some theoretical models predict asymmetries of significantly less than 10^{-4}, one would like to obtain a precision of $\lesssim 10^{-5}$, which requires the detection of $\gtrsim 10^{10}$ scattered electrons. If we were to perform a traditional counting experiment, the limitation of the SLAC duty cycle to $\lesssim 1$ event per beam pulse would then require ~ 3 years of actual running time to obtain the required statistics. (Furthermore, if the events were recorded on magnetic tape, then even a modest detector arrangement would require 10^5 magnetic tapes).

The alternative adopted was to detect approximately 1000 scattered electrons per 1.5 μsec beam pulse (at 120 pulses/sec) by measuring an integrated signal proportional to the "flux" of scattered electrons, rather than to count individual electrons.

As shown in fig. 1, two electron detectors were used. The first was a nitrogen-filled Cerenkov counter, which was followed by a 9-radiation-length lead glass shower counter. For each pulse (i) the anode current of each detector was integrated to provide a flux Y_i. When normalized to the incident beam intensity I_i for that pulse (obtained from the beam-induced signal in a resonant toroid monitor), this provided a quantity proportional to the cross section:

$$\sigma_i = \frac{Y_i}{I_i} \qquad (6)$$

Clearly the two counters could not be placed in coincidence because of the high rates in the detectors. The purpose of using two detectors was to obtain two separate (although not statistically independent) measurements of the asymmetry. The agreement of the results between the two detectors, which used separate electronics and had significantly different responses to pion and soft photon backgrounds, provides an important consistency check.

A third detector, not shown in fig. 1, was used to measure pion backgrounds. This detector was a lead glass counter placed behind 27 radiation lengths of lead, which in turn was located behind the shower counter. Electrons were absorbed in the shower counter and the lead, so that only hadrons (principally pions) and muons could penetrate to the pion counter. By searching for an asymmetry in this counter, we could verify that the asymmetry observed in the electron detectors was not due to the hadron background.

Characteristics of the detectors operated in the flux mode are shown in Table II. A further characteristic, which I wish to discuss in somewhat more detail, is the question of

statistical accuracy. This is important both in verifying that the detectors were operating properly, and in understanding the definition of the statistical uncertainty of the measurements.

Table II
Flux counter characteristics

Non-linearity	$\lesssim 1\times10^{-4}$ /%
Stability	$\sim$0.5% over 3.5 hour run
Pion contamination	
Shower counter	2%
Cerenkov counter	4%
Stray background	<< pion contamination

For an ideal counter the statistical uncertainty in the measurement of the cross section σ_i for a single pulse is determined by the number of detected electrons N_i for that pulse:

$$\frac{\delta\sigma_i}{\sigma_i} = \frac{1}{\sqrt{N_i}} = \frac{C}{\sqrt{I_i}} \qquad (7)$$

where I_i is the incident beam intensity, and C is a constant relating the incident and scattered beam intensities. The constant C was measured by running with a very low beam intensity and operating the detectors in the counting mode to determine the number of scattered electrons per unit of incident beam. (Note that the constant C was used purely for calibration purposes, and was not used in the data analysis.) Operating the detectors in the flux mode at higher intensities one could measure $\delta\sigma_i/\sigma_i$ at a given intensity simply by measuring the rms fluctuations in the value of σ_i over many pulses. Thus we could compare the performance of the detectors with that expected from eq. (7). The measured values of $\delta\sigma/\sigma$ for the shower counter are shown in fig. 8 plotted against $1/\sqrt{I}$. The solid line shows the behavior expected from the independently measured calibration constant C. The agreement between the observed and expected behavior is quite good, indicating that the statistical behavior of the detectors is indeed dominated by the statistical fluctuations in the number of detected electrons.

To combine the cross section measurements of many pulses (of perhaps different beam intensity) we wish to weight each pulse by $1/\delta\sigma_i^2$, which we have now verified to be proportional to incident beam intensity I_i. The average measured cross section $\langle\sigma\rangle$ and its statistical uncertainty $\delta\sigma$ are then given by

$$\langle\sigma\rangle = \frac{\sum_i \sigma_i I_i}{\sum_i I_i} = \frac{\sum_i N_i}{\sum_i I_i} \qquad (8)$$

$$\delta\sigma^2 = (\langle\sigma^2\rangle - \langle\sigma\rangle^2)/n \qquad (9)$$

where n is the number of measured pulses.

By maintaining separate sums over beam pulses with each helicity (which we designate by super-scripts + and - (5)) we define the experimentally measured asymmetry A_{Exp} and its relationship to the desired physics asymmetry A as

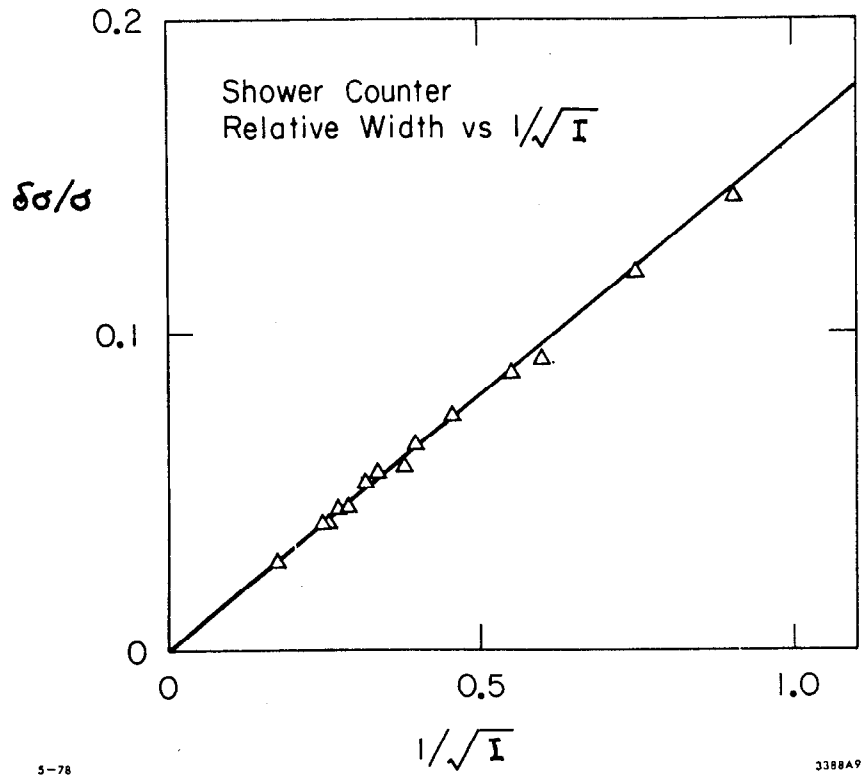

Fig. 8. Relative width of the shower counter distributions as a function of beam intensity, compared to the behavior expected from counting statistics.

$$A_{Exp} = \frac{\langle\sigma^+\rangle - \langle\sigma^-\rangle}{\langle\sigma^+\rangle + \langle\sigma^-\rangle} = P_e A \qquad (10)$$

$$\delta A_{Exp} = \frac{\delta\sigma}{\langle\sigma\rangle} \qquad (11)$$

At this point I wish to emphasize that, because of long-term drifts in the system, we could not measure the absolute cross section to within the statistical errors of $<10^{-5}$. However, because of the cancellation of drifts obtained by the frequent helicity reversals, the requisite accuracy could be obtained in the relative asymmetry measurement given by eqs. (10) and (11). Two tests were made to verify the legitimacy of the quoted statistical uncertainties in the asymmetry measurements.

The first test was to measure a null asymmetry using the normal SLAC unpolarized "gun" beam, rather than that from the polarized source. The same random bit generator as was used to set the source helicity was used to tag each beam pulse as having + or - "helicity", and an asymmetry was measured according to equation (10). The resulting asymmetry obtained was

$$A_{Exp}/0.37 = (-2.5\ 2.2)\times 10^{-5}$$

which is consistent with the expected value of 0. Here 0.37 is the average value of the beam polarization obtained with the polarized source, averaged over the entire experiment. (We divide by this average polarization so that the results

may be compared with the observed physics asymmetry of -16×10^{-5}.)

One can further test the statistical consistency of the data by looking at the data on a run by run basis, where a single run consisted of a few hours of data taking. The individual asymmetry measurements for the gun beam data are shown as a function of run sequence in fig. 9, from which it can be seen that there are no gross departures from the calculated statistical uncertainties. This is shown more quantitatively in fig. 10, which shows the distribution of variances, $\Delta/\delta A$, of the individual measurements. This distribution should be a gaussian of unit standard deviation, consistent with the results obtained. In particular, we obtain a standard deviation of 1.02 ± 0.13, corresponding to a χ^2 of 27 with 26 degrees of freedom for the agreement of the individual runs with zero.

The second test of the statistical consistency of the data also measured a null asymmetry, but in this case used the polarized beam data itself. In this test, the "helicities" of the beam pulses were artificially juggled such that a false asymmetry was measured between sets of beam pulses which in reality had the same helicity. The resulting observed asymmetry was

$$A_{Exp} / P_e = (1.1 \pm 1.2) \times 10^{-5} .$$

The result is again consistent with the expected value of zero, and with run to run distributions about zero consistent with the calculated statistical uncertainties of the

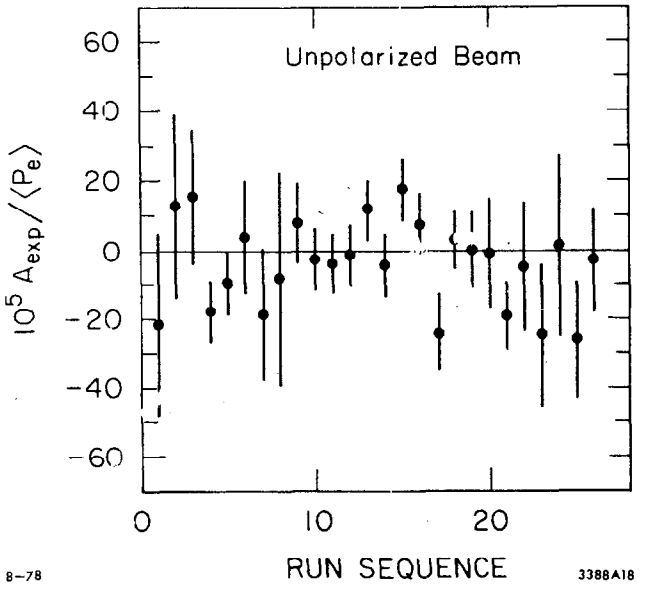

Fig. 9. Individual asymmetry measurements using an unpolarized beam.

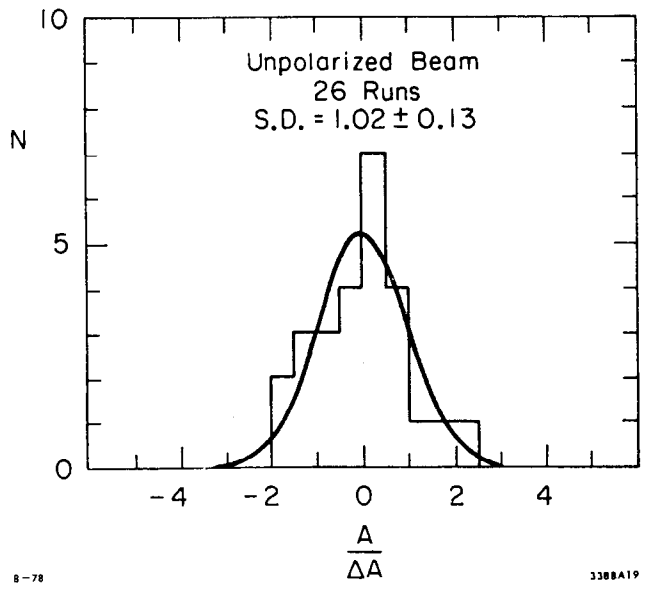

Fig. 10. Distribution of variances about zero of asymmetry measurements using an unpolarized beam.

measurements.

VI. BEAM MONITORING

While the tests just described establish that the statistical uncertainties of the asymmetry measurements are being properly calculated, they do not address the potentially more serious problem of systematic errors. Since the observed cross section clearly depends upon parameters such as beam energy and position at the target, as well as upon beam helicity, it is important to establish that there are no significant changes in these parameters which are correlated with beam helicity. An extensive beam monitoring system was used for this purpose. A list of beam parameters which were measured for each beam pulse is given in Table III and shown schematically in fig. 11.

Table III
Beam monitors and corrections

Parameter	Device	Resolution per pulse	δX	10^5 $\delta A/Q^2$ (correction)
I_1	Resonant toroid	0.02%	0.01%	-0.03
I_2	Resonant toroid	0.02%	0.01%	-0.03
E_1	μwave position monitor	0.01%	2×10^{-4} %	-0.35
E_2	μwave phase difference	0.01%	2×10^{-4} %	-0.35
x	μwave position monitor	10 μ	0.09 μ	<0.06
y	μwave position monitor	10 μ	0.03 μ	-0.03
θ_x	μwave position monitor	0.3 μrad	2×10^{-3} μrad	<0.05
θ_y	μwave position monitor	0.3 μrad	2×10^{-5} μrad	<0.01

The beam intensity was measured using two independent resonant toroid monitors (6). In these devices, which have been in use for a number of years, a signal is induced which

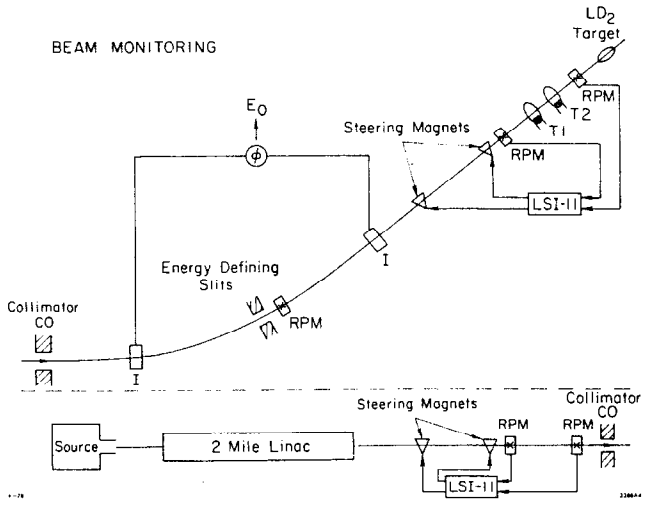

Fig. 11. Schematic illustration of the beam monitoring system.

is proportional to the the electric charge of the beam passing through the toroid. At the beam intensities used in this experiment, resolutions of $\sim 0.02\%$ for a single beam pulse were obtained.

The horizontal and vertical beam positions just upstream of the target were measured using resonant microwave beam position monitors (7). In these devices the 2856 MHz structure of the SLAC beam is used to induce a signal in a tuned microwave cavity. The cavity operates in the TM120 mode, giving a node at the center of the cavity (located on the beam axis) in the plane of interest (horizontal or vertical). The operation of the monitor can best be understood by analogy with a piano wire. If the wire is struck exactly in the center, no first harmonic will be generated. If the wire is struck a small distance off-center, however, a first harmonic will be generated which is proportional to the distance off-center and to the strength of the impulse applied. By analogy, the microwave position monitors produce a signal proportional to the distance off-axis of the beam and to the beam intensity. Resolutions of $\sim 10\mu m$ in position were obtained at typical beam intensities.

The angle of incidence of the beam was measured using a second set of microwave position monitors $\simeq 50m$ further upstream. A fifth horizontal position monitor, placed in the beam switchyard at a point where the beam is momentum dispersed, was used to measure the beam energy with a single

pulse resolution of $\delta E/E \lesssim 0.01\%$. An additional measurement of the energy, with comparable resolution, was obtained using microwave intensity monitors located before and after the beam switchyard (8). The relative phase of the two monitors gave a measure of the pathlength through the switchyard, which is determined almost solely by the beam energy.

In addition to being read by the main online computer, the beam monitors were also read by an LSI-11 microcomputer used to drive vernier steering magnets and a pair of vernier klystrons in order to stabilize the average beam position and energy. Because most steering changes were associated with changes in the accelerator rather than in the switchyard, an additional set of four position monitors and vernier correction magnets were installed at the exit of the accelerator in order to stabilize the beam steering going into the beam switchyard.

The correction to the physics asymmetry due to an asymmetry in some beam parameter X is given by

$$\delta A = \frac{-1}{P_e \sigma} \frac{d\sigma}{dX} \frac{\delta X}{2} \qquad (12)$$

where $\delta X = \langle X^+ \rangle - \langle X^- \rangle$. Hence in addition to measuring the difference between the average parameter values for the two beam helicities, one must also know $1/\sigma \; d\sigma/dX$. This cross section coefficient could be determined in several ways. For most of the beam parameters, the coefficient could be calculated from the known kinematic dependence of the cross section, using a Monte Carlo program to include geometrical and acceptance effects. The coefficients could also be measured experimentally by changing the beam parameters by known amounts and observing the associated change in cross section.

The cross section coefficients could also be measured experimentally using the data of the experiment itself. To see that this can easily be accomplished, we simplify slightly to the case in which the only important beam parameters are helicity and energy. (This simplified picture is, in fact, a reasonable approximation to the actual physical situation.) Typical pulse to pulse changes in the cross section due to helicity flips were $\sim 5 \times 10^{-5}$, whereas changes due to random fluctuations in energy were $\sim 3 \times 10^{-3}$. Because the correlation between energy and helicity was extremely small, one could measure the helicity dependence of the cross section by averaging over energy. It should be clear, however, that one could also measure the energy dependence by averaging over helicity.

The simultaneous measurement of the cross section coefficients in addition to the energy is somewhat more complicated because of the presence of strong correlations between beam parameters. Consequently, the simultaneous determination of multiple coefficients required the accumulation and inversion of a corelation matrix between beam parameters.

Agreement among cross section coefficients as determined by the three methods was quite satisfactory. The agreement of the coefficients determined from the matrix inversion with those obtained by more straight-forward means was important in establishing the absence of unmeasured beam parameters which significantly affect the cross section. If such parameters were present, one would expect the matrix inversion to result in artificially large values of some of the coefficients because of correlations between these beam parameters and the unmeasured parameters.

Corrections to the final asymmetry (divided by Q^2) due to asymmetries in beam parameters are shown in Table III, from which it can be seen that the only significant correction is that due to beam energy. This asymmetry was due to a small intensity difference between the two beams of opposite helicity. Because of the presence of beam loading in the accelerator this resulted in a small ($\sim 2 \times 10^{-6}$) energy difference at the target. For some of the beam parameters we could determine only an upper limit on the corrections. However, the limits were significantly stringent to demonstrate that corrections for these parameters were negligible. The net correction due to beam parameter asymmetries was only 4% of the final measured asymmetry, which is $\sim 1/2$ of the statistical uncertainty of the experiment (9). We thus conclude that beam parameter asymmetries, while present, are not important. The correction has been applied to the final answer obtained for the experiment, but not to the other figures shown in this paper. We have assigned a systematic uncertainty to the correction of 100% of itself.

VII. CONSISTENCY CHECKS

The asymmetry measured at a beam energy of 19.4 GeV is shown on a run by run basis in fig. 12, where a single run typically consisted of 3.5 hours of data taking. It can be seen that an asymmetry is clearly present, and that the effect is present throughout the data rather than being due to isolated anomolous runs. The distribution of variances about the mean, $(A-\langle A\rangle)/\delta A$, is shown in fig. 13. Again the data are consistent with a gaussian of unit standard deviation, and give a χ^2 of 44 with 43 degrees of freedom for the agreement of the individual runs with the mean.

It should be noted that the data shown consist of two separate periods of running, between which the source was almost completely dismantled and reassembled. The consistent behavior of the measured asymmetry is in marked contrast to the behavior of asymmetries in the beam parameters, which were quite sensitive to the alignment of the source optics and showed large variations over the course of the experiment.

To further verify that the measured asymmetry was indeed due to beam helicity, it was desireable to devise tests in which the observed effect could be made to change in predictable ways. Two such tests were performed.

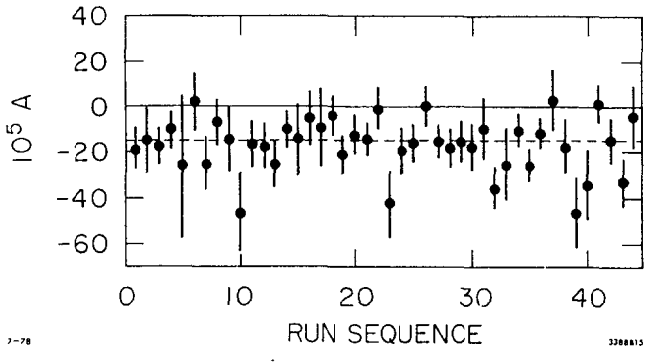

Fig. 12. Individual asymmetry measurements using the polarized beam.

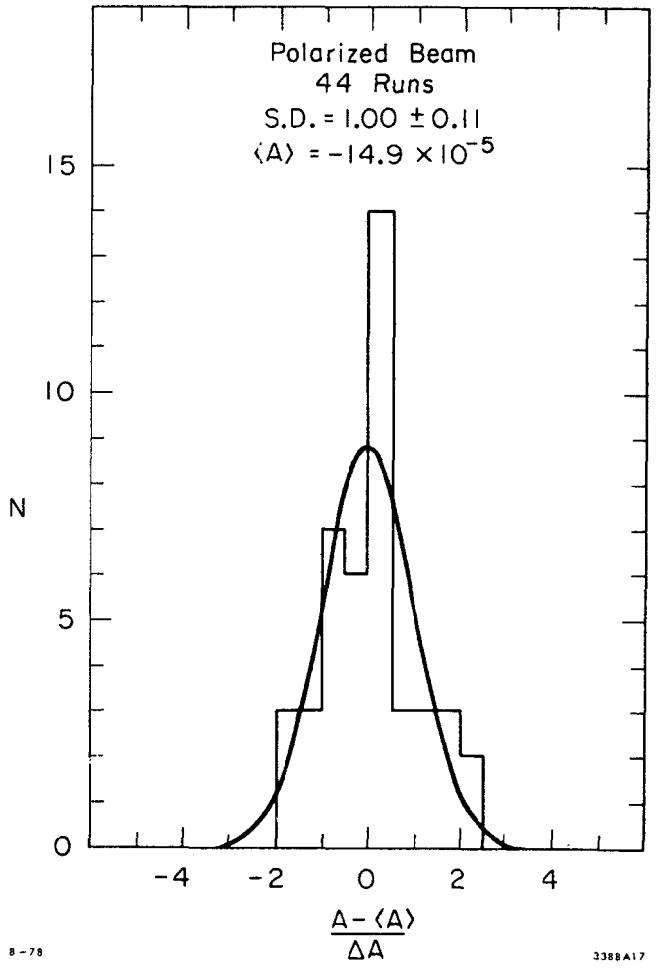

Fig. 13. Distribution of variances about the mean of asymmetry measurements using the polarized beam.

The first test utilized the rotation of the source calcite prism to change the beam helicity by a means independent of the Pockels cell. The helicity of the beam at the source is determined by the plane of linear polarization incident on the Pockels cell as well as by the voltage applied to the cell. In particular, referring to fig. 4, the plane of polarization must be at 45° with respect to the fast and slow axes of the cell in order to obtain circular polarization. If the prism (and consequently the plane of polarization) is rotated by 90° about the beam axis, then, for a given sign of voltage on the Pockels cell, the sense of circular polarization is reversed. Furthermore, if the prism is rotated by 45°, the plane of linear polarization is parallel to either the fast or slow axis of the Pockels cell, and the beam remains linearly polarized. This results in an unpolarized electron beam from the GaAs crystal and provides an opportunity to measure a null asymmetry in the presence of any systematics associated with the reversal of the Pockels cell voltage.

The experiment was run with roughly equal amounts of data taken in the nominal 0° and 90° prism orientations. The prism was rotated approximately once per day. In the data of fig. 12, the orientation of the prism has been taken into account in calculating the asymmetry. Fig. 14 shows the same data, in which only the sign of the Pockels cell voltage, but not the prism orientation, is used to determine the beam "helicity". It is clear that, as expected, the 90° rotation

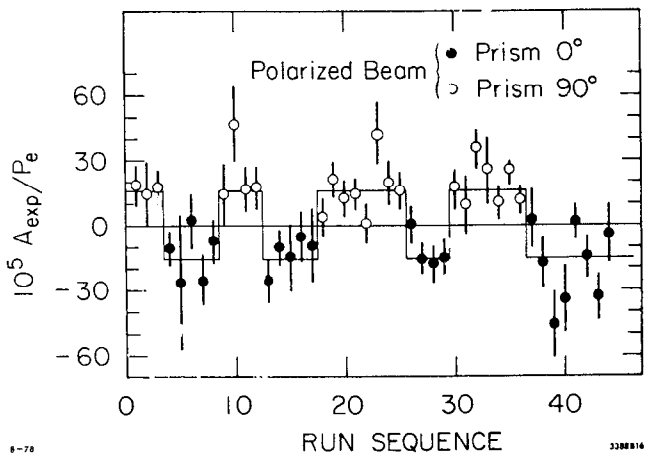

Fig. 14. Individual asymmetry measurements using the polarized beam, in which the prism orientation has not been taken into account.

of the prism reverses the experimentally observed effect.

A set of special runs was also taken with the prism in the 45° orientation in order to measure the expected null asymmetry. The measured value obtained was $A_{Exp}/0.37 = (1.0 \pm 3.0) \times 10^{-5}$, again consistent with the expected value of 0.

The data for the three different prism orientations are summarized in fig. 15, in which the prism orientation has again been ignored in determining the beam "helicity". As can be seen, good agreement is obtained with the expected behavior. The asymmetries measured by both the shower counter and the Cerenkov counter are shown in the figure, giving good consistency.

The second test in which the experimentally observed effect was made to change in a predictable fashion also involved changing the beam helicity. In this case, however, the helicity change was completely independent of the polarized source, and utilized the the spin precession of the electrons in the beam switchyard. The electron beam is deflected by 24.5° in going from the accelerator to the experimental area. The anomolous magnetic moment of the electron causes the electron spin to precess relative to the momentum direction by an amount

$$\theta_{prec} = \gamma\left(\frac{g-2}{2}\right)\theta_{bend} = \frac{E\,\pi}{3.237}. \qquad (13)$$

Consequently the electron beam at the target is

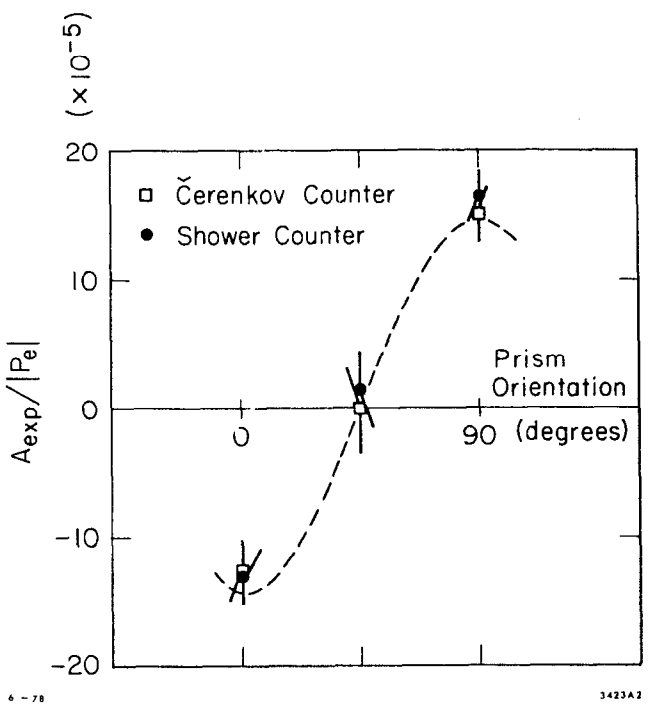

Fig. 15. Behavior of the observed experimental asymmetry as a function of prism orientation.

longitudinally polarized only for energies which are multiples of 3.237 GeV. Transverse components of the spin at high energies are expected to have a negligible effect in electron scattering (10) so that only the longitudinal component is of importance, and the effective beam polarization becomes

$$P_{eff} = P_e \cos\left(\frac{E\pi}{3.237}\right) \qquad (14)$$

The energies (E) and spectrometer momenta (E') at which data were taken are shown in Table IV. If the spin precession is neglected in determining the beam "helicity", then the experimentally observed asymmetry for these four kinematic settings should show the $\cos(E\pi/3.237)$ dependence of eq. (14). In particular, for the point at E=17.8 GeV, the longitudinal beam polarization is 0., and we again expect a null asymmetry. The measured asymmetry for this point was $A_{exp}/0.37 = (-1.2\pm2.1)\times10^{-5}$

Table IV
Kinematic operating points

E (GeV)	θ_{prec} (rad)	E' (GeV)	$\langle Q^2 \rangle$ (GeV^2)	$\langle \nu \rangle$
16.18	5.0 π	12.5	1.05	0.18
17.80	5.5 π	13.5	1.25	0.19
19.42	6.0 π	14.5	1.46	0.21
22.20	6.9 π	17.0	1.91	0.21

Because the data points at the other energies have different kinematics, some assumptions concerning the physics of the asymmetry are required to relate the data at different energies. In most current models, the asymmetry for a deuterium target is expected to be of the form

$$A \propto Q^2 f(y) \qquad (15)$$

where $y = (E-E')/E$. Because the function $f(y)$ is highly model dependent, the spectrometer momentum settings were chosen to maintain constant y, allowing Q^2 to vary. To compare the data at different energies we then remove the Q^2 dependence by plotting $A_{Exp}/(P_e Q^2)$, which is shown in fig. 16. Good agreement is obtained between the data and the expected energy dependence of the experimentally observed effect.

The final tests required are to demonstrate that the observed effect arises from the scattered electron signal, and not from the small hadron background seen by the detectors (although we have no reason to expect such a hadron asymmetry). From the lack of asymmetry in the pion counter, we were able to place a limit of $\lesssim 10^{-6}$ on the contribution of hadrons to the measured value of A/Q^2. A second test, which gave a similar limit, was obtained from special runs in which the spectrometer was set to accept positively charged particles. These runs were sensitive both to hadron asymmetries and to asymmetries in pair produced positrons.

VIII: RESULTS AND CONCLUSIONS

The final result obtained by combining the shower counter data at beam energies of 19.4 and 22.2 GeV is

$$A/Q^2 = (-9.5\pm0.9\pm0.8)\times10^{-5} = (-9.5\pm1.6)\times10^{-5},$$

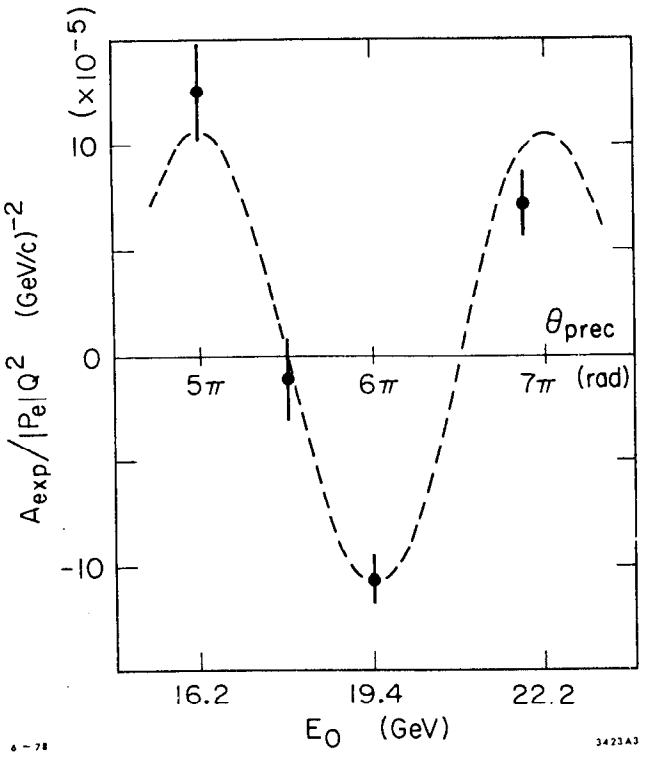

Fig. 16. Behavior of the observed experimental asymmetry as a function of beam energy.

where the first error quoted is the statistical uncertainty, and the second error is the estimated systematic uncertainty. The measurements made at a beam energy of 16.2 GeV have not been included because of uncertainties in the elastic and resonance region contributions, which are significantly larger than at higher energies. The average value of Q^2 for the combined data is 1.6 GeV^2 and the average value of y is 0.21. In addition to the 3% correction for beam parameter asymmetries, the result also includes corrections of 2% for the hadron background and 3% for radiative corrections. The systematic error was obtained by linearly adding the 3% uncertainty due to beam parameter asymmetries and the 5% ($\delta P_e/P_e$) uncertainty in the beam polarization. The quoted total error of 1.6×10^{-5} was obtained by adding the statistical and systematic errors linearly rather than in quadrature. It should be emphasized that the results are based on a preliminary analysis, and, while we do not expect the answer to change significantly, the quoted systematic error represents more of a guess than a scientific determination. However, on the basis of the consistency checks which I have already described, we feel confident that the systematic errors cannot be significantly larger than the statistical errors.

In addition to the measurements from the deuterium target, a limited amounted of data was taken with a hydrogen target at a beam energy of 19.4 GeV, giving a result of

$$A/Q^2 = (-9.7\pm2.7)\times10^{-5}.$$

Current theoretical models (2) predict a somewhat smaller

asymmetry from hydrogen than from deuterium. Our results are not inconsistent with this expectation, but are not of sufficient statistical precision to verify the expected difference.

The most important conclusion of the experiment is that parity violation has been observed in electron scattering. Certain classes of gauge theory models predict (at least to first order) no parity violation in experiments such as ours. Among these are left-right symmetric models in which the difference between neutral current neutrino and anti-neutrino scattering cross sections is explained as a consequence of the handedness of the neutrino and anti-neutrino, while the underlying dynamics are parity conserving. Such models are incompatible with our results.

The simplest gauge theories are based on the gauge group $SU(2)xU(1)$. Within this framework the original Weinberg-Salam (W-S) model (11) makes specific weak isospin assignments: left-handed electrons and quarks are are assigned to doublets ; right-handed electrons and quarks are assigned to singlets. Other assignments are possible, however. Specific predictions for a variety of isospin assignments have been made by Cahn and Gilman (2). The authors consider either singlet or doublet assignments for right-handed electrons and u or d quarks, allowing all possible singlet and doublet combinations (for a total of 8). In addition to the original W-S model, the most interesting of these, which cannot be ruled out by neutrino data, and which is compatible with those atomic experiments which fail to observe parity violation (12), is the "hybrid" model in which right-handed electrons are assigned to a doublet, while right-handed quarks are assigned to singlets.

To make specific predictions for the asymmetry one must have a model for the nucleon, the simplest of which is the naive quark model. For a deuterium target the quark distribution functions for u and d quarks are the same. Consequently, to the extent that one can neglect contributions from the quark-antiquark sea, the x-dependence of the asymmetry cancels out. Thus the predictions are not strongly affected by the details of the model. For a given set of isospin assignments the magnitude and y-dependence of A/Q^2 can then be specified in terms of the Weinberg angle θ_w.

The asymmetry measured in this experiment gives a Weinberg angle of $\sin^2\theta_w = 0.20\pm0.03$ in the W-S model, and a value of $\sin^2\theta_w = -0.14\pm0.1$ for the hybrid model. Comparison with values determined from neutrino data clearly favors the W-S model. The predicted y-dependence of the asymmetry in the two models for various values of $\sin^2\theta_w$ is shown in fig. 17. It can be seen that a measurement of the y-dependence of the asymmetry would provide a further means of distinguishing between the two (or other) models. Plans for such a measurement are in progress.

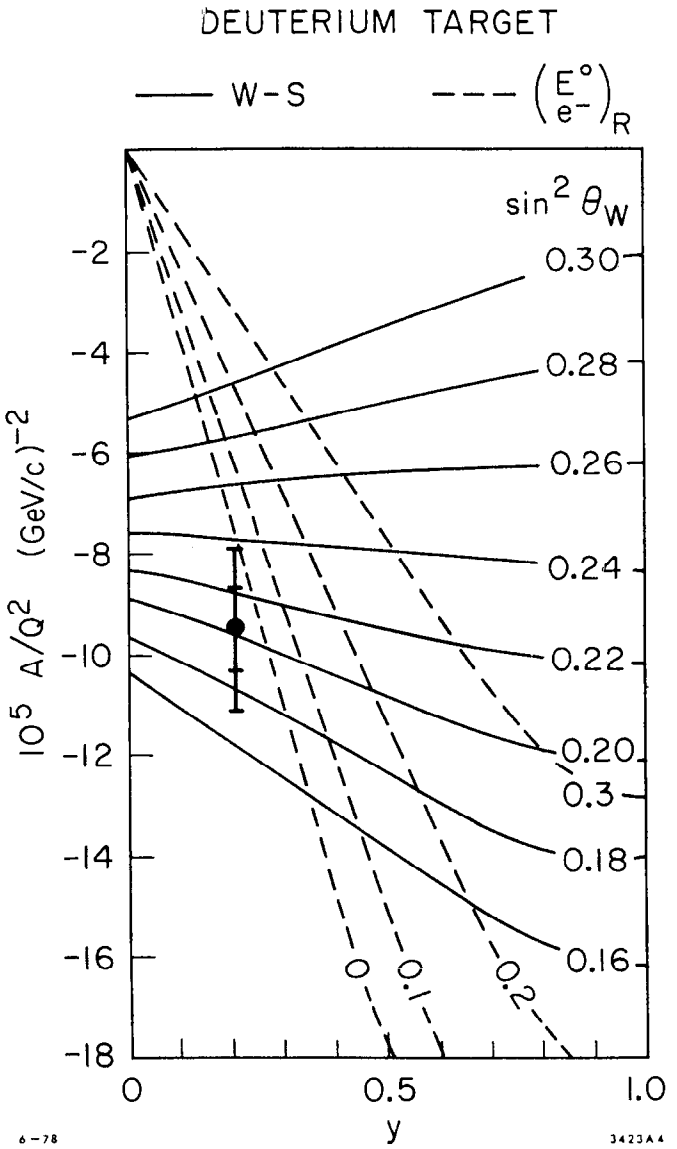

Fig. 17. y-dependence of A/Q^2 for the Weinberg-Salam model and the hybrid (electron doublet) model, parameterized by $\sin^2\theta_W$, and compared to our measured data point.

REFERENCES

(1) C.Y. Prescott, et al. Phys. Lett. B77,347(1978).

(2) R.N. Cahn and F.J. Gilman, Phys. Rev. D17,1313(1978). Further references to the theory may be found in this reference.

(3) The factor $GQ^2/4\pi\alpha$ is simply the overall ratio of weak to electromagnetic amplitudes, and thus sets the overall scale of the expected asymmetry.

(4) E.L. Garwin et al, SLAC-PUB-1576 (1975). D.T. Pierce et al, Phys. Lett. 51A,465(1975) ; Appl. Phys. Lett. 26,670(1975).

(5) I use the notation σ^+ and σ^- rather than σ^R and σ^L because a). experimentally, the polarization of the beam is not 100%, and b). for reasons which will become clear later, I am being intentionally vague in the definition of the experimental "helicity", which, in fact, will change throughout the paper. The meaning, however, should be clear from the context in which it is used.

(6) R.S. Larsen and D. Horelick, SLAC-PUB-398 (1968).

(7) Z.D. Farkas, et al, SLAC-PUB-1823 (1976).

(8) Z.D. Farkas, et al, SLAC-PUB-1970 (1977).

(9) This correction is slightly different from that quoted in ref. 1. The final asymmetry quoted has not been corrected for this difference, however, and remains that of ref. 1.

(10) In the one photon exchange approximation effects of transverse electron polarization on the virtual photon polarization matrix are supressed by a Lorentz factor $1/\gamma \simeq 5\times10^{-5}$. For those who demand experimental proof, we note that the scattering plane of the experiment is vertical and the electron spin precession is in the horizontal plane. Hence the point at 17.8 GeV provides direct confirmation that $\vec{\beta}\cdot\vec{n}$ terms are small.

(11) S. Weinberg, Phys. Rev. Lett. 19,1264 (1967) ; A. Salam, in Elementary Particle Theory: Relativistic Groups and Analyticity (Nobel Symposium No. 8), edited by N. Svartholm, (Almqvist and Wiskell, Stockholm, 1968), p.367.

(12) P.E.G. Baird, et al, Phys. Rev. Lett. 39,798(1977) ; L.L. Lewis et al, Phys. Rev. Lett. 39,795(1977) ; L.M. Barkov and M.S. Zolotorev, Zh. Eskp. Teor. Fiz. Pis'ma Red. 26,379(1978) (also available as SLAC-TRANS-180, 1978). The first two experiments see no parity violation, while the third experiment does.

EXPERIMENTAL SEARCH FOR PARITY NON-CONSERVATION IN ATOMIC THALLIUM[†]

By

E. D. Commins

Physics Department
University of California
and
Materials and Molecular Science Division
Lawrence Berkeley Laboratory
Berkeley, California 94720

In this lecture I will describe an experimental search for parity nonconservation (PNC) in the $6^2P_{1/2} - 7^2P_{1/2}$ transition in atomic thallium (see the energy level diagram fig. 1). A somewhat similar experiment on cesium is being done in Paris[1].

Our group consists of P. Bucksbaum, S. Chu, R. Conti, and myself, with new students P. Drell and L. Hunter. I will first explain why we chose this particular transition then describe our method, give results to date, and conclude with a brief description of our future plans.

1. Why the $6^2P_{1/2} - 7^2P_{1/2}$ Transition in Thallium?

In an atom, according to the Weinberg-Salam model, an electron and the nucleus are coupled not only by the usual electromagnetic interaction, but also by a neutral weak interaction of very short range arising from Z_0 exchange. The latter interaction has both scalar and pseudoscalar

---

[†] This work supported by the Division of Chemical Sciences, Office of Basic Energy Sciences, U.S. Department of Energy

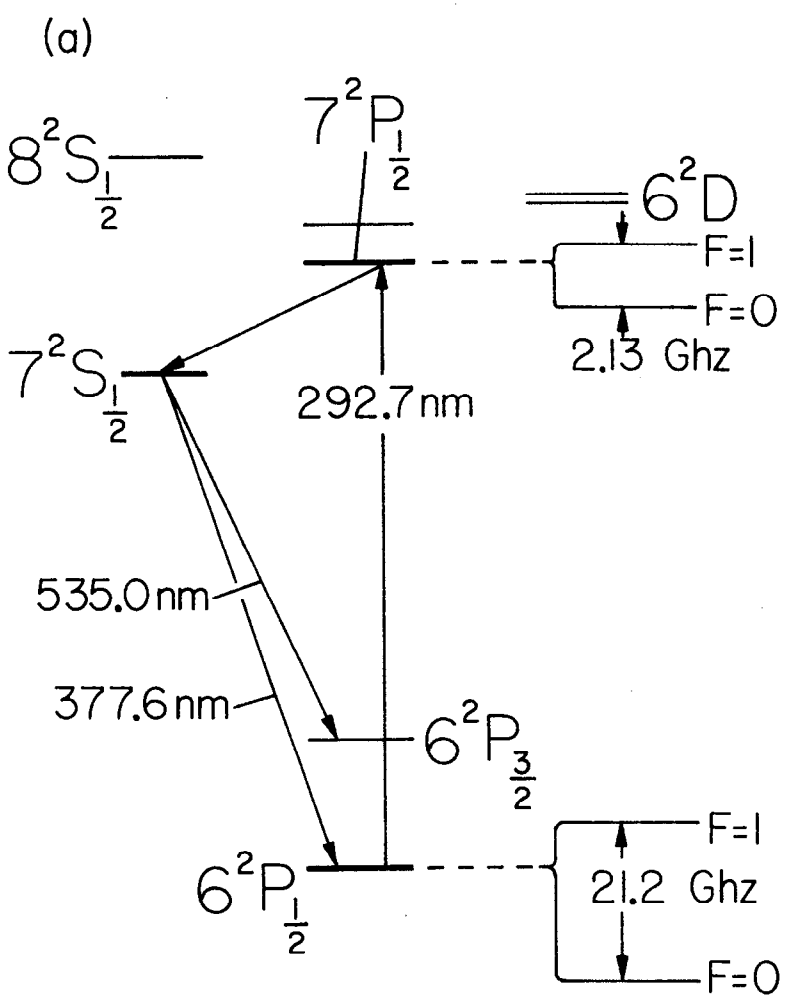

Fig. 1

parts, the pseudoscalar portion arising from coupling of the axial hadronic current to the vector electronic current, and the vector hadronic current to the axial electronic current. (A similar effect couples atomic electrons to one another but it is too small for observation at present.) In a heavy atom the portion $V_{hadron} \times A_{electron}$ is dominant. It gives rise in the nucleon non-relativistic limit to an effective PNC potential V_p which takes the approximate form:

$$V_p = \frac{G}{4\sqrt{2}} Q_w [\underset{\sim}{\sigma} \cdot \underset{\sim}{p}\, \delta^3(r) + \delta^3(r) \underset{\sim}{\sigma} \cdot \underset{\sim}{p}] \tag{1}$$

where $$Q_w = (1-4 \sin^2\Theta_w)Z - N, \tag{2}$$

G is Fermi's coupling constant, Θ_w is Weinberg's angle, $\underset{\sim}{\sigma}$, $\underset{\sim}{p}$ and $\underset{\sim}{r}$ refer to the electron and we employ units $m_e = \hbar = c = 1$.

Since V_p is pseudoscalar and of zero range it couples only those atomic states of opposite parity with finite magnitude/gradient at the origin ($^2P_{1/2}$,$^2S_{1/2}$ states). Thus, for example, the $6^2P_{1/2}$, $7^2P_{1/2}$ states of thallium are perturbed as follows:

$$|6^2P_{1/2}\rangle \rightarrow |6^2P'_{1/2}\rangle = |6^2P_{1/2}\rangle + \sum_n \frac{|n^2S_{1/2}\rangle\langle n^2S_{1/2}|V_p|6^2P_{1/2}\rangle}{E_{6p} - E_{nS}} \tag{3}$$

$$|7^2P'_{1/2}\rangle = |7^2P_{1/2}\rangle + \sum_n \frac{|n^2S_{1/2}\rangle\langle n^2S_{1/2}|V_p|7^2P_{1/2}\rangle}{E_{7p} - E_{nS}} \tag{4}$$

Let's now consider the magnetic dipole transition $6^2P_{1/2} \rightarrow 7^2P_{1/2}$. To first order in V_p, the transition amplitude is, from (3) and (4):

$$A = \langle 7^2P'_{1/2}|H_{EM}|6^2P'_{1/2}\rangle = \langle 7^2P_{1/2}|H_{EM}|6^2P_{1/2}\rangle + \sum_{nS} \frac{\langle 7P|H_{em}|nS\rangle\langle nS|V_p|6P\rangle}{E_{6p} - E_{nS}} + \sum_{nS} \frac{\langle 7P|V_p|nS\rangle\langle nS|H_{EM}|6P\rangle}{E_{6p} - E_{nS}} \qquad (5)$$

The first term on the RHS of (5) is the ordinary magnetic dipole amplitude M. For an allowed M1 transition as in the bismuth experiments, this would be of order $\mu_0 = e\hbar/2m_e c$. However, the $6P_{1/2} \to 7P_{1/2}$ transition in thallium is forbidden (in the non-relativistic limit M would be zero); in fact $M \sim v/c\ \mu_0 \sim (10^{-4}\text{-}10^{-5})\mu_0$ (a more precise estimate of M is given in ref 2). The second and third terms on the RHS of (5) together constitute the parity non-conserving electric dipole moment $\mathcal{E}_p$. At first sight one would guess that because it is proportional to G, $\mathcal{E}_p$ is extremely small. However, on account of the Z^3 effect (Z = 81 here) $\mathcal{E}_p$ is in fact not hopelessly minute -- a crude estimate is $|\mathcal{E}_p| \sim 10^{-10}\, ea_0$ (again, a more precise estimate is given in ref 2).

Now when both M and $\mathcal{E}_p$ are present, one has the possibility of observing circular dichroism, which is a dependence of the absorption cross section on the circular polarization of the incoming photons. Employing the optics convention, according to which L, R circular polarization correspond to +,- helicity respectively, we can easily show that

$$\delta = \frac{\sigma(L) - \sigma(R)}{\sigma(L) + \sigma(R)} = \frac{+2\ \mathrm{Im}\,(\mathcal{E}_p M^*)}{|M|^2 + |\mathcal{E}_p|^2} \approx \frac{2\ \mathrm{Im}\,(\mathcal{E}_p^*)}{M} \qquad (6)$$

the last approximation being valid since $|\mathcal{E}_p| \ll M$. Furthermore, time reversal invariance implies that M is real and $\mathcal{E}_p$ is pure imaginary. Using the crude estimates for M, $|\mathcal{E}_p|$ given above, we are thus led to expect $\delta \approx 10^{-3}$.

Let us now consider the atomic structure of thallium a bit more carefully, in order to sharpen this estimate. The ground configuration of Tl (Z = 81) is $1s^2 2s^2 \ldots 5d^{10} 6s^2 6p$ and as has been understood for many years, all low-lying levels (see fig. 1) are described to a reasonably good approximation in terms of the spherically symmetric core ($1s^2 \ldots 5d^{10} 6s^2$) and the single valence electron in one or another state of excitation. (Thallium thus resembles an alkali atom.) This one-electron central field approximation is the basis for detailed numerical calculations carried out by Neuffer and myself.[2] Specifically, the Dirac equation is solved numerically for the valence electron in a central potential of the Tietz type whose two free parameters are chosen to give a fit to the $6^2P_{1/2}$, $7^2P_{1/2}$ energy levels. Many other energy levels, hyperfine splittings, allowed electric dipole transition strengths, and Stark matrix elements and the g_J anomaly in the ground state are all calculated and compared with abundant spectroscopic and atomic beam data on thallium. The agreement is in all cases very good. In addition, the amplitude M is calculated and agrees well with observations of M made in the course of this experiment[3]. Thus to summarize, the agreement between calculations and observations are so good that we have reasonable confidence in our ability to estimate $\mathcal{E}_p$ and δ with fair accuracy on the basis of the Weinberg-Salam model. We find $\delta = (2.6 \pm 6) \times 10^{-3}$. The main conclusion from this exercise, and answer to the question "Why the

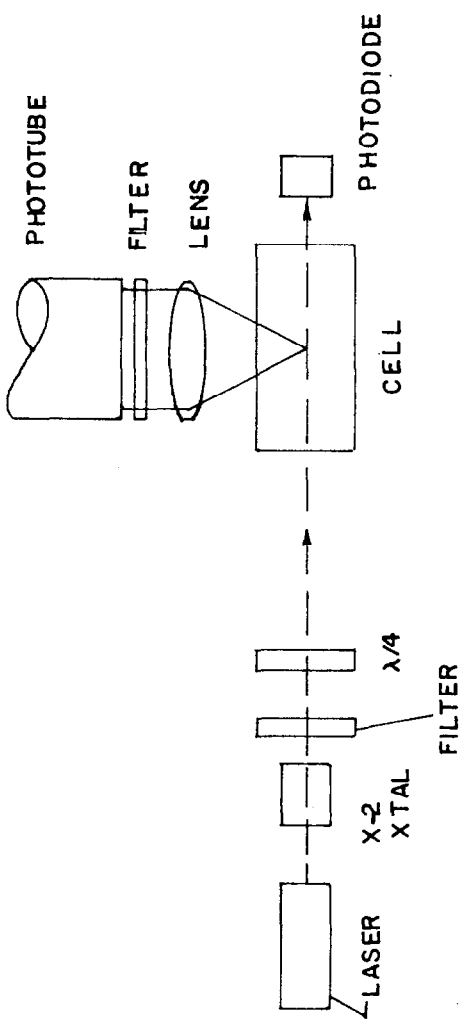

Fig. 2

$6^2P_{1/2} - 7^2P_{1/2}$ transition in Tl?" is that the atomic physics of thallium is reasonably "clean" and δ is encouragingly large.

2. Experimental Method

Our first naive attempt to observe PNC is illustrated in figure 2. We simply illuminated a quartz cell containing Tl vapor ($T \sim 950°$ K, $n \sim 2 \times 10^{14}$ atoms/cm^3) with UV light from a flash-lamp-pumped dye laser transmitted through an ADA doubling crystal, to give 2927 Å photons corresponding to the $6^2P_{1/2} - 7^2P_{1/2}$ resonance.

By observing the fluorescence at 5350 Å corresponding to the $7^2S_{1/2} \rightarrow 6^2P_{3/2}$ decay as we switched back and forth between left- and right-circular polarization, we hoped to determine δ. This did not work -- we could not even observe the M1 transition by this method, let alone determine the asymmetry -- because of background fluorescence at 5350 Å hundreds of times larger than the M1, which did not go away when we turned off the resonance, and which is proportional to laser power and varies approximately as n^2. This non-resonant background -- which is still with us, incidentally, albeit in diminished size, -- we call the "molecular" background, because it is presumably due to broadening and strengthening of the $6^2P_{1/2} - 7^2P_{1/2}$ transition due to the random, momentary electric fields (Stark effect) which occur when Tl atoms collide, (and sometimes stick together to form "Rydberg" molecules or even real, bound molecular states).

In order to overcome this difficulty we have found it necessary to make use of the Stark effect <u>in a controlled way</u> by imposing a uniform external electric field. In such a field the

$6^2P_{1/2}$, $7^2P_{1/2}$ states are mixed with $n^2S_{1/2}$, $n^2D_{3/2}$ states and the $6^2P_{1/2} \rightarrow 7^2P_{1/2}$ transition acquires a Stark-induced parity-conserving electric dipole component. The transition intensity becomes observable at a finite E field because it varies as E^2. In addition we are able to observe interference effects between M and the Stark amplitude; and also very recently between δ_p and the Stark amplitude.

Let us consider these effects in some detail. Fig. 3 shows a linearly polarized 2927 Å laser beam along x with polarization $\hat{\varepsilon}$ parallel to the external field E, along y. The quantization-detection axis is along z. For $\hat{\varepsilon} \parallel E$, the allowed hyperfine components of the $6^2P_{1/2} - 7^2P_{1/2}$ Stark transition are F=0 → F=0 and F=1 → F=1, $\Delta m_f = 0$. Because M is also present and interferes with the Stark matrix element α, one obtains a polarization of the $7^2P_{1/2}$ state, as indicated in fig. 3, of:

$$1 \rightarrow 1 \; : \quad P = \frac{4}{3}\frac{\alpha M}{|\alpha|^2 + 2|M|^2} \approx \frac{4M}{3\alpha} \quad \text{for } |\alpha| >> |M| \tag{7}$$

$$0 \rightarrow 0 \; : \quad P = 0$$

Similarly, one can choose linear polarization $\hat{\varepsilon} \perp$ to E (see fig. 4.). In this case the hyperfine transitions which can occur are F=0 → F=1 ($\Delta m_f = \pm 1$), F=1 → F=0 ($\Delta m_f = \pm 1$) and F=1 → F=1 ($\Delta m_f = \pm 1$). In particular, the polarization of the $7^2P_{1/2}$ state, again along z, for the F=0 → F=1 transition, is:

$$P = \frac{-2}{|\beta|^2 + |M|^2}\frac{\beta M}{} \approx \frac{-2}{|\beta|} \tag{8}$$

where β is another Stark amplitude. According to our calculations,

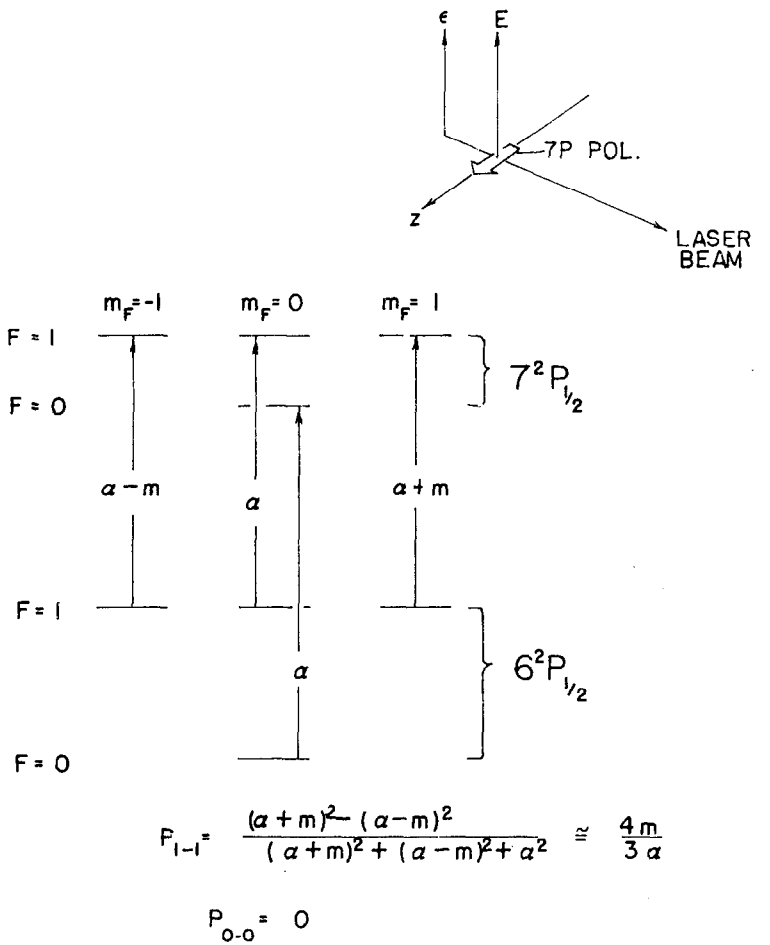

Fig. 3

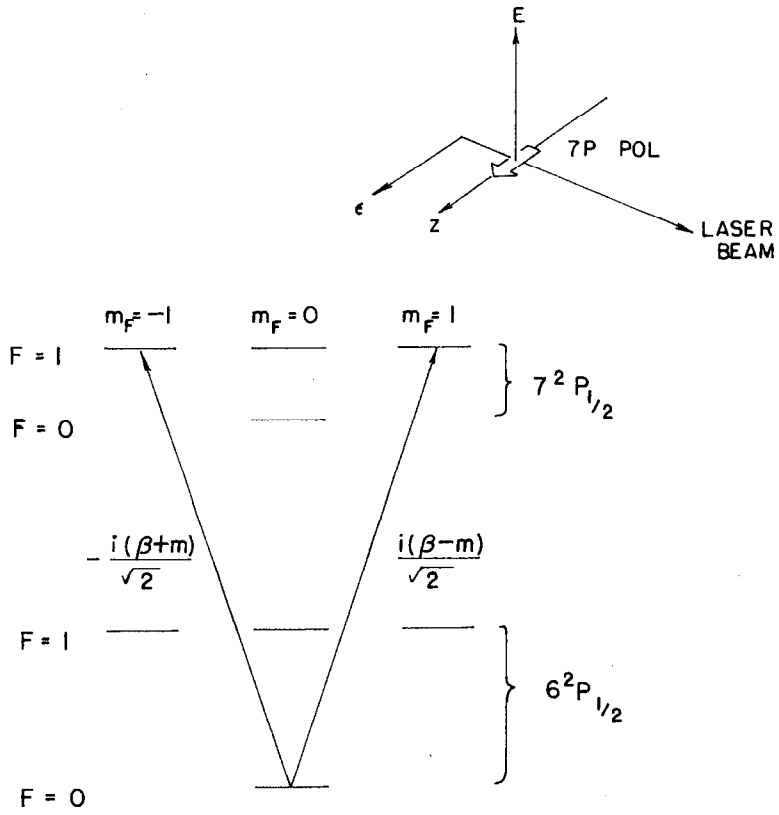

XBL 778-9845

Fig. 4

$$\left.\begin{aligned} \alpha_{calc} &= +7.4 \times 10^{-8}\ E \\ \beta_{calc} &= +6.0 \times 10^{-8}\ E \end{aligned}\right\} \text{ in atomic units, but E in volts/cm} \qquad (9)$$

with an uncertainty in each number of no more than 20%.

In an early version of our experiment,[3] we observed the polarizations of equations (7), (8) by detecting the circular polarization of the ensuing decay fluorescence at 5350 Å along the ±z axis (see fig. 1 and figs 5,6), at various values of electric field. As expected, the circular polarization varies as 1/E, and the ratio of polarizations observed for the F=1 → F=1 (Δm_F=0) transition and the F=0 → F=1 transition (Δm_F=±1) is in agreement in sign and magnitude with formulae 7,8, with α,β given by formulae (9). Also as expected, the 0-0 line gives zero polarization. In this early experiment we calibrated our detectors by observing an effect illustrated in fig. 7. Here, for the 1 → 1 transition, using circularly polarized laser light, we obtain a polarization of the $7^2P_{1/2}$ state along the x axis, due to interference of the amplitudes α,β, both of which participate in this particular transition. This polarization

$$P = \frac{\mp 4\alpha\beta}{3\alpha^2 + 2\beta^2} \qquad (10)$$

(where ∓ refers to L(R) circular polarization) is independent of the sign and magnitude of E (eq. 10 valid in the limit α,β >> M). It was first observed by applying a static B field along y to cause precession of the polarization of the $7^2P_{1/2}$ to line up with the z axis. The results of this experiment were in good agreement with calculations, as shown in figure 8. Thus we were able to determine that $M = (-2.11 \pm .30) \times 10^{-5}\ \mu_0$.[3]

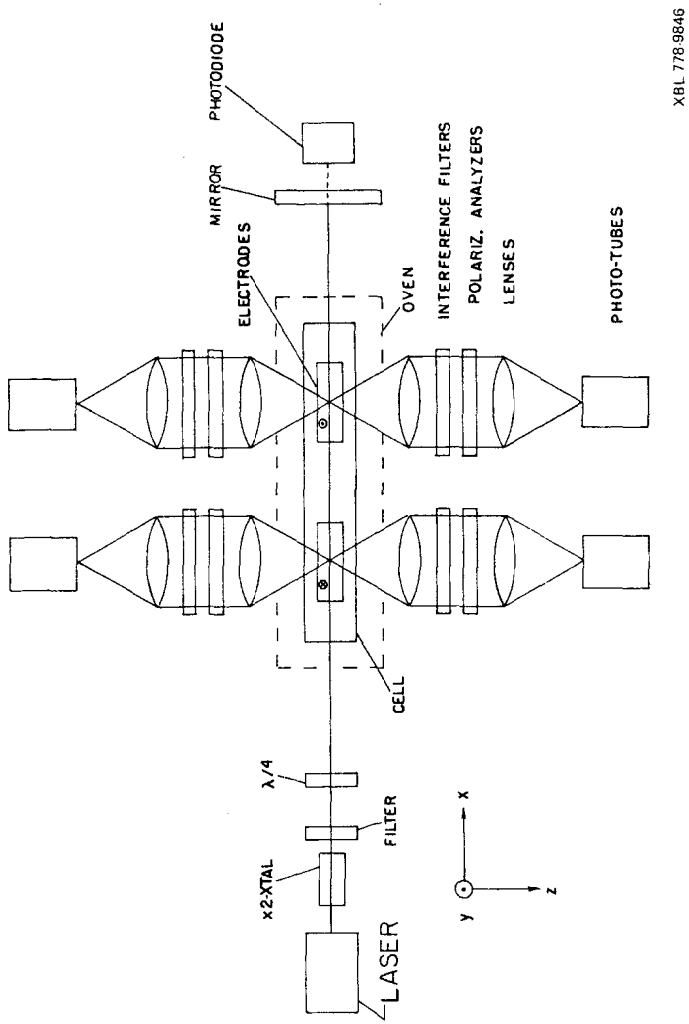
PHOTODIODE
MIRROR
ELECTRODES
OVEN
INTERFERENCE FILTERS
POLARIZ. ANALYZERS
LENSES
PHOTO-TUBES
CELL
λ/4
FILTER
x2-XTAL
LASER
x
y
z
XBL 778-9846

Fig. 5

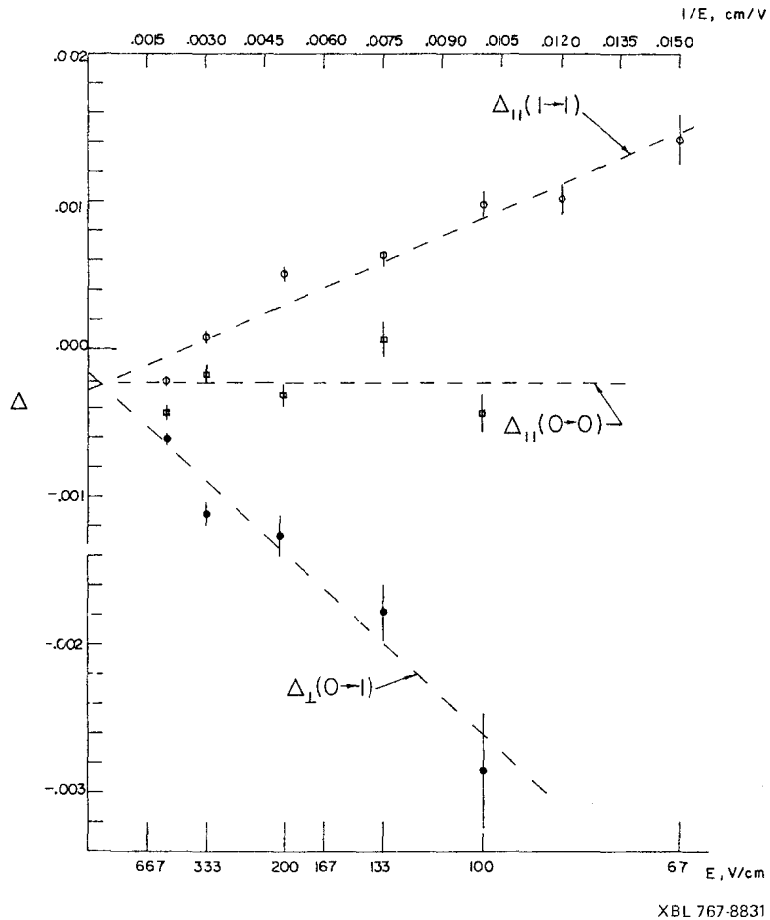
1/E, cm/V
.0015 .0030 .0045 .0060 .0075 .0090 .0105 .0120 .0135 .0150
.002
.001
.000
-.001
-.002
-.003
Δ
$\Delta_{11}(1\leftarrow1)$
$\Delta_{11}(0\leftarrow0)$
$\Delta_{\perp}(0\leftarrow1)$
667 333 200 167 133 100 67
E, V/cm
XBL 767-8831

Fig. 6

HANLE EFFECT

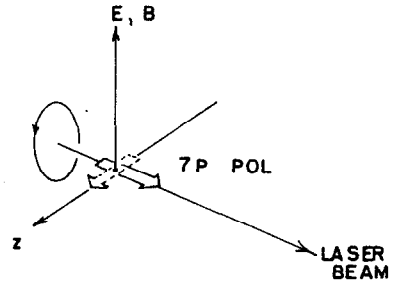

$$\langle P(z) \rangle = \frac{\int_0^\infty P\, e^{-\lambda t}\, dt}{\int_0^\infty e^{-\lambda t}\, dt}$$

$$P = \mp \frac{4\alpha\beta}{3\alpha^2 + 2\beta^2} \cdot \sin\omega t$$

FOR 1-1 TRANSITION

XBL 778-9841

Fig. 7

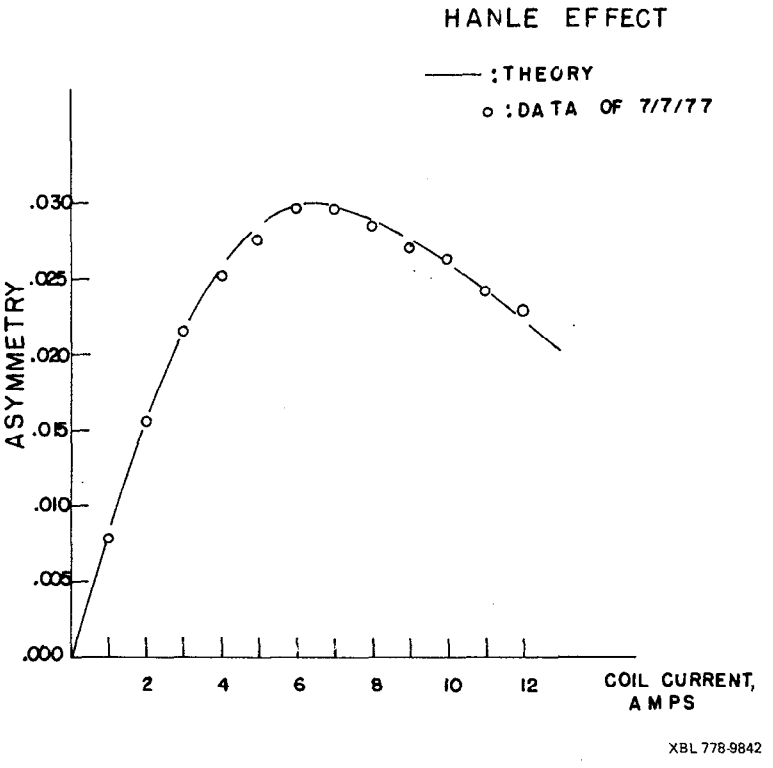

XBL 778-9842

Fig. 8

Now, what modifications must be introduced when one takes into account the presence of δ_p? It can be shown (see fig. 9) that if one uses circularly polarized 2927 Å radiation, the polarization of the $7^2P_{1/2}$ state along z becomes for the 1 → 1 transition:

$$P = \frac{(4\alpha - 2\beta)M(1 \mp \delta/2)}{3\alpha^2 + 2\beta^2} \qquad (11)$$

while for the 0 → 1 transition, one has

$$P = \frac{-2\beta M(1 \mp \delta/2)}{\beta^2} \qquad (12)$$

where $\delta_{THEO} = 2.6 \times 10^{-3}$ and we use $\mp$ for L(R) 2927 Å circular polarization, respectively. Thus parity nonconservation brings in the additional factor $(1 \mp \delta/2)$. The 0 → 1 transition is particularly attractive for observation of PNC because the polarization is relatively large, [$P = \frac{-2.57}{E}(1 \mp \delta/2)$, E in volts/cm] the 0 - 1 line can readily be compared with the nearby 0 - 0 line, which should exhibit no polarization, and finally the 0 - 1 line suffers less from possible dangerous systematic effects than the 1 → 1 line.

One major defect of the original method of detection ($7^2S_{1/2} \rightarrow 6^2P_{3/2}$ fluorescence at 5350 Å) is as follows: there is a factor of 12 dilution in the $7^2P_{1/2}$ polarization. This comes about as follows:

a) A factor of 3 is lost in going from $7^2P_{1/2}$ to $7^2S_{1/2}$,

b) Another factor of 2 is lost in going from $7^2S_{1/2}$ to $6^2P_{3/2}$.

c) The branching ratio $7^2S_{1/2} \rightarrow 6^2P_{1/2}$ is about 0.5. However, this transition is resonantly trapped. The corresponding 3776 Å

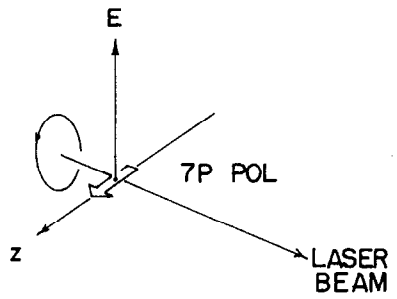

TEST FOR PARITY NON CONSERVATION

$$F_{1-1} = \frac{(4\alpha - 2\beta)m}{3\alpha^2 + 2\beta^2}(1 \mp \tfrac{\delta}{2}) = \frac{.56}{E}(1 \mp \tfrac{\delta}{2})$$

$$P_{0-1} = -\frac{2m}{\beta}(1 \mp \tfrac{\delta}{2}) = -\frac{2.57}{E}(1 \mp \tfrac{\delta}{2})$$

$$W\text{-}S: \quad \delta = 2.6 \times 10^{-3}$$

XBL 778-9843

Fig. 9

photons are depolarized and converted to 5350 Å photons, with a further loss of polarization of about a factor 2.

To overcome this difficulty we now measure the $7^2P_{1/2}$ polarization by a different method, illustrated in fig. 10. The transition $7^2P_{1/2} \rightarrow 8^2S_{1/2}$ (allowed El) is induced by a circularly polarized infra-red beam tuned to the resonance at 2.18 m, directed along the z axis with right or left circular polarization, and with sufficient power to saturate the transition. The population of the $8^2S_{1/2}$ level depends on the polarizations of the $7^2P_{1/2}$ and the circular polarization of the infra-red. It is detected by observation of the decay $8^2S_{1/2} \rightarrow 6^2P_{3/2}$ at 3230 Å. A careful analysis of the rate equations for this process, including resonance trapping of the $8^2S_{1/2} \rightarrow 6^2P_{1/2}$ line (2580 Å) and other small effects, shows that our analyzing power is now almost unity instead of a mere 1/12. This is confirmed by the following calibration experiment, see fig. 11. We observe 3230 Å decay photons, using the $6^2P_{1/2} \rightarrow 7^2P_{1/2}$ 1 → 1 line with circularly polarized UV and the infra-red beam directed anti-parallel to the UV beam. The expected polarization arising from α,β interference as in equation (10) is

$$P_{THEO} = \mp \frac{4\alpha\beta}{3\alpha^2 + 2\beta^2} = \mp 0.75 \qquad (13)$$

We observe:

$$P_{EXPT} = \mp 0.58 \qquad (14)$$

which is consistent with an analyzing power of

$$A = P_{EXPT}/P_{THEO} = \frac{0.58}{0.75} = .76 \qquad (15)$$

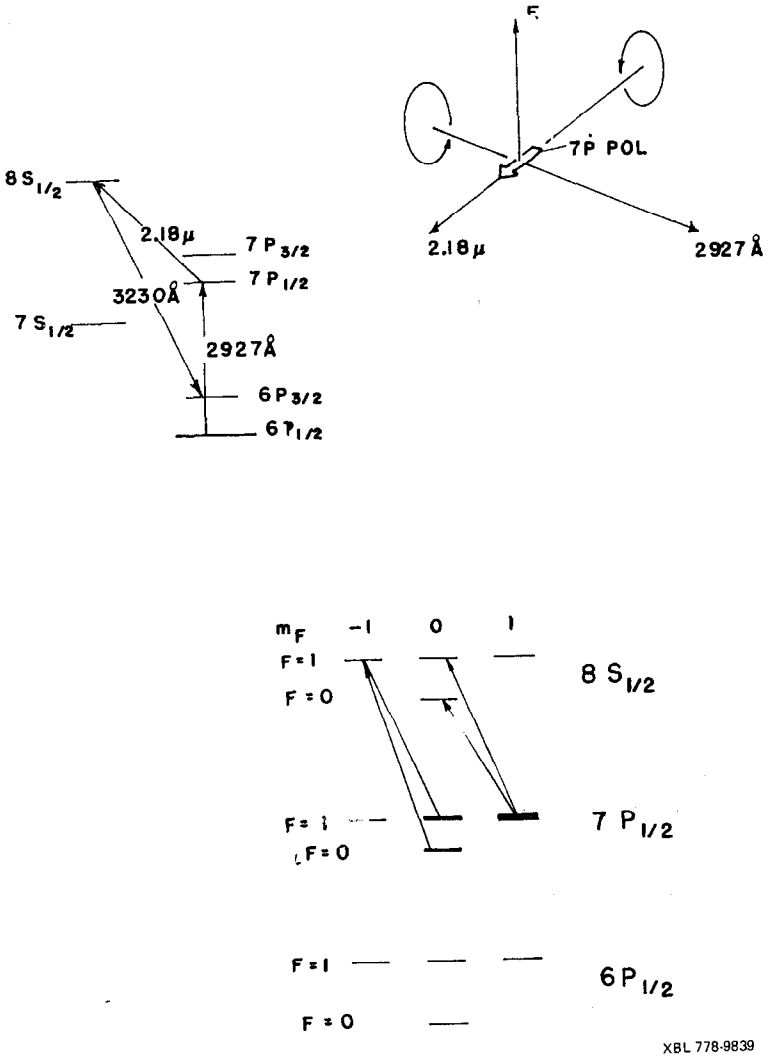

Fig. 10

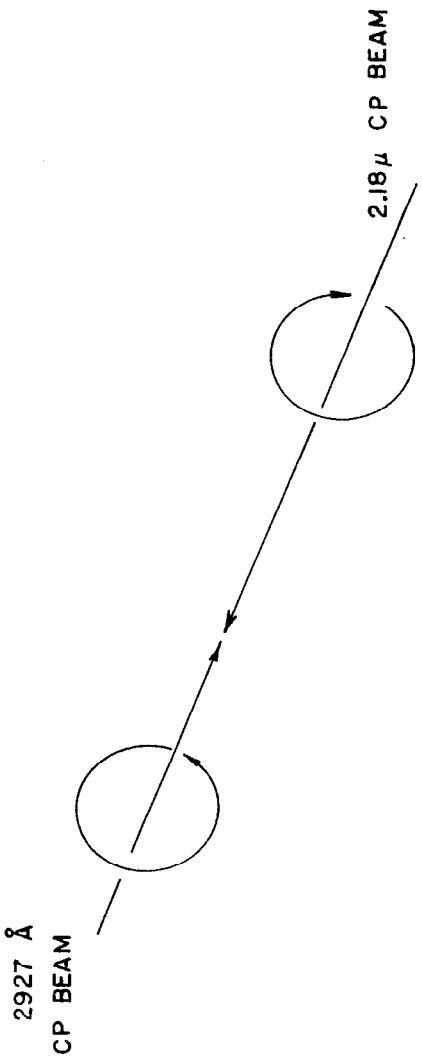

Fig. 11

Now we describe the actual parity experiment, illustrated in figure 12. The IR beam intersects the UV beam twice. Thus we have two interaction regions, each viewed separately by a pair of lenses, filters and photo-tubes for detection of 3230 Å radiation. Since the infra-red polarization is opposite in the two regions, the asymmetries from the two regions are of opposite sign. Thus, when we take the difference between the signals in regions 1 and 2, infra-red pulse-to-pulse intensity fluctuations cancel to a large degree, but the asymmetries add. Both lasers are pulsed synchronously 20 times per second. The UV and IR polarizations and E field direction are reversed periodically as follows:

0 - 1 line: Pulse #	UV CP	E	IR CP
1	L	+	L
2	R	+	L
3	L	-	L
4	R	-	L
5	L	+	L
	.....		
128	R	-	L
129	L	+	R
	.....		
256	R	-	R

etc.

After 1024 pulses the data which has been computer-analyzed on-line is printed out. After 25 print-outs, the frequency is changed to the 0 - 0 line, and the sequence is repeated. A given run (approx. 48 hours) consists of about 40 groups of 0 - 1, 0 - 0 sets of

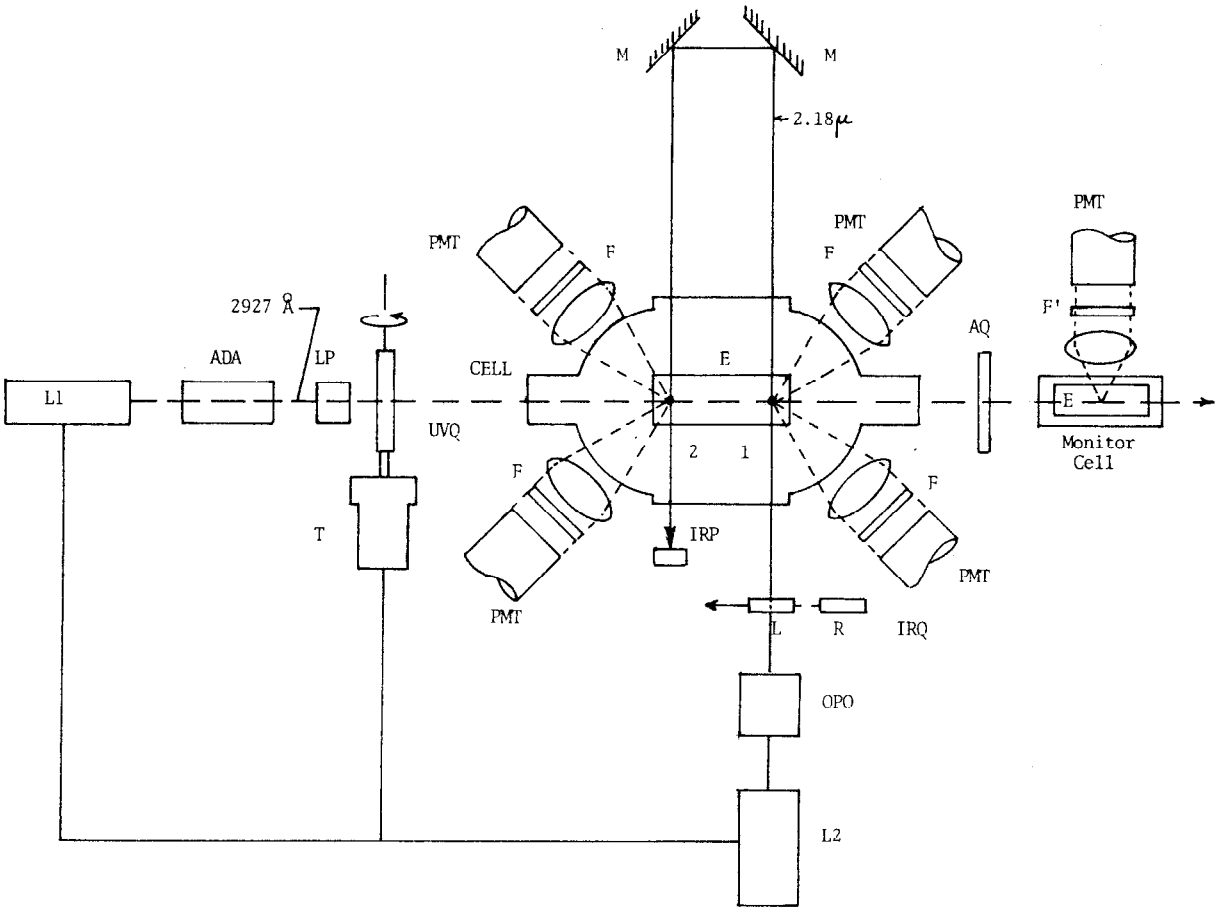

Fig. 12

Schematic diagram of apparatus used to observe parity non-conservation in the $6P_{1/2} - 7P_{1/2}$ transition in thallium. The apparatus consists of:

L1: Flashlamp-pumped pulsed dye laser , generating a pulsed beam at 585nm, part of which is converted to 2927 Å pulses in the ADA crystal. The linear polarization of this UV light is precisely defined in LP, a calcite Glan- air prism. UVQ is the rotating UV quarter - wave plate(sense of rotation indicated). T is the driving motor and timing mechanism which is coupled to the computer and the two lasers. L2 is a second flashlamp pumped pulsed dye laser essentially identical to the first, which drives an Optical Parametric Oscillator. The latter generates 2.18 micron radiation. CELL is the quartz cell heated to about 1050 ^{o}K by a stainless steel oven, not shown. A pair of tantalum plane parallel electrodes defines the static Stark field E, whose direction can be reversed. The infra red circular polarization is determined by one of two quartz quarter wave plates IRQ which can be translated into or out of the beam by an automatic mechanical device. The infra red photons have opposite polarization in regions 1 and 2, which are separately viewed by lenses, filters (F) and photomultiplier tubes PMT. IRP is an infra red power monitoring device. The circular polarization of the UV light is converted into linear polarization which shifts back and forth between the y and z directions on alternate pulses by a fixed analyzing quarter wave plate AQ. In this way we monitor the frequency of the UV by comparing the 0-0 resonance (y linear polarization) with the 0-1 resonance (z linear polarization). These two transitions are well resolved(splitting = 2.13 Ghz.) in the Monitor cell.

observations. The data is analyzed in such a way that we separate the PNC and M1 dependent portions of the polarization. Thus we continuously observe the M1 polarization in the 0 - 1 and 0 - 0 lines and use it to normalize any observed PNC asymmetry.

Great care has been taken to avoid possible sources of systematic error. We note especially our method of producing circularly polarized 2927 Å photons. This is done with a rotating crystalline quartz plate ground to extreme flatness, aligned with unusual care and rotated in a manner such as to cancel several possible sources of systematic error. Detailed analysis shows that a false PNC asymmetry arising from the M1 asymmetry due to imperfect UV polarization would affect both 0 - 0 and 0 - 1 lines with the same sign and approximately the same magnitude, given our conditions of observation. Also such an effect is expected to be at least an order of magnitude smaller in each line than the expected difference in in asymmetries $\Delta(0,1 \text{ -- } 0\ 0)$ between 0 - 1 and 0 - 0 lines due to PNC according to Weinberg/Salam. It is in fact the difference Δ which we measure.

On the basis of data taken so far at E = 300 V/cm we find:

$$\Delta\ (0,1 \text{ -- } 0,0) = -13 \pm 5 \times 10^{-6} \qquad (16)$$

Comparing to our observed M1 asymmetry we obtain:

$$\delta_{EXPT} = (4.2 \pm 1.6) \times 10^{-3} \qquad (17)$$

which is to be compared, in turn with the theoretical predic tion

$$\delta = (2.6 \pm .6) \times 10^{-3} \qquad (18)$$

These values agree; therefore our very preliminary results suggest that the Weinberg-Salam model correctly describes PNC effects in atoms.

In the immediate future we intend to continue taking data in the manner indicated both to improve the precision and to check for possible systematic errors. Major improvements in our UV and IR lasers, which are now being prepared together with a new cell and light collection system, should enable us to collect data much more rapidly at various Stark fields within the next 3 or 4 months. In addition we hope to observe the $6^2P_{1/2} \rightarrow 8^2P_{1/2}$ transition in Tl (2417 Å). The M1 and PNC effects in this transition are quite comparable to that of $6^2P_{1/2} \rightarrow 7^2P_{1/2}$, and a comparison between the two should be useful in reducing uncertainties due to atomic theory.

1. M.A. Bouchiat and C. Bouchiat
   Phys. Lett. 48 B 111, 1974
   Jour. Phys. 35 899, 1974
   Jour. Phys. 36 493, 1975

2. D.V. Neuffer and E.D. Commins
   Phys. Rev. A 16, 844, 1977

3. S. Chu, E.D. Commins and R. Conti
   Phys. Lett. 60A, 96, 1977

Search for Parity Non Conserving Neutral Current Effects in Atomic Bismuth

Norval Fortson

University of Washington

Seattle, Washington 98195

The Weinberg-Salam theory of Weak Interactions[1,2] predicts the existence of observable parity non-conservation (PNC) in atoms. Experiments to search for atomic PNC effects have been underway for many years,[3-10] and of these, the most accurate thus far have been the searches for optical rotation associated with magnetic-dipole transitions in atomic bismuth vapor. Two of the latter experiments, one at Oxford[9] using the 6476 Å line and the other at the University of Washington[8] using the 8757 Å line have reported no observable PNC effects at well below the level calculated[11-14] for bismuth on the basis of the Weinberg-Salam model.

More recently, however, a group at Novosibirsk[9] using the 6476 Å line has claimed to see a PNC effect in bismuth at a level consistent with the Weinberg-Salam prediction. It is important to clear up the discrepancy among the atomic experiments, especially since outside of these experiments the Weinberg-Salam theory has been remarkably successful.

As a step in this direction, we report here early results[15] from a new and more accurate bismuth experiment at the University of Washington. These results show no optical rotation of the size reported in the Novosibirsk experiment, but instead are consistent with the earlier UW experiments. There is possibly a small effect that appears at the barely resolved level.

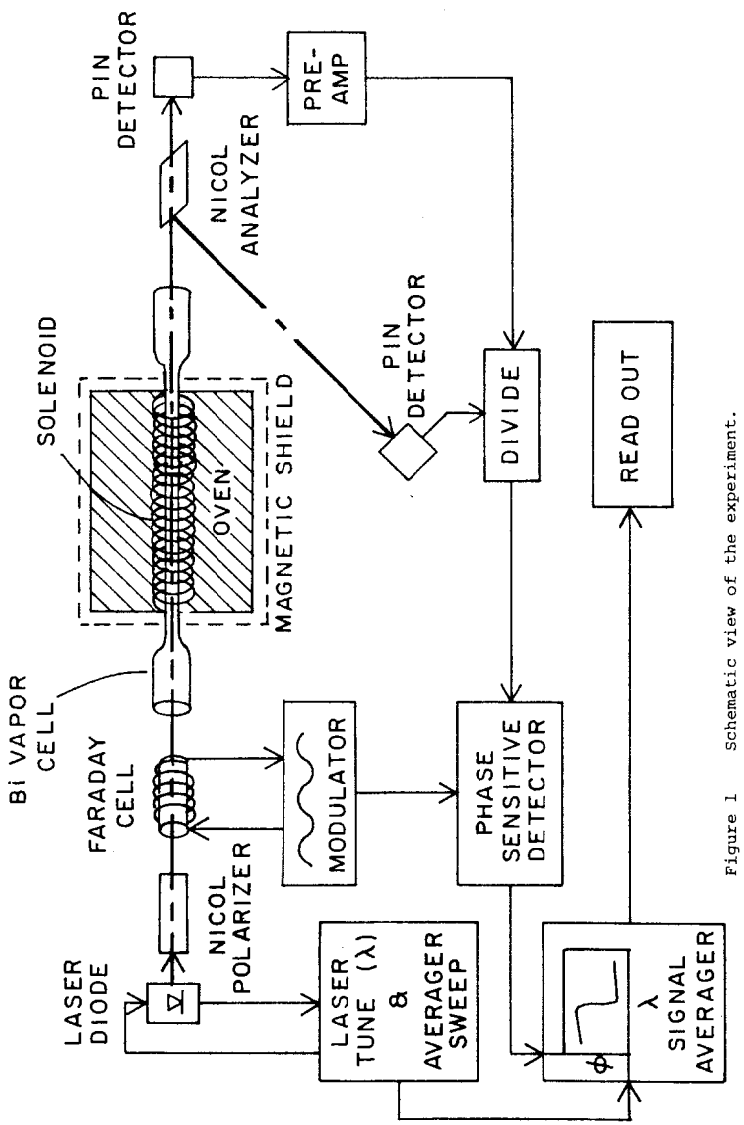

Figure 1 Schematic view of the experiment.

Although we have almost completely rebuilt our apparatus, the conceptual basis of our new experiment is the same as before. A PNC Weak Interaction between the atomic electrons and nucleons would mix the parity of the electronic states of the atom, and couple a normally forbidden electric-dipole (E_1) transition into the observed magnetic-dipole (M_1) optical transition. The E_1 - M_1 interference causes an optical rotation of the plane of polarized light in the bismuth vapor by an angle $\phi_{pnc} = 4\ell\lambda^{-1}(n-1)\ E_1/M_1$ where n is the refractive index of the vapor and ℓ the path length. We look for the sharp dispersive change in ϕ_{pnc} that should occur at each component of the magnetic-dipole line. At each dispersion peak the rotation is typically about $1/2\ E_1/M_1$ for unit absorption at line-center.

The plan of our experiment is shown in Figure 1. We send a beam of light from a tunable laser through two nearly crossed plane polarizing prisms which are located at either end of a heated bismuth vapor cell. An optical rotation of the light passing through the cell causes a change in intensity transmitted by the second prism. As the tunable laser wavelength is varied near the bismuth absorption line at 8757 Å, a dispersive dependence of ϕ is looked for as evidence of a PNC effect.

One of the major changes in our experiment is the use of a recently developed CW gallium-arsenide laser diode to replace the pulsed parametric laser used in our earlier work. The stability of the light intensity, optical characteristics, and wavelength resolution are vastly improved with the new laser. The different hfs components are now clearly resolved down to their doppler-widths.

Figure 1 gives the overall plan of the experiment. The laser wavelength is tuned across the Bi line by varying either the temperature of the diode or the current through it. The laser beam, after being polarized by the first Nicol prism, enters a water-filled tube

inside a magnetic coil which produces a Faraday modulation of the beam polarization angle. The beam then passes through the bismuth cell within a magnetically-shielded oven, and finally through the second "analyzing" prism, after which it is detected and compared with the reference beam level. The resulting signal is matched with the Faraday modulation in a phase sensitive detector and then stored as a function of laser wavelength.

Figure 2 shows the expected Bi Faraday rotation pattern ϕ_f, together with a portion of the observed pattern, with which it agrees in size and shape. Figure 2 also shows the shape of the dispersive rotation that is expected if there is a PNC effect. It is seen that there are many points of zero ϕ_f where ϕ_{pnc} should be nearly maximum. By stepping the laser wavelength to each of these points we obtain maximum changes in ϕ_{pnc} while virtually eliminating the ϕ_f background.

Our remaining background comes from a residual angle which changes very slowly with wavelength due to interference effects in the polarizers and in other optical components. This background is rejected quite adequately for the accuracies we report here by looking for the more rapid λ dependence shown in Figure 2.

The first data from this new experiment, taken in 8 hours of running time, consists of 50,000 sweeps over a portion of the 8757 Å line having 4 alternating maxima and minima of ϕ_{pnc}. The data yields a new experimental value of $R = E_1/M_1 = -1.8 \pm 1.6 \times 10^{-8}$. The quoted error is one standard deviation computed from the statistical variation of the measured values of R from sweep to sweep. Improved accuracy is expected in the coming months.

The present result is shown below together with the results of the Oxford, Novosibirsk, and earlier Washington experiments, and also with the average of calculated values[16] expected in bismuth on the basis of

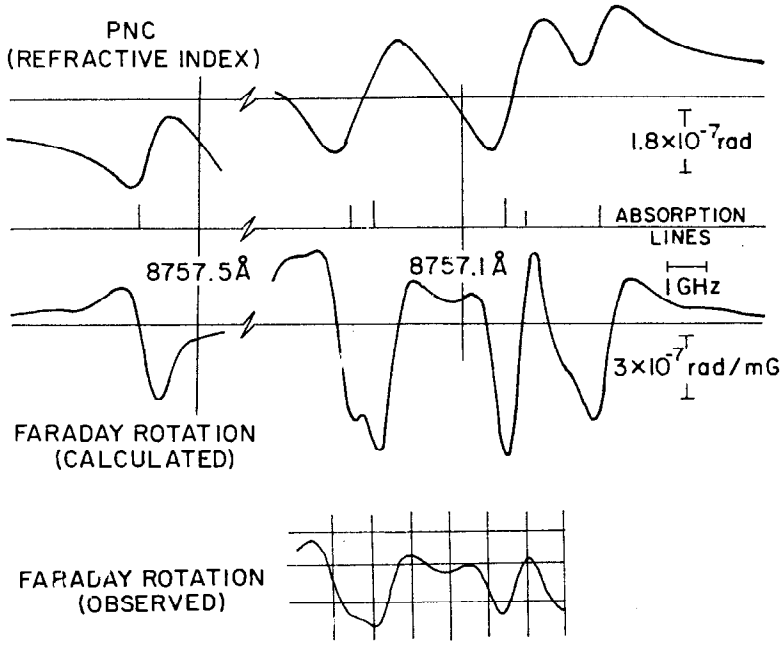

Figure 2 Form of the PNC and Faraday rotation curves expected for the 8757 Å line in Bi. The vertical scale assumes unit absorption on the strongest hfs component, and for the PNC curve, a value of $R = 2.5 \times 10^{-7}$. The observed Faraday rotation is also shown, but with a different vertical scale.

the Weinberg-Salam theory.

	R (87.7 Å) (10^{-8})	R (6476 Å)
Theory	-14	-19
Experiment	-0.7 ± 3.2 (UW, old)	+2.7 ± 4.7 (Oxford)
	-1.8 ± 1.6 (UW, new)	-22 ± 6 (Novosibirsk)

It is clear that more work needs to be done in order to resolve the experimental situation. Also, there remains a discrepancy between our results and the predicted value of R.

1. S. Weinberg, Phys. Rev. Lett. 19, 1264 (1967).
2. A. Salam, in Proceedings of the Eighth Nobel Symposium, edited by Svartholm (Almkvist and Wiksell, Stockholm, 1968).
3. M. A. Bouchiat and C. C. Bouchiat, Phys. Lett. 48B, 111 (1974).
4. D. C. Soreide and E. N. Fortson, Bull. Am. Phys. 50c, 20, 491 (1975), D. C. Soreide et al., Phys. Rev. Lett. 36, 352 (1976).
5. P. G. H. Sandars, in Atomic Physics 4 edited by G. zu Putlitz, E. W. Weber, and A. Winnacker (Plenum, New York, 1975).
6. I. B. Khriplovich, Pis' ma Zh. Eksp. Teor. Fiz. 20, 686 (1974) [JETP Lett. 20, 315 (1974)].
7. P. E. G. Baird et al., Phys. Rev. Lett. 39, 798 (1977).
8. L. L. Lewis et al., Phys. Rev. Lett. 39, 795 (1977).
9. L. M. Barkov and M. S. Zolatoryov, Pis' ma Zh. Eksp. Teor. Fiz., 27, 379 (1978) [JETP Lett., to be published].
10. S. Chu, R. Conti, and E. D. Commins, Phys. Lett. A 60A, 96 (1977).
11. E. M. Henley and L. Wilets, Phys. Rev. A14, 1411 (1976).
12. V. N. Novikov, O. P. Sushkov and I. B. Khriplovich, Zh. Eksp. Teor. Fiz. 71, 1665 (1976) [JETP 44, 872 (1976)].
13. M. Brimicombe, C. Loving, and P. Sandars, J. Phys. B9, L1 (1976).
14. C. E. Loving and P. G. H. Sandars, Private Communication.
15. Earlier results given at the Neutrinos-78 Conference at Purdue.
16. L. Wilets, International Conference on Neutrino Physics and Neutrino Astrophysics, Purdue (1978) to be published.

CHARM AND TAU MEASUREMENTS FROM DELCO[1*]

Jasper Kirkby
Stanford University

I. INTRODUCTION

DELCO has just completed its data-taking period of eighteen calendar months at SPEAR. The detector has distinguished itself from other '4π' spectrometers by emphasizing clean electron identification over a broad energy range at the expense of poorer momentum resolution. This characteristic allows a general purpose probe of both charm and τ decays via the transitions $c \to s\, e^+\nu_e$ and $\tau^- \to \nu_\tau\, e^-\bar{\nu}_e$ respectively. Both decays have the merit of large ($\geq$ 10%) branching ratios and consequently we have accumulated relatively strong data samples (1K eX events from τ decays and 5K multiprong electron events from charm and τ decays).

Most of our analysis so far has emphasized τ studies (which are discussed in section V). However, I will also show you what we know from cross sectional measurements (section III) and from preliminary studies of D semileptonic decays at the ψ'' (section IV). There will be very little discussion of the interesting subject of di-electron events (2 electrons + $\geq$ 1 charged particle $\neq$ e) since our analysis is in an early stage.

Finally, I refer the reader to the excellent series of lectures by Stanley Wojcicki at this Summer Institute. These contain both a general discussion of how our measurements fit into the overall picture of weak decays and a far more thorough list of references on this broad subject. As a result I can, and will, primarily concentrate on simply presenting the experimental data.

* Work supported by the U.S. National Science Foundation and Department of Energy.
(Presented to the SLAC Summer Institute on Particle Physics, Stanford California 94305, July 1978)

II. APPARATUS

The apparatus (Figs. 1a) and 1b)) consists of a tracking system of cylindrical multiwire proportional chamber and planar magnetostrictive wire spark chambers (WSC) separated by a one-atmosphere ethane threshold Cerenkov counter. The latter provides clean electron identification ($P_{\pi \to e} < 10^{-3}$) down to a momentum of 0.2 GeV (below which the Cerenkov light images are displaced off the phototubes). A magnet provides an analyzing field integral of 1.7 kG-m which results in a momentum accuracy of $\sigma_p/P = 8P$ (GeV)% due to measurement errors and 5.2% due to multiple Coulomb scattering. The outer-most detector layers are an array of Pb/scintillator shower counters which cover 60% of 4π steradians and a pair of Pb walls, followed by scintillation counters and WSC, which allow π/μ separation over 20% of 4π steradians.

III. THE R AND R_e PLOTS

A. Hadronic Cross-Section

Historically the R plot has been the single most fruitful measurement made in e^+e^- annihilations. (R is defined by $R = \sigma(e^+e^- \to \text{hadrons})/\sigma(e^+e^- \to \mu^+\mu^-)$ and its variation is measured with centre-of-mass energy.) It was the first indicator of a new flavour, charm, it supports the colour hypothesis and measures the quark charges, it revealed an extra contribution due to the τ lepton and led to the spectacular observations of the ψ and ψ'.

For the last couple of years or so it has been used as a R(oad) map to lead experimentalists to productive centre-of-mass energies. The most notable success has been the ψ''[2] which is found just above charm threshold at E_{CM}=3.77 GeV. At this energy 30% of the hadronic events are due to

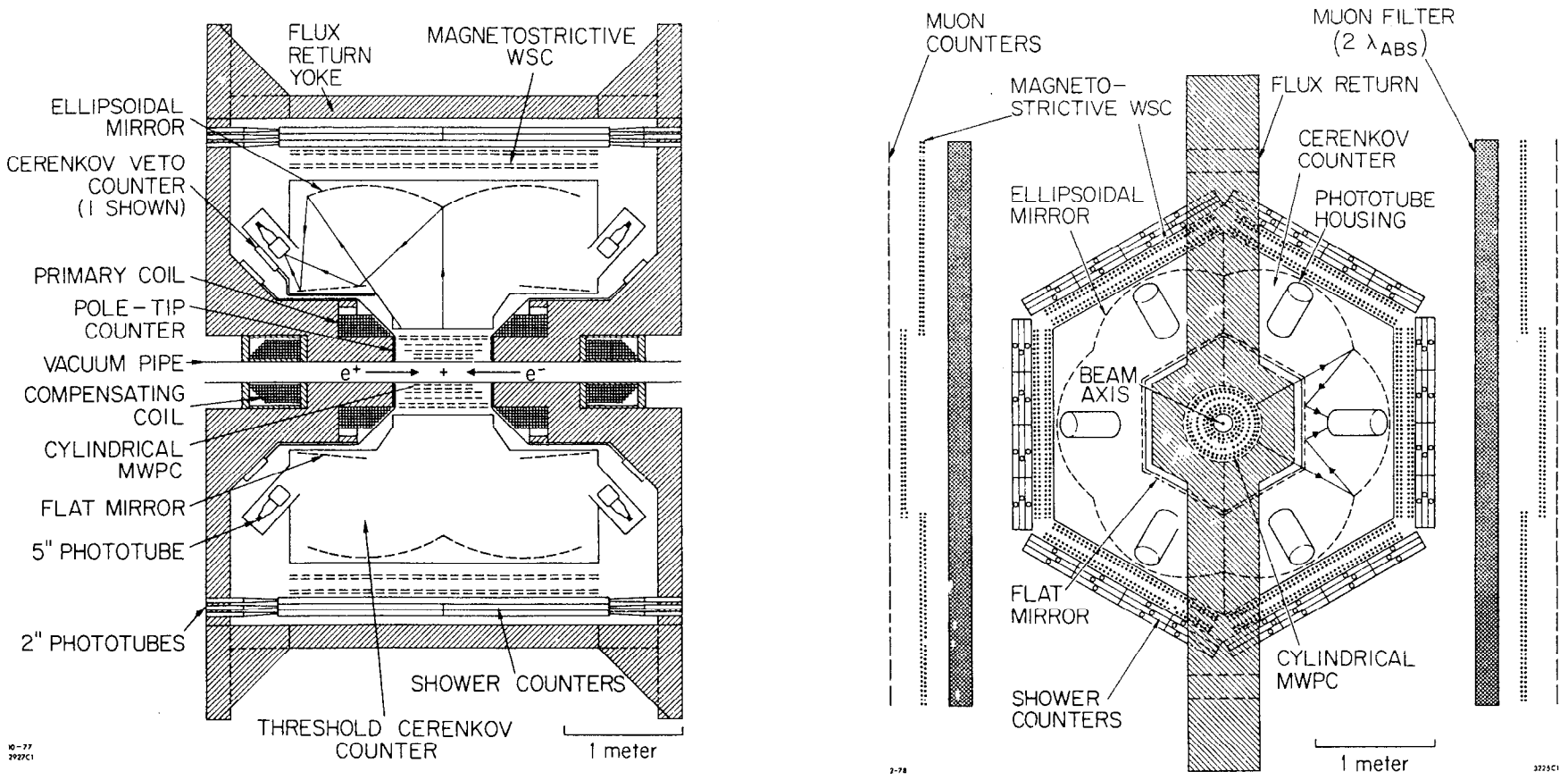

Fig. 1. a) Polar and b) Azimuthal projections of the apparatus.

pure $D\bar{D}$ initial states (roughly half $D^{o}\bar{D}^{o}$). Furthermore the D's have a low velocity ($\beta \sim 0.14$) so there are rather small differences between LAB and CM quantities. The studies of D semi-leptonic decays discussed in Section IV were made at this resonance.

The value of R in the range $3.50 < E_{CM} < 4.8$ GeV, after removal of the ψ and ψ' radiative tails, is shown in Fig. 2. No further radiative corrections have been applied to these data since they exagerate fluctuations which may be both statistical and authentic. This in turn leads to difficulties in identifying resonances and in making comparisons with other experiments.

The hadronic detection efficiency has been determined from the observed prong and photon distributions and is $0.85^{+0.05}_{-0.10}$ over this range. The bars indicate only statistical errors and thereby do not reflect an overall systematic error of ±15% due to model uncertainties, event losses and backgrounds such as those due to beam gas scattering. Any variation in systematic erros vs. E_{CM} is smooth and so the statistical error bars are appropriate indicators of structure.

The value of R below charm and τ thresholds at E_{CM}=3.50 and 3.52 is $2.0 \pm 0.1 \pm 0.3$[3] in good agreement with the coloured quark prediction of $3(Q_u^2 + Q_d^2 + Q_s^2) = 2$. The dashed line in Fig. 2 represents the constant contribution from 'old physics' at higher energies.

Beyond the resonance region, R again assumes an approximately constant energy dependence with the new value $4.4 \pm 0.2 \pm 0.6$. From our τ measurements we determine a contribution (indicated by the dot-dashed line) of 0.85 ± 0.15 to this increase and thereby infer a residue due to charm of $4.4 - 2.0$ (old physics) $- 0.85(\tau) = 1.55 \pm 0.2 \pm 0.2$. Once more

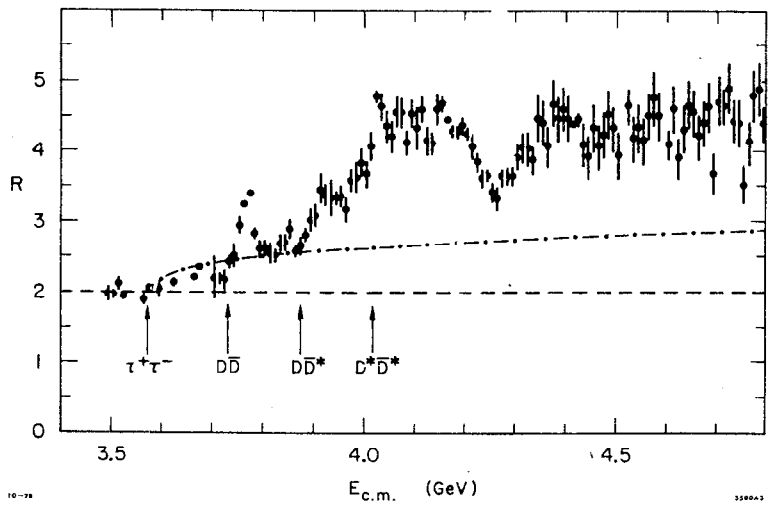

Fig. 2. The hadronic cross section, R in the range $3.50 < E_{CM} < 4.8$ GeV after removal of the ψ and ψ' radiative tails. The dashed line represents the contribution from old physics and the dot-dashed line is the τ contribution. Also indicated are the energy thresholds for τ and D production.

this is compatible with the quark model prediction of 4/3.

The residual charm component of the hadronic cross section (R^c) is shown in Fig. 3. The data display considerable structure: sharp rises just above thresholds for production of $D\bar{D}$ (centered at 3.77 GeV), $D\bar{D}^*$ (3.92 GeV) and $D^*\bar{D}^*$ (4.03 GeV) and a sharp dip at E_{CM} = 4.25 GeV. The region between 4.03 and 4.2 GeV is reasonably flat and the 4.4 GeV peak is rather modest in contrast with the observations[4] of other experiments (Fig. 4). Part of these discrepancies is due to the afore-mentioned application of radiative corrections. The theoretical models for these structures include both s-channel poles due to a $c\bar{c}$ state[5] (charmonium) and bound states of two quarks and two anti-quarks[6] ($D\bar{D}$ molecules).

B. Multi-Prong Electronic Cross-Section

Both the τ and the lightest charmed particles will give rise to 'prompt' single electrons since they have weak-decay lifetimes ($\sim$few 10^{-13}sec) which are much shorter than those familiar from kaon decay ($\sim 10^{-8}$sec). Since electromagnetic sources produce electrons in pairs, which can thereby be identified and rejected, the study of inclusive electron production provides a sensitive technique for observing the new particles.

The inclusive electron cross section is expressed as $R_e = \sigma(e^+e^- \to e^\pm + \geq 2 \text{ charged particles})/\sigma(e^+e^- \to \mu^+\mu^-)$. The variation of this quantity in the range $3.5 < E_{CM} < 4.8$ GeV is shown in Fig. 5. Events containing two or more prompt electrons have been excluded from these data. A prompt electron is identified as a single track which appears to originate from the interaction region and possesses in-time Cerenkov and shower counter pulses. The minimum pulse heights correspond to 0.7 photo-electrons for the Cerenkov counter and 0.3 minimum ionizing particles for the shower counter.

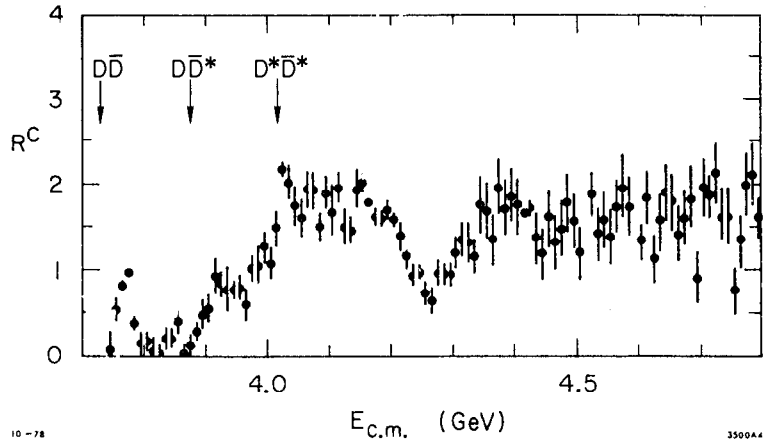

Fig. 3. The charm hadronic cross-section, R^c. The contributions from old physics, $\tau^+\tau^-$ pairs and the ψ and ψ' radiative tails have been removed.

The track is required to have at least one hit in either the first (innermost) or second cylindrical proportional chambers in order to decrease photon conversion backgrounds.

We will now discuss the backgrounds to these data. The dominant electron source is pair production both by externally and internally converted photons from π^o decay. We can estimate this background assuming 3 π^o's per hadronic event and a 1% beam-pipe radiator. The number of external γ conversions per hadronic event is $\sim$ 6x .01 x 0.5(Ω) $\sim$ 0.03 which is approximately equal to the charm signal rate $\sim$(1.3/5)x2x0.1x0.5$\sim$0.03 per hadronic event (assuming a semileptonic branching ratio of 0.1). Most Dalitz pairs and photons which convert in the beam pipe are removed by requiring that the candidate electrons are unaccompanied by another track of opposite charge and small relative ('opening') angle. A fake signal is also generated by the spatial coincidence of a charged track with a photon conversion in the 'blind' region at the entrance to the Cerenkov counter or in the ethane radiator itself. We measure this process to occur at the level $(4.2\pm0.3)10^{-3}$ per hadronic event and have applied this correction to Fig. 5. The probability for a non-electron to be detected by the Cerenkov counter is $(0.8\pm0.3)10^{-3}$, as determined from $\mu^+\mu^-$ events. This is consistent with the production rate of δ rays above the electron Cerenkov threshold in ethane (14 MeV). This background is very small (<3% of the charm signal) since the majority of the pion momenta are below 500 MeV/c and thereby cannot give rise to δ rays exceeding 14 MeV.

After removal of these backgrounds, the value of R_e at E_{CM}=3.50, 3.52 GeV is 0.03±0.01 which represents the residue from unsubtracted backgrounds such as asymetric Dalitz decays and two-photon electron production. Until we have a better understanding of the nature of this residual background

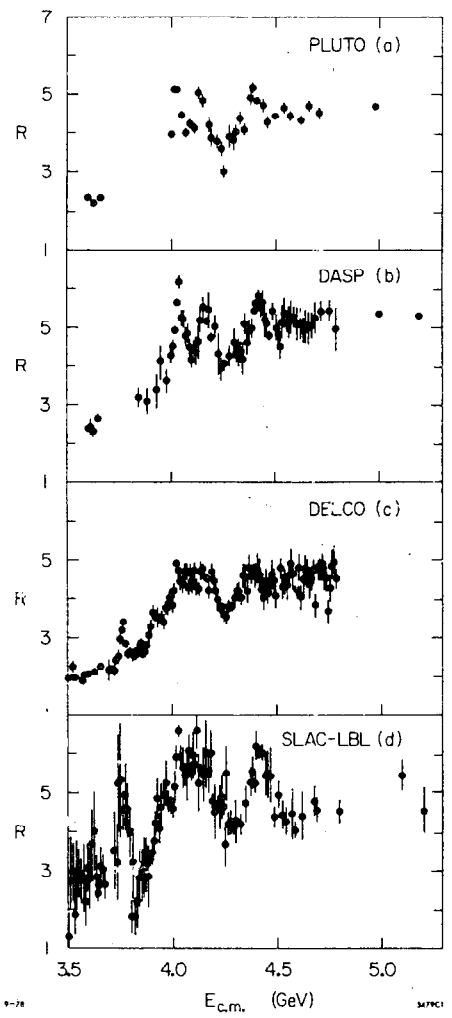

Fig. 4. A comparison of the hadronic cross sections from a) PLUTO b) DASP c) DELCO and d) SLAC-LBL. Complete radiative corrections have been applied to all data with the exception of those from DELCO (which displays the raw data after removal of the ψ and ψ' radiative tails).

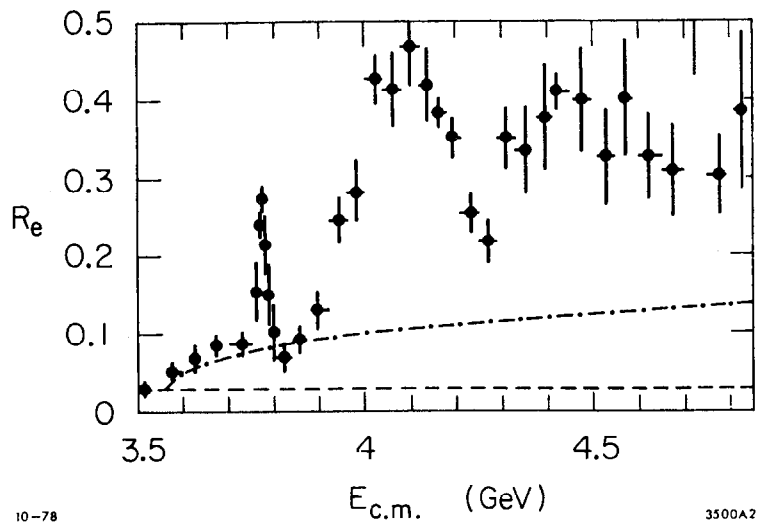

Fig. 5. The multi-prong electronic cross-section, R_e. The residual background is indicated by the dashed line and the dot-dashed line is the τ contribution.

we will naively assume it has a constant energy dependence as indicated by the dashed line. Above the τ and D thresholds the data exhibit a striking increase and a structure similar to the hadronic production. These data contain a large contribution from τ decays (dot-dashed-line) according to measurements described in Section V.

It is instructive to compare quantitatively the electron production from charm R_e^c (Fig. 6) with the total charm cross section (Fig. 3). This comparison is made by plotting the ratio R_e^c/R^c (Fig. 7). The value at E_{CM}=3.77 GeV provides a direct measurement of the semileptonic branching ratio, b_e^D, averaged over an equal flux of D^o and D^+. In a 4 MeV energy range which is centred on the ψ'', we find $R^c = 0.97 \pm 0.02$ and $R_e^c = 0.192 \pm 0.021$, where the quoted errors are statistical and events involving two detected electrons are excluded. We therefore measure,

$$2b_e^D\,(1-0.25\,b_e^D) = R_e^c/R^c = 0.20 \pm 0.023$$

$$\text{i.e.} \qquad b_e^D = 0.10 \pm 0.02.$$

The final result includes an estimation of systematic errors.

The data of Fig. 7 display, within systematic errors, a constant or perhaps slightly falling electron contribution from charm. It is especially interesting to note that electron production at the energies 4.16 and 4.4 GeV, which are associated with F production, shows no significant departure from the D regions. This implies either a small F cross-section or semileptonic branching ratio similar to the D.

C. Two-Electron Multiprong Cross Section

Events which contain two prompt electrons in addition to hadrons cannot arise from the decay of a sequential heavy lepton pair but will be generated by the simultaneous semi-leptonic decays of a pair of charmed particles. As such they provide good sensitivity to certain features of the charm semileptonic decays despite a statistical reduction by a factor of 20 relative to

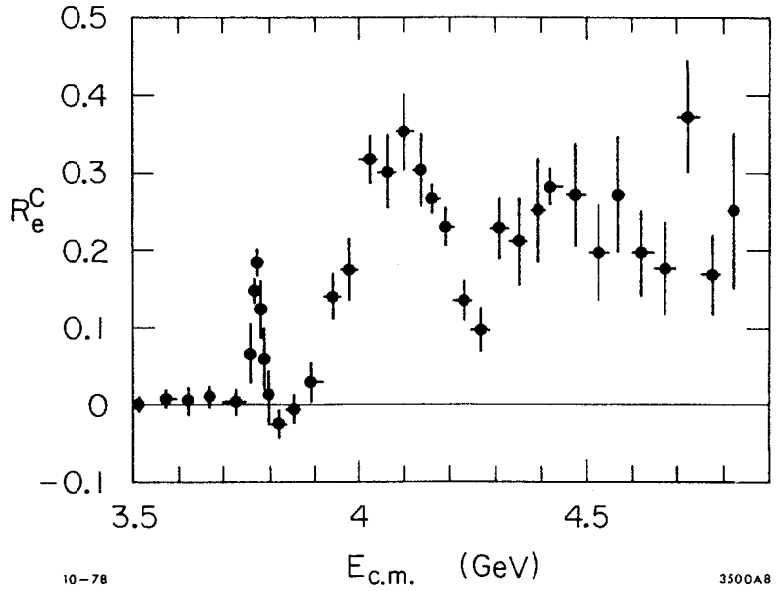

Fig. 6. The charm multi-prong electronic cross-section, R_e^c. The contributions from backgrounds and τ leptons have been removed.

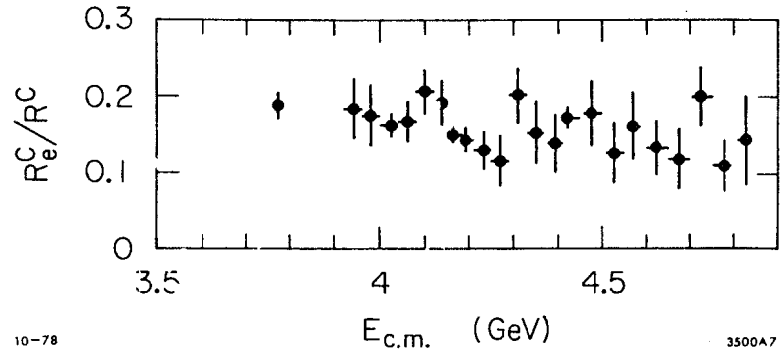

Fig. 7. The ratio R_e^c/R^c. The data are plotted where the ratio can be well determined (at E_{CM}=3.77 GeV and above E_{CM}=3.95 GeV). The error bars are statistical and do not reflect possible smooth energy-dependent systematic errors.

the one-electron events.

The important backgrounds are π^o Dalitz decays, the cascade decays $\psi' \to X\,\psi \to e^+e^-$ and electrons from the two-photon process. These are inhibited by the requirements that the e^+e^- pair mass exceed 135 MeV/c^2, the coplanarity angle $\phi_{ee} < 160^o$ and that at least one non-electron track is present with a momentum above 200 MeV/c and with a polar angle $55^o < \theta < 125^o$.

After applying these restrictions there remain 75 events in the range $3.1 < E_{CM} < 4.25$ (ψ' excluded). The cross section $R_{2e} = \sigma(e^+e^- \to e^+e^- + \geq 1$ prong $\neq e)/\sigma(e^+e^- \to \mu^+\mu^-)$ is shown in Fig. 8. We have arbitrarily allowed the rate in the range $3.5 < E_{CM} < 3.67$ GeV to define the background level.

The data are consistent with the charm production energy-dependence we saw earlier. At the ψ'' we measure,

$$R_{2e}/R^c = (b_e^D)^2 = 0.015 \pm 0.005$$

or,
$$b_e^D = 0.12 \pm 0.02 \pm 0.04$$

where the second (systematic) error reflects model uncertainties. For example, if the dominant decay mode is $D \to Ke\nu$ then the acceptance of D^+D^- events is almost a factor of two lower than $D^o\bar{D}^o$ events. (This follows from the poor detection efficiency of neutral kaons.) The data of Fig. 8 assume equal contributions from $D^o\bar{D}^o$ and D^+D^- events and equal $Ke\nu$ and $K^*e\nu$ partial rates; if we make the extreme assumption that only D^+D^- events contribute then $b_e^+ = 0.14 \pm 0.02 \pm 0.04$.

This measurement can be used to set limits on the separate D^+ and D^o semileptonic branching ratios (b_e^+ and b_e^o, respectively). For example, in the extreme case that $b_e^+ \sim 20\%$ and $b_e^o \sim 0\%$, the one-electron data at the ψ'' would lead to a measurement $b_e^D = 10\%$. However we would observe an anomalously large (by a factor of two) di-electron yield since this is proportional to

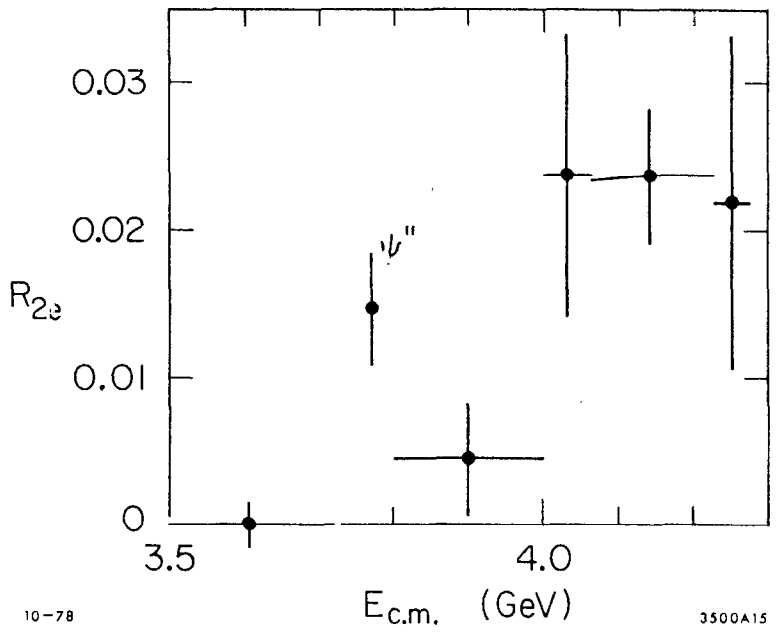

Fig. 8. The two-electron multi-prong cross-section, R_{2e}.

$(b_e^+)^2 + (b_e^o)^2$. Unfortunately, the present errors in R_{2e} do not allow a useful measurement.

The presence of a charm-changing neutral current would result in the decay $D \to e^+e^-X$. The two-electron cross section therefore measures,

$$(b_e^D)^2 + 2\, b_{ee}^D = R_{2e}/R^c$$

where b_{ee}^D is the branching ratio for $D \to e^+e^-X$ and we assume equal D^o and D^+ semileptonic branching ratios (given by $b_e^D = 0.10 \pm 0.02$). At the ψ'' we find,

$$(.10 \pm .02)^2 + 2\, b_{ee}^D = .015 \pm .005$$

or,

$$b_{ee}^D < 0.008 \text{ (95\% CL)}.$$

This measurement is an order-of-magnitude weaker than the limit determined by the Columbia-BNL group from the ratio $\mu^-e^+e^-/\mu^-e^+$ from ν_μ interactions in the FNAL 15' bubble chamber.[7]

IV. D SEMI-LEPTONIC DECAYS

A. Electron Spectrum

Since the basic charmed quark electronic decay is $c \to s\, e^+\, \nu_e$ we expect the following channels to contribute to the semi-leptonic decays of D mesons:[8)9)]

$D \to Ke\nu$

$D \to K^*(890)\, e\nu$

$D \to K^{**}(1420)\, e\nu$

$D \to Q\,(1290)\, e\nu$

$D \to K\,(n\pi)\, e\nu$

The decays are unlikely to contain three kaons due to phase-space suppression. This argument also applies to $K^{**}(1420)$ and Q(1290). The decays to $K(n\pi)$ with n larger than 2 or so are not only suppressed by the available phase space but also by the low energy theorem which says that the semi-leptonic decay rate vanishes if any one of the pions is soft.[8] The anticipated D semileptonic decays are therefore $D \to Ke\nu$, $K^*e\nu$ and $K(n\pi)e\nu$ $(n \leq 2)$, with some prejudice that the $K\pi$ channel is dominated by the K^* pole.

In addition there will be smaller contributions from the Cabibbo-suppressed modes:

$D \to \pi e\nu$

$D \to \rho e\nu$

$D \to A_1\, e\nu$

Of these only the $\pi e\nu$ mode may be significant since, in contrast with the other decays, it benefits from a modest phase-space enhancement so that,

$$\frac{\Gamma\,(D \to \pi e\nu)}{\Gamma\,(D \to Ke\nu)} = 1.6\, \tan^2\theta_c$$

where θ_c is the Cabibbo angle.

The most direct experimental quantity which distinguishes between the various semi-leptonic decays is the electron momentum spectrum. The effect of decay to a higher-mass hadronic state is of course to soften the electron momenta (as illustrated in Fig. 9).

The electron spectrum obtained in the multiprong events at the ψ'' (Fig. 10) must be corrected for backgrounds before it can provide information about the D decays. The τ background (dot-dashed line) is well-determined and is the predominant source of high-energy electrons. The residual hadronic background spectrum (dashed line) has been determined from data taken in the energy range $3.50 < E_{CM} < 3.67$ GeV (after removal of the τ electrons) and from hadronic events at the ψ''. The final spectrum

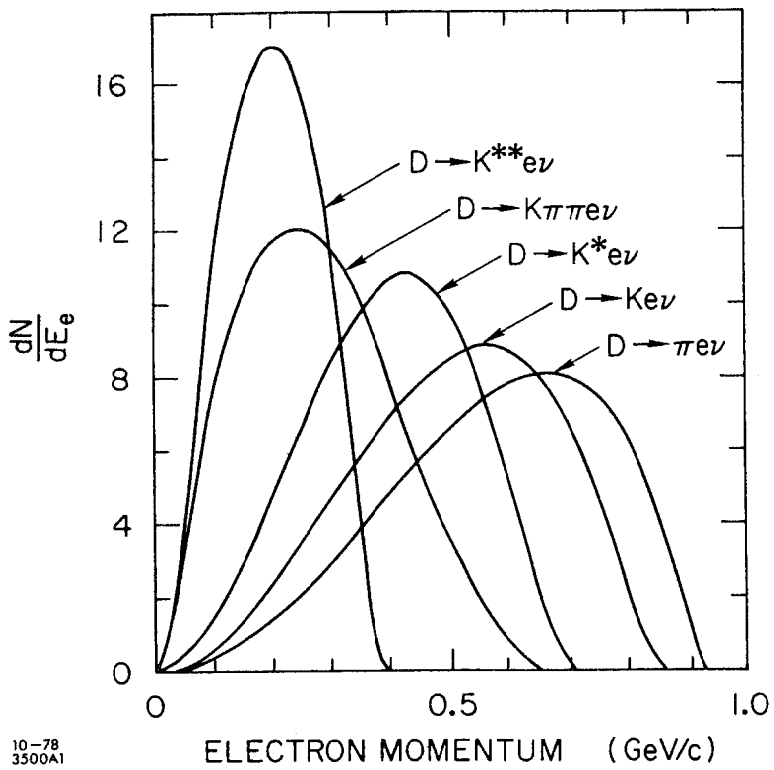

Fig. 9. The electron momentum spectra from several semi-leptonic decay modes of the D at rest.

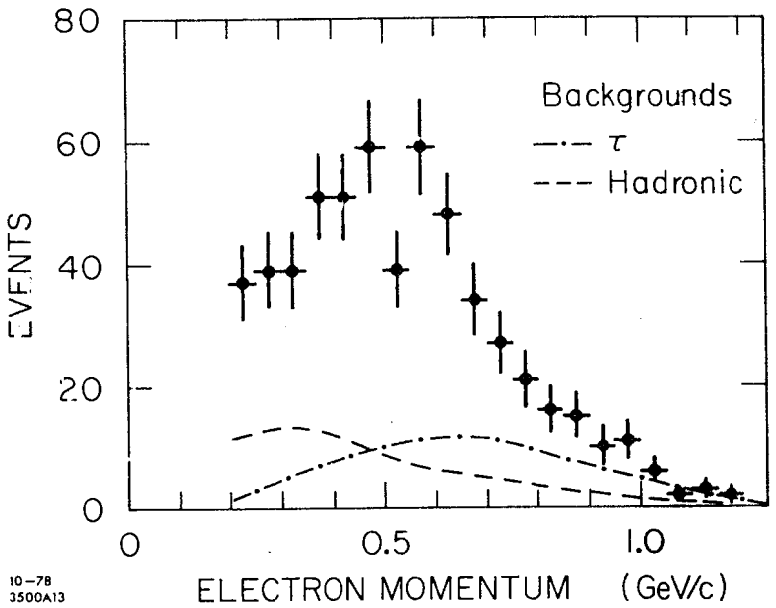

Fig. 10. The unsubtracted electron momentum spectrum obtained in the multiprong events at the ψ". The backgrounds from the τ and other processes are indicated, respectively, by the dot-dashed and dashed lines.

after removal of these backgrounds is shown in Fig. 11.

We will use these data to determine the relative contributions from $K^*e\nu$ and $Ke\nu$ on the assumption that these are the dominant semi-leptonic decay modes. The results of the fit (which includes a fixed $\pi e\nu$: $Ke\nu$ fraction of 1.6 $\tan^2\theta_c$) are illustrated in Fig. 11 and provide the following measurements:

$$\Gamma(D \to Ke\nu)/\Gamma(D \to Xe\nu) = 0.37 \pm 0.20$$

and, $$\Gamma(D \to K^*e\nu)/\Gamma(D \to Xe\nu) = 0.60 \pm 0.20$$

where the errors include an estimate of systematic effects. Under the assumption that the major semi-leptonic decays are $K^*e\nu$ and $Ke\nu$ we therefore measure the branching ratios,

$$BR\ (D \to Ke\nu) = (3.7 \pm 2.1)\%$$

and, $$BR\ (D \to K^*e\nu) = (6.0 \pm 2.3)\%$$

These errors are, of course, highly correlated.

In a separate fit we have varied the $\pi e\nu$ fraction while holding the $K^*e\nu$: $Ke\nu$ ratio equal to 0.60:0.37. This sets a limit,

$$\Gamma(D \to \pi e\nu)/\Gamma(D \to Xe\nu) < 0.20\ (95\%\ CL)$$

or, $$BR\ (D \to \pi e\nu) < 2.0\%\ (95\%\ CL)$$

B. D Lifetime

We may combine the results obtained from the branching ratio determinations and the electron spectra to measure the lifetime of the D mesons.

As input we need a theoretical calculation of the $\Gamma(D \to Ke\nu)$[8)9)]. This decay can be fairly rigorously calculated in contrast with purely hadronic channels, as demonstrated by the successful analogous treatment applied to K_{e3} and $K_{\mu 3}$ decays. The result is $\Gamma(D \to Ke\nu) = (1.4 \pm 0.3)\ 10^{11}\ sec^{-1}$ where the error reflects form factor uncertainties.

If we make the assumption that the D^0 and D^+ lifetimes (τ_D) are equal then by combining this theoretical calculation with our experimental branching ratio measurement we find,

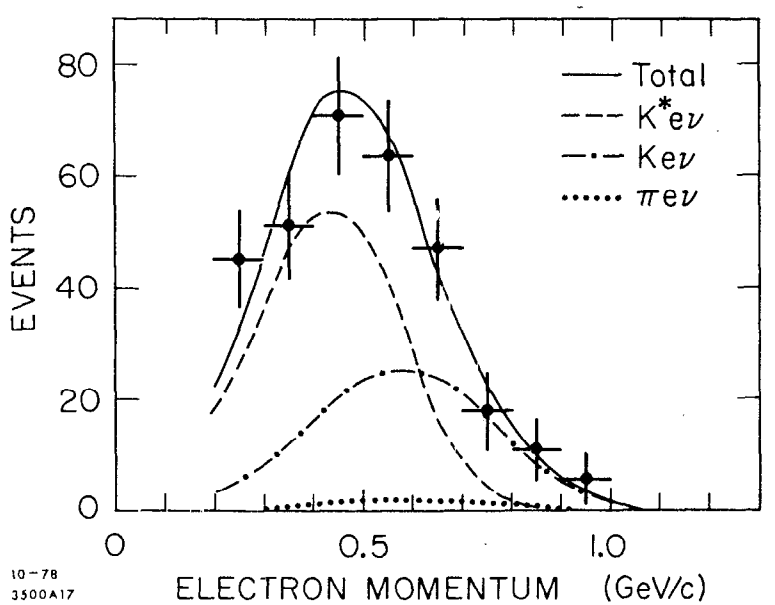

Fig. 11. The D electron momentum spectrum at the ψ''. The fits indicate the contributions from $K^*e\nu$ (dashed line), $Ke\nu$ (dot-dashed line) and $\pi e\nu$ (dotted line) to the total (solid line).

$$\tau_D = (0.037 \pm 0.021)/((1.4 \pm 0.3)\ 10^{11})$$
$$= (2.6 \pm 1.5)\ 10^{-13} \text{ sec}$$

However, it may be invalid to assume that the hadronic decay rate of the D^0 and the D^+ are equal since the D^0 can decay to both I=1/2 and 3/2 final states whereas the D^+ can decay only to I=3/2 states. The conjecture of several authors[10] in fact is that $\Gamma(D^+ \to \text{all}) << \Gamma(D^0 \to \text{all})$. Since the semi-leptonic decay rates of both the D^+ and D^0 must be equal we may test this hypothesis by measuring the separate semi-leptonic branching ratios.

An alternative technique to that involving the two electron events is to compare single electron production at the ψ'' and in the range $4.0 < E_{CM} < 4.2$. At each centre-of-mass energy we write,

$$R^0\, b_e^0 + R^+\, b_e^+ = R_e$$

where R^0 and R^+ are, respectively, the D^0 and D^+ cross sections. In principle therefore, the separate semi-leptonic branching ratios may be determined if R^0, R^+ and R_e are known at two centre-of-mass energies which involve different relative amounts of D^0 and D^+. This is the case for E_{CM}=3.77 and 4.03 GeV and the measurements are summarized in Table 1 Here we have used Mk I data[11] for the relative D^0:D^+ production at E_{CM}=4.03 GeV and our absolute cross-section measurements in order to provide cancellation of some systematic errors.

Table 1

Input Data Used to Determine the D^0 and D^+ Semileptonic Branching Ratios

E_{CM}(GeV)	R^0	R^+	R_e^c
3.77	1.08 ± 0.14	0.86 ± 0.14	0.192 ± 0.21
4.03	2.92 ± 0.36	1.14 ± 0.36	0.399 ± 0.64

The results are,

$$b_e^0 = 0.10 \pm 0.05$$
and $$b_e^+ = 0.10 \pm 0.08$$

The values are very sensitive to input assumptions and the errors are highly correlated. Clearly at present the data are unable to test the hypothesis that the D^+ and D^0 lifetimes are different. This conclusion may be reversed after a more careful analysis has been completed on both these measurements and the detailed characteristics of the two-electron events.

C. $D^0\overline{D^0}$ Mixing

In analogy with the K^0-$\overline{K^0}$ system, it is expected that the D^0 and $\overline{D^0}$ can transform into one another via intermediate states. However since these states must have zero strangeness the process is inhibited by $\tan^4\theta_c$ ($\sim 10^{-3}$) and the mixing will be negligible within the short D^0 lifetime.[12] On the other hand, complete mixing occurs if $|\Delta C|=2$ neutral currents exist at the level of $\geq 10^{-3}$ of the normal weak coupling. A consequence of mixing is the observation of like-sign di-electron events resulting from the process,

$$e^+e^- \to X\, D^{0,+}\overline{D^0} \longrightarrow D^0 \longrightarrow X e^+ \nu_e$$
$$\qquad\qquad\qquad\qquad\quad \hookrightarrow X\, e^+ \nu_e$$

In the D region ($3.72 < E_{CM} < 4.14$ GeV) we observe 46 two-electron events which satisfy the cuts described earlier. Of these, 1 event has like-sign electrons. In the background region, below charm threshold, we observe 7 events of which 2 are like-sign. After adjusting for the relative luminosities we find the single like-sign event in the charm region is consistent with background. On the assumption that half of the observed

electrons are produced by neutral D decay we find,

$$\text{Probability } (D^0 \to \overline{D^0}) < 0.05 \text{ (90\% CL)}$$

V. τ DECAYS

A. Cross Sections

Since a large fraction (70%) of τ decays involve only one-charged particle, they have primarily been studied by means of the anomalous two-prong lepton events, eμ, eX and μX. In our case we have isolated a sample of eX ($X \neq e$) events which have survived certain requirements in order to remove backgrounds. The most important of these are that the X particle does not possess either a Cerenkov tag or a large shower counter pulse-height and that both tracks are acoplanar by at least 20^o. (The acoplanarity angle is defined as the angle between the two planes containing a track and the beam axis). A minimum momentum of 0.3 GeV/c is allowed for the X particle and 0.2 GeV/c for the electron in order to ensure efficient Cerenkov detection. These cuts result in a very clean sample of τ events: the background from misidentified radiative e^+e^- events is about 4% and the charm contamination is <5%, averaged over the full energy range.

The production cross section ratios, $R_{ex}^{2p} = \left(\sigma(e^+e^- \to eX)/\sigma(e^+e^- \to \mu^+\mu^-)\right)$ for eX events with no detected photons are shown in Fig. 12a) and for all eX events in Fig. 12b). The data exhibit a sharp rise at threshold followed by a smooth increase up to a constant high-energy value. This is precisely the energy dependence expected from leptonic pair-production and is in striking contrast with the multi-prong electron data (Fig. 5) which characterizes a charmed hadronic origin.

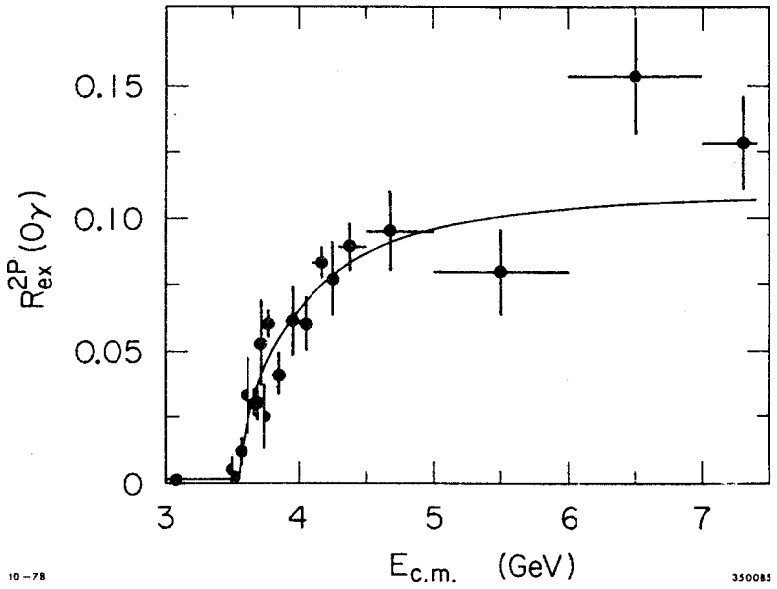

Fig. 12. a) The two-prong electronic cross section, R_{eX}^{2P} for eX events with no detected photons.

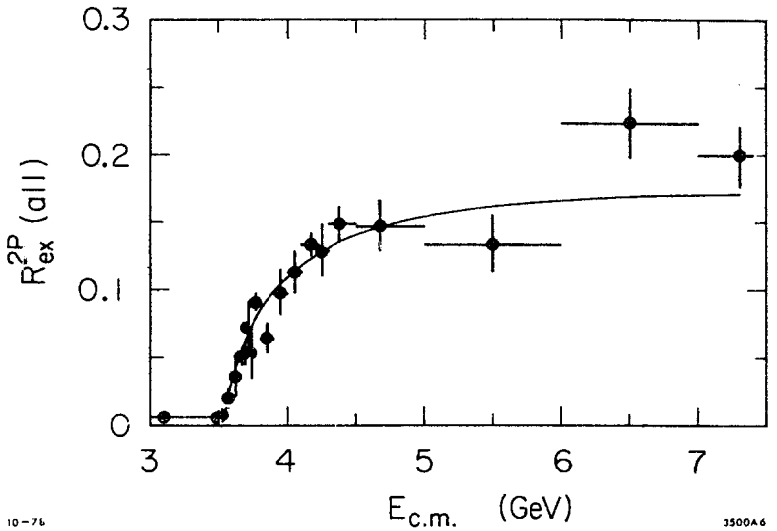

b) The two-prong electronic cross section, R_{ex}^{2P} for all eX events. The fitted curves indicates the cross sections expected from a spin 1/2 τ lepton after accounting for radiative corrections. Both fits have excluded the ψ'' point because of possible charm contamination.

The fitted curves indicate the (radiatively-corrected) cross section expected for a spin 1/2 τ lepton superimposed on a constant background term. The latter predicts a background of (5±3)% due to particle misidentification in agreement with an independent shower counter pulse height study.

The shape of the anomalous two-prong lepton cross-section has been a corner-stone in the argument for the existence of the τ lepton. These data have been statistically limited until the past year and, given the proximity of the charm and two-prong lepton cross sections, the τ was not considered to be completely established. The remaining doubts were eliminated by the observation[13] of eX events below charm threshold ($E_{CM}= 2M_{D^0}=3726.6\pm1.8$ MeV) An expanded view of the threshold behaviour of the eX events (Fig. 13) clearly distinguishes them from charm.

The data of Fig. 13 are sufficient to exclude all τ spin asignments other than J=1/2.[14] The solid line indicates a spin 1/2 fit after accounting for radiative corrections. These have the effect of reducing the annihilation centre-of-mass energy and thereby decreasing the cross-section (to a level which may reach zero for the collisions which suffer large radiative losses.). If these data result from a pair of integer spin particles then they must be produced in a relative p-state since a boson and its anti-particle have the same parity. The resultant gentle increase in cross section at threshold is in contradiction with observation. (An example of a pair of spin 1 particles is indicated by the dashed line.) However the data are well fit by the steep s-wave threshold resulting from half-integer spins. Spins other than J=1/2 are excluded since they lead to divergent high energy behaviour (an example, J=3/2, is illustrated by the dot-dashed line).

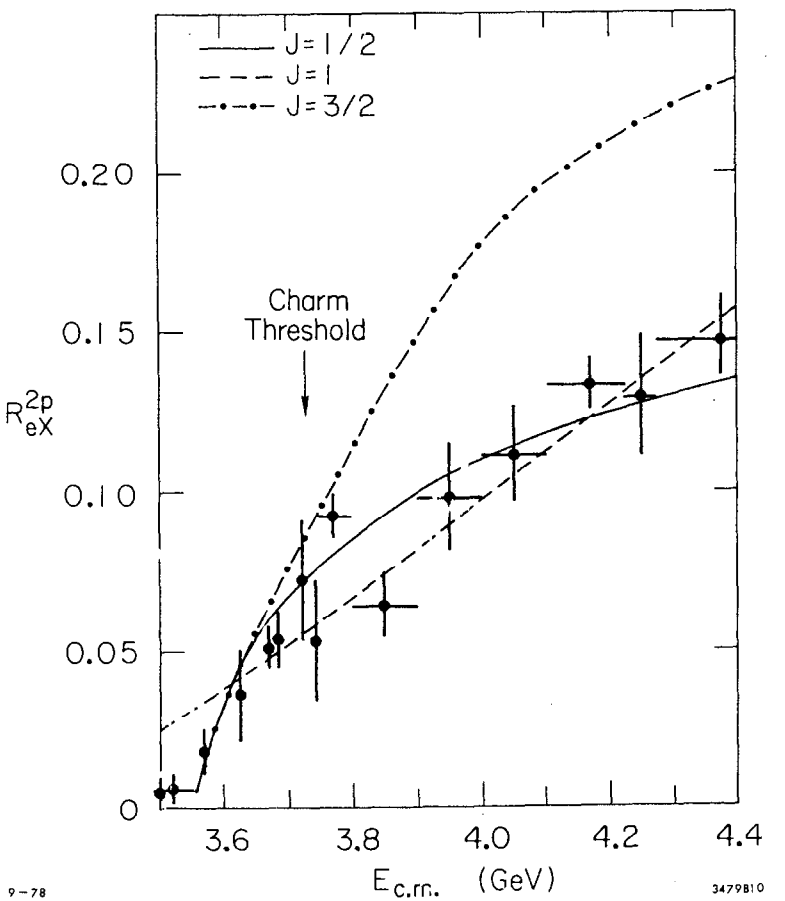

Fig. 13. R_{ex}^{2p} for all eX events with $3.50<E_{CM}<4.40$ GeV. The fitted curves indicate the (radiatively-corrected) threshold behaviour of a pair of particles with spin 1/2 (solid), 1 (dashed) and 3/2 (dot-dashed).

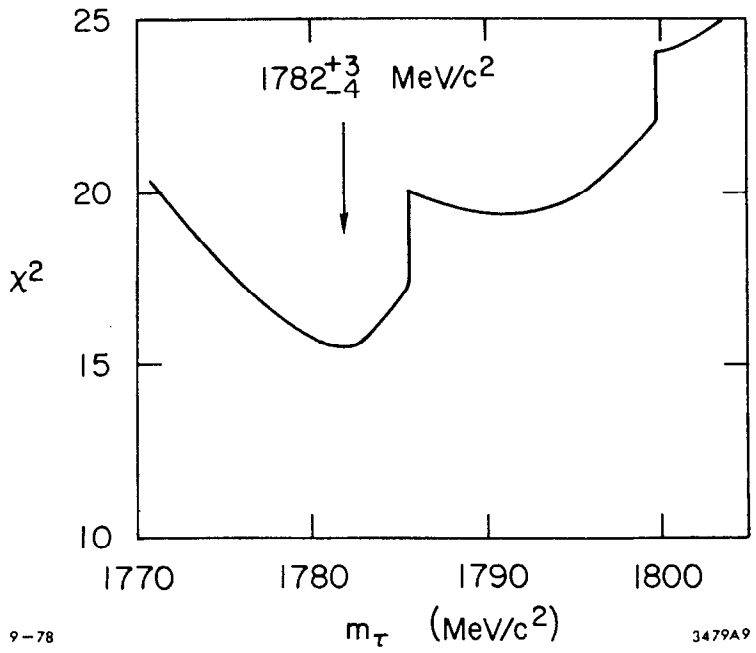

Fig. 14. Total χ^2 of the fit to the data of Fig. 12b) vs. τ mass ($E_{CM}/2$). The fit has 17 degrees-of-freedom.

We have determined the precise threshold energy by fitting a radiatively-corrected spin 1/2 curve and constant background term to the data of Fig. 12b). The χ^2 variation of this fit vs. threshold beam energy (Fig. 14) measures the τ mass as,

$$m_\tau = 1782^{+3}_{-4} \quad \text{MeV}/c^2$$

Although the two-prong electron data is relatively free of charm at all energies the same is certainly not true of the multi-prong electron data (Fig. 5). However there is a brief window between the τ and charm thresholds where we can observe any τ decay with zero charm contamination. The τ cross-section is rather small ($R_{\tau\tau} \lesssim 0.3$) and so the hadronic and two-photon backgrounds are substantial. A small systematic rise in the multi-prong electron production below charm threshold can be seen in Fig. 5. These data were selected automatically and a small improvement in background rejection is possible by manually scanning a computer reconstruction of each event. This has been carried out for events in the range $3.50 < E_{CM} < 3.725$ GeV and the resultant R_e plot (Fig. 15) provides direct evidence for the existence of τ decays into three-or-more charged particles.

B. Branching Ratios

The majority of the τ decay rates can be calculated and so branching-ratio measurements test whether the standard weak current participates in τ decays. The muon decay rate determines $\Gamma(\tau^- \to e^- \bar{\nu}_e \nu_\tau)$ and $\Gamma(\tau^- \to \mu^- \bar{\nu}_\mu \nu_\tau)$ and the pion lifetime measures $\Gamma(\tau^- \to \pi^- \nu_\tau)$. The experimental measurements of $e^+e^- \to n\pi$ (n-even) at $\sqrt{s} < m_\tau$ are related to $\tau^- \to (n\pi)^- \nu_\tau$ (n-even) via CVC. The τ axial-vector decay rates involving odd numbers of pions are less well-known

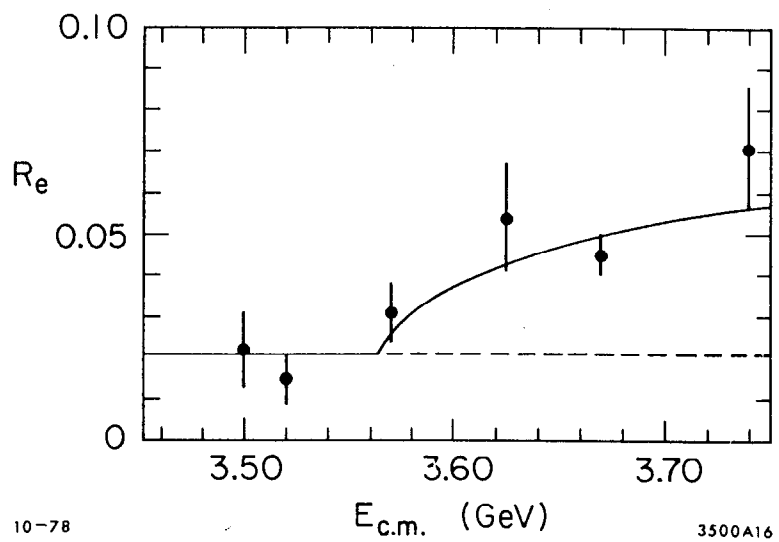

Fig. 15. R_e for the multi-prong electron data below charm threshold. The ψ' point is excluded. (The nearby point was taken below the ψ' at E_{CM}=3.67 GeV.) The fitted curve (χ^2/dof=4.1/4) corresponds to a spin 1/2 τ lepton, of mass 1782 MeV/c^2, superimposed on a constant background term.

but are estimated using Weinbergs sum rules.[16] The small decay rates involving strange particles are related to the multi-pion calculations via $\tan^2\theta_c$. Recent theoretical calculations,[17] are summarized in Table 2 for τ decays into one-charged-particle plus neutrals.

Table 2

τ One-Prong Relative Rates and Branching Ratios

$\tau^- \to \nu_\tau$ +	Relative Rate	Branching Ratio (normalized to b_e = 0.160)
$e^- \bar{\nu}_e$	1.00	0.160
$\mu^- \bar{\nu}_\mu$	0.97	0.155
π^-	0.59	0.094
$\pi^- \pi^o$	1.24	0.198
π^- + $\geq 2\pi^o$	0.27	0.043
K^-	0.03	0.005
$K n \pi$	0.05	0.008
		0.66 (Total)

The leptonic branching ratios are the most precisely measured among τ decays. The branching ratio for $\tau^- \to e^- \bar{\nu}_e \nu_\tau$ (denoted b_e) is provided by the fit in Fig. 12a) which yields $2 b_e b_{x,0\gamma} = 0.105 \pm 0.007$, where $b_{x,0\gamma}$ is the branching ratio for $\tau^- \to \nu_\tau$ + 1 charged particle ($\neq e$) + no detected photons. The value of $b_{x,0\gamma}$ requires theoretical input of the rates, relative to $\tau^- \to e^- \bar{\nu}_e \nu_\tau$, of the decay modes $\mu^- \bar{\nu}_\mu \nu_\tau$, $\pi^- \nu_\tau$ and $\pi^- \pi^o \nu_\tau$. Approximately one-third of the $\pi^- \pi^o$ decays contribute, corresponding to events where both photons escape detection. After accounting for small contributions from decays involving larger pion multiplicities we determine,

$$b_e = 0.160 \pm 0.013$$

The error, which is largely systematic, is rather small since this determination of the cross section is proportional to b_e^2.

The validity of this approach depends on the existence of the three specified decay modes with the correct relative rates. Each are considered to be on solid theoretical ground and consequently the apparent absence of $\tau^- \to \pi^- \nu_\tau$, reported[18] by DASP at the Hamburg Conference last year, led to a variety of new descriptions of the nature of the τ.

The measurement of the branching ratio for $\tau^- \to \pi^- \nu_\tau$ (denoted b_π) clearly became an important goal. However, experimentally it is difficult since not only is the branching ratio low but also muon backgrounds must be removed, and this substantially reduces the data sample.

The first step in our analysis involves the isolation of a clean sample of τ decays by selecting two-prong eX events according to the previous criteria. In addition, the X particle is required to aim within a restricted sensitive area of the muon detector and have sufficient momentum to penetrate (typically 0.7 GeV/c).

There are 54 events which survive the selection criteria, corresponding to a sample of 27,800 $\tau^+\tau^-$ decays in the energy range, $3.57 < E_{CM} < 7.4$ GeV. We summarize these data in Table 3 according to particle composition.

Table 3

Predicted and Observed Event Category of the eX events

Event Category	Predicted Events $\tau^+ \to \bar{\nu}_\tau e^+ \nu_e$, $\tau^- \to \nu_\tau Y$				Observed Events (ee background previously subtracted)
	$Y=\mu^- \bar{\nu}_\mu$	$Y=\pi^-$	$Y=\rho^-, A_1^-, K^-$ etc.	Total	
$e\mu$	14.7	2.0	1.0	17.7	23 (0)
$e\mu+\geq 1\gamma$	0	0	1.0	1.0	2 (0)
$e\pi$	0.8	12.4	6.1	19.3	17.4(0.6)
$e\pi+\geq 1\gamma$	0	0	6.4	6.4	9.5(1.5)

The predicted numbers of events in Table 3 are based on the previous branching ratios (Table 2) and include small additional contributions from multi-prong τ decays (0.2 events) and charm semi-leptonic decays (0.3 events). The experimental data show good agreement with the theoretical expectations. In particular, if the $\pi\nu_\tau$ (and $K\nu_\tau$) decay modes are absent, the predicted signal of $e\pi+0\gamma$ events would be $6.9-0.7\ (K\nu_\tau) = 6.2$ in contrast to 17.4 events observed. The probability for this to be a fluctuation is $\ll 10^{-3}$.

We conclude that the decay $\tau^- \to \pi^- \nu_\tau$ exists and measure its branching ratio, $b_\pi = 0.094\ (17.4-6.9)/12.4$ i.e.

$$b_\pi = 0.080 \pm 0.032 \pm 0.013$$

Similarly we measure, $b_\mu = 0.155\ (23-3.0)/14.7$ i.e.

$$b_\mu = 0.21 \pm 0.05 \pm 0.03$$

The observed μ and π momentum spectra (Figs 16a) and 16b) are consistent with those expected from τ decays and in particular we observe that the pions do not cluster at the low momentum cut, which would suggest large

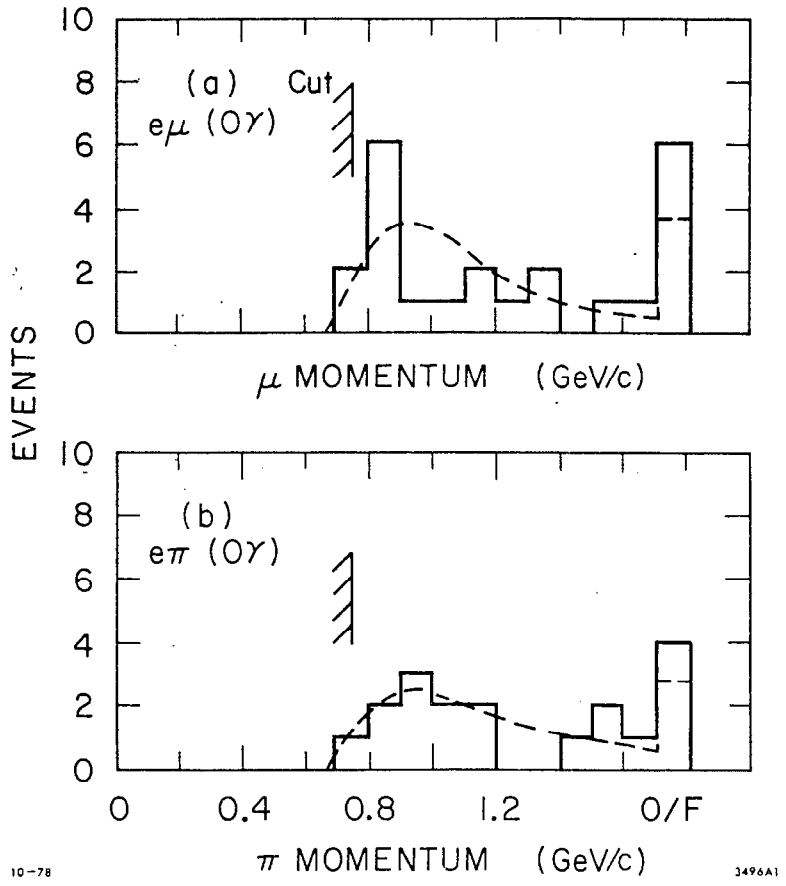

Fig. 16. a) Momentum spectrum of the μ in the eμ(0γ) events.

b) Momentum spectrum of the π in the eπ(0γ) events.

The dashed lines indicate the predicted shapes expected from τ decays. The cut indicated corresponds to the average amount of material a track must penetrate to be identified by the muon detector.

μ or multipion contamination. Both these branching ratio measurements are consistent with the hypothesis that the τ couples to the standard weak current.

We will now consider b_{mp}, the branching ratio for $\tau^- \to \nu_\tau + \geq$ (3 charged particles)$^-$. This has been determined in three independent ways. The fit to the data of Fig. 12b) determines $2b_e\,(1-b_e-b_{mp}) = 0.168 \pm 0.008$ which yields (for $b_e = 0.160$),

$$b_{mp} = 0.32 \pm 0.05$$

The direct observation of multi-prong τ decays (Fig. 15) gives a quantitatively somewhat weaker result, $2b_e\, b_{mp} = 0.092 \pm 0.021$ or,

$$b_{mp} = 0.29 \pm 0.07$$

Finally, we may plot (Fig. 17) the ratio of observed multi-prong to two-prong electron events, $R' = N(e^\pm + \geq 2\text{-prongs})/N(e^\pm + 1\text{ prong})$ above a minimum electron momentum. This ratio falls as the cutoff momentum is raised reflecting the relatively soft electron spectrum resulting from charm decays. Above ~1.1 GeV/c momentum the ratio has the constant value of 1.9 ± 0.2 and indicates a common source for the electrons in both the multiprong and twoprong data. The value of b_{mp} is given by $(b_{mp}\,\varepsilon_{mp})/(b_x\,\varepsilon_x) = 1.9 \pm 0.2$, where $\varepsilon_{mp,x}$ are the appropriate detection efficiencies and $b_x = 1-b_e-b_{mp}$. (Note that the electron detection efficiency cancels and the dependency on b_e is fairly weak.) The result is,

$$b_{mp} = 0.34 \pm 0.05$$

All three determinations agree within errors and are averaged to give the final result,

$$b_{mp} = 0.32 \pm 0.04.$$

At present we have not made detailed studies of the composition of the τ multiprong decays. However it is clear from the uncorrected prong distribution of multiprong electron data taken below charm threshold (Fig. 18a) that the majority involve only three charged particles. The total pion

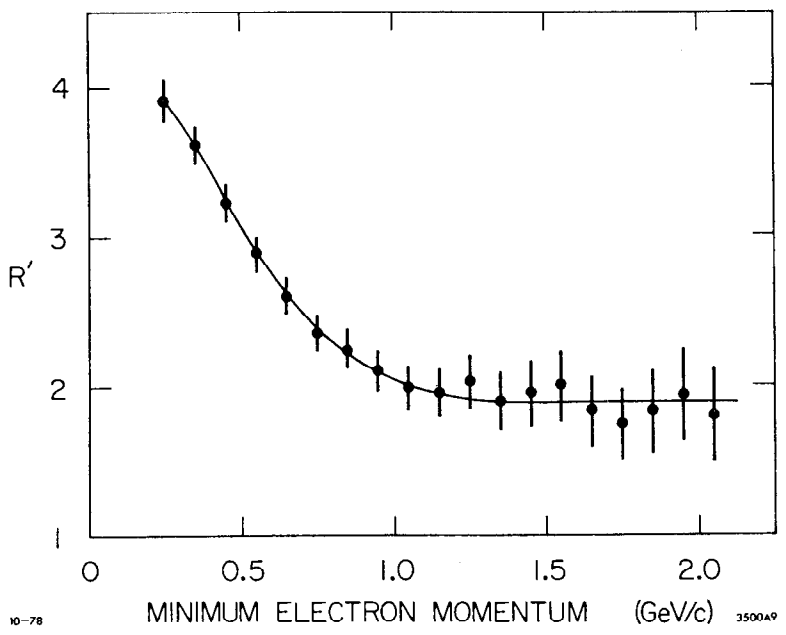

Fig. 17. The ratio, R', of the observed multi-prong electron events to the observed two-prong electron events at electron momenta above the value indicated on the horizontal axis. The curve is hand-drawn.

multiplicity will require a measurement of π^0 production as indicated by the observed photon distribution (Fig. 18b)). (In order to decrease backgrounds these data have the additional requirement that the electron momenta exceed one third of the beam energy).

C. Characteristics of the τ-ν_τ-W Vertex

So far we have seen that the data support the hypothesis that the τ is a spin 1/2 lepton which, according to branching ratio measurements, couples to the conventional intermediate vector boson. It is therefore natural to assume that the e-ν_e vertex in the decay $\tau \to \nu_\tau e\nu_e$ is pure V-A and to use the electron energy spectrum to measure the V, A structure of the τ-ν_τ vertex. The most general coupling is a linear combination of V and A amplitudes but, for a massless ν_τ, the anticipated couplings are pure V-A or V+A which correspond, respectively, to a left-handed ν_τ and a right-handed ν_τ.

The shape of the electron spectrum in the τ rest frame is determined by the one-parameter Michel formula:

$$d\Gamma(x) = G_1 \left(3(1-x) + 2\rho\left(\tfrac{4}{3}x-1\right) + r(x)\right) x^2\, dx$$

where $G_1 = G^2 m_\tau^5/48\pi^3$

and $x = 2p_e/m_\tau$ is the scaled energy of the electron ($0 < x < 1$). A V-A coupling is characterized by a Michel parameter, $\rho = 0.75$ and results in the spectral shape, $d\Gamma(x) \propto (3-2x)x^2 dx$. In the case of V+A, $\rho=0$ and the electron spectrum becomes $d\Gamma(x) \propto (1-x)\, x^2\, dx$. We see that a V-A coupling results in the most probable electron energy at $x=1$ (as familiar in μ decay) whereas a V+A spectrum peaks at $x=2/3$ and is indeed zero at $x=1$. (Physically, the reason for this zero is that a

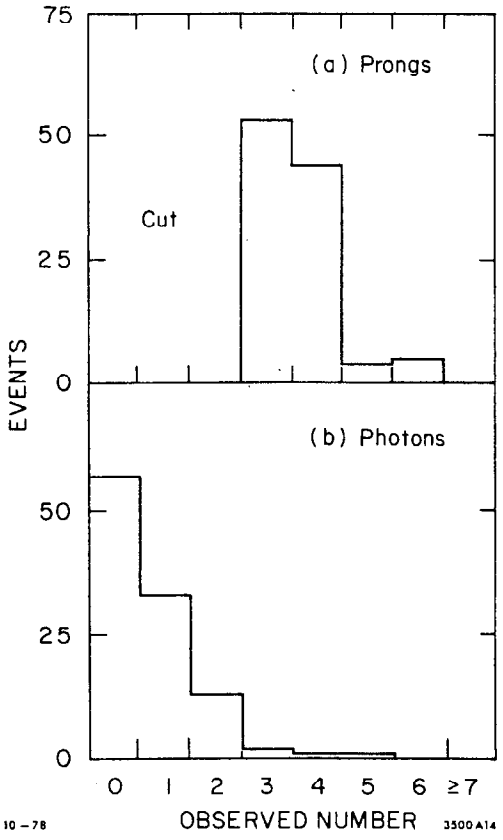

Fig. 18. a) The observed prong distribution of the multiprong electron events in the energy range $3.625 < E_{CM} < 3.72$ GeV (ψ'' excluded).

b) The observed photon distribution in the same energy range.

right-handed ν_τ leads to a total angular momentum 3/2 at x=1.) Other combinations of V and A are characterised by intermediate values of ρ e.g. pure V or pure A, corresponding to equal left-right amplitudes, implies $\rho = 3/8$.

The function r(x) accounts for radiative corrections to the standard spectral formula. Ali and Aydin[19] point out that the corrections can be approximately accommodated into the bare formula by using an effective Michel parameter, ρ_{eff}. They determine a substantial softening of the electron energies e.g. in the range $0.2 \leq x \leq 0.95$, $\rho_{eff} = 0.66$ for V-A and $\rho_{eff} = -0.18$ for V+A.

The experimental electron spectrum (Fig. 19a)) has been obtained from a sample of 621 $eX + \geq 0\gamma$ events in the range $3.17 \leq E_{CM} \leq 7.4$ GeV (ψ'' excluded). The spectrum observed below charm threshold (Fig. 19b)) is statistically weaker but benefits from a reduced Lorentz smearing and consequent higher sensitivity. The events were selected according to the criteria described earlier with a further requirement of at least one associated spark on the outer WSC for each track in order to provide a momentum measurement. In addition events were rejected if $|\vec{P}_e|+|\vec{P}_x|+|\vec{P}_e - \vec{P}_x| > 0.85\ E_{CM}$ in order to remove residual $e^+e^-\gamma$ and grossly mis-measured events. (The latter occur if a spark in the outer WSC is incorrectly assigned to a track in the MWPC.)

We summarize in Table 4 the fit results[20] for pure V-A and V+A and for the ρ parameter giving the minimum χ^2. At this stage we have not explicitly included radiative corrections in the Monte-Carlo-generated spectra and so it is appropriate to compare the observed Michel parameter approximately with $\rho_{eff} \sim 0.64$(V-A) and -0.17 (V+A).

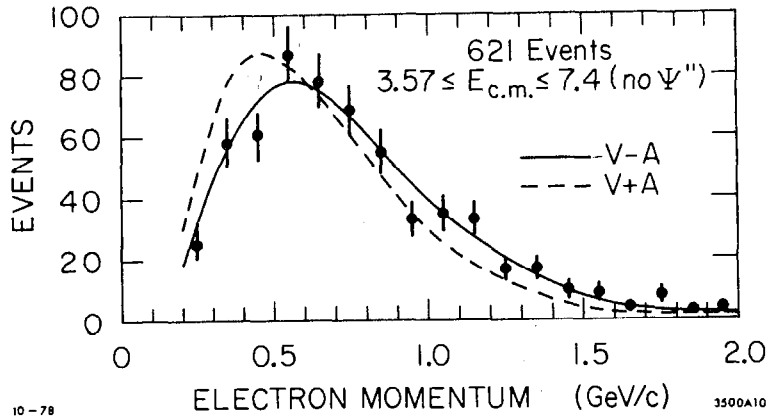

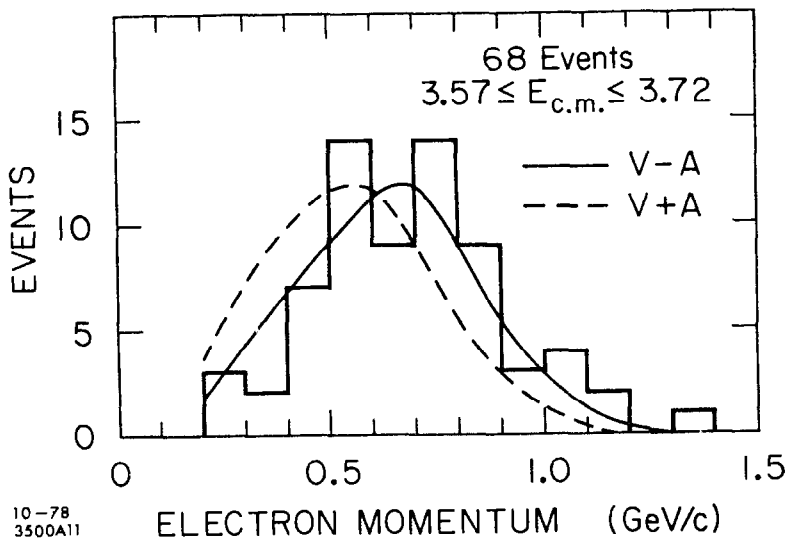

Fig. 19. a) The electron momentum spectrum of the eX events in the range $3.57 \leq E_{CM} \leq 7.4$ GeV after excluding data taken at the ψ".

b) The spectrum observed below charm threshold in the range $3.57 \leq E_{CM} \leq 3.725$ GeV. The solid (dashed) lines are V-A (V+A) fits with zero ν_τ mass and without radiative corrections. Events with $p_e > 1.9$ GeV/c in spectrum b) are excluded from the fit.

Table 4

Summary of the Fits to the Data of Fig. 19

Hypothesis	a) All Data			b) Below Charm Threshold		
	ρ	χ^2	# dof	ρ	χ^2	# dof
V-A	0.75	13.8	17	0.75	8.1	7
V+A	0.0	57.9	17	0.0	21.7	7
Free Fit	$0.86 \pm 0.12 \pm 0.15$	13.0	16	$0.99 \pm 0.26 \pm 0.17$	7.2	6

We conclude that there is good agreement with a V-A coupling whereas V+A is completely excluded and pure V or pure A are disfavoured.

It is interesting to note[21] that these data are the first to exclude the Pati-Salam integer-charged quark[22] interpretation of the anomalous two-prong lepton events. In this model the events arise by decay of a pair of unconfined, pointlike, spin 1/2 quarks through intermediate real vector gluons in the process,

$$e^+e^- \to q^+ q^- \begin{cases} \to \nu_e V^- \to \nu_e e^- \bar{\nu}_e \\ \to \bar{\nu}_e V^+ \to \bar{\nu}_e \begin{cases} \mu^+ \nu_\mu \\ \text{hadrons} \end{cases} \end{cases}$$

The model is excluded on two counts:

i) Below q threshold there should remain a signal of eX events, with an electron spectrum characteristic of two-body decay, arising from direct pair production of vector gluons,

$$e^+e^- \to V^+V^- \to e^+ \nu_e \mu^- \bar{\nu}_\mu$$

This contradicts the observations made at $E_{CM} = 3.50$ and 3.52 GeV (Fig.13).

ii) The observed electron spectra (Fig. 19a) particularly below 0.5 GeV/c, are in complete disagreement with gluon decay for any value of its mass.[21]

The effect of a non-zero ν_τ mass is to soften the electron spectrum. Since the V+A hypothesis is ruled out for any value of m_{ν_τ} we set the ρ parameter at 0.64 (V-A) and 0.86 (minimum χ^2) for this study. From the measured χ^2 variations with non-zero ν_τ masses[23] we determine,

$$m_{\nu_\tau} < 0.25 \text{ GeV/c}^2 \text{ (95\% CL)}$$

To summarize, it appears that the τ^- couples to a neutral object which is consistent with being massless and purely left-handed. However before simply introducing a new neutrino it is important to investigate whether the 'ν_τ' is actually one of the old neutrinos. Experimentally, the assignment $\nu_\tau = \nu_\mu$ has been excluded by neutrino experiments. Unfortunately, since ν_e beams are poor, they have not provided a test of the electron neutrino assignment. The latter possibility is unlikely since the branching ratio for $\tau^- \to e^-\gamma$ is small ($\leq$ 2.6% (90%CL) as measured by the SLAC-LBL group).

The exclusion of the old-neutrino assignment assumes a full-strength τ-ν_τ-W vertex. In a heavy-neutrino model with $m_{\nu_\tau} > m_\tau$ the τ would decay via a small mixing[24] between ν_e, ν_μ and ν_τ consistent with the experimental constaints from the neutrino experiments and μ-e-β universality.

An immediate consequence is that the τ lifetime (τ_o) is longer than that expected in the standard model, which predicts $\tau_o = \tau_\mu (m_\mu/m_\tau)^5 b_e$. For an electronic branching ratio of 0.16 this lifetime is $2.6\ 10^{-13}$ sec which allows a flight path of about 0.1 mm at a beam energy of 3 GeV.

The experimental technique for measuring the lifetime is to determine the apparent origin of the individual prongs in the eX events. In order to increase the sensitivity, the following additional cuts are imposed. Only data above E_{CM}=6 GeV are considered and both tracks must be well-measured geometrically ($\geq$ 5 hits in the MWPC and at least one WSC spark in the ϕ and θ views) and have a minimum momentum of 300 MeV/c. Events are selected containing a high-energy prong (P > 1.35 GeV/c) and another track making a coplanarity angle between 60^o and 140^o. The high-energy prong presumably results from a forward decay of one τ and can therefore define the direction of the second τ. The apparent projected flight path of the second τ is determined by the distance of closest approach of the second prong from the beam centre. This technique has the merit of a known τ flight direction and, as a result of the angular cuts, the maximum sensitivity to a finite flight path.

The 35 events which survive these criteria do not display a systematic displacement away from the beam centre (Fig. 20b)). (The mean (μ) of the distribution is μ=0.025±0.19 mm). As a check of the procedure, the same analysis of multi-prong hadronic events (Fig. 20a)) also produced a centred distribution. (The latter check is really only meaningful in the absence of null result for the τ.) From Monte-Carlo studies we determine that a true $c\tau$ value of 1 mm leads to projected flight distance of 0.37 mm integrated over the E_{CM} range. We thereby determine the τ lifetime limit,

$$\tau_o < 2.8\ \ 10^{-12} \text{ sec (95\% CL)}$$

The heavy τ-neutrino model assumes that the ν_e-e and ν_μ-μ couplings are reduced by factors $(1-\epsilon_e^2)$ and $(1-\epsilon_\mu^2)$ due to a small coupling between the τ and the old neutrinos. The upper limit on the τ lifetime provides a

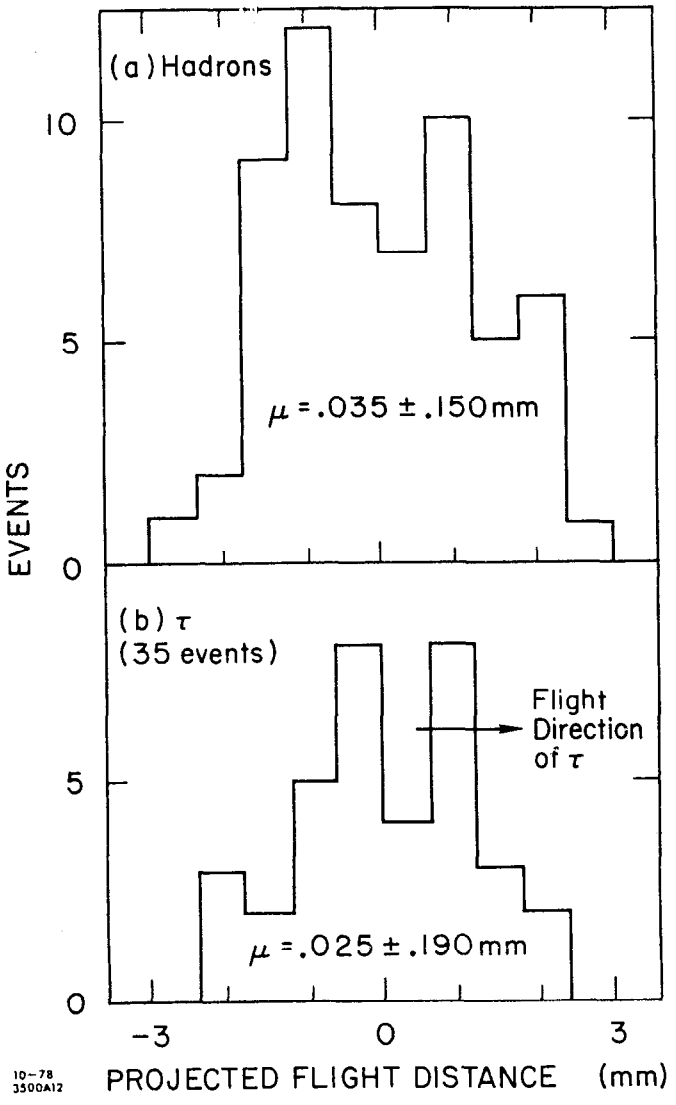

Fig. 20. The projected flight distances using a) a control sample of hadronic events and b) eX events. A measurable τ flight path would lead to a shift in the mean (μ) of the lower distribution in the positive direction.

lower bound on the coupling strength to ν_e and ν_μ given by,

$$\tau_o = \frac{2.6\ 10^{-13}\ \text{sec}}{\varepsilon_e^2 + \varepsilon_\mu^2}$$

$$\text{i.e.} \quad \varepsilon_e^2 + \varepsilon_\mu^2 > 0.09$$

The tight experimental limits on μ-e-β universality place upper bounds on the mixing amplitudes For example, the ratio of the coupling strengths (G´),

$$\frac{G'(K_{e3}) + G'(0^{14}\ \beta\ \text{decay})}{G'(\mu\ \text{decay})} = 1.003 \pm 0.004$$

This comparison removes the Cabibbo angle and indicates,

$$\varepsilon_\mu^2 = 0.003 \pm 0.004$$

In addition,

$$\frac{\Gamma(\pi \to e\nu)}{\Gamma(\pi \to \mu\nu)} = \text{theory} \times (1.03 \pm 0.02)$$

$$\text{i.e.} \quad \varepsilon_\mu^2 - \varepsilon_e^2 = 0.03 \pm 0.02$$

The combination of these two results measures,

$$\varepsilon_\mu^2 = 0.003 \pm 0.004 \text{ and } \varepsilon_e^2 = -0.027 \pm 0.02$$

Therefore the total 'missing' coupling strength is

$$\varepsilon_e^2 + \varepsilon_\mu^2 = -0.024 \pm 0.02$$

We observe this is in contradiction with the lower bound provided by the τ lifetime measurement and hence the heavy τ neutrino possibility is excluded.

In conclusion, there is now a very solid case for the existence of the third charged lepton, τ, with all properties compatible with a coupling to its own massless neutrino and the standard intermediate vector boson. The τ is indeed ready to receive that ultimate accolade, 'ready for the text-books'.

Acknowledgements: I would like to thank my colleagues in the DELCO collaboration for their most enjoyable and informative company. In addition I acknowledge the invaluable services of the Experimental Facilities Division, SPEAR Operations Group and SLAC Computing Center.

References

1) The members of the DELCO collaboration are:
W. Bacino, T. Ferguson, L. Nodulman, W. Slater, H. K. Ticho, University of California, Los Angeles, California 90024, A. Diamant-Berger, G. J. Donaldson, M. Duro, A. Hall, G. M. Irwin, J. Kirkby, F. S. Merritt, S. G. Wojcicki, Stanford Linear Accelerator Center and Physics Department, Stanford University, Stanford, California 94305, R. Burns, P. Condon, P. Cowell, University of California, Irvine, California 92664, J. Kirz, State University of New York, Stony Brook, N.Y. 11794.

2) P. Rapidis et al., Phys. Rev. Lett. 39, 526 (1977).
W. Bacino et al., Phys. Rev. Lett. 40, 671 (1978).

3) Wherever two errors are quoted the first is statistical and the second is systematic.

4) G. Feldman. Raporteurs talk at the XIX International Conference on High Energy Physics, Tokyo, Japan (August 1978).

5) K. Gottfreid. Proceedings of the International Conference on Lepton and Photon Interactions at High Energies, (August 1977), edited by F. Gutbrod and published by DESY, Hamburg, Germany.

6) A. De Rujula and R. Jaffe, Proceedings of the Conference on Experimental Meson Spectroscopy, Northeastern University, Boston (April 1977).

7) C. Baltay, Proceedings of the International Conference on Neutrino Physics and Neutrino Astrophysics, Purdue University, (April 1978).

8) M. K. Gaillard, B. W. Lee and J. L. Rosner, Rev. Mod. Phys. 47, 277 (1975).

9) There has been extensive discussion of D semi-leptonic decays in the literature. The following is a partial list from which further references may be derived. J. Ellis, M.K. Gaillard and D.V. Nanopoulos, Nucl. Phys. B100, 313 (1975), A. Ali and T. C. Yang, Phys. Lett. 65B 275 (1976), I. Hinchliffe and C. M. Llewellyn-Smith, Nuc. Phys. B114 45 (1976), V. Barger, T. Gottschalk and R. Phillips, Phys. Rev. D16, 746 (1977), W. Wilson, Phys. Rev. D16, 742, F. Bletzacker, M. T. Nieh and A. Soni, Phys. Rev. D16, 732 (1977), D. Fabirov and B. Stech, Nucl. Phys. B133, 315 (1978).

10) G. Altorelli et al., Phys. Rev. Lett. 35, 635 (1975) and Nucl. Phys. B88, 285 (1975), Y. I. Wasak, Phys. Rev. Lett. 34, 1407 (1975), M. Einhorn et al., Phys. Rev. D12, 2013 (1975) and Phys. Rev. Lett. 35, 1407 (1975), M. Katuya et al., Nuovo Cimento Lett. 16, 357 (1976).

11) G. Feldman, Proceedings of the SLAC Summer Institute on Particle Physics SLAC-204 (1977).

12) R. L. Kingsley et al., Phys. Rev. D11, 1919 (1975).

13) R. Brandelik et al., Phys. Lett. 73B, 109 (1978).
W. Bacino et al., Phys. Rev. Lett. 41, 13 (1978).
W. Bartel et al., submitted to Phys. Lett.

14) Y. S. Tsai, SLAC-PUB-2105.

15) For clarity we shall only refer to one charged state of the τ.

16) Y.S. Tsai, Phys. Rev. D4, 2821 (1971),
H. B. Thacker and J. J. Sakurai, Phys. Lett. 36B, 103 (1971).

17) F. J. Gilman and D. H. Miller, Phys. Rev. D17, 1846 (1978),
N. Kawamoto and A. I. Sanda, DESY 78/14 (1978).

18) S. Yamada, Proceedings of the International Conference on Lepton and Photon Interactions at High Energies, (August 1977), edited by F. Gutbrod and published by DESY, Hamburg, Germany.

19) A. Ali and Z. Z. Aydin, Nuov. Cim. 43A, 270 (1978).

20) These measurements possess rather large systematic errors since, at present, the Monte-Carlo-generated spectra do not include radiative corrections or a detailed accounting of momentum measurement-error tails.

21) A. W. Ball and C. D. Froggatt, Glasgow University preprint 78-0953 (1978).

22) J. C. Pati and A. Salam, Proceedings of the 1976 Aachen Neutrino Conference, edited by H. Faissner et al.

23) We thank Y. S. Tsai for providing the analytic expressions for $m_{\nu_\tau} \neq 0$.

24) N. Cabibbo, XV Ettore Majorna School for Subnuclear Physics, Erice (1977), C. W. Kim, Johns Hopkins preprint HET-7804 (1978).

MULTIMUON PRODUCTION BY HIGH ENERGY NEUTRINOS AND ANTINEUTRINOS

by

M. G. D. Gilchriese
Department of Physics
University of Pennsylvania
Philadelphia, Pa. 19104

Abstract

Results on multimuon production by neutrinos and antineutrinos are presented. Opposite sign dimuon rates have been determined and distributions are compared with a model of charm production. We present evidence for a prompt signal for $\mu^-\mu^-$ events seen in neutrino interactions. Preliminary results on a new sample of trimuon events will be presented and a tetramuon candidate is described.

Talk presented at the SLAC Summer Institute on Particle Physics, July 1978

I. Introduction

The observation of opposite sign dimuon events in neutrino interactions was one of the first indications of the production of new hadrons.[1] The first observations have been confirmed by later experiments[2] and the new hadrons are now known to be charmed particles. The observation of same sign dimuons and subsequently of trimuon[3] and tetralepton events[4] also may provide information about or set limits to the production of new heavy quark states or heavy leptons.[5] It is therefore interesting to study these rare processes and compare the different rates and distributions.

In this paper we first discuss opposite sign dimuon production by neutrinos and antineutrinos and use the measured rates to extract the fraction of strange quark sea in the nucleon. Distributions are also compared with a charm model to obtain some information about charm particle production dynamics and to set approximate limits to the amount of non-charm signal in the $\mu^-\mu^+$ data. We also present evidence for the production of prompt $\mu^-\mu^-$ events by neutrinos and discuss $\mu^+\mu^+$ production by antineutrinos. Preliminary results on a new sample of trimuon events are given and a new tetramuon candidate will be described.

II. Beams and Detector

The data discussed here were obtained in four runs in the Quadrupole Triplet (QT) and Bare Target Sign Selected ν and $\bar{\nu}$ beams (BTSSν and BTSS$\bar{\nu}$) at Fermilab. In the QT beam the pions and kaons produced by the 400 GeV proton beam are focussed by a triplet of quadrupoles but not charge selected before decay.[6] The result is a beam with high mean energy but substantial $\bar{\nu}$ event content (16%). The BTSS beams employ a "dog-leg" arrangement to select the charge of the pion or kaon and thereby reduce the wrong sign background.[7] Beam fluxes are given in Fig. 1.

The E-310 detector is shown in Fig. 2. There are three separate targets of different densities; a three segment target of iron (250 tons); twelve modules of liquid scintillator calorimeter (50 tons); and an iron plate-scintillator calorimeter (120 tons). Wide gap optical spark chambers are interspersed between calorimeter modules in both the liquid and iron plate calorimeters.

Following the three targets is a muon spectrometer composed of three 7.3 m diameter, .61 m thick iron toroidal magnets and four 3.7 m diameter, 1.2 m thick toroids. Wide gap optical spark chambers located between each toroid provide the means to track muons. Scintillation counter hodoscopes are located in the first two gaps of both the large and small toroid spectrometers.

The energy response and resolution of the liquid and iron-plate calorimeters has been measured between 10 and 100 GeV. The liquid (iron) calorimeter resolution varies between 7-12% (15-23%). Muon beams of known momentum were used to calibrate the muon spectrometer with a resultant error of $\pm$ 3% on the absolute momentum calibration.

The primary emphasis of the experiment was to detect multimuon events. Under normal conditions, the high neutrino flux in either the QT or BTSS beams would result in multiple charged current interactions in our detector during the 2 ms beam spill. Since the spark chambers could obviously be fired only once per spill, triggering on each charged current event would cause a large dead-time resulting in the loss of the rare multimuon events. The single

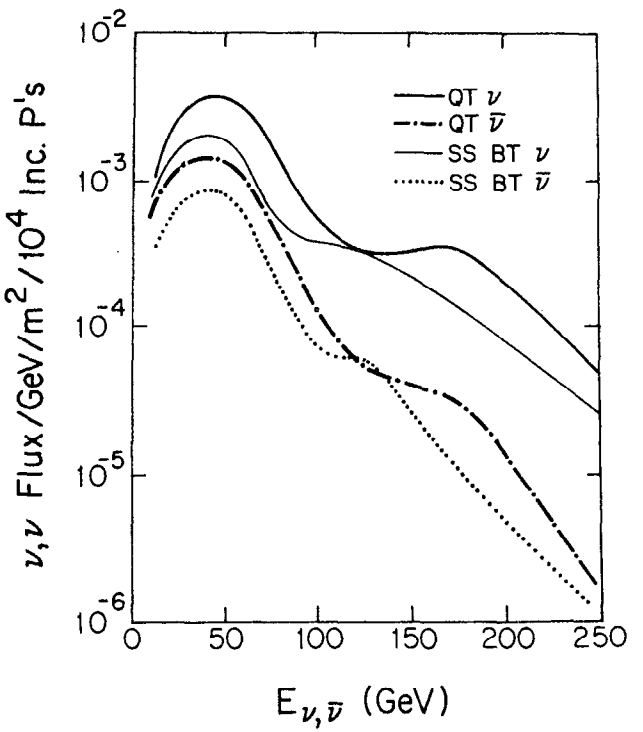

Fig. 1. Neutrino and antineutrino fluxes for the Quadrupole Triplet and Bare Target Sign Selected beams.

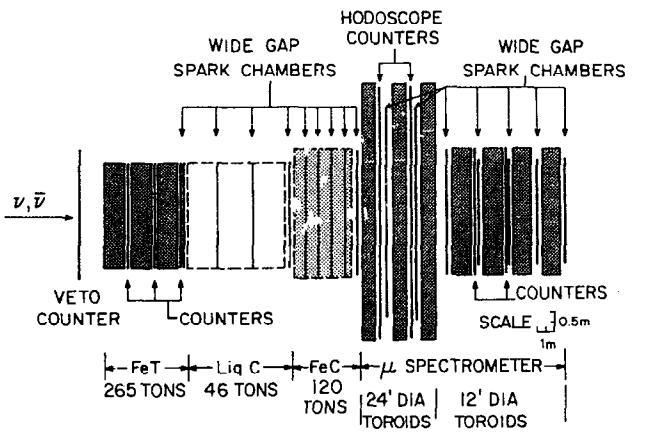

Fig. 2. The E-310 detector.

muon triggers were, therefore, prescaled by different factors (2-32) for each of the three targets.

The counter hodoscopes in the gaps of the 7.3 m toroids, in coincidence with energy deposited in the calorimeters or with the counters in the iron target, generated the primary multimuon trigger. An additional trigger was formed by requiring a 1.5x minimum ionizing pulse height in a majority of the liquid calorimeter modules together with one penetrating muon.

The extent of our multimuon data sample is given in Table 1. The data obtained during the first QT run (QT I) and the BTSSν ($\bar{\nu}$) runs have been completely analyzed. Preliminary results will be reported here on trimuons and a small sample of energetic dimuons obtained during the second QT run (QT II).

III. Opposite Sign Dimuons

We report here on 199 $\mu^-\mu^+$ events obtained in the QT I and BTSSν runs and 49 $\mu^+\mu^-$ events from the BTSS$\bar{\nu}$ run. The distributions and rates of the dimuons have been compared with calculations based on the standard model of charm in order to more fully understand the dynamics of charm production.[8] In the comparison, the effects of geometrical acceptance, counter and chamber efficiencies and the background from pion and kaon decay have been taken into account. The fraction of dimuons arising from π and K decay ($\sim$25%) was calculated by a Monte Carlo program based on measured distributions of pions and kaons produced in neutrino (or antineutrino) interactions.[9] The calculations were consistent with our measurement of the decay fraction using different density targets.

E-310 Data Sample

Beam	POT x 10^{18}	Dimuons opp.	Dimuons same	Trimuons (P_μ >2 GeV/c)	Tetramuon (candidates)
QT I	0.8	136	27	5	0
BTSS$\bar{\nu}$	2.5	49	2	0	0
BTSSν	0.4	63	19	3	1
QT II	3.7	$\sim$2000	$\sim$300	41	1

Table 1. Multimuon data sample. The number of dimuon events for QT II is an estimate based on a small sample.

In Fig. 3 the distribution of the momentum asymmetry, $\alpha = (P_- - P_+)/(P_- + P_+)$ is shown for the QT I and BTSS(ν) samples for $P_\mu > 5$ GeV/c. The curves, including charm meson production and π and K decay, show the contributions from ν and $\bar{\nu}$ separately and the sum. The $\bar{\nu}$ contamination in the ν sample is reduced to 4% or less by requiring $\alpha > -0.3$ and similarly the ν in the $\bar{\nu}$ sample to 8% by requiring $\alpha < 0.3$. These cuts have been applied to the distributions described below.

The distributions of X_{vis} and Y_{vis} for ν and $\bar{\nu}$ events are shown in Fig. 4. $\left(X_{vis} = (E_{\mu_1}/M_p)(1 - \cos\theta_{\mu_1})/Y_{vis}\right.$ and $Y_{vis} = (E_{\mu_2} + E_H)/E_{vis}$ where for $\nu(\bar{\nu})$ μ_1 is $\mu^-(\mu^+)$ and μ_2 is $\mu^+(\mu^-).\left.\right)$ In the charm model, neutrinos produce charmed particles from interactions with valence d quarks and sea strange quarks. Antineutrinos will produce charm essentially only from the strange antiquark component of the sea. After correcting for π, K decay the average values of X_{vis} from the ν and $\bar{\nu}$ data are 0.20 ± 0.03 and 0.11 ± 0.03, respectively. As anticipated, the $\bar{\nu}$ sample has a lower average value of X_{vis}, while the ν data is consistent with approximately equal contributions from valence and sea quarks

In Fig. 5 we show the distribution of $Z_+ = P_+/(P_+ + E_H)$ for the neutrino data along with curves assuming two different forms of the charm fragmentation function, F(Z) ($Z = E_D/E_H$). The distribution favors an approximately flat distribution and rejects a distribution falling faster than e^{-3Z} or rising faster than e^Z. The measured $P_\perp$ distribution for the ν sample is shown in Fig. 6 ($P_\perp$ is the component of momentum of the μ^+ perpendicular to the ν-μ scattering plane). The superimposed curve was

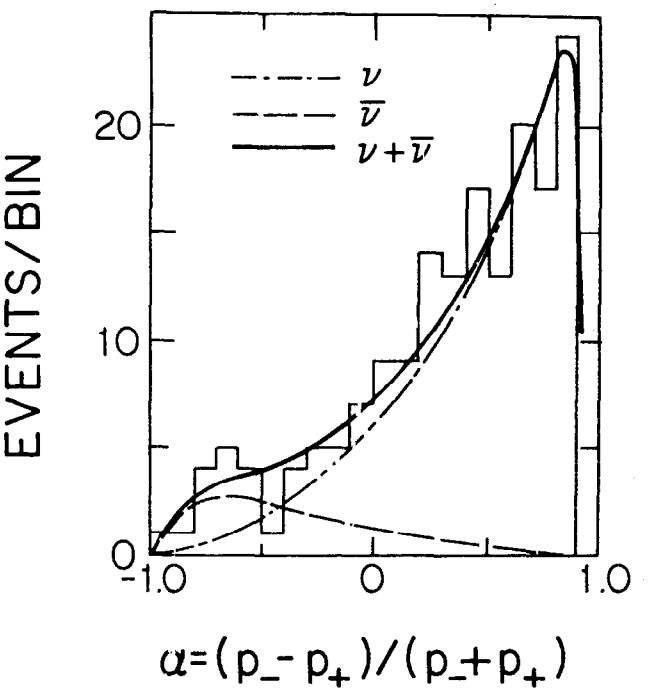

Fig. 3. The momentum asymmetry parameter $\alpha = (P_- - P_+)/(P_- + P_+)$.

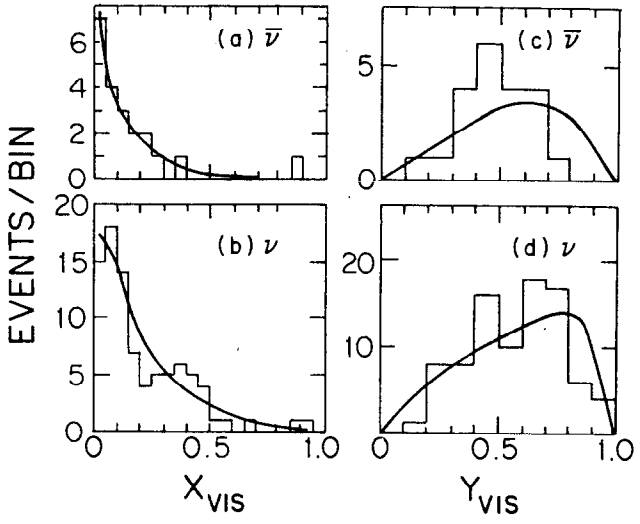

Fig. 4. X_{vis} and Y_{vis} distributions for ν and $\bar{\nu}$ produced dimuons.

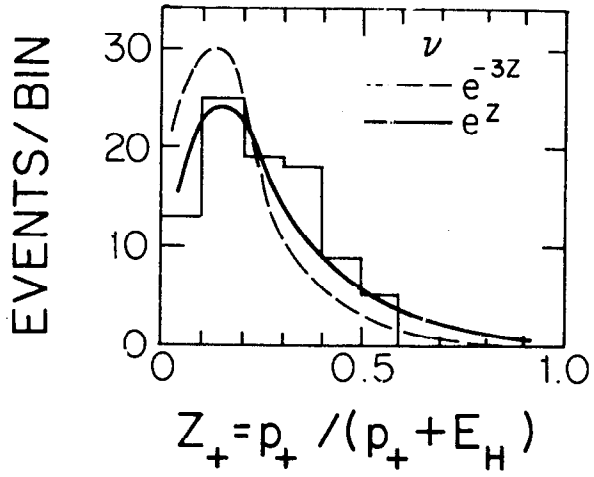

Fig. 5. The distribution of $Z_+ = P_+/(P_+ + E_H)$ for the neutrino data.

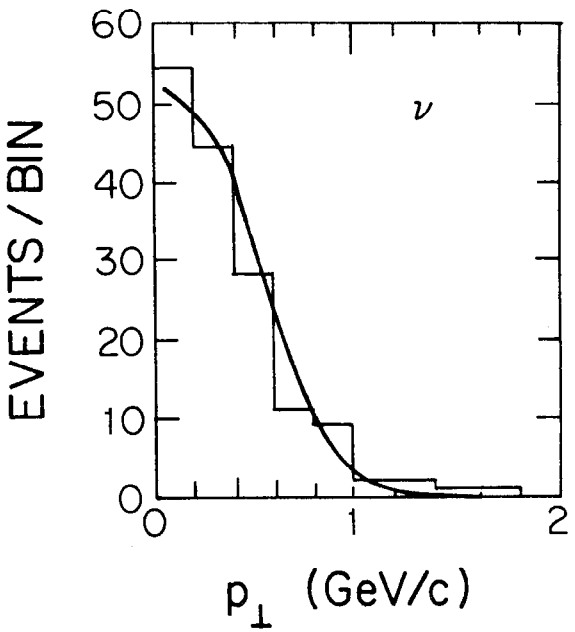

Fig. 6. The transverse momentum out of the ν-μ scattering plane.

obtained with the assumption that D mesons are produced with a $P_\perp$ to the exchanged W direction of the form $dN/dP_\perp^2 \alpha\ e^{-6[P_\perp^2 + M_D^2]^{1/2}}$. The good agreement between Fig. 6 and the charm model calculation suggests that the contribution from non-charm sources, particularly heavy new quarks, is small in the energy range covered by the experiment. A more quantitative statement awaits further data and comparison with specific heavy quark production models.

The energy dependence of the dimuon/single muon ratio is shown in Fig. 7a and 7b for the ν and $\bar{\nu}$ data. The predictions of the charm model calculation are shown with and without a 5 GeV/c minimum momentum requirement.[10] The observed energy dependence arises from the momentum cut. With this cut, above 100 GeV, $R(\mu^-\mu^+)/R(\mu^-)$ is $0.6 \pm 0.13 \times 10^{-2}$ for ν and $R(\mu^+\mu^-)/R(\mu^+)$ is $0.70 \pm 0.25 \times 10^{-2}$ for $\bar{\nu}$.

The fraction of strange quark sea (S or $\bar{S}$) may be extracted from the measured dimuon rates and single muon production. The ratios $\bar{S}/U$ and S/D (U (D) is the fractional momentum carried by the u(d) quarks) may be determined independently from the $\bar{\nu}$ and ν data after correcting for the minimum muon momentum requirement. This correction is sensitive to the Z distribution of charmed particle production.[11] With the assumption of a flat Z distribution, one obtains $\bar{S}/U = 0.076 \pm 0.027$ and $S/D = 0.099 \pm 0.035$ for $E_\nu > 100$ GeV. If one uses the ratio $[\sigma(\mu^+\mu^-)/\sigma(\mu^+)]/[\sigma(\mu^-\mu^+)/\sigma(\mu^-)]$ a value of $\bar{S}/D = 0.066 \pm 0.061$ is obtained and is independent of the dimuon correction factor and hence of the assumed Z distribution.

IV. Same Sign Dimuon Production

Unlike opposite sign dimuons which are now known to arise predominantly, if not completely, from charm, the origin of like sign

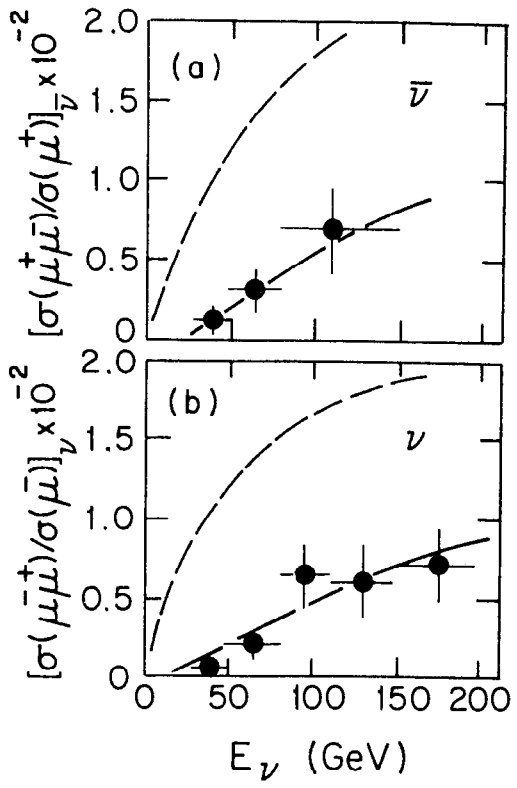

Fig. 7. Energy dependence of the dimuon rate for neutrinos and antineutrinos.

dimuon events is uncertain. The observed rate for such events is small and therefore the contribution from pion and kaon decay in ordinary charged current interactions is a substantial background. We present here an analysis of 49 $\mu^-\mu^-$ events from the QT I and BTSSν runs, 2 $\mu^+\mu^+$ events from the BTSS$\bar{\nu}$ and preliminary results on a small sample of the data from QT II.

It is important to emphasize two features of the E-310 detector. First, the neutrino interactions occur in three targets of different hadronic absorption lengths (λ). The effective absorption lengths for each target were calculated including gaps and end effects. They are: iron target = 31 cm; iron calorimeter = 61 cm; and liquid calorimeter = 120 cm. Second, the 7.3 meter diameter toroids provide a very large acceptance that is independent of muon sign.

The relative rates for $R(\mu^-\mu^-)/R(\mu^-)$ are difficult to determine because of acceptance and trigger differences. The ratio $N(\mu^-\mu^-)/N(\mu^-\mu^+)$, however, is independent of vertex position, triggering, etc. The observed numbers of events (from QT I and BTSSν) from each target are given in Table 2. A cut of 5 GeV/c (10 GeV/c) reduces the number of $\mu^-\mu^-$ events to 38 (18). The ratio $N^{obs}(\mu^-\mu^-)/N^{obs}(\mu^-\mu^+)$ is shown in Figs. 8a and 8b. This ratio may also be written as

$$N^{obs}(\mu^-\mu^-)/N^{obs}(\mu^-\mu^+) = [N^{prompt}(\mu^-\mu^-) + N^{decay}(\mu^-\mu^-)]/[N^{prompt}(\mu^-\mu^+) + N^{decay}(\mu^-\mu^+)]$$

The quantity $N^{decay}(\mu^-\mu^+)$ has been calculated by a Monte Carlo program.[9] The known distributions of pions and kaons produced by ν (or $\bar{\nu}$) have been used as input to the program. The primary pions and kaons are followed up to the fourth reinteraction. At present we estimate a 25% error in the calculation which primarily comes from uncertainties in the input data on neutrino interactions.

TARGET	FIDUCIAL MASS (Tons)	ABS. LENGTH (cm)	$N^{obs}(\mu^-\mu^+)$		$N^{decay}(\mu^-\mu^+)$		$N^{obs}(\mu^-\mu^-)$		$N^{decay}(\mu^-\mu^-)$	
			$p_\mu>5$ GeV	$p_\mu>10$ GeV	$p_\mu>5$ GeV	$p_\mu>10$ GeV	$p_\mu>5$ GeV	$p_\mu>10$ GeV	$p_\mu>5$ GeV	$p_\mu>10$ GeV
IRON (FeT)	198	31	75	50	11.7	3.1	12	8	8.1	1.9
IRON CAL. (FeC)	42	61	42	23	11.1	2.3	10	4	7.8	1.8
LIQ. CAL. (LiqC)	36	120	56	32	23.5	6.9	16	6	16.3	3.8
TOTAL			173	105	46.3	12.3	38	18	32.2	7.5

Table 2. Fiducial masses, absorption lengths and numbers of observed dimuon events in the three targets. Also shown are the calculated numbers of dimuon events from pion and kaon decays.

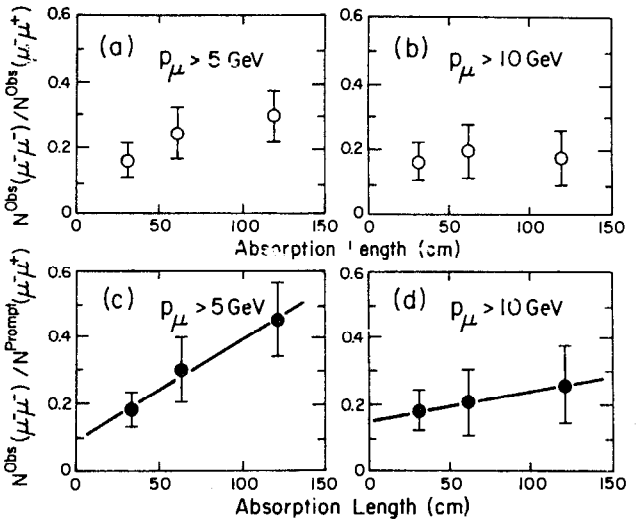

Fig. 8. Ratios of $\mu^-\mu^-$ events/$\mu^-\mu^+$ events before [(a), (b)] and after [(c), (d)] correcting the $\mu^-\mu^+$ events for π, K decay.

For $P_\mu > 10$ GeV/c, the fraction of $\mu^-\mu^+$ from decay is 6-22%, depending upon the target (column labelled $N^{decay}(\mu^-\mu^+)$ in Table 2). After this subtraction, the ratio $N^{obs}(\mu^-\mu^-)/N^{prompt}(\mu^-\mu^+)$ should depend linearly on λ and a finite intercept at $\lambda = 0$ would indicate a prompt source. This ratio is shown in Figs. 8c and 8d and the data are well described by linear fits. Clearly for the 5 GeV/c cut data, a significant fraction of the observed $\mu^-\mu^-$ signal is from decay. The intercepts, however, are finite at $\lambda = 0$ for both the 5 GeV/c (0.09 ± 0.09) and 10 GeV/c (0.15 ± 0.10) cut data. Also the fitted slopes are in reasonable agreement with the values obtained from the numbers $N^{decay}(\mu^-\mu^-)$ shown in Table 2. In particular for the 5 GeV/c cut, the fitted value is $3.0 \pm 1.3 \times 10^{-3}$ cm^{-1} and the predicted value is $4.0 \pm 1.0 \times 10^{-3}$ cm^{-1}. One may then use the Monte Carlo values of $N^{decay}(\mu^-\mu^-)$ to obtain $N^{prompt}(\mu^-\mu^-)$.

Averaging over all three targets, we obtain $N^{prompt}(\mu^-\mu^-)/N^{prompt}(\mu^-\mu^+) = 0.06 \pm 0.05$ for the 5 GeV/c cut and 0.12 ± 0.05 for the 10 GeV/c cut which indicates that a prompt signal may exist. It is somewhat more statistically powerful to observe that we see, for $P_\mu > 10$ GeV/c, 18 events and expect only 7.5 ± 1.9 events.

Some of the properties of the $\mu^-\mu^-$ events are shown in Figs. 9a and 10a. The same distributions for $\mu^-\mu^+$ events (from ν) are shown in Figs. 9b and 10b for comparison. One observes that there is no striking difference between the properties of $\mu^-\mu^+$ and $\mu^-\mu^-$ events. The $\Delta\varphi$ distribution suggests that the $\mu^-\mu^-$ events are predominantly of hadronic origin. The E_{vis} plot indicates a production energy dependence of a nature similar to charm production. Of course the substantial background from decay is included in the plots which would dilute any energy dependence dissimilar from charm.

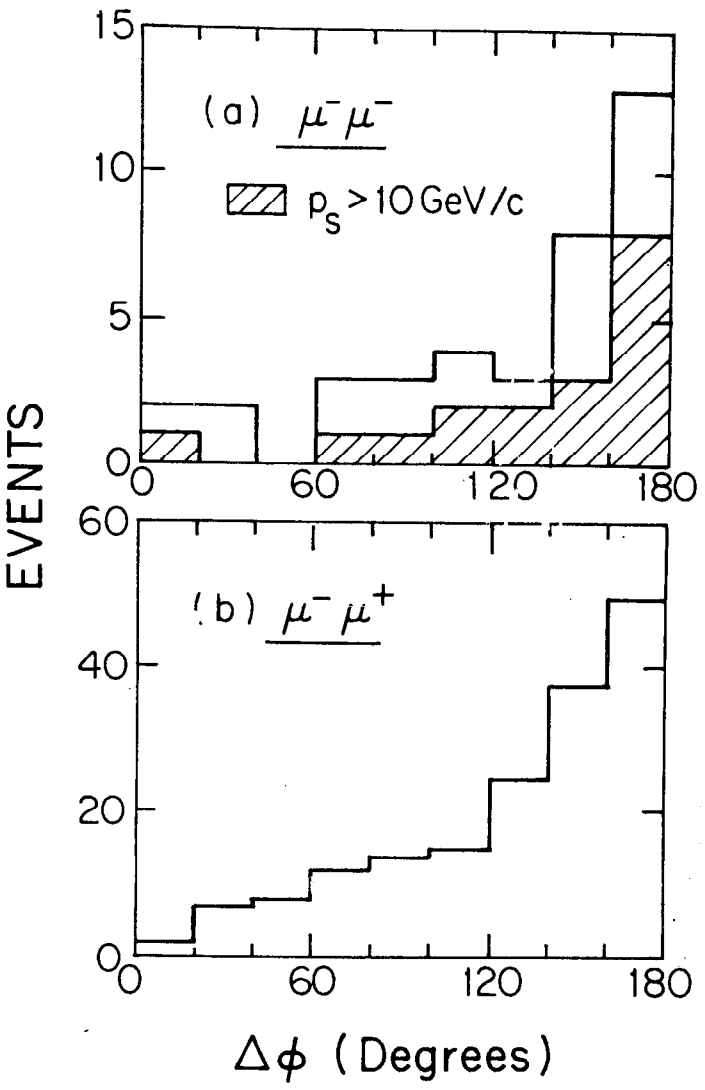

Fig. 9. The $\Delta\varphi$ distribution for (a) $\mu^-\mu^-$ and (b) $\mu^-\mu^+$ events.

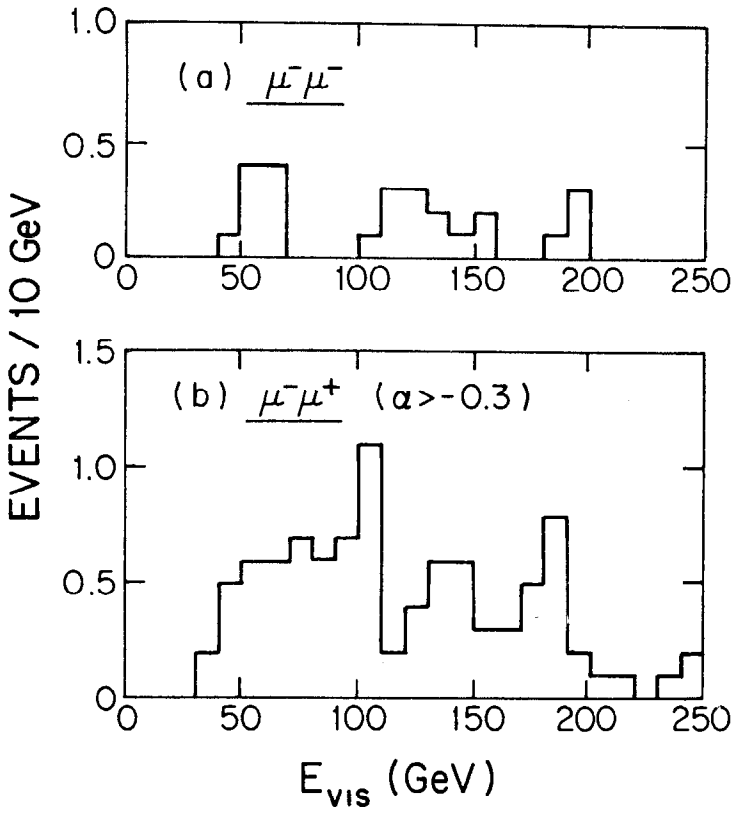

Fig. 10. The visible energy distribution for (a) $\mu^-\mu^-$ and (b) $\mu^-\mu^+$ events.

There are at least two conventional origins for $\mu^-\mu^-$ events. First, the same processes which yield trimuon events ($\mu^-\mu^-\mu^+$) may also result in $\mu^-\mu^-$ events if the μ^+ is lost as a result of detection inefficiency. Second, the production of charm-anticharm pairs and subsequent decay could also result in same sign dimuons. It is presently believed that the majority of trimuon events ($\geq$ 80%) arise from radiative or direct muon pair production. If these virtual photon processes were entirely responsible for the prompt $\mu^-\mu^-$ signal, one would expect $R(\mu^-\mu^-)/R(\mu^-\mu^-\mu^+) < \frac{1}{2}$, particularly for $E_\nu > 100$ GeV where the trimuon acceptance is good. At present, the data do not support this hypothesis as $R(\mu^-\mu^-)$ is 6 ± 3 times the trimuon rate. Current theoretical estimates for the production of charm-anticharm would predict rates lower than the measured value.[12] It is unlikely that the majority of the prompt $\mu^-\mu^-$ events come from production of hadronic flavors beyond charm. We do not observe a rate increase as E_ν increases as one would anticipate for a heavy new quark. Also the $P_\perp$ (out of the ν-μ plane) shown in Fig. 11 is consistent with the decay of particles with masses $\leq$ charm.

At present we have analyzed a small fraction of the dimuon data obtained during the QT II run. In particular we have currently processed events of the type in which both muons penetrate to at least the first spark chamber in the 3.7 meter toroid spectrometer. This yields 170 $\mu^-\mu^+$ and 32 $\mu^-\mu^-$ events with $P_\mu > 10$ GeV/c. Unfortunately this sample is not free of biases as was the old data since the acceptance now depends on muon sign. We have attempted to correct for acceptance by using a charm-like model of $\mu^-\mu^-$ production with the result that a correction factor of 2 is necessary. With this assumption, and after combining with the old QT and BTSS ν

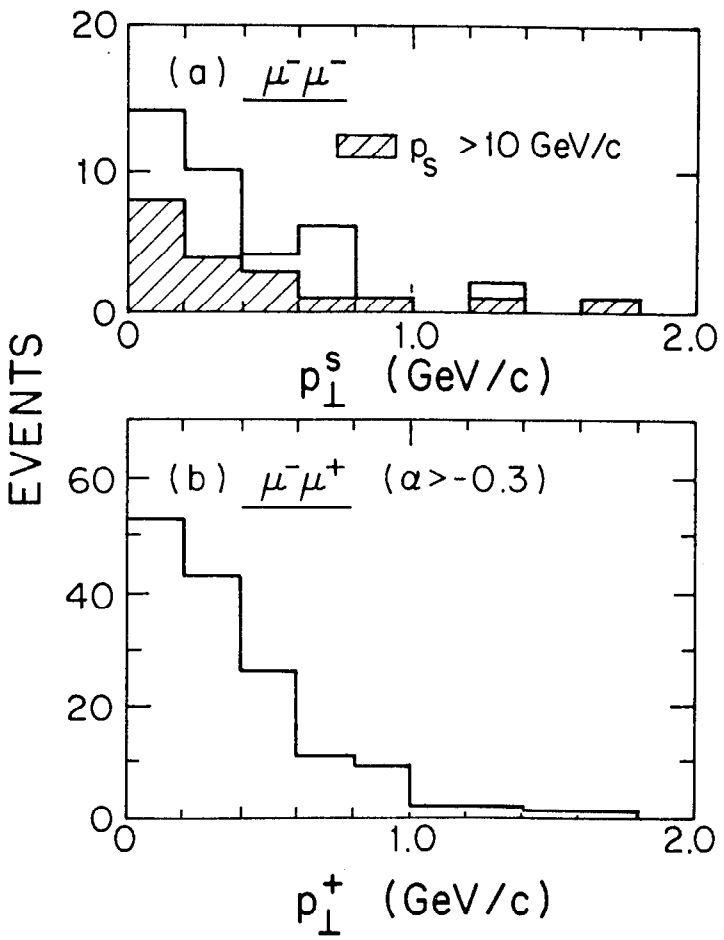

Fig. 11. Transverse momentum of $\mu^-\mu^-$ and $\mu^-\mu^+$ events out of the ν-μ scattering plane.

samples, we find 50 events and expect 28 $\pm$ 7 for all three targets and 20 events and 8 $\pm$ 2 expected for the iron target.

We have observed two $\mu^+\mu^+$ events in the BTSS$\bar{\nu}$ run. Neither of these events satisfies the 5 GeV/c minimum momentum cut and both events are consistent with arising from π or K decay.

V. Trimuon Data Sample and Distributions

The number of trimuon events observed from each target is given in Table 3 for a $P_\mu > 2$ GeV/c cut and for a $P_\mu > 4.5$ GeV/c momentum cut as indicated. There are an additional 15 events with at least one muon below 2 GeV/c that have not been included in the distributions that follow. The column labelled "3Q" corresponds to events where all three charges are known. The two observed - ++ events are completely consistent with the expectations of dimuon production plus pion or kaon decay.[9] For the events labelled "2Q", one of the muon momenta has been determined by range. In all distributions - - + production has been assumed, i.e. - - ? becomes - - + and - + ? becomes - - -.

The distributions of muon momenta are shown in Fig. 12. The leading μ^- (P_μ^L-) is defined by the μ^- with the larger transverse momentum with respect to ν direction. In the plots that follow the leading μ^- is labelled "1", non-leading μ^- "2" and the μ^+ "3". The shaded area in all distributions corresponds to a 4.5 GeV/c momentum cut. One observes in Fig. 12 that the soft μ^- and μ^+ have similar momentum distributions.

Distributions are shown in Fig. 13 for three of the possible muon mass combinations. There is no striking feature. The M_{12} and M_{13} distributions are similar. A plot of visible energy is shown in Fig. 14. We see no events below E_{vis} of 40 GeV and the majority of

	3Q		2Q		
	- - +	- + +	- - ?	- + ?	+ + ?
FeT	10 (9)	1 (1)	5 (2)	7 (1)	0
LiQ	10 (5)	0	7 (0)	4 (0)	0
FeC	6 (4)	1 (0)	0	0	0

Table 3. Number of trimuon events for each target for $P_\mu > 2$ GeV/c. Numbers in parentheses indicate a 4.5 GeV/c cut.

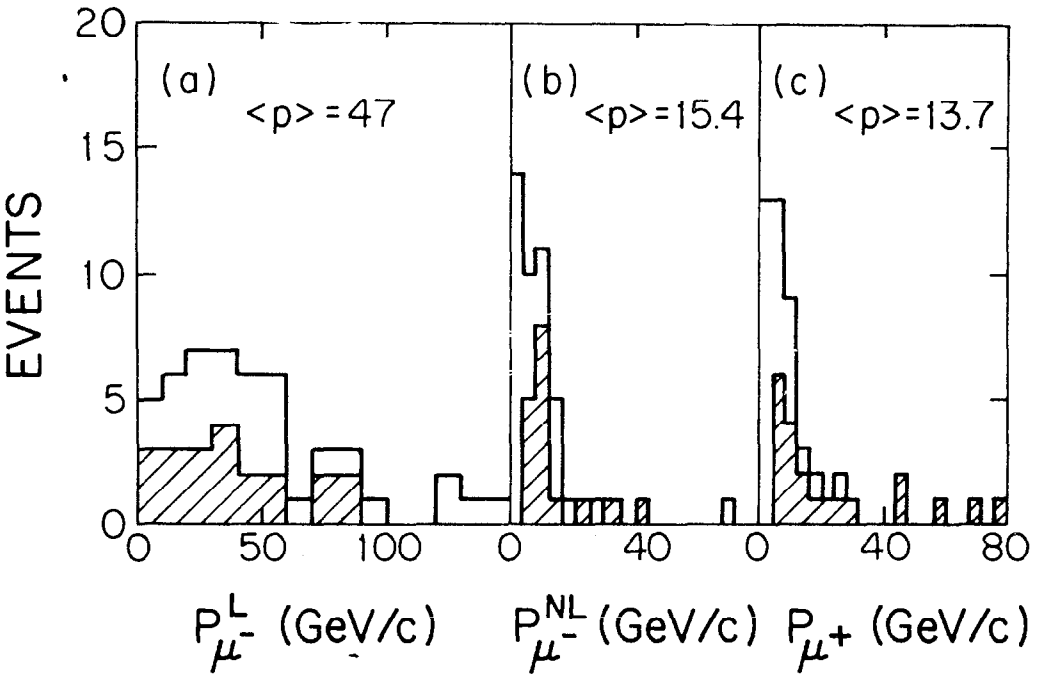

Fig. 12. Muon momentum distributions: (a) leading μ^-; (b) non-leading μ^-; and (c) μ^+. The shaded area corresponds to a 4.5 GeV/c cut for all trimuon distributions.

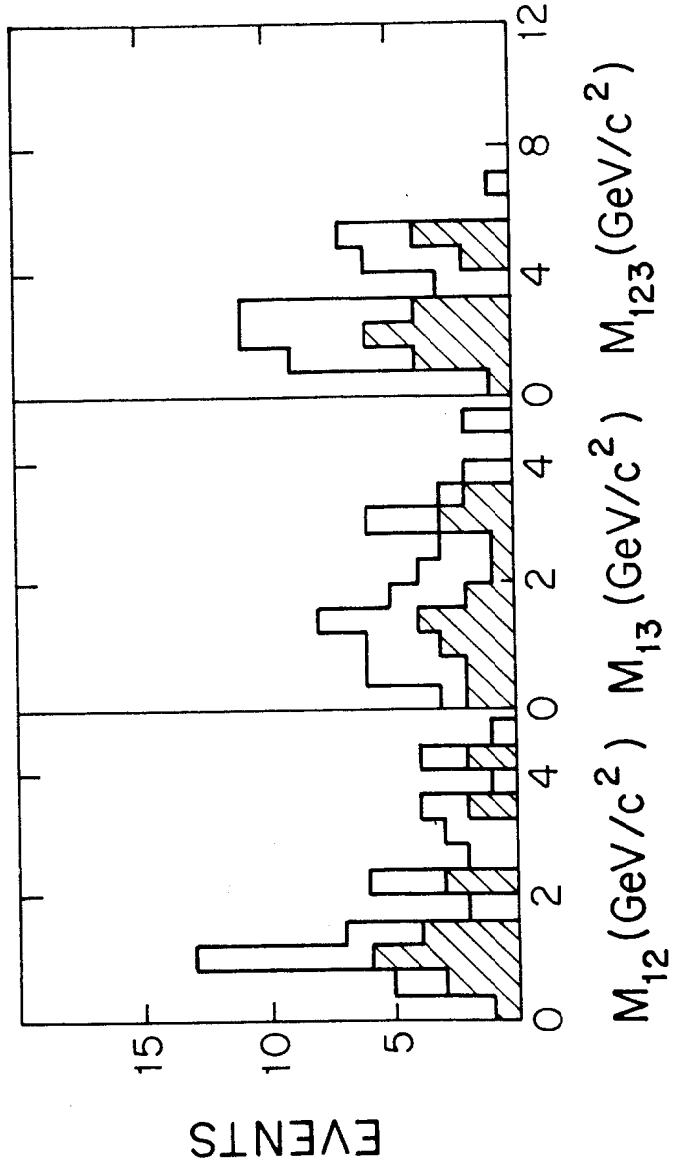

Fig. 13. Various muon pair mass combinations.

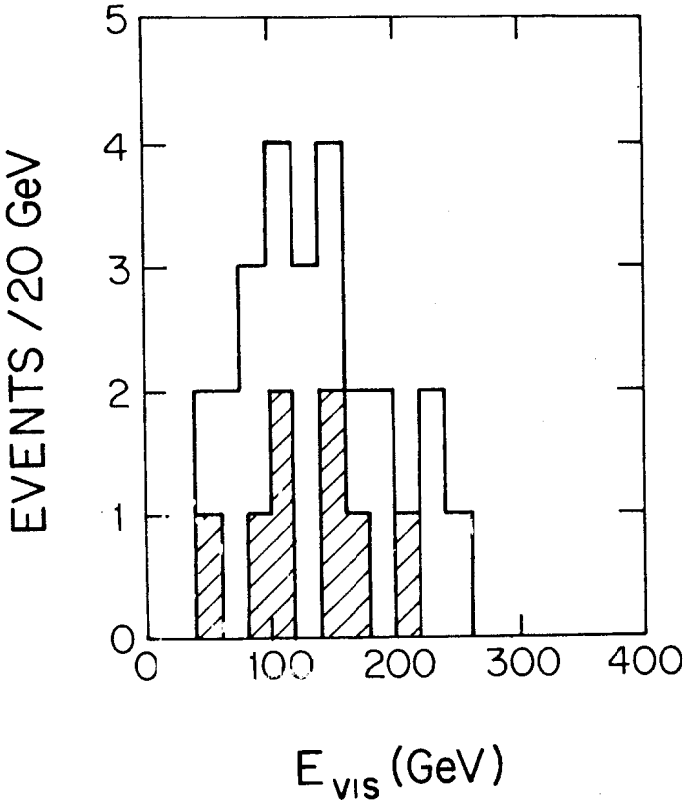

Fig. 14. Visible energy of the trimuon events.

the events have $E_{vis} > 100$ GeV. The fraction of energy that goes into hadrons is shown in Fig. 15. On average, slightly more than one-half the energy in the interaction is contained in the hadronic shower. In Fig. 16 we show a scatter plot of X_{vis} and Y_{vis}. The X_{vis} distribution is typically neutrino like and the Y_{vis} is consistent with being flat. The cutoff in Y_{vis} results from a minimum muon momentum cut.

Azimuthal angular distribution between various muons are shown in Figs. 17 and 18. The angle $\Delta\varphi$ is defined by projecting the muon momenta onto a plane perpendicular to the neutrino direction. The μ^+ tends to be produced opposite to the leading $\mu^-(\Delta\varphi = 180^o)$ and the non-leading μ^- in the same direction as the $\mu^+(\Delta\varphi = 0)$. There are, however, events in which the μ^+ is produced in the same direction as the leading μ^-.

In Fig. 18 we show the $\Delta\varphi$ between the leading μ^- and the vector sum of the other μ^- and μ^+. Most of the μ pairs are produced at the hadron vertex ($\Delta\varphi \approx 180^o$) although there is some contribution at the lepton vertex as well.

The invariant mass of the non-leading μ^- and μ^+ is given in Fig. 19. There is a low mass peak, similar to that observed in hadronic production of muon pairs. Our mass resolution is approximately 250 MeV/c^2 at 1 GeV/c^2 and therefore we are unable to resolve any structure such as ρ production. The same mass combination is plotted in Fig. 20 for "lepton-like" ($\Delta\varphi < 60^o$) and "hadron-like" ($\Delta\varphi > 120^o$). The distributions are similar with the lepton-like possibly being somewhat flatter.

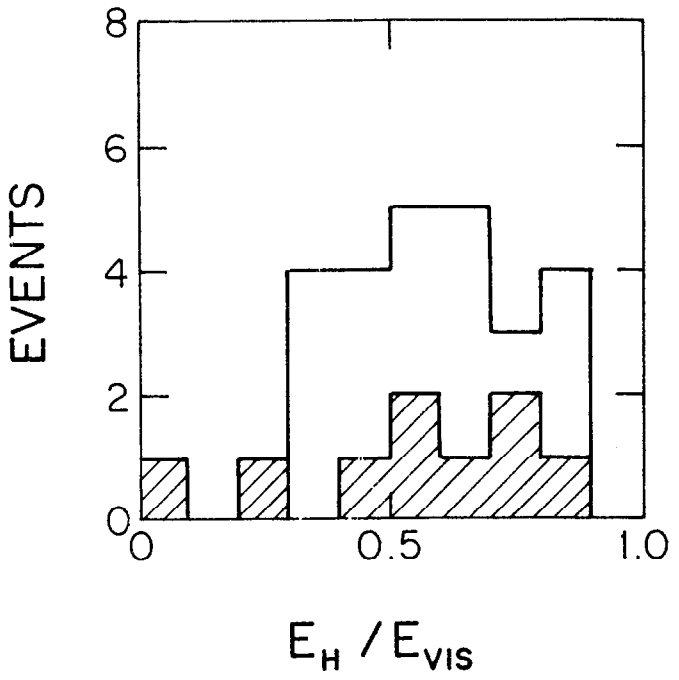

Fig. 15. The fraction of hadronic energy for trimuon events.

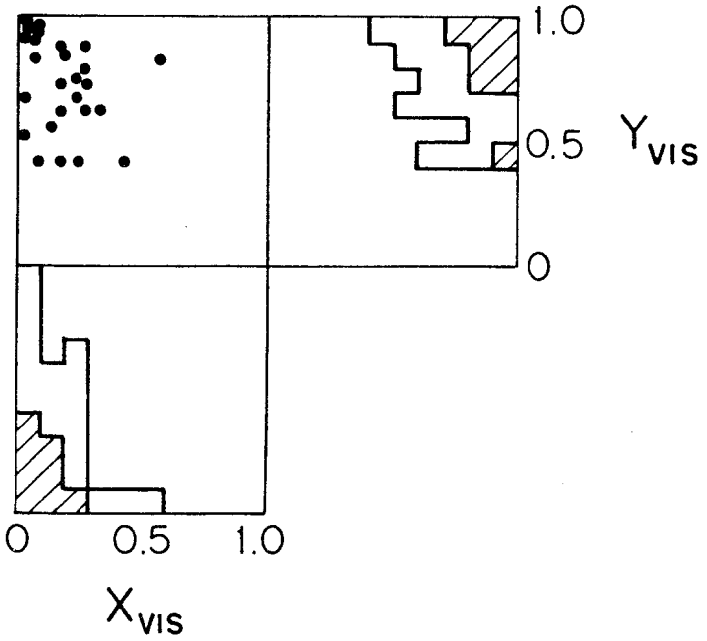

Fig. 16. Scatter plot of X_{vis} and Y_{vis}.

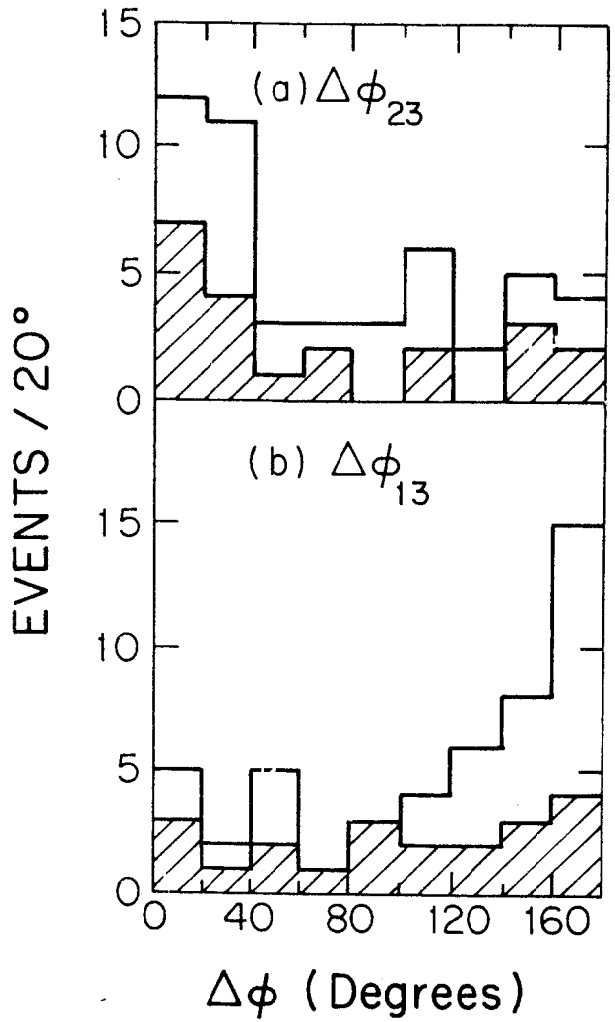

Fig. 17. Azimuthal angular differences between (a) non-leading μ^- and μ^+ and (b) leading μ^- and μ^+.

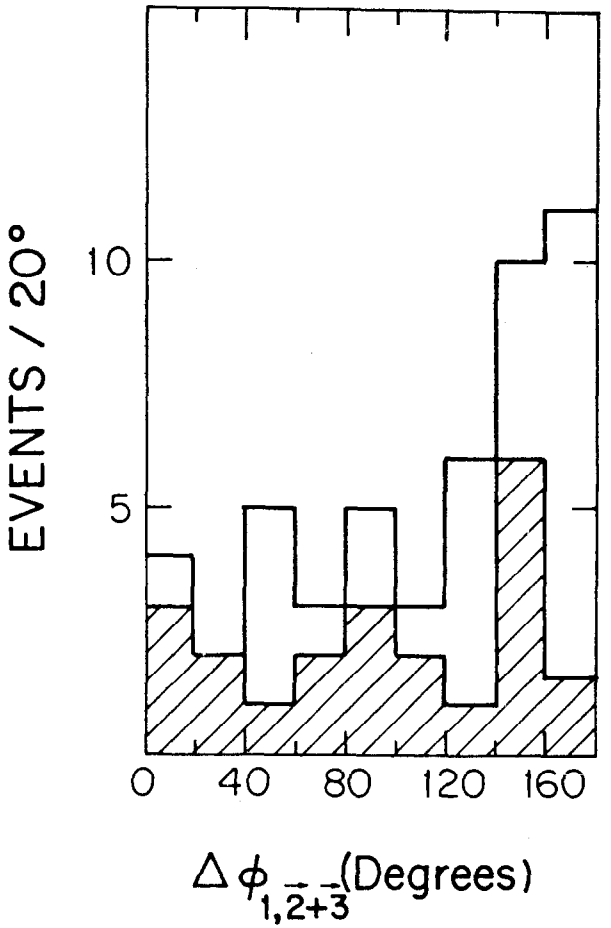

Fig. 18. $\Delta\varphi$ between the leading μ^- and muon pair.

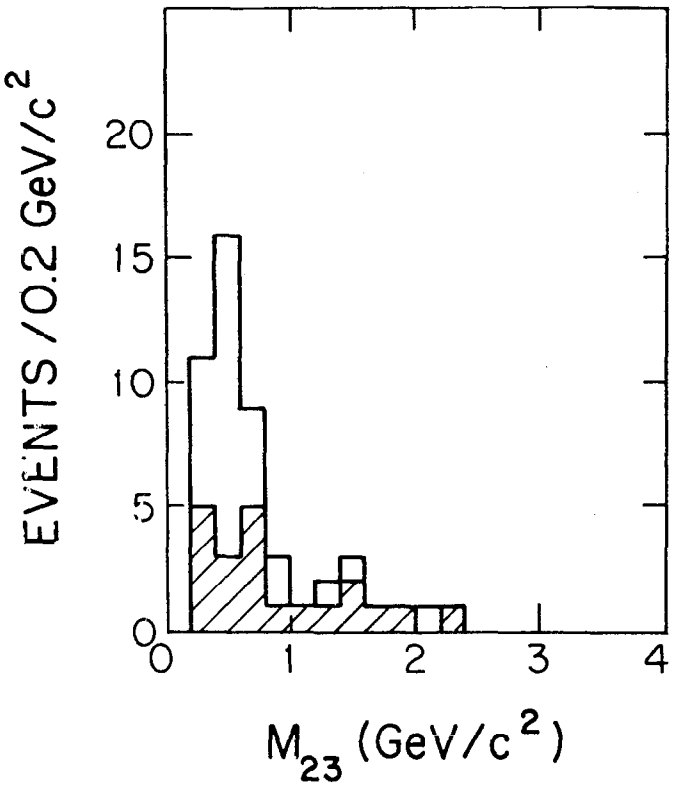

Fig. 19. Muon pair mass for non-leading μ^- and μ^+.

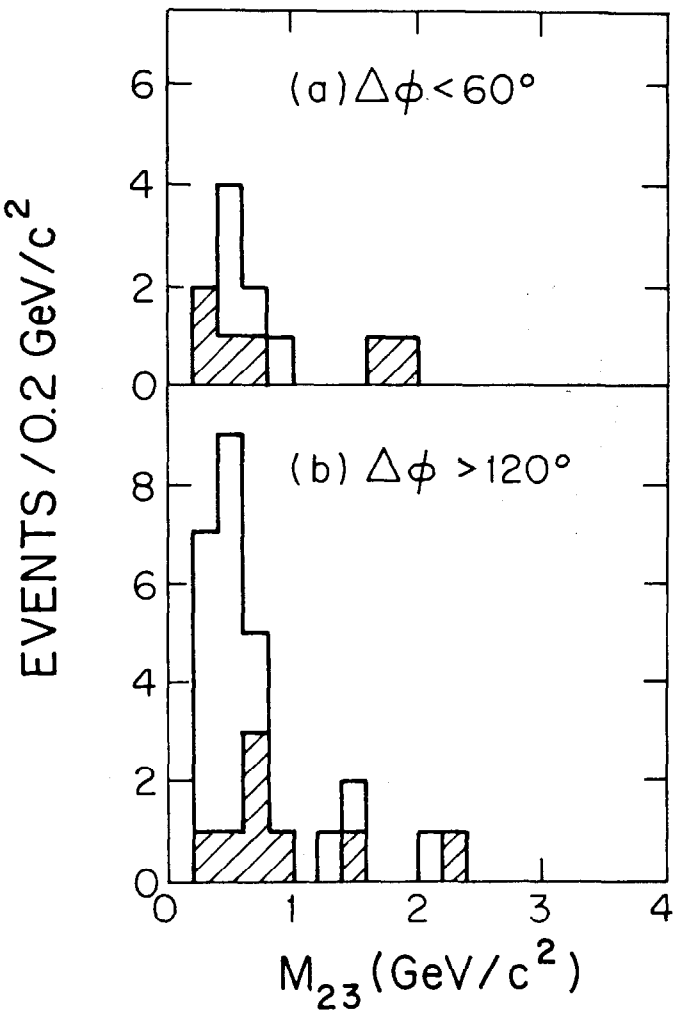

Fig. 20. Muon pair mass for (a) $\Delta\varphi < 60^{\circ}$ and (b) $\Delta\varphi > 120^{\circ}$.

VI. Trimuon Rate Estimates

We have estimated the production rate of trimuons compared to ordinary charge current neutrino induced events. Only events occurring in the two calorimeter targets are used as we wish to investigate the energy dependence of the rate. For the QT II data the total number of single muon events has been obtained by scaling up from a small analyzed sample ($\sim 3\%$) of the data. The error in this estimate together with possible scanning and triggering biases is estimated to be 25% and has not been included in the preliminary rate calculations that follow.

The trimuon rate for a $P_{\mu} > 4.5$ GeV/c cut is shown as a function of visible energy in Fig. 21. The contribution from π and K decay has been subtracted. One sees that the rate above E_{ν} of 100 GeV is constant at a value of $1.2 \pm 0.5 \times 10^{-4}$. The smaller rate below 100 GeV may be accounted for by reduced acceptance resulting from a fixed 4.5 GeV/c cut.

There are a number of processes which may contribute to trimuon production. These may be divided into two convenient categories: virtual photon production; and charm-anticharm, heavy new quark (b, t) or heavy lepton production. Low mass muon pairs may be created by an internal bremstrahlung-like process from the μ^- or entering or exiting quarks in the interaction.[5, 13] This would lead to a $\Delta\varphi$ distribution peaked both at 0° and 180° depending upon the particular subprocess. Direct muon pair production at the hadron vertex would also create low mass pairs and $\Delta\varphi$ would be peaked at 180°. The production of charm-anticharm pairs and subsequent double decay would also result in events of apparent hadronic origin. New hadronic flavor production could also lead to

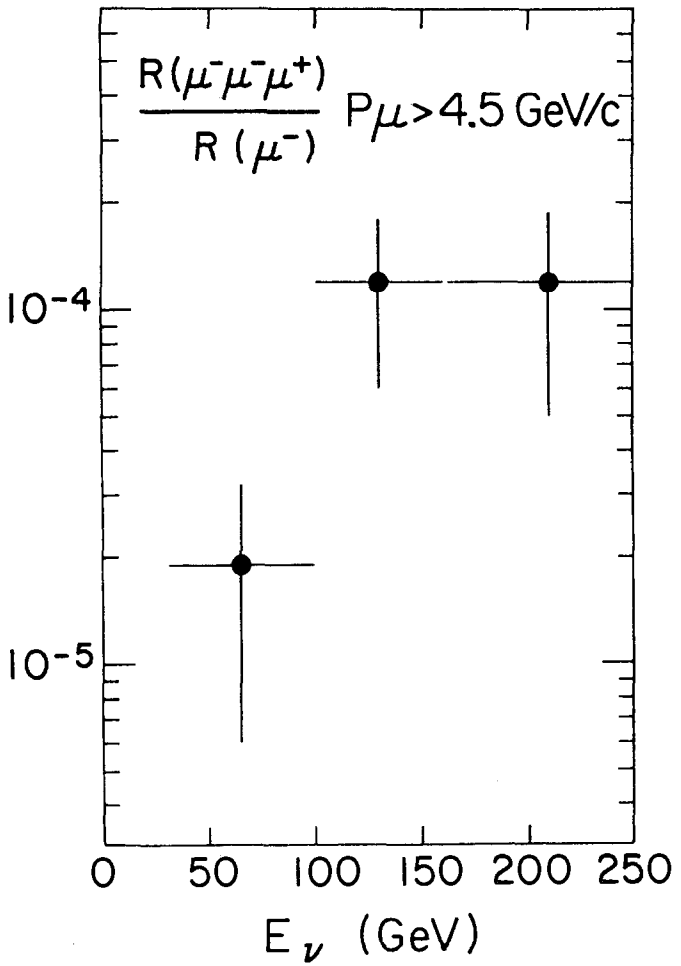

Fig. 21. Trimuon rate as a function of visible energy.

trimuons via a cascade of semileptonic decays.[13] Such events would tend to have larger pair masses as a result of the heavy parent particle. Similarly, new heavy lepton cascades would produce multimuon events, again with larger pair mass than is observed. As yet we have not done quantitative multicomponent fits to our distributions, but qualitatively the data are consistent with coming from a mixture of the two virtual photon processes. If one interprets our observation of prompt $\mu^-\mu^-$ events as coming from charm-anticharm production, then we would predict that 20 ± 20% of the trimuons come from the same source after taking into account the additional branching ratio (.10) and detection efficiency ($\sim$ 1/3) for the third muon.

VII. Tetramuon Candidate

We have observed one tetramuon candidate in the QT II run. The properties of this event are given in Table 4. We estimate the probability that this event comes from a trimuon plus decay or a dimuon and a double decay is 20%. We cannot, therefore, unambiguously tell if the event is evidence for prompt four muon production. If the event is assumed to be a result of prompt production, then the origin of the other three muons is hadronic as they are produced opposite to the leading μ^-.

VIII. Summary of Rates and Conclusions

In Table 5 we summarize our measurements of multimuon rates. The opposite sign dimuon events are consistent with the production and semileptonic decay of charmed particles. New sources of such events are not required although they cannot be completely excluded. We have presented evidence for the prompt production of $\mu^-\mu^-$ events by neutrinos at a rate of 10 ± 5% of the opposite sign events. The like

P_x	P_y	P_z	QP
- 3.1	- 1.0	43.9	- 44 ± 5
1.0	- .1	60	+60 ± 26
- .01	.5	3.8	+3.8 ± 1
- .33	.23	3.0	? 3.0 ± 1
	E_H = 178 GeV		
	E_{vis} = 289 GeV		

Table 4. Tetramuon event

	all E_ν	$E_\nu > 100$
$R(\mu^-\mu^+)/R(\mu^-)$	$4.0 \pm 0.8 \times 10^{-3}$	$6.5 \pm 1.3 \times 10^{-3}$
$R(\mu^+\mu^-)/R(\mu^+)$	$2.7 \pm 0.9 \times 10^{-3}$	$7.0 \pm 2.5 \times 10^{-3}$
$R(\mu^-\mu^-)/R(\mu^-)$	$4.0 \pm 2.0 \times 10^{-4}$	$6.5 \pm 3.5 \times 10^{-4}$
$R(\mu^+\mu^+)/R(\mu^+)$	$\leq 10^{-4}$	—
$R(\mu^-\mu^-\mu^+)/R(\mu^-)$	$6 \pm 2 \times 10^{-5}$	$1.2 \pm 0.5 \times 10^{-4}$
$R(4\mu)/R(\mu^-)$	$\leq 7 \times 10^{-6}$	—
$R(>4\mu)/R(\mu^-)$	$< 5 \times 10^{-6}$	—

Table 5. Multimuon rates with momentum cuts given in the text.

sign events are predominantly, if not completely, of hadronic origin. We have no evidence for prompt $\mu^+\mu^+$ products by antineutrinos. Trimuon production, is at present, consistent with arising entirely from radiative or direct muon pair production and charm-anticharm production. The production of new heavy quarks or leptons certainly is not the sole source of the trimuon events but cannot be ruled out at about the 20% level. Our new tetramuon candidate has a substantial probability to come from a trimuon plus π or K decay (20%). If interpreted as a prompt event, it is clear that the source of the non-leading muons is hadronic. Finally, we have no candidates for events with more than four muons.

The results presented here were obtained by members of the E-310 collaboration from Fermilab, Harvard, Ohio State, University of Pennsylvania, Rutgers, and University of Wisconsin. The members are: A. Benvenuti, F. Bobisut, D. Cline, P. Cooper, S. M. Heagy, R. Imlay, T. Y. Ling, A. K. Mann, S. Mori, D. D. Reeder, J. Rich, R. Stefanski, and D. R. Winn.

References and Footnotes

1. A. Benvenuti et al, Phys. Rev. Lett. 34, 419 (1975).

2. B. C. Barish et al, Phys. Rev. Lett. 36, 939 (1976); M. Holder et al, Phys. Lett. 69B, 377 (1977).

3. B. C. Barish et al, Phys. Rev. Lett. 36, 939 (1976); A. Benvenuti et al, Phys. Rev. Lett. 38, 1110 (1977); A. Benvenuti et al, Phys. Rev. Lett. 40, 488 (1978); M. Holder et al, Phys. Lett. 70B, 393 (1977); T. Hansl et al, submitted to Nucl. Phys. B.

4. M. Holder et al, Phys. Lett. 73B, 105 (1978); R. J. Loveless et al, UW preprint COO-088-29.

5. See for example, C. H. Albright, J. Smith and J. A. M. Vermaseren, FNAL PUB-78/14-THY.

6. A. Skuja, R. Stefanski and W. Windelbon, FNAL TM469(1974).

7. R. Stefanski and H. B. White, FNAL TM26A(1976).

8. J. D. Bjorken and S. L. Glashow, Phys. Lett. 11, 255 (1964); S. L. Glashow, J. Iliopolous, and L. Maiani, Phys. Rev. D2, 1285 (1970); We have assumed an equal mixture of $D \to K \mu \nu$ and $D \to K^* \mu \nu$.

9. The decay calculations are described in an E-310 memo, Muons from Pions and Kaons, by R. Imlay.

10. The uncut curve is for slow rescaling; R. M. Barnett, Phys. Rev. Lett. 36, 1163 (1976); H. Georgi and H. D. Politzer, Phys. Rev. Lett. 36, 1281 (1976).

11. For a fragmentation function e^{-3z}, $\bar{S}/U$ and S/D would increase by 50% and a factor of two, respectively.

12. H. Goldberg, Phys. Rev. Lett. 39, 1598 (1977); B. L. Young, T. F. Walsh and T. C. Yang, Phys. Lett. 74B, 111 (1978).

13. J. Smith, talk presented at Neutrinos-78, Purdue (1978).

RECENT RESULTS FROM THE CDHS* EXPERIMENT

presented by M. Holder, CERN

Abstract

Results are presented on two topics: charged current reactions and trimuon events.

The charged current data consist of approximately 23 00 neutrino and 6 000 antineutrino events after all cuts. They were collected in narrow band beam runs with 200 GeV secondaries derived from 400 GeV proton - Al collisions. The neutrino spectrum extends from 30 GeV to 90 GeV for neutrinos from π-decays and from 90 GeV to 200 GeV for neutrinos from K-decays. The detector consists of a fiducial mass of 500 tons of magnetized iron, sandwiched with scintillators and drift chambers.

The preliminary results are:

1. The total cross sections per unit energy (σ/E) are approximately constant in the indicated energy range, with a possible change of ±10 % between the upper and the lower end, mainly due to the present uncertainty in the K/π - ratio. The average values are, in units of 10^{-38} cm^2 GeV^{-1}:

$$(\sigma/E)^{\nu} = 0.62\pm0.03, \qquad (\sigma/E)^{\bar{\nu}} = 0.30\pm0.02$$

with the ratio

$$\sigma^{\bar{\nu}}/\sigma^{\nu} = 0.48\pm0.02.$$

*T. Hansl, M. Holder, J. Knobloch, J. May, H.P. Paar, P. Palazzi, F. Ranjard, D. Schlatter, J. Steinberger, H. Suter, W. von Rüden, H. Wahl, S. Whitaker, E.G.H. Williams (CERN); F. Eisele, K. Kleinknecht, H. Lierl, G. Spahn, H.-J. Willutzki (Dortmund); W. Dorth, F. Dydak, C. Geweniger, V. Hepp, K. Tittel, J. Wotschack (Heidelberg); P. Bloch, B. Devaux, S. Loucatos, J. Maillard, B. Peyaud, J. Rander, A. Savoy-Navarro, R. Turlay (Saclay); F.L. Navarria (Bologna).

2. The differential cross sections $f^{\nu} = \frac{d\sigma^{\nu}}{dy}\Big|_{y=0}$ and $f^{\bar{\nu}} = \frac{d\sigma^{\bar{\nu}}}{dy}\Big|_{y=0}$ are consistent with being equal (charge symmetry of F_2). The values are:

$$f^{\bar{\nu}}/f^{\nu} = \begin{cases} 1.05 \pm 0.07 \text{ for } 30 \text{ GeV} < E < 90 \text{ GeV} \\ 1.06 \pm 0.11 \text{ for } 90 \text{ GeV} < E < 200 \text{ GeV} \end{cases}$$

3. The Callan-Gross relation (spin 1/2 partons) is valid within about 10 %. From a fit to the average y distributions $\delta = 1 - \int 2xF_1 dx / \int F_2 dx < 0.05$. Radiative corrections, not included in this analysis, will probably raise δ to a value of less than 0.10.

4. The momentum carried by quarks and antiquarks is $\int F_2 dx = 0.44 \pm 0.03$ for 30 GeV < E < 90 GeV and $\int F_2 dx = 0.47 \pm 0.05$ for 90 GeV < E < 200 GeV. This result is from $d\sigma/dy\Big|_{y=0}$.

5. The average amount of antiquarks, measured from the y distributions in neutrino and antineutrino reactions, is $(\bar{q}-s+c)/(q+\bar{q}) = 0.08 \pm 0.04$ and $(\bar{q}+s-c)/(q+\bar{q}) = 0.16 \pm 0.02$ with the mean $\bar{q}/(q+\bar{q}) = 0.12 \pm 0.02$, where $q=u+d+s+c$ represents the sum of the quark densities in the proton.

6. The ratio of antiquarks to quarks is consistent with being constant in the energy range 30 GeV < E < 200 GeV, with a maximum change of ± 0.04 from the average of $\bar{q}/(q+\bar{q}) = 0.12$.

7. If the average x- distributions for valence quarks and for antiquarks are parameterized by $xF_3(x) \propto \sqrt{x}(1-x)^n$ and $\bar{q}(x) \propto (1-x)^m$, the best values for the parameters are $n=3.5 \pm 0.5$ and $m=6.7 \pm 0.5$.

8. Scaling deviations are observed, most directly in the shape of $F_2(x)$ as a function of neutrino energy. $F_2(x,Q^2)$ decreases with increasing Q^2 for $x \gtrsim 0.2$ and increases for $x<0.1$.

9. The values of F_2 at low Q^2 agree within about 10 % with the values expected on the basis of the quark model and the e-d data at the same Q^2.

10. The scaling violations in the Q^2- range accessible to this experiment (roughly $2 \leq Q^2 \leq 100$ $(GeV/c)^2$) seem to be in agreement with QCD calculations.

The second topic discussed is the interpretation of trimuon events. 75 events have been observed in the CDHS detector during wide band beam neutrino running. For a detailed discussion of the results the reader is referred to ref. 1 and ref. 2. The events are consistent with being due to charged current reactions with additional creation of a low mass $\mu^+\mu^-$ pair. This pair can be understood as being either produced from the hadron system, analogous to μ-pair production in hadron-hadron collisions, or as being created by internal Bremsstrahlung from the muon. Heavy leptons or heavy quarks can also contribute to trimuons through their leptonic decay modes, but the average kinematical configuration would be different from that of the observed events. Upper limits for the production of these particles are given.

References:

1. T. Hansl et al., Phys. Letters 77B (1978) 114.

2. T. Hansl et al., Characteristics of trimuon events etc., submitted to Nucl. Physics B.

Recent Results from the FNAL 15 Foot Bubble Chamber

M.J. Murtagh

TABLE OF CONTENTS

Recent Results from the FNAL 15 Foot Bubble Chamber

M.J. Murtagh
Physics Department, Brookhaven National Laboratory

I. Introduction

Recent results from the Fermilab 15' Bubble Chamber on charm production by neutrinos and antineutrinos and on the measurement of the elastic scattering of muon neutrinos on electrons are discussed. All the results come from exposures of the chamber filled with a heavy neon-hydrogen (64% at. neon) mixture. In this liquid electrons are easily identified through visible bremsstrahlung since the radiation length is only 40 cms. With any reasonably defined fiducial volume and the requirement that electrons are identified by at least two signatures, the detection efficiency for electrons is $\gtrsim$ 85%. The interaction length for hadrons is 125 cms, so that hadrons typically interact while muons leave the chamber without interacting and can, in general, be identified on the scan table. From the comparison of interacting and non-interacting tracks of both signs the background of fake μ^{-} from hadron punchthrough is estimated to be about 10%.

The neutrino results presented (unless otherwise stated) are from the Brookhaven National Laboratory-Columbia University experiment (Exp. 53A).[1] The total exposure of 134,000 pictures contains 106,000 charged current neutrino interactions. The present dilepton ($\mu^{-}e^{+}$) sample which is double the published data from this experiment[2] is clearly consistent with the GIM charm model. In addition, the non-leptonic

charm decay $K^{o}\pi^{+}\pi^{-}$ of the D^{o} has been observed.[3] The current status of the search for charmed baryons is presented.

The cross-section for $\nu_\mu - e^-$ elastic scattering has been measured.[4] When analyzed in terms of the Weinberg-Salam model this result yields a value of $\sin^2\theta_w = 0.2$ which is consistent with the value obtained from neutrino hadron scattering. This is in contrast to the recent GARGAMELLE results[5] which gave a Weinberg-Salam angle $\sin^2\theta_w \sim 0.73$.

Recently two groups[6,7] have reported on dilepton (μ^+e^-) production by antineutrinos. While the number of events is still small, the results are clearly consistent with the expectations of the GIM model.

II. Charm Production

Dilepton production by neutrinos was first reported almost four years ago.[8] Since then many arguments have been advanced as to why dilepton events are manifestations of GIM charm production.[9] However, these counter experiments were unable to investigate one of the basic premises of the GIM scheme; the strong correlation between charm and strangeness. This information is the province of bubble chambers and the current situation on the strange particle content of dilepton events will be emphasized in the following discussion.

a) By Neutrinos

Charm particles[10] can be produced in charged current neutrino interactions either by interactions on d quarks or on s quarks in the $s\bar{s}$ sea.

Valence:

$d(x)\sin^2\theta_c$

1 S.P. per event

Sea:

$s(x)\cos^2\theta_c$

2 S.P. per event

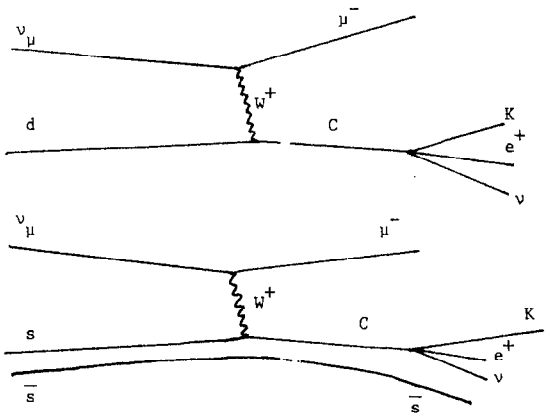

When they decay semileptonically, e^+ particles are produced. Thus, one expects to find μ^-e^+ events. In charm production from valence quarks, the total charm production rate is $\sin^2\theta_c$ (5%), where θ_c is the Cabibbo angle. Since charm couples preferentially to strangeness, one expects one strange particle per event. In charm production from $s\bar{s}$ pairs in the sea, the production rate is $\sim s(x)\cos^2\theta_c$, where $s(x)$ is the probability of finding an s quark with fractional momentum x. Here one expects $\sim$ two strange particles per event (one from the decay of c, the other from the leftover $\bar{s}$). These two mechanisms may have comparable rates. They can be distinguished by their characteristic x- distributions. The production on s quarks is expected to have a distribution peaked at small x, while production on a valence quark has a broader x distribution. In addition, the total strange particle content should be between one and two strange particles per event depending on the mixture of valence

and sea production.

b) By Antineutrinos

Antineutrinos can produce only anti-charm particles[10] either by interactions on $\bar{d}$ or $\bar{s}$ quarks in the sea.

Sea:
$d(x)\sin^2\theta_c$
1 S.P. per event

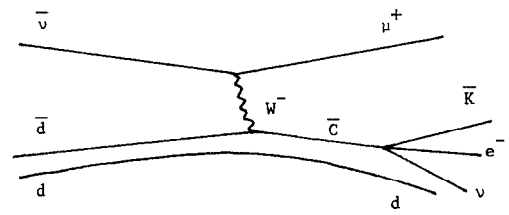

Sea:
$s(x)\cos^2\theta_c$
2 S.P. per event

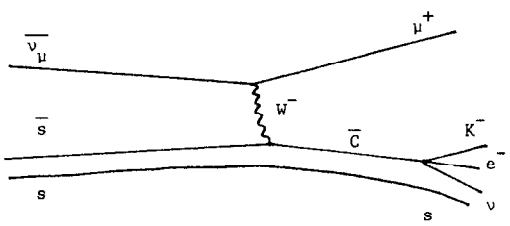

Since the production is always from sea quarks, the production from $\bar{s}$ should dominate since its rate is proportional to $\cos^2\theta_c$. Consequently, one expects antineutrinos to give μ^+e^- events with a characteristic "sea" x-distribution and approximately two strange particles per event.

III. Dilepton Production

a) By Neutrinos

A total of 164 events with at least a μ^- and an e^+ in the final state have been found in the analysis of 100,000 pictures, corresponding to 60,000 charged current neutrino interactions. The e^+ is required to have two signatures and a momentum over 300 MeV/c. With these cuts, the background from asymmetric Dalitz pairs is a few percent. The μ^- is identified as the fastest negative leaving track. No momentum cut is made. From a comparison of interacting and noninteracting tracks of both signs, the background due to fake μ^- (hadron punchthrough) is determined to be about 10%. After correcting for these backgrounds, scan efficiency (~90%), and e^+ identification efficiency (~85%), the calculated dilepton rate is

$$R = \frac{\nu_\mu + Ne \to \mu^- + e^+ + \ldots}{\nu_\mu + Ne \to \mu^- + \ldots} = (0.5 \pm 0.15)\%.$$

This rate is calculated for half of the events for which there is an accurate normalization. Figure 1 shows the momentum distribution of the e^+, the μ^- and the total visible energy.

Various opening angles between selected particles as projected on the plane perpendicular to the beam direction are shown in Fig. 2. In general, one expects these angles to be shifted toward 0° for particles coming from the same production vertex and 180° for those particles emitted at opposite vertices. These results are consistent with the premise that the e^+ is associated with the hadron rather than the lepton vertex.

The 164 μ^-e^+ events were examined for associated $K_S \to \pi^+\pi^-$ and $\Lambda \to p\pi^-$ decays. A total of 33 such vees (25 events with a single vee, 4 with a double vee) were found. After resolving the K^o/Λ ambiguities (10 of the 33 vees were ambiguous) there were 23 K^o_S and 10 Λ decays. This corresponds to 0.6 ± 0.2 neutral strange

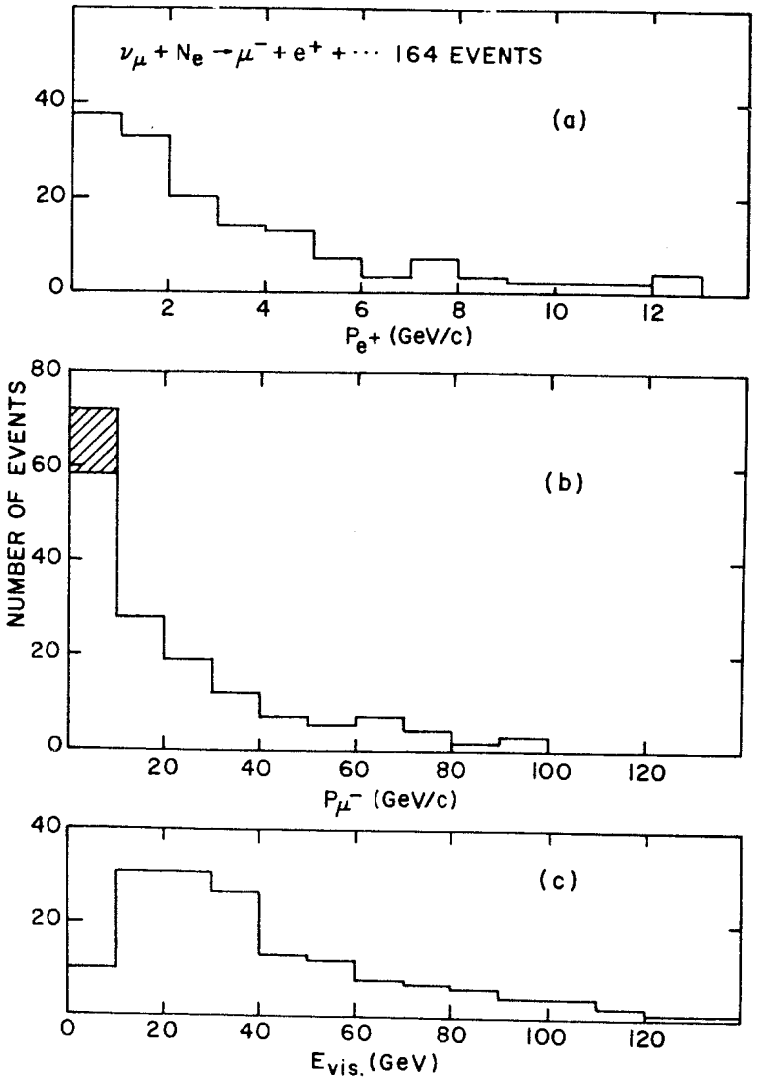

Fig. 1 Momentum of a) the e^+; and b) the μ^-, in the dilepton sample. The shaded events are the background from hadron punchthrough; c) the total visible energy.

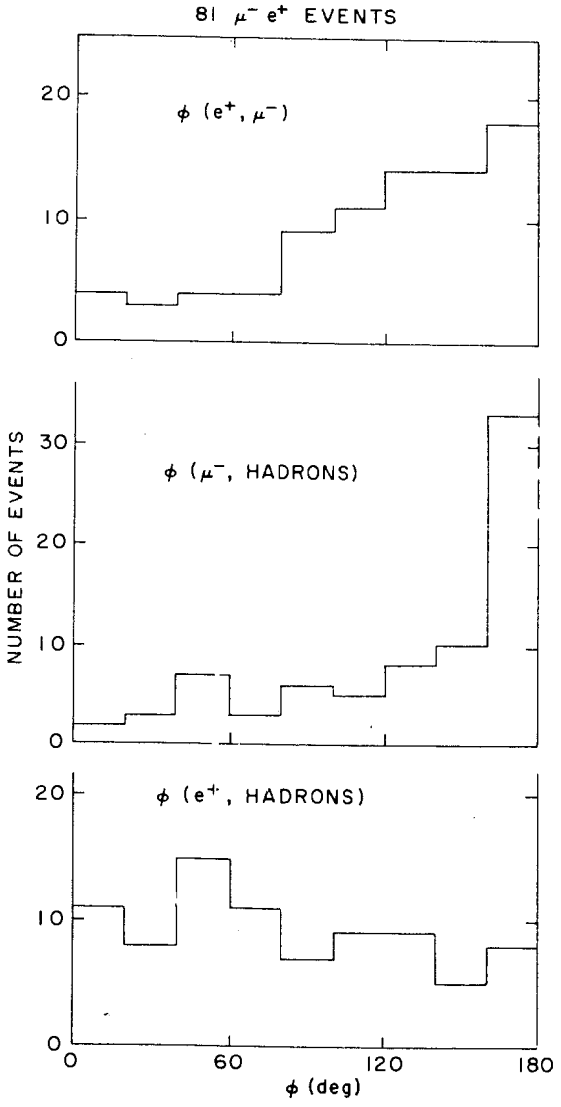

Fig. 2 Opening angles as projected onto the plane normal to the ν_μ beam direction.

particles per dilepton event. The visible vee production rate in normal charged current interactions is measured to be 6%. Therefore, one expects only 10 vees in 164 events, whereas 33 are observed. This excess of strange particles in dilepton events is as expected in the GIM charm model. Recently a number of other bubble chamber experiments have reported the observation of dilepton events in neutrino interactions (Table I, Fig. 3). Both the rate for dilepton production and the number of neutral strange particles per event are consistent with the results of the Brookhaven National Laboratory-Columbia University experiment.

The x distribution for the 164 $\mu^- e^+$ events (Fig. 4) can be fit to a mixture of the x distributions measured at SLAC and GARGAMELLE for valence and sea quarks. The best fit indicates that charm production by neutrinos is about 2/3 from valence and 1/3 from sea quarks. This ratio between charm production on valence and sea quarks implies that the sea s quark content is 3% of the valence d quark content in a neon target. The number of strange particles expected per event is, therefore, (2/3 x 1 strange particle) + (1/3 x 2 strange particles) = 1.33. On the assumption that charged and neutral strange particles are equally likely in charm decay, the observed total strange particle production rate is ∿1.2 strange particles per event.

The characteristics of these dilepton events strongly supports the conjecture that they are predominantly from the decay of charmed particles.

Figure 5 shows the $K^o e^+$ effective mass from the 19 $\mu^- e^+$ events

TABLE I

$\mu^- e^+$ From Other Experiments

Experiment	$\langle E_\nu \rangle$ BeV	Liquid	Events Observed	Vees* Observed	$\mu^- e^+/\mu^-$ Rate (%)
Gargamelle(11) CERN PS	1-8	Freon	14 $\mu^- e^+$	3	
Wisconsin-CERN-Hawaii-Berkeley (12) Fermilab 15 foot B.C., E28	∿30	21% Ne	17 $\mu^- e^+$	11	0.8 ± 0.3
Columbia-Brookhaven Fermilab 15 foot B.C., E53	∿30	64% Ne	164 $\mu^- e^+$	33	0.5 ± 0.15
Berkeley-Seattle-LBL-Hawaii (6) Fermilab 15 foot B.C., E172	∿30	64% Ne	6 $\mu^- e^+$	1	$0.34 \pm 0.23 \atop - 0.13$
Fermilab-LBL-Hawaii (13) Fermilab 15 foot B.C., E546	∿30	50% Ne	40 $\mu^- \mu^+$	5	0.43 ± 0.16
BEBC Narrow band(14) CERN SPS	∿75	60% Ne	11 $\mu^- \mu^+$ 5 $\mu^- e^+$	6 2	0.7 ± 0.3
BEBC Wide band(15) CERN SPS	∿30	60% Ne	21 $\mu^- e^+$	6	0.5 ± 0.17
GARGAMELLE Wide band(16) CERN SPS	∿30	Freon Propane	46 $\mu^- \mu^+$	6	0.7 ± 0.2

*Vees stand for $K^o_s \to \pi^+ + \pi^-$ or $\Lambda^o \to p + \pi^-$ decays

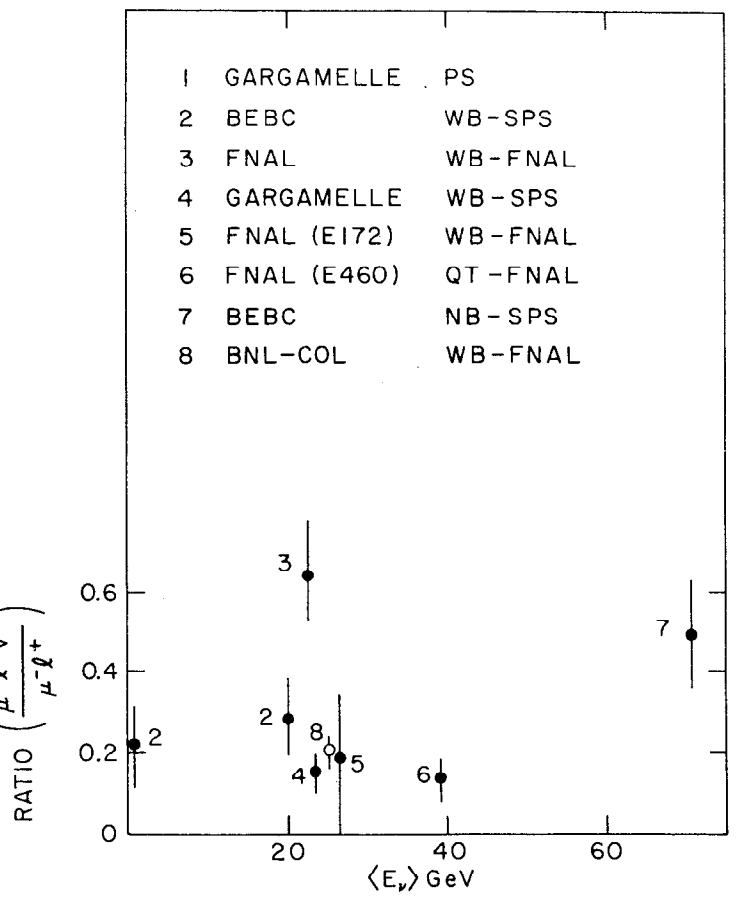

Fig. 3 Visible V^0 content in various dilepton experiments.

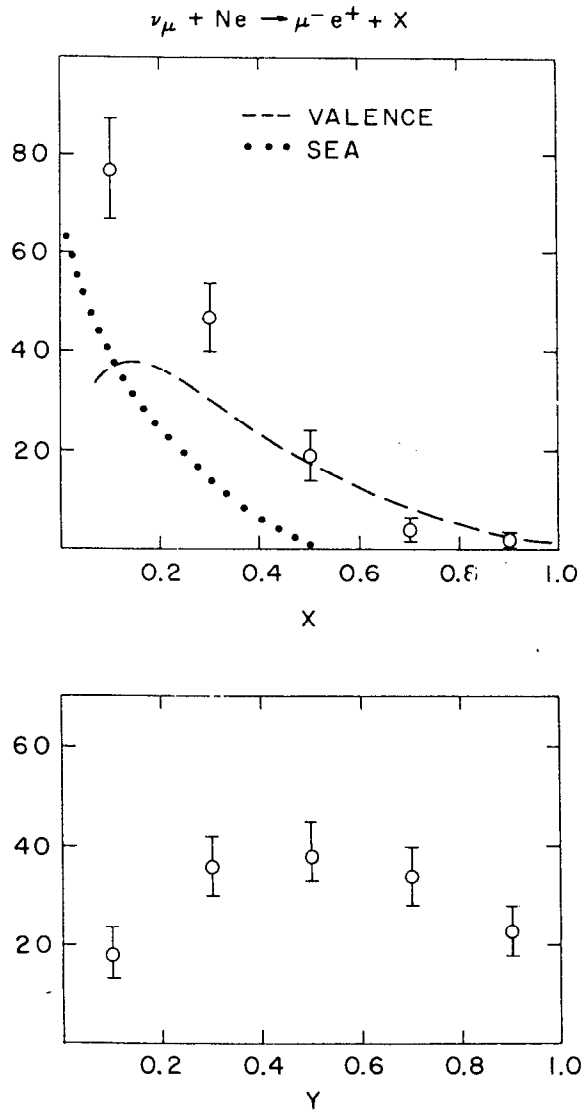

Fig. 4 X and Y variables for dilepton events. The curves represent fitted contributions from valence and sea quarks.

with a single K^o. The data are not in good agreement with the distribution expected from the $K^o e^+ \nu_e$ decay of a spin zero D^+ meson at 1868 MeV. The distribution is consistent with a calculation by Barger et al.[17] assuming a $K\pi e\nu$ decay. However, 3-body decay modes are not excluded (the only 3-body D^o decay mode $D^o \to K^- e^+ \nu$ can not contribute to the plot).

b) By Antineutrinos

Recently two groups working at FNAL have presented results on dilepton production ($\mu^+ e^-$) by antineutrinos.[6,7] The statistics in each case (Table II) are low but the situation relative to neutrino produced dileptons is rather clear. The strange particle content is higher $\sim$ 0.5 ($K_S \to \pi^+\pi^- + \Lambda^o \to p\,\bar{\pi}$) per event which, when corrected for missing neutrals and with reasonable assumptions on the relative production of charged and neutral strange particles, yields $\sim$2 strange particles per event.[7] The x-distribution peaks at small x-values consistent with production from sea quarks. The rate is probably lower than for neutrino production of dileptons. In all cases the results are in accord with the expectations of the GIM charm model. However, it is clear that improved statistics will greatly facilitate the comparison with the model.

IV. Search for Non Leptonic Charm Decays

All events with possible vees ($K_S \to \pi^+\pi^-$ or $\Lambda^o \to p\pi^-$ decays) in about 80,000 pictures, corresponding to 46,000 charged current events with a muon momentum over 2 GeV/c, were measured. Good 2 or 3 constraint fits for 1815 $K_S \to \pi^+\pi^-$ and 1367 $\Lambda \to p\pi^-$ decays

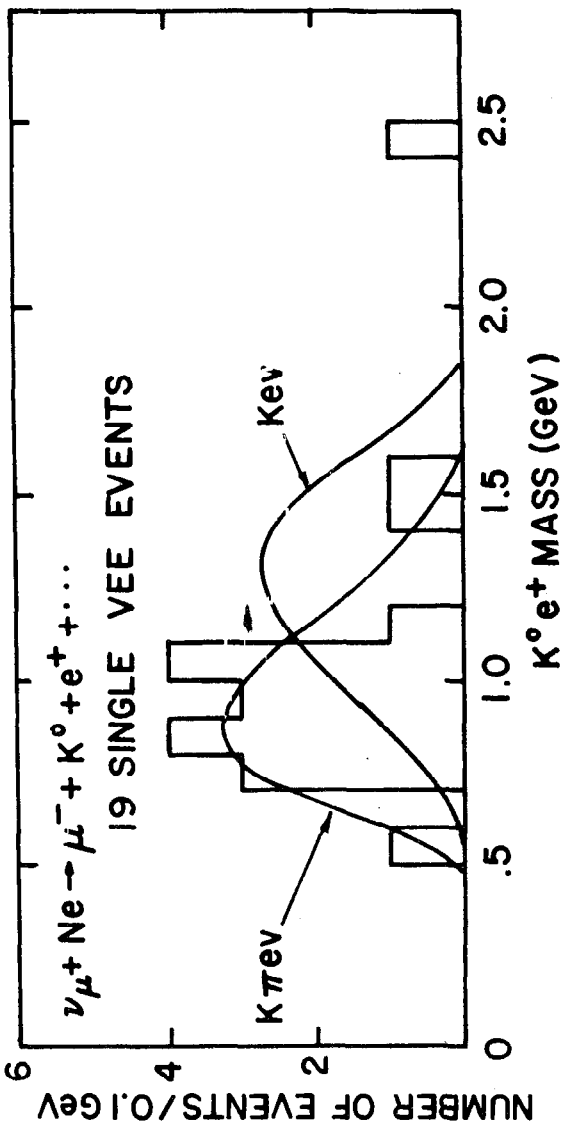

Fig. 5 $K^o e^+$ mass from dilepton sample.

TABLE II

μ^+e^- Events in Antineutrino Interactions

	Berkeley Hawaii-Seattle[6]	Fermilab-IHEP ITEP-Michigan[7]
$\bar{\nu} \to \mu^+ \ldots$Events	2800	6320
$\bar{\nu} \to \mu^+e^- \ldots$Events	4	12
$\bar{\nu} \to \mu^+e^-V^o$ Events*	2	7
Rate $\mu^+e^-/\mu^+ \ldots$	$(0.15\ ^{+0.14}_{-0.08})\%$	$(0.22 \pm 0.07)\%$

*V^o stands for $K^o_s \to \pi^+\pi^-$ or $\Lambda^o \to p\pi^-$ decay associated with the primary vertex.

were obtained. Correcting for branching ratios and detection efficiencies, this corresponds to a $(K^o + \bar{K}^o)$ rate of $(13.6 \pm 1.5)\%$ of all charged current events, and a $(\Lambda^o + \Sigma^o)$ rate of $(5.0 \pm 0.5)\%$.

Figures 6a and 6b show the $K^o_S\pi^+$ and the $K^o_S\pi^+\pi^-$ mass distributions, respectively. There is a peak in the $K^o\pi^+\pi^-$ distribution in the mass region of the charmed D^o meson seen at SPEAR.[18] The best fit of a polynomial background plus a Gaussian, shown by the curve on Fig. 7a gives the following parameters:

$$M = 1850 \pm 15 \text{ MeV}, \quad \sigma = 20 \pm 8 \text{ MeV}$$

corresponding to 64 events above a background of 180, with a statistical significance of four standard deviations. The width is consistent with the experimental mass resolution of 20 MeV. No corresponding peak is apparent near the D mass in the events without a μ^- (Fig. 7b). This is consistent with the prediction of the GIM model that the charm charging neutral current interactions are absent. If the peak were due to K^* production, then one might expect it to be present in events with and without a μ^-.

Correcting for branching ratios and detection efficiencies, the measured rate is

$$\frac{\nu_\mu + Ne \to \mu^- + D^o + \ldots,\ D^o \to K^o\pi^+\pi^-}{\nu_\mu + Ne \to \mu^- + \ldots} = (0.7 \pm 0.2)\%.$$

There is no significant peak at the D^+ mass in the $K^o\pi^+$ mass distribution. Fitting to a Gaussian with the width of the mass resolution centered on the D^+ mass gives a result of 11 ± 8 $D^+ \to K^o\pi^+$ events, which is clearly not a significant signal. Using the branching ratios measured at SPEAR[19] of $4 \pm 1.3\%$ for

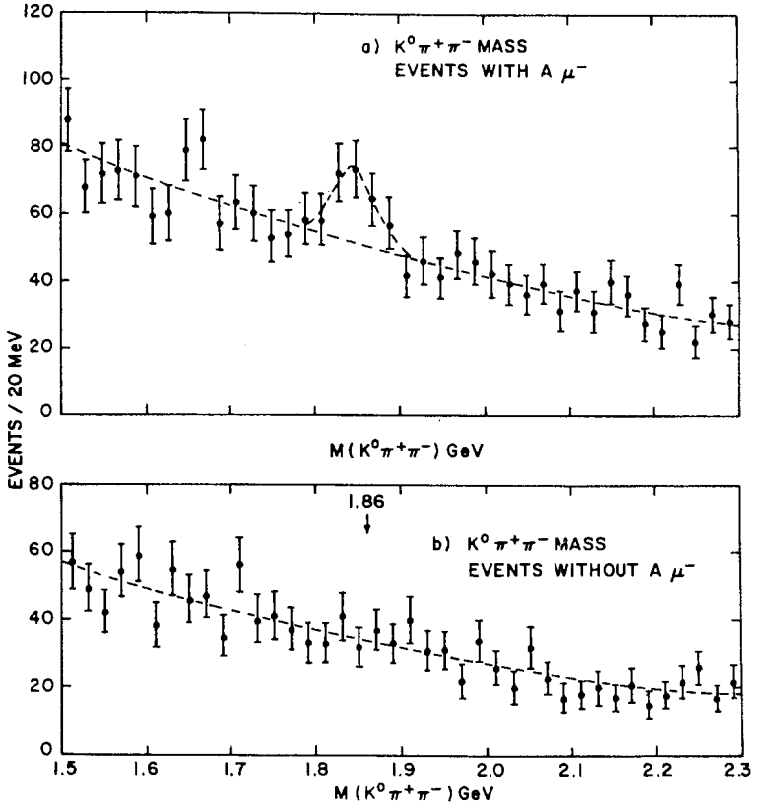

Fig. 6 $K^0\pi^+\pi^-$ invariant mass distributions for a) events with μ^- candidates; and b) events without μ^- candidates.

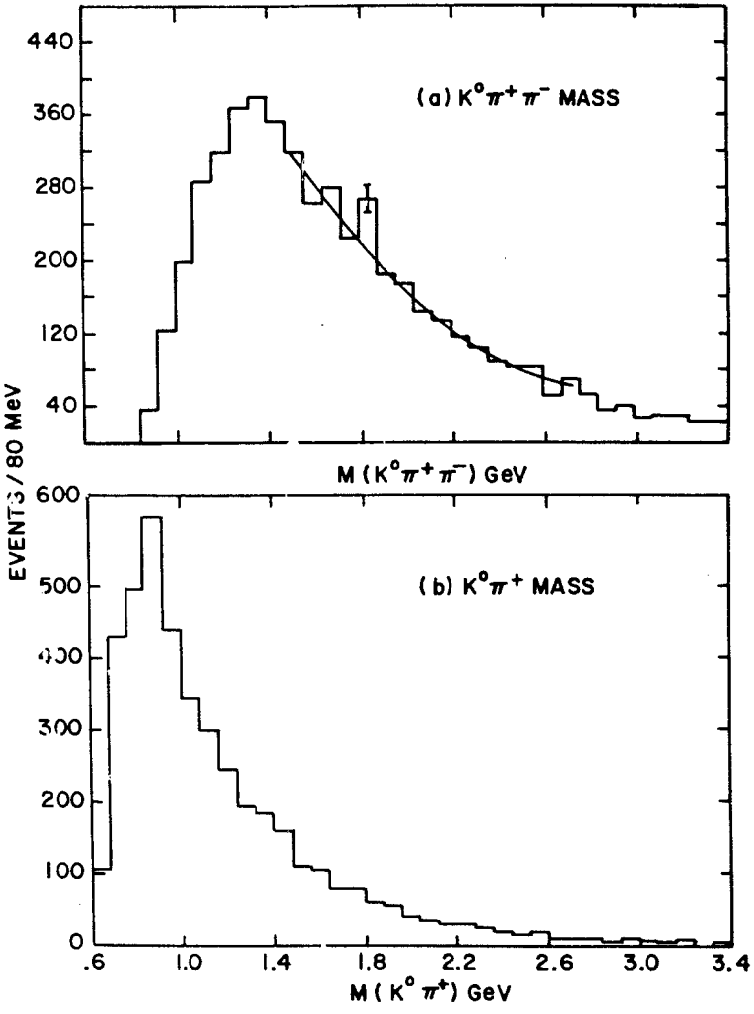

Fig. 7 a) $K^0\pi^+\pi^-$ and b) $K^0\pi^+$ invariant mass distributions from charged current events.

$D^o \to K^o\pi^+\pi^-$ and 1.5 ± 0.6% for $D^+ \to K^o\pi^+$, the ratio of D^+ to D^o production by neutrinos is $D^+/D^o = 0.5 \pm 0.4$.

The D^o rate can be compared with the previously measured rate for $\nu_\mu + Ne \to \mu^- + e^+ + .../\nu_\mu + Ne \to \mu^- + ...$ of (0.5 ± 0.15)%[2] It is not possible to obtain an exact value for the ratio of semileptonic to $K^o\pi^+\pi^-$ decays of the D^o since it is not known what fraction of the μ^-e^+ events come from D^o decays. If it is assumed that all of the μ^-e^+ events are due to semileptonic D^o decays, $D^o \to e^+ + ...$, then the ratio $R = (D^o \to e^+ + ...)/(D^o \to K^o\pi^+\pi^-)$ is $R = 0.7 \pm 0.3$. If, on the other hand, only a fraction of the μ^-e^+ events is due to D^o decays, which is more reasonable since there is likely to be some D^+ and charmed baryon decays contributing to the μ^-e^+ events, then the value for R is less than that given above. Recent measurements at SPEAR yield the branching ratios of (4.0 ± 1.3)% for $D^o \to K^o\pi^+\pi^-$,[19] and (7.2 ± 2.8)% for $D \to e^+ + ...$,[20] which correspond to a value of $R = 1.8 \pm 0.9$, assuming equal semileptonic branching ratios for the D^o and the D^+. The Brookhaven-Columbia values, with any assumption about the D^o contribution to the μ^-e^+ events, are lower than the SPEAR value for R. However, the errors on all of these numbers are rather large at the present.

V. Search for Charmed Baryons

There is an indication of charmed baryon production in the dilepton sample. Since 10 events of the type $\nu_\mu + Ne \to \mu^- + e^+ + \Lambda^o + ...$ are observed where about five events are expected from associated production. These Λ^o's can not come from D meson decay nor from the $\bar{s}$ quark left over when the e^+ comes from charm produced on an s quark in the sea.

The hadronic decays of charmed baryons into Λ's were searched for. Figures 8a and 8b show the $\Lambda^o\pi^+$ and the $\Lambda^o\pi^+\pi^+\pi^-$ mass distribution from events of the type $\nu_\mu + Ne \to \mu^- + \Lambda^o +$ hadrons. There is no enhancement in the $\Lambda\pi^+\pi^+\pi^-$ mass at 2250 MeV. A small peak with 20 ± 9 events is present in the $\Lambda\pi^+$ mass at 2250 MeV but the signal is not present if a cut in helicity angle (require $\cos\theta^* > -0.6$) is made. This cut was chosen to remove a background of events with a slow Λ and a fast π and should have enhanced the Λ_c^+ signal to background. Thus, this is considered at this time to be a statistical fluctuation. From these results the 90% confidence level limit for $\Lambda_c^+ \to \Lambda\pi^+\pi^+\pi^-$ is $\leq$ 0.2% while the $\Lambda\pi^+$ signal, if real, leads to a rate for the $\Lambda_c^+ \to \Lambda\pi^+$ mode of (0.1 ± 0.5)%.

VI. $\nu_\mu - e^-$ Elastic Scattering

The observation of neutral current induced neutrino interactions gave strong support to the gauge theories unifying weak and electromagnetic interactions. Presently all neutrino-hadron neutral current interactions are consistent with the SU(2) x U(1) gauge model proposed by Weinberg[21] and Salam[22] with a Weinberg angle $\sin^2\theta_w \approx 1/4$. One of the theoretically most stringent tests of this theory is provided by the purely leptonic process, $\nu_\mu e^- \to \nu_\mu e^-$ which can proceed only via the weak neutral current interaction,

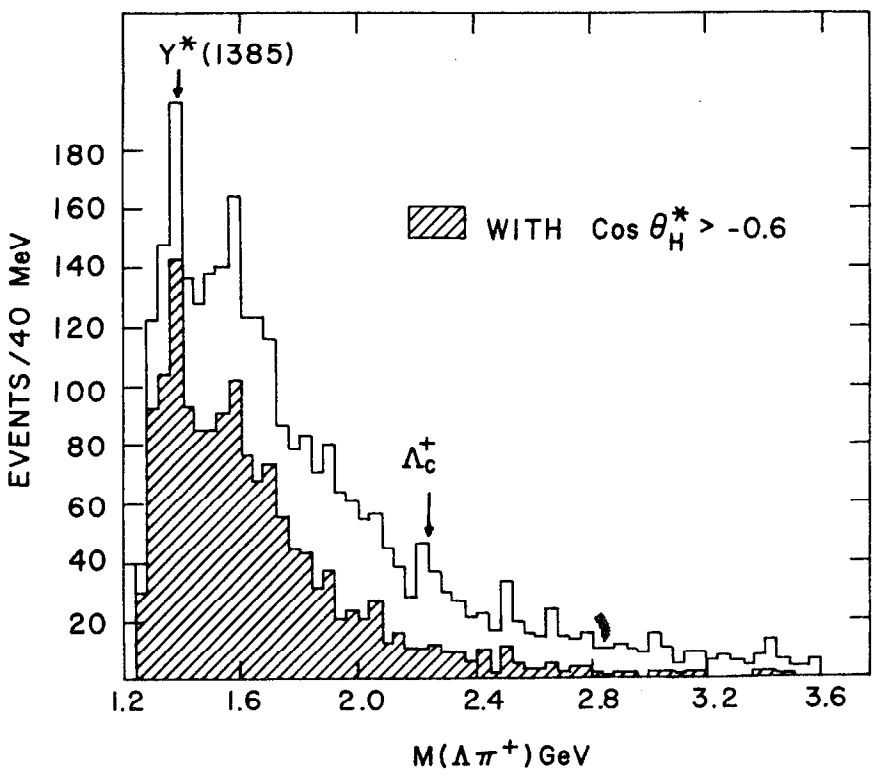

Fig. 8 a) $\Lambda\pi^+$ invariant mass distributions from charged current events.

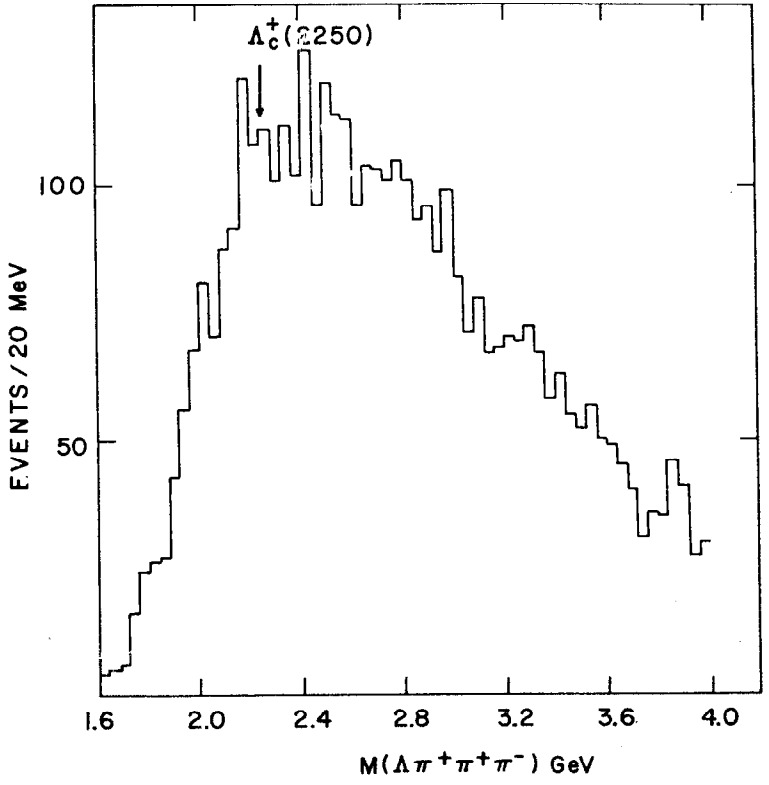

Fig. 8 b) $\Lambda\pi^+\pi^+\pi^-$ invariant mass distribution from charged current events.

and the theory can be compared to experimental measurement without uncertainties introduced by using hadronic targets. Early experimental results on this reaction at neutrino energies of a few GeV[23,24,25] are consistent with the Weinberg-Salam model. A recent result at higher energies[5] indicates a significantly higher cross section for this process than that expected from the Weinberg-Salam model. The Brookhaven-Columbia experiment, which has four times the charged current data sample, is in good agreement with the Weinberg-Salam model.

The entire data sample of 134,000 photographs containing 106,000 charged current ν_μ interactions was subjected to a dedicated scan for isolated electromagnetic showers; 93,000 of the pictures were double scanned. All forward energetic single e^-, single e^+, or $\gamma \to e^+e^-$ pairs with no other tracks originating at the interaction vertex were recorded. Electrons of either sign were identified by at least two signatures. All such events were examined by a physicist, measured, and geometrically reconstructed using the program, TVGP. By using the 93,000 double-scanned pictures the scanning efficiency was determined[26] to be (61 ± 15)% for a single scan, giving an overall scan efficiency of (78 ± 15)%.

Events which had energy $E \geq 2$ GeV and angle $\theta \leq 3^\circ$ and which were not associated with other events were retained for further consideration. The subsequent procedures adopted were guided by the philosophy of retaining single electron events and rejecting γ-ray conversions. An event was defined to be a single e^- if there was no visible radiation on a negative track before there was observable curvature so that the event clearly had a single track at the origin. If there was early radiation within a short distance of the origin such that it was not possible to determine whether the event began as a single or double track (in all ambiguous cases this distance was less than 10 cm), then the event was still classified as a single e^- if, a) the fastest track was negative, b) the fastest positron coming from the confused region was less than 25% of the electron energy ($E^+/E^- < 1/4$), and c) the energy of the second fastest electron was greater than 10% of the positron energy. Condition (b) removes fast symmetric pairs while condition (c) obviates the problem of low energy δ rays on asymmetric pairs. In most instances the identification was clear cut; the spatial resolution and lack of confusion being sufficient to clearly distinguish among the noted categories. In three cases it was not possible to distinguish between a single e^- with early conversion and the production of a delta ray from a converted γ pair before clear separation of the lepton tracks. Adoption of the above rules relegated these three events to the γ category (two of the three are consistent with $\nu_\mu e^- \to \nu_\mu e^-$ kinematics). Corrections are made for real e^- events being classified as γ's by these procedures. The probability of an e^- radiating more than 1/4 of its energy in a single radiation within the first 10 cm sufficiently asymmetrical to be classified as a γ has been calculated to be 3%.

The final sample contains 11 unambiguous e^- events, 5 unambiguous e^+ events, and 22 γ pairs. The number of single e^+ events is quite consistent with what we expect from the reaction $\bar{\nu}_e p \to e^+ n$

induced by the small $\bar{\nu}_e$ contamination in the beam.[27] The energies and angles of the 11 single e^- events, listed in Table III, are compared to the kinematics of $\nu_\mu e^- \to \nu_\mu e^-$ scattering on Fig. 9. The curves show the expected correlation between E and θ of the electrons in the lab frame for E_ν = 30 GeV, the peak of our spectrum, and E_ν = 10 and 100 GeV, which are the approximate limits of our spectrum. All 11 e^- events are consistent with the kinematics of this reaction. The single e^+ and the γ events are not sharply peaked like the e^- events but are spread out up to the 52 mrad angle cut. An appropriate variable to illustrate this difference is $E\theta^2$, since the kinematic limit in $\nu_\mu e^- \to \nu_\mu e^-$ scattering, $E\theta^2 \leq 2\, m_e$ (electron mass) is independent of the incident neutrino or outgoing electron energies. The distributions in $E\theta^2$ for the e^-, e^+ and γ events are shown in Fig. 10. The e^- events are peaked below the $2\, m_e$ (~1 MeV) kinematic limit, while the e^+ and γ events are much more spread out.

Three sources of background that could produce single electrons in this experiment were considered:

a) Photons which Compton scatter or convert to e^+e^- pairs so asymmetrically that the e^+ is not seen are a negligible background. Another background comes from photons which convert into asymmetric e^+e^- pairs and have an early energetic δ so as to be classified as an e^- and not as a γ by the criteria noted above. The probability for this is calculated to be ~1%. When multiplied by the total number of unassociated γ's that are consistent with the kinematics of $\nu_\mu e^- \to \nu_\mu e^-$ (8 events with $E\theta^2 < 3$ MeV) this yields .08 events which is negligible.

TABLE III

List of $\nu_\mu + e^- \to \nu_\mu + e^-$ Events

Event	E_{e^-} (GeV)	θ_{e^-} (mrad)	$E\theta^2$ (MeV)
1	3.7 ± 1.6	10 ± 5	0.4
2	4.7 ± 0.3	5 ± 8	0.1
3*	5.6 ± 2.6	5 ± 7	0.1
4	6.5 ± 1.6	8 ± 4	0.4
5*	8.8 ± 1.7	4 ± 3	0.1
6	9.0 ± 1.0	8 ± 5	0.6
7	14.0 ± 3.0	14 ± 10	2.7
8*	15.8 ± 2.6	8 ± 5	1.0
9*	20.8 ± 5.6	2 ± 3	0.1
10	27.5 ± 9.0	8 ± 4	1.8
11	34.6 ± 4.0	4 ± 4	0.6

*Event cut of fiducial volume used for the cross section calculation.

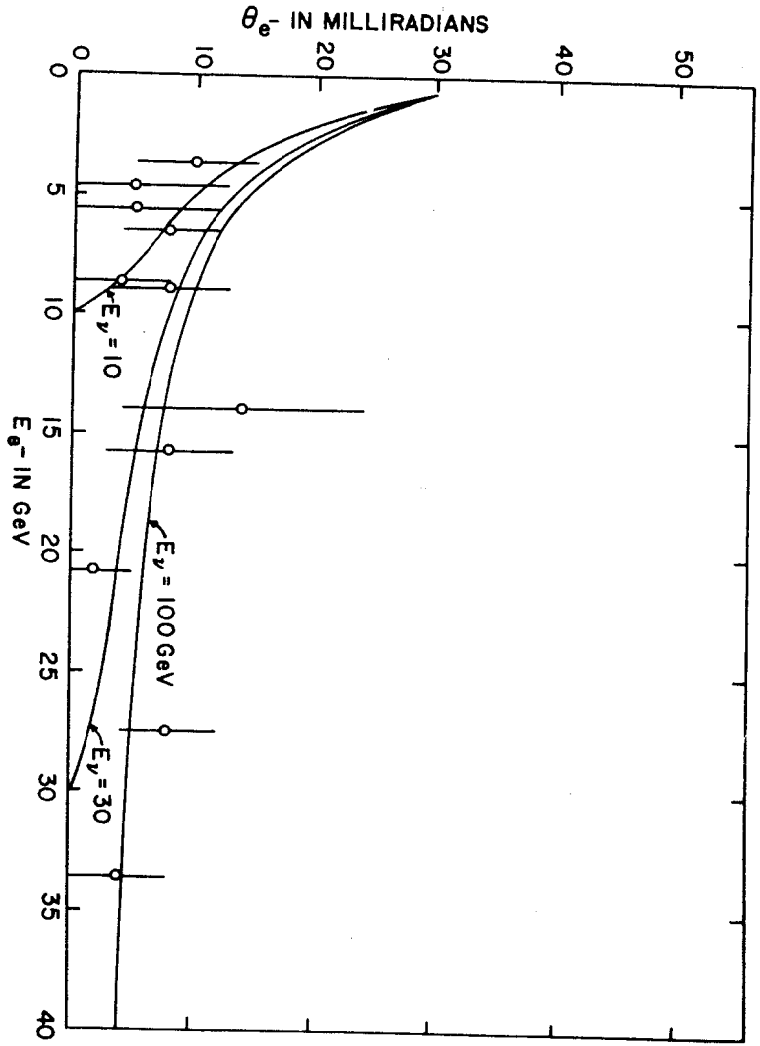

Fig. 9 Electron angle vs. energy of the 11 observed single electron events compared to the kinematics of the reaction $\nu_\mu e^- \rightarrow \nu_\mu e^-$ for various neutrino energies E.

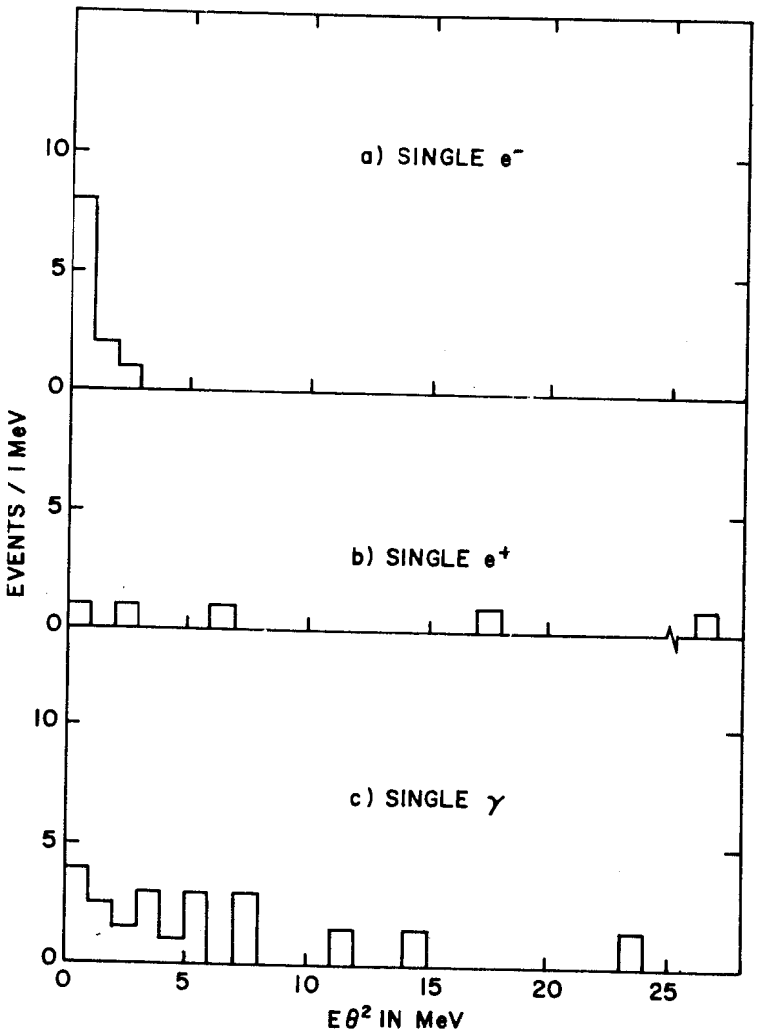

Fig. 10 Distribution in the variable $E\theta^2$ for a) the single e^- events; b) the single e^+ events; and c) the single $\gamma \rightarrow e^+e^-$ pairs.

b) The process $\nu_e n \to e^- p$ and $\nu_e n \to e^- p \pi^o$, where the proton is too low in energy to be seen, and the γ's from the π^o are mixed in with the shower of the e^-. In this experiment, they also scanned for and measured events with an e^- and hadrons,[27] and found 22 events with an e^- and a proton (with additional stubs which could be nuclear fragments) and possibly γ's from a π^o. From the expected q^2 distributions for these events, it was calculated[28] that 3% of these events would have an invisible proton and an e^- at a small enough angle to be consistent with the kinematics of $\nu_\mu e^- \to \nu_\mu e^-$. This background is calculated to be 0.7 events or (6 ± 6)% of the $\nu_\mu e^- \to \nu_\mu e^-$ signal.

c) The reactions $\bar{\nu}_\mu e^- \to \bar{\nu}_\mu e^-$, $\nu_e e^-$, and $\bar{\nu}_e e^- \to \bar{\nu}_e e^-$ are indistinguishable from the $\nu_\mu e^- \to \nu_\mu e^-$ reaction. However, since the relative fluxes in the beam are $\nu_\mu/\bar{\nu}_\mu/\nu_e/\bar{\nu}_e \simeq 100/3/1/0.1$, the contribution of these reactions in any reasonable model is expected to be small in this experiment.

The 11 $\nu_\mu e^- \to \nu_\mu e^-$ events and the corresponding 106,000 charged current ν_μ interactions are in a volume visible to all three cameras. To calculate the cross section for this process, one imposes a more restricted fiducial volume to insure a uniform (and essentially 100%) detection efficiency for high energy electrons.[29] Then 8 of the 11 $\nu_\mu e^- \to \nu_\mu e^-$ events and 79% of the charged current ν_μ interactions are in this fiducial volume. After subtracting (6 ± 6)% for the $\nu_e n \to e^- p$ background, correcting for the (78 ± 15)% scan efficiency, and for the following losses of single electrons: 10% for the 2 GeV cut[30] on E_e, 3% for loss of e^- classified as γ, and 3% miscellaneous losses such as a false association with another ν event etc., one obtains the ratio

$$\frac{\nu_\mu + e^- \to \nu_\mu + e^-}{\nu_\mu + Ne \to \mu^- + \ldots} = (1.36 \pm 0.54) \times 10^{-4}.$$

One can calculate the total cross section for this process by using the total charged current cross section $\sigma_{tot} = (0.67 \pm 0.06) \times 10^{-38} E_\nu$ cm^2/nucleon measured in the energy range of 20 to 60 GeV in a BEBC experiment[31] and by noting that the electron to total nucleon ratio in neon is 1/2. The result is

$$\sigma(\nu_\mu + e^- \to \nu_\mu + e^-) = (1.8 \pm 0.8) \times 10^{-42} E_\nu \text{ cm}^2$$

where E_ν is the incident neutrino energy in units of GeV.

This result is in disagreement with a recent measurement in the GARGAMELLE experiment[5] at the CERN SPS. On the other hand, our result is in good agreement with the Weinberg-Salam model. Figure 11a shows a comparison of the results with the prediction of the model as a function of the mixing angle $\sin^2\theta_w$. The data restrict the value of $\sin^2\theta_w$ to be $0.20^{+.16}_{-.08}$ or $0.57^{+.07}_{-.17}$, the former value being in excellent agreement with several previous neutral current measurements.[32] Figure 3b shows the energy distribution of the 11 $\nu_\mu e^- \to \nu_\mu e^-$ events. The curve on the figure is the prediction of the Weinberg-Salam model with $\sin^2\theta_w = .25$ integrated over the incident neutrino energy spectrum. The agreement is quite good.

This research was supported by the U.S. Department of Energy and the National Science Foundation.

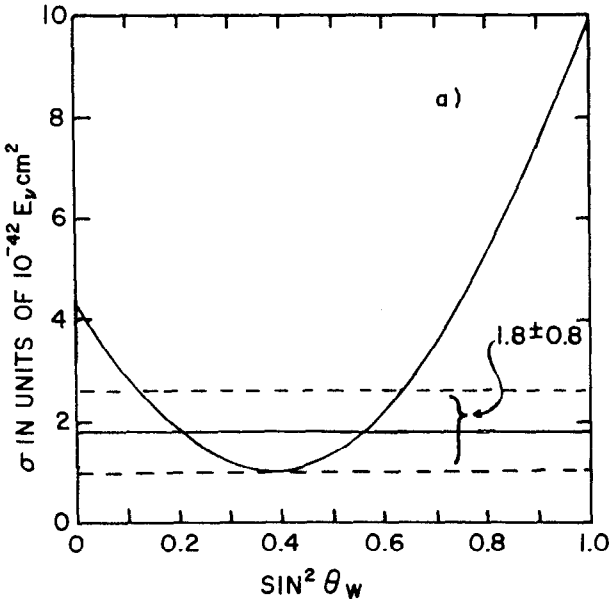

Fig. 11 a) Comparison of the prediction of the Weinberg-Salam model with the measured cross section for $\nu_\mu e^- \rightarrow \nu_\mu e^-$.

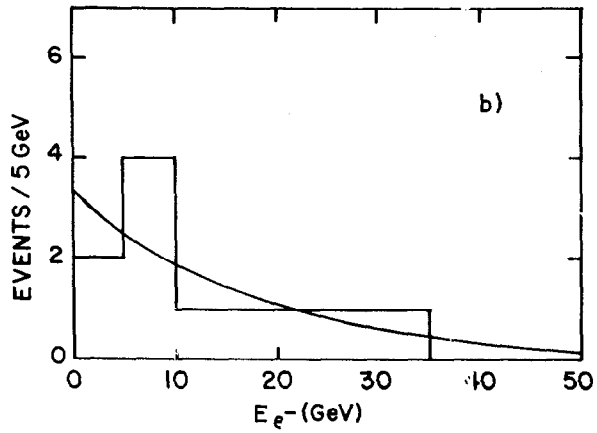

Fig. 11 b) Distribution in the electron energy of the 11 $\nu_\mu e^- \rightarrow \nu_\mu e^-$ events. The curve is the prediction of the Weinberg-Salam model with $\sin^2\theta_w = 1/4$ integrated over the incident neutrino energy spectrum of the experiment.

References

1. Brookhaven National Laboratory-Columbia University Group:

   A.M. Cnops, P.L. Connolly, S.A. Kahn, H.G. Kirk, M.J. Murtagh, R.B. Palmer, N.P. Samios and M. Tanaka, Brookhaven National Laboratory, Upton, N.Y. 11973
   C. Baltay, D. Caroumbalis, H. French, M. Hibbs, R. Hylton, M. Kalelkar and W. Orance, Columbia University, New York, N.Y. 10027.

2. C. Baltay et al., Phys. Rev. Lett. 39, 62 (1977).

3. C. Baltay et al., Phys. Rev. Lett. 41, 73 (1978).

4. A.M. Cnops et al., Phys. Rev. Lett. 41, 357 (1978).

5. P. Alibran et al., Phys. Lett. 74B, 422 (1978).

6. H.C. Ballagh et al., Phys. Rev. Lett. 39, 1650 (1977).

7. J.P. Berge et al., Submitted to Phys. Rev. Lett.

8. A. Benvenuti et al., Phys. Rev. Lett. 34, 419 (1975).

9. S.L. Glashow, J. Iliopoulos, L. Maiani, Phys. Rev. D2, 1285 (1970).

10. Associated charm production will yield $\mu^- e^- (\mu^+ e^+)$ events in neutrino (antineutrino) interactions. Since there is no significant bubble chamber data on these final states no discussion of associated charm production is included.

11. H. Deden et al., Phys. Lett. 67B, 474 (1977).

12. P. Bosetti et al., Phys. Rev. Lett. 38, 1248 (1977).

13. F. Harris, Presented at Topical Conference on Neutrino Physics at Accelerators, Oxford University, England, July 3-7, 1978.

14. P.C. Bosetti et al., Phys. Lett. 73B, 380 (1978).

15. O. Erriquez et al., Phys. Lett. 77B, 227 (1978).

16. A. Blondel, Presented at Topical Conference on Neutrino Physics at Accelerators, Oxford University, England, July 3-7, 1978.

17. V. Barger et al., Phys. Rev. D16, 746 (1977).

18. G. Goldhaber et al., Phys. Rev. Lett. 37, 255 (1976).

19. I. Peruzzi et al., Phys. Rev. Lett. 39, 1301 (1977).

20. J.M. Feller et al., Phys. Rev. Lett. 40, 274 (1978). There have been other results on the semileptonic branching ratio (W. Bacius et al., Phys. Rev. Lett. 40, 671 and R. Brandelik et al., Phys. Lett. 70B, 387). We use the results of J.M. Feller et al. since they were obtained in the same experiment as the $K\pi\pi$ branching ratio of Ref. 18.

21. S. Weinberg, Phys. Rev. Lett. 19, 1264 (1967).

22. A. Salam, in Elementary Particle Theory, N. Swartholm, Ed. (Stockholm 1969).

23. F.J. Hasert et al., Phys. Lett. 46B, 131 (1973); J. Blietschau et al., Nucl. Phys. B114, 189 (1976).

24. J. Blietschau et al., Phys. Lett. 73B, 232 (1978).

25. H. Faissner et al., Phys. Rev. Lett. 41, 213 (1978).

26. To determine the scan efficiency a sample of 134 high energy forward e^+, e^-, and γ's was used. The result is consistent with an (86 ± 20)% efficiency obtained from the 11 single e^- events alone.

27. In a sample of 27,600 total $\nu_\mu \to \mu^-$ interactions, 187 ± 14 and 28 ± 6 total $\nu_e \to e^-$ and $\bar{\nu}_e \to e^+$ interactions, respectively, were found (A. Cnops et al., Phys. Rev. Lett. 40, 144). Scaling these numbers by 106,000/27,600 one obtains 723 ± 54 and 108 ± 23 total ν_e and $\bar{\nu}_e$ interactions, respectively, in the present sample. From these numbers there should be 15 $\nu_e n \to e^- p$ and 6 $\bar{\nu}_e p \to e^+ n$ events, consistent numbers actually seen.

28. This estimate is in good agreement with the measurement in the GARGAMELLE experiment of $R_\mu = (\mu^- \text{ within } 3^\circ)$ (proton unseen)/ $(\mu^- + p) = (5 \pm 3)\%$, assuming $\nu_e - \nu_\mu$ universality. ibid Ref. 5.

29. The fiducial volume is defined by $R \leq 170$ cm, $|z| \leq 125$ cm, and $D \geq 78$ cm, where R is the distance from the center of the chamber, z is the vertical distance from the median plane, and D is the distance from the back wall of the chamber along the beam direction.

30. The 10% loss due to the $E_e \geq 2$ GeV cut was calculated using the Weinberg-Salam model with a $\sin^2\theta_w = 1/4$. However, this loss is only weakly dependent on the model used.

31. K. Schultze, Proceedings of the Symposium on Lepton and Photon Interactions, p. 359. Hamburg (1977).

32. M. Holder et al., Phys. Lett. 71B, 222 (1977); B.C. Barish et al., Proceedings of the International Neutrino Conference, Aachen 1976, 289; P. Wanderer et al., Phys. Rev. D17, 1679 (1978).

WEAK NEUTRAL-CURRENT INTERACTIONS*

R. Michael Barnett

Stanford Linear Accelerator Center
Stanford University, Stanford, California 94305

I. INTRODUCTION

The structure of gauge theories of the weak and electromagnetic interactions can be studied with the weak neutral-current interactions of quarks and leptons. In gauge theories, the charged currents (CC) are related to the neutral currents (NC). In SU(2) × U(1) models, for example, the determination of the neutral currents follows from the relation (where for simplicity right-handed charged currents are ignored):

$$J_\mu^{NC} = \bar{q}\, C^o\, \gamma_\mu\, (1 + \gamma_5)\, q - 2 \sin^2 \theta_W\, J_\mu^{em} \tag{1.1}$$

where q is the vector (u, c, d, s, ...) and J_μ^{em} is the electromagnetic current. C^o is a matrix obtained from

$$C^o = \left[C,\, C^\dagger\right] \tag{1.2}$$

where C is a matrix giving the appropriate charged current of a given SU(2) × U(1) model, i.e.,

$$J_\mu^{CC} = \bar{q}\, C\, \gamma_\mu\, (1 + \gamma_5)\, q. \tag{1.3}$$

Thus information about neutral currents can determine the existence or non-existence of charged currents such as $\bar{u}b_R$, $\bar{t}d_R$ or $\bar{E}^o e_R$ where m_t, m_b and m_{E^o} can be arbitrarily large.

*Research supported in part by the Department of Energy.

With the data now available, it is possible to establish uniquely the values of the neutral-current couplings of u and d quarks. The roles of each type of experiment in the determination of these couplings are analyzed in Section II. The section concludes with a discussion of the implications of these results for gauge models of the weak and electromagnetic interactions. Section III contains an analysis of the neutral-current couplings of electrons. The first part of this section presents an analysis of the data based on the assumption that only one Z^o boson exists. The second part discusses a model-independent analysis of parity-violation experiments. The conclusions are given in Section IV.

II. DETERMINATION OF QUARK COUPLINGS

A model-independent analysis[1] of neutrino scattering data has shown that the neutral-current couplings of u and d quarks could be uniquely determined. The input involved four types of experiments which will be discussed separately. The work[1] described here was done together with Larry Abbott.

It is assumed here that there are only V and A currents. The currents of s and c quarks are neglected. The notation used in this section has u_L, d_L, u_R and d_R (L ≡ left and R ≡ right) as the coefficients in the effective neutral-current coupling:

$$\mathcal{L} = \frac{G}{\sqrt{2}} \bar{\nu}\gamma_\mu(1+\gamma_5)\nu\Big[u_L\,\bar{u}\gamma_\mu\,(1+\gamma_5)u + u_R\,\bar{u}\gamma_\mu\,(1-\gamma_5)\,u + d_L\,\bar{d}\gamma_\mu\,(1+\gamma_5)\,d + d_R\,\bar{d}\,\gamma_\mu\,(1-\gamma_5)\,d\Big], \tag{2.1}$$

In the Weinberg-Salam (WS) model[2] with the Glashow-Iliopoulos-Maiani (GIM) mechanism[3] incorporated, u_L is equal to $\frac{1}{2} - \frac{2}{3}\sin^2\theta_W$ with θ_W a free parameter of the theory; u_R, d_L and d_R have similar forms.

Note that there is no assumption about the bosons carrying the neutral current, only an assumption that the effective Lagrangian (2.1) holds.

A. Neutrino-Nucleon Inclusive Scattering

The calculation of deep-inelastic neutrino scattering off nucleons ($\nu N \to \nu X$) is done using the parton model. For sake of discussion only, let us neglect sea contributions and scaling violations (from QCD). For an isoscalar target, one finds that the neutral-current (NC) and charged-current (CC) cross sections for neutrinos are:

$$\sigma_\nu^{NC} = \frac{G^2 mE}{\pi}\int dx\ F(x)\ \left[\left(u_L^2 + d_L^2\right) + \frac{1}{3}\left(u_R^2 + d_R^2\right)\right] \tag{2.2}$$

$$\sigma_\nu^{CC} = \frac{G^2 mE}{\pi}\int dx\ F(x)\ [1] \tag{2.3}$$

Then the ratios for neutrinos and for antineutrinos are

$$R_\nu \equiv \frac{\sigma^{NC}}{\sigma^{CC}} = \frac{\left(u_L^2 + d_L^2\right) + \frac{1}{3}\left(u_R^2 + d_R^2\right)}{(1)} \tag{2.4}$$

$$R_{\bar{\nu}} \equiv \frac{\sigma^{NC}}{\sigma^{CC}} = \frac{\frac{1}{3}\left(u_L^2 + d_L^2\right) + \left(u_R^2 + d_R^2\right)}{\left(\frac{1}{3}\right)} \tag{2.5}$$

Therefore, one can determine the values of $\left(u_L^2 + d_L^2\right)$ and of $\left(u_R^2 + d_R^2\right)$, which are the radii in the left (L) and right (R) coupling planes. The available data[4] are shown in Fig. 1 along with the predictions of the WS model.

Using the data[4] of the CERN-Dortmund-Heidelberg-Saclay (CDHS) group ($R_\nu = 0.295 \pm 0.01$ and $R_{\bar{\nu}} = 0.34 \pm 0.03$), the values of the radii in the L and R planes allowed at the 90% confidence level are shown in Fig. 2.

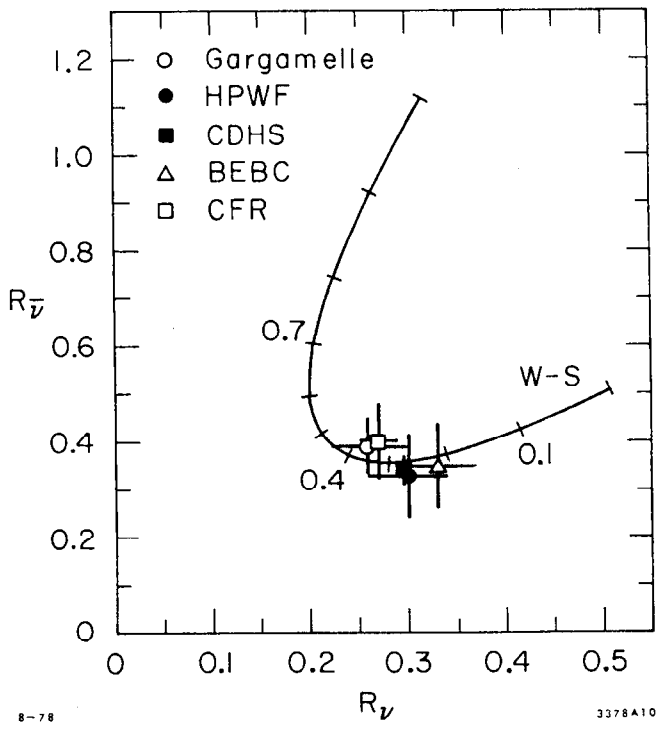

Fig. 1. The ratio of neutral to charged-current deep-inelastic scattering cross sections for antineutrinos versus that ratio for neutrinos. The curve shows the predictions of the WS model as a function of $\sin^2\theta_W$ (each tick mark indicates a tenth value of $\sin^2\theta_W$). The data are from Ref. 4.

An overall sign ambiguity among the four couplings is resolved by requiring $u_L > 0$.

B. Inclusive Production of Pions by Neutrinos

The allowed radii are well determined by deep-inelastic scattering. It remains to determine the allowed angles in the left and right planes. Let us define

$$\theta_L \equiv \arctan\ (u_L/d_L)$$
$$\theta_R \equiv \arctan\ (u_R/d_R) \qquad (2.6)$$

One means of determining the angles is through use of inclusive pion production ($\nu N \to \pi X$). Again parton model assumptions are involved in the calculations. This analysis has been discussed by Sehgal, Hung and Scharbach.[5] It is assumed that pions produced in the current-fragmentation region (leading pions) are decay products of the struck quark. If z is defined as E_π/E_{had} (where E_{had} = [total hadron energy] = energy of the struck quark), then $D_q^\pi(z)$ describes the probability that a given pion has a fraction z of energy of the struck quark q. The calculations are similar to those for inclusive deep-inelastic scattering except that the limited specification of the final state requires that the u couplings be multiplied by $D_u^\pi(z)$ and d couplings by $D_d^\pi(z)$. Then the ratio of π^+ to π^- production for neutrinos is (neglecting sea contributions for discussion only):

$$\frac{N_{\pi^+}}{N_{\pi^-}} = \frac{\left(u_L^2 + \frac{1}{3}u_R^2\right)F_u^{\pi^+} + \left(d_L^2 + \frac{1}{3}d_R^2\right)F_d^{\pi^+}}{\left(u_L^2 + \frac{1}{3}u_R^2\right)F_u^{\pi^-} + \left(d_L^2 + \frac{1}{3}d_R^2\right)F_d^{\pi^-}} \qquad (2.7a)$$

with

$$F_q^\pi \equiv \int_{z_1}^{z_2} dz\, D_q^\pi \tag{2.7b}$$

where one requires $z > z_1$ (leading pions), $z < z_2$ (avoids resonance region) and $E_{had} > E_0$; the values of z_1, z_2, and E_0 depend on the particular experiment.

There are isospin relations

$$D_u^{\pi^+} = D_d^{\pi^-} \quad \text{and} \quad D_u^{\pi^-} = D_d^{\pi^+} \tag{2.8}$$

which help simplify Eq. (2.7). Furthermore, the ratio of $D_u^{\pi^+}$ to $D_u^{\pi^-}$ can be measured in ep scattering and in charged-current neutrino scattering; the relevant ratio is

$$\eta \equiv \int_{z_1}^{z_2} dz\, D_u^{\pi^+}(z) \Big/ \int_{z_1}^{z_2} dz\, D_u^{\pi^-}(z) \tag{2.9}$$

Using Eq. (2.8) and (2.9) in Eq. 2.7, one obtains

$$\left(\frac{N_{\pi^+}}{N_{\pi^-}}\right)_\nu = \frac{\left(u_L^2 + \frac{1}{3}u_R^2\right)\eta + \left(d_L^2 + \frac{1}{3}d_R^2\right)}{\left(u_L^2 + \frac{1}{3}u_R^2\right) + \left(d_L^2 + \frac{1}{3}d_R^2\right)\eta} \tag{2.10}$$

For antineutrinos, Eq. (2.10) holds if one interchanges L and R. There are corrections to Eq. (2.10) from sea contributions and from experimental efficiencies.

The data used here are low energy data from Gargamelle[6] at the CERN PS. These data are $\left(N_{\pi^+}/N_{\pi^-}\right)_\nu = 0.77 \pm 0.14$ and $\left(N_{\pi^+}/N_{\pi^-}\right)_{\bar\nu} = 1.64 \pm 0.36$ for $0.3 < z < 0.7$ and $E_{had} > 1$ GeV. These are shown in Fig. 3 along with the predictions of the WS model.

Recently, high energy data have become available. The neutrino data[6] are not for pions but for all charged particles (within the prescribed cuts); Abbott and I have used electroproduction data to estimate K and p contamination in the signal and find that the results are consistent with the Gargamelle results. The preliminary antineutrino data[6] are also consistent with the low energy data.

We find that the high energy data do not change our conclusions or the final values of the neutral-current couplings obtained from our analysis. However, the error bars would be increased; this is due in part to the fact that the actual quantity used (see Eq. B3 and B4 in the second paper of Ref. 1) involves differences between numbers of the same magnitude.

As can be seen in Fig. 2, the Gargamelle pion-inclusive data (even with 90% confidence levels) place severe restrictions on the allowed angles. However, since the ratios (Eq. 2.10) are functions of the squares of the couplings, there are various sign ambiguities.

C. Elastic Neutrino-Proton Scattering

Further determination of the allowed angles along with resolution of some sign ambiguities can be obtained from analysis[1,7] of elastic neutrino-proton scattering ($\nu p \to \nu p$). Unlike the calculations of Sections IIA and B, no parton model assumptions are needed here. The matrix element for the process is

$$\langle p'|J_\mu|p\rangle = \bar u(p')\left[\gamma_\mu F_1 + \frac{i\sigma_{\mu\nu}q^\nu}{2m}F_2 + \gamma_5\gamma_\mu F_A\right]u(p) \tag{2.11}$$

The vector form factors $\left[F_i(q^2) \text{ and } F_2(q^2)\right]$ are related via CVC to

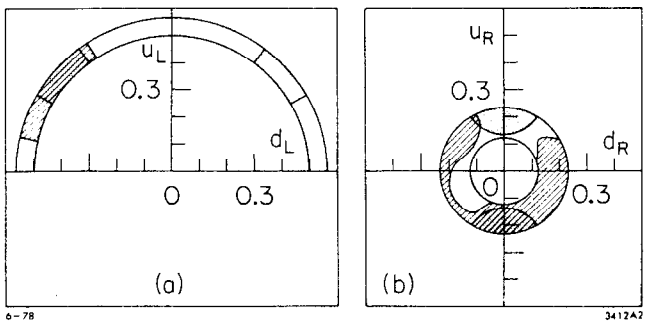

Fig. 2. The left (a) and right (b) coupling-constant planes. The lower half of (a) is omitted due to our sign convention $u_L \geq 0$. The annular regions are allowed by deep-inelastic data. The regions shaded with dots are allowed by inclusive-pion results, and the region shaded with lines is allowed by elastic and exclusive-pion data. Unique determination of the quark coupling values is given by the region shaded with both dots and lines.

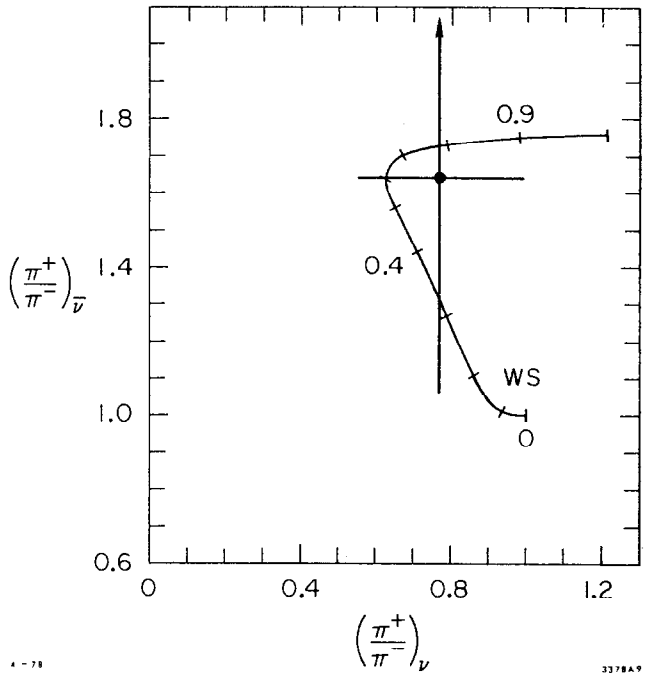

Fig. 3. The ratio of π^+ to π^- multiplicities from inclusive-pion data for antineutrinos versus that ratio for neutrinos. The curve shows the predictions of the Weinberg-Salam model as a function of $\sin^2\theta_W$. The data are from Ref. 5, and 90% confidence limits are shown.

the electromagnetic form-factors of protons and neutrons:

$$\text{Isovector} \quad F_i = F_i^p - F_i^n \tag{2.12}$$

$$\text{Isoscalar} \quad F_i = F_i^p + F_i^n \tag{2.13}$$

The isovector part of the axial-vector form-factor has been measured and has the form:

$$F_A(q^2) = \frac{1.23}{(1 + Q^2/m_A^2)^2} \tag{2.14}$$

where $m_A^2 \approx 0.79$ GeV^2 (our results are not very sensitive to variation of m_A). The isoscalar part of the axial-vector form factor is assumed to have the same Q^2 dependence.

The appropriate factors between these four terms are obtained using the SU(6) wavefunctions of nucleons. The data of the Harvard-Pennsylvania-Wisconsin (HPW) group[8] are $R_\nu \equiv \sigma^{NC}/\sigma^{CC} = 0.11 \pm 0.02$ and $R_{\bar{\nu}} = 0.19 \pm 0.05$ (statistical errors shown). These are shown in Fig. 4 along with the predictions of the WS model.

The resolution of the sign ambiguities remaining from the pion-inclusive data is difficult to see in Fig. 2, since correlations between the left and right planes are not evident. From the pion-inclusive data shown in Fig. 2, one might think that there are 2, 3, or 4 allowed regions. The correlations can be made evident by plotting θ_L vs θ_R (see Eq. 2.6) as in Fig. 5; this can be done "uniquely," because the radii in the left and right planes are well determined. The pion-inclusive data result in four allowed regions (appearing as ellipses in Fig. 5); there would be eight regions except that $d_R \approx 0$ so that four pairs of regions coalesce.

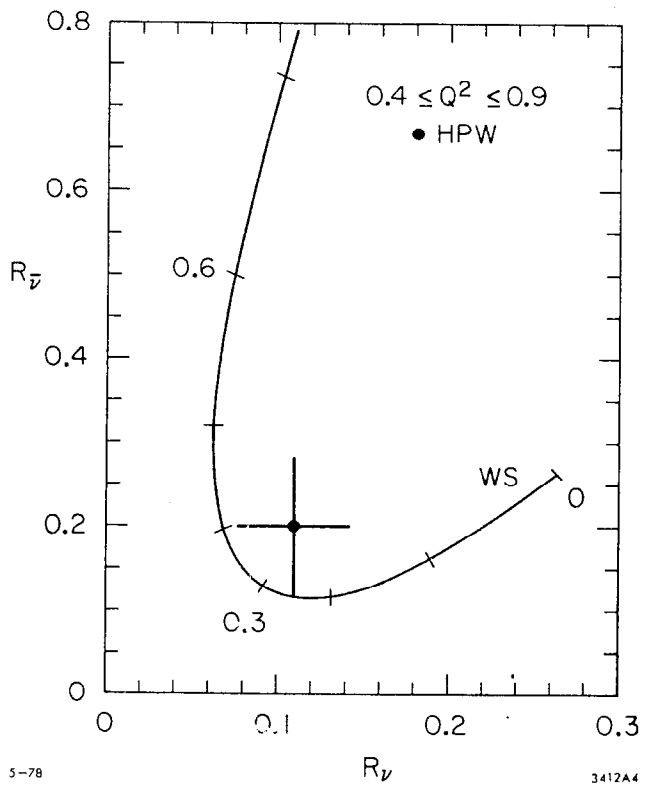

Fig. 4. The ratio of neutral to charged-current elastic νp scattering cross sections for antineutrinos versus that ratio for neutrinos where $0.4 \leq Q^2 \leq 0.9$ GeV^2. The curve shows the predictions of the Weinberg-Salam model as a function of $\sin^2\theta_W$. The data are from Ref. 8, and only statistical uncertainties are shown (at the 90% confidence level).

By "inverting" the νp elastic scattering data (with the analysis described above), one can rule out two of these four regions completely and can rule out substantial portions of one other. Varying portions of two regions do remain allowed. Independent of the pion-inclusive data, the elastic data severely limit the allowed regions in coupling space.

D. Production of Exclusive Pion Modes by Neutrinos

Two of the three remaining allowed regions in Fig. 5 can be ruled out by consideration of the cross-section ratios for six exclusive channels containing a pion:

$$\sigma(\nu p \to \nu p\pi^0)/\sigma_1 \tag{2.15}$$

$$\sigma(\nu n \to \nu n\pi^0)/\sigma_1 \tag{2.16}$$

$$\sigma(\nu n \to \nu p\pi^-)/\sigma_1 \tag{2.17}$$

$$\sigma(\nu p \to \nu n\pi^+)/\sigma_1 \tag{2.18}$$

$$\left[\sigma(\bar{\nu}p \to \bar{\nu}p\pi^0) + \sigma(\bar{\nu}n \to \bar{\nu}n\pi^0)\right]/\sigma_2 \tag{2.19}$$

$$\sigma(\bar{\nu}n \to \bar{\nu}p\pi^-)/\sigma_2 \tag{2.20}$$

with

$$\sigma_1 \equiv \sigma(\nu n \to \mu^- p\pi^0) \tag{2.21}$$

$$\sigma_2 \equiv \sigma(\bar{\nu}p \to \mu^+ n\pi^0) \tag{2.22}$$

where recent Gargamelle data[9] were used.

To analyze the data, the detailed pion-production model developed by Adler[10] was used. This model is superior to all other pion-production models; it includes non-resonant production (an important feature), incorporates excitation of the Δ(1232) resonance, and satisfies current algebra constraints. The model gives quite good descriptions of a variety of data and is crucial for analysis of the Gargamelle data.

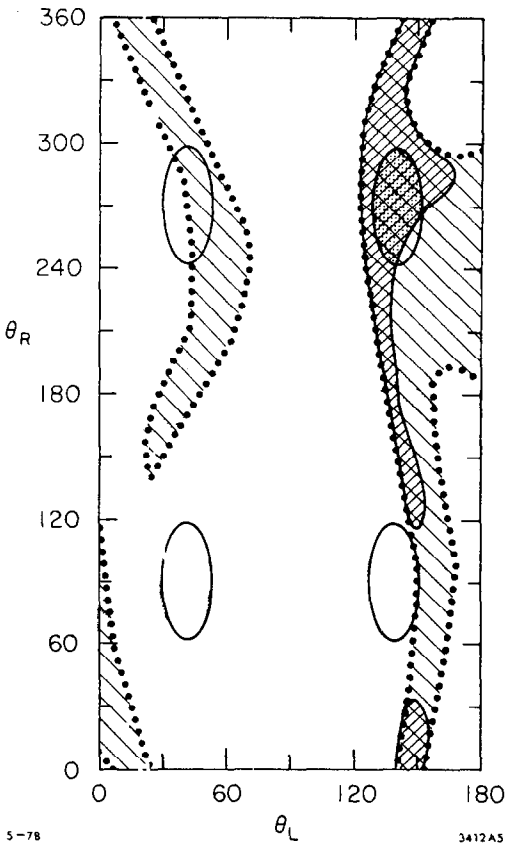

Fig. 5. The allowed angles in the coupling planes of Fig. 2 for fixed radii taken at the center of the allowed annulus ($r_L = 0.53$) in the left-coupling plane and at the outer edge of the allowed annulus ($r_R = 0.22$) in the right-coupling plane. The ellipses indicate the regions allowed by inclusive-pion data; going clockwise from the upper-right, they are regions A, B, C and D, respectively. The area shaded with lines and enclosed with a dotted curve is allowed by elastic data. The region which is cross-hatched is allowed by elastic and exclusive-pion results. The area shaded with dots is the only region allowed by all data.

One begins with the Born amplitudes shown in Fig. 6 which are given in terms of the form factors F_1, F_2 and F_A (described in Section IIIC), F_π (coming from Fig. 6c) and g_r (the pion-nucleon coupling). There are two types of corrections applied.

One comes from using the current algebra relation:

$$T\left\{\partial^\mu J^5_\mu \mathcal{J}\right\} = -\delta(x_0)\left[J^5_0, \mathcal{J}\right] + \partial^\mu T\left\{J^5_\mu \mathcal{J}\right\} \qquad (2.23)$$

(where T indicates time-ordered product, and $\mathcal{J}$ is the weak current of interest). Taking the Fourier transforms and then the matrix element between nucleon states for each piece of Eq. (2.23, one finds from PCAC that the left side is proportional to the desired matrix element $\langle N\pi|\,\mathcal{J}(0)\,|N\rangle$. The first term on the right side leads to additional form factor terms. The second term containing the J^5 current with axial-vector couplings, rather than the pseudo-scalar coupling assumed for the pion, implies certain vertex corrections.

The second type of correction is for final-state interactions; the outgoing pion and nucleon can resonate. In particular, for the appropriate $I = \frac{3}{2}$ terms, one must account for the $\Delta(1232)$ resonance. There are the usual phase shifts ($e^{i\delta_R}$) and enhancement effects for this P_{33} resonance. It is <u>crucial</u> to keep the non-resonant (including $I = \frac{1}{2}$) pieces; both the analysis and the data say those pieces are significant.

To avoid other (higher mass) resonances and for consistency with the soft-pion assumptions of current algebra, it is necessary to require that the invariant mass W of the pion-nucleon system be less than 1.4 GeV. Unfortunately, the data are not available with this cut, and for modes with final-state neutrons it is, of course, quite difficult to obtain the invariant mass. However, the relevance of the cut to our conclusions is

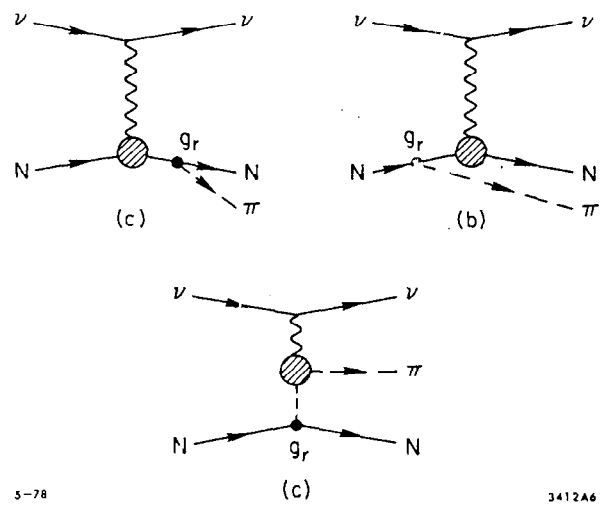

Fig. 6. Born diagrams for the exclusive-pion-production analysis. g_r is the pion-nucleon coupling constant.

minimized because: (1) most data are below the W = 1.4 GeV cut; (2) ratios of cross sections are used; (3) application of the cut to the limited experimental mass plots available indicates a strengthening of our conclusions; and (4) the model predictions are assumed to be valid only to within 30% and the data to the 90% confidence level (this is somewhat different from the procedure followed in the first paper of Ref. 1). This fourth point is approximately equivalent to allowing any theoretical values which lie within a factor of two of the various data.

Our analysis of the six exclusive pion-production channels shows that small values of $\theta_L (\theta_L < 90^\circ)$ are totally forbidden by these data. Recall that there were four regions in Fig. 5 allowed by pion-inclusive data, and that two were ruled out by the elastic data. A third region (with $\theta_L \approx 40^\circ$ and $\theta_R \approx 270^\circ$ in Fig. 5) is now completely ruled out. The region with $\theta_L \approx 140^\circ$ and $\theta_R \approx 90^\circ$, which was forbidden by elastic data, is not allowed by these data either. The exclusion of this latter region by these data alone would be much more marginal than for the regions with $\theta_L \approx 40^\circ$. What remains is a single region (with $\theta_L \approx 140^\circ$ and $\theta_R \approx 270^\circ$) which is in good agreement with all four types of neutrino experiments. This unique determination can be expressed in terms of the coupling constants so that the allowed region (see Fig. 2) is

$$u_L = 0.35 \pm 0.07 \qquad u_R = -0.19 \pm 0.06$$
$$d_L = -0.40 \pm 0.07 \qquad d_R = 0.0 \pm 0.11 \tag{2.24}$$

where the errors are 90% confidence levels and an overall sign convention ($u_L \geq 0$) has been assumed.

E. Implications for Gauge Models

In examining the structure of gauge models of weak and electromagnetic interactions, one of the important questions is whether, in the context of SU(2) × U(1) models, there is any evidence for right-handed charged currents. The neutral-current results are directly relevant to this question and indicate that there are no right-handed charged currents for u or d quarks in SU(2) × U(1) models.

This conclusion can be obtained by consideration of Fig. 7 which shows the allowed regions from Fig. 2. All SU(2) × U(1) models with the left-handed coupling doublet $\bar{u}d_L$ have values in the left-coupling plane (Fig. 7a) which are indicated by the line with tick marks. These models have $\sin^2 \theta_W$ as a free parameter so that the position on the line (i.e., the value of $\sin^2 \theta_W$) is determined solely from the data. Clearly from Fig. 7a, the allowed value of $\sin^2 \theta_W$ is between 0.2 and 0.3.

Now looking at the right coupling plane, Fig. 7b, one sees that for the WS model the values of $\sin^2 \theta_W = 0.2 - 0.3$ are also allowed there. The overall magnitude of these neutral-current couplings was dependent on the mass ratio of $m(Z^\circ)/m(W^\pm)$ which is predicted by the WS model[2] with the minimal Higgs boson structure (one or more doublets) to be:

$$m_{Z^\circ} = m_{W^\pm}/\cos \theta_W \tag{2.25}$$

If this mass ratio were not as predicted, then the model would be ruled out (for example, one might find that $\sin^2 \theta_W = 0.1$ was required by the left-coupling plane, Fig. 7a, but $\sin^2 \theta_W = 0.4$ by the right-coupling plane, Fig. 7b). The success of these predictions of the WS model is remarkable.

For other SU(2) × U(1) models, if one chooses $\sin^2 \theta_W = 0.3$ from the

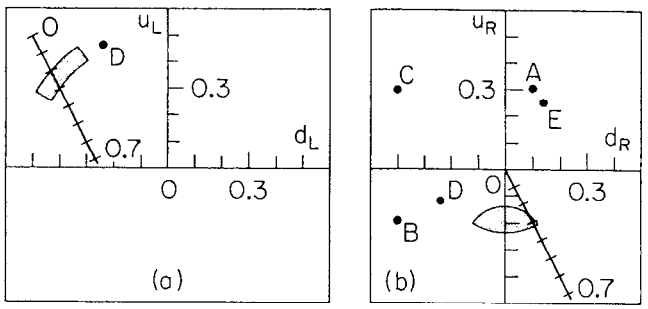

Fig. 7. Various gauge models compared with the allowed coupling-constant region. The lines mark the Weinberg-Salam model for values of $\sin^2\theta_W$ from 0.0 to 0.7. The points labeled A-E are the predictions of various models discussed in the text. For A, B, C, and E, u_L and d_L lie within the allowed region in the left-coupling plane.

left-coupling plane, then the resulting points in the right plane are determined. Shown in Fig. 7b are the points for the cases where the models have the right-handed doublets $\bar{u}b_R$ (labeled A),[11] $\bar{t}d_R$ (B)[12], and both $\bar{u}b_R$ and $\bar{t}d_R$ (C). The latter model (C)[13] has been called the "vector" model. As can be seen, these models are ruled out by the data. Varying the ratio $m(Z^o)/m(W^{\pm})$ moves the points toward or away from the origin, but these models still cannot survive. There are other SU(2) × U(1) models[14] involving $-\frac{4}{3}$ and 5/3 charged quarks, and these are also ruled out.

The applicability of these results is not limited to SU(2) × U(1) models. For example, there are two SU(3) × U(1) models which are ruled out by these data. One[15] (labeled D in Fig. 7b) has the u quark in a right-handed singlet and the other[16] (E) has the u quark in a right-handed triplet (for this latter case the parameters of the model were chosen to place u_L and d_L in the allowed region in Fig. 7a).

These results also apply to the $SU(2)_L \times SU(2)_R \times U(1)$ model.[17] Since that model can be chosen to have the same values of u_L, d_L, u_R and d_R as the WS model, it is allowed by the analysis of quark couplings. In fact, Georgi and Weinberg[18] have generalized this conclusion by showing that at zero-momentum transfer, the neutral-current interactions of neutrinos in an SU(2) × G × U(1) gauge theory are the same as in the corresponding SU(2) × U(1) theory if neutrinos are neutral under G.

III. DETERMINATION OF ELECTRON COUPLING

A. Analysis of Neutrino and Parity Violation Experiments

There are two types of experiments which are used to obtain information about the weak neutral-current coupling of the electron. The first

is neutrino-electron scattering which can be analyzed in a model-independent fashion as was done for quarks. The second involves searches for parity-violation in electron-nucleon interactions. This analysis requires use of the uniquely determined quark couplings obtained in Section II. However, if the results from analysis of parity-violation experiments are to be compared with those from νe scattering (i.e., if g_A and g_V are to be calculated), then one must make the assumption that there is only one Z^o boson which can carry the relevant weak neutral currents.

One type of experiment involves the search for parity-violation in atomic transitions in bismuth. The details of these experiments have been given elsewhere.[19] Clearly such effects are proportional to the VA interference terms, and, in the case of bismuth, the $(V_{hadron}\, A_{electron})$ term is completely dominant. The optical rotation ρ which is measured is then proportional to this term, i.e., $\rho = KQ_w$, where K is a constant and (with the one Z^o assumption)

$$Q_w = -4\, V_{had}\, g_A \tag{3.1}$$

If one defines e_L and e_R as the coefficients in the effective neutral-current coupling:

$$\mathscr{L} \propto \frac{G}{\sqrt{2}}\left[e_L\, \bar{e}\, \gamma_\mu(1+\gamma_5)\, e + e_R\, \bar{e}\, \gamma_\mu(1-\gamma_5)e\right] \tag{3.2}$$

then

$$\begin{aligned} g_A &\equiv (e_L - e_R) \\ g_V &\equiv (e_L + e_R) \end{aligned} \tag{3.3}$$

and

$$\begin{aligned} V_{had} = {} & (2u_L + d_L + 2u_R + d_R)Z \\ & + (u_L + 2d_L + u_R + 2d_R)N \end{aligned} \tag{3.4}$$

where Z and N are the numbers of protons and neutrons (for bismuth, Z=83 and N = 126).

Although there is some question[20] about the atomic and nuclear calculations of K (where $\rho = KQ_w$), present theoretical estimates for K are such that the optical rotations ρ for the two transitions that have been measured are

$$\rho \approx 1.1 \times 10^{-9}\, Q_w \text{ radians} \quad \text{(for 8757 Å)} \tag{3.5}$$

$$\rho \approx 1.5 \times 10^{-9}\, Q_w \text{ radians} \quad \text{(for 6476 Å)} \tag{3.6}$$

Two experiments report results consistent with zero: the Washington group[20] reports $\rho = (-0.5 \pm 1.7) \times 10^{-8}$ for the 8757 Å transition while the Oxford group[21] reports $\rho = (+2.7 \pm 4.7) \times 10^{-8}$ for the 6476 Å transition. By contrast, the Novosibirsk experiment[22] found $\rho = (-21 \pm 6) \times 10^{-8}$ for the 6476 Å transition.

Assuming that there exists only one Z^o boson, then the quark couplings (Eq. 2.24) imply that $g_A \approx 0 \pm 0.06$ for the first two experiments, and $g_A \approx -0.4 \pm 0.17$ for the Novosibirsk experiment.

The other type of experiment for which results have been reported[23] involves νe elastic scattering (with $\nu_\mu e$, $\bar{\nu}_\mu e$ and $\bar{\nu}_e e$ measured by various groups). The cross sections for $\nu_\mu e$ and $\bar{\nu}_\mu e$ scattering are (no Z^o assumption is involved here):

$$\frac{d\sigma^{\nu,\bar{\nu}}}{dE_e} = \frac{G\, m_e}{2\pi}\left[\left(g_V \pm g_A\right)^2 + \left(g_V \mp g_A\right)^2 \left(1 - \frac{E_e}{E_\nu}\right)^2 + \left(g_A^2 - g_V^2\right)\frac{m_e E_e}{E_\nu^2}\right] \tag{3.7}$$

where bottom signs are for antineutrinos. For $\bar{\nu}_e e$ elastic scattering, there is an annihilation term (through a W^- boson), so that in Eq. (3.7) $g_V \to g_V + 1$ and $g_A \to g_A + 1$. Knowledge of these cross sections leads to

allowed regions in a g_A-g_V plot which are ellipsoidal annuli.

Results have been reported for a SLAC experiment[24] involving the deep-inelastic scattering of polarized electrons off deuterium and hydrogen targets. In this experiment one measures the asymmetry between the cross sections σ_p and σ_a with electrons polarized parallel and antiparallel to the beam. If there are weak parity-violating effects, the asymmetry will be non-zero. The asymmetry is sensitive to both the $V_{had}\, A_{elec}$ and $A_{had}\, V_{elec}$ terms, and furthermore involves no difficult atomic or nuclear calculations.

For an isoscalar target (deuterium) the asymmetry (see Ref. 25) is, with the one Z^o assumption:

$$\frac{d\sigma_p - d\sigma_a}{d\sigma_p + d\sigma_p} = 64 \times 10^{-5}\, Q^2 \left\{ \left[\frac{2}{3}(u_L + u_R) - \frac{1}{3}(d_L + d_R) \right] g_A + \left[\frac{1 - (1-y)^2}{1 + (1-y)^2} \right] \left[\frac{2}{3}(u_L - u_R) - \frac{1}{3}(d_L - d_R) \right] g_V \right\} \qquad (3.8)$$

The SLAC experiment on the inelastic scattering of polarized electrons from deuterium has reported an asymmetry of $(-9.5 \pm 1.6) \times 10^{-5}\, Q^2$ where Q^2 is about 1.6 GeV^2 and y = 0.21. This is shown in Fig. 8 along with the predictions of the WS model and the "hybrid" model (described later). Similar results were obtained with hydrogen. A run at a higher value of y may be made in the future.

B. Model Independent Analysis of Parity Violation Experiments

Bjorken[26] has shown how to analyze parity violation experiments in a model-independent fashion (in particular, there is no need to assume that there is only one Z^o boson). One defines the parity-violation

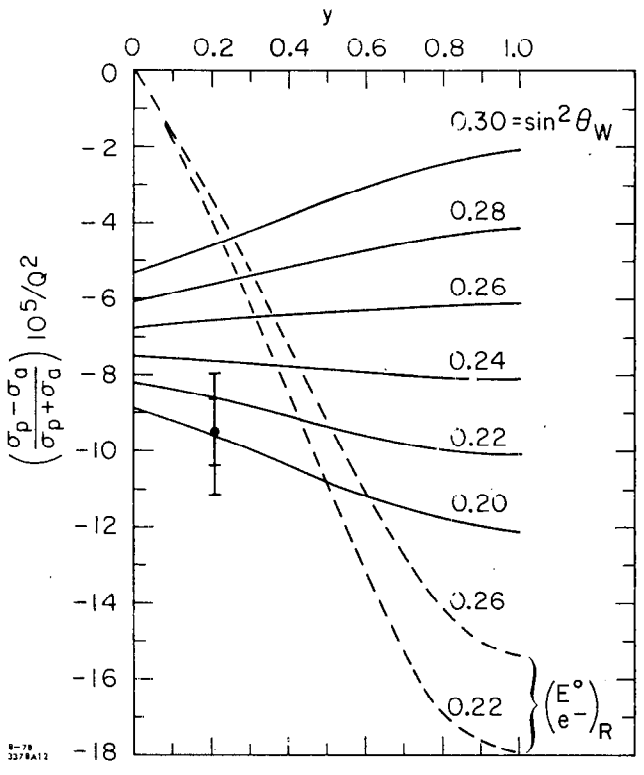

Fig. 8. The asymmetry in the SLAC experiment in which polarized electrons are inelastically scattered off deuterons, shown as a function of $y \equiv (E_e - E_e')/E_e$. The solid (dashed) curves are the predictions of the WS ("hybrid") model for various values of $\sin^2\theta_W$. The data are from Ref. 24 and have Q^2 = 1.6 GeV^2 and y = 0.21. σ_p and σ_a refer to cross sections for electrons polarized parallel and antiparallel to the beam.

parameters $\varepsilon_{VA}^{e,q}$ and $\varepsilon_{AV}^{e,q}$ as the coefficients in the effective Lagrangian

$$\mathcal{L} = \frac{G}{\sqrt{2}}\left[\bar{e}\gamma^{\mu}\, e\left\{\varepsilon_{VA}^{e,u}\,\bar{u}\gamma_{\mu}\gamma_5\, u + \varepsilon_{VA}^{e,d}\,\bar{d}\gamma_{\mu}\,\gamma_5\, d\right\}\right. \\ \left. + \bar{e}\gamma^{\mu}\,\gamma_5\, e\left\{\varepsilon_{AV}^{e,u}\,\bar{u}\gamma_{\mu}\, u + \varepsilon_{AV}^{e,d}\,\bar{d}\gamma_{\mu}\, d\right\}\right] \tag{3.9}$$

It turns out that more information can be obtained about $\varepsilon_{AV}^{e,q}$ than about $\varepsilon_{VA}^{e,q}$ from present data. The implications of the results of the Novosibirsk, Oxford and Washington experiments[20-22] in bismuth and of a "hypothetical" y = 0 polarized-electron deuterium experiment are shown in Fig. 9, along with the predictions of the WS model.

C. Implications for Gauge Models

The WS model predicts $g_A = -0.5$ (independent of $\sin^2\theta_W$) which is not consistent with the results of the Oxford and Washington experiments, but it is consistent with the results of the Novosibirsk experiment. There is an SU(2) × U(1) model which predicts $g_A \approx 0$. This model, called the "hybrid" model, is identical to the WS model except that in addition to the coupling $(\bar{\nu}e)_L$ there is a right-handed coupling $(\bar{E}^0 e)_R$. However, Marciano and Sanda[27] have shown that higher order corrections in the hybrid model make g_A large enough to already be in marginal conflict with the Oxford and Washington experiments. Furthermore, as can be seen in Fig. 8, measurements of the polarized-electron deuteron scattering asymmetry at different values of y should clearly distinguish the hybrid and WS models (it can already be said that the hybrid model is in some conflict with the y = 0.21 measurement).

The three varieties of νe scattering lead to an allowed region in the $g_A - g_V$ plot as shown in Fig. 10. The WS model with $\sin^2\theta_W = 0.2$-0.3

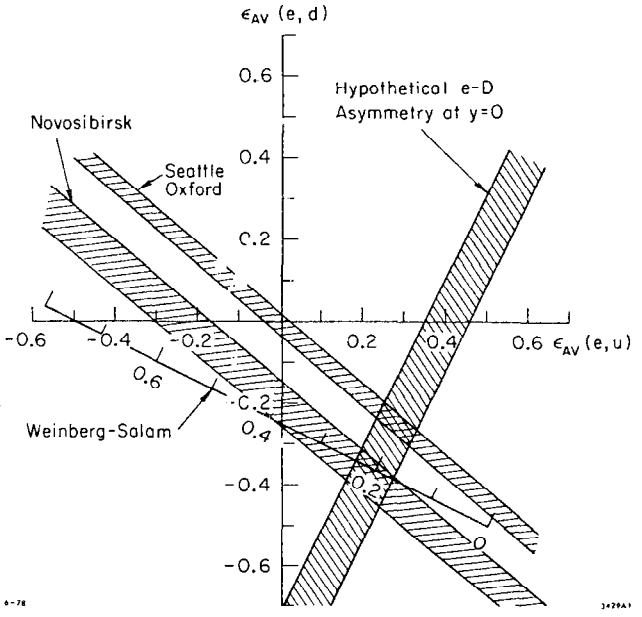

Fig. 9. Allowed values of $\varepsilon_{AV}^{e,q}$, assuming that the measured deep-inelastic polarized-electron deuteron scattering asymmetry represents its value at y = 0.

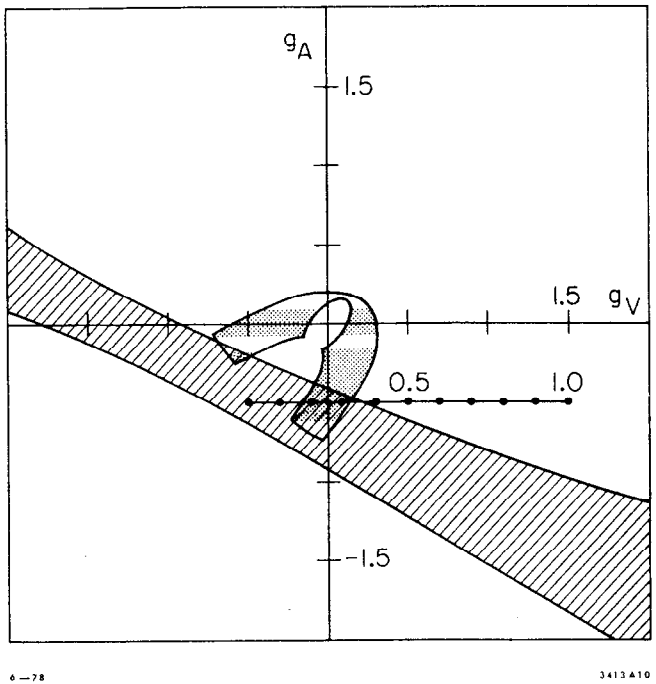

Fig. 10. Ninety percent confidence limits on g_A and g_V of the electron. The horseshoe-shaped area at the center of the figure is the overlap region allowed by the three types of νe scattering experiments. The band shaded with lines is the allowed region from the SLAC polarized-electron-deuteron scattering experiment (Ref. 24) assuming a single Z^o boson and values from Sec. II of quark couplings (including quark error bars). The upper (lower) band shaded with dots is for the Washington-Oxford (Novosibirsk) parity-violation experiments. The predictions of the WS model are shown for tenth values of $\sin^2\theta_W$.

is clearly consistent with the data. Using the single Z^o boson assumption, one can also plot the regions allowed by the two types of parity violation experiments.

The SLAC data rule out that version of the $SU(2)_L \times SU(2)_R \times U(1)$ model which predicted no parity-violation (to lowest order); however, other versions of that model reproduce the WS model's predictions for all neutral-current phenomena.

IV. CONCLUSIONS

The discussion in Sections II and III indicated that most models are ruled out by present analyses, but that the WS model and certain corresponding $SU(2) \times U(1) \times G$ models survive. In general, those models which fail are ruled out by many standard deviations. In contrast, the $SU(2) \times U(1)$ model of Weinberg and Salam agrees within 90% confidence levels with 17 different experimental numbers as shown in the Table. Note that at the 90% confidence level one would expect about 2 of the 17 numbers to disagree with the theory; the fact that none disagrees may indicate that the error bars are conservative. Clearly one should not use only one standard deviation since then 6 numbers would be expected to disagree with theory. Left out of the Table are the results from the atomic parity-violation experiments since there are conflicting experimental results.

If one chooses to believe <u>both</u> the Oxford-Washington result and the SLAC result (and assuming there is no large y dependence), then the standard WS model fails. However, there is a simple extension[28] of the model which can account for all of these phenomena. Consider the group $SU(2) \times U(1) \times U(1)_R$ where neutrinos are neutral under $U(1)_R$. Then all

TABLE

Comparison of WS Theory with Experiment. The theoretical numbers for exclusive pion production contain 30% errors as discussed in the text.

Process	Quantity Measured	90% Confidence Experimental Limits (Statistical + Systematics)	WS Theory $\sin^2\theta_W = 0.25$
$\nu N \to \nu X$	R	.295 ± .02	.31
$\bar{\nu} N \to \bar{\nu} X$	R	.34 ± .05	.36
$\nu N \to \nu \pi X$	N_{π^+}/N_{π^-}	.77 ± .22	.82
$\bar{\nu} N \to \bar{\nu} \pi X$	N_{π^+}/N_{π^-}	1.64 ± .58	1.18
$\nu p \to \nu p$	R	.11 ± .05	.11
$\bar{\nu} p \to \bar{\nu} p$	R	.19 ± .10	.12
$\nu p \to \nu p \pi^0$	R	.56 ± .16	.42 ± .13
$\nu n \to \nu n \pi^0$	R	.34 ± .15	.43 ± .13
$\nu n \to \nu p \pi^-$	R	.45 ± .20	.28 ± .08
$\nu p \to \nu n \pi^+$	R	.34 ± .12	.28 ± .08
$\bar{\nu} N \to \bar{\nu} N \pi^0$	R	.57 ± .16	.39 ± .12
$\bar{\nu} n \to \bar{\nu} p \pi^-$	R	.58 ± .26	.29 ± .09
$\nu_\mu e \to \nu_\mu e$	$\frac{\sigma}{E}\left(\frac{cm^2}{GeV}\right)$	$(1.5 \pm 1.5) \times 10^{-42}$	1.4×10^{-42}
$\bar{\nu}_\mu e \to \bar{\nu}_\mu e$	$\frac{\sigma}{E}\left(\frac{cm^2}{GeV}\right)$	$(1.9 \pm 1.8) \times 10^{-42}$	1.4×10^{-42}
$\bar{\nu}_e e \to \bar{\nu}_e e (1.5 < E_e < 3.0)$	σ (cm^2)	$(5.96 \pm 2.7) \times 10^{-43}$	5.94×10^{-43}
$\bar{\nu}_e e \to \bar{\nu}_e e (3.0 < E_e < 4.5)$	σ (cm^2)	$(3.21 \pm 1.3) \times 10^{-43}$	2.53×10^{-43}
$e_{pol}\, D \to e\, X$	A/Q^2	$(9.5 \pm 2.6) \times 10^{-5}$	7.2×10^{-5}

charged-current interactions and all neutrino interactions are unaffected. The parity-violation experiments here reflect the current

$$J_\mu^{WS} + \rho\, J_\mu^I = 0 \qquad (4.1)$$

where the current resulting from $U(1)_R$ is isoscalar ($\bar{u}u + \bar{d}d$), and ρ is a free parameter which is taken to be small (say 0.1 or 0.2). Since the SLAC result involves differences between u_L and d_L (u_R and d_R), it is little affected by an isoscalar piece (which is multiplied by a small number). However, in the bismuth experiment one measures sums of u_L and d_L, and one finds that it is possible to cancel the effect due to the WS current. While it is possible to achieve this cancellation, it might seem to be a rather artificial or "unnatural" solution to this problem--obtaining zero by cancelling two large numbers against each other.

For the time, it might be best to wait for further atomic physics results on bismuth, thallium and hydrogen before reaching final conclusions. Nonetheless, the essential nature of the weak neutral-current interactions has become quite clear and the success of the Weinberg-Salam model is evident.

ACKNOWLEDGMENTS

The work described here was completed with Larry Abbott. I have benefited from discussions with S. Adler, J. Bjorken, F. Gilman, B. Kayser, W. Kozanecki, W. Marciano, J. Marriner, C. Matteuzzi, E. Monsay, F. Nezrick, Y.-J. Ng, E. Paschos, B. Roe, D. Sidhu, J. Strait, L. Sulak, S. Weinberg, and T. C. Yang. I would like to thank the Aspen Center for Physics (where this talk was prepared) and the Brookhaven National Laboratory theory group (where the written version was prepared) for the stimulating atmosphere each provided and for their hospitality.

REFERENCES

1. L. F. Abbott and R. M. Barnett, Phys. Rev. Lett. 40, 1303 (1978) and SLAC-PUB-2136 (1978) (submitted to Physical Review D). There are many other general discussions of neutral currents; among them are: D. P. Sidhu and P. Langacker, report No. BNL-24393 (1978) and Phys. Lett. 74B, 233 (1978); E. A. Paschos, report No. BNL-24619 (1978) and Phys. Rev. D15, 1966 (1977); F. E. Paige et al., Phys. Rev. D15, 3416 (1977); B. Kayser, NSF report (1978), invited talk at Int. Conf. on Neutrino Physics and Neutrino Astrophysics, Lafayette, Ind., April 28 - May 2, 1978; J. J. Sakurai, report No. UCLA/78/TEP/18 (1978), invited talk at Topical Conf. on Neutrino Physics at Accelerators, Oxford, England, July 4-9, 1978; UCLA/78/TEP/9 (1978), presented at Current Trends in Theory of Fields - 50 years of the Dirac Equation, Tallahassee, Fla., April 6-7, 1978; UCLA/77/TEP/23 (1977), presented at Irvine Conf. on Leptons and Quarks, Irvine, CA, Dec. 2-3, 1977; UCLA/77/TEP/15 (1977), invited talk at Neutrino 77, Elbrus, USSR, June 18-24, 1977; UCLA/76/TEP/21 (1976), invited lectures at Int. School of Subnuclear Physics, Erice, Sicily, June 23 - Aug. 8, 1976; Phys. Rev. Lett. 35, 1037 (1976); in Proc. 4th Int. Conf. on Neutrino Physics and Astrophysics, Dowington, PA., Apr. 26-28, 1974; P. Q. Hung and J. J. Sakurai, Phys. Lett. 72B, 208 (1977), 69B, 323 (1977) and 63B, 295 (1976); G. Ecker, Phys. Lett. 72B, 450 (1978); R. E. Hendrick and L.-F. Li, Carnegie-Mellon report (June 1978); see also Ref. 5, 7 and 10.

2. S. Weinberg, Phys. Rev. Lett. 19, 1264 (1967); A. Salam, in Elementary Particle Physics: Relativistic Groups and Analyticity, edited by N. Svartholm (Almquist and Wiksell, Stockholm, 1968), p. 367.

3. S. L. Glashow, J. Iliopoulos and L. Maiani, Phys. Rev. D2, 1285 (1970).

4. M. Holder et al. (CDHS), Phys. Lett. 72B, 254 (1977); J. Blietschau et al. (Gargamelle), Nucl. Phys. B118, 218 (1977); A. Benvenuti et al. (HPWF), Phys. Rev. Lett. 37, 1039 (1976); P. Wanderer et al. (HPWF), Phys. Rev. D17, 1979 (1978); F. S. Merritt et al. (CF), Phys. Rev. D17, 2199 (1978); P. C. Bosetti et al. (BEBC), Phys. Lett. 76B, 505 (1978).

5. L. M. Sehgal, Phys. Lett. 71B, 99 (1977); P. Q. Hung, Phys. Lett. 69B, 216 (1977); P. Scharbach, Nucl. Phys. B82, 155 (1974); and Ref. 1; recent work: S. Sarkar, Pennsylvania preprint, July 1978.

6. H. Kluttig et al., Phys. Lett. 71B, 446 (1977); J. Marriner, report No. LBL-6438 (1977), Univ. of California Ph. D. Thesis; B. Roe, invited talk at the Topical Conf. on Neutrino Physics at Accelerators, Oxford, England, July 4-9, 1978.

7. Analyses of elastic scattering have been done by S. Weinberg, Phys. Rev. D5, 1412 (1972); M. Barnett, Phys. Rev. D14, 2990 (1976); C. H. Albright et al., Phys. Rev. D14, 1780 (1976); V. Barger and D. V. Nanopoulos, Nucl. Phys. B124, 426 (1977); D. P. Sidhu, Phys. Rev. D14, 2235 (1976); F. Martin, Nucl. Phys. B104, 111 (1976); J. J. Sakurai and L. F. Urrutia, Phys. Rev. D11, 159 (1975).

8. L. Sulak, Harvard report, to appear in the Proc. of the Neutrinos-78 Conf., Purdue University, April 28 - May 2, 1978; J. B. Strait and W. Kozanecki, Harvard University Ph. D. theses (1978); D. Cline et al., Phys. Rev. Lett. 37, 252 and 648 (1976); see also W. Lee et al., Phys. Rev. Lett. 37, 186 (1976); M. Pohl et al., Phys. Lett. 72B, 489 (1978).

9. W. Krenz et al., report No. CERN/EP/PHYS 77-50 (1977); O. Erriques et al., Phys. Lett. 73B, 350 (1978); see also S. J. Barish et al., Phys. Rev. Lett. 33, 448 (1974); W. Lee et al., Phys. Rev. Lett. 38, 202 (1977).

10. S. L. Adler, Ann. Phys. 40, 189 (1968), and Phys. Rev. D12, 2644 (1975); S. L. Adler et al., Phys. Rev. D12, 3501 (1975) and Phys. Rev. D13, 1216 (1976); see also E. H. Monsay, Argonne report ANL-HEP-PR-78-08 (1978); G. Ecker in Ref. 7; and Ref. 1.

11. R. M. Barnett, Phys. Rev. Lett. 34, 41 (1975), Phys. Rev. D11, 3246 (1975); P. Fayet, Nucl. Phys. B78, 14 (1974); F. Gürsey and P. Sikivie, Phys. Rev. Lett. 36, 775 (1976); P. Ramond, Nucl. Phys. B110, 214 (1976).

12. R. M. Barnett, Phys. Rev. D13, 671 (1976).

13. A. De Rújula et al., Phys. Rev. D12, 3589 (19.6); F. A. Wilczek et al., Phys. Rev. D12, 2768 (1975); H. Fritzsch et al., Phys. Lett. 59B, 256 (1975); S. Pakvasa et al., Phys. Rev. Lett. 35, 702 (1975).

14. R. M. Barnett, Phys. Rev. D15, 675 (1977).

15. B. W. Lee and S. Weinberg, Phys. Rev. Lett. 38, 1237 (1977); B. W. Lee and R. E. Shrock, Phys. Rev. D17, 2410 (1978); G. Segre and J. Weyers, Phys. Lett. 65B, 243 (1976).

16. R. M. Barnett and L. N. Chang, Phys. Lett. 72B, 233 (1977); R. M. Barnett et al., Phys. Rev. D17, 2266 (1978); P. Langacker and G. Segre, Phys. Rev. Lett. 39, 259 (1977).

17. J. Pati and A. Salam, Phys. Rev. D10, 275 (1974); H. Fritzsch and P. Minkowski, Nucl. Phys. B103, 61 (1976); R. N. Mohapatra and D. P. Sidhu, Phys. Rev. Lett. 38, 667 (1977); A. De Rújula, H. Georgi and S. L. Glashow, Ann. Phys. 109, 242 and 258 (1977).

18. H. Georgi and S. Weinberg, Phys. Rev. D17, 275 (1978); R. Gatto and F. Strocchi, Geneva report (1978).

19. P. E. G. Baird et al., Nature 264, 528 (1976).

20. N. Fortson, to appear in the Proc. of the Neutrinos-78 Conf., Purdue University, April 28 - May 2, 1978; E. Henley ibid.; W. J. Marciano and A. I. Sanda, Phys. Rev. D17, 3055 (1978) and Rockefeller report No. COO-2232B-153 (1978); G. Feinberg, Columbia report No. CU-TP-111, to appear in the Proc. of the Ben Lee Memorial Int. Conf., Batavia, Ill., Oct. 20-22, 1977.

21. P. G. H. Sandars, in Proc. 1977 Int. Symp. on Lepton and Photon Interactions at High Energies, edited by F. Gutbrod (DESY, Hamburg, 1977) p. 599.

22. L. M. Barkov and M. S. Zolotorev, Pisma Zh. Eksp. Teor. Fiz. (JETP Lett) 26, 379 (1978).

23. F. J. Hasert et al., Phys. Lett. 46B, 121 (1973); J. Blietschau et al., Nucl. Phys. B114, 189 (1976); H. Faissner et al., Phys. Rev. Lett. 41, 213 (1978); A. M. Cnops et al., Phys. Rev. Lett. 41, 357 (1978); P. Alibran et al., Phys. Lett. 74B, 422 (1978); F. Reines et al., Phys. Rev. Lett. 37, 315 (1976).

24. C. Y. Prescott et al., report No. SLAC-PUB-2148 (1978).

25. R. N. Cahn and F. J. Gilman, Phys. Rev. D17, 1313 (1978) and references therein.

26. J. D. Bjorken, report No. SLAC-PUB-2146 (1978).

27. W. J. Marciano and A. I. Sanda, Rockefeller report No. COO-2232B-142 (1978).

28. Private communications from J. D. Bjorken and T. C. Yang. It is possible that other people have also considered such an extension and its application to these two experiments.

FERMILAB-Conf-78/64-THY
August 1978

Weak Decays of Heavy Quarks*

MARY K. GAILLARD†
Fermi National Accelerator Laboratory, Batavia, Illinois 60510
and
Laboratoire de Physique Théorique et Particules Elémentaires,‡ Orsay

---

*Lecture presented at the 1978 SLAC Summer Institute.

†Mailing address: CERN, Geneva, Switzerland.

‡Laboratoire Associé au CNRS.

1. INTRODUCTION

It is generally anticipated that at least two more quark flavors will be discovered sooner or later, and I will discuss some of the properties that may help to identify them: lifetime, branching ratios, selection rules, lepton decay spectra. In addition, there is the exciting possibility that CP violation may manifest itself more strongly in heavy particle decays than elsewhere, providing a new probe of its origin.

Predictions of these properties, however, require some understanding of the dynamics of non-leptonic transitions, and I will first try to convince the reader that theorists have made considerable progress in the understanding of non-leptonic transitions among lighter quarks. As the technology of QCD has been developing there has been a feed-back of application to the long standing problems of non-leptonic K- and hyperon-decay, and a rather staisfactory description of these decay amplitudes has emerged. Within the same framework predictions were made for the decays of the Ω^- and of charmed particles; we shall see how they compare with the data now available.

In addition to a framework for treating strong interaction effects, we need a model for the weak coupling of heavy quarks; I will restrict my discussion to the Kobayashi-Maskawa model. After a brief justification of this choice, I will go into details of its implications for topology and bottomology.

2. DYNAMICS OF NONLEPTONIC DECAYS

The first step is to find the effective local operators which can induce transitions among the quarks in the hadron wave function. For strangeness changing processes the most important operators are four fermion couplings. For example, the quark scattering process

$$s + u \to u + d$$

for all external momenta $<<m_W$ is obtained by summing diagrams of the type shown in Fig. 1. Since gluon exchange conserves helicity, the primary V-A coupling structure is unchanged, but the effective fermi coupling constant gets renormalized, the renormalization factor depending on the color representation of the scattering channel. For a V-A pointlike interaction, scattering occurs in an s-wave spin zero channel which is antisymmetric in the quarks. The color and flavor wave functions must therefore have the same symmetry properties: the final state u and d quarks will have I = 0 for color $\bar{3}$ scattering and I = 1 for color 6 scattering. Since the initial (s, u) state has I = ½, the $\bar{3}$ scattering amplitude is pure $\Delta I = ½$, while the 6 amplitude is a mixture of I = ½ and I = 3/2. It turns out that renormalization effects enhance the effective Fermi coupling constant in the $\bar{3}$ channel and suppress it in the 6 channel. In the leading log approximation,[1] i.e. up to $O\left(\ln(m_W^2/\Lambda^2)^{-1}\right)$

$$G_{F_i}^{eff} = \left(\frac{\alpha_s(\mu^2)}{\alpha_s(m_W^2)}\right)^{\gamma_i} G_F \tag{1}$$

$$\gamma_{\bar{3}} = -2\gamma_6 = 12/(33 - 2N_f) \tag{2}$$

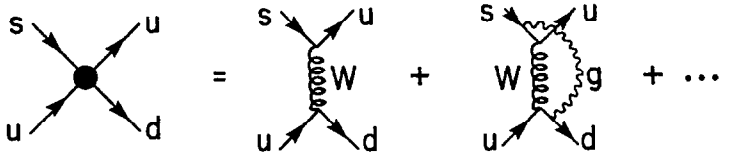

Fig. 1. Effective local $|\Delta S| = 1$ quark scattering operator

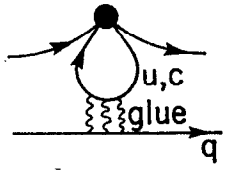

Fig. 2. Generic penguin diagram

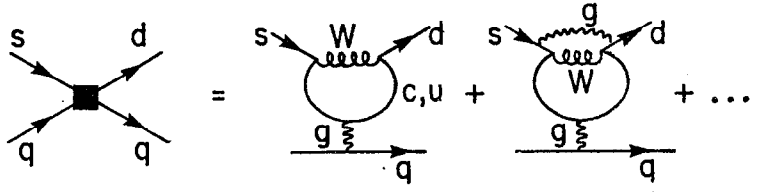

Fig. 3. Dominant effective local $|\Delta S| = 1$ operator generated by a penguin diagram.

$$\alpha_s(Q^2) = \frac{12\pi}{33 - 2N_f} \frac{1}{\ln(Q^2/\Lambda^2)} \tag{3}$$

where m_W is the intermediate boson mass, μ is a typical hadron mass, O(1 GeV), N_f is the number of quark flavors and Λ should be approximately the same as the parameter measured in deep inelastic lepton-hadron scattering experiments.[2] Assuming $N_f = 6$, $\Lambda = 500$ MeV, the numerical results are

$$G_F^{eff}(\bar{3}) \simeq 2.6\, G_F$$

$$G_F^{eff}(6) \simeq 0.6\, G_F \tag{4}$$

giving a factor 4-5 enhancement of $\Delta I = 1/2$ over $\Delta I = 3/2$ amplitudes, which is not by itself sufficient to explain the observed amplitude enhancement factor of about 20.

If the u and c quarks were degenerate (and the mixing with a t quark negligible), the operators discussed above (and denoted by a black circle as in Fig. 1) would be the only operators contributing to $O(1/m_W^2)$. However there is a class of diagrams,[3] generically referred to as "penguin diagrams,"[4] which arise when the external u or c quarks of Fig. 1 are connected and communicate via gluon exchange with other quarks in the hadron wave function as shown in Fig. 2. All these diagrams are pure $\Delta I = \frac{1}{2}$ because gluons cannot transmit isospin. Since these diagrams are unimportant for large internal momenta where the u, c mass difference can be neglected, their strength is characterized by m_c^2 rather than m_W^2. To leading order in μ^2/m_c^2, the dominant effective operator is again a 4-quark operator.[5] (In the valence quark model used below the only other relevant operator is a 6-quark local operator which may have a small matrix element, and operators involving external gluons vanish for soft gluons, so the approximation of

retaining only the 4-quark operator may not be too bad even for penguins.) It will be denoted by a solid square, and the effective coupling is obtained by summing diagrams of the type shown in Fig. 3. The effective quark operator is local because by gauge invariance the s-d-gluon vertex must have a q^2 factor which cancels the pole in the gluon propagator. Again in the leading log approximation (this time to $O\left(\ln(m_c^2/\Lambda^2)^{-1}\right)$, the effective Fermi coupling is given by the value of the lowest order diagram of Fig. 3 times a renormalization factor coming from the sum over extra gluon exchange:

$$G_F^{\text{eff}}(\text{penguin}) \simeq \ln\left(\frac{m_c^2}{\mu^2}\right) \frac{\alpha_s(m_c^2)}{6\pi}\left(\frac{\alpha(\mu^2)}{\alpha(m_c^2)}\right)^{2\gamma_{\bar{3}}} G_F$$

$$\simeq G_F/12 \quad . \tag{5}$$

The effective Fermi coupling is small but the structure of the operator is not of the V-A type:

$$O_{\text{penguin}} = (\bar{d}\lambda_i s)_{V-A}(\bar{q}\lambda^i q)_V \tag{6}$$

where the λ^i are color SU(3) matrices. In order to express the operator in terms of color singlet bilinears, we must perform a Fierz transformation. Writing

$$(\bar{q}\lambda^i q)_V = (\bar{q}\lambda^i q)_{V-A} + (\bar{q}\lambda^i q)_{V+A} \quad , \tag{7}$$

the (V-A)× (V-A) structure is invariant under a Fierz transformation, but

$$(\bar{d}\lambda_i s)_{V-A}(\bar{q}\lambda^i q)_{V+A} \xrightarrow[\text{Fierz}]{} (\bar{d}q)_{S+P}(\bar{q}s)_{S-P} \quad . \tag{8}$$

For q = u, d, the bilinear $(\bar{d}q)_P$ has the quantum numbers of the pion, and this results in a considerable enhancement for certain matrix elements.

The second step is to evaluate the matrix elements of the operators obtained above. This has been done[5] assuming a simple valence quark model for the hadron wave functions. First consider baryon decays: $B \to B' + \pi_c$. The penguin operator has enhanced matrix elements only when two quark lines are attached to the external pion, and we shall neglect it elsewhere. Then the relevant amplitudes are those shown in Fig. 4. Since the baryon wave function is totally antisymmetric under color SU(3), any quark pair is in a $\bar{3}$, and only the enhanced, $\Delta I = \frac{1}{2}$ part, of the quark scattering operator contributes if two quark lines are connected to the same baryon state.[6] Therefore the diagrams 4a-4c are predominantly $\Delta I = \frac{1}{2}$; they can be evaluated in the standard soft pion treatment[7] which relates both s and p wave amplitudes to the baryon-baryon transition matrix elements shown in Fig. 5. In the non-relativistic SU(6) model these are determined in terms of a single parameter, the probability $|\psi(0)|^2$ for finding two quarks at the same point in the baryon wave function. Fig. 4d is pure $\Delta I = 1/2$; Fig. 4e is a mixture of $\Delta I = 1/2$ and 3/2. It vanishes in the chiral symmetry limit ($m_{u,d}, m_\pi^2 \to 0$) while Fig. 4d does not. Neglecting gluon exchange effects other than those included in the renormalized fermi coupling constants the amplitudes can be factorized in terms of matrix elements of quark bilinears:

$$M^{4e} \propto \langle B|J_\mu|B'\rangle\langle\pi|J_\mu|0\rangle \simeq f_\pi \langle B'|\partial_\mu J_\mu|B\rangle$$

$$M^{4d} \propto \frac{1}{m_s m_{u,d}} \langle B|\partial_\mu J_\mu|B'\rangle\langle\pi|\partial_\mu J_\mu|0\rangle \simeq \frac{f_\pi m_\pi^2}{m_s m_{u,d}} \langle B'|\partial_\mu J_\mu|B\rangle \tag{9}$$

where J_μ is the usual V-A current operator and we have used the standard assumption (required in most gauge theories) that they are conserved up to quark mass terms. The pion decay constant f_π is defined by

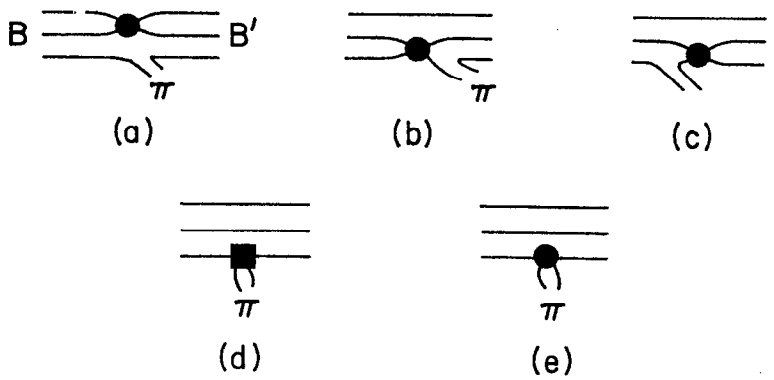

Fig. 4. Matrix elements for baryon decay: $B \to B'\pi$.

Fig. 5. Matrix element for weak baryon to baryon transition.

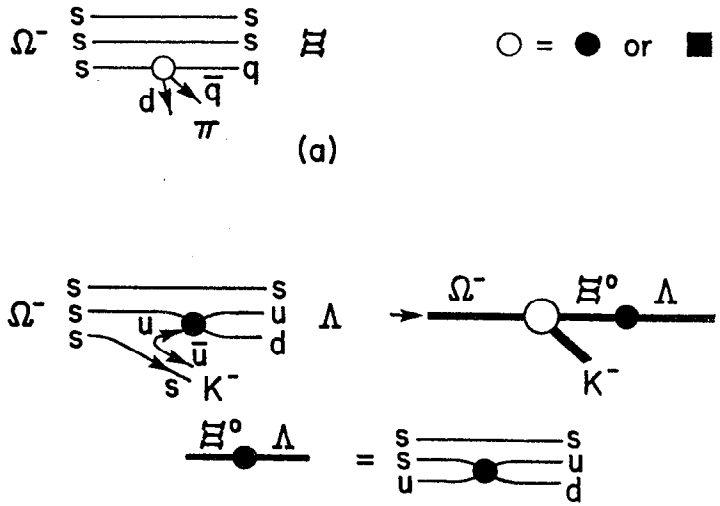

Fig. 6. Matrix elements for Ω^- decay: (a) $\Omega^- \to \Xi\pi$, (b) $\Omega^- \to \Lambda K^-$.

$$\langle \pi | J_\mu | 0 \rangle = f_\pi p_{\pi\mu} \tag{10}$$

As a first remark we see that the $\Delta I = 3/2$ amplitudes, arising solely from Fig. 4e in this approximation are completely determined in terms of the known matrix elements relevant to semi-leptonic decays. They agree[5] with experiment in both sign and magnitude up to a common factor of about 1.5, for both K- and baryon decay (with the possible exception of $\Lambda \to p\pi$). Secondly, using conjectured values[8] for the "current quark" masses:

$$m_u \simeq m_d \simeq 5 \text{ MeV} \quad , \quad m_s \simeq 150 \text{ MeV} \tag{11}$$

we see that matrix element ratio of 4d to 4e is considerably enhanced:

$$M^{4d}/M^{4e} \simeq \frac{m_\pi^2}{m_s m_{u,d}} \simeq 26 \quad . \tag{12}$$

Absorbing this factor into the effective Fermi coupling constant Eq. (5) we get

$$G_F^{\text{eff}}(\text{penguin}) \simeq 2.2 \quad , \tag{13}$$

a coupling comparable to the enhanced $\Delta I = \frac{1}{2}$ part of the quark scattering operator, Eq. (4). Putting everything together, a fit to all baryon decay amplitudes can be made,[5] which determines the single unknown parameter $|\psi(0)|^2$.

Applying the above model to Ω^- decay,[9] the decay amplitudes are uniquely determined by the parameters used to fit baryon decay. In the Ω^- case the amplitudes are particularly simple. For $\Omega^- \to \Xi\pi$ only diagrams of the type 4d and 4e can contribute (see Fig. 6a) because only one strange quark can participate in the quark scattering of Fig. 1. The matrix element factorizes:

$$A(\Omega^- \to \Xi\pi) \propto \langle \Xi | J_\mu | \Omega \rangle \langle \pi | J_\mu | 0 \rangle$$

or $$J_\mu \to \partial_\mu J_\mu \quad .$$

In the SU(3) limit only the axial current contributes to the $\Omega - \Xi$ transition at low q^2 (here $q^2 = m_\pi^2$), and since only the axial current contributes to the π-vacuum transition, the amplitudes are predicted to be nearly parity conserving. For $\Omega^- \to \Lambda K$ the only diagram is that of Fig. 4c. Phenomenologically, it should be dominated by the Ξ^0 pole diagram of Fig. 6b, because of both the proximity of the pole and the large wave function overlap for the spectator baryon. It then depends on the wave function overlap $|\psi(0)|^2$, and will again be predominantly parity conserving. The predicted rates[9] agree with the experimental value[10] within about a factor two. This is well within the theoretical uncertainties on both $|\psi(0)|^2$ and the $\Omega^- \to \Xi^-$ current matrix element. Free of these uncertainties are the predictions of vanishing asymmetry parameters

$$\alpha_{\Omega^-} = 0$$

and the violation of the $\Delta I = \frac{1}{2}$ rule[9]

$$\Gamma(\Xi^0\pi^-)/\Gamma(\Xi^-\pi^0) \simeq 3$$

which are in remarkable agreement with the experimental results[10]

$$\alpha_{K\Lambda} = 0.06 \pm 0.14$$

$$\Gamma(\Xi^0\pi^-)/\Gamma(\Xi^-\pi^0) = 2.93 \pm 0.45 \quad .$$

It should be emphasized that the large (20%) violation of the $\Delta I = \frac{1}{2}$ rule found in $\Omega^- \to \Xi\pi$ strongly supports the idea of a dynamical origin of the approximate $\Delta I = \frac{1}{2}$ rule. In the picture described here, it can be understood by the absence of the $\Delta I = \frac{1}{2}$ dominated diagrams of Figs. 4a-4c.

We turn now to meson decays. The $K \to 3\pi$ decay is successfully determined[11] by soft pion theorems from the $K \to 2\pi$ decay, so we need only consider the latter. The possible diagrams all factorize and are shown in Fig. 7. Fig. 7a gets a contribution only from the operator of Fig. 2 because the strangeness conserving part of the weak current is conserved and cannot create two pions in a zero angular momentum state:

$$\langle \pi\pi(J = 0) | J_\mu | 0 \rangle = 0 \quad .$$

Fig. 7b is given by amplitudes similar to those of Eq. (9). The operator of Fig. 1 gives an amplitude ratio $1/2 : 3/2 \simeq 4\text{-}5$, while the penguin operator of Fig. 2 gives a contribution (Eq. (13)) similar to the enhanced part of Fig. 1, so the overall $\Delta I = \frac{1}{2}$ enhancement for 7b is about a factor 10 (modulo the appropriate Clebsh Gordan factors). Adding 7a and 7b, one finds[5] the experimental enhancement factor of 20 if one suppresses the $\Delta I = 3/2$ part by an extra factor of 1.5 as needed for baryon decays. (This could be due to extra gluon exchange effects.)

Next we turn to charm decays.[3,5,12] First we note several reasons why strong interaction effects should be weaker than for strange particle decays.

a) There are no penguins for the dominant $\Delta C = \Delta S = \pm 1$ transitions, since the basic four-fermi coupling (Fig. 8) involves no identical quarks.

b) The coupling constant renormalization is weaker since the average momentum transfer is characterized by the charmed quark mass:

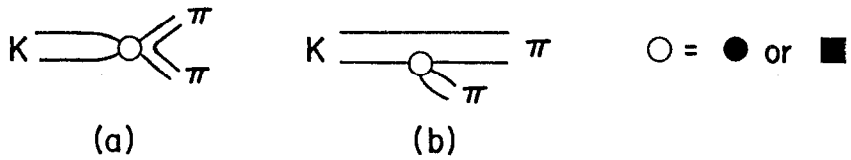

Fig. 7. Matrix elements for $K \to \pi\pi$.

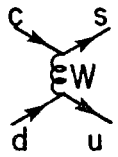

Fig. 8. Dominant $|\Delta C| = 1$ transition process.

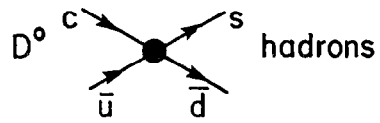

Fig. 9. Matrix element for D^0 annihilation decay channel.

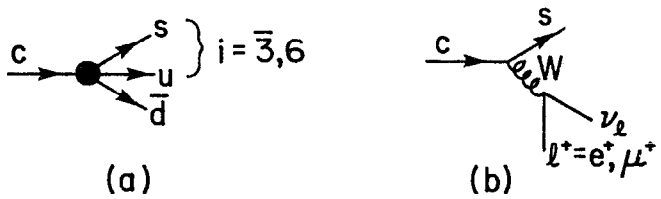

Fig. 10. Matrix elements for inclusive charm decays: (a) non-leptonic and (b) semileptonic.

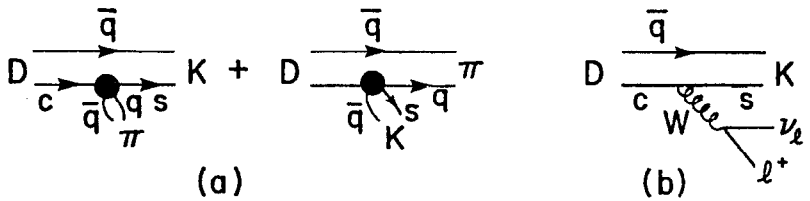

Fig. 11. Matrix elements for exclusive charm decays: (a) $D \to K\pi$, (b) $D \to K\ell^+\nu_\ell$.

$$1 - G^{eff}/G = O\left(\ln(m_W^2/m_c^2)\right) \text{ instead of } O\left(\ln(m_W^2/\mu^2)\right) \quad .$$

c) Because of increased phase space, there is no dynamical suppression of diagrams of the type of Fig. 7b since pion emission, which is suppressed by approximate chiral symmetry, can be replaced by ρ emission, or more generally any spin-1 hadronic system with a mass $\sim$1 GeV.

The processes which can be most readily estimated using QCD technology are inclusive decays and the exclusive channels $D \to K\ell\nu$, $D \to K\pi$. We shall neglect the contribution of Fig. 9 which has branching ratio $\approx f_D^2 m_s^2/m_c^4$ and should be small unless $f_D \gg f_\pi$, where f_D is defined similarly to f_π, Eq. (10). Then the inclusive hadronic and leptonic decay rates, Figs. 10a and 10b, respectively, are given by*

$$\Gamma(D \to \text{hadrons}) \approx \sum_i \left(G_i^{eff}/G_F\right)^2 \left(\frac{m_c}{m_\mu}\right)^5 \Gamma_\mu$$

$$\Gamma(D \to h + \ell\nu) = 2\left(\frac{m_c}{m_\mu}\right)^5 \Gamma_\mu \qquad (14)$$

where Γ_μ is the muon decay rate. The total lifetime prediction

$$\tau_D \approx (1 - 4)\ 10^{-13}$$

is sensitive to the value (1.5 - 2 GeV) used for m_c, but this uncertainty disappears in the total leptonic branching ratio

$$B_e = B_\mu \approx (10\text{-}13)\%$$

where we have again used a 6-flavor model and $\Lambda = 500$ MeV to evaluate the G_i^{eff}. The exclusive decay amplitudes, Fig. 11, are given by*

*Color factors for the hadronic decays are implicit.

$$A(D \to K\pi) = \sum_i G_i^{eff}/\sqrt{2} \langle K|J_\mu|D\rangle\langle\pi|J_\mu|0\rangle$$

$$A(D \to K\ell\nu) = G_F/\sqrt{2} \langle K|J_\mu|D\rangle\langle\ell\nu|J_\mu|0\rangle \quad . \qquad (15)$$

The D-K current matrix element may have large SU(4) breaking corrections. However the relative ratios for different K-π channels are sensitive only to the G_i^{eff}. We find

$$B(D^+ \to \bar{K}^0\pi^+)/B(D^0 \to K^-\pi^+) = 0.77 \quad ,$$

to be compared with the experimental value 0.68 ± 0.33. If we assume SU(4) symmetry we predict

$$B(D^0 \to K^-\pi^+) \simeq (1-4)\% \quad .$$

Using the experimental value of 2.2% to eliminate the uncertainty in the ratio $(m_c/m_\mu)^5/|\langle D|J|K\rangle|^2$, we can predict the fraction of 3-body leptonic decays, finding:

$$B(K\ell\nu)/B(h\ell\nu) \simeq 0.44 \quad .$$

We conclude this section with an optimistic view of our present understanding of non-leptonic decays, and turn to the decays of still heavier quarks. As the quark mass increases, the effects of strong interactions should become weaker still:

$$G_F^{eff}/G_F - 1 \simeq 0\left[\ln(m_Q^2/m_W^2)\right] \to 0$$

as the quark mass approaches the W-mass. Penguin diagrams may be present, but they contain explicit factors of $\alpha_s(m_Q^2)$ which vanish with increasing quark mass. However, before discussing dynamics we must have a model for the weak couplings, which we shall first present and discuss.

3. THE KOBAYASHI-MASKAWA MODEL

This model[14] is a simple extension of the Cabibbo-GIM model[15,16] from four quarks to six. The charged current couplings are pure V-A and are given by

$$\mathcal{L}_{CC} = g W_\mu^\dagger \bar{q}_L \gamma_\mu \frac{\tau^-}{2} U q_L + hc \qquad (16)$$

where U is a 3 x 3 generalized Cabibbo matrix. The phenomenological motivations for restricting our discussion to this model are by now many:

a) It incorporates CP violation in a way which is consistent with low energy phenomenology.[17-19]

b) A V-A coupling is now strongly favored[13] for the τ and its neutrino. Renormalizability of the Weinberg-Salam[20] model then requires[21] a new quark doublet (t, b) with a V-A coupling.

c) With the demise of the high-y anomaly, there is no evidence for right-handed charged couplings (e.g. a $(\bar{u}b)_R$ coupling of the usual strength is ruled out).

d) There is now evidence for parity violation in neutral currents.[22,23] While the situation in atomic physics is still controversial,[24] the SLAC result[23] gives clear evidence for parity violation, removing another motivation for the introduction of right-handed couplings.

e) There are experimental limits[25,10] in the lifetime of the $B^-(b\bar{u})$, expected to be the lightest naked bottom state with a mass around 5 GeV:

$$\tau_B \gtrsim 5 \cdot 10^{-8} - 5 \cdot 10^{-9} \quad \text{if} \quad \sigma_B \gtrsim \sigma_T$$

as expected. This result argues against a new conserved quantum number associated with the b quark which has been suggested in the context of larger flavor groups than SU(2) × U(1) (unless the B decays into a lighter stable lepton). On more speculative theoretical grounds, the K-M model, as embedded in the Weinberg-Salam gauge model, provides the simplest viable possibility for the unification of strong, weak and electromagnetic interactions, namely the Georgi-Glashow SU(5) model.[26] This model has had a certain amount of phenomenological success; it predicts vanishing masses for all neutrinos, and determines the Weinberg angle to be[27,28]

$$\sin^2 \theta_W = 0.20 \quad .$$

Assuming there are only 6 quarks, the "constituent" masses (roughly defined as half the threshold mass for production of the corresponding naked flavor) have been estimated to be[28]

$$m_b \simeq (4.8 - 5.6)\ \text{GeV}$$

$$m_s \simeq (380 - 500)\ \text{MeV} \quad .$$

What concerns us here are the charged current couplings as defined by Eq. (16). The U matrix acts between the quark vectors

$$q_L \to \begin{pmatrix} d \\ s \\ b \end{pmatrix}_L \quad , \qquad \bar{q}_L \to (\bar{u}\ \bar{c}\ \bar{t})_L \tag{17}$$

and can be written explicitly as

$$U = \begin{pmatrix} c_1 & s_1 c_3 & s_1 s_3 \\ -s_1 c_2 & c_1 c_2 c_3 + s_2 s_3 e^{i\delta} & c_1 c_2 s_3 - s_2 c_3 e^{i\delta} \\ -s_1 s_2 & c_1 s_2 c_3 - c_2 s_3 e^{i\delta} & c_1 s_2 s_3 + c_2 c_3 e^{i\delta} \end{pmatrix} . \tag{18}$$

where $s_i \equiv \sin\theta_i$, $c_i = \cos\theta_i$. If $s_i \ll 1$ for all the mixing angles, the matrix (18) simplifies to

$$U \simeq \begin{pmatrix} 1 & s_1 & s_1 s_3 \\ -s_1 & 1 & s_3 - s_2 e^{i\delta} \\ -s_1 s_2 & s_2 - s_3 e^{i\delta} & 1 \end{pmatrix} . \tag{19}$$

In the limit where the t and b quarks decouple, $s_2, s_3 \to 0$, we recover the Cabibbo-GIM matrix with $s_1 = \sin\theta_C$.

Are there any empirical limits on s_2 and s_3? The experimental verification of Cabibbo universality for the ud and us couplings:

$$c_1^2 + s_1^2 c_3^2 \simeq 1 \tag{20}$$

forbids s_3^2 to be too large. Taking into account the experimental errors[29] on the relation (20), one gets the constraint[19]

$$s_3 \lesssim s_1 \simeq \sin\theta_C \simeq 0.23 \quad . \tag{21}$$

A constraint on s_2 is provided by the K_L-K_S mass difference which receives a contribution from top quark exchange:

$$\frac{\Delta m_K}{m_K} \propto s_1^2 \left[m_c^2 + s_2^4 m_t^2 + 2\frac{s_2^2 m_t^2 m_c^2}{m_t^2 - m_c^2} \ln \frac{m_t^2}{m_c^2} \right] \quad . \qquad (22)$$

Since the exchange of a charmed quark of mass 1.5-2 GeV accounts by itself ($s_1^2 = s_c^2$, $s_2^2 = 0$ in Eq. (22)) for the observed mass difference, the top quark contribution cannot be arbitrarily large. Assuming it to be no larger than the charm contribution gives[30]

$$s_2 \lesssim 0.36 \qquad (23)$$

if $m_t > 8$ GeV as suggested by dimuon data.[31] In the 6-quark model CP violation is described by the single parameter δ. From the analysis of CP violation in the kaon system, one finds[30]

$$\frac{1}{2}\left|\frac{\mathrm{Im}\, m_K}{\Delta m_K}\right| \simeq 10^{-3} \simeq s_2 s_3 \sin\delta\, f(m_t^2/m_c^2, s_2^2) \quad . \qquad (24)$$

Since s_2 and s_3 are bound from above, Eq. (24) bounds δ from below, but the bound is very weak:

$$\delta \gtrsim 10^{-3} \qquad \text{for} \qquad 8\ \text{GeV} \lesssim m_t \lesssim m_W \qquad (25)$$

However, an arbitrarily large value of the parameter δ is permitted by present phenomenology.

4. VERY HEAVY QUARK DECAYS

We now turn to the analysis of naked top and bottom decays. To simplify the discussion we

a) ignore the renormalization of the effective coupling constant for the $\Delta B = \pm 1$ analogue of the operator in Fig. 1, since this effect is small. Using the same parameters as in section 2, we find

$$G_F^{\mathrm{eff}}/G_F = 1.4 \quad \text{and} \quad 0.85$$

for the $\bar{3}$ and 6 channels, respectively;

b) characterize the mixing parameters s_2 and s_3 by a common parameter s, expected to be no larger than $s_c \equiv \sin\theta_c \approx 0.2$, and discount the possibility of a strong cancellation between s_2 and s_3 in the elements $s_3 - s_2 e^{i\delta}$, $s_2 - s_3 e^{i\delta}$ in the matrix (19);

c) ignore phases.

Then the mixing matrix (19) is of the approximate form:

$$U \approx \begin{pmatrix} 1 & s_c & s_c s \\ s_c & 1 & s \\ s_c s & s & 1 \end{pmatrix} \quad . \qquad (26)$$

We further assume that the T(9.4) is a $b\bar{b}$ bound state, so that

$$m_t > m_b \simeq 5\ \text{GeV} \quad . \qquad (27)$$

We then obtain immediately a prediction for the relative strengths of different flavor changes in heavy quark decays:

$$\Gamma(t \to b)/\Gamma(t \to s)/\Gamma(t \to d) \simeq F\left(m_b^2/m_t^2\right)/s^2/s^2 s_c^2$$

$$\Gamma(b \to c)/\Gamma(b \to u) \simeq s^2 F\left(m_c^2/m_b^2\right)/s^2 s_c^2 \simeq \frac{1}{3 s_c^2} \simeq 6 \qquad (28)$$

where F(x) is the V-A phase space factor for the decay of a fermion of mass m into a fermion of mass xm and two massless fermions. The $t \to b$ branching ratio is very sensitive to the top quark mass; we find

$$F\left(m_b^2/m_t^2\right) \simeq \begin{cases} 0.05 \\ 1 \end{cases} \text{ if } m_t = \begin{cases} 8 \text{ GeV} \\ m_W \end{cases} . \qquad (29)$$

But since we expect $s^2 \lesssim s_c^2 \simeq 0.06$, we expect in any case a significant $t \to b$ branching ratio:

$$\Gamma(t \to b) \gtrsim \Gamma(t \to s) \simeq 20\,\Gamma(t \to d) . \qquad (30)$$

Since the b-quark is expected to decay predominantly into charm, we anticipate spectacular multilepton events, for example:

$$t \to b + (\text{hadrons or } \ell^+ \nu_\ell)$$
$$\quad\; \downarrow$$
$$\quad\; c + (\text{hadrons or } \ell^- \bar{\nu}_\ell)$$
$$\quad\quad\; \downarrow$$
$$\quad\quad\; s + (\text{hadrons or } \ell^+ \nu_\ell)$$

with a (20-40)% probability for lepton emission at each step. The leptons will be characterized by a high transverse momentum; if the average decay c.m. lepton energy is a third of the energy release we find

$$\langle p_\perp \rangle \simeq \langle E_\ell \rangle_{c.m.} = Q/3 \simeq \begin{cases} 400 \text{ MeV} & c \to s\ell\nu \\ 1 \text{ GeV} & B \to c\ell\nu \\ 3 \text{ GeV} & T(9 \text{ GeV}) \to s\ell\nu \\ 2 \text{ GeV} & T(11 \text{ GeV}) \to b\ell\nu \end{cases} .$$

(For charm decay we would naively predict $\langle E_\ell \rangle_{c.m.} \simeq m_c/3 \simeq$ (500-600) MeV. The observed value of about 400 MeV may be attributable to gluon bremsstrahlung[32] which should be less important for higher mass systems.)

Since the specifics of heavy quark decays are highly mass dependent, we shall hereafter concentrate on b-decay, under the assumptions (27). In Figs. 12 we show[33] the lepton spectra for the process

$$e^+e^- \to \bar{b}b \to \text{hadrons}$$

at a c.m. energy of 20 GeV, assuming an elementary 4-fermion V-A coupling for the decay, and under several assumptions for the quark fragmentation functions. While the precise shape of the spectra are model dependent, their qualitative features are not and the leptons originating at the $b \to c$ vertex (primary) and $c \to s$ vertex (secondary) appear to be separable. Fig. 13 shows transverse momentum distributions using different models for the decay processes. Again the primary and secondary leptons appear separable.

Aside from observing multi-lepton events and measuring lepton decay spectra, we may hope to study final state quantum numbers and look for particular final state configurations such as[34] two-jet decay channels. The basic decay mechanisms are shown in Fig. 14, and the corresponding final state characteristics and estimated branching ratios[30] are given in Table 1. Figs. 14a, b show the dominant free 3-body quark decay mechanism dominated by charmed final states as discussed above, Eq. (28).

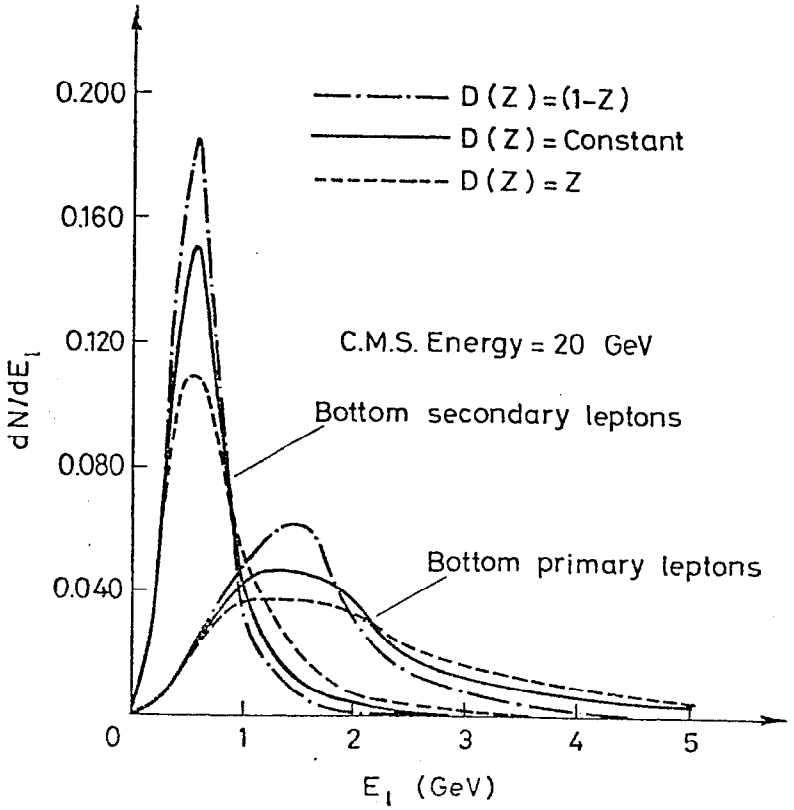

Fig. 12. Energy spectra[33] for primary and secondary leptons from bottom decay in the reaction $e^+e^- \to B^0\bar{B}^0 + X$ at $\sqrt{s}$ = 20 GeV assuming m_B = 5.1 GeV, m_C = 2.0 GeV, m_s = 0.7 GeV, and a V-A four fermion interaction, for different assumptions on the quark fragmentation functions.

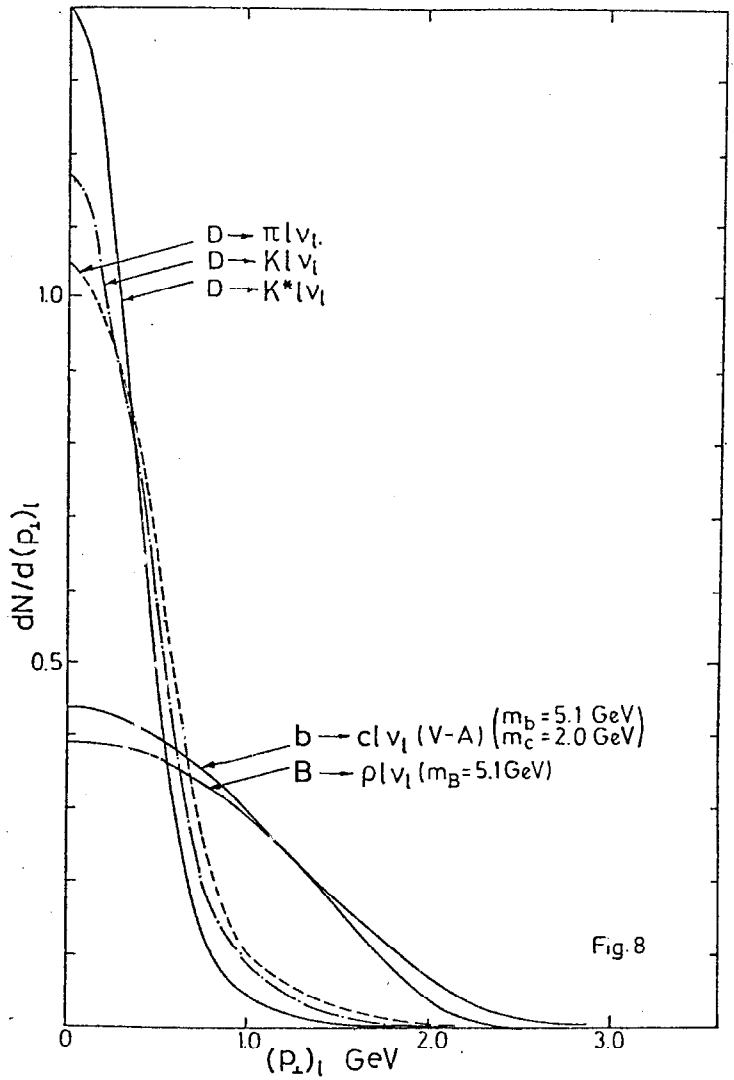

Fig. 8

Fig. 13. Transverse lepton distributions[33] for secondary and primary leptons from bottom decay under different assumptions for decay mechanisms.

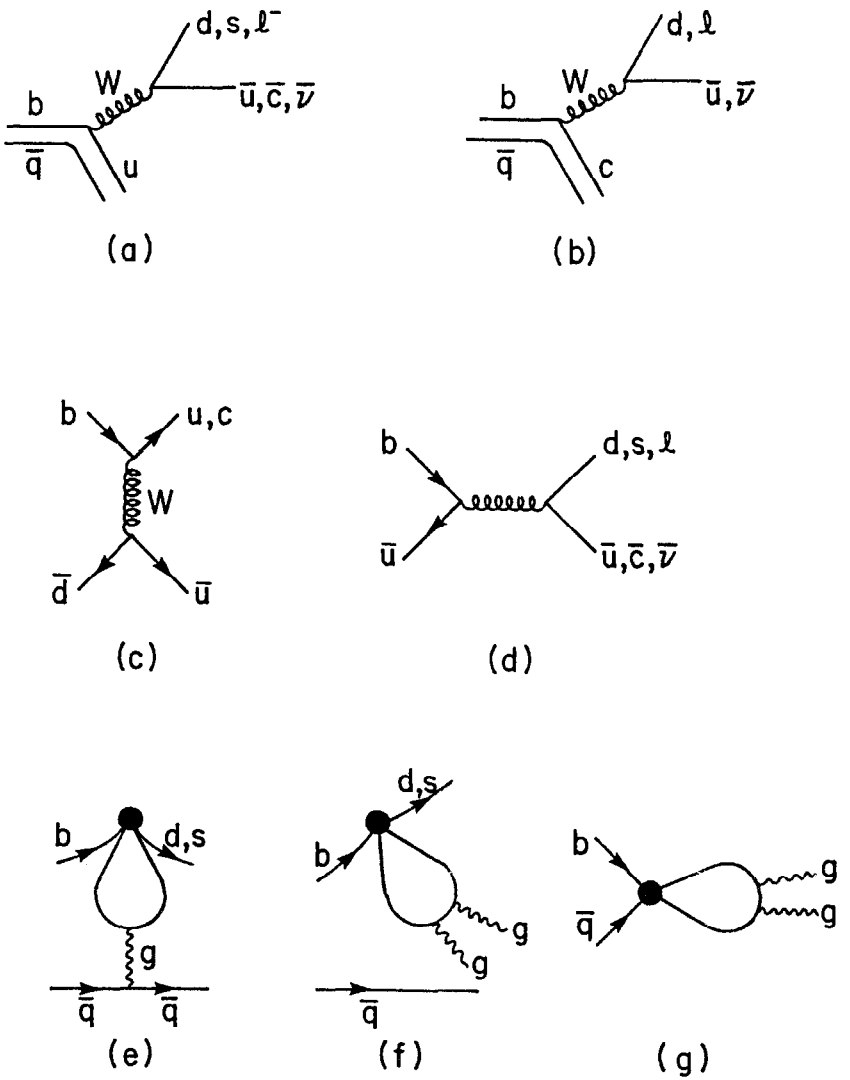

Fig. 14. Diagrams for B($b\bar{q}$) decay.

Figs. 14c, d are annihilation processes which can be more important than for charm decay (cf. Fig. 9) because of the relatively heavy charmed quark which suffers little helicity suppression and because the decay constant f_B (analogue of f_π, Eq. (10)) may be large. Various estimates[34,35] suggest

$$f_B \simeq 500 \text{ MeV} \quad . \tag{31}$$

Figs. 14e-g are the penguin diagrams. Fig. 14g is the bottom-changing analogue of the 4-quark operator of Fig. 3. Its importance depends on the t-quark mass, i.e. on the effectiveness of the generalized GIM cancellation[16] involving t-quark exchange. In any case, there is an explicit factor $\alpha_s(m_b^2)/\pi$ for these diagrams, and their contribution is not expected to exceed several percent of the total decay width. While operators containing external gluons are negligible in the valence quark model used to describe exclusive $|\Delta S| = 1$ decay channels, they need not be a negligible contribution to inclusive decays of a heavy quark. However explicit calculations[30] suggest their contribution is quite small.

Adding up the contributions of table 1, one expects a total branching ratio into charmed particles of (80-85)% and a total semi-leptonic branching ratio of about 35%. Depending on the top quark mass, one can expect a 2-jet configuration in the final state (including one fattish charmed jet) at a level of 5 or 10 percent. In addition there should be[30] $B^- \to \tau^- \nu_c$ decays at a level of about one percent, and semi-leptonic decays into a $(\tau \nu_e)$ pair at a similar level.

The total lifetime is estimated to be[30]

$$\tau_B \simeq 4 \times 10^{-15} (s_2^2 + s_3^2 + 2 s_2 s_3 \cos\delta)^{-1} \quad . \tag{32}$$

Table 1

Mechanisms for bottom decay

Diagram (Fig. 14)	Final State	$\left(\frac{\text{Amplitude}}{G_F s}\right)^2$	Branching Ratio (%)
(a)	$B \to$ hadrons	$3s_c^2 \simeq 0.15$	7
	$B \to \bar{c}$ + hadrons	$s_c^2 \simeq 0.05$	2
	$B \to \ell^- \bar{\nu}_\ell$ + hadrons	$2s_c^2 \simeq 0.10$	5
(b)	$B \to c$ + hadrons	$3 \times \frac{1}{3} \simeq 1$	45
	$B \to c + \ell^- \nu_\ell$ + hadrons	$2 \times \frac{1}{3} \simeq \frac{2}{3}$	30
(c)	$B^0 \to$ 2 jets	$\frac{f_B^2 m_u^2 s_c^2}{m_b^4} \sim 10^{-4}$	-
	$B^0 \to c$ + jet	$f_B^2 \frac{m_c^2}{m_b^4}\left(1 - \frac{m_c^2}{m_b^2}\right)^2 \sim 0.10$	5
(d)	$B^- \to$ 2 jets	10^{-3}	-
	$B^- \to c$ + jet	$s_c^2 \simeq 0.05$	2
	$B^- \to \ell\nu$	~ 0	-
	$B^- \to \tau\nu$	0.02	1
(e)	$B \to$ 2 jets	$\left[\frac{\alpha_s(m_b^2)}{\pi} \ln\left(\frac{m_t^2}{m_b^2}\right)\right]^2 \lesssim .13$	<6
(f)	$B \to$ hadrons ($\Delta S \neq 0$)	10^{-3}	-
(g)	$B \to$ 2 fat jets ($\Delta S \neq 0$)		

Using the upper bounds on s_3 and s_2 Eqs. (21) and (23), we obtain a lower limit on the lifetime:

$$\tau_B \gtrsim 10^{-13} \quad . \tag{33}$$

The upper limit obtained by exploiting (21) and (23)-(25) is one or two order of magnitudes longer.

The above analysis applies to the pseudoscalar $B^-(b\bar{u})$ and $B^0(b\bar{d})$ states which are expected to be the lightest naked bottom states. A similar analysis can be carried out for the strange state $B_s(b\bar{s})$, which should be very close in mass to the B^0, B^- doublet.

5. MASS MIXING AND CP VIOLATION

Second order weak interaction effects induce the flavor changing ($|\Delta F| = 2$) transitions responsible for neutral particle mixing: $K^0 \leftrightarrow \bar{K}^0$, $D^0 \leftrightarrow \bar{D}^0$, $B^0 \leftrightarrow \bar{B}^0$, etc. Just as in the cases of non-leptonic decays the effective local quark operator can be derived[36] from the (gluon radiative-corrected[37]) quark scattering diagrams as indicated in Fig. 15. The leading operator is again a V-A four fermion operator, and in the valence quark approximation for meson wave functions its matrix element factorizes:

$$\Delta m_P \propto \langle \bar{P}^0 | J_\mu | 0 \rangle \langle 0 | J_\mu | P^0 \rangle = f_p^2 m_p^2$$

$$P = K, D, B, \ldots \quad . \tag{34}$$

However in the K-M model the effective Fermi coupling constant is in general complex; the strength of the amplitudes of Fig. 15 determines the amount of mass mixing, while their imaginary part governs the CP violation.

Mass mixing and CP violation in the $B^0\bar{B}^0$ system might be measurable by studying dilepton production in the process

$$e^+e^- \rightarrow B^0\bar{B}^0$$

near threshold. Mass mixing will produce "same sign" dilepton pairs:

$$\begin{array}{l} e^+e^- \rightarrow B^0\bar{B}^0 + X \\ \quad \hookrightarrow \bar{c}\ell^+\nu_e \\ \quad \hookrightarrow \bar{B}^0 \rightarrow \bar{c}\ell^+\nu_e \end{array} \quad .$$

and CP violation would produce a charge asymetry:

$$N(\ell^+\ell^+) \neq N(\ell^-\ell^-) \quad .$$

However if B decays predominantly into charm as anticipated, a same sign dilepton background would arise from cascade decays:

$$\begin{array}{l} e^+e^- \rightarrow B^0\bar{B}^0 \\ \quad \hookrightarrow \bar{c}\ell^+\nu_e \\ \qquad \hookrightarrow \text{hadrons} \\ \quad \hookrightarrow c + \text{hadrons} \\ \qquad \hookrightarrow \ell^+\nu_e + \text{hadrons} \end{array} \quad .$$

The determination of the mass mixing will then depend on the feasibility of separating primary and secondary leptons as discussed above (Fig. 12); CP violating effects will be measurable only to the extent that the mass mixing is appreciable.

This may indeed be the case, in contrast to $D^0 - \bar{D}^0$ mixing which is predicted to be negligible. In terms of the same sign dilepton rate, the mixing parameter can be expressed as[38]

$$r_1 = \frac{\sqrt{N^{++}N^{--}}}{N^{+-}} = \frac{\Delta}{1+\Delta}$$

$$\Delta = \frac{(\Delta\Gamma)^2/4 + (\Delta m)^2}{2\Gamma + (\Delta m)^2 - (\Delta\Gamma)^2/4} \qquad (35)$$

where if $m_{1,2}$ and $\Gamma_{1,2}$ are the physical mass and width of the decay eigenstates:

$$\Delta m = m_1 - m_2 \;,\quad \Delta\Gamma = \Gamma_1 - \Gamma_2 \;,\quad 2\Gamma = \Gamma_1 + \Gamma_2 \quad . \qquad (36)$$

We see that the effect will be important if $\Delta m/\Gamma$ and/or $\Delta\Gamma/\Gamma$ is large. For the neutral kaon system, mixing is maximal because both the total decay rate and the mixing amplitude (Fig. 16a) are characterized by small angles:

$$\Gamma_K, \Delta\Gamma_K \propto s_c^2 \quad , \quad \Delta m_K \propto s_c^2 m_c^2 \;,\; s_c^2 s^4 m_t^2 , \qquad (37)$$

and because the GIM mechanism which acts to suppress mixing is badly broken by the c-u mass difference. In fact it is totally ineffective in suppressing $\Delta\Gamma$ since charmed final states are energetically forbidden; the nonleptonic decay modes carry no net flavor and are common to both K^0 and $\bar{K}^0$ decay. In contrast, charm decay is not suppressed by a small angle while the mixing parameters are: the decay modes common to D^0 and $\bar{D}^0$ are the Cabibbo suppressed uncharmed ones. In addition, to the extent that the bottom quark coupling can be neglected ($s^2 << 1$), the GIM cancellation is more effective, broken only by the s-d mass difference (Fig. 16b)

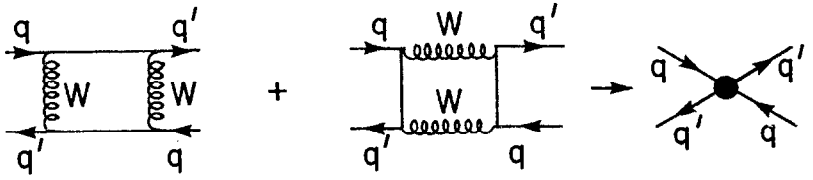

Fig. 15. Effective local operator for $|\Delta F| = 2$ transitions.

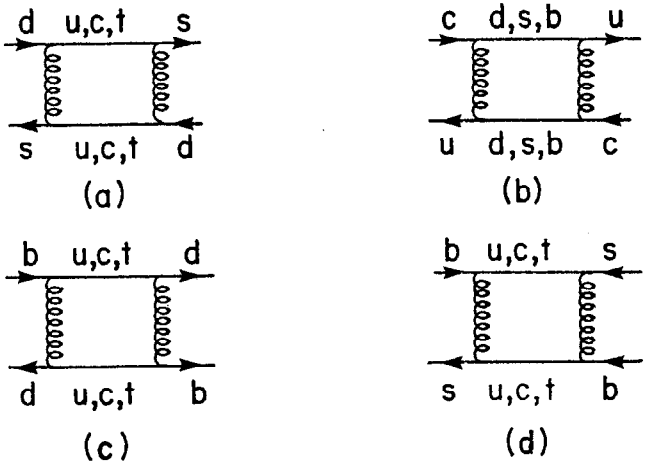

Fig. 16. Diagrams contributing to (a) $K^o - \bar{K}^o$, (b) $D^o - \bar{D}^o$, (c) $B^o - \bar{B}^o$, and (d) $B_s^o - \bar{B}_s^o$ mixing.

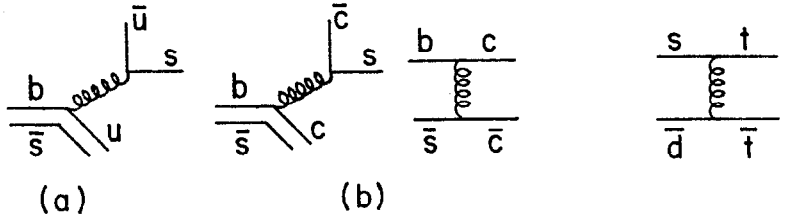

Fig. 17. B_s decays into flavor neutral final states which are suppressed by (a) angles or (b) phase space.

Fig. 18. Zweig suppressed CP violating contribution to $|\Delta S| = 1$ decay amplitudes.

$$\Gamma_D \propto 1, \ \Delta\Gamma_D \propto s_c^2, \Delta m_D \propto s_c^2 m_s^4/m_c^2, \ s_c^2 s^4 m_b^2 \quad . \tag{38}$$

For the neutral B-system, the situation is more analogous to the kaon case; the decay rates are suppressed by the same small angles as the mass mixing (Fig. 16c), or by phase space for the favored decay into charm. $\Delta\Gamma$ arises only from non-charmed final states, and so should not be too large:

$$\Gamma_B \propto s_c^2 s^2 \ , \ \tfrac{1}{3} s^2 \quad ; \quad \Delta\Gamma_B \propto s_c^2 s^2 \quad ; \quad \Delta m_B \propto s_c^2 s^2 m_t^2 \quad . \tag{39}$$

For the strange neutral bottom state $B_s(b\bar{s})$, mixing will be enhanced even further since the Cabibbo suppression of b-s mixing (Fig. 16d) is weaker than for b-u mixing, while Cabibbo favored decay channels are still suppressed by phase space. $\Delta\Gamma$ will be very small, since the final states common to B_s^o and $\bar{B}_s^o$ are highly suppressed by angles (Fig. 17a) or by phase space (Fig. 17b):

$$\Gamma_{B_s} \propto s_c^2 s^2, \ \tfrac{1}{3} s^2 \quad ; \quad \Delta\Gamma_{B_s} \propto s_c^4 s^2 \quad ; \quad \Delta m_{B_s} \propto s^2 m_t^2 \quad . \tag{40}$$

For the kaon system, the measured mixing parameters are

$$\frac{\Delta m_K}{\Gamma_K} \simeq \frac{1}{2} \quad , \quad \frac{\Delta\Gamma_K}{\Gamma_K} \simeq 1 \quad . \tag{41}$$

The measured value of Δm_K agrees in sign and magnitude with the value calculated[36] neglecting top exchange if $m_c \simeq 1.5$ GeV. For neutral heavy quark systems, the predictions obtained from the analysis of the mixing (Fig. 16) and decay (e.g. Figs. 14 and 17) amplitudes are

$$\frac{\Delta m_c}{\Gamma_c} \simeq \frac{\Delta \Gamma_c}{\Gamma_c} \propto 10^{-4} \tag{42}$$

for the $D^o - \bar{D}^o$ system,[39,19]

$$\frac{\Delta m_B}{\Gamma_B} \simeq \left(\frac{m_t}{26\ \text{GeV}}\right)^2 \gtrsim 0.1 \quad , \quad \frac{\Delta \Gamma_B}{\Gamma_B} \simeq (0.10 - 0.15) \tag{43}$$

for the $B^o(b\bar{d})$ system,[30] and

$$\frac{\Delta m_{B_s}}{\Gamma_{B_s}} \simeq \left(\frac{m_t}{6\ \text{GeV}}\right)^2 > 1 \quad , \quad \frac{\Delta \Gamma_{B_s}}{\Gamma_{B_s}} \lesssim 10^{-2} \quad . \tag{44}$$

for the $B_s^o(b\bar{s})$ system.[40]

The six quark model was introduced by Kobayashi and Maskawa in 1973 as a mechanism for incorporating CP violation into the standard Weinberg-Salam-GIM model.[20,16] Their observation[14,18] was the following. For a theory with n weak isospin quark doublets, the mixing matrix U will be an n x n unitary matrix which is specified by n^2 real parameters. Of these, $(n^2 - n)/2$ define a real orthogonal matrix, so there will be $(n^2 + n)/2$ phases. However since all couplings in the theory are flavor diagonal except for the charged current coupling, Eq. (16), the matrix U can be redefined by any flavor diagonal phase transofrmation

$$u \to e^{i\alpha_u} u \quad , \quad d \to e^{i\alpha_d} d, \quad \text{etc.} \quad ,$$

which leaves invariant the remainder of the Lagrangian. Any phase which can be removed from U by such a transformation is unobservable. There are a total of 2n quark flavors, and therefore 2n independent invariant phase transformations. However a phase common to all the charge 2/3 quarks has the same effect on U as a phase common to all the charge -1/3 quarks, so there are 2n - 1 independent transformations which can be made to redefine U, leaving as the number of observable phases:

$$\frac{n^2 - 3n + 2}{2} = \begin{cases} 0 & n = 2 \\ 1 & n = 3 \\ >1 & n > 3 \end{cases} \quad . \tag{45}$$

There is no observable phase in the 4-quark model, while CP violation in the KM model is uniquely specified[41] by a single phase parameter. It will vanish in the limit where

a) any quark pair decouples, since then the mixing matrix reduces to the 2 x 2 case, and

b) any two quarks of the same charge are degenerate in mass, since then there is an extra invariance which can be exploited to remove the remaining phase.

For low energy CP violation phenomenology, the model mimics the super weak model. In order for CP violation to occur, the mixing of the light quarks to the heavy (t, b) doublet has to play a role. For lowest order $|\Delta S| = 1$ decay amplitudes, CP violation will depend on the highly Zweig suppressed component of a $(t\bar{t})$ sea in the hadron wave functions, and the CP violating amplitude, Fig. 18, is purely $\Delta I = \frac{1}{2}$. CP violation in higher order weak transitions as in Fig. 16a arise from virtual top exchange. While it vanishes in the limit of quark mass degeneracy, $\Delta m_q^2/m_W^2 \to 0$, the large top mass splitting makes CP violation in the kaon mass matrix the dominant effect for transitions among light quarks. In particular the neutron dipole moment is predicted to be even smaller than in the super weak model.[19,42] In all processes involving light quarks, CP violating amplitudes are characterized by the suppression factor

$$s_2^2 s_3^2 \sin^2\delta \quad , \tag{46}$$

which knows about the coupling to heavy quarks as well as the CP violating phase.

CP violation in the $B^0\bar{B}^0$ system can be much larger than in the $K^0\bar{K}^0$ system. For kaons, the dominant contribution to $|\Delta m_K|$ comes from u, t exchange, $\propto \sin^2\theta_c$, while the top quark contribution, necessary to generate a phase is suppressed by the additional factor (46). On the other hand, for the $B^0(b\bar{d})$ system, the contributions from u, c, and t exchange are all of order $s_c^2 s^2$, so the system "knows" maximally about the full quark mixing. If we define the complex parameters $\Delta\bar{m}_P$ and $\Delta\bar{\Gamma}_P$ respectively as the dispersive (virtual intermediate states as in Fig. 16) and absorptive (real intermediate states) of the $P^0 \leftrightarrow \bar{P}^0$ mixing amplitude:

$$A(P^0 \leftrightarrow \bar{P}^0) = \Delta\bar{m}_P - i\frac{\Delta\bar{\Gamma}_P}{2} \quad , \tag{47}$$

the CP violating charge asymmetry in same sign dilepton events in e^+e^- annihilation can be expressed as[38]

$$r_2 = \sqrt{\frac{\bar{N}^{--}}{\bar{N}^{++}}} = \left| \frac{\Delta\bar{m} - i\Delta\bar{\Gamma}/2}{\Delta\bar{m}^* - i\Delta\bar{\Gamma}^*/2} \right| \quad . \tag{48}$$

If CP violation is present, r_2 can differ from unity. The effect will vanish if Δm and $\Delta\Gamma$ have the same phase, but also if $|\Delta m/\Delta\Gamma|$ or $|\Delta\Gamma/\Delta m| \ll 1$. The effect is therefore maximal if $|\Delta m|$ and $|\Delta\Gamma|$ are comparable. In order for it to be measurable, there must be an appreciable same sign dilepton rate; r_1 in Eq. (35) cannot be too small.

For the $B^0(b\bar{d})$ system, if $m_t \simeq 8$ GeV, we find

$$|\Delta m_B| \backsim \left|\frac{\Delta\Gamma_B}{2}\right| \backsim 0.1\,\Gamma_B$$

$$r_1 \backsim 10^{-2} \quad , \quad r_2 = \frac{1+\sin\delta}{1-\sin\delta} \quad . \tag{49}$$

As m_t increases, $|\Delta m_B|$ increases relative to Γ_B and $|\Delta\Gamma_B|$, so the mixing gets more important but the CP violation decreases for fixed δ. For $m_t \gg 8$ GeV:

$$|\Delta\Gamma_B| \ll |\Delta m_B| \backsim \Gamma_B$$

$$r_1 = O(1) \quad , \quad r_2 \simeq 1 - 2\sin\delta\left(\frac{8\ \text{GeV}}{m_t}\right)^2 \quad . \tag{50}$$

Since δ is arbitrary, there are at least some values of m_t where these effects may be large enough to be measured. For the $B_s(b\bar{s})$ system[40] the mixing is expected to be large, but the CP violating effects are expected to be small

$$|\Delta m_{B_s}| \gtrsim \Gamma_{B_s} \gg |\Delta\Gamma_{B_s}|$$

$$r_1 = O(1) \quad , \quad r_2 \lesssim O(10^{-2}) \quad . \tag{51}$$

In conclusion, there is a case for putting some effort into an experimental study of $B^0\bar{B}^0$ mixing, since it offers some hope of shedding new light on the elusive problem of the origin of CP violation.

ACKNOWLEDGMENT

I am happy to thank Chris Quigg and the Fermilab theory group for the hospitality extended while these notes were prepared.

REFERENCES

[1] M.K. Gaillard and B.W. Lee, Phys. Rev. Letters 33, 108 (1974); G. Altarelli and L. Maiani, Phys. Letters 52B, 351 (1974).

[2] See the lectures by D. Perkins, these proceedings.

[3] J. Ellis, M.K. Gaillard and D.V. Nanopoulos, Nucl. Phys. B100, 313 (1975).

[4] M. Franklin, private communication.

[5] M.A. Shifman, A.I. Vainstein, V.I. Zakharov, JETP Letters 22, 55 (1975); Nucl. Phys. B120, 316 (1977); ITEP preprints 63 and 64 (1975).

[6] J.C. Pati and C.H. Woo, Phys. Rev. Letters D3, 2920 (1971).

[7] For a review and references see B.W. Lee, Proc. Topical Conference on Weak Interactions, CERN yellow report 69-7 (1969).

[8] H. Leutwyler, Phys. Letters 48B, 269 (1975).

[9] J. Finjord, Phys. Letters 76B, 116 (1978).

[10] J.M. Gaillard, these proceedings.

[11] For a review and references, see V.I. Zakharov, Proc. 16th International Conference on High Energy Physics (Batavia, 1972), vol. II, p. 263.

[12] Farikov and Steck, Nucl. Phys. B133, 315 (1978); N. Cabibbo and L. Maiani, Phys. Lett. 73B, 418 (1978).

[13] For recent reviews see B. Wiik and G. Wolf, DESY report (1978) and S. Wojcicki, these proceedings.

[14] M. Kobayashi and K. Maskawa, Progr. Theor. Phys. 49, 652 (1973).

[15] N. Cabibbo, Phys. Rev. Letters 10, 531 (1964).

[16] S.L. Glashow, J. Iliopoulos and L. Maiani, Phys. Rev. D2, 1285 (1970).

[17] S. Pakvasa and H. Sugawara, Phys. Rev. D14, 305 (1976).

[18] L. Maiani, Phys. Letters 62B, 183 (1976).

[19] J. Ellis, M.K. Gaillard and D.V. Nanopoulos, Nucl. Phys. B109, 213 (1976).

[20] S. Weinberg, Phys. Rev. Letters 19, 1264 (1967); A. Salam, Proc. 8th Nobel Symposium, Stockholm 1968, ed. N. Svartholm (Almqvist and Wiksells, Stockholm, 1968), p. 37.

[21] H. Harari, Proc. Int. Symposium on lepton and photon interactions at high energies, Stanford 1975, ed. W.T. Kirk, p. 317 (SLAC, Stanford, 1975), p. 317.

[22] L.M.B. Barkov and M.S. Zolotorev, Pisma JETP 26, 379 (1978).

[23] D.J. Sherden, these proceedings.

[24] N. Fortson, this conference.

[25] D. Cutts, et al., Phys. Rev. Letters 41, 363 (1978); R. Vidal, et al., Fermilab preprint (1978).

[26] H. Georgi and S.L. Glashow, Phys. Rev. Letters 32, 438 (1974).

[27] H. Georgi, H.R. Quinn and S. Weinberg, Phys. Rev. Letters 33, 451 (1974).

[28] M.S. Chanowitz, J. Ellis, and M.K. Gaillard, Nucl. Phys. B128, 506 (1977); A.J. Buras, J. Ellis, M.K. Gaillard and D.V. Nanopoulos, Nucl. Phys. B135, 66 (1978).

[29] C. Jarlskog, et al., Nucl. Phys. B109, 1 (1976).

[30] J. Ellis, M.K. Gaillard, D.V. Nanopoulos and S. Rudaz, Nucl. Phys. B131, 285 (1977).

[31] K. Ueno, et al., Fermilab preprint in preparation.

[32] M. Suzuki, LBL Report LBL-7948 (1978).

[33] A. Ali, CERN preprint TH-2411 (1977) to appear in Nucl. Phys. B.

[34] R.N. Cahn and S.D. Ellis, Phys. Rev. D16, 1484 (1977).

[35] S.S. Gerstein and M. Yu. Klopkov, JETP Letters 23, 338 (1976); V.A. Novikov, et al., Phys. Rev. Lett. 38, 626 and 791(E) (1977).

[36] A.I. Vainshtein and I.B. Khriplovich, JETP Letters 18, 83 (1973); M.K. Gaillard and B.W. Lee, Phys. Rev. D10, 897 (1974).

[37] Effects of radiative corrections were first studied by D.V. Nanopoulos and G.G. Ross, Phys. Letters 56B, 219 (1975). For the most recent discussion with references, see V.A. Novikov, et al., Phys. Rev. D16, 223 (1977).

[38] A. Pais and S.B. Treiman, Phys. Rev. 176, 2744 (1975).

[39] F.A. Wilczek, A. Zee, R.L. Kingsley and S.B. Treiman, Phys. Rev. D12, 2768 (1975).

[40] A. Ali and Z.Z. Aydin, DESY preprint 78/17 (1978).

[41] CP violation can also be introduced by increasing the number of Higgs doublets. T.D. Lee, Phys. Reports 9, 143 (1973); S. Weinberg, Phys. Rev. Letters 37, 657 (1976).

[42] E.P. Shabalin, ITEP preprint 31 (1978).

SEARCH FOR $\mu^+ \to e^+ \gamma$

Martin D. Cooper

Los Alamos Scientific Laboratory

University of California, Los Alamos, New Mexico 87545

Abstract

Using the Stopped Muon Channel at LAMPF to produce a surface muon beam, 2.3×10^{12} muons were stopped in a 50 mg/cm^2 target. The solid angle-efficiency product of the detector for the rare decay $\mu^+ \to e^+ \gamma$ was 1.2%. Hence, 3×10^{10} μ^+ decays were examined. There is no indication of any signal, the data being consistent with a small background of random electron and gamma coincidences. The new upper limit on the branching ratio is $\Gamma(\mu^+ \to e^+ \gamma)/\Gamma(\mu^+ \to e^+ \nu_e \bar{\nu}_\mu) < 2 \times 10^{-10}$ with 90% confidence.

The development of guage theories of weak and electromagnetic interactions has renewed interest in searching for the flavor violating decays of the muon. In particular, new searches for $\mu^+ \to e^+ \gamma$[1,2] and $\mu^- Z \to e^\pm Z'$ [3] have taken place in the last two years. The theories predict that if all the masses of the neutrinos are not zero, then the flavors will not necessarily be eigenstates of mass and the physical particles will have admixtures of several flavors. Through these admixtures, muon number conservation will be violated. The upper limit one obtains from using the known limits on the mass of the muon and electron neutrinos is $\sim 10^{-24}$ and is experimentally uninteresting.

The discovery[4] of the τ tells us that the spectrum of lepton flavors is richer than previously believed. Various theories involving

heavy neutral leptons predict branching ratios as high as 10^{-8} for the muon number violating decays. The "standard" model uses the upper limit on the neutral τ mass of less than 250 MeV to predict branching ratios of less than 10^{-11}. This level of sensitivity has not yet been experimentally reached.

Other possibilities are still not experimentally ruled out. For example, the right handed electron and muon could be coupled to heavy right handed neutrinos as suggested by Cheng and Li.[5] Mixing of these heavy neutral leptons would possibly produce muon number violation at higher levels. Additionally, having more than one set of Higgs doublets which are mixed[6] would do the same. Other possibilities exist to produce muon number violation.

These theories all involve unknown particles with unknown mixing between particles. Hence, muon number violation may be at a level which is experimentally unobservable, or nature may have made it an exact symmetry for reasons we do not understand. Thus, if it is found, it is a useful testing ground for guage theories; if not, it only puts a weak limit on theories. The present published upper limits on muon number violation are given in Table 1.

The experiment described here was performed at the Clinton P. Anderson Meson Physics Facility (LAMPF) by a collaboration of scientists from Los Alamos, the University of Chicago, and Stanford University. They are listed in Table 2.

To search for the decay $\mu^+ \to e^+\gamma$ with a sensitivity of 10^{-10}, one must rely on kinematic separation from more favored processes. Normal muon decay produces a positron spectrum, the Michel Spectrum, which is peaked near half the muon mass, 1/2 x 105.6 MeV. In itself, it cannot be

Table 1. Present published upper limit on muon number violating decays.

Decay	Upper Limit (90% Confidence)	Reference
$\mu^+ \to e^+\gamma$	2×10^{-10}	This work
	1.1×10^{-9}	2
$\mu^- + Z \to e^- + Z$ (Sulfer)	4×10^{-10}	3
$\mu^- + Z \to e^+ + (Z-2)$ (Sulfer)	1×10^{-9}	3
$\mu^+ \to e^+\gamma\gamma$	5×10^{-8}	7
$\mu^+ \to e^+e^+e^-$	1.9×10^{-9}	8

Table 2. Participants in present work.

Name	Institutions
H. L. Anderson	University of Chicago, Los Alamos
J. D. Bowman	Los Alamos
R. Carrington	Stanford University
M. D. Cooper	Los Alamos
R. Eichler	Stanford University
M. E. Hamm	Los Alamos
C. M. Hoffman	Los Alamos
R. Hofstadter	Stanford University
E. B. Hughes	Stanford University
W. W. Kinnison	University of Chicago
H. S. Matis	University of Chicago, Los Alamos
T. McPharlane	Stanford University
R. E. Mischke	Los Alamos
D. E. Nagle	Los Alamos
J. S. Sarracino	Los Alamos
P. A. Thompson	Los Alamos
S. C. Wright	University of Chicago

mistaken for $\mu^+ \to e^+\gamma$ because it does not decay with a photon emission. However, it provides the high electron rate which can be in random coincidence with "photons" to simulate $\mu^+ \to e^+\gamma$. A prompt background comes from the radiative decay or internal bremsstrahlung in which a μ^+ decays into $e^+\gamma\bar{\nu}\nu$. Being a bremsstrahlung process, the angular correlation between the photon and positron is peaked near zero degrees and vanishes as one approaches the $\mu^+ \to e^+\gamma$ kinematics of positron and photon energy equal to 52.8 MeV and $\theta_{e\gamma} = 180^{\circ}$.

The experimental "tools" which have been used to distinguish between signal and background are a gamma ray resolution of 7.5%, a positron energy resolution of 8.3%, a timing resolution of 2.5 nsec, and an angular resolution of 5°. Using these resolutions, we can demonstrate that the process $\pi^+ + Z \to (Z+1) + \pi^0 + e^+\gamma$ is rejected at a level of 10^{-17}. The radiative decay is rejected at a level of 10^{-12}. Random backgrounds are only rejected at about a level of 10^{-10} and provide the major background for the experiment.

To discriminate against random coincidences, one must reduce the source of "photons" to a minimum. Cosmic rays and accelerator neutrons doing (n,p) reactions in the photon detector have been eliminated with shielding. The use of the surface muon beam, to be described below, eliminates positron annihilation-in-flight and external bremsstrahlung of positrons interacting in the target. Photons from radiative decay are always there and must be defeated with good energy resolution.

A critical part of the experiment was the surface muon beam. This beam of 30 MeV/c muons was derived from stopped pion decay in the last 50 mg/cm^2 of the proton production target. The 800 MeV beam of LAMPF was passed through a 6 gm/cm^2 C target. The low energy muons were

transported through a magnetic channel where pions decayed away. The beam was momentum analyzed and, then, purified by using the differential energy loss of positrons and muons in a 40 mg/cm^2 CH_2 degrader. Such a beam had the following advantages for a $\mu^+ \to e^+\gamma$ experiment: 1) Positron and pion contaminations of 10% and $<10^{-4}$ respectively, 2) Contaminent positron momentum substantially less than 52.8 MeV, 3) A rate of 2.5×10^6 Hz, and 4) A residual range of 30 mg/cm^2. The ability to use a 50 mg/cm^2 target eliminated the backgrounds from external bremsstrahlung and positron annihilation-in-flight as well as preserved the collinearity of e^+ and γ from $\mu^+ \to e^+\gamma$ which might otherwise be lost due to multiple scattering in the target.

The experimental apparatus for detecting $\mu^+ \to e^+\gamma$ is shown in Fig. 1. The beam enters the target through an iron shield to prevent deflection by the magnetic fields of the spectrometers. The target is supported by a cone shaped piece of 50 mg/cm^2 polyethylene shielding. This shielding catches any stray muons so that their decay positrons cannot pass through a thick piece of matter on the way toward the photon detector. Both arms of the detector are filled with He.

The positron arm consists of a magnetic spectrometer which bends 52.8 MeV/c particles by 40°. The incident and exiting angles are measured in four sets (x and y coordinates) of multiwire proportional counters (MWPC). Behind the MWPC's is a hodoscope of scintillation counters which are used both for timing and the trigger.

The photon arm consists of a photon detector and a sweeping magnet which prevents charged particles from hitting the photon counter. The photon detector is a multi-cellular array of NaI(Tl) made up of 45 hexagonal elements. A front view of these is shown in Fig. 2. Each

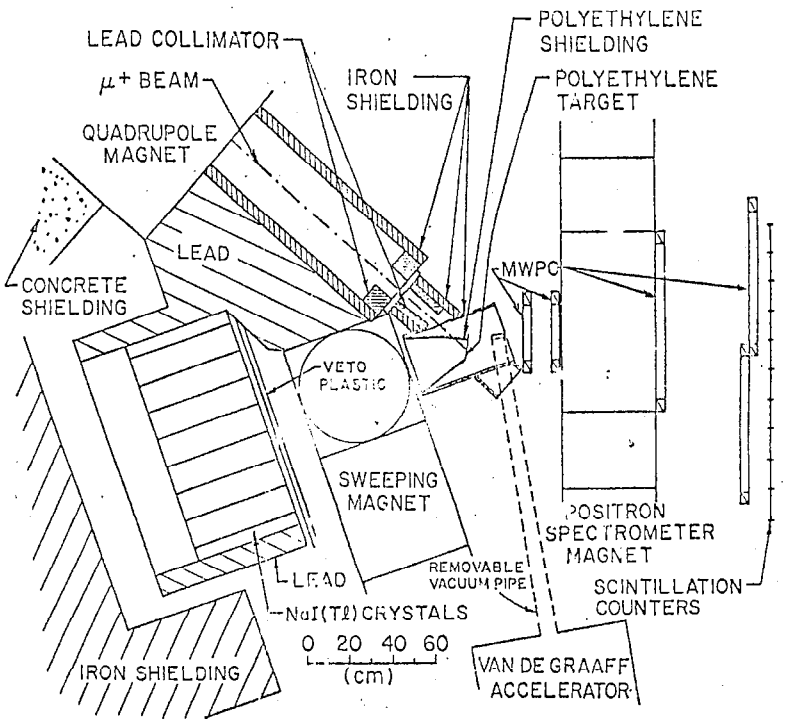

Figure 1. The experimental apparatus.

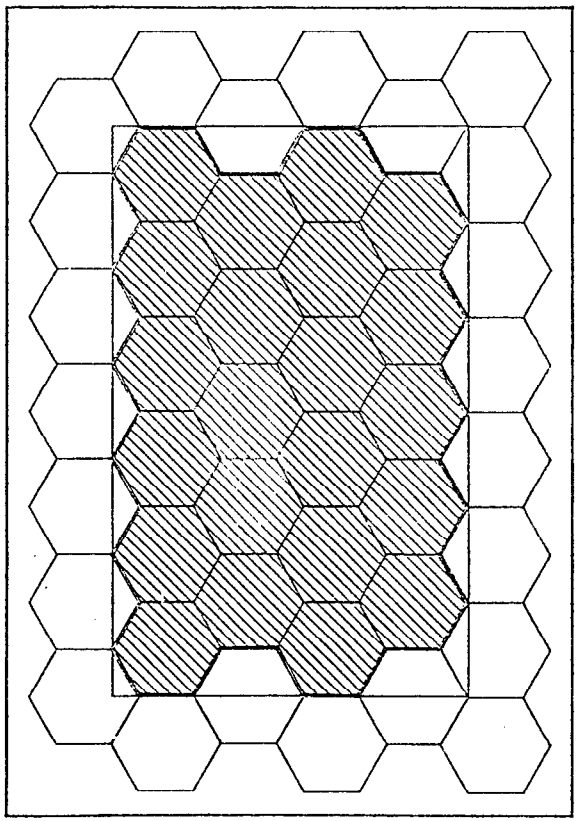

Figure 2. The front face of the NaI detector. The shaded region is the fiducial area and the inner rectangle represents the boundary of region shadowed by the field clamp.

crystal is 7.68 cm on a side and 20 radiation lengths deep. The edge crystals are shadowed by the sweeping magnet and its field clamp. They serve to contain showers which impinge on the fiducial crystals, which are cross hatched in the figure. The sweeping magnet keeps the singles rate in each crystal quite modest. The stack is also fronted by a charged particle veto counter.

The data from a typical trigger consists of timing information from the NaI and positron scintillators, sparks from the MWPC's, and pulse height information from the NaI array. The identification of $\mu^+ \to e^+\gamma$ candidates is dependent on finding time coincidence between the arms and a positron and photon, each of which has an energy $\gtrsim$ 30 MeV. The positron track is then reconstructed to give its initial positron and momentum at the target. The spread of the electromagnetic shower in the NaI is used to give an interaction point for the photon in the NaI. Assuming the same origin for both the photon and positron, the acollinearity angle is calculated.

With this description of how the apparatus is designed to work, it is now possible to understand the details of the experiment. The elements of a good $\mu^+ \to e^+\gamma$ experiment are examining enough μ decays and having enough background suppression to observe an effect at the level of the number of observed μ decays. In this experiment, both of these limitations occur around a level of 10^{-10}.

The number of μ decays in the experiment were measured in two ways. The first was to calculate the number of single positrons observed in the spectrometer. For an experiment dominated by random coincidences, the number of μ decays observed is just

$$N_\mu = N_\mu \text{ (observed in } e^+ \text{ arm)} \frac{fG}{R_\gamma \tau} \quad (1)$$

where f corrects N_μ (observed) for the energy acceptance of the spectrometer, G is the solid angle overlap of the arms, R_γ is the rate of γ singles, and τ is the resolving time of the trigger. The second measurement was taken from the number of decays into a calibrated counter times the acceptance of the spectrometer, which is calculated by Monte Carlo techniques. The two techniques agree to better than 10%. For the sample of data reported in this talk, the number of μ stops was 2.3×10^{12} and the number of μ decays which were examined was 3×10^{10}. This latter number is the denominator of the branching ratio calculation.

In order to know the level of background suppression, it is necessary to calibrate the detector and measure the resolution functions. The four quantities for which this must be done are the relative time between the arms t, the positron energy E_e, the γ-ray energy E_γ, and the acollinearity angle $\theta_{e\gamma}$.

To accomplish these measurements, an auxilliary calibration experiment was performed. The channel was reset to stop π^- in a liquid hydrogen target, where the reaction $\pi^- p \to \pi^0 n$ produced two high energy γ-rays from π^0 decay. One γ-ray was converted by pair production to a positron for observation in the positron spectrometer. The kinematics of the π^0 decay is dominated by Doppler shift from the π^0 motion. Here $\theta_{e\gamma}$ is restricted to be greater than 157°. For 180° decays, the two γ-rays have an energy of 55 and 82 MeV. The auxiliary experiment helps with the measurement of t, E_γ, and $\theta_{e\gamma}$.

The timing calibration was made with the π^0 decays. Relative offsets for each of the 45 NaI crystals and 10 hodoscopes were found so that the coincidence peak lay at the zero of time. The timing resolution obtained from hydrogen was 2.2 nsec(FWHM). By relaxing the conditions on collinearity, a coincidence peak was observable in the data due to internal bremsstrahlung. The resolution of the peak was 2.5 nsec(FWHM) and is shown in Fig. 3. This resolution represents the coincidence requirement for the rejection of randoms since it is observed during the actual data taking.

The calibration of the electron spectrometer was accomplished by an optical survey of the position of the MWPC's, a map of the magnetic field along the entirety of the positron's path, and an analysis of field off data to demonstrate that, within the limits of multiple scattering, the positrons traced out straight lines. Then, regular data was analyzed to measure the Michel spectrum, shown in Fig. 4. Folding a bremsstrahlung corrected Michel spectrum with a Gaussian, a resolution of 8.3% (FWHM) and an offset of 0.3 MeV was obtained.

The energies and position algorithms for the NaI detector rely on the information from the crystal with the highest pulse height and its six adjacent neighbors as shown in Fig. 5. The choice of which crystals to include is a compromise between obtaining good resolution and preventing pile up. The energy algorithm consists of determining the energy deposited in each crystal as a function of the pulse amplitude. These functions are ideally linear, but may contain nonlinearities due to the phototubes and analog-to-digital converters. Once the crystal with the maximum energy is determined, events outside the feducial region are rejected. For the remaining events, the energy is the sum over the seven crystals.

Since the modular nature of the detector implies that the energy is divided over a large dynamic range, an elaborate calibration was

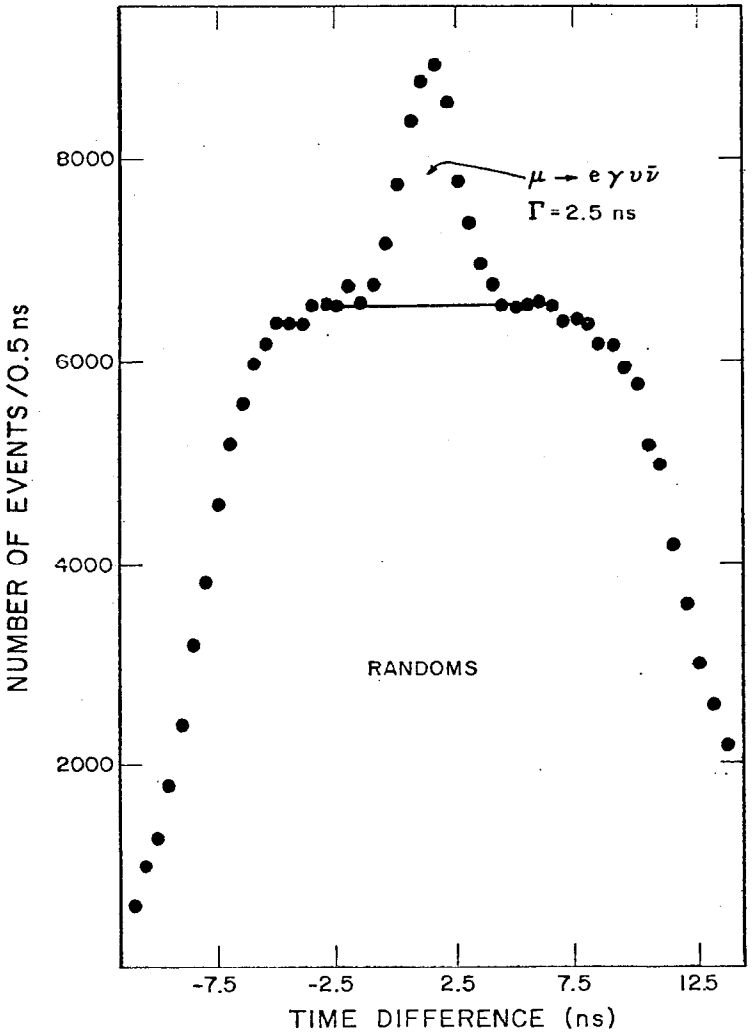

Figure 3. On line time spectrum with relaxed cuts on collinearity.

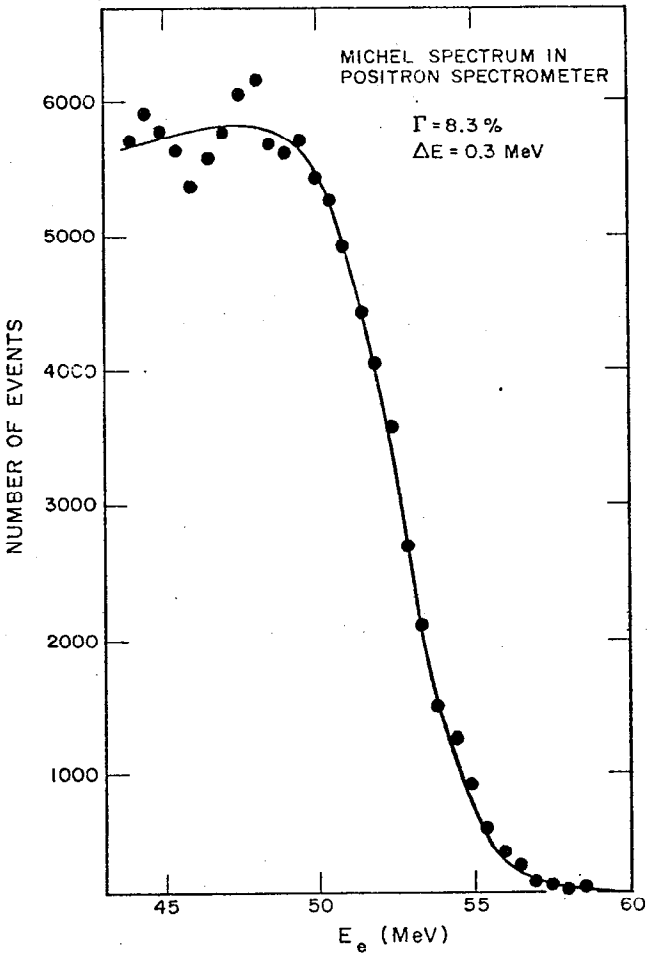

Figure 4. Michel spectrum in positron spectrometer.

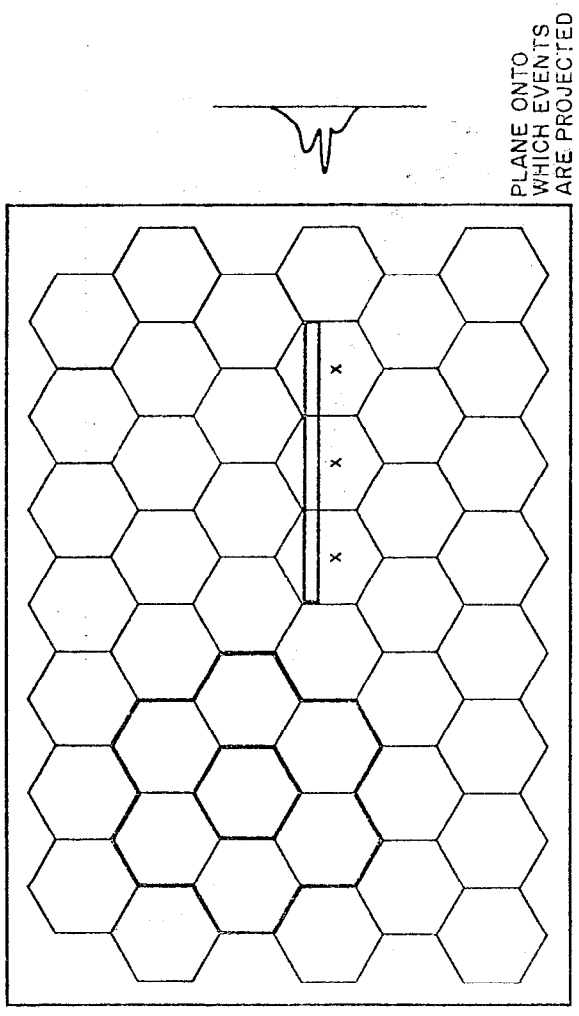

Figure 5. The front face of the NaI detector. Outlined in heavy ink is a typical sum of seven crystals used in the energy and position algorithms. The slot shows the location of the polyethylene slot in a Pb wall used to test the position algorithm. On the right is a sketch of the projection of the position data.

done with sufficient frequency to prevent drifts. In Table 3, each of the calibration points are listed, along with their fitted energy, resolution and frequency. As an example, the Michel spectrum obtained with the beam intensity reduced and sweeping magnet off is shown in Fig. 6. The fit with a Michel spectrum folded with a Gaussian gives a 7.0% (FWHM) resolution. As a check, the NaI spectrum from the normal data was fit with a combination of sources including internal and external bremsstrahlung, positron annihilation in flight and a constant background from accelerator neutrons and cosmic rays. The results are shown in Fig. 7, where the fit region is above 45 MeV and the deviation at lower energies is most likely due to thick target bremsstrahlung from the sweeping magnet's pole faces. In the fit region, the χ^2/F is 1.1, the resolution is consistent with the calibrations (7.2% FWHM), and the normalization is consistent with the stop rate to 10%.

The angular correlation measurement depends on both the positron and photon arms. Although it is expected that the MWPC's will give accurate reconstruction of the positrons, multiple scattering will introduce a non-negligible uncertainty. The resolution of the MWPC's was measured by looking at decays of muons which were stopped in horizontal and vertical line targets (1 cm wide). The reconstructed targets are shown in Fig. 8, and these spectra lead to a resolution of better than 1 cm. Since the line targets were surveyed, the locations are a check on the absolute position of the chambers.

The algorithm for the entrance point of the γ-rays into the NaI crystals depends very heavily on a Monte Carlo simulation of the electromagnetic shower which leads to the pulses. The algorithm used was a weighting of the crystal coordinates by the observed energy

Table 3. NaI calibration points.

Source	Energy	Fitted Energy	Resolution (%)	Frequency of Measurement
$Pu \rightarrow \alpha + Be \rightarrow {}^{12}C + \gamma$	4.43	4.33	10.0	1/day
$p + {}^{19}F \rightarrow {}^{20}Ne \rightarrow {}^{16}O + \alpha + \gamma$	6.13	5.90	8.0	1/week
$p + {}^{7}Li \rightarrow {}^{8}Be + \gamma$	17.64	17.26	6.7	1/week
$\mu^+ \rightarrow e^+ \nu\bar{\nu}$ (endpoint)	52.83	52.83	7.0	1/day
$\pi^- + p \rightarrow \pi^o + n$, $\pi^o \rightarrow \gamma\gamma$ (collinear)	55.10	55.05	7.5	twice
	82.65	82.43	6.5	twice
$\pi^- + p \rightarrow n + \gamma$	129.36	128.30	5.5	twice

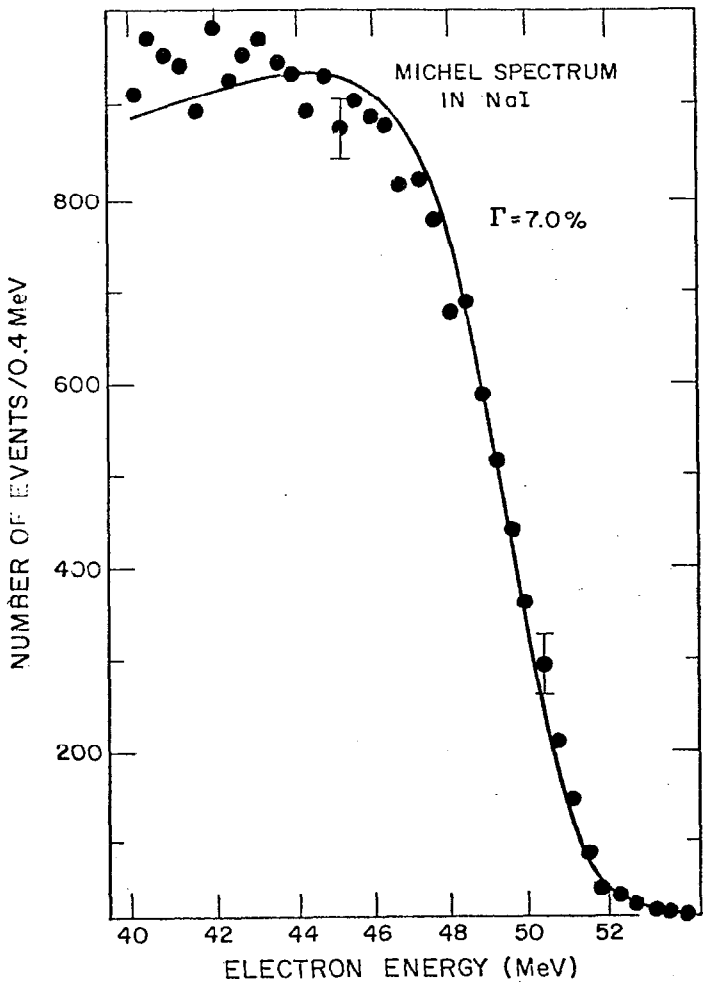

Fig. 6. Michel spectrum in the NaI with the sweeping magnet off.

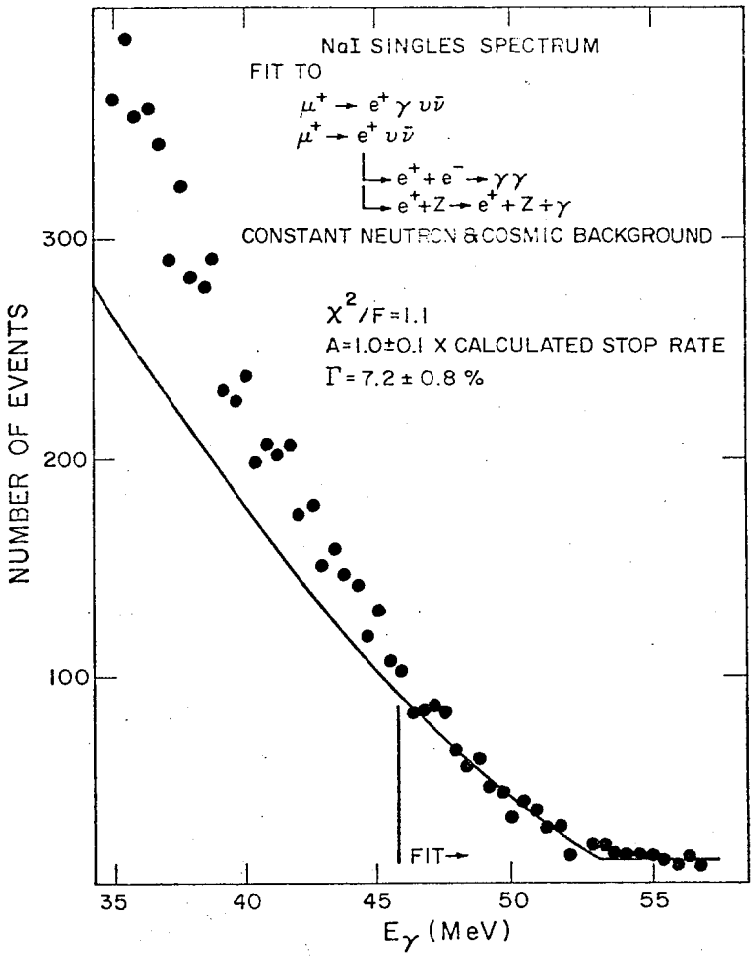

Figure 7. NaI singles spectrum and a fit from known sources of photons.

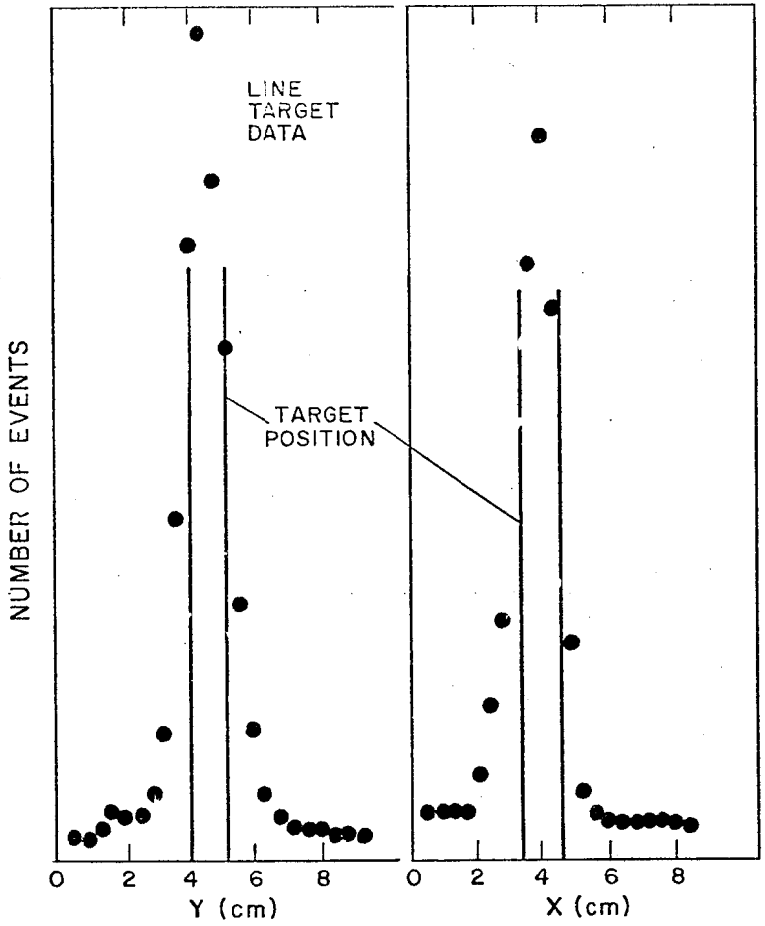

Figure 8. Reconstructions of 1 cm wide horizontal and vertical line targets as determined from detecting the positrons from muon decay.

deposition

$$\vec{x} = \sum_{i=1}^{7} \vec{x}_i E_i^S \Big/ \sum_{i=1}^{7} E_i^S \quad , \tag{2}$$

where S is determined by the matching of mean lateral shower spread to the size of the NaI modules. Monte Carlo calculations suggest $s \simeq 0.4$ and that the mean interaction depth is 4 radiation lengths into the crystals.

In order to fine tune the algorithm empirically for 55 MeV γ-rays, the face of the NaI was covered with a 5 cm thick wall of Pb. In the wall a 2.5 cm high slot of CH_2 was left for coincident photons from π^0 decay to pass. The setup is illustrated in Fig 5. For a substantial fraction of the events, no shower leakage into neighboring crystals occurs. The best estimator for these events is a crystal center, and this produces a peak in the projected position spectrum. The spectrum, when projected to the right, is given in Fig. 9. The best Monte Carlo prediction for the data ($s \simeq 0.36$) is also shown. The Monte Carlo is then used to calculate the positron resolution, and the projected resolution is 7 cm FWHM.

With the resolutions and calibrations in hand, the data analysis may proceed. The operating conditions of the experiment are listed in Table 4, and the results reported here represent an analysis of about half the data. A first editing of that part of the data has yielded 8518 events for use with the most refined algorithms and likelihood analysis.

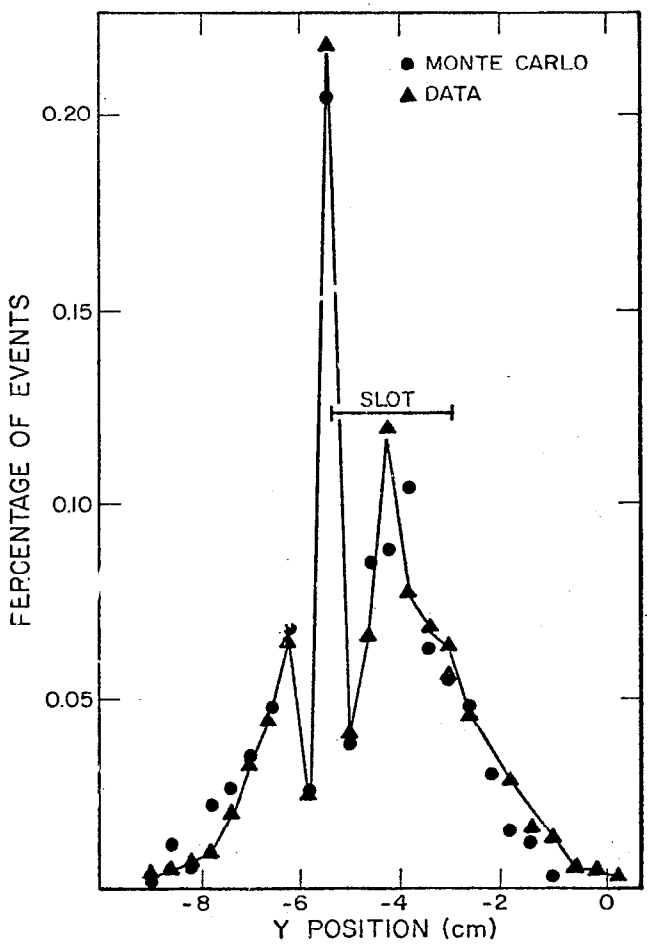

Figure 9. Position data and Monte Carlo simulations for the CH_2 slot in the Pb wall.

Table 4. Typical operating characteristics of the apparatus.

Rates	
Instantaneous μ^+ stops	3.3×10^7/sec
Average μ^+ stops	2.0×10^6/sec
Electron contamination	10%
Instantaneous e^+ triggers	1.4×10^6/sec
Instantaneous γ triggers/NaI crystal	10^3/sec
Triggers	10/sec
Solid Angle	2%
Efficiency for reconstruction	x 60%
	1.2%
μ^+ stops in sample reported	2.3×10^{12}
μ^+ examined in sample reported	3×10^{10}
Events on tape	6×10^6
400 Tapes production data	
250 Tapes calibration data	
Hardware Cuts	E_γ>35 MeV
	-10 nsec < t < 10 nsec

If one were to make sharp cuts on all the kinematic variables at 1.5 σ, then one finds 8 events fall in the window. A background of 9 events are expected and this yields a net for $\mu^+\to e^+\gamma$ of $-1\pm\sqrt{8}$ events. The branching ratio upper limit at 90% confidence is then given as 1.5 times the number of $\mu^+\to e^+\gamma$ events divided by the cut efficiency and the number of μ decays examined. This would yield $\Gamma(\mu^+\to e^+\gamma)/\Gamma(\mu^+\to \text{all}) \leq 2.9 \times 10^{-10}$.

The proper way to set the limit is to do a maximum likelihood analysis. The experiment is sensitive to three processes: $\mu^+\to e^+\gamma$, $\mu^+\to e^+\gamma\nu\bar{\nu}$, and random coincidences. Hence, the likelihood function may be written

$$L(\alpha,\beta) = \frac{1}{N^N}\prod_{i=1}^{N}\left[\alpha P(x_i)+\beta Q(x_i)+(N-\alpha-\beta)R(x_i)\right], \qquad (3)$$

where N is the total number of events (8518), α is the number of $\mu^+\to e^+\gamma$ events, β is the number of internal bremsstrahlung events, and x_i are the measured properties of the i^{th} event (E_e, E_γ, $\theta_{e\gamma}$, t). P(x), Q(x), and R(x) are probability density functions for $\mu\to e\gamma$, internal bremsstrahlung, and random events, respectively. P(x) is taken as a product of the measured resolution functions; Q(x) is taken from Q.E.D. calculations of internal bremsstrahlung smeared with the measured resolution functions; R(x) is taken as the product of the shapes of the spectra of the individual parameters. $L(\alpha,\beta)$ can than be interpreted at the joint probability density for α and β.

Figure 10 shows the likelihood contours for α and β. The amount of internal bremsstrahlung observed is consistent with the geometry

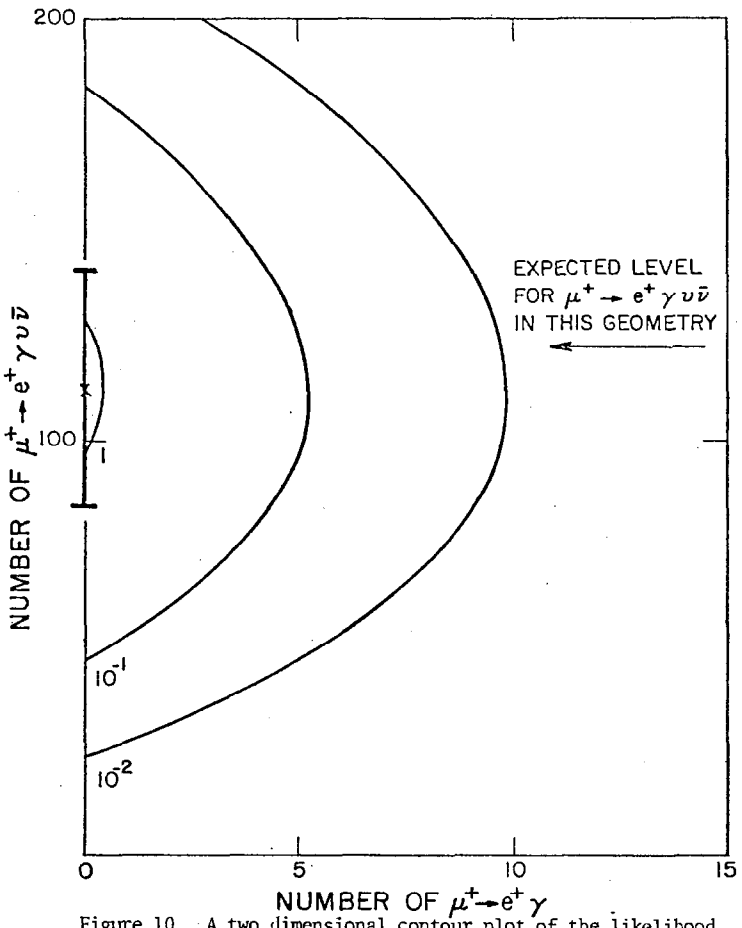

Figure 10. A two dimensional contour plot of the likelihood function's dependence on α, the number of $\mu^+ \to e^+ \gamma$, and β, the number of $\mu^+ \to e^+ \gamma \nu \nu$.

for observing that decay. The fact that the contours are symmetric about horizontal and vertical axis shows that α and β are linearly independent; i.e., the signature for internal bremsstrahlung is distinct from that for $\mu^+ \to e^+ \gamma$.

Figure 11 shows the projection of Fig. 10 which displays the dependence on α, and is labeled t=0. The curve labeled t=5 nsec is a likelihood function for purely random events and is consistent with the t=0 curve in accordance with the statistics of small numbers. The 90% confidence limit is the point where the area under the curve is 90% of the total area. This occurs at α=6 events. Hence, after dividing by the number of examined decays, the upper limit for $\mu^+ \to e^+ \gamma$ is $\Gamma(\mu^+ \to e^+ \gamma)/\Gamma(\mu^+ \to \text{all}) \leq 2.0 \times 10^{-10}$ with 90% confidence.

The physicists who have performed this experiment would like to acknowledge the encouragement and support of Dr. Louis Rosen and the LAMPF administration as well as the many people who provided invaluable technical support throughout the experiment. This project was carried out under the auspices of the U.S. Department of Energy, the National Science Foundation (Grants #PHY77-20610 and #PHY76-10287) and the U.S. National Aeronautics and Space Administration (Grant NGR452).

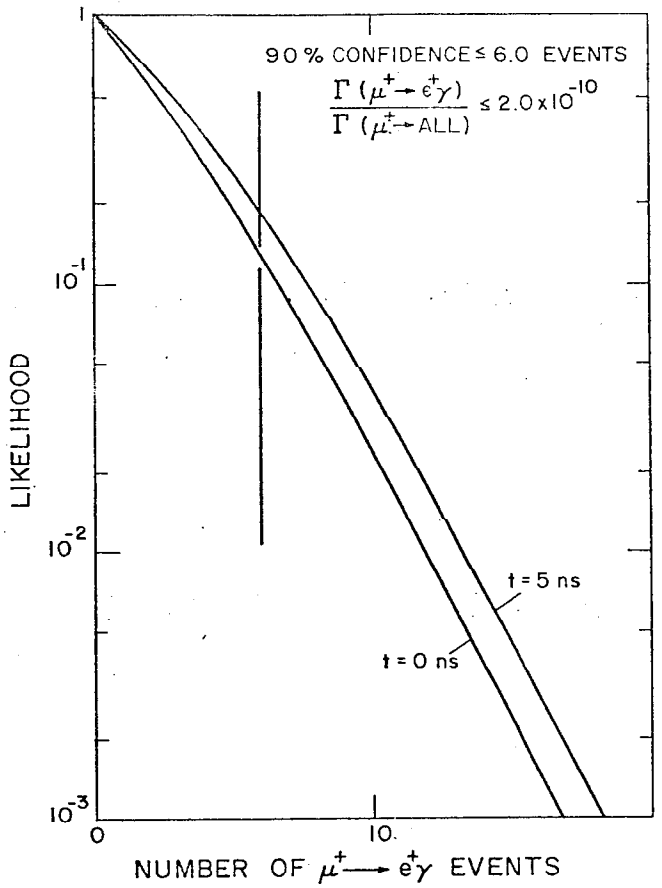

Figure 11. The likelihood function's dependence on α, the number of $\mu^+ \to e^+\gamma$ for coincidence and random events. The vertical line indicates the point where 90% of the likelihood occurs; i.e., at 6 events.

REFERENCES

1. P. Depommier, J. P. Martin, J. M. Poutissou, R. Poutissou, D. Berghofer, M. D. Hasinoff, D. F. Measday, M. Solomon, D. Bryman, M. Dixit, J. A. McDonald, and G. I. Opat, Phys. Rev. Lett. 39, 1113 (1977).

2. J. P. Pevel, W. Dey, H. K. Walter, H. J. Pfeiffer, V. Sennhauser, J. Egger, H. J. Gerber, M. Salzmann, A. Van der Schaat, W. Eichenberger, R. Engfer, F. Hermes, F. Schleputz, V. Weidmann, C. Petitjean and W. Hesselink, Phys. Lett. 72B, 183 (1977).

3. A. Badertscher, K. Borer, G. Czapek, A. Flückiger, H. Hänni, B. Hahn, E. Hugentobler, A. Markees, U. Moser, R. P. Redwine, J. Schacher, H. Scheidiger, P. Schlatter, and G. Viertel, Phys. Rev. Lett. 39, 1385 (1977).

4. M. L. Perl, G. S. Abrams, A. M. Boyarski, M. Breidenbach, D. D. Briggs, F. Bulos, W. Chinowsky, J. T. Dakin, G. J. Feldman, C. E. Friedberg, D. Fryberger, G. Goldhaber, G. Hanson, F. B. Heile, B. Jean-Marie, J. A. Kadyk, R. R. Larsen, A. M. Litke, D. Lüke B. A. Lulu, V. Lüth, D. Lyon, C. C. Morehouse, J. M. Paterson, F. M. Pierre, T. P. Pun, P. A. Rapidis, B. Richter, B. Sadoulet, R. F. Schwitters, W. Tanenbaum, G. H. Trilling, F. Vannucci, J. S. Whitaker, F. C. Winkelmann, and J. E. Wiss, Phys. Rev. Lett. 35, 1489 (1975).

5. T. P. Cheng and L. F. Li, Phys. Rev. D16, 1425 (1977).

6. J. D. Bjorken and S. Weinberg, Phys. Rev. Lett. 38, 622 (1977).

7. J. D. Bowman, T. P. Cheng, L. F. Li, and H. S. Matis, Phys. Rev. Lett. 41, 442 (1978).

8. S. M. Korenchenko, B. F. Kostin, G. V. Mitsel'makher, K. G. Nekrasov, and V. S. Smirnov, JETP 43, 1 (1976).

EUROPEAN ORGANIZATION FOR NUCLEAR RESEARCH

Ω^- DECAYS AND OTHER RARE HYPERON PROPERTIES(*)

Jean-Marc Gaillard
Laboratoire de L'Accélérateur Linéaire, F-91405 Orsay

Invited talk presented at the SLAC Summer Institute
July 1978

Geneva - 16 October 1978

(*) The results presented in this talk have been obtained by a group composed of:

M. Bourquin, R.M. Brown, Y. Chatelus, J.C. Chollet, A. Degré, J. Froidevaux, A.R. Fyfe, C.N.P. Gee, J-M. Gaillard, M. Gibson, P. Igo-Kemenes, P.W. Jeffreys, B. Merkel, R. Morand, H. Plothow, J-P. Repellin, B.J. Saunders, G. Sauvage, B. Schiby, H.W. Siebert, V.J. Smith, K.P. Streit, R. Strub and J.J. Thresher.

The SPS charged hyperon beam has been in operation for a year and a half. After a detailed study of the beam performance and of particle spectra an important fraction of running time was used to collect large samples of semi-leptonic hyperon decays. That data is presently being analysed. In this talk after a brief description of the properties of the hyperon beam, I will present results on Ω^- decays obtained from data taken during a special run in March-April 1978. I will also briefly discuss our results on hyperon and anti-hyperon production.

THE SPS CHARGED HYPERON EXPERIMENT [1]

The set up can be divided into three parts:

- the magnetic channel,
- the DISC Cerenkov counter,
- the spectrometer.

The magnetic channel and the DISC counter are shown schematically in fig. 1. The magnetic channel is composed of three bending magnets M_1, M_2, M_3, with special tapered poles and a 4 cm gap, and two supra-conducting quadrupoles Q_1 and Q_2. It has been designed to achieve in the shortest possible length the momentum selection and the beam optical properties required for particle identification in the DISC counter.

A branch of the extracted proton beam of the SPS is focussed onto a BeO target 32 cm long and 2 mm in diameter. The proton energy, initially 200 GeV, was upgraded to 210 GeV at the time of the Ω^- run. The primary protons transmitted through the target are absorbed in the left tungsten lip of collimator C_1. To achieve maximum separation between the transmitted protons and the secondary beam an extra coil is wound within the pole tip of M_1 to boost the field to 3.5 Tesla. The variable collimators allow an adjustment of the horizontal acceptance (C_1 or C_2) and of the momentum bite (C_3) of the secondary beam. Under typical running conditions the collimator apertures are ± 1 mm for C_1 and ±10 mm for C_3 corresponding to

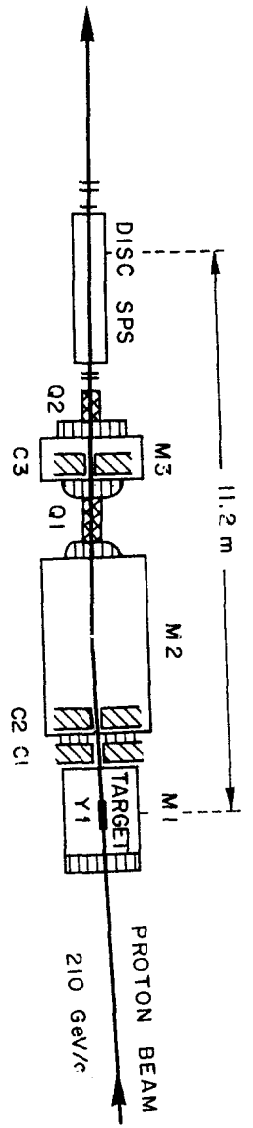

Fig. 1 The magnetic channel and the DISC counter.

a $\Delta p/p$ of 7.5% (FWHM). The supraconducting quadrupoles are tuned to give a parallel beam at the exit of the magnetic channel for each value of the momentum. The direction of the beam particle is measured to an accuracy of ± 0.05 mrad in both projections before and after the DISC counter. The horizontal angle measurement corresponds to a determination of $\Delta p/p$ to an accuracy of ± 1%.

The DISC is a differential Cerenkov counter in which the light focussed onto a narrow diaphragm is viewed by eight phototubes. The shape and the width of the diaphragm can be modified according to the requirements of the experiment. Fig. 2 shows the particle spectrum measured in a negative beam of 100 GeV/c with a narrow circular diaphragm. In order to identify the less abundant particles with optimal efficiency and a low contamination, special shaped diaphragms have been constructed: a diaphragm to identify concurrently Σ^- and Ξ^- for the leptonic experiment and a diaphragm shaped for the Ω^- run.

The DISC is followed by a ten meter decay region and a spectrometer to analyse the decay products. The spectrometer is shown in fig. 3. It is composed of an analysing magnet of 2.2 Tm with two sets of drift chambers DC 1-4 and DC 5-8 placed before and after the magnet. The angles of the charged decay particles are measured to an accuracy better than 0.1 mrad in the chambers DC 1-4. From the measurement of the bending angles in the horizontal plane with DC 5-8 the particle momentum is measured to an accuracy of ± 2% at 100 GeV/c. The chambers DC 5-8 also provide a less accurate measurement of the vertical angle. From the reconstructed tracks of the decay products the parameters of the parent particle are obtained. For instance, in the decay $\Xi^- \to \Lambda^o\pi^-$ we obtain FMHM of 4 MeV/c^2 and 6 MeV/c^2 for the Λ^o and Ξ^- mass distributions respectively.

Fig. 3 also shows the electron detectors: two transition radiation detectors, a lead glass array, a gas Cerenkov counter and a shower counter. In front of the lead glass array, two successive gamma ray detectors, each composed of 1 R.L. lead sheet and a multiwire proportional chamber, measure the position of the converted gamma rays. An hodoscope of

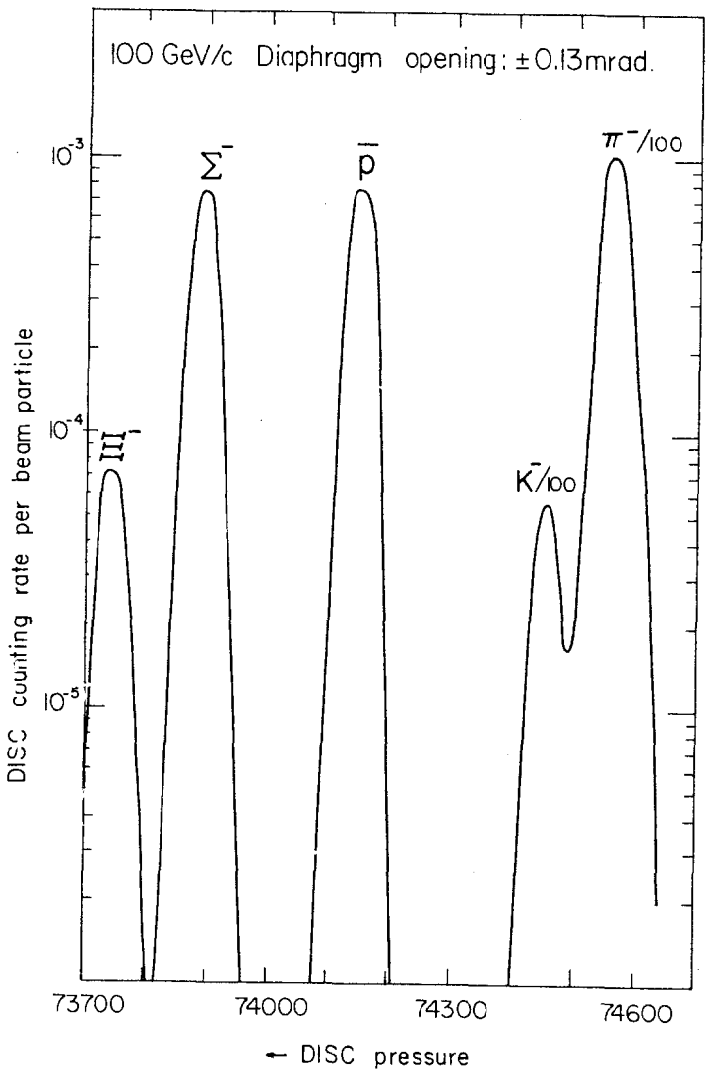

Fig. 2 DISC pressure curve at 100 GeV/c.

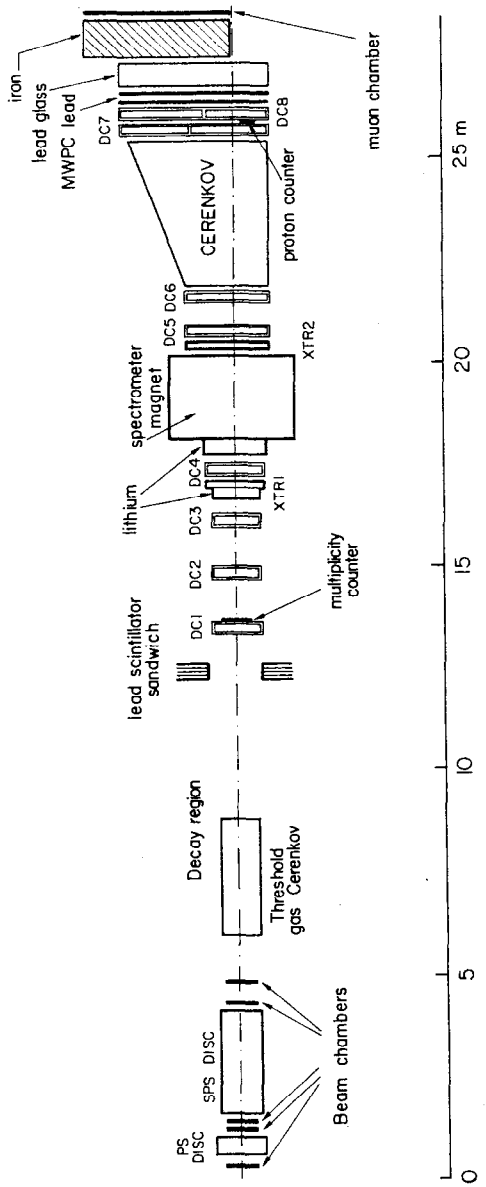

Fig. 3 The spectrometer and the electron and gamma detectors.

interleaved lead and scintillator counters is placed in front of the chamber DC_1 to catch the gamma rays which cannot reach the gamma chamber.

Under typical running conditions we work with a flux of 10^6 particles per burst. This corresponds to about 3×10^{10} protons incident on the target at 100 GeV/c and for a negative beam.

2. Ω^- DECAYS

Early test runs in 1977 established the existence of a significant flux of Ω^- in the CERN SPS charged hyperon beam. The results reported here correspond to 2/3 of the statistics obtained during a 25 day production run.

We restricted our search to events which include a $\Lambda^0 \to p\pi^-$ amongst the decay products. Thus the trigger requirements were a coincidence between a signal from the DISC set at the pressure corresponding to Ω^-, a pulse corresponding to more than one charged particle in a multiplicity counter situated 10 m downstream from the DISC and a pulse from a proton counter which is located downstream from the spectrometer and covers the spot of protons from Λ^0 decays. With these requirements the trigger rate was about 12 for 10^6 particles entering the DISC. This rate was further reduced by a factor of 4 by rejecting high multiplicity charged particle showers using the on line computer. Under these conditions, we have collected 360 000 triggers which are still mainly multitrack events or true Ξ^- whose early decay triggered the DISC and fulfilled the other trigger requirements.

We have studied the following decay modes where we measure the momenta of all charged particles

$$\Omega^- \to \Lambda^0 K^- \quad \Lambda^0 \to p\pi^-$$

$$\Omega^- \to \Xi^0 \pi^- \quad \Xi^0 \to \Lambda^0 \pi^0 \quad \Lambda^0 \to p\pi^-$$

$\Omega^- \to \Xi^- \pi^0$
$\quad \hookrightarrow \Lambda^0 \pi^-$
$\quad\quad \hookrightarrow p\pi^-$

$\Omega^- \to \Lambda^0 \pi^-$

$\Omega^- \to \Xi^- \pi^+ \pi^-$

$\Omega^- \to \Xi^0 e^- \bar{\nu}$

The presence of a Λ^0 particle decaying into a proton and a π^- being a common feature of these channels, the reconstruction program starts the event search by computing the (p, π^-) effective mass and a possible vertex for these two tracks. Only those events having a (p, π^-) effective mass within $\pm$ 10 MeV/c^2 of the Λ^0 mass, a vertex located before the multiplicity counter and at least one additional negative track are considered for further analysis. For each decay mode additional cuts are then made to reduce the background and the efficiency for the signal is determined. The central momentum of the sample analysed was measured to be 98.5 GeV/c.

2.1 The $\Omega^- \to \Lambda^0 K^-$ decay mode

For this mode the additional requirements are:

- the momentum balance between the beam particle momentum measured with the beam telescope and the (Λ^0, K^-) momentum measured by the spectrometer is smaller than 10 GeV/c. The standard deviation for that momentum balance is about 2 GeV/c.
- The (Λ^0, K^-) effective mass is within $\pm$ 50 MeV/c^2 of the Ω^- mass.

For the other decay modes we will apply an additional cut requiring that the Ω^- decay occurs after the end of the DISC counter to reduce the background for these decays. Fig. 4 shows the scatter plot of the $(\Lambda^0 K^-)$ mass versus the $(\Lambda^0 \pi^-)$ mass with the Ω^- decay vertex cut applied. It clearly shows that the selected sample contains two main contributions: the $\Omega^- \to \Lambda^0 K^-$ decays and the $\Xi^- \to \Lambda^0 \pi^-$ background. The projection of the events with a $(\Lambda^0 \pi^-)$ mass > 1.35 GeV/c^2 on the $(\Lambda^0 K^-)$ axis is shown

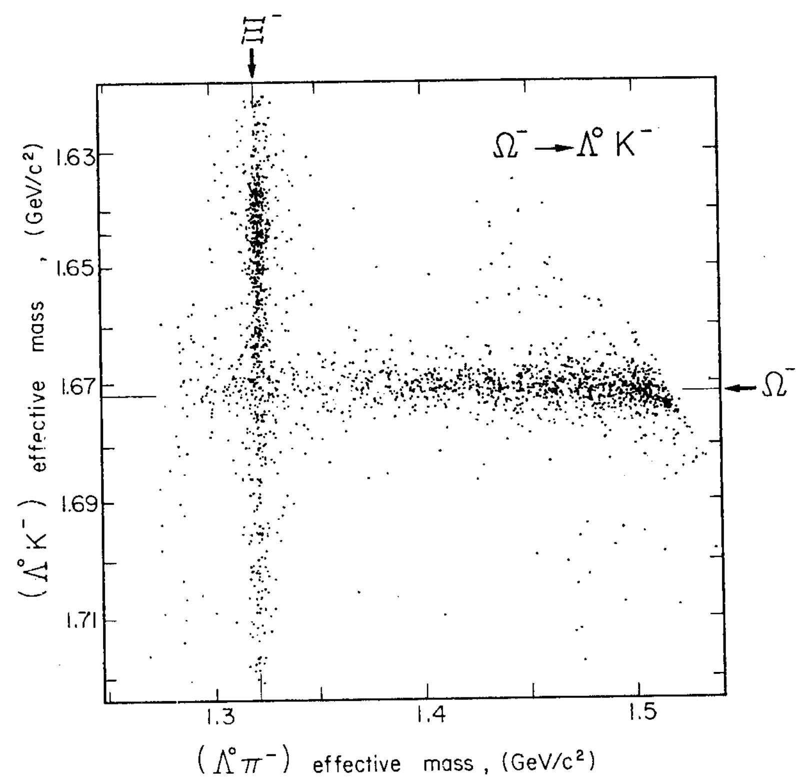

Fig. 4 Scatter plot of the (Λ^0, K^-) and (Λ^0, π^-) effective masses for the $\Omega^- \to \Lambda^0 K^-$ candidates.

in fig. 5. Within a mass range of ± 10 MeV/c^2 centered at the Ω^- mass there are 1244 events with an estimated background of 20 events. This sample is used for the branching ratio measurement.

For the Ω^- lifetime measurement reported below, the Ω^- decay vertex cut has not been applied, and with the kinematic selection criteria given above we obtain a sample of 1410 events with an estimated background of 23 events. One half of the background is due to $\Omega^- \to \Xi^0\pi^-$ decays, the other half is the residual $\Xi^- \to \Lambda^0\pi^-$ contamination.

2.2 The $\Omega^- \to \Xi^0\pi^-$ decay mode

The selection of the $\Xi^0\pi^-$ candidates is made requiring that:

- the $(\Omega^- - \pi^-)$ missing mass is within ± 150 MeV/c^2 of the Ξ^0 mass,
- the Ω^- decay takes place downstream from the end of the DISC counter,
- the beam particle momentum is within ± 10 GeV/c of the mean beam momentum,
- the momentum of the missing π^0 is greater than 2 GeV/c.

In fig. 6 the scatter plot of the $(\Omega^- - \pi^-)$ missing mass versus the (ΛK^-) effective mass shows a clear signal at the Ξ^0 mass with the main background coming from the $\Omega^- \to \Lambda^0 K^-$ decays. Fig. 7 is a projection of these events on the $(\Omega^- - \pi^-)$ axis. The solid curve drawn in the figure represents the background estimate derived from a study of the $\Lambda^0 K^-$ events. We obtain a signal of 240 ± 22 $\Omega^- \to \Xi^0\pi^-$ events.

The π^0 detection will be essential to extract a measurement of the $\Omega^- \to \Xi^-\pi^0$ mode. We have used the $\Omega^- \to \Xi^0\pi^-$ to determine the capability to detect a π^0 accompanied by three charged tracks. The dashed histogram of fig. 7 is obtained by requiring the detection of at least one photon in the gamma detectors. The efficiency for the signal is 90% while the background is reduced by a factor of 3. Fig. 8 shows the π^0 missing mass squared computed for the $\Xi^0\pi^-$ candidates which satisfy the one photon requirement. The π^0 detection efficiency has also been measured by inverting the beam polarity and detecting the $\Sigma^+ \to p\pi^0$ decays. The solid curve of

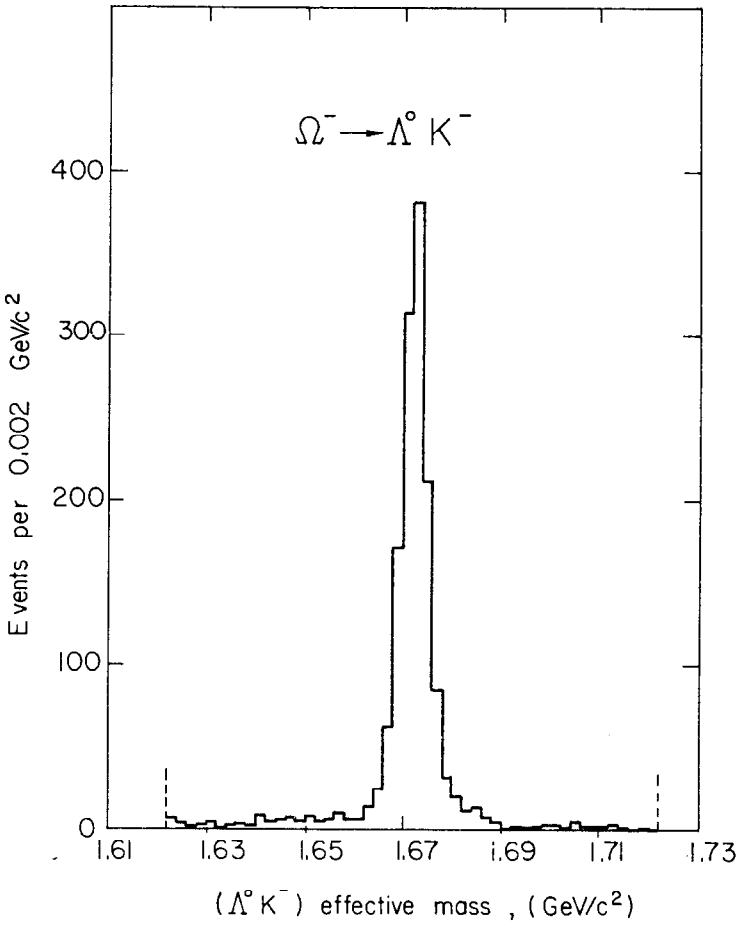

Fig. 5 (Λ^0, K^-) effective mass distribution for events with (Λ^0, π^-) mass > 1.35 GeV/c^2.

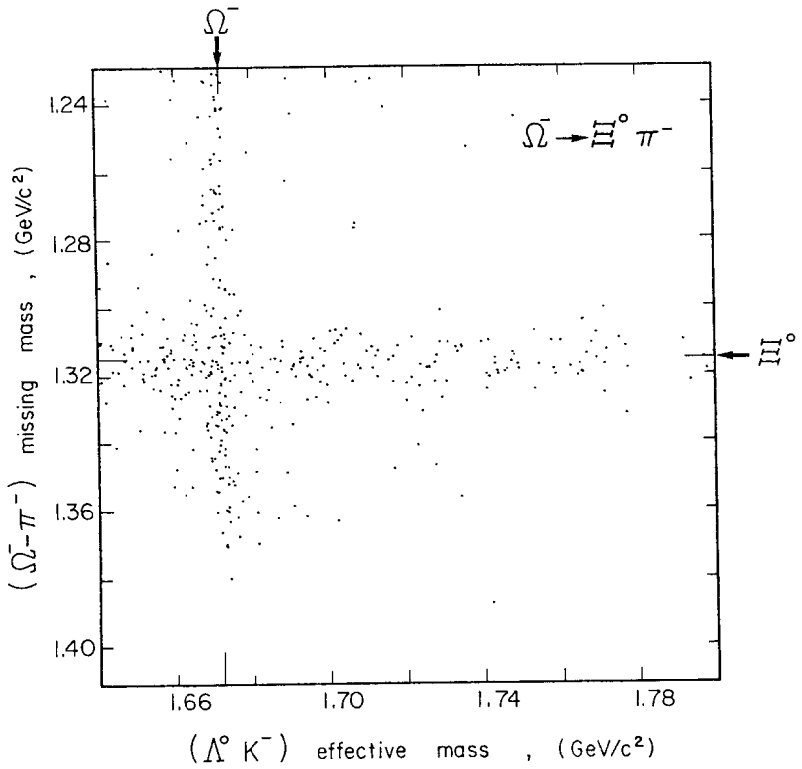

Fig. 6 Scatter plot of the $(\Omega^-\text{-}\pi^-)$ missing mass and the (Λ^0,K^-) mass for the $\Omega^- \to \Xi^0\pi^-$ candidates.

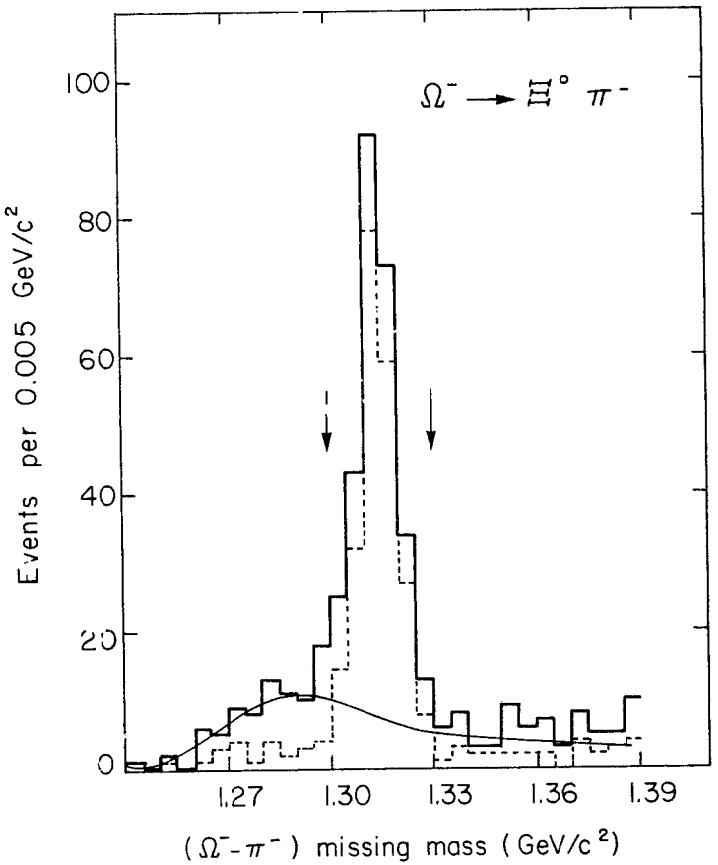

Fig. 7 The solid line is the $(\Omega^-\text{-}\pi^-)$ missing mass for $\Omega^- \to \Xi^0\pi^-$ candidates. The dashed line is the same distribution for the events which have at least one measured photon.

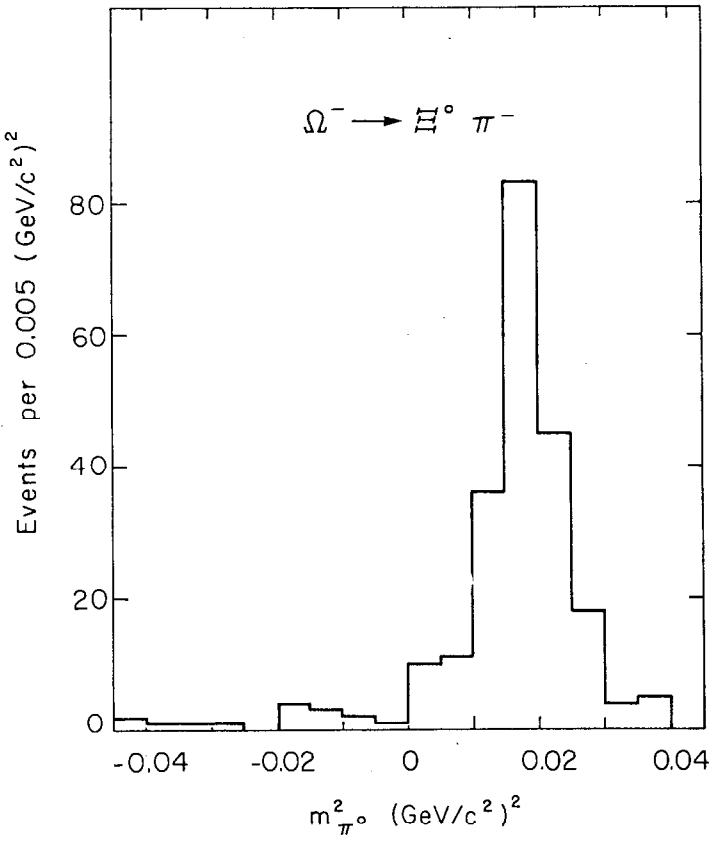

Fig. 8 π^0 missing mass squared for $\Xi^0\pi^-$ events with at least one measured photon.

fig. 9 shows the efficiency for detecting at least one phot decays as a function of the π^0 momentum. For comparison fi also shows the photon detection efficiency measured from th themselves.

2.3 The $\Omega^- \to \Xi^-\pi^0$ decay mode

The selection of the $\Xi^-\pi^0$ is made requiring that:

- the (Λ^0, π^-) effective mass is equal to the Ξ^- mass ±
- the beam momentum is within ± 10 GeV/c of the mean bea
- the supposed missing π^0 has a longitudinal momentum p_L 1 GeV/c,
- the different decay vertices are ordered as follows

$$z_{\Omega^-} < z_{\Xi^-} < z_{\Lambda}.$$

The background in this sample comes from the $\Xi^- \to \Lambda^0\pi^-$ is mainly concentrated at low p_L (p_L < 10 GeV/c) as shown i For a $\Xi^- \to \Lambda^0\pi^-$ event interpreted as $\Omega^- \to \Lambda^0\pi + x^0$ one gets

$$m_x^2 \simeq [(m_\Omega^2 - m_{\Xi^-}^2)/p_{beam}] \times p_L \simeq 0.01\ p_L.$$

The scatter plot of fig. 10 shows clearly the correlation $\Xi^- \to \Lambda^0\pi^-$ background events. To eliminate most of this ba a cut at p_L = 10 GeV/c. Fig. 11 shows the projection of th events on the $(\Omega^- - \Xi^-)$ missing mass squared axis. The ha are those which do not satisfy the photon requirements. U measured 90% photon detection efficiency and a background 3.5, we obtain a $\Xi^-\pi^0$ signal of 86 ± 12 events for p_L > 10

2.4 Ω^- Lifetime

The lifetime measurement is done using the $\Omega^- \to \Lambda^0K^-$ which is the most abundant. The event selection has been sect. 2.1. We measure the Ω^- decay vertex distribution. a lifetime can be deduced from this distribution has been

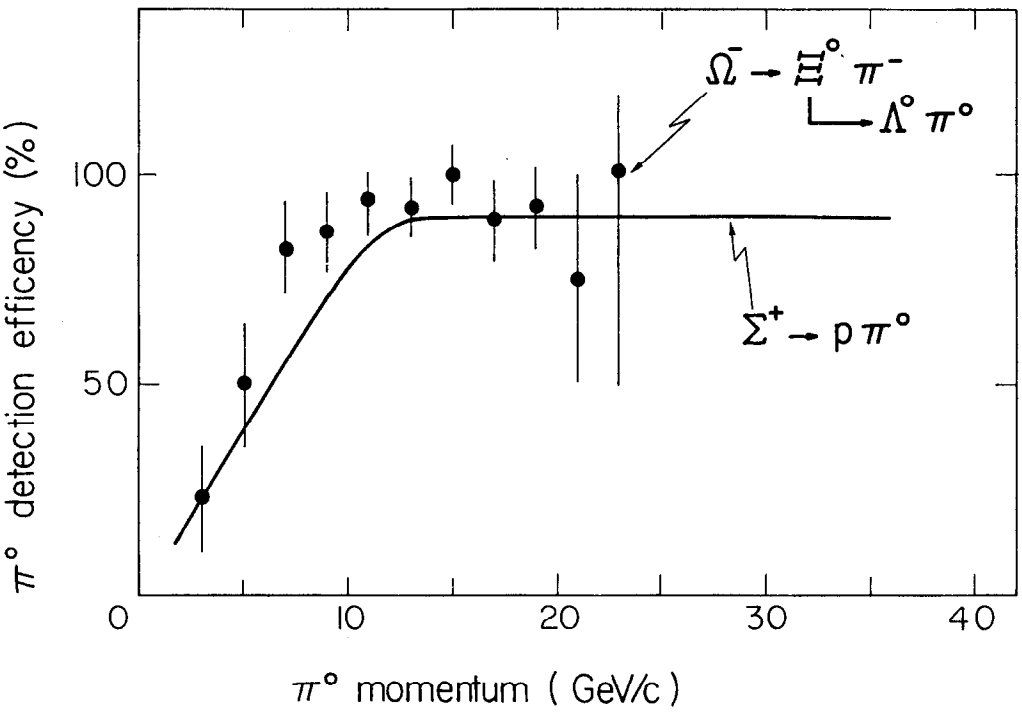

Fig. 9 Probability to detect at least one photon as a function of π^0 momentum. The solid line comes from the photon detection efficiency determined from $\Sigma^+ \to p\pi^0$. The points are obtained from $\Omega^- \to \Xi^0\pi^-$.

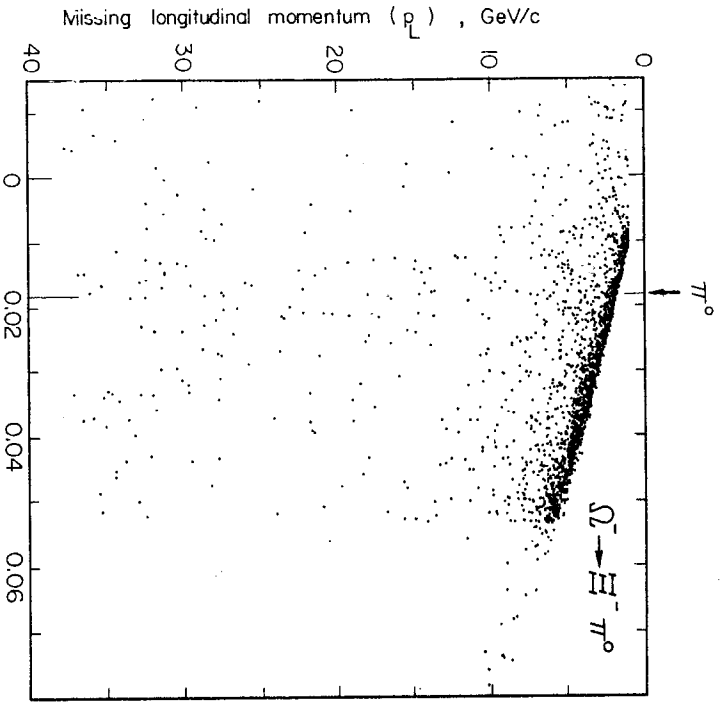

Fig. 10 Correlation between the $(\Omega^- - \Xi^-)$ missing mass squared and the longitudinal momentum of the missing π^0 for $\Omega^- \to \Xi^-\pi^0$ candidates.

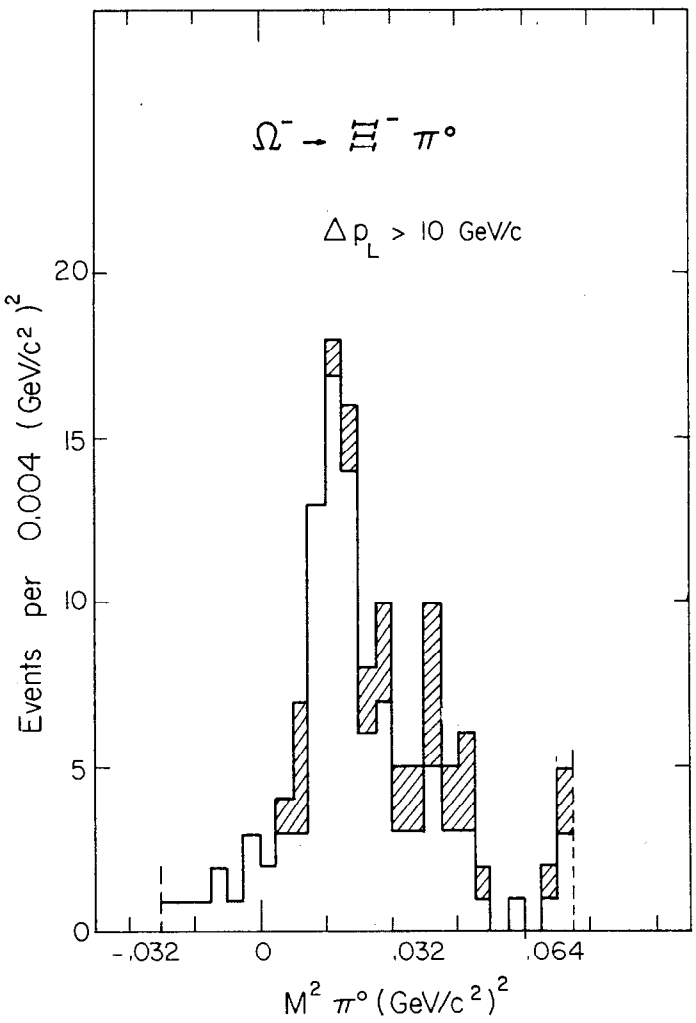

Fig. 11 $(\Omega^- - \Xi^-)$ missing mass squared for $\Omega^- \to \Xi^- \pi^0$ after elimination of the events with $p_L \leq 10$ GeV/c. The dashed events have no measured photon.

comparing a Monte-Carlo (M - C) simulation with the decay vertex distribution of $\Xi^- \to \Lambda^0 \pi^-$ events measured in the same apparatus.

The M - C simulation includes:

- the momentum and spatial distributions of the beam particles,
- the trigger requirements,
- the event selection criteria,
- the tracking of charged particles through the magnet,
- the measurement errors,
- the effect of confusion between very close tracks in the wire chamber telescope located before the magnet.

Fig. 12 shows the vertex position distribution of the Ξ^- from a sample of 22 000 events. The dashed curve corresponds to a M - C simulation which does not include the effect of confusion between close tracks. There is clearly a loss of events in the data for large values of the decay vertex coordinate which gets more pronounced when the vertex gets closer to the chamber telescope located before the magnet. That deficit of events is due to the effect of confusion between very close tracks. The parametrization of the confusion effect has been optimized on the $\Xi^- \to \Lambda^0 \pi^-$ decays and the complete M - C simulation gives the full curve of fig. 12. Fig. 13 displays the vertex position distribution for $\Omega^- \to \Lambda^0 K^-$ and the χ^2 of the fit between the data points and the Monte-Carlo tried for different lifetime hypotheses is shown in fig. 14. The best fit is obtained for $\tau_{\Omega^-} = 0.82 \times 10^{-10}$ sec with a χ^2 of 15 for 11 degrees of freedom and a statistical error of 0.03×10^{-10} sec. The full curve in fig. 13 corresponds to the best fit. The dashed curve is the fit obtained for a lifetime of 1.4×10^{-10} sec.

The value obtained for τ_{Ω^-} is stable if the start of the decay region is varied between 175 and 375 cm. The correction due to the confusion effect is small in the region where the Ω^- decays occur as can be seen from fig. 12. It corresponds to a change of 6% in the logarithmic slope. Taking into account possible systematic effects, we obtain:

$$\tau_{\Omega^-} = (.82 \pm .06) \times 10^{-10} \text{ sec.}$$

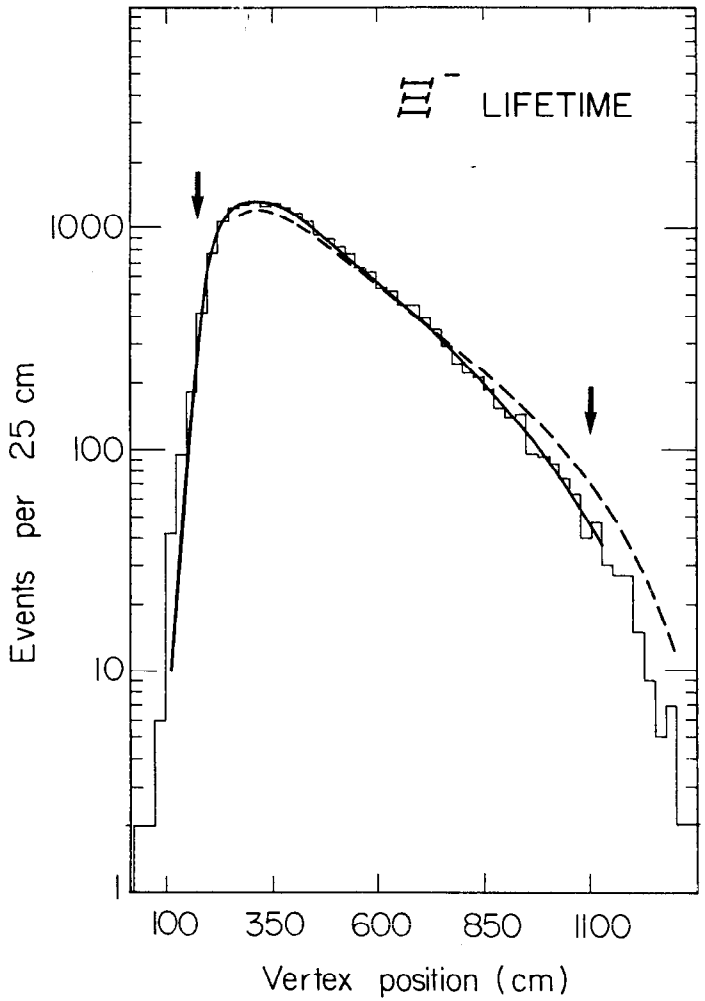

Fig. 12 Vertex position distribution for $\Xi^- \to \Lambda^0\pi^-$. The two curves correspond to M - C simulations taking $\tau_{\Xi^-} = 1.65 \times 10^{-10}$ sec. The dashed curve does not include the effect of the loss due to close tracks. The parametrisation of this effect yields the full M - C curve. The arrows delimit the range of decay points used for the calculation.

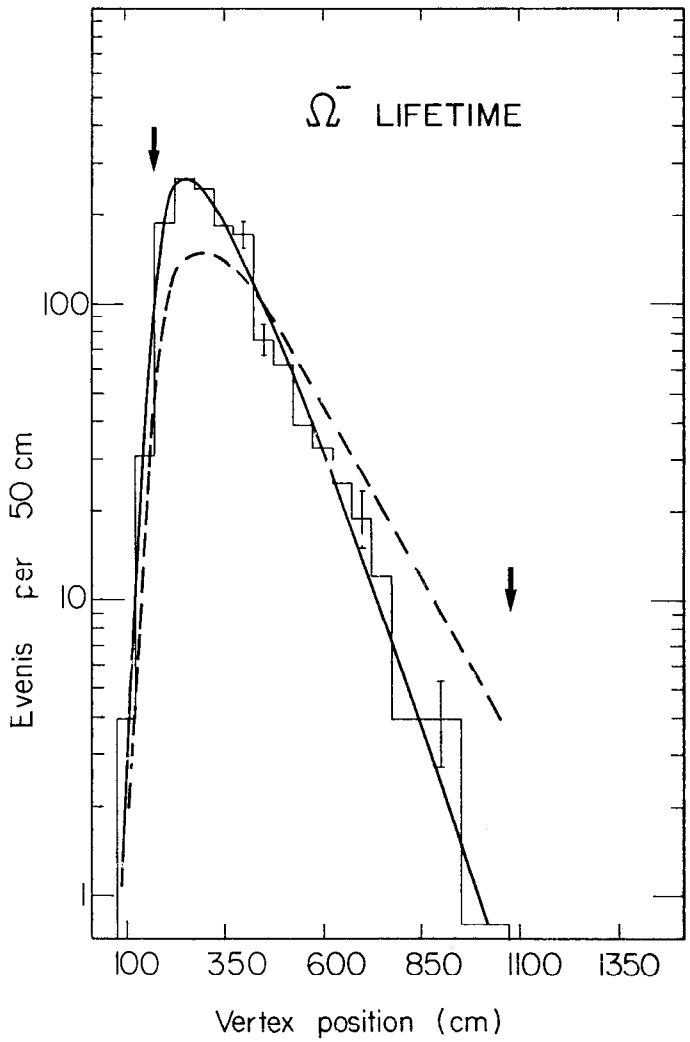

Fig. 13 Vertex position distribution for $\Omega^- \to \Lambda^0K^-$. The solid line is the Monte-Carlo fit for $\tau_\Omega = 0.82 \times 10^{-10}$ sec. The dashed curve correspond to $\tau_\Omega = 1.4 \times 10^{-10}$ sec. The arrows delimit the range of decay points used for the calculation.

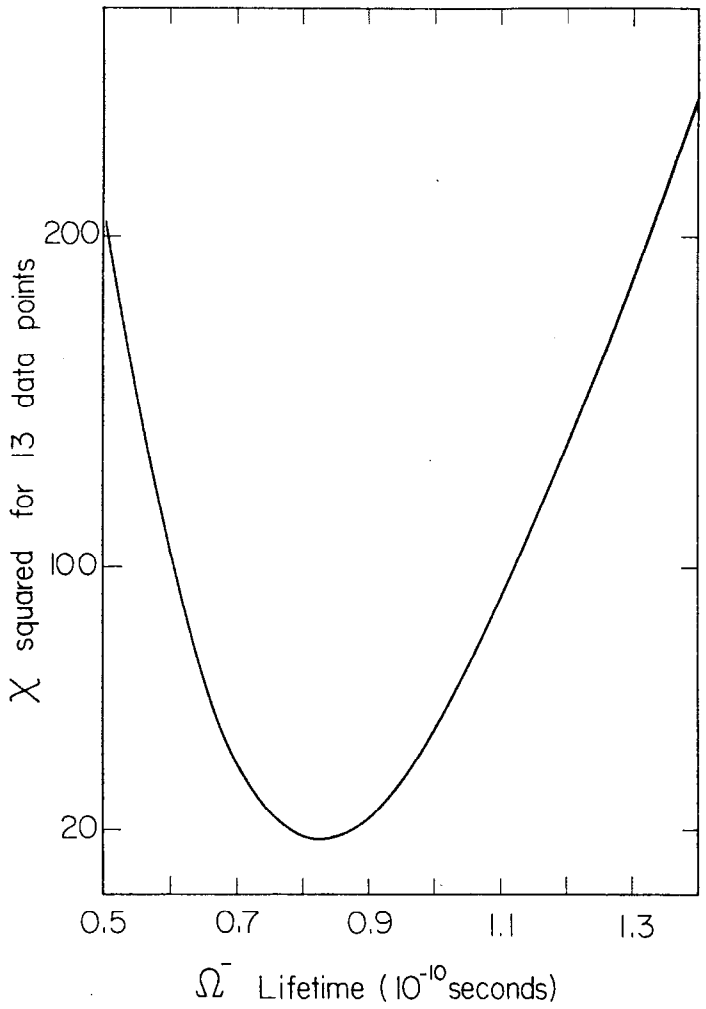

Fig. 14 Chi-squared of the fit between the data points and the Monte-Carlo for different Ω^- lifetime hypotheses.

This value is in disagreement with the Particle Data Group average [2] and the measurement of M. Deutschmann et al. [3] who get a value of $(1.41 \,^{+\,0.15}_{-\,0.24}) \times 10^{-10}$ sec. It agrees with the recent results of two bubble chamber experiments [4,5] each based on about 40 events.

2.5 Branching ratios for the main Ω^- decay modes

We have computed the selection efficiency and the relative acceptances using the M - C simulation with our own measured value of the Ω^- lifetime. From the data described above, assuming $\Gamma(\Lambda K) + \Gamma(\Xi^0\pi^-) + \Gamma(\Xi^-\pi^0) = \Gamma$ (all) i.e. neglecting rarer decay modes, we obtain the following ratios:

$$\frac{\Gamma(\Lambda K)}{\Gamma(\text{all})} = (67.0 \pm 2.2) \times 10^{-2}$$

$$\frac{\Gamma(\Xi^0\pi^-)}{\Gamma(\text{all})} = (24.6 \pm 1.9) \times 10^{-2}$$

$$\frac{\Gamma(\Xi^-\pi^0)}{\Gamma(\text{all})} = (8.4 \pm 1.1) \times 10^{-2}$$

The systematic uncertainties being negligible, the quoted errors are statistical only. We also get:

$$\Gamma(\Xi^0\pi^-)/\Gamma(\Xi^-\pi^0) = 2.93 \pm 0.50.$$

If the Ω^- decay proceeded through a pure $\Delta I = \frac{1}{2}$ amplitude a ratio of 2 would be expected. But within the framework of QCD, the $\Delta I = \frac{1}{2}$ contribution to the Ω^- decay amplitude is expected to be less important than for other hyperon decays and in a recent theoretical paper J. Finjord [6] predicts $\Gamma(\Xi^0\pi^-)/\Gamma(\Xi\,\pi^0) \simeq 3$.

2.6 The decay asymmetry parameter α for $\Omega^- \to \Lambda^0 K^-$

As we measure completely all the particles involved in the $\Lambda^0 K^-$ decay, we have used these events to compute the weak decay asymmetry parameter $\alpha_{\Lambda K}$ This parameter describes the interference of the two partial waves $a_{j-\frac{1}{2}}$ and $a_{j+\frac{1}{2}}$ which contribute to the transition matrix. It is a measure of the parity violation in that decay. Let θ be the angle

between the direction of the proton in the Λ^0 rest frame and the direction of the Λ^0 in the Ω^- rest frame. The proton angular distribution is given by:

$$I(\cos\theta) \sim 1 + \alpha_\Lambda \alpha_{\Lambda K} \cos\theta,$$

knowing α_Λ ($\alpha_\Lambda = .642 \pm .013$) and fitting the angular distribution with such a representation, we obtain:

$$\alpha_{\Omega \to \Lambda K} = .06 \pm .14,$$

where we quote the statistical uncertainty only. As a check we have also measured α_Ξ with the $\Xi^- \to \Lambda^0\pi^-$ events. We obtain $\alpha_\Xi = -.312 \pm .078$ in good agreement with the world average ($-.392 \pm .021$).

Our measurement is in good agreement with theoretical expectations [6] that the $\Omega^- \to \Lambda^0 K^-$ decay mode be nearly parity conserving.

2.7 The rare decay modes

We have made a search in our data sample for the decay $\Omega^- \to \Lambda\pi^-$ which would correspond to a $\Delta S = -2$ transition. We have found no events and conclude that:

$$\frac{\Gamma(\Omega \to \Lambda\,\pi)}{\Gamma(\text{all})} < 1.5 \times 10^{-3} \text{ at 90\% confidence level.}$$

The decay channel $\Omega^- \to \Xi^-\pi^+\pi^-$ has been analysed. At the present stage of the analysis, one clear event has been found with coherent vertices and a $(\Xi^-\pi^+)$ effective mass of 1533 MeV/c^2 near the $\Xi^*(1530)$ mass. The $\Xi^*(1530)\pi$ is expected to dominate in the 3 body decay mode and with a $\Delta I = \frac{1}{2}$ decay amplitude the analysed channel represent 4/9 of all $\Xi^*\pi$ decays. Thus the observed event corresponds to a branching ratio of about 2×10^{-3} for $\Omega^- \to \Xi^*\pi$.

We have searched for the decay $\Omega^- \to \Xi^0 e^- \bar{\nu}$ followed by $\Xi^0 \to \Lambda^0\pi^0$. We have found 3 candidates which have an identified electron, a reconstructed π^0 and correct π^0 and $(\Lambda^0\pi^0)$ masses. We are still investigating possible residual backgrounds from the decays $\Omega^- \to \Xi^0\pi^-$ and $\Omega^- \to \Xi^-\pi^0$. With the relative efficiency for that decay mode, 3 events would correspond to a branching ratio $\Gamma_{lept}/\Gamma_{all} \simeq 10^{-2}$.

3. HYPERON AND ANTIHYPERON PRODUCTION [1]

In this section I will briefly review the main features of the production of hyperon and antihyperon by 200 and 210 GeV protons at $x = 0.48$. Fig. 15 shows the ratios baryon/π^- and antibaryon/baryon as a function of the baryon strangeness. For the ratios baryon/π^- we have assigned 15% uncertainties which account for the reproducibility of the measurements under different beam conditions. For the Ω^-/π^- ratio, the larger uncertainty is almost entirely due to the 6% lifetime uncertainty. The ratio baryon/π^- decreases rapidly with the strangeness from 10 for p/π^- to 2.9×10^{-4} for Ω^-/π^-. In contrast the antibaryon/baryon ratio increases rapidly with the strangeness. Hyperons can be produced through the decay of an excited state of the incoming baryon (leading particle effect) or as a pair with an antihyperon. The observed ratios reflect the progressive disappearance of the first process when the strangeness and the mass of the produced hyperon increase.

4. CONCLUSIONS

From a large sample (1713 events) of Ω^- decays we have obtained a precise determination of:

(i) The Ω^- lifetime $\tau_\Omega = (.82 \pm .06)\ 10^{-10}$ sec.

(ii) The Ω^- branching ratios into Λ^0K^-, $\Xi^0\pi^-$, $\Xi^-\pi^0$

$$\Gamma(\Lambda K)/\Gamma_{all} = (67.0 \pm 2.2)\ 10^{-2}$$
$$\Gamma(\Xi^0\pi^-)/\Gamma_{all} = (24.6 \pm 1.9)\ 10^{-2}$$
$$\Gamma(\Xi^-\pi^0)/\Gamma_{all} = (8.4 \pm 1.1)\ 10^{-2}.$$

(iii) The weak decay asymmetry parameter for $\Omega^- \to \Lambda^0K^-$

$$\alpha_{\Lambda K} = .06 \pm .14.$$

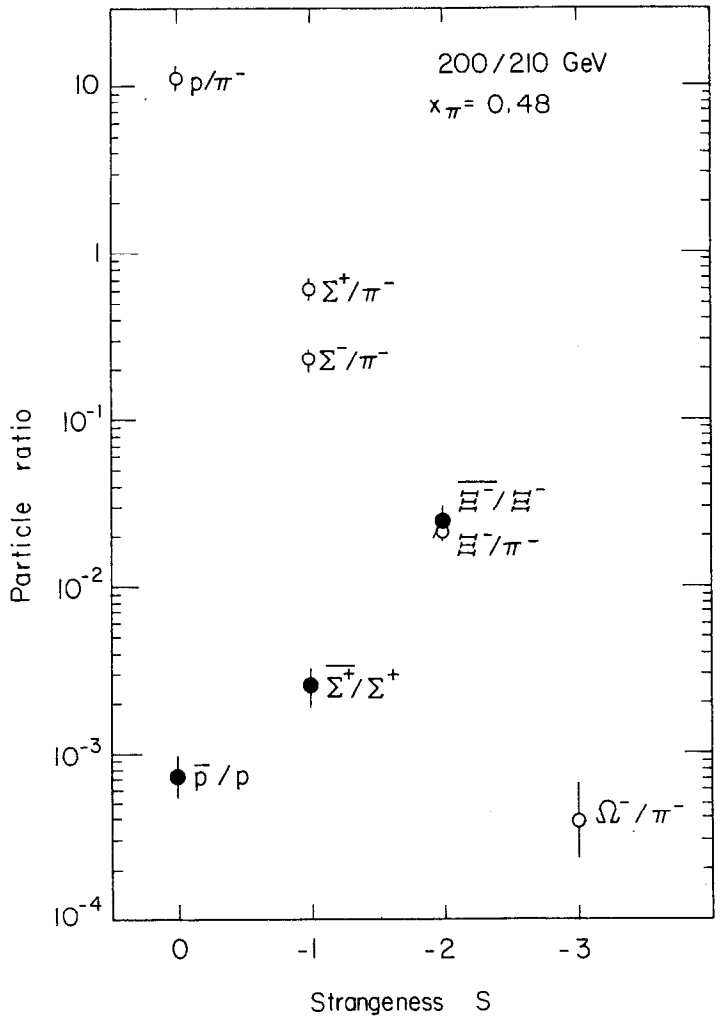

Fig. 15 Particle ratios as a function of strangeness.

The fact that the $\Omega^- \to \Lambda^0 K^-$ is nearly parity conserving and the observed ratio $\Gamma(\Xi^0\pi^-)/\Gamma(\Xi^-\pi^0) = 2.93 \pm 0.50$ are in good agreement with theoretical expectations within the QCD framework. The importance of the Ω^- decay parameters as a test of current theoretical ideas will be discussed in detail by M.K. Gaillard [7] in her talk.

The search for rare decay modes has allowed us to set an upper limit on the $\Delta S = -2$ forbidden transition, $\Omega^- \to \Lambda^0\pi^-$.

$$\frac{\Gamma(\Omega^- \to \Lambda^0\pi^-)}{\Gamma(\text{all})} < 1.5 \times 10^{-3} \text{ at 90\% confidence level.}$$

REFERENCES AND FOOTNOTES

[1] Particle and antiparticle production by 200 and 210 GeV protons in the CERN-SPS charged hyperon beam. To be submitted to Nucl. Phys. This paper describes in detail the hyperon beam and gives the production rates.

[2] Particle Data Group, Rev. Mod. Phys. 48 (1976) no. 2 part II.

[3] M. Deutschmann et al., Phys. Lett. B73 (1978) 96.

[4] R.J. Hemingway et al., to be published in Nucl. Phys.

[5] M. Baubillier et al., to be published in Phys. Lett.

[6] J. Finjord, Phys. Lett. 76B (1978) 116.

[7] M.K. Gaillard, Proceedings of the SLAC Summer Institute (1978).

PARTICIPANTS

A:

L. Abbott
SLAC - Bin 81
P.O. Box 4349
Stanford, Ca. 94305

Gregory Adkins
U. of California
Physics Dept.
Los Angeles, Ca. 90024

M. Aelion
SLAC - Bin 81
P.O. Box 4349
Stanford, Ca. 94305

S. Alam
SLAC - Bin 95
P.O. Box 4349
Stanford, Ca. 94305

David Aschman
Princeton University
Physics Dept.
Princeton, N.J. 08540

W. B. Atwood
SLAC - Bin 96
P.O. Box 4349
Stanford, Ca. 94305

R. Avakian
SLAC - Bin 96
P. O. Box 4349
Stanford, Ca. 94305

B:

B. Baaquie
61, D.O.H.S.
Dacca Cantt.
Dacca-6, Bangladesh

David Badtke
Johns Hopkins Univ.
Physics Dept.
Baltimore, Md. 21218

J. Ballam
SLAC - Bin 80
P.O. Box 4349
Stanford, Ca. 94305

Rose Mary Baltrusaitis
Fermilab
P.O. Box 500
Batavia, Ill. 60510

Uzi Bar-Gadda
SLAC - Bin 81
P.O. Box 4349
Stanford, Ca. 94305

Michael Barnett
SLAC - Bin 81
P.O. Box 4349
Stanford, Ca. 94305

Shahar Ben-Menahem
SLAC - Bin 81
P.O. Box 4349
Stanford, Ca. 94305

Vinod Bharadwaj
U. of California
Physics Dept.
Santa Barbara, Ca. 93106

David L. Bintinger
Fermilab
P.O. Box 500
Batavia, Ill. 60510

James Bjorken
SLAC - Bin 81
P.O. Box 4349
Stanford, Ca. 94305

Richard Blankenbecler
SLAC - Bin 81
P.O. Box 4349
Stanford, Ca. 94305

Craig Blocker
Lawrence Berkeley Laboratory
University of California
Berkeley, Ca. 94720

David Blockus
Johns Hopkins Univ.
Physics Department
Baltimore, Md. 21218

Elliott Bloom
SLAC - Bin 98
P.O. Box 4349
Stanford, Ca. 94305

Furio Bobisut
Istituto di Fisica
Via Marzola 8
35100 Padua, Italy

Arthur Bowling
Agnes State College
Physics Dept.
Decatur, Ga. 30030

James Brau
SLAC - Bin 78
P.O. Box 4349
Stanford, Ca. 94305

David Brayshaw
SLAC - Bin 81
P.O. Box 4349
Stanford, Ca. 94305

Marty Breidenbach
SLAC - Bin 95
P.O. Box 4349
Stanford, Ca. 94305

Stanley Brodsky
SLAC - Bin 81
P.O. Box 4349
Stanford, Ca. 94305

Richard Brower
Univ. of California
Div. of Natural Sciences
Santa Cruz, Ca. 95064

John L. Brown
SLAC - Bin 71
P.O. Box 4349
Stanford, Ca. 94305

Karl Brown
SLAC - Bin 94
P.O. Box 4349
Stanford, Ca. 94305

R. M. Brown
CERN
1211 Geneva 23
Switzerland

Fatin Bulos
SLAC - Bin 98
P.O. Box 4349
Stanford, Ca. 94305

Kirk Bunnell
SLAC - Bin 65
P.O. Box 4349
Stanford, Ca. 94305

David Burke
SLAC - Bin 61
P.O. Box 4349
Stanford, Ca. 94305

Gerd Buschhorn
Max-Planck Institute
Föhringer Ring 6
D-8 Munchen 40
Germany

Paolo Butera
SLAC - Bin 81
P.O. Box 4349
Stanford, Ca. 94305

C:

Robert N. Cahn
U. of California
Physics Dept.
Davis, Ca. 95616

Michael Cain
U. of California
Physics Dept.
Santa Barbara, Ca. 93106

Robert Carnegie
Carleton University
Physics Dept.
Ottawa, Ontario, Canada K1S 5B6

Giorgio Carnesecchi
CERN
1211 Geneva 23
Switzerland

J. Terry Carroll
SLAC - Bin 78
P.O. Box 4349
Stanford, Ca. 94305

Victor Cautis
SLAC - Bin 78
P.O. Box 4349
Stanford, Ca. 94305

Matteo Cavelli-Sforza
SLAC - Bin 78
P.O. Box 4349
Stanford, Ca. 94305

George B. Chadwick
SLAC - Bin 78
P.O. Box 4349
Stanford, Ca. 94305

Vlada Chaloupka
SLAC - Bin 78
P.O. Box 4349
Stanford, Ca. 94305

Lai-Him Chan
Louisiana State Univ.
Physics & Astronomy Dept.
Baton Rouge, La. 70803

Mark Coles
Lawrence Berkeley Laboratory
University of California
Berkeley, Ca. 94720

Eugene D. Commins
U. of California
Physics Department
Berkeley, Ca. 94720

Flavio Costantini
Istituto Di Fisica
2 Piazza Torricelli
56100 Pisa, Italy

M. D. Cooper
Los Alamos Scientific Lab.
P.O. Box 1663
Los Alamos, N.M. 87544

Susan Cooper
Lawrence Berkeley Laboratory
University of California
Berkeley, Ca. 94720

R. L. A. Cottrell
SLAC - Bin 96
P.O. Box 4349
Stanford, Ca. 94305

Don Coyne
Princeton University
Physics Dept.
Princeton, N.J. 08540

D:

Kamala Prasad Das
Univ. of Oregon
Inst. of Theoretical Science
Eugene, Oregon 97403

Jan Dash
Centre de Physique Theorique
CNRS
31 Chemin J. Aiguier
F-13274 Marseille
CEDEX 2, France

M. Daumens
Univ. de Bordeaux I
Lab. de Physique Theorique
Chemin du Solarium
F-33170 Gradignan, France

Michel Davier
Univ. Paris XI
Lab de l'Accelerateur Lineaire
Batiment 200
F-91405 Orsay, France

Christopher M. Debeau
Univ. of California
Physics Department
Irvine, Ca. 92664

N. G. Deshpande
Univ. of Oregon
Inst. of Theoretical Science
Eugene, Oregon 97403

H. DeStaebler
SLAC - Bin 96
P.O. Box 4349
Stanford, Ca. 94305

Walter Dey
TRIUMF
Univ. of British Columbia
Vancouver, BC, Canada V6T 1W5

Alain-Michel Diamont-Berger
SLAC - Bin 63
P.O. Box 4349
Stanford, Ca. 94305

Robert Diebold
Argonne National Lab.
9700 So. Cass Ave.
Argonne, Ill. 60439

Patrick Dishaw
SLAC - Bin 63
P.O. Box 4349
Stanford, Ca. 94305

Peter N. Dobson, Jr.
Univ. of Hawaii
Dept. of Physics & Astronomy

Greg Donaldson
SLAC - Bin 63
P.O. Box 4349
Stanford, Ca. 94305

W. Van Doninck
Vrije Univ. Brussel
Theoretische Natuurkunde
Pleinlaan 2
B-1050 Brussels, Belgium

J. Dorenbosch
SLAC - Bin 95
P.O. Box 4349
Stanford, Ca. 94305

Jonathan Dorfan
SLAC - Bin 61
P.O. Box 4349
Stanford, Ca. 94305

P. J. Dornan
Imperial College
Physics Dept.
London SW 7 2A2, England

William Dunwoodie
SLAC - Bin 62
P.O. Box 4349
Stanford, Ca. 94305

Stanley Durkin
SLAC - Bin 62
P.O. Box 4349
Stanford, Ca. 94305

Marsha Duro
SLAC - Bin 63
P.O. Box 4349
Stanford, Ca. 94305

E:

T. Eguchi
Fermi Institute
Univ. of Chicago
5640 S. Ellis Ave.
Chicago, Ill. 60637

Martin B. Einhorn
Univ. of Michigan
Physics Dept.
Ann Arbor, Mi. 48104

Alan M. Eisner
Univ. of California
Physics Dept.
Santa Barbara, Ca. 93106

John Ellis
CERN
1211 Geneva 23
Switzerland

A. Engler
Carnegie Mellon Univ.
Physics Dept.
Pittsburgh, Pa. 15213

F:

Ralph Fabrizio
Univ. of Michigan
Physics Dept.
Ann Arbor, Mi. 48109

Edward Fahri
SLAC - Bin 81
P.O. Box 4349
Stanford, Ca. 94305

Graham Farmelo
Open Univ.
Walton Hall, Faculty of Science
Physics Dept.
Milton Keynes, England

Gary Feldman
SLAC - Bin 61
P.O. Box 4349
Stanford, Ca. 94305

Joe Feller
Lawrence Berkeley Lab.
Univ. of California
Berkeley, Ca. 94720

Thomas Ferguson
SLAC - Bin 98
P.O. Box 4349
Stanford, Ca. 94305

Ted Fieguth
SLAC - Bin 20
P.O. Box 4349
Stanford, Ca. 94305

Clive Field
SLAC - Bin 78
P.O. Box 4349
Stanford, Ca. 94305

N. Fortson
U. of Washington
Physics Dept.
Seattle, Wa. 98195

William R. Francis
Michigan State Univ.
Physics Dept.
East Lansing, Mi. 48823

Melissa Franklin
SLAC - Bin 61
P.O. Box 4349
Stanford, Ca. 94305

David Freyberger
SLAC - Bin 20
P.O. Box 4349
Stanford, Ca. 94305

Yasutaka Fukushima
Fermilab
P.O. Box 500
Batavia, Ill. 60510

Miguel A. Furman
Lawrence Berkeley Lab.
U. of California
Berkeley, Ca. 94720

G:

J. M. Gaillard
Univ. of Paris
Lab de l'Accelerateur Lineaire
Batiment 200
91405 Orsay, France

M. K. Gaillard
CERN
1211 Geneva 23
Switzerland

John Gaiser
SLAC - Bin 98
P.O. Box 4349
Stanford, Ca. 94305

Roger Gearhart
SLAC - Bin 20
P.O. Box 4349
Stanford, Ca. 94305

Murdock Gilchriese
Cornell Univ.
Newman Lab.
Ithaca, N.Y. 14853

Roscoe Giles
Mass. Institute of Technology
Physics Dept.
Cambridge, Ma. 02139

Frederick Gilman
SLAC - Bin 81
P.O. Box 4349
Stanford, Ca. 94305

Thomas Glanzman
Duke University
Physics Dept.
Durham, N.C. 27706

Austin M. Gleeson
Univ. of Texas
Center for Particle Theory
Austin, Tx. 78712

Gary Godfrey
SLAC - Bin 98
P.O. Box 4349
Stanford, Ca. 94305

T. J. Goldman
Los Alamos Scientific Lab.
P.O. Box 1663
Los Alamos, N.M. 87544

George Gollin
Princeton University
Physics Dept.
Princeton, N.J. 08540

A. Gonidec
Lab d'Annecy-le-Vieux
B.P. 909
F-74019 Annecy-le-Vieux
CEDEX
France

Francesco Grancagnolo
Univ. of California
Div. of Natural Sciences
Santa Cruz, Ca. 95064

Jean-Yves Grandpeix
SLAC - Bin 78
P.O. Box 4349
Stanford, Ca. 94305

Martin Green
Univ. of Southampton
Physics Dept.
Highfield
Southampton SO9 5NH, England

T. Gregorian
Bedford College
Univ. of London
40 Mornington Terrace
London NW 1, England

Pavel Grossman
Univ. of Oxford
Nuclear Physics Lab.
Keble Road
Oxford OX1 3RH, England

J. P. Guillaud
Univ. of Indiana
Physics Dept.
Bloomington, Ind. 47401

H:

Baruch Haber
SLAC - Bin 65
P.O. Box 4349
Stanford, Ca. 94305

Howard Haber
Univ. of Michigan
Physics Dept.
Ann Arbor, Mi. 48104

Leopold Halpern
Florida State Univ.
Physics Dept.
Tallahassee, Fl. 32306

Brian Haltsley
SLAC - Bin 94
P.O. Box 4349
Stanford, Ca. 94305

Gail Hanson
SLAC - Bin 61
P.O. Box 4349
Stanford, Ca. 94305

Kenneth Hayes
SLAC - Bin 61
P.O. Box 4349
Stanford, Ca. 94305

A. W. Hendry
Lawrence Berkeley Lab.
Univ. of California
Berkeley, Ca. 94720

B. Hermannsfeldt
SLAC - Bin 33
P.O. Box 4349
Stanford, Ca. 94305

Thomas Himel
SLAC - Bin 95
P.O. Box 4349
Stanford, Ca. 94305

Ian Hinchliffe
Lawrence Berkeley Lab.
Univ. of California
Berkeley, Ca. 94720

David Hitlin
SLAC - Bin 95
P.O. Box 4349
Stanford, Ca. 94305

M. Holder
CERN
1211 Geneva 23
Switzerland

Alan Honma
SLAC - Bin 62
P.O. Box 4349
Stanford, Ca. 94305

R. Horgan
Theory Division
CERN
1211 Geneva 23
Switzerland

David Hutchinson
SLAC - Bin 62
P.O. Box 4349
Stanford, Ca. 94305

I:

George Irwin
SLAC - Bin 63
P.O. Box 4349
Stanford, Ca. 94305

David Iskandar
Univ. of Oregon
Inst. of Theoretical Science
Eugene, Ore. 97403

J:

A. Jabs
SLAC - Bin 81
P.O. Box 4349
Stanford, Ca. 94305

Fritz Janata
DESY
Notkestieg 1
D-2000 Hamburg 52, Germany

John Jaros
SLAC - Bin 61
P.O. Box 4349
Stanford, Ca. 94305

P. Jenni
SLAC - Bin 95
P.O. Box 4349
Stanford, Ca. 94305

Karl J. Johnson
Lawrence Berkeley Lab.
Univ. of California
Berkeley, California 94720

James Johnson
SLAC - Bin 94
P.O. Box 4349
Stanford, Ca. 94305

William B. Johnson
SLAC - Bin 62
P.O. Box 4349
Stanford, Ca. 94305

E. Jones
SLAC - Bin 81
P.O. Box 4349
Stanford, Ca. 94305

U. Joshi
Univ. of California
Physics Dept.
Santa Barbara, Ca. 93106

K:

Vladimir Kadyshevsky
Joint Institute for Nuclear Research
Head P. O. Box 79
101000 Moscow, U.S.S.R.

Sinan Kaptanoglu
Institute for Theoretical Physics
SUNY at Stony Brook
Stony Brook, N.Y. 11794

Inga Karliner
Fermilab
P.O. Box 500
Batavia, Ill. 60510

Alan Katz
SLAC - Bin 81
P.O. Box 4349
Stanford, Ca. 94305

Boris Kayser
Div. of Physics
National Science Foundation
Washington, D. C. 20550

Yoichi Kazama
Fermilab
P.O. Box 500
Batavia, Ill. 60510

Lewis Keller
SLAC - Bin 20
P.O. Box 4349
Stanford, Ca. 94305

Robert Kelly
Lawrence Berkeley Laboratory
U. of California
Berkeley, Ca. 94720

Rosemary G. Kennett
California Inst. Tech.
Physics Dept.
Pasadena, Ca. 91125

Joel Kent
Lawrence Berkeley Lab.
U. of California
Berkeley, Ca. 94720

Wai-Yee Keung
Univ. of Wisconsin
Physics Dept.
Madison, Wisc. 53706

S. Kheifets
SLAC - Bin 12
P.O. Box 4349
Stanford, Ca. 94305

Chris Kiesling
SLAC - Bin 98
P.O. Box 4349
Stanford, Ca. 94305

I. Kimel
Univ. de Sao Paulo
Inst. de Fisica
Cidade Univ.
C.P. 20516
Sao Paulo, Brazil

Jasper Kirkby
Stanford University
Physics Dept.
Stanford, Ca. 94305

Janos Kirz
State Univ. of New York
Physics Dept.
Stony Brook, N.Y. 11794

Helmut Koch
CERN - EP Div.
1211 Geneva 23
Switzerland

Herman F. Kolanoski
Stanford Univ.
High Energy Physics Lab.
Stanford, Ca 94305

Wolf D. Kollmann
SLAC - Bin 98
P.O. Box 4349
Stanford, Ca. 94305

Takahiko Kondo
Fermilab
P.O. Box 500
Batavia, Ill. 60510

Ivan Kramer
Univ. of Maryland
Physics Dept.
5401 Wilken Ave.
Baltimore, Md. 21228

Philip Kraushaar, Jr.
Univ. of Michigan
Physics Dept.
Ann Arbor, Mi. 48104

Clara Keuhn
Univ. of Wisconsin
Physics Dept.
Madison, Wisc. 53706

Paul Kunz
SLAC - Bin 62
P.O. Box 4349
Stanford, Ca. 94305

Darmadi Kusno
Univ. of Oregon
Inst. of Theoretical Science
Eugene, Oregon 97403

N. Kwak
Univ. of Kansas
Physics & Astronomy Dept.
Lawrence, Ka 66044

L:

Kwan Wu Lai
Brookhaven National Lab.
Upton, Long Island, N.Y. 11973

Wolfgang Langguth
State Univ. of New York
Physics Dept.
Albany, N. Y. 12222

Rudy R. Larsen
SLAC - Bin 95
P.O. Box 4349
Stanford, Ca. 94305

Thomas Lasinski
SLAC - Bin 62
P.O. Box 4349
Stanford, Ca. 94305

David W. G. S. Leith
SLAC - Bin 62
P.O. Box 4349
Stanford, Ca. 94305

P. Lepage
Cornell Univ.
Lab. of Nuclear Studies
Ithaca, N.Y. 14850

Pat Leung
SLAC - Bin 94
P.O. Box 4349
Stanford, Ca. 94305

Lorne Levinson
SLAC - Bin 62
P.O. Box 4349
Stanford, Ca. 94305

Ling-Fong Li
Carnegie Mellon Univ.
Physics Dept.
Pittsburgh, Pa. 15213

J. Lindesay
SLAC - Bin 81
P.O. Box 4349
Stanford, Ca. 94305

C. Litwin
SLAC - Bin 61
P.O. Box 4349
Stanford, Ca. 94305

Nigel Lockyer
Argonne National Lab.
9700 So. Cass Ave.
Argonne, Ill. 60439

Eugene Loh
Univ. of Utah
Physics Dept.
Salt Lake City, Utah 84112

M. A. Lohe
Adelaide Univ.
Math-Physics Dept.
Adelaide, S.A. 5001
Australia

Michael J. Losty
Lawrence Berkeley Lab.
U. of California
Berkeley, California 94720

Wolfgang Luhrsen
Univ. Hamburg
II. Inst. Physik
Luruper-Chaussee 149
D-2000 Hamburg 50, Germany

Dieter Luke
DESY - F35
Notkestrasse 85
D-2 Hamburg 52
Germany

Vera Luth
SLAC - Bin 95
P.O. Box 4349
Stanford, Ca. 94305

Rick Lytel
Stanford Univ.
Physics Dept.
Stanford, Ca. 94305

M:

Ernest Ma
Univ. of Hawaii
Physics Dept.
Honolulu, Hi. 96822

Z. Ming Ma
SLAC - Bin 65
P.O. Box 4349
Stanford, Ca. 94305

Ebrahim Mahdavi-hez
Bedford College
Univ. of London
40 Mornington Terrace
London NW 1, England

Margaret Malone
Univ. of Melbourne
School of Physics
Parkville, Victoria
3052, Australia

Kim Maltman
Univ. of Toronto
Dept. of Physics
Toronto, On, Canada M5S 1A7

Thomas W. Markiewicz
Lawrence Berkeley Laboratory
Univ. of California
Berkeley, Ca. 94720

Francois Martin
SLAC - Bin 81
P.O. Box 4349
Stanford, Ca. 94305

Michael Marx
Brookhaven National Lab.
Upton, L.I., New York 11973

George E. Masek
U. of California, San Diego
Physics Department
La Jolla, Ca. 92093

Chris May
Johns Hopkins Univ.
Physics Dept.
Baltimore, Md. 21218

Robert McKee
Carleton Univ.
Physics Dept.
Ottawa, On., Canada K1S 5B6

Larry McLerran
SLAC - Bin 81
P.O. Box 4349
Stanford, Ca. 94305

Frank Merritt
SLAC - Bin 63
P.O. Box 4349
Stanford, Ca. 94305

Pierre Mery
Centre de Physique Theorique
Centre Univ. de Luminy
70 Route Leon Lachamp
13009 Navseille, France

Hinrich Meyer
DESY
Notkestieg 1
D2000 Hamburg 52, Germany

Thomas Meyer
SLAC - Bin 62
P.O. Box 4349
Stanford, Ca. 94305

Peter D. Meyers
Lawrence Berkeley Lab.
U. of California
Berkeley, Ca. 94720

Stefan Michalowski
SLAC - Bin 94
P.O. Box 4349
Stanford, Ca. 94305

D. Miller
SLAC - Bin 81
P.O. Box 4349
Stanford, Ca. 94305

Ross Millikan
Lawrence Berkeley Lab.
U. of California
Berkeley, Ca. 94720

T. Minamikawa
SLAC - Bin 81
P.O. Box 4349
Stanford, Ca. 94305

Marie-Noelle Minard
L.A.P.P. Chemin du Bellevue
74019 Annecy le Vieux
France

I. Miroshnichenko
SLAC - Bin 78
P.O. Box 4349
Stanford, Ca. 94305

Michiko Miyamoto
Kobe College
Physics Dept.
4-1, Okadayama
Nishinomiya, Japan 622

Kenneth C. Moffeit
SLAC - Bin 78
P.O. Box 4349
Stanford, Ca. 94305

Rollin Morrison
U. of California
Physics Dept.
Santa Barbara, Ca. 93106

Robert Morse
U. of Wisconsin
Physics Dept.
Madison, Wisc. 53706

Robert Mozley
SLAC - Bin 65
P.O. Box 4349
Stanford, Ca. 94305

Michael J. Murtagh
Brookhaven National Lab.
Upton, L.I., New York 11973

N:

M. Nakamura
4-10-15 Minami
Yukigaya, Ohta, Tokyo
Japan

Charles A. Nelson
State Univ. of New York
Physics Dept.
Binghamton, N.Y. 13901

Y. J. Ng
U. of North Carolina
Physics & Astronomy Dept.
Chapel Hill, N.C. 27514

Larry Nodulman
U. of California
Physics Dept.
Los Angeles, Ca. 90024

O:

Jack O'Reilly
Stanford University
Physics Dept.
Stanford, Ca. 94305

F. G. Oakham
Carleton Univ.
Physics Dept.
Ottawa, On., Canada K1S 5B6

Allen Odian
SLAC - Bin 65
P.O. Box 4349
Stanford, Ca. 94305

Arthur Ogawa
Lawrence Berkeley Lab.
U. of California
Berkeley, Ca. 94720

Harry Orbach
SLAC - Bin 81
P.O. Box 4349
Stanford, Ca. 94305

Mark Oreglia
SLAC - Bin 98
P.O. Box 4349
Stanford, Ca. 94305

P:

Sandid Pakvasa
Univ. of Hawaii
Physics Dept.
Honolulu, HI 96822

Lalit Panda
Yale Univ.
Physics Dept.
New Haven, Ct. 06520

W. K. H. Panofsky
SLAC - Bin 80
P.O. Box 4349
Stanford, Ca. 94305

Sherwood Parker
Lawrence Berkeley Lab.
U. of California
Berkeley, Ca. 94720

Richard Partridge
California Institute Tech.
Physics Dept.
Pasadena, Ca. 91125

James F. Patrick
Lawrence Berkeley Lab.
U. of California
Berkeley, Ca. 94720

D. Perkins
Univ. of Oxford
Nuclear Physics Lab.
Keble Road
Oxford OX1 3RH, England

Martin Perl
SLAC - Bin 61
P.O. Box 4349
Stanford, Ca. 94305

B. Petersson
Univ. Bielefeld
Faculty of Physics
Postfach 8640
D-4800 Bielefeld 1, Germany

Kaori Maeshima Petrini
U. of California
Physics Dept.
Davis, Ca. 95616

William Petro
SLAC - Bin 63
P.O. Box 4349
Stanford, Ca. 94305

T. N. Pham
Ecole Polytechnique
Centre de Physique Theorique
Route de Saclay
F-91120 Palaiseau, France

E. Picasso
CERN
1211 Geneva 23
Switzerland

Venetis Polychronakos
Fermilab
P.O. Box 500
Batavia, Ill. 60510

Frank Porter
California Inst. Tech.
Physics Dept.
Pasadena, Ca. 91125

Richard Prepost
SLAC - Bin 94
P.O. Box 4349
Stanford, Ca. 94305

Charles P. Prescott
SLAC - Bin 96
P.O. Box 4349
Stanford, Ca. 94305

Thomas H. Pringle
Univ. of Oregon
Inst. of Theoretical Science
Eugene, Ore. 97403

Q:

Helen Quinn
SLAC - Bin 81
P.O. Box 4349
Stanford, Ca. 94305

R:

Jeff Rabin
Stanford Univ.
Physics Dept.
Stanford, Ca. 94305

Monroe S. Z. Rabin
Univ. of Massachusetts
Physics Dept.
Amherst, Ma. 01002

John P. Ralston
Univ. of Oregon
Inst. of Theoretical Science
Eugene, Ore. 97403

L. K. Rangan
Purdue Univ.
Physics Dept.
Lafayette, In. 47907

Petros Rapidis
SLAC - Bin 61
P.O. Box 4349
Stanford, Ca. 94305

Blair Ratcliff
SLAC - Bin 62
P.O. Box 4349
Stanford, Ca. 94305

David Reiss
California Inst. Tech.
Physics Dept.
Pasadena, Ca. 91125

J. Richardson
SLAC - Bin 81
P. O. Box 4349
Stanford, Ca. 94305

Mark L. Richardson
SLAC - Bin 98
P.O. Box 4349
Stanford, Ca. 94305

Leon Rochester
SLAC - Bin 96
P.O. Box 4349
Stanford, Ca. 94305

Michael Ronan
Lawrence Berkeley Lab.
U. of California
Berkeley, Ca. 94720

Carlo Rubbia
Harvard Univ.
Physics Dept.
Cambridge, Ma. 02138

S:

Hartmut Sadrozinski
Princeton Univ.
Physics Dept.
Princeton, N.J. 08540

H. G. Sander
Tech. Hochsch., Aachen
I. Physikalisches Institut
Schinkelstrasse 2
D-5100 Aachen, Germany

J. Sapirstein
SLAC - Bin 81
P.O. Box 4349
Stanford, Ca. 94305

P. Scharbach
Rutherford Lab.
Theoretical Physics Dept.
Chilton, Didcot, England

Daniel Scharre
SLAC - Bin 61
P.O. Box 4349
Stanford, Ca. 94305

Rafe Schindler
SLAC - Bin 95
P.O. Box 4349
Stanford, Ca. 94305

C. Schmid
Eidgenossische Tech. Hochsch.
Theoretische Physik
Honggerberg
CH-8093 Zurich, Switzerland

William Schreiber
The College of Staten Island
City Univ. of N.Y.
Sunnyside Campus
Physics Dept.
Staten Island, N.Y. 10301

Jonas Schultz
U. of California, Irvine
Physics Dept.
Irvine, Ca. 92664

Mel Schwartz
Stanford University
Physics Department
Stanford, Ca. 94305

B. Schwarzschild
U. of Toronto
Physics Department
Toronto, Canada M5S 1A7

Roy Schwitters
SLAC - Bin 95
P.O. Box 4349
Stanford, Ca. 94305

Frank Sciulli
California Inst. Tech.
Physics Dept.
Pasadena, Ca. 91125

Steve Shapiro
SLAC - Bin 62
P.O. Box 4349
Stanford, Ca. 94305

Gordon Shaw
U. of California, Irvine
Physics Dept.
Irvine, Ca. 92664

Marc Sher
U. of Colorado
Physics & Astrophysics Dept.
Boulder, Co. 80302

David Sherden
SLAC - Bin 60
P.O. Box 4349
Stanford, Ca. 94305

Thomas N. Sherry
International Center for Theor. Physics
Miramare-Grignano
P.O. Box 586
I-34100 Trieste, Italy

Kirk A. Shinsky
Cornell Univ.
Lab of Nuclear Studies
Ithaca, N. Y. 14853

Ken-ichi Shizuya
Fermilab
P.O. Box 500
Batavia, Ill. 60510

James Siegrist
SLAC - Bin 95
P.O. Box 4349
Stanford, Ca. 94305

Pierre Sikivie
SLAC - Bin 81
P.O. Box 4349
Stanford, Ca. 94305

D. Silverman
SLAC - Bin 81
P.O. Box 4349
Stanford, Ca. 94305

Patrick Skubic
Rutgers Univ.
Physics Dept.
New Brunswick, N.J. 08903

W. E. Slater
U. of California
Physics Dept.
Los Angeles, Ca. 90024

A. Gordon Smith
Stanford University
Physics Department
Stanford, Ca. 94305

Wesley H. Smith
Lawrence Berkeley Lab.
U. of California
Berkeley, Ca. 94720

Gregory R. Snow
Rockefeller Univ.
Physics Dept.
New York, N.Y. 10021

Miguel Socolovsky
SLAC - Bin 81
P.O. Box 4349
Stanford, Ca. 94305

A. Soni
U. of California, Irvine
Physics Dept.
Irvine, Ca. 92664

Stephen B. Sontz
Northwestern Univ.
Physics Dept.
Evanston, Il. 60201

Cherrill Spencer
Florida State Univ.
Physics Dept.
Tallahassee, Fl. 32306

Robin Staffin
SLAC - Bin 81
P.O. Box 4349
Stanford, Ca. 94305

Thomas H. Sterling
U. of Michigan
Physics Dept.
Ann Arbor, Mi. 48104

James Strait
Lawrence Berkeley Lab.
U. of California
Berkeley, Ca. 94720

Ryszard Stroynowski
SLAC - Bin 62
P.O. Box 4349
Stanford, Ca. 94305

Robert Sugar
U. of California
Physics Dept.
Santa Barbara, Ca. 93106

Pamela Surko
Princeton Univ.
Physics Dept.
Princeton, N.J. 08540

M. Suzuki
Lawrence Berkeley Lab.
U. of California
Berkeley, Ca. 94720

Benjamin Svetitsky
SLAC - Bin 81
P.O. Box 4349
Stanford, Ca. 94305

Zenon M. Szalata
American University
Physics Department
Washington, D.C. 20016

T:

Yoshinobu Takaiwa
Univ. of Tsukuba
Physics Dept.
Ibaraki, Japan 300-31

Eiichi Takasugi
Univ. of Texas
Center for Particle Theory
Austin, Tx. 78712

Richard Talaga
Lawrence Berkeley Lab.
U. of California
Berkeley, Ca. 94720

Hans Taureg
SLAC - Bin 95
P.O. Box 4349
Stanford, Ca. 94305

Richard E. Taylor
SLAC - Bin 96
P.O. Box 4349
Stanford, Ca. 94305

Jon J. Thaler
Univ. of Illinois
Physics Dept.
Urbana, Ill. 61801

Manfred Tonutti
SLAC - Bin 95
P.O. Box 4349
Stanford, Ca. 94305

Y. S. Tsai
SLAC - Bin 81
P. O. Box 4349
Stanford, Ca. 94305

Tom Tsao
SLAC - Bin 81
P.O. Box 4349
Stanford, Ca. 94305

Peter Turner
SLAC - Bin 81
P.O. Box 4349
Stanford, Ca. 94305

U:

David G. Unger
U. of Colorado
Physics & Astrophysics Dept.
Boulder, Co. 80302

V:

Yaroslav Va'vra
Carleton Univ.
Physics Dept.
Ottawa, On., Canada K1S 5B6

Harsh Venkataramania
Yale Univ.
Physics Dept.
New Haven, Ct. 06520

Richard Vidal
SLAC - Bin 95
P.O. Box 4349
Stanford, Ca. 94305

Francesco Villa
SLAC - Bin 65
P.O. Box 4349
Stanford, Ca. 94305

T. Virdee
Imperial College, Sci. Tech.
Physics Department
London, SW 7 2B2 England

W:

Walter W. Wada
Ohio State Univ.
Physics Dept.
Columbus, Oh. 43210

Bennie Ward
SLAC - Bin 81
P.O. Box 4349
Stanford, Ca. 94305

Bruce G. Weeks
U. of Michigan
Physics Dept.
Ann Arbor, Mi. 48104

Marvin Weinstein
SLAC - Bin 81
P.O. Box 4349
Stanford, Ca. 94305

J. Weiss
SLAC - Bin 95
P.O. Box 4349
Stanford, Ca. 94305

N. Weiss
SLAC - Bin 81
P. O. Box 4349
Stanford, Ca. 94305

Jorge Willemsen
U. of California
Div. of Natural Sciences
Santa Cruz, Ca. 95064

Raymond Willey
U. of Pittsburgh
Physics Dept.
Pittsburgh, Pa. 15260

M. Wise
SLAC - Bin 81
P.O. Box 4349
Stanford, Ca. 94305

David Wiser
U. of Wisconsin
Physics Dept.
Madison, Wisc. 53706

Stanley Wojcicki
Stanford Univ.
Physics Department
Stanford, Ca. 94305

Lincoln Wolfenstein
Carnegie Mellon Univ.
Physics Dept.
Pittsburgh, Pa. 15213

T. F. Wong
Rutgers Univ.
Physics Dept.
New Brunswick, N. J. 08903

Craig Woody
Johns Hopkins Univ.
Physics Dept.
Baltimore, Md. 21218

K. Wyatt-Brown
California Inst. Tech.
Physics Dept.
Pasadena, Ca. 91125

Y:

Masaki Yasue
Carleton Univ.
Physics Dept.
Ottawa, On., Canada K1S 5B6

Jae Hyung Yee
Yonsei University
Physics Dept.
Seoul, Korea

Z:

Henri Zaccone
SLAC - Bin 95
P.O. Box 4349
Stanford, Ca. 94305

M. S. Zahir
Univ. of Oregon
Inst. of Theoretical Science
Eugene, Ore. 97403

Y. Zambre
Yale University
Physics Dept.
New Haven, Conn. 06520